

66TH INTERNATIONAL



OPEN READINGS

CONFERENCE FOR STUDENTS OF
PHYSICS AND NATURAL SCIENCES

ANNUAL
ABSTRACT BOOK

2023



Vilnius
University

VILNIUS UNIVERSITY PRESS

Editors

Martynas Keršys
Šarūnas Mickus

Cover and Interior design
Milda Stancikaitė

Vilnius University Press
9 Saulėtekio Av., III Building, LT-10222 Vilnius
info@leidykla.vu.lt, www.leidykla.vu.lt/en/
www.knygynas.vu.lt, www.journals.vu.lt

Bibliographic information is available
on the Lithuanian Integral Library Information System (LIBIS) portal ibiblioteka.lt.

ISBN 978-609-07-0883-5 (PDF)

© Vilnius University, 2023

Dear Participants,

Welcome to Open Readings 2023, the 66th International Conference for students of Physics and Natural Sciences!

As the organizing team, we are excited to bring together young researchers from all around the world for this year's live event. Open Readings offers a platform for sharing your work, exchanging ideas, and connecting with fellow scientists.

With a diverse range of topics, distinguished speakers, and enthusiastic young researchers like yourselves, this conference promises a memorable and enriching experience. We encourage you to approach this opportunity with curiosity and creativity, fostering collaboration and pushing the boundaries of knowledge.

Good luck on your scientific journey, and may Open Readings 2023 inspire you to stay curious and innovative.

Sincerely,

The Open Readings 2023 Organizing Team



Conference Chair:

Šarūnas Mickus, *Faculty of Physics, Vilnius University, SPIE Chapter of Vilnius University, OPTICA*

Organizing Committee:

Lukas Naimovičius, *Vilnius University, Institute of Materials Science of Barcelona, SPIE Chapter of Vilnius University, OPTICA*

Gabrielė Stanionytė, *Faculty of Physics, Vilnius University*

Radvilas Bendorys, *Life Sciences Center, Vilnius University*

Martynas Keršys, *Faculty of Physics, Vilnius University*

Goda Grybauskaitė, *Faculty of Physics, Vilnius University*

Dominykas Augulis, *Faculty of Physics, Vilnius University*

Milda Stancikaitė, *Faculty of Physics, Vilnius University*

Erikas Atkočaitis, *Faculty of Physics, Vilnius University*

Uršulė Tarvydytė, *Faculty of Physics, Vilnius University*

Ūla Lauciūtė, *Faculty of Physics, Vilnius University*

Domantas Klumbys, *Faculty of Physics, Vilnius University*

Rimantas Naina, *Faculty of Physics, Vilnius University*

Goda Mažeikaitė, *Faculty of Physics, Vilnius University, SPIE Chapter of Vilnius University*

Giedrius Puidokas, *Faculty of Physics, Vilnius University, SPIE Chapter of Vilnius University*

Ieva Baltrukonytė, *Faculty of Physics, Vilnius University, SPIE Chapter of Vilnius University*

Povilas Užtupys, *Faculty of Physics, Vilnius University*

Dovydas Špukas, *Faculty of Physics, Vilnius University*

Programme Committee:

Dr. Agnė Kalnaitytė, *Laser Research Center, Faculty of Physics, Vilnius University*

Dr. Aldona Balčiūnaitė, *Department of Catalysis, Center for Physical Sciences and Technology*

Dr. Algirdas Mikalkėnas, *Institute of Biosciences, Life Sciences Centre, Vilnius University*

Dr. Andrius Gelžinis, *Institute of Chemical Physics, Faculty of Physics, Vilnius University*

Dr. Andrius Žemaitis, *Department of Laser Technologies, Center for Physical Sciences and Technology*

Bernadeta Masiulionytė, *Institute of Biotechnology, Life Sciences Center, Vilnius University*

Dr. Brigita Abakevičienė, *Institute of Materials Science, Faculty of Mathematics and Natural Sciences, Kaunas University of Technology*

Dr. Dovydas Banevičius, *Institute of Photonics and Nanotechnology, Faculty of Physics, Vilnius University*

Dr. Edvinas Orentas, *Department of Organic Chemistry, Faculty of Chemistry and Geosciences, Vilnius University*

Dr. Edvinas Radiunas, *Institute of Photonics and Nanotechnology, Faculty of Physics, Vilnius University*

Enrika Celitan, *Department of Biochemistry and Molecular Biology, Life Sciences Center, Vilnius University*

Dr. Greta Bigelytė, *Institute of Biotechnology, Life Sciences Center, Vilnius University*

Dr. Ieva Matulaitienė, *Department of Organic Chemistry, Center for Physical Sciences and Technology*

Dr. Ilja Ignatjev, *Department of Organic Chemistry, Center for Physical Sciences and Technology*

Dr. Irina Buchovec, *Institute of Photonics and Nanotechnology, Faculty of Physics, Vilnius University*

Dr. Julius Vengelis, *Laser Research Center, Faculty of Physics, Vilnius University*

Dr. Jurga Būdienė, *Department of Organic Chemistry, Center for Physical Sciences and Technology*

Dr. Jurga Juodkazytė, *Department of Chemical Engineering and Technology, Center for Physical Sciences and Technology*

Dr. Justinas Čeponkus, *Institute of Chemical Physics, Faculty of Physics, Vilnius University*

Kotryna Skardžiūtė, *Institute of Biotechnology, Life Sciences Center, Vilnius University*

Kristina Žukauskaitė, *Institute of Biosciences, Life Sciences Centre, Vilnius University*

Dr. Linas Vilčiauskas, *Department of Chemical Engineering and Technology, Center for Physical Sciences and Technology*

Dr. Mažena Mackoit-Sinkevičienė, *Institute of Theoretical Physics and Astronomy, Vilnius University*

Dr. Mindaugas Karaliūnas, *Optoelectronics Department, Center for Physical Sciences and Technology*

Dr. Nina Urbelienė, *Institute of Biochemistry, Life Sciences Center, Vilnius University*

Dr. Paulius Baronas, *Department of Superconducting Materials and Nanostructure at Large Scale, Institute of Materials Science of Barcelona*

Dr. Rasa Pauliukaitė, *Department of Nanoengineering, Center for Physical Sciences and Technology*

Dr. Rasa Platakytė, *Institute of Chemical Physics, Faculty of Physics, Vilnius University*

Dr. Renata Butkutė, *Optoelectronics Department, Center for Physical Sciences and Technology*

Dr. Steponas Raišys, *Institute of Photonics and Nanotechnology, Faculty of Physics, Vilnius University*

Dr. Tadas Malinauskas, *Institute of Photonics and Nanotechnology, Faculty of Physics, Vilnius University*

Dr. Tomas Čeponis, *Institute of Photonics and Nanotechnology, Faculty of Physics, Vilnius University*

Dr. Tomas Šalkus, *Institute of Applied Electrodynamics and Telecommunications, Faculty of Physics, Vilnius University*

Dr. Tomas Serevičius, *Institute of Photonics and Nanotechnology, Faculty of Physics, Vilnius University*

Dr. Tomas Tamulevičius, *Institute of Materials Science, Faculty of Mathematics and Natural Sciences, Kaunas University of Technology*

Dr. Virginija Kalcienė, *Institute of Biosciences, Life Sciences Centre, Vilnius University*

Dr. Vytautas Jakštas, *Department of Physical Technologies, Center for Physical Sciences and Technology*

Dr. Vytautas Klimavičius, *Institute of Chemical Physics, Faculty of Physics, Vilnius University*

Chairmen:

Dr. Mažena Mackoit-Sinkevičienė, *Institute of Theoretical Physics and Astronomy, Vilnius University*

Dr. Tomas Serevičius, *Institute of Photonics and Nanotechnology, Faculty of Physics, Vilnius University*

Dr. Dovydas Banevičius, *Institute of Photonics and Nanotechnology, Faculty of Physics, Vilnius University*

Dr. Edvinas Radiunas, *Institute of Photonics and Nanotechnology, Faculty of Physics, Vilnius University*

Dr. Jurga Būdienė, *Department of Organic Chemistry, Center for Physical Sciences and Technology*

Dr. Aldona Balčiūnaitė, *Department of Catalysis, Center for Physical Sciences and Technology*

Dr. Vytautas Klimavičius, *Institute of Chemical Physics, Faculty of Physics, Vilnius University*

Dr. Vytautas Jukna, *Laser Research Center, Faculty of Physics, Vilnius University*

Dr. Domas Paipulas, *Laser Research Center, Faculty of Physics, Vilnius University*

Dr. Mikas Vengris, *Laser Research Center, Faculty of Physics, Vilnius University*

Dr. Algirdas Mekys, *Institute of Photonics and Nanotechnology, Faculty of Physics, Vilnius University*

Dr. Kęstutis Ikamas, *Institute of Applied Electrodynamics and Telecommunications, Faculty of Physics, Vilnius University*

Dr. Mangirdas Malinauskas, *Laser Research Center, Faculty of Physics, Vilnius University*

Dr. Gintaras Valušis, *Optoelectronics Department, Center for Physical Sciences and Technology*

Dr. Wanessa De Cassia Martins Antunes De Melo, *Department of Functional Materials and Electronics, Center for Physical Sciences and Technology*

Dr. Greta Bigelytė, *Institute of Biotechnology, Life Sciences Center, Vilnius University*

ELECTRICITY AND FUELS FROM THE SUN: UNDERSTANDING AND CONTROLLING ELECTRON AND ENERGY TRANSFER REACTIONS IN SOLAR ENERGY CONVERSION MATERIALS

Maria Abrahamsson

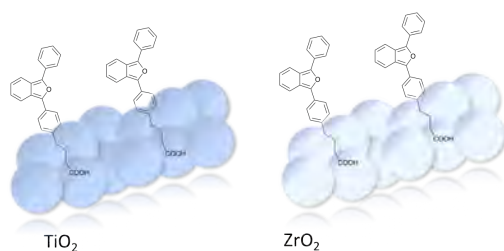
Chalmers University of Technology
abmaria@chalmers.se

Ca 160 years ago, the first scientific article that showed that CO₂ is a greenhouse gas was published. And about 125 years ago, Swedish chemist Svante Arrhenius predicted that an increased amount of CO₂ in the atmosphere would lead to increased temperatures. Jump ahead to 1912 and the Italian photochemist Giacomo Ciamician stated that we should not use coal, but the sun, for our energy supply.

Solar energy has tremendous potential to be a central part of the transition to a more sustainable society. If we can increase the efficiency of direct conversion of solar energy into useful energy forms for us by just 1%, it corresponds to more than the entire combined potential of all other types of renewable energy (nuclear power not included).

In my research group we are concerned with conversion of solar energy into fuels and electricity and especially with the (multi)-electron and energy transfer processes that govern the energy conversion reactions. One of the avenues we are exploring concerns how we can manipulate the incoming solar radiation so that we can increase the efficiency of solar cells. This means we look into the process of singlet fission to better utilize sunlight with *higher-than-necessary* energies and photon upconversion to use the red part of the solar spectrum. Another avenue of our research concerns how we can store solar energy – in chemical bonds. Simply a way to make fuel from sunlight. One can think of several different end products, it could be hydrogen, or methanol or methane. These processes require moving a lot of charges. Issues with stability, and unwanted reactions occurring are common.

In the talk, I will give examples of how the environment and choice of material affects the electron and energy transfer rates and yields. For example, we have shown that by changing the polarity of the surrounding solvent, we can control the singlet fission dynamics. In order to further understand the environmental effects, we have also studied well-known singlet fission chromophores in gels, aiming at an understanding on how self-assembly in the solid state can be used to achieve efficient singlet fission.



References

Sundin, E., Ringström, R., Johansson, F., Küçüköz, B., Ekebergh, A., Gray, V., Albinsson, B., Mårtensson, J., Abrahamsson, M. *J. Phys. Chem. C* **2020**, 124, 20794–20805.

TRIPLET-TRIPLET ANNIHILATION MEDIATED PHOTON UPCONVERSION IN CONFINED NANO DOMAINS OF BIOPOLYMER-SURFACTANTS-CHROMOPHORES CO-ASSEMBLY

Pankaj Bharmoria^{1,2,3}, Nobuhiro Yanai,^{2*} Nobuo Kimizuka,^{2*} Kasper Moth-Poulsen^{1,3*}

¹ The Institute of Materials Science of Barcelona, ICMAB-CSIC, Barcelona, Spain

² Department of Chemistry and Biochemistry, Graduate School of Engineering, Kyushu University, Japan

³ Department of Chemistry and Chemical Engineering, Chalmers University of Technology, Sweden
pbharmoria@icmab.es

Triplet-triplet annihilation mediated photon upconversion (TTA-UC) materials are emerging for applications in biology to drive non-invasive low energy excitation based biochemical processes, and in photovoltaics (PV) to avoid transmission losses.^[1] However, realization of efficient TTA-UC materials in aqueous environments and solid-state faces issues of chromophores aggregation and deactivation of excited triplets by dissolved oxygen molecules. We overcame these issues by developing a generalized approach of biopolymer surfactant-chromophore coassembly where TTA-UC chromophores are confined inside surfactant nano-domains coated with thick fiber networks of biopolymers in hydrogels or bioplastic frameworks (Fig. 1). Consequently, air-stable green to blue TTA-UC with high UC efficiency of 13.5% and a long annihilator triplet lifetime of 4.9 ms was achieved in the hydrogel.^[2] Interestingly, drying of this hydrogel in air resulted in phase separation of liquid surfactant domains containing chromophores inside the transparent solid bioplastic film. The film showed even higher UC efficiency of 15.6 % in air with an unprecedented durability of two years.^[3] Further, to expand the photon harvesting window of bioplastics, red to blue TTA-UC bioplastics with record UC efficiency of 17.6 % and proof-of-concept Far-red to blue bioplastics were developed.^[4] The key is two-fold. First, biopolymer and the surfactant self-assemble in water to give a developed hierarchical structure with hydrophobic domains which accommodate chromophores up to high concentrations to drive efficient triplet energy transfer and TTA. Second, thick hydrogen-bonding networks of biopolymer backbone prevent O₂ inflow to the interior chromophores region, as evidenced by long triplet lifetimes both in hydrogels (4.9 ms) and bioplastic films (1.6 to 2.5 ms). Later, the developed NIR to blue hydrogel was successfully applied for optogenetic genome engineering of light responsive hippocampal gene to induce neuronal dendrite growth with unconverted blue light upon excitation with NIR light in vitro.^[5]

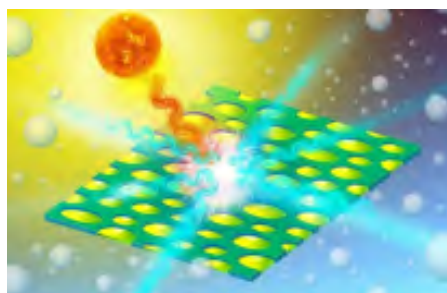


Fig. 1. Air Stable triplet-triplet annihilation mediated photon upconversion in confined nano-domains

- [1] **P. Bharmoria**,* H. Bildirir and K. Moth-Poulsen,* Triplet–triplet annihilation based near infrared to visible molecular photon upconversion, *Chem. Soc. Rev.* **49**, 6529–6554 (2020).
- [2] **P. Bharmoria**, S. Hisamitsu, H. Nagatomi, T. Ogawa, M.-aki Morikawa, N. Yanai* and N. Kimizuka,* Simple and Versatile Platform for Air Tolerant Photon Upconverting Hydrogels by Biopolymer–Surfactant–Chromophore Co-assembly, *J. Am. Chem. Soc.* **140**, 10848–10855 (2018) [3] **P. Bharmoria**, S. Hisamitsu, Y. Sasaki, T. S. Kang, M.-aki Morikawa, B. Joarder, H. Bildirir, A. Mårtensson, K. Moth-Poulsen, N. Yanai and N. Kimizuka,* *J. Mater. Chem. C* 2021, **9**, 11655–11661 (2021).
- [4] **P. Bharmoria**, F. Edhborg, H. Bildirir, Y. Sasaki, S. Ghasemi, A. Mårtensson, N. Yanai, N. Kimizuka, B. Albinsson, K. Börjesson, K. Moth Poulsen,* Recyclable optical bioplastics platform for solid state red light harvesting via triplet–triplet annihilation photon upconversion *J. Mater. Chem. A* **10**, 21181–21752 (2022).
- [5] Y. Sasaki, M. Oshikawa, **P. Bharmoria**, H. Kouno, A. Hayashi-Takagi, M. Sato, I. Ajioka,* N. Yanai,* and N. Kimizuka* Near-Infrared Optogenetic Genome Engineering Based on Photon Upconversion Hydrogels. *Angewandte Chemie Int. Ed.* **58**, 17827 -17833 (2019)

LASER PRINTING

Boris N. Chichkov

Leibniz University Hannover, Institute of Quantum Optics

In this lecture, I will start from a discussion of photon properties (mass, momentum, and energy) in a dielectric medium. Then, I will turn to the discussion of laser-based techniques which can be applied for the generation of complex 2D and 3D structures by printing very small and delicate objects like nanoparticles, living cells, and microorganisms. I will consider a few application examples of this technology for printing of metasurfaces, 3D scaffolds for tissue engineering, and biofabrication of biological systems.

POLARITONIC NONLINEAR METASURFACES FOR FLAT NONLINEAR OPTICS

Mikhail A. Belkin

Walter Schottky Institute, Technical University of Munich, Garching, Germany

mikhail.belkin@wsi.tum.de

Nonlinear optical metasurfaces – planar structures made of a large number of sub-wavelength elements with engineered nonlinear optical response – can enable frequency mixing without phase-matching constraints of bulk nonlinear crystals and manipulation of the shape of the output beam via phase control of the nonlinear response of an individual sub-wavelength element. However, efficient frequency mixing in nonlinear metasurfaces requires nonlinear response orders of magnitude higher than that of traditional materials.

Intersubband transitions in n-doped coupled semiconductor coupled quantum wells allow one to quantum-engineer nonlinear response in semiconductor materials and produce very large optical nonlinearities. This large nonlinear optical response can be further enhanced if intersubband transitions are coupled to electromagnetic modes of optical nanoresonators fabricated in the semiconductor heterostructures to form intersubband nonlinear polaritonic metasurfaces. In this presentation, I will share our results on developing metasurfaces that display second- and third-order nonlinear susceptibility values 4-7 orders of magnitude higher than that of traditional nonlinear materials. In particular, I will present metasurfaces designed for efficient mid-infrared second harmonic and difference-frequency generation with second-order nonlinear susceptibility of $\sim 10^6$ pm/V with controllable phases of the nonlinear optical response and metasurfaces designed for saturable absorption and power limiting.

THE CALTECH OPTICAL OBSERVATORIES

Jonas Zmuidzinas

California Institute of Technology

Caltech has a long and rich tradition in astronomy and astrophysics, especially in optical astronomy, where Caltech has developed and operated forefront observatories for many decades. This year - 2023 - marks the 75th anniversary of the 5-meter Hale Telescope at Palomar CA as well as the 30th anniversary of the Keck Observatory on Mauna Kea, HI. I will trace the history of the Palomar and Keck Observatories, review some key scientific accomplishments, describe current efforts to construct and deploy leading-edge instrumentation, and conclude with a few words on the next-generation observatory, the Thirty Meter Telescope (TMT) project.

About the author:

Jonas Zmuidzinas is the Merle Kingsley Professor of Physics at Caltech and currently serves as the Director of the Caltech Optical Observatories. A native of Southern California, he received his B.S. in physics from Caltech in 1981 and his Ph.D. in physics from U.C. Berkeley in 1987. He has served on the Caltech faculty since 1990 and has also concurrently held positions at the Caltech/NASA Jet Propulsion Laboratory including Chief Technologist. His father, Jonas Stasys Zmuidzinas, was born in Lithuania, as were his wife Vilia's parents, Adomas and Lina Mickeviciai.

QUANTUM METROLOGY WITH NON-CLASSICAL STATES OF LIGHT

Michèle Heurs

Leibniz University Hannover

Nowadays, non-classical (fixed-quadrature „squeezed“) light is routinely used in second-generation interferometric gravitational wave detectors such as aLIGO and AdVirgo to increase their detection sensitivity, leading to some of the most exciting astrophysical discoveries of the past years. Beyond this well-known application example, squeezing is a quantum technique that can benefit precision metrology in many other areas. It can be useful whenever the signal-to-noise ratio of the measurement is fundamentally limited by the quantum noise of the employed and technically already ultra-stabilised laser light.

This talk will highlight exemplary applications of squeezed light, ranging from interferometric gravitational wave detection to sub-shot-noise limited spectroscopy. The latter example makes use of high-frequency squeezed light sources, so-called *squeezing combs*, which will be introduced in this talk. These squeezing combs exhibit entanglement between the individual upper and lower squeezing sidebands, which occur at the free spectral ranges of the squeezing cavity. This feature makes squeezing combs a promising resource for applications in quantum information.

THE MODERN RESPONSE TO INFECTIOUS DISEASE OUTBREAKS USING GENETIC SEQUENCING

Gytis Dudas

Vilnius University, Life Sciences Center

The modern response to infectious disease outbreaks has become unimaginable without sequencing, the reading of the genetic code that makes up the pathogen. Due to increasingly cheaper sequencing technologies, it is now trivial to diagnose genetic conditions in humans and many infectious disease outbreaks caused by bacterial, viral, and even fungal pathogens can be dissected with a remarkable degree of precision, revealing information that would be impossible or unfeasible to get via any other means. You'll hear about a few outbreaks and epidemics from the headlines of the last decade (e.g. Ebola virus in West Africa 2013-2016) whose investigations using pathogen genetic sequence data spearheaded the ongoing revolution in epidemiology, how such information was used in Lithuania during the SARS-CoV-2 pandemic, and how methods developed in this field are now being applied in entirely new areas, like looking at infections in mosquitoes.

Conference Programme:

	APRIL 18		APRIL 19	
09:00-09:15	OPENING CEREMONY (A101)		BORIS CHICHKOV (A101) Leibniz Universität Hannover	
09:15-10:00	MARIA ABRAHAMSSON (A101) Chalmers University of Technology		Laser printing	
10:00-10:15	Electricity and Fuels from the Sun: Understanding and controlling electron and energy transfer reactions in solar energy conversion materials		EKSPLA (A101)	
10:15-11:00	BREAK		BREAK	
11:00-12:15	O1 (A101) Chemistry and Chemical physics	O2 (D401) Nanomaterials and Nanotechnology	O5 (A101) Material Science and Modern Technologies	O6 (D401) Laser Physics and Optical Technologies
12:15-13:00	LUNCH		LUNCH	
13:00-14:00	O3 (A101) Chemistry and Chemical physics	O4 (D401) Nanomaterials and Nanotechnology	O7 (A101) Material Science and Modern Technologies	O8 (D401) Laser Physics and Optical Technologies
14:00-14:15				
14:15-14:45	BREAK		BREAK	
14:45-15:00				
15:00-16:00	PANKAJ BHARMORIA (A101) Institute of Materials Science of Barcelona (ICMAB-CSIC) Triplet-Triplet Annihilation Mediated Photon Upconversion in Confined Nano- domains of Biopolymer-Surfactants-Chromophores Co-Assembly		MIKHAIL BELKIN (A101) Walter Schottky Institute, Technical University of Munich Polaritonic Nonlinear Metasurfaces for Flat Nonlinear Optics	
16:00-16:15	LIGHT CONVERSION (A101)		BROLIS SENSOR TECHNOLOGY (A101)	
16:15-17:15	P1 (MAIN HALL) Chemistry and Chemical physics /Functional Materials and Derivatives	AŠ - DAKTARAS. KAS IŠ TO?(A101)	P2 (MAIN HALL) Material Science and Modern Technologies/Nanomaterials and Nanotechnology/Semiconductor and Condensed Matter/Laser Physics and Optical Technologies/Spectroscopy/Theoretical Physics	
17:15-18:00				
18:00-19:00			VILNIUS CITY TOUR (FTMC LOBBY)	
19:00				

	APRIL 20	APRIL 21		
09:00-09:15	JONAS ŽMUIDZINAS (A101) California Institute of Technology The Caltech Optical Observatories	GYTIS DUDAS (A101) Vilnius University The modern response to infectious disease outbreaks using genetic sequencing		
09:15-10:00				
10:00-10:15	NANOAVIONICS (A101)			
10:15-11:00	BREAK	BREAK		
	INSIDE NATURE COMMUNICATIONS			
11:00-12:15	O9 (A101) Theoretical Physics	O10 (D401) Spectroscopy, Methods and Devices for Physical Diagnostics	O13 (A101) Biochemistry, Biophysics and Biotechnology	O14 (D401) Biology, Genetics and Biomedical Sciences
12:15-13:00	LUNCH		LUNCH	
13:00-14:00	O11 (A101) Astrophysics and astronomy	O12 (D401) Spectroscopy, Methods and Devices for Physical Diagnostics	P3 (MAIN HALL) Biochemistry, Biophysics and Biotechnology/Biology, Genetics and Biomedical Sciences	
14:00-14:15			BREAK	
14:15-14:45	BREAK		CLOSING REMARKS (A101)	
14:45-15:00				
15:00-16:00	MICHELE HEURS (A101) Leibniz Universität Hannover Quantum metrology with non-classical states of light			
16:00-16:15				
16:15-17:15	SPECIAL EVENT (A101) Artificial intelligence and academic publishing			
17:15-18:00				
18:00-19:00				
19:00	SOCIAL EVENING			

O1 Session:

TRANSIENT ABSORPTION SPECTROSCOPY OF EXCITATION DYNAMICS AND RADICAL FORMATION IN DIFFERENT PHOTOINITIATORS	38
Marius Navickas, Edvinas Skliutas, Mangirdas Malinauskas, Mikas Vengris	
INVESTIGATION OF NEW TADF MATERIALS DERIVATIVE OF THE 1,3,5- TRIAZINE MOLECULE	39
Eyad Al Souki, Ikbal Marghad, Mathieu Sauthier	
ONE-STEP IMIDAZO[2,1-<i>b</i>][1,3]THIAZINE AND IMIDAZO[2,1- <i>c</i>][1,4]THIAZEPINE SCAFFOLD SYNTHESIS FROM 2- ALKYNYLTHIOIMIDAZOLES	40
Indrė Misiūnaitė, Algirdas Brukštus, Ieva Žutautė	
SYNTHETIC PATHWAY INVESTIGATION OF BENZIMIDAZOLE DERIVATIVES AS POTENTIAL INHIBITORS FOR HSP90	41
Lukas Neverdauskas, Paulina Kaziukonytė, Algirdas Brukštus	
FEMTOSECOND LASER WAVELENGTH INFLUENCE ON THE FORMATION OF SINGLE-SHOT GOLD NANOSTRUCTURES	42
Kernius Vilkevičius, Evaldas Stankevičius	

O2 Session:

NITROGEN-MODIFIED REDUCED GRAPHENE OXIDE AS A PLATFORM FOR SENSITIVE AND SELECTIVE ELECTROCHEMICAL DETECTION OF DOPAMINE.....	43
Rūta Aukštakojytė, Justina Gaidukevič, Rasa Pauliukaitė, Jurgis Barkauskas	
INVESTIGATION OF THE DEPENDENCE OF LASER PULSE ENERGY ON THE STABILITY OF GOLD, SILVER AND HYBRID NANOPARTICLES GENERATED FROM THIN FILM TARGETS	44
Vita Petrikaitė, Evaldas Stankevičius	
ENHANCED BIOIMAGING PROPERTIES OF NANOSIZED FLUOROAPATITE COMPOSITES, DOPED WITH EUROPIUM(III) IONS <i>VIA</i> INCORPORATION OF RUBIDIUM(I) IONS	45
Nicole Nowak, Dominika Czekanowska, Tomasz Gebarowski, Rafal J. Wiglusz	
PROBING METHYL GROUP TUNNELING IN [(CH₃)₂NH₂][Zn(HCOO)₃] HYBRID PEROVSKITE USING Co²⁺ EPR.....	46
Gediminas Usevičius, Ignas Pocius, Vidmantas Kalendra, Mirosław Mączka, Jūras Banys, Mantas Šimėnas	

O3 Session:

INVESTIGATION OF TES-ADT BASED NIR-TO-VIS PHOTON UPCONVERSION SYSTEM	47
Justas Lekavičius, Edvinas Radiunas, Karolis Kazlauskas	
MICROSCOPIC ANALYSIS OF MAGNETISATION PROCESSES USING THE ISING MODEL.....	48
Jorūnas Dobilas	
MODELLING GLIBENCLAMIDE IN AQUEOUS MIXTURES OF BIOACTIVE IONIC LIQUIDS	49
Žyginta Einorytė, Vytautas Klimavičius, Kęstutis Aidas	
SYNTHESIS OF AROMATIC <i>N</i>-OXIDES AND EPOXIDES BY BIOCATALYTIC METHODS	50
Greta Mačiūitytė, Vytautas Petkevičius	
GARNETS FOR SCINTILATION APPLICATION.....	51
Greta Inkrataitė, Jan-Niklas Keil, Thomas Jüstel, Ramūnas Skaudžius	

O4 Session:

ADSORPTION MECHANISM OF METHYLENE BLUE DYE ON POLYMER CLAY NANOCOMPOSITE.....	52
Yao Mawuena Tsekpo, Augustine Nana Sekyi Appiah, Lucas Nana Wiredu Damoah, Daniel Amusah and Ebenezer Annan	
TYROSINE KINASE INHIBITORS COMBINED WITH NANOHYDROXYAPATITE FOR TARGETED THERAPIES - PHYSICO-CHEMICAL AND IN VITRO STUDIES	53
Paulina Sobierajska, Anna Serwotka-Suszczak, Sara Targonska, Damian Szymanski, Krzysztof Marycz and Rafal J. Wiglusz	
MULTI- LEVEL HIERARCHICAL CONSTRUCTION OF NANO- AND MICRO- COMPOSITE PARTICLES SUPPORTED BY MICROFLUIDICAL SYNTHESIS.....	54
Raminta Mazetyte, Johann Michael Köhler	

O5 Session:

INVESTIGATION OF FANO RESONANCE NATURE IN SPLIT-RING RESONATOR ARRAY METASURFACE.....	55
Darius Urbonis, Žilvinas Kancleris, Paulius Ragulis	
BANDGAP MODULATION BY CATIONIC SUBSTITUTION IN QUASI-ONE- DIMENSIONAL SnZrS₃-SnTiS₃ ALLOY SYSTEM	56
Rokas Kondrotas, Vidas Pakštis, Artūras Suchodolskis, Katri Muska, Marit Kauk-Kuusik	
NMR CHARACTERIZATION OF NOVEL Y_{3-x}Na_xAl_{5-y}VyO₁₂ GARNETS	57
Carlos Martin Signes, Diana Vištorskaja, Aivaras Kareiva, Vytautas Klimavičius	
PRUSSIAN WHITE AS CATHODE MATERIAL FOR AQUEOUS SODIUM ION BATTERIES.....	58
Gintarė Gečė, Jurgis Pilipavičius, Linas Vilčiauskas	
BEHAVIOUR OF 3D PRINTING FILAMENTS IN ENVIRONMENTS WITH VARIOUS RELATIVE HUMIDITY	59
Leons Stankevics, Olga Bulderberga, Andrey Aniskevich	

O6 Session:

INVESTIGATIONS OF NONLINEAR ABSORPTANCE AND FATIGUE EFFECT IN HFO₂, ZRO₂, AND AL₂O₃ DIELECTRIC COATINGS	60
Erikas Atkočaitis, Simonas Kičas, Vaida Grašytė, Justinas Galinis, Austėja Aleksiejūtė, Andrius Melninkaitis	
EFFECT OF MICROMACHINING PARAMETERS ON GEOMETRICAL	61
Mohamed A. Baba, Gazy Rodowan, Brigita Abakevičienė, Sigita Tamulevičius, Sebastian Molin, Tomas Tamulevičius	
LASER IRRADIATION BY SHORT PULSES FOR WETTABILITY MODIFICATION OF COPPER SURFACE	62
Saulė Steponavičiūtė, Andrius Žemaitis, Paulius Gečys, Mindaugas Gedvilas	
SUPERCONTINUUM GENERATION IN KGW CRYSTAL AT HIGH REPETITION RATE	63
Kawthar Reggui, Vaida Marčiulionytė, Gintaras Tamošauskas, Audrius Dubietis	

O7 Session:

DLC:CU THIN FILM STABILITY TESTING IN CELL CULTURE MEDIUM.....	64
Shahd Elkhider, Mohamed A. Baba, Andrius Vasiliauskas, Šarūnas Meškėnis, Dainius Zienius,	
TEMPERATURE DRIVEN PHASE TRANSITIONS IN METASTABLE Sc DOPED HEXAGONAL LuFeO₃.....	65
Andrius Pakalniškis, Gediminas Niaura, Dmitry Karpinsky, Guillaume Rogez, Pierre Rabu, Shih-Wen Chen, Thomas Chung-Kuang Yang, Ramūnas Skaudžius, Aivaras Kareiva	

INVESTIGATION OF CHARGE CARRIER DYNAMICS IN Mg DOPED GAN LAYERS BY LIGHT-INDUCED TRANSIENT GRATING TECHNIQUE	66
Mantas Vaičiulis, Arūnas Kadys, Ramūnas Aleksiejūnas	

RESEARCH OF NON-EQUILIBRIUM CHARGE CARRIER DYNAMICS IN GAN FILMS WITH VARYING IMPURITY DENSITIES	67
Mantas Auruškevičius, Kazimieras Nomeika	

O8 Session:

DEVELOPMENT AND INVESTIGATION OF SUBNANOSECOND PULSE COMBINED OPTICAL PARAMETRIC AMPLIFIER SYSTEM	68
--	-----------

Augustė Stravinskaitė, Gabrielė Stanionytė, Jonas Banyš, Julius Vengelis

PHOTOLUMINESCENCE MAPPING OF INGAAS/GAAS MULTI- QUANTUM WELL SYSTEM FOR VCSEL FABRICATION	69
--	-----------

Andrea Zelioli, Arnas Pukinskas, Silvija Keraitytė, Augustas Vaitkevičius, Sandra Stanionytė, Monika Jokubauskaitė, Bronislovas Čechavičius, Aurimas Čerškus, Evelina Dudutienė, Renata Butkutė

THE DEPENDANCE OF MAGNETO-OPTICAL SIGNALS ON THE RELATIVE PUMP-PROBE BEAM INTENSITY IN Cs ATOMS FOR ZERO MAGNETIC FIELD DETECTION	70
--	-----------

A. Nikolajevs, A. Mozers, L. Busaite, D. Osite, F. Gahbauer, M. Auzinsh

THIN MICROWAVE ANTENNA DESIGN FOR WIDE FREQUENCY RANGE OPTICALLY DETECTED MAGNETIC RESONANCE MEASUREMENTS	71
--	-----------

Emils Smits, Reinis Lazda, Florian Gahbauer and Marcis Auzinsh

APPLICATION OF A NV BASED MAGNETOMETER AS A HIGH DC	72
--	-----------

Antra Asare, Reinis Lazda, Oskars Rudzitis, Florian Gahbauer, and Marcis Auzinsh

O9 Session:

COMPLEX S_3-SYMMETRIC THREE-HIGGS-DOUBLET MODELS	73
--	-----------

Anton Kunčinas, Odd Magne Øgreid, Per Osland, Margarida Nesbitt Rebelo

MAGNETIC PROPERTIES OF $L1_0$ FENI THIN FILMS WITH SURFACES (010), (111), AND (001): DENSITY FUNCTIONAL THEORY CALCULATIONS	74
---	-----------

Joanna Marciniak, Mirosław Werwiński

TOPOLOGICAL CHARGE PUMPING IN SUBWAVELENGTH OPTICAL LATTICES	75
---	-----------

Domantas Burba, Mantas Račiūnas, Ian B. Spielman, Gediminas Juzeliūnas

EXCITED STATES OF CHLOROPHYLL MOLECULES IN LIGHT-HARVESTING ANTENNA OF PSI	76
---	-----------

Gabrielė Rankelytė, Jevgenij Chmeliov, Andrius Gelžinis, Leonas Valkūnas

KINETICS OF THE CONFORMATIONAL CHANGES OF THE NITROGEN MATRIX ISOLATED DISUBSTITUTED SILACYCLOHEXANES: EXPERIMENT MEETS THEORY AT FINITE TEMPERATURE RANGE	77
---	-----------

Joanna Stocka, Pawel Rodziewicz, Valdas Sablinskas, Gamil A. Guirgis

O10 Session:

SOLID STATE NMR SPECTROSCOPY STUDY OF CALCIUM PYROPHOSPHATE ($Ca_2P_2O_7$) POLYMORPHS EXPOSED TO X-RAY RADIATION	78
--	-----------

Aurimas Dubauskas, Diana Griesiūtė, Andris Antuzevics, Aleksej Žarkov, Vytautas Klimavičius

THE MIEYE: BENCH-TOP SUPER-RESOLUTION MICROSCOPE WITH COST-EFFECTIVE EQUIPMENT	79
---	-----------

Mohammad Nour Alsamsam, Aurimas Kopūstas, Meda Jurevičiūtė, Marijonas Tutkus

ROA-CPL SPECTROSCOPY CAN CLEARLY DISTINGUISH POST- TRANSLATIONAL MODIFICATIONS OF PEPTIDES	80
---	-----------

Agnieszka Domagała, Grzegorz Zajac, Małgorzata Barańska

MAPPING VISCOSITIES OF LIPID BILAYERS IN LIVE CELLS AND MODEL MEMBRANES THROUGH FLIM 81

Artūras Polita, Gintaras Valinčius

EFFECT OF UV AND IR WAVELENGTHS ON PLASMA CHARACTERISTICS FOR FEMTOSECOND LIBS ON COPPER AND82

Gytis Zaremba, Ona Balachninaite, Domas Paipulas

O11 Session:

HST APERTURE PHOTOMETRY OF THE STAR CLUSTERS IN M3183

Eimantas Kriščiūnas, Rima Stonkutė, Vladas Vansevicius

AGN OUTFLOW-INDUCED STAR FORMATION IN GALACTIC DISC 84

Martynas Laužikas, Kastytis Zubovas

STOCHASTICITY OF STAR CLUSTER PARAMETERS.....85

Karolis Daugevičius, Rima Stonkutė, Vladas Vansevicius

A FAST GRID-BASED FEEDBACK INJECTION METHOD IN NUMERICAL AGN SIMULATIONS 86

Matas Tartėnas, Kastytis Zubovas

SPATIAL DIVERSITY IN COMPETING DYNAMICS ISING MODEL87

Justas Kvedaravicius, Aleksejus Kononovicius

O12 Session:

SODIUM SILICATE PARTICLE SIZE MEASUREMENTS USING TIME - RESOLVED FLUORESCENCE ANISOTROPY88

Daniel Doveiko, Simon Stebbing, Yu Chen, David J. Birch, Vladislav Vyshemirsky, Olaf Rolinski

DYNAMIC FORCE SPECTROSCOPY OF HEMOGLOBIN-INOSITOL PHOSPHATES INTERACTION SIMULATED BY STEERED MOLECULAR DYNAMICS 89

Wojciech Marciniak, Joanna Marciniak, Arkadiusz Ptak

STUDY OF THE ANTIVIRAL PROPERTIES OF SURFACE COATINGS USING THE SERS SPECTROSCOPY TECHNIQUE 90

Marius Balodis, Sonata Adomavičiūtė-Grabusovė, Valdas Šablinskas

GAS FLOW DYNAMICS AND PURIFICATION FROM ULTRAFINE PARTICULATE MATTER IN A NEWLY DEVELOPED APPARATUS 91

Aleksandras Chlebnikovas, Artūras Kilikevičius

O13 Session:

CRYO-EM STRUCTURES OF *STREPTOCOCCUS THERMOPHILUS* CAS9 BOUND TO TARGET AND NON-TARGET DNA92

Ugne Gaizauskaite, Arunas Silanskas, Giedrius Sasnauskas

STRUCTURAL CHARACTERIZATION OF A TYPE II CRISPR-CAS INTEGRASE COMPLEX93

Rugilė Ivanickaitė, Giedrius Sasnauskas

PROPIDIUM IODIDE, OLIGO- AND POLYNUCLEOTIDE SIZE INFLUENCE ON CELL ELECTROTRANSFER EFFECTIVENESS 94

Aras Rafanavičius, Rūta Palepšienė, Saulius Šatkauskas

THERMODYNAMIC CHARACTERISTICS OF THE SOLID DISPERSION SYSTEM OF DIOSMIN95

Artem Kharchenko, Vadym Lisovyi, Volodymyr Bessarabov, Olga Kovalevska, Andriy Goy, Iryna Povshedna

O14 Session:

DECREASE IN P53 FUNCTION IS AN EARLY STEP TOWARDS CHEMORESISTANCE IN COLORECTAL CANCER CELLS	96
Julius Žukas, Nadežda Dreizė, Silvija Urnikytė, Mantas Špakovas	
THE EFFICACY OF GEMCITABINE ON VIABILITY AND SURVIVAL OF PANCREATIC CANCER CELLS POST AHR GENE SILENCING, IN VITRO	97
Gabrielė Karvelytė, Darius Stukas, Aldona Jasukaitienė, Jason Matthews, Antanas Gulbinas, Žilvinas Dambrauskas	
SIALIDASE GENE EXPRESSION AND ENZYMATIC ACTIVITY ASSESSMENT IN THE DEVELOPING MOUSE HIPPOCAMPUS.....	98
Rimas Prokopovicius, Ugne Kuliesiute , Urte Neniskyte	
FOLICULOGENESIS-RELATED GENE EXPRESSION IN CHEMOTHERAPY-INDUCED PREMATURE OVARIAN FAILURE MODEL	99
Indrė Krastinaitė, Veronika Viktorija Borutinskaitė, Rūta Navakauskienė	

P1 Session:

CARBON FROM COCONUT SHELLS FOR EFFICIENT REMOVAL OF NITROBENZENE FROM AQUEOUS SOLUTION.....	100
Aleksandar M. Đorđević, Jadranka Milikić, Aldona Balčiūnaitė and Biljana Šljukić	
ASCORBATE STABILIZED SYNTHESIS OF TIN SULFIDE AND THE APPLICATION FOR SUPERCAPACITORS.....	101
Asta Bronusiene, Anton Popov, Ieva Barauskiene, Ingrida Ancutiene	
PRUSSIAN BLUE – MODIFIED ELECTRODES IN FORMATION OF BIOSENSORS	102
Gabija Kavaliauskaitė, Aušra Valiūnienė	
CRYO-FOCUSING IN GC ANALYSIS: A NEW APPROACH FOR MEASURING TERPENES IN CANNABIS SATIVA.....	103
Audrius Sadaunykas, Audrius Zolumskis, Evaldas Naujalis	
SYNTHESIS OF CALCIUM CHLORAPATITE THROUGH THE PHASE CONVERSION OF AMORPHOUS CALCIUM PHOSPHATE IN MOLTEN CHLORIDES	104
Erlandas Kabasinskas, Jonas Stadulis, Diana Griesiute, Dovydas Karoblis, Eva Raudonyte-Svirbutaviciene, Aleksej Zarkov	
EVALUATION OF THE INTERACTION BETWEEN SARS-COV-2 SPIKE GLYCOPROTEINS AND THE MOLECULARLY IMPRINTED POLYPYRROLE	105
Ernestas Brazys, Vilma Ratautaitė, Raimonda Bogužaitė, Arūnas Ramanavičius	
INVESTIGATION OF THE CORONAVIRUS SARS-CoV-2 STRUCTURAL PROTEINS AND SPECIFIC ANTIBODIES INTERACTIONS USING OPTICAL AND PIEZOELECTRIC METHODS.....	106
Silvija Juciūtė, Vincentas M. Mačiulis, Ieva Plikusienė	
ELECTRONIC EXCITED STATES OF CHLOROPHYLLS IN PHOTOSYNTHETIC COMPLEX CP29	107
Sandra Barysaitė, Andrius Gelzinis, Jevgenij Chmeliov, Leonas Valkunas	
OPTIMIZATION OF SOL-GEL SYNTHESIS PROCEDURE FOR DEPOSITION OF BIVO₄ COATINGS.....	108
Pamela Rivera, Milda Petrulevičienė, Irena Savickaja, Kamila Turuta, Jurga Juodkazytė, Arūnas Ramanavičius	
PHOTOPOLYMERIZATION OF GLYCEROL ACRYLATES AND THEIR MIXTURES WITH VANILLIN STYRENE	109
Evelina Saunoryte, Aukse Navaruckiene, Jolita Ostrauskaite	
REMOVAL EFFICIENCY AND DISTRIBUTION OF MICROPLASTIC PARTICLES AT WASTEWATER TREATMENT PLANT	110
Sonata Pleskytė, Ieva Uogintė, Steigvilė Byčėnienė	

SYNTHESIS AND ANALYSIS OF GdPO₄·H₂O:Eu FUNCTIONALIZED WOOD.....	111
Monika Baublytė, Denis Sokol, Ramūnas Skaudžius	
STUDY OF EUROPIUM-DOPED SODIUM ALUMINUM GERMANATE.....	112
Marius Dzvinka, Martynas Misevičius	
STUDY OF FORMATION OF 1-ARYL-3<i>a</i>,8<i>b</i>-DIHYDRO-1<i>H</i>- BENZOFURO[2,3-<i>d</i>]IMIDAZOLES DURING THE VAN LEUSEN REACTION	113
Vilius Petraška, Paulina Kaziukonytė, Ieva Žutautė, Algirdas Brukštus	
PROGRESS TOWARDS SYNTHESIS OF BICYCLO[3.3.1]NONANE-BASED POLYAROMATIC RECTANGULAR CAVITANDS	114
Nojus Radzevičius, Edvinas Orentas	
PREPARATION OF HEXAGONAL RARE EARTH MANGANITES BY MOLTEN SALT SYNTHESIS.....	115
Dovydas Karoblis, Aleksej Zarkov, Aivaras Kareiva	
SYNTHESIS AND INVESTIGATION OF ACRYLATED EPOXIDIZED SOYBEAN OIL AND VANILLIN DIMETHACRYLATE BASED PHOTOPOLYMER	116
Vilte Šereikaite, Aukse Navaruckiene, Jolita Ostrauskaite	
MOLECULAR DYNAMICS AND RAMAN STUDY FOR LYCOPENE AND CYCLODEXTRIN COMPLEXES.....	117
Goda Bankovskaitė, Mindaugas Mačernis	
DETERMINATION OF PPY LAYER STABILITY FOR THE DEVELOPMENT OF THE SENSOR	118
Raimonda Bogužaitė, Vilma Ratautaitė, Greta Pilvenytė, Arūnas Ramanavičius	
FABRICATION OF CoFe, CoFeMn, CoFeMo COATINGS AND THEIR APPLICATION FOR HYDROGEN EVOLUTION REACTION.....	119
Karina Vjūnova, Zita Sukackienė, Jūratė Vaičiūnienė, Loreta Tamašauskaitė-Tamašiūnaitė	
SYNTHESIS AND CHARACTERIZATION OF CoFe, CoFeMn, CoFeMo COATINGS AND THEIR APPLICATION FOR OXYGEN EVOLUTION REACTION	120
Huma Amber, Zita Sukackienė, Jūratė Vaičiūnienė, Loreta Tamašauskaitė-Tamašiūnaitė	
LUMINESCENCE OF EUROPIUM, DYSPROSIUM AND BISMUTH DOPED.....	121
NaAlGeO₄.....	121
Gabija Janusauskaite, Martynas Misevičius	
SYNTHESIS OF NOVEL 6-(5-ARYL-1,2,3-THIADIAZOL-4-YL)-4- ARYLBENZENE-1,3-DIOLS IN SEARCH FOR POTENTIAL HSP90.....	122
Urtė Milerytė, Algirdas Brukštus, Ieva Žutautė	
FRASS – UNTRADITIONAL RAW MATERIAL FOR PRODUCTION OF FERTILIZERS.....	123
Goda Gudinskaitė, Rasa Paleckienė, Rasa Šlinkšienė	
MODIFICATION OF PINE WOOD WITH Mg₂/Al₁-CO₃ AND Zn₂/Al₁-CO₃ LAYERED DOUBLE HYDROXIDE: SYNTHESIS AND ANALYSIS.....	124
Neringa Gailiūtė, Denis Sokol	
SYNTHESIS AND CHEMICAL PROPERTIES OF 1-(2,4- DIFLUOROPHENYL)-5-OXOPYRROLIDINE-3-CARBOXYLIC ACID.....	125
Guoda Pranaitytė, Birutė Grybaitė, Vytautas Mickevičius	
SYNTHESIS AND CHEMICAL PROPERTIES OF 1-(2-HYDROXY-5- METHYLPHENYL)-5-OXOPYRROLIDINE-3-CARBOXYLIC ACID.....	126
Karolis Krikštonis, Birutė Grybaitė	
STRUCTURAL ANALYSIS OF BIS-2-HYDROXYETHYLENE TEREPHTHALATE OBTAINED FROM DEPOLYMERIZATION OF POLYETHYLENE TEREPHTHALATE	127
Diana Masiulionytė, Monika Čekavičiūtė, Laura Pečiulytė, Joana Bendoraitienė	
CONFORMATIONAL STUDY OF 1,1-DICHLORGERMACYCLOPENTANE BY MEANS OF VIBRATIONAL SPECTROSCOPY.....	128
Tautvydas Taraškevičius, Jogilė Mačytė, Gamil A.Guirgis, Valdas Šablinskas	

EFFICIENT BIMETALLIC NICKEL-MANGANESE/TITANIUM BIFUNCTIONAL ELECTROCATALYST FOR ALKALINE WATER.....	129
Sukomol Barua, Aldona Balčiūnaitė, Jūrate Vaičiūnienė, Loreta Tamašauskaitė-Tamašiūnaitė, Eugenijus Norkus	
SYNTHESIS AND CHEMICAL PROPERTIES OF 3-(1-(4-METHOXY-2-.....	130
Roberta Gelminauskaitė, Birutė Grybaitė, Vytautas Mickevičius	
INVESTIGATIONS ON APPLICATION OF BiVO₄ PHOTOANODE FOR GLYCEROL DEGRADATION	131
Rūta Baltaragytė, Milda Malakauskaitė-Petrulevičienė, Irena Savickaja, Jurga Juodkazytė, Alvydas Zagorskis, Arūnas Ramanavičius	
INVESTIGATION OF BIOACTIVE FILMS BASED ON NATURAL POLYSACCHARIDES AND PLANT EXTRACTS.....	132
Emilija Galkauskaite, Ramune Rutkaite, Vaida Kitryte-Syrpa, Dovile Liudvinaviciute, Michail Syrpas	
POLYETHYLENE TEREPHTHALATE GLYCOLYSIS USING MAYENITE AS CATALYST.....	133
Klaudija Bojanauskaite, Diana Masiulionyte, Laura Peculyte, Joana Bendoraitiene	
INFLUENCE OF DODECENYLSUCCINATE CONTENT ON PROPERTIES OF ACETYLATED POTATO STARCH DODECENYLSUCCINATE.....	134
Jonas Luneckas, Laura Peculyte, Joana Bendoraitiene, Ramune Rutkaite	
ELECTRONIC EXCITATION DEACTIVATION PATHWAYS OF BODIPY MOLECULAR ROTORS WITH ROTATING HYDROCARBON GROUP	135
Delianas Palinauskas, Stepas Toliautas	
BIOREFINING OF THREE <i>VINCETOXICUM</i> SPECIES INTO VALUABLE COMPONENTS BY DIFFERENT EXTRACTION METHODS	136
Jovita Jovaišaitė, Laura Jūrienė, Audrius Pukalskas, Petras Rimantas Venskutonis	
SYNTHESIS AND PROPERTIES OF OCTENYL SUCCINIC ANHYDRIDE.....	137
Emilija Morkvėnaite, Ramune Rutkaite, Vesta Navikaite-Snipaitiene	
BIOREFINING OF TAGETES PATULA BY INNOVATIVE EXTRACTION METHODS.....	138
Laura Jūrienė, Audrius Pukalskas, Petras Rimantas Venskutonis	
ENHANCING SCOTS PINE WOOD WITH CALCIUM PHOSPHATE BIOCERAMICS SYNTHESIZED FROM EGGSHELLS FOR IMPROVED STRENGTH AND FIRE RESISTANCE	139
Gabija Navašinskaitė, Denis Sokol	
STATISTICAL ANALYSIS OF BODIPY DERIVATIVES ROTATIONAL ENERGY TRANSITIONS AND GEOMETRY.....	140
Rokas Garbačas, Stepas Toliautas	
STUDY OF VISCOSITY AND FRICTION OF POLYURETHANE ADHESIVES.....	141
Paulina Nemaniutė, Dalia Bražinskienė, Tadas Matijošius, Svajus Asadauskas	
COVALENT RADII DERIVATION FROM OPEN CRYSTALLOGRAPHIC DATA.....	142
Eglė Šidlauskaitė, Andrius Merkys, Antanas Vaitkus	
PHASE TRANSITION STUDIES OF CALCIUM-SUBSTITUTED La₂Mo₂O₉ CERAMIC PREPARED BY AN AQUEOUS SOL-GEL METHOD	143
Giedrė Gaidamavičienė, Artūras Žalga	
ESTIMATION OF CARBONACEOUS AEROSOL PARTICLE SOURCES AT TWO LOCATIONS IN METRO MANILA, PHILIPPINES	144
Touqeer Gill, , Simonas Kecorius, Kamilė Kandrotaitė, Vadimas Dudoitis, Leizel Madueno, Alfred Wiedensohler, Steigvilė Byčėnkiėnė and Kristina Plauškaite	
SYNTHESIS OF POTENTIAL HSP90 INHIBITORS 4-(CYCLOALKYL)-6-(1-(4-SUBSTITUTED)-1H-IMIDAZOL-5-YL OR -1,2,3- THIADIAZOL)BENZENE-1,3-DIOLS	145
Kamilė Venskūnaitė, Algirdas Brukštus	
CONTROLLED CARBON COATING OF ANODE MATERIALS THROUGH IN-SITU POLYMERIZATION.....	146
Nadežda Traškina, Jurgis Pilipavičius, Jurga Juodkazytė, Linas Vilčiauskas	

SYNTHESIS AND CHARACTERIZATION OF IRON DOPED CALCIUM PHOSPHATE WITH WHITLOCKITE STRUCTURE.....	147
Diana Griesiute , Jonas Stadulis, Aleksej Zarkov	
NEUTRALIZATION OF THE SIMULANTS OF VESICANT/BLISTER CHEMICAL AGENTS IN THE PRESENCE OF MONTMORILLONITE	148
Drizhd Varvara, Vakhitov Ramil	
DESIGN AND SYNTHESIS OF STRUCTURALLY SIMPLE SUPRAMOLECULAR CAPSULE	149
Domantas Valčekas, Edvinas Orentas	
SYNTHESIS AND PROPERTIES OF TRIPHENYLETHYLENE DERIVATIVES AS HOLES TRANSPORTING MATERIALS	150
Julius Petrulevičius, Marytė Daškevičienė, Egidijus Kamarauskas, Kristijonas Genevičius, Vygintas Jankauskas, Vytautas Getautis	
THE PSEUDO-POLY (AMINO ACIDS) AS COMPONENTS OF PERFUMERY-COSMETIC TOOLS	151
Daria Botsula, Roman Taras, Natalia Bukartyk, Valeriia Shabikova	
CASCADE CYCLISATION OF PYRAZOLE-4-CARBALDEHYDES AND PHENYLENDIAMINES: ACCESS TO NOVEL PYRAZOLOOXAZEPANES	152
Agnė Užupytė, Gabrielė Antulytė, Eglė Arbačiauskienė, Algirdas Šačkus	
DESIGN AND SYNTHESIS OF PHOTOCLEAVABLE RESIN FOR PREPARATION OF OBOC DNA-ENCODED CHEMICAL LIBRARIES	153
Alberta Jankūnaitė, Edvinas Orentas	
CONTINUOUS FLOW SYNTHESIS OF SILICON DIOXIDE MICROSPHERES	154
Lukas Šerpytis, Matas Damonskis, Lukas Taujenis, Simas Šakirzanovas	
FORMATION OF MACROPOROUS HYDROGEL MATERIAL FOR MEDICAL PURPOSES BASED ON SODIUM ALGINATE.....	155
Valeriia Shabikova, Iryna Dron, Daria Botsula, Zoriana Nadashkevych, Volodymyr Samaryk	
ESSENTIAL PREPARATIONS FOR THE DELIVERY OF TRACE ELEMENTS BASED ON N-DERIVATIVES OF GLUTAMIC ACID WITH A HYDROPHILIC SUBSTITUENT	156
Alona Sachuk, Viktoriia Oleksa, Serhii Varvarenko, Roman Matiishyn	
STUDY OF THE PROCESS OF OBTAINING CROSS-LINKED POLYACRYLAMIDE MESH REINFORCED WITH MODIFIED POLYPROPYLENE FIBER.....	157
Solomiia Kapatsila, Olena Bordeniuk, Alona Sachuk, Nataliia Nosova	
BISMUTH SULFIDE STUDY USING X-RAY DIFFRACTION ANALYSIS.....	158
Aistis Melnikas, Skirma Žalenkienė	
THE INVESTIGATION OF FLUORINATED SECONDARY BENZENSULFONAMIDES BINDING MECHANISM AND STRUCTURE FOR CARBONIC ANHYDRASES.....	159
Aivaras Vaškevičius, Denis Baronas, Virginija Dudutienė, Vaida Paketurytė, Visvaldas Kairys, Alexey Smirnov, Vaida Juozapaitienė, Elena Manakova, Saulius Gražulis, Asta Zubrienė, Daumantas Matulis	
DIBLOCK COPOLYMERS WITH GRADIENT DISTRIBUTION OF ZWITTERIONIC AND BRUSH FRAGMENTS, AND CONTAINING.....	160
Marijus Jurkūnas, Vaidas Klimkevičius, Ričardas Makuška	
TIME-RESOLVED SPECTROSCOPIC CHARACTERIZATION OF THE PORPHYRIN-CONTAINING MOLECULAR DIMERS	161
Ivan Halimski, Vidmantas Jašinskas, Ally Aukauloo, Renata Karpicz, Jevgenij Chmeliov, Vidmantas Gulbinas	
SYNTHESIS OF THE ROD-SHAPE CARBAZOLE-BASED PHOSPHONIC ACID	162
Kotryna Gumauskaitė, Aida Drevilkauskaitė, Vytautas Getautis, Artiom Magomedov	
STUDY OF CHEMICAL AND ELECTROCHEMICAL DEGRADATION OF VANADIUM-BASED PHOSPHATE FRAMEWORKS AS AQUEOUS NA-ION BATTERY CATHODES.....	163
Davit Tediashvili, Linas Vilčiauskas	
SYNTHESIS AND INVESTIGATION OF TETRAHYDROFURFURYL ACRYLATE-BASED PHOTOCROSS-LINKED POLYMERS	164

Justinas Jaras, Aukse Navaruckiene, Jolita Ostrauskaite

DEPOSITION AND INVESTIGATION OF SELENIDES THIN FILMS ON POLYAMIDE FOR OPTOELECTRONIC APPLICATIONS	165
Emilija Skuodaitė, Henrieta Markevičiūtė, Valentina Krylova	
DEPOSITION AND INVESTIGATION OF SILVER OXIDE THIN FILMS ON POLYVINYLCHLORIDE TEXTILE SURFACE.....	166
Emilija Skuodaitė, Valentina Krylova	
MIXED Zn-Co OXIDE (Zn:Co 1.25:1) LAYERS FOR PHOTOCATALYTIC APPLICATIONS	167
Agnietė Juciūtė, Dovilė Sinkevičiūtė, Nerita Žmuidzinaičienė, Agnė Šulčiūtė	
FERROELECTRIC, PIEZOELECTRIC, AND BROADBAND DIELECTRIC STUDIES OF LEAD-FREE $x(\text{Bi}(\text{Zn}_{2/3}\text{Nb}_{1/3})\text{O}_3)-(1-x)\text{BaTiO}_3$.....	168
Žygimantas Logminas, Artyom Plyushch, Jessica Marshall, David Walker, Pam Thomas, Jūras Banys	
SYNTHESIS OF THERMORESPONSIVE COPOLYMERS BASED ON CHITOSAN AND N-ISOPROPYLACRYLAMIDE	169
Vesta Navikaite-Snipaitiene, Arminta Kairyte, Migle Babelyte, Ramune Rutkaite, Laura Peculyte, Volodymyr Samaryk	
SYNTHESIS AND APPLICATION OF TiO₂ NANOTUBE ARRAYS FOR WASTEWATER TREATMENT.....	170
Maria-Anthoniette Onoriode-Afunezie, Agne Sulciute, Vytautas Abromaitis	
MIXED Zn-Co OXIDE LAYERS FORMATION AND THEIR ELECTROCHEMICAL PROPERTIES	171
Vasaris Statkevičius, Dovilė Sinkevičiūtė, Agnė Šulčiūtė, Nerita Žmuidzinaičienė	
DETERMINATION OF MAGNESIUM WHITLOCKITE STRUCTURAL PROPERTIES: RIETVELD MODELING	172
Agnė Kizalaitė, Jonas Stadulis, Aleksej Žarkov	
CYANO-SUBSTITUTED 1,2-DIPHENYLBENZOIMIDAZOLE DERIVATIVES AS HOSTS FOR OLED APPLICATIONS.....	173
Simas Macionis, Murad Najafov, Jurate Simokaitiene, Juozas V. Grazulevicius, Jiun-Haw Lee, Chia-Hsun Chen, Bo-Yen Lin, Tien-Lung Chiu	
INVESTIGATION OF THERMAL PROPERTIES OF DIFFERENT COMPOSITION CAFFEIC ACID AND CHITOSAN COMPLEXES	174
Dovilė Liudvinavičiūtė, Vesta Navikaite-Šnipaitienė, Ramunė Rutkaitė, Joana Bendoraitienė	
SYNTHESIS AND CHARACTERIZATION OF ACENAPHTHYLENE LABELLED CHITOSAN-GRAFT-POLY(N-ISOPROPYLACRYLAMIDE) COPOLYMERS.....	175
Migle Babelyte, Ramune Rutkaite, Dovile Liudvinaviciute, Vesta Navikaite-Snipaitiene, Volodymyr Samaryk	
ULTRAVIOLET-C PERSISTENT LUMINESCENCE OF Sr₂MgSi₂O₇: Pr³⁺	176
Dace Nilova, Andris Antuzevics, Guna Doke, Guna Kriekē, Pavels Rodionovs, Jekabs Cirulis, Andris Fedotovs, Uldis Rogulis	
SOLID DISPERSION SYSTEMS AS THE BASIS OF A SUCCESSFUL STRATEGY FOR IMPROVING THE BIOPHARMACEUTICAL PROPERTIES OF ACTIVE PHARMACEUTICAL INGREDIENTS	177
Volodymyr Yaremenko, Olena Ishchenko, Viktoriia Plavan	
ELECTROSPINNING POSSIBILITIES OF KERATIN MODIFIED WITH HERBAL EXTRACTS AND SILVER NANOPARTICLES	178
Ugnė Zaslaurinskaitė, Akvilė Andziukevičiūtė-Jankūnienė, Aistė Balčiūnaitienė, Jonas Viškėlis, Erika Adomavičiūtė, Virgilijus Valeika, Virginija Jankauskaitė	
EXPLORING THE STRUCTURE AND DYNAMICS OF CAVITAND –	179
Benjaminas Malmiga, Kęstutis Aidas	
IMPACT OF MICROSECOND PULSED ELECTRIC FIELDS ON ENDOPLASMIC RETICULUM MEMBRANE PERMEABILIZATION	180
Virginija Siaurusevičiūtė, Viktorija Juščenko, Gintarė Dalmantaitė, Aušra Baradoke, Arūnas Stirkė	

Overview of the first LHCb Open Data Release	181
Mindaugas Šarpis	
PERSONAL EXPOSURE AND DEPOSITION OF BLACK CARBON ON HUMAN LUNGS IN VILNIUS, LITHUANIA	182
Abdullah Khan, Lina Davulienė, Sergej Šemčuk, Kamilė Kandrotaitė, Agnė Minderytė, Mehri Davtalab, Ieva Uogintė, Martynas Skapas, Vadimas Dudoitis, Julija Pauraitė, Inga Garbarienė, and Steigvilė Byčenkienė	
MOLECULARLY IMPRINTED POLYMER-BASED BIOSENSORS FOR THE DETECTION OF ALZHEIMER'S DISEASE BIOMARKERS.....	183
Greta Pilvenytė, Raimonda Bogužaitė, Vilma Ratautaitė, Arūnas Ramanavičius	
MODELING CAROTENOID-CHLOROPHYLL COMPLEXES WITH MOLECULAR DYNAMICS.....	184
Justyna Kalaševska, Mindaugas Macernis	
SYNTHESIS OF 4-AMINO-1,2,4-TRIAZOLE-3-THIONES BEARING 2- PYRIDINYLAMINO MOIETY.....	185
Aida Šermukšnytė, Kristina Kantminienė, Zigmuntas Jonas Beresnevičius, Ingrida Tumosienė	
DONOR-ACCEPTOR-DONOR TYPE ENAMINES FOR PEROVSKITE SOLAR CELLS	186
Šarūnė Daškevičiūtė-Gegužienė, Yi Zhang, Kasparas Rakštys, Marytė Daškevičienė, Vygintas Jankauskas, Mohammad Khaja Nazeeruddin, Vytautas Getautis	
MOLECULAR DYNAMICS SIMULATIONS OF BIOMOLECULES ENCAPSULATED IN MACROMOLECULAR MATRICES	187
Mykolas Jerutis, Einaras Sipavičius, Kęstutis Aidas	
 P2 Session:	
SYNTHESIS AND INVESTIGATION OF VITRIMERS FROM RENEWABLE RESOURCES.....	188
Sigita Grauzėlienė, Marius Kastanauskas, Jolita Ostrauskaitė	
DYNAMIC HOT EMBOSsing PROCESS OF MICROSTRUCTURES FORMATION.....	189
Justas Ciganas, Giedrius Janusas	
TRIPHENYLETHENE-CARBAZOLE DERIVATIVES FOR AGGREGATION-INDUCED EMISSION IN OLEDs.....	190
Gintare Krucaite, Cheng-Yung Ho, Raminta Beresnevičiute, Dovydas Blazevičius, Wei- Han Lin, Jhao-Cheng Lu, Chang-Yu Lin, Saulius Grigalevičius, Chih-Hao Chang, Ernestas Zaleckas	
MULTIFUNCTIONAL BICARBAZOLE-BASED TWISTED D-A-D DERIVATIVES FOR BLUE AND GREEN OLEDs.....	191
Dovydas Blaževičius, Gintarė Kručaitė, Daiva Tavgenienė, Saulius Grigalevičius, Prakalp Gautam, Shahnawaz Shahnawaz, Iram Siddiqui, Jwo-Huei Jou	
INDUCED ENERGY BAND BENDING OF PTAA BY USING SELF- ASSEMBLED MOLECULES FOR WIDE BANDGAP LEAD PEROVSKITE SOLAR CELLS WITH INVERTED STRUCTURE	192
Raminta Beresnevičiute, Huan Bi, Jiaqi Liu, Gaurav Kapil, Daiva Tavgeniene, Beata Achramovic, Zheng Zhang, Liang Wang, Chao Ding, Shahrir Razey Sahamir, Yoshitaka Sanehira, Ajay Kumar Baranwal, Kitamura Takeshi, Dandan Wang, Yuyao Wei, Yongge Yang, Dong-Won Kang, Saulius Grigalevičius, Qing Shen, Shuzi Hayase	
DIELECTRIC PROPERTIES OF [NH₄][ZN(HCOO)₃] METAL FORMATE FRAMEWORK DOPED WITH ALKALI METALS	193
Barbora Škėlaitė, Sergejus Balčiūnas, Mantas Šimėnas, Mirosław Mączka, Juras Banys	
DIELECTRIC AND PIEZOELECTRIC PROPERTIES IN (1 - x)Na_{0,5}Bi_{0,5}TiO₃-xCdTiO₃ SOLID SOLUTIONS	194
Eglė Martinaitytė, Eriks Birks, Šarūnas Svirskas	
NUMERICAL CALCULATIONS OF THE HEAT CONDUCTIVITY OF SiO₂ GLASS SUBJECTED TO ULTRA-HIGH PRESSURE USING MOLECULAR DYNAMICS	195
Adam Puchalski, Mateusz Ślusarczyk, Paweł Keblinski, Tomasz K. Pietrzak	
SIMULATING MICROWAVE FIELD DISTRIBUTION IN A NOVEL SUPERCONDUCTING EPR MICRORESONATOR	196

Ignas Pocius, Paulina Verbaitytė, Jūras Banys, Mantas Šimėnas	
SECOND-HARMONIC GENERATION IN A PERIODICAL POLARITY GaN.....	197
Gustas Petrusevicius, M. Kolenda, D. Kezys, T. Grinys, A. Vaitkevicius, A. Kadys, I. Reklaitis, V. Vaicaitis, R. Petruskevicius, R. Tomasiunas	
EMOTION RECOGNITION USING A GENERAL-PURPOSE OBJECT DETECTION ALGORITHM	198
Arvydas Lozys, Ema Spiliauskaite, Migle Skystimaite, Daichi Tsujimoto, Antanas Zinovicius, Vytautas Bucinskas	
ANNEALING EFFECTS ON IMPLANTED SILICON FOR SPIN-BASED QUANTUM TECHNOLOGIES.....	199
Justinas Turčak, Jūras Banys, Mantas Šimėnas	
ENHANCING MECHANICAL PROPERTIES OF ALSI10MG ALLOY VIA EQUAL CHANNEL ANGULAR PRESSING POST-PROCESSING	200
Augustine Nana Sekyi Appiah, Przemysław Snopiński, Marcin Adamiak	
INDOOR RADIO FREQUENCY ENERGY HARVESTING.....	201
Justina Žemgulytė, Paulius Ragulis, Gediminas Šlekas, Romualdas Trusovas, Karolis Ratautas, Rimantas Simniškis, Žilvinas Kancleris, Gediminas Račiukaitis	
SIMULATION OF DIFFRACTIVE OPTICS INTEGRATION IN A THZ BOWTIE DETECTOR	202
Karolis Redeckas, Linas Minkevičius, Vytautas Jakštas, Ignas Grigelionis	
THE INFLUENCE OF SYNTHESIS CONDITIONS ON LITHIUM-COBALT BORATE STRUCTURAL PROPERTIES	203
Alicja Kadziela, Przemysław Piotr Michalski	
THE DEVELOPMENT OF TECHNOLOGY OF A NEW GENERATION IDENTIFICATION ELEMENT	204
Erika Rajackaitė, Andrius Žutautas, Rasa Žostautienė, Pranas Narmontas	
SELECTIVE FORMATION OF METALLIC MICROSTRUCTURES ON THE SURFACE OF POLYTETRAFLUOROETHYLENE USING LASER.....	205
Šarūnas Mickus, Vytautas Vosylius, Evaldas Kvietkauskas, Viktorija Vrubliauskaitė, Karolis Ratautas	
BIOCOMPATIBLE HYDROXYAPATITES CO-DOPED WITH TERBIUM(III) AND RUBIDIUM(I) IONS AS HIGHLY FUNCTIONAL MATERIALS FOR BIOMEDICAL APPLICATIONS	206
Dominika Czekanowska, Nicole Nowak and Rafal Wiglusz	
STUDY OF THE EFFECT OF VIBRATION ON FLUID FLOW IN ALUMINUM OXIDE NANOPORES.....	207
Urte Cigane, Arvydas Palevicius	
MULTIFUNCTIONAL NANOSYSTEMS: ASSESSMENT OF UPCONVERTING NANOPARTICLES FOR BIOIMAGING, TEMPERATURE SENSING, AND MRI.....	208
Egle Ezerskyte, Augustas Morkvenas, Arturas Katelnikovas, Vitalijus Karabanovas and Vaidas Klimkevicius	
INVESTIGATION OF THERANOSTIC PROPERTIES OF SILICATE-SUBSTITUTED HYDROXYAPATITE CO-DOPED WITH Eu³⁺ Gd³⁺ AND Li⁺ IONS	209
Natalia Charczuk, Sara Targońska and Rafal J. Wiglusz	
TITANIUM ADHESION LAYER INFLUENCE ON LASER DIRECT WRITING FOR THE FORMATION OF GOLD MICROBUMPS ARRAYS	210
Rodrigas Liudvinavičius, Evaldas Stankevičius	
SYNTHESIS OF SILVER NANOWIRES	211
Gytautė Sirgėdaitė, Lina Mikoliūnaitė	
PHOTOCHEMICAL SYNTHESIS OF SILVER NANOPARTICLES AND STUDY OF THEIR STRUCTURAL PROPERTIES.....	212
Mindaugas Illickas, Asta Guobienė, Brigita Abakevičienė	
METAL OXIDE NANOSTRUCTURES IN CHEMICAL SENSORS AND BIOSENSORS.....	213
Vincentas Mačiulis, Almira Ramanavičienė, Miglė Stančiauskaitė, Ieva Plikusienė	

ELECTROCHEMISTRY-DRIVEN AFFINITY SENSOR FOR THE DETECTION OF ANTIBODIES AGAINST SARS-COV-2	214
Maryia Drobysh, Viktorija Liustrovaite, Alma Rucinskiene, Ausra Baradoke, Almira Ramanaviciene, Ieva Plikusiene, Urte Samukaite-Bubniene, Roman Viter, Chien-Fu Chen, Arunas Ramanavicius	
POLYANILINE AND POLYPYRROLE NANOCOMPOSITES WITH EMBEDDED GLUCOSE OXIDASE AND GOLD NANOPARTICLES.....	215
Natalija German, Anton Popov, Almira Ramanaviciene, Arunas Ramanavicius	
RESISTIVITY AND LOW-FREQUENCY NOISE CHARACTERISTICS OF HYBRID COMPOSITES WITH CARBON NANOTUBES AND GRAPHENE.....	216
Frydrichas Mireckas	
Investigation of crystals growth in ZnO thin films made by Sol-Gel technique.....	217
Deividas Vainauskas, Vidas Pakštas, Arnas Naujokaitis, Rokas Kondrotas	
IRON AND COPPER NANOPARTICLES DEPOSITED ON REDUCED GRAPHENE OXIDE FOR OXYGEN EVOLUTION REACTION	218
Jadranka Milikić , Ana Nastasić, Kristina Radinović, Aldona Balčiūnaitė and Biljana Šljukić	
IRON AND COPPER NANOPARTICLES DEPOSITED ON REDUCED GRAPHENE OXIDE FOR ORR IN ALKALINE MEDIA	219
Ana Nastasić, Jadranka Milikić, Kristina Radinović, Aldona Balčiūnaitė and Biljana Šljukić	
INVESTIGATION OF STABILITY OF SILVER NANOPARTICLES UNDER DIFFERENT STORAGE CONDITIONS	220
Mantas Mikalkevičius, Nadzeya Khinevich, Tomas Tamulevičius, Asta Tamulevičienė	
THE IMPACT OF DIFFERENT GOLD NANOSTRUCTURES ON THE PERFORMANCE OF ELECTROCHEMICAL IMMUNOSENSORS	221
Katazyna Blazevic, Kristina Sobol, Benediktas Brasiunas, Almira Ramanaviciene	
HARNESSING THE POWER OF GOLD NANORODS: A JOURNEY THROUGH SYNTHESIS AND CHARACTERIZATION	222
Viktorija Lisyte, Anton Popov, Almira Ramanaviciene	
EXPERIMENTAL STUDY ON ACOUSTIC AGGLOMERATION OF ULTRAFINE ASH PARTICULATE MATTER UNDER VARIOUS ENVIRONMENTAL CONDITIONS.....	223
Kristina Kilikevičienė, Aleksandras Chlebnikovas, Artūras Kilikevičius	
THERMAL ANALYSIS OF GRAPHENE/n-Si(100) DIODE, FORMED USING TRANSFER-LESS METHOD	224
Šarūnas Jankauskas, Rimantas Gudaitis, Šarūnas Meškinis	
STUDY OF RECOMBINATION AND ELECTRICAL CHARACTERISTICS IN HIGH ENERGY RADIATION Si SENSORS.....	225
Rytis Markevičius, Tomas Čeponis, Laimonas Deveikis, Eugenijus Gaubas, Jevgenij Pavlov, Vytautas Rumbauskas	
THERMODYNAMIC ANALYSIS OF NITROGEN DOPED GALLIUM OXIDE - COMPARATIVE STUDY	226
Ana Kurtanidze, Tamar Tchelidze	
RELATION BETWEEN DESIGN OF GaAsBi PARABOLIC QUANTUM WELLS AND OPTICAL PROPERTIES	227
Monika Jokubauskaitė, Evelina Dudutienė, Bronislovas Čechavičius, Arnas Pukinskas, Simona Pūkiene, Sandra Stanionytė, Martynas Skapas, Renata Butkutė	
STUDY OF ELECTRICAL CHARACTERISTICS IN SILICON PARTICLE SENSORS IRRADIATED WITH PROTONS OF DIFFERENT FLUENCES	228
Margarita Biveinytė, Tomas Čeponis, Laimonas Deveikis, Eugenijus Gaubas	
RELATIONSHIP BETWEEN CARRIER LIFETIME AND CATHODOLUMINESCENCE WAVELENGTH IN InGaN COMPOUNDS.....	229
Viktorija Mickūnaitė, dr. Žydrūnas Podlipskas, Mantas Migauskas	
EXTENDED DEFECT RELATED LEAKAGE CURRENT IN InGaN LIGHT EMITTING DIODE	230
Kristupas Karčemarskas, Žydrūnas Podlipskas, Virginijus Bukauskas, Tomas Grinys	

HIGH-DIMENSIONAL TOPOLOGICAL PUMPING IN TIME-SPACE CRYSTALLINE STRUCTURES	231
Yakov Braver, Egidijus Anisimovas, Krzysztof Sacha	
GaN/Graphene STRUCTURES THROUGH A LENS OF SEM-CL MICROSCOPE.....	232
Mantas Migauskas, Viktorija Mickūnaitė, Žydrūnas Podlipskas	
LUMINESCENCE CHARACTERISTICS IN MOCVD GaN STRUCTURES WITH A CHEMICALLY ETCHED SURFACE	233
Gertrūda Pociūtė, Tomas Čeponis, Jevgenij Pavlov	
INVESTIGATING THE QUALITY OF PHOTOVOLTAIC PANELS BY MEANS OF AN ELECTROLUMINESCENCE CONTROL SYSTEM	234
Adomas Vasiliauskas, Artūras Jukna, Gražina Grigaliūnaitė-Vonsevičienė	
LUMINESCENCE PROPERTIES OF CERIUM DOPED GARNET EPITAXIAL SCINTILATORS CODOPED WITH MAGNESIUM	235
Mikas Iršėnas, Augustas Vaitkevičius, Saulius Nargelas, Žydrūnas Podlipskas, Pavel Bohacek, Martin Nikl, Gintautas Tamulaitis	
OPTICAL PROPERTIES OF InGaAs/GaAs MULTIPLE QUANTUM WELLS FOR NEAR- INFRARED LASERS.....	236
Patricija Šleiniūtė, Monika Jokubauskaitė, Andrea Zelioli, Bronislovas Čechavičius, Sandra Stanionytė, Evelina Dudutienė, Renata Butkutė	
MANY BODY LOCALIZATION PHASE TRANSITION, MOBILITY EDGE AND UNIVERSALITY OF SPECTRAL FORM FACTOR IN QUANTUM SUN MODEL	237
Konrad Pawlik, Piotr Sierant, Jakub Zakrzewski	
ANNEALING EFFECT ON QUANTUM DOTS FORMATION IN MBE.....	238
Arnas Pukinskas, Kipras Mažeika, Augustas Vaitkevičius, Aivaras Špokas, Arnas Naujokaitis, Martynas Skapas, Bronislovas Čechavičius, Monika Jokubauskaitė, Evelina Dudutienė, and Renata Butkutė	
EXTREMELY NARROW, SHARP-PEAKED RESONANCES AT THE EDGE OF THE CONTINUUM	239
Ignas Lukosiunas, Lina Grineviciute, Julianija Nikitina, Darius Gailevicius, Kestutis Staliunas	
MEASUREMENT OF NONLINEAR REFRACTIVE INDEX DISPERSION IN PHOTONIC CRYSTAL FIBER	240
Jokūbas Pimpė, Miglė Kuliešaitė, Vygandas Jarutis, Julius Vengelis	
LOW-FREQUENCY NOISE SPECTROSCOPY OF GaAsBi-BASED QUANTUM WELL LASER DIODES.....	241
Richard Pinkrah, Sandra Pralgauskaitė	
OPTICAL RESPONSE OF THE HYBRID TAMM-SURFACE PLASMON POLARITON MODES ON THE SURFACE LATTICE ARRAY OF GOLD NANO-BUMBS	242
Justina Anulytė, Ernesta Bužavaitė-Vertelienė, Vilius Vertelis, Evaldas Stankevičius, Kernius Vilkevičius, Zigmas Balevičius	
HIGH-ENERGY 90 PS PULSES FROM PERFLUOROCTANE SBS-COMPRESSOR.....	243
Auguste Cerneckyte, Paulius Mackonis, Aleksej M. Rodin	
STRONG COUPLING BETWEEN SURFACE PLASMON RESONANCE AND EXCITON OF LABELED PROTEIN-DYE COMPLEX FOR IMMUNOSENSING APPLICATIONS.....	244
Povilas Jurkšaitis, Ernesta Bužavaitė-Vertelienė, Zigmas Balevičius	
INVESTIGATION OF THZ IMAGING WITH STRUCTURED BEAMS IN A DIGITAL EXPERIMENT.....	245
Karolis Mundrys, Paulius Kizevičius, Sergejus Orlovas	
INVESTIGATION OF OPTICAL PARAMETRIC GENERATOR PUMPED WITH SUBNANOSECOND PULSES BASED ON FAN-OUT GRATING DESIGN MgO:PPLN CRYSTAL	246
Simona Armalytė, Jonas Banys, Julius Vengelis	
MODULATION OF PHASE MAP SEGMENTS TO FORM HOMOGENOUS ILLUMINATION	247
Mateusz Surma Mateusz Kałuża, Paweł Komorowski, Agnieszka Siemion	

LASER 3D PRINTING OF INORGANIC AND OPTICALLY ACTIVE WHISPERING GALLERY MODE MICRO-RESONATOR.....	248
Giedrius Balčas, Maria Androulidaki, Dimitra Ladika, Vasileia Melissinaki, Darius Gailevičius, Maria Farsari, Mangirdas Malinauskas	
RAPID LASER MICROMACHINING OF SILICON DIFFRACTIVE OPTICAL ELEMENTS DESIGNED FOR TERAHERTZ IMAGING	249
Ernestas Nacius, Justinas Minkevičius, Orestas Ulčinas, Sergej Orlov, Vytautas Jukna	
SURFACE HARDNESS MEASUREMENTS OF STEEL SAMPLES USING FEMTOSECOND LASER INDUCED BREAKDOWN SPECTROSCOPY, COMPARISON OF ULTRAVIOLET AND INFRARED IRRADIATION.....	250
Aušrys Vaitiekūnas, Ona Balachninaite	
LASER-INDUCED GRAPHENE FORMATION FOR ELECTROCHEMICAL SENSOR APPLICATIONS	251
Aivaras Sartanavičius, Vytautas Žutautas, Rasa Pauliukaitė, Romualdas Trusovas	
DEVELOPMENT OF SELECTIVE LASER SINTERING FOR CERAMIC ADDITIVE MANUFACTURING.....	252
Alireza Shahidi, Karolis Stravinskas, Genrik Mordas	
TERAHERTZ PASSIVE OPTICAL COMPONENTS REALIZING FREQUENCY-DIVISION DEMULTIPLEXING	253
Mateusz Kaluza, Mateusz Surma, Pawel Komorowski, and Agnieszka Siemion	
MULTIWAVELENGTH SURFACE-ENHANCED RAMAN SPECTROSCOPIC STUDY OF MAGNETO-PLASMONIC NANOPARTICLES.....	254
Aikaterini-Maria Gkouzi, Martynas Talaikis, Lina Mikoliūnaitė, Evaldas Stankevičius, Gediminas Niaura	
INVESTIGATION OF CONCENTRATION QUENCHING OF DYSPROSIUM IONS IN SILICATE-SUBSTITUTED FLUORAPATITE	255
Sara Targońska and Rafal J. Wignusz	
HIGH RESOLUTION NMR STUDY OF 1-BUTYL 3-	256
Lukas Mikalauskas, Vytautas Klimavičius	
SPECTRAL PECULIARITIES OF HOT CARRIER PHENOMENON IN A SOLAR CELL	257
Ihor Zharchenko, Oleksandr Masalskyi, Jonas Gradauskas, Steponas Ašmontas, Algirdas Suziedėlis, Aldis Šilėnas, Aurimas Cerskus, Aleksej Rodin	
THE WAVE CLIMATE PARAMETERS CHANGE IN NEARSHORE ALONG THE CURONIAN SPIT SEA COAST IN 2003-2019	258
Pranciškus Brazdžiūnas, Donatas Pupienis	
STRUCTURAL ANALYSIS OF VALERIC ACID STRUCTURE USING MATRIX ISOLATION FTIR SPECTROSCOPY AND <i>AB INITIO</i> CALCULATIONS.....	259
Jogilė Mačytė, Rasa Platakyte, Joanna Stocka, Valdas Šablinskas	
SOLAR CELL PERFORMANCE EVALUATION PECULIARITIES WITH LED – BASED SOLAR SIMULATORS	260
Darius Antonovič, Žygimantas Vosylius, Algirdas Novičkovas, and Vincas Tamošiūnas	
FEATURES OF FLUORESCENCE PROPERTIES OF NANODIAMONDS.....	261
Yaraslau Padrez, Lena Golubewa, Renata Karpicz	
ANALYSIS OF TIME-RESOLVED FLUORESCENCE SPECTRA FOR MOLECULAR SYSTEMS	262
Laura Lelevičiūtė, Andrius Gelžinis, Jevgenij Chmeliov, Leonas Valkūnas	
AEROSOL PARTICLE NUMBER CONCENTRATION AND SIZE DISTRIBUTION DURING MIDSUMMER EVENT	263
Kamilė Kandrotaitė, Agnė Minderytė, Audrė Kalinauskaitė, Lina Davulienė, Lucja Janicka, Vadimas Dudoitis, Iwona S. Stachlewska, Steigvilė Byčenkienė	
A CASE STUDY OF EXTENSIVE BIOMASS BURNING RELATED BLACK CARBON EMISSIONS DURING MIDSUMMER EVE IN VILNIUS, LITHUANIA.....	264
Agnė Minderytė, Kamilė Kandrotaitė, Audrė Kalinauskaitė, Lina Davulienė, Lucja Janicka, Vadimas Dudoitis, Iwona S. Stachlewska, Steigvilė Byčenkienė	

CHARACTERIZATION OF Eu³⁺ ION-DOPED Sr₁₀(PO₄)₆F₂ FOR LUMINESCENCE-BASED TEMPERATURE SENSING.....	265
Katarzyna Szyszka and Rafal J. Wiglusz	
POLARIZATION-BASED IDLER ELIMINATION: ENHANCING THE EFFICIENCY OF OPTICAL PARAMETRIC AMPLIFICATION.....	266
Gaudenis Jansonas, Rimantas Budriūnas, Gintaras Valiulis, Arūnas Varanavičius	
STUDY OF THE CALIBRATION OF CROC PIXEL DETECTORS WITH SENSORS.....	267
Kristijonas Mikas Silius, Marijus Ambrozas	
APPLICATION OF 3D VECTOR BUILDING DATA FOR DIFFRACTION MODELING IN WIRELESS NETWORKS.....	268
Karolis Stankevičius, Steponas Pilkauskas, Rimvydas Aleksejūnas	
DIGITAL SIMULATION OF AGGLOMERATION OF SOLID PARTICLES FORMED DURING BIODIESEL COMBUSTION USING DEM	269
Darius Vainorius, Artūras Kilikevičius, Algis Džiugys	
RELATIVE OSCILLATOR STRENGTHS FOR LOW-LYING LEVELS OF Tm: EXPERIMENT AND THEORY	270
Adams Lapins, Maris Tamanis, Ilze Klincare, Ruvin Ferber, Gönül Başar, Sophie Kröger, Andrey I. Bondarev, Mikhail G. Kozlov	
CREATING FLUORESCENCE SPECTRA BASED ON THE FRANCK- CONDON FACTOR	271
Jaba Shainidze, Nugzar Gomidze	
ANALYSIS OF SPECTRAL LINES FOR STARS VIA SYNTHETIC SPECTRA.....	272
Dzmitry Viarbitski	
MULTITARGET REACTIVE MAGNETRON SPUTTERING TOWARDS THE PRODUCTION OF STRONTIUM MOLYBDATE THIN FILMS	273
Mindaugas Andrulevičius , Evgenii Artiukh , Gunnar Suchanek , Sitao Wang , Nikolai A. Sobolev ,*, Gerald Gerlach , Asta Tamulevičienė , Brigita Abakevičienė , and Sigitas Tamulevičius	
STUDY OF ELECTRICAL CHARACTERISTICS OF SILICON SENSORS FOR RADIOTHERAPY DOSE CONTROL	274
Augustas Baliukonis, Tomas Čeponis, Eugenijus Gaubas, Vytautas Rumbauskas, Marius Burkanas, Jonas Venius	
ELECTROKINETIC PROPERTIES OF PLATINUM NANOPARTICLE MONOLAYERS DEPOSITED ON SOLID SURFACES	275
Kristina Sobol, Monika Wasilewska, Almira Ramanaviciene, Magdalena Ocwieja	
HIGH-SPEED DETECTION OF WATER CONTENT IN CRUDE OIL BY USING TERAHERTZ TIME-DOMAIN SPECTROSCOPY	276
Ihor Krapivin, Ramūnas Adomavičius	
AgAl mixed films for space applications	277
Ignas Bitinaitis, Alexandr Belosludtsev, Edvinas Petraitis, Anna Sytchkova	
PEROVSKITE SOLAR CELLS WITH MONOLAYER MODIFIED PTAAs AND APPLICATION TO ALL-PEROVSKITE TANDEM SOLAR CELLS WITH EFFICIENCY OVER 25%	278
Daiva Tavgenienė, Huan Bi, Yasuhiro Fujiwara, Chao Ding, Shahrir Razey Sahamir, Yoshitaka Sanehira, Ajay Kumar Baranwal, Kitamura Takeshi, Guozheng Shi, Gaurav Kapil, Zheng Zhang, Liang Wang, Takeru Bessho, Hiroshi Segawa, Saulius Grigalevicius, Qing Shen, Shuzi Hayase	

P3 Session:

MATERNAL HIGH-FAT DIET: THE CHANGES OF OFFSPRING GUT MICROBIOTA AND BEHAVIOR.....	279
Adomas Smalskys, Gintarė Urbonaitė, Urtė Neniškytė	
THE IMPACT OF STORAGE CONDITIONS AND EXTRAHERT CONCENTRATION ON THE CONTENT OF BIOACTIVE COMPOUNDS IN BEE BREAD AND POLLEN	280
Liveta Muliulytė, Vilma Kaškonienė, Audrius Maruška	
ASSESSMENT OF THE INFLUENCE OF FERMENTATION WITH KOMBUCHA SCOBY ON	

THE BIOLOGICAL ACTIVITY OF PLANT MATERIAL	281
Greta Raškauskienė, Vilma Kaškonienė, Rūta Mickienė, Audrius Maruška	
FORMATION OF CALPROTECTIN (S100A8/S100A9) INHIBITS AGGREGATION OF S100A9 INTO AMYLOID COMPLEXES	282
Ieva Baronaitė, Darius Šulskis, Vytautas Smirnovas	
PLASMA MI RNAs AS POTENTIAL BIOMARKERS FOR PREDICTING RADIATION-INDUCED HEART DISEASES IN LUNG CANCER PATIENTS.....	283
Paulina Kazlauskaitė, Ieva Vaicekauskaitė, Rasa Sabaliauskaitė, Sonata Jarmalaitė, Jonas Venius, Rita Steponavičienė	
ISOLATION OF ENDOPHYTIC MICROORGANISMS FROM BLUEBERRY FRUIT AND IDENTIFICATION BY SURFACE-ENHANCED RAMAN SPECTROSCOPY	284
Sofiya Asadchaya, Dorotėja Vaitiekūnaitė, Ingrida Bružaitė, Valentinas Snitka	
QUANTUM DOTS TOXIC EFFECTS ON BROWN TROUT (<i>SALMO TRUTTA FARIO</i>)	285
Toma Černauskaitė, Gintarė Sauliūtė, Živilė Jurgelėnė	
THE ACTIVITY OF HUMAN ANTIOXIDANT PROTECTION ENZYMES AFTER INFLUENCE OF TiO₂	286
Maryia Sadaunichuk, Aliaksandra Skarabahačava, Elena Venskaya, Natalia Aliakhnovich	
SYNTHESIS OF LIPOSOMAL CURCUMIN AND ITS CHARACTERIZATION IN VITRO	287
Austėja Kvedaraitė, Simona Steponkienė, Vitalijus Karabanovas, Ričardas Rotomskis	
RELEASE STUDIES OF NISIN FROM NISIN-LOADED FUCOIDAN PARTICLES.....	288
Aiste Galinskaite, Ruta Gruskiene, Jolanta Sereikaite	
THE APPLICATION OF PECTIN FOR THE PROTEOLYTIC STABILIZATION OF NISIN.....	289
Justė Čeičytė, Aistė Galinskaitė, Rūta Gruškienė	
ISOLATION AND CULTURE METHOD OF DERMAL CANINE FIBROBLASTS CELL LINE.....	290
Dawid Jeżewski, Nicole Nowak, Tomasz Gębarowski, Joanna Bubak	
ANTIMICROBIAL EXTRACTS AND ESSENTIAL OIL APPLICATION IN O/W EMULSION FORMATION.....	291
Jurga Andreja Kazlauskaite, Inga Matulyte, Jurga Bernatoniene	
COLLAGEN-CONTAINING ENZYME-ELECTROPHORESIS IN DETECTION OF PROTEOLYTIC ACTIVITY IN BLOOD PLASMA OF DONORS WITH DIFFERENT TITERS OF ANTI-SARS-COV-2 IGG.....	292
Maryna Kalashnikova, Daryna Krenytska, Olexiy Savchuk	
INHIBITOR PROTEINS OF CRISPR-CAS BACTERIAL IMMUNITY	293
Dovydas Januška, Tomas Šinkūnas	
CLONING, PURIFICATION AND <i>IN VIVO</i> ACTIVITY OF A NOVEL BACTERIAL DEFENSE SYSTEM	294
Marija Duchovskytė, Dalia Smalakyte, Gintautas Tamulaitis	
INVESTIGATION OF ANTIMICROBIAL PEPTIDE PEDIOCIN	295
Julija Petravičiūtė, Ramunė Stanevičienė, Elena Servienė, Jolanta Sereikaitė	
YEAST SURFACE DISPLAY OF <i>ACINETOBACTER BAUMANNII</i> BLP1 PROTEIN C-TERMINAL FRAGMENT	296
Ieva Šapronytė, Arūnė Verbickaitė, Indrė Dalgėdienė, Julija Armalytė, Rasa Petraitytė-Burneikienė	
TOWARDS SIDE-EFFECT FREE ANTICANCER THERAPY	297
Reda Rulinskaitė, Rūta Palepšienė, Saulius Šatkauskas, Renaldas Raišutis, Martynas Maciulevičius	
MICROFLUIDIC CHIP FABRICATION FOR ELECTROPORATION OF CELLS.....	298
Kamilė Kasperavičiūtė, Eivydas Andriukonis, Arūnas Stirė	
IDENTIFICATION AND HETEROLOGOUS BIOSYNTHESIS OF NOVEL BACTERIOCINS WITH THE ANTI-PHYTOPATHOGENIC BACTERIAL	299
Gabija Smulkaitė, Arnoldas Kaunietis	
CHARACTERIZATION OF NOVEL CRISPR-CAS12 EFFECTOR COMPLEXES.....	300

Brigita Duchovska, Greta Bigelytė, Rimantė Žedaveinytė, Arūnas Šilanskas, Tautvydas Karvelis	
INHIBITION OF BACTERIAL ANTIVIRAL CRISPR-CAS SYSTEM.....	301
Melita Grauzinytė, Tomas Šinkūnas	
VIABILITY OF E. COLI COMPETENT CELLS USING CRYOPROTECTANTS.....	302
Saulė Rapalytė, P. Šimonis, Greta Gančytė, Arūnas Stirkė	
MILK PERMEATE AS AN ALTERNATIVE TO ISOPROPYL B-D-1-THIOGALACTOPYRANOSIDE FOR THE INDUCTION OF RECOMBINANT PROTEIN SYNTHESIS.....	303
Aurimas Greičius, Renata Gudiukaitė	
IMAGING OF GLUCOSE OXIDASE ACTIVITY BY SCANNING ELECTROCHEMICAL MICROSCOPY.....	304
Tomas Mockaitis, Wojciech Nogala, Agnė Boguševičė, Kasparas Kižys, Inga Morkvėnaitė-Vilkončienė	
DEVELOPMENT OF MONOCLONAL ANTIBODIES AGAINST ANTIBIOTIC RESISTANCE PROTEINS OXA-48, OXA-134, SME-3, ADC-144 AND SHV-42	305
Gabija Laučiūtė, Vytautas Rudokas, Laima Čepulytė, Karolina Juškaitė, Martynas Simanavičius, Aurelija Žvirblienė	
PRO-INFLAMMATORY PROTEIN S100A9 ALTERS MEMBRANE ORGANIZATION BY DISPERSING ORDERED DOMAINS	306
Rimgailė Tamulytė, Evelina Jankaitytė, Zigmantas Toleikis, Darius Šulskis, Marija Jankunec	
SYNTHESIS OF SACCHAROMYCES CEREVISIAE L-BC VIRUS-LIKE PARTICLES IN ESCHERICHIA COLI.....	307
Kamilė Vaišaitė, Erika Celitan, Saulius Serva	
ACTION POTENTIALS IN NITELLOPSIS OBTUSA RHIZOIDS	308
Ilvika Maleckaitė, Vilmantas Pupkis, Indrė Lapeikaitė, Vilma Kisnierienė	
Formation of tethered bilayer lipid membranes on gold surface probed by SEIRAS	309
Vaidas Pudžaitis, Martynas Talaikis, Gediminas Niaura	
GLUCOSE DECORATED BOVINE SERUM ALBUMINE STABILIZED GOLD NANOCCLUSERS	310
Šantalė Šaliūtė, Greta Jarockytė, Vilius Poderys	
LOCALISED IMPEDANCE OF ANTI - HUMAN GROWTH HORMONE ANTIBODIES FOR THE DEVELOPMENT OF AN IMPEDIMETRIC IMMUNOSENSOR	311
Timas Merkelis, Antanas Zinovičius, Inga Morkvėnaitė - Vilkončienė, Arūnas Ramanavičius	
LIPOPOLYSACCHARIDES AND PROPERTIES OF THEIR AQUEOUS.....	312
Aistė Stičinskaitė, Lina Ragelienė	
INVESTIGATION OF TETRAPHENYLPHOSPHONIUM CATION UPTAKE BY ELECTROPORATED S. CEREVISIAE YEASTS	313
Greta Gančytė, Povilas Šimonis, Aurelijus Zimkus, Arūnas Stirkė	
EFFECTS OF HUMAN CHORIONIC GONADOTROPIN ON ENDOMETRIAL STROMAL CELLS DECIDUALIZATION.....	314
Deimante Zukauskaite, Erika Girniute, Ruta Navakauskiene	
ATTEMPTS TO INHIBIT EFFLUX OF ANTIFUNGALS IN CANDIDA SPP. YEASTS	315
Eglė Vanseviciūtė, Guoda Jarašiūtė, Rimantas Daugelavičius	
TRICHODERMA REESEI AND PRODUCTION OF HYDROLYTIC ENZYMES	316
Augustinas Andziulis, Rimantas Daugelavičius	
AUTOFLUORESCENCE	317
Aušrinė Navickaitė, Vilmantas Pupkis, Saulius Bagdonas	
ACTIVITY AND CRYSTALLIZATION OF TYPE III CRISPR-CAS ASSOCIATED RING NUCLEASE	318
Danas Klimavičius, Dominik Rafalski, Matthias Bochtler, Gintautas Tamulaitis	
STUDIES ON ENERGY TRANSFORMATION IN HALOARCUA HISPANICA IN LIGHT AND	

DARK PHASES	319
Tomas Stanevičius, Rimantas Daugelavičius	
EXPRESSION OF SELECTED HISTONE METHYLATION-ASSOCIATED GENES IS ASSOCIATED WITH ADVANCED PROSTATE CANCER	320
Greta Meidutė, Rūta Maleckaitė, Kristina Daniūnaitė	
CRISPR-CAS PROTOSPACER INTERACTION WITH ADAPTATION COMPLEX.....	321
Viktoras Ragožius, Inga Songailienė, Lina Malinauskaitė	
INVESTIGATION OF DEEP EUTECTIC SOLVENTS FOR LIGNOCELLULOSIC BIOMASS PRE-TREATMENT	322
Monika Paulauskaitė, Justinas Babinskas, Inga Matijošytė	
PROTEIN AND ALGAE EFFECT ON THE PHOTOSTABILITY OF Cd- AND Cu-BASED QUANTUM DOTS.....	323
Emilija Januškaitė, Agnė Kalnaitytė, Saulius Bagdonas	
OVARIAN CANCER CELL LINES EXHIBIT DIFFERENTIAL STEMNESS-RELATED PROTEIN AND GENE EXPRESSION IN 2D AND 3D.....	324
Eglė Žymantaitė, Agata Mlynska	
PLASMA INDUCED CHANGES IN STEVIA REBAUDIANA ANTIOXIDANT ACTIVITY	325
Augustė Judickaitė, Erika Endriulaitytė, Rasa Žūkienė	
PHYSICOCHEMICAL CHARACTERIZATION AND RELEASE PROPERTIES OF HYDROGEL WITH NIMESULIDE LOADED ON NANOHYDROXYAPATITE.....	326
Katarzyna Wiglusz and Rafal J. Wiglusz	
APPLICATION OF MOUSE ORGANOTYPIC HIPPOCAMPAL SLICE CULTURES TO INVESTIGATE NEURONAL SIALYLATION.....	327
Ugne Kisielute, Ugne Kuliesiute, Urte Neniskyte	
STRUCTURAL VARIABILITY OF PRION PROTEIN AMYLOID FIBRILS UNDER DIFFERENT AGITATION CONDITIONS	328
Egle Pociute, Kamile Mikalauskaite, Vytautas Smirnovas	
THE EFFECT OF dGAE FRAGMENT CONCENTRATION ON ITS SELF- AGGREGATION AND ASSOCIATION WITH TAU PROTEIN.....	329
Urte Venclovaite, Kamile Mikalauskaite, Vytautas Smirnovas	
ACTION POTENTIAL EXCITATION THRESHOLD HYPERPOLARIZATION IN <i>NITELLOPSIS OBTUSA</i> CELL AFTER EXPOSURE TO IP₃	330
Judita Januzaitė, Vilmantas Pupkis, Indre Lapeikaite, Vilma Kisnieriene	
ELECTROCHEMICAL METHOD FOR HYBRIDISATION SIGNAL AMPLIFICATION OF METHYLENE BLUE-LABELLED DNA OLIGONUCLEOTIDES.....	331
Justina Gineitytė, Dalius Ratautas	
EVALUATION OF THE INFLUENCE OF SOLVENT AND STEPWISE EXTRACTION ON THE AMOUNT OF PHENOLIC AND FLAVONOID COMPOUNDS IN OAK ACORN EXTRACTS	332
Aurelija Kondratavičiūtė, Vilma Kaškonienė, Rūta Mickienė, Audrius Maruška	
EVALUATION OF THE IMPACT OF VARIOUS TREATMENT METHODS ON BEE-COLLECTED POLLEN BIOLOGICAL ACTIVITY.....	333
Lukas Asanavičius, Ieva Krivaitė, Vilma Kaškonienė, Nicola Tiso, Audrius Sigintas Maruška	
INVESTIGATING BODIPY-BASED SENSORS FOR MEASURING MICROVISCOSITY IN HUMAN BREAST CANCER CELLS	334
Džiugas Jurgutis , Greta Jarockytė , Aurimas Vyšniauskas, Ričardas Rotomskis, Vitalijus Karabanovas	
BIOCHEMICAL CHARACTERIZATION OF SARS-COV-2 3-CHYMOTRYPSIN-LIKE PROTEASE	335
Kamilė Čerepenkaitė, Aurelija Mickevičiūtė, Asta Zubrienė	
PROTOTYPE OF ANTIMICROBIAL PHOTOINACTIVATION TO PROTECT AGAINST FUNGI PHYTOPATHOGENS AND EXTEND THE.....	336
Goda Mažeikaitė, Irina Buchovec, Pranciškus Vitta	

FERREDOXIN:NADP⁺ OXIDOREDUCTASE FROM <i>RHODOPSEUDOMONAS PALUSTRIS</i>: STEADY-STATE KINETICS AND POTENTIOMETRIC CHARACTERISTICS.....	337
Gintarė Maurutytė, Mindaugas Lesanavičius, Daisuke Seo, Narimantas Čėnas	
CRYSTALLIZATION AND X-RAY STRUCTURAL ANALYSIS OF THSB PROTEINS FROM BACTERIAL ANTIVIRAL SYSTEM THOERIS	338
Deividas Vilutis, Arūnas Šilanskas, Mindaugas Zaremba, Giedrė Tamulaitienė	
UNCOVERING THE ROLE OF 5'-NAD-RNA HYDROLYSIS-ASSOCIATED PROTEINS IN <i>ESCHERICHIA COLI</i>	339
Gytė Tupikaitė, Gabrielė Olendraitė, Renatas Krasauskas, Milda Mickutė, Giedrius Vilkaitis	
SIGNIFICANCE OF NOTCH SIGNALING PATHWAY IN COLORECTAL CANCER HCT116 AND ENDOMETRIAL CANCER KLE CELL LINES	340
Darija Šachova, Viktorija Stučytė, Eglė Žalytė, Violeta Jonušienė	
STRUCTURAL AND FUNCTIONAL STUDIES OF THOERIS ANTIPHAGE DEFENSE SYSTEM	341
Dziugas Sabonis, Giedrius Sasnauskas, Audrone Ruksenaite, Arunas Silanskas, Gal Ofir, Rotem Sorek, Mindaugas Zaremba, Virginijus Siksnyš, Giedre Tamulaitiene	
INVESTIGATION OF THE PHOTOPHYSICAL PROPERTIES OF THE CHLOROPHYLLIN- CHITOSAN COMPLEX.....	342
Gabrielė Vasiliauskaitė, Irina Buchovec	
<i>LACTICASEIBACILLUS CASEI</i> BL23 NON-CODING SLCB2236- SMALL RNA – MEDIATED RESPONSE TO ENVIRONMENTAL STRESSES	343
Odilija Safinaitė, Renatas Krasauskas, Giedrius Vilkaitis	
STUDY OF NEW ANTI-PHAGE DEFENSE SYSTEMS	344
Viktorija Rainytė, Paulius Toliušis, Mindaugas Zaremba	
SYNTHESIS OPTIMIZATION OF ADOMET ANALOGUE FOR PHOTOCLEAVABLE GENE LABELING.....	345
Mindaugas Matonis, Martynas Malikėnas	
APPLICATION OF IMMOBILIZED FRUCTOSE DEHYDROGENASE ONTO MODIFIED GOLD NANOPARTICLES FOR D-TAGATOSE BIOSENSOR	346
Milda Stachnevičiūtė, Julija Razumienė, Marius Butkevičius	
THE DEVELOPMENT AND CHARACTERIZATION OF AN L-AMINO.....	347
Deimantė Stakelytė, Justas Miškinis, Dalius Ratautas	
A FLUORIMETRIC METHOD FOR NUCLEIC ACID CONTENT DETERMINATION BASED ON PROPIDIUM IODIDE STAINING	348
Rammukund Kishore Kumar, Dr. Baltramiejus Jakštys	
SYNTHESIS OF AMINO ACID AND NUCLEOSIDE CONJUGATES	349
Kamilė Butkutė, Martyna Koplūnaitė, Rolandas Meškys	
ELECTROCHEMICAL INVESTIGATION OF PHOSPHOLIPID MEMBRANE DAMAGE INDUCED BY S100A9 PROTEIN.....	350
Evelina Jankaitytė, Darius Šulskis, Vytautas Smirnovas, Rima Budvytytė, Gintaras Valinčius	
<i>ARCHAEOGLOBUS FULGIDUS</i> ARGONAUTE PROTEIN RECOGNIZES GUIDE AND TARGET STRANDS IN A SEQUENCE-SPECIFIC MANNER.....	351
Reda Pocevičiūtė, Edvardas Golovinas, Elena Manakova, Mindaugas Zaremba	
STUDY OF THE STABILITY OF POTENTIAL DRUG CARRIERS, GRAPHENE QUANTUM DOTS AND DOXORUBICIN AGGREGATES BY	352
Martynas Zalieckas, Vilius Čirgelis, Renata Karpicz	
MODULATION OF SPECIFIC DNMT1 ACTIVITY BY KINASE INHIBITORS IN MURINE EMBRYONIC STEM CELLS.....	353
Radvilas Bendorys, Liepa Gasiulė, Vaidotas Stankevičius	
HALIDE METHYLTRANSFERASE AS AN EFFICIENT TOOL FOR CHEMOENZYMATIC COFACTORS SYNTHESIS.....	354

Goda Jankauskaitė, Bernadeta Masiulionytė, Giedrius Vilkaitis	
RESEARCH ON CELL PLASMA MEMBRANE PERMEABILIZATION, RESEALING AND CELL VIABILITY AFTER ELECTROPORATION.....	355
Dominykas Makarovas, Baltramiejus Jakštys, Saulius Šatkauskas	
TITANIUM VS STAINLESS-STEEL ELECTRODES IN ELECTROPORATION: COMPARING CELL TRANSFECTION, PERMEABILITY, PORE RESEALING AND VIABILITY	356
Dominyka Gabulaitė, Baltramiejus Jakštys, Saulius Šatkauskas	
LYSOZYME AMYLOID FIBRIL STRUCTURAL VARIABILITY DEPENDENCE ON INITIAL PROTEIN FOLDING STATE.....	357
Kamilė Mikalauškaite, Mantas Ziaunys, Vytautas Smirnovas	
ENZYMATIC ELECTROCHEMICAL BIOSENSOR FOR EXTRACELLULAR GLUTAMATE DETECTION IN BIOFLUIDS	358
Roberta Stefanovič, Vidutė Gurevičienė, Julija Razumienė	
STAT3 SIGNALING PATHWAY AS A POTENTIAL PREDICTIVE TARGET IN TRIPLE-NEGATIVE BREAST CANCER.....	359
Aistė Gerulaitytė, Justas Burauskas, Agnė Šeštokaitė, Monika Drobnienė, Rasa Sabaliauskaitė, Sonata Jarmalaitė	
THE EFFECT OF SOWING DENSITY ON THE CHEMICAL COMPOSITION AND ANTIOXIDANT ACTIVITY OF INDUSTRIAL HEMP (<i>CANNABIS SATIVA</i> L.) ROOTS.....	360
Dovilė Motiejauskaitė, Karolina Barčauskaitė	
GENOTOXICITY AND CYTOTOXICITY ASSESSMENT OF MICROPLASTICS ON FISH	361
Agnė Bučaitė, Milda Stankevičiūtė	
EFFECTS OF PATHOGENIC OOMYCETES ON ATLANTIC SALMON EMBRYOS.....	362
Eglė Gadeikytė, Gintarė Sauliutė, Arvydas Markuckas, Milda Stankevičiūtė	
BIOANALYTICAL METHOD FOR THE DETERMINATION OF PSYCHOACTIVE SUBSTANCES IN BIOLOGICAL SPECIMENS	363
Nerijus Karlonas	
STUDY OF THE EFFECT OF CHEMOTHERAPEUTICS ON HUMAN COLORECTAL CANCER CELL SUBLINES	364
Ieva Norkaitytė, Eglė Žalytė, Aušra Sasnauskienė	
THE ANALYSIS OF ANTIBIOTIC RESISTANCE AND VIRULENCE GENES IN CLINICAL AND ENVIRONMENTAL ISOLATES OF	365
Radvilė Drevinskaitė, Laurita Klimkaitė, Julija Armalytė	
MECHANISM OF CRISPR-CAS3 HELICASE USING MAGNETIC TWEEZERS.....	366
Miglė Šarpilo, Algirdas Toleikis	
ACUTE TOXIC EFFECTS CAUSED BY THE CO-EXPOSURE OF NANO/MICROPARTICLES AND HYDROXYCHLOROQUINE IN <i>SALMO TRUTTA</i> AT EARLY DEVELOPMENT	367
Augustas Morkvėnas, Živilė Jurgelėnė, Reda Dzingelevičienė, Nerijus Dzingelevičius, Małgorzata Szultka-Młyńska, Bogusław Buszewski, Vitalijus Karabanovas	
EVALUATION OF CHEMICAL COMPOSITION AND RADICAL SCAVENGING OF MEDICAL PLANTS ACCUMULATING BIOACTIVE COMPOUNDS USING SPECTROMETRIC AND CHROMATOGRAPHIC METHODS	368
Domantas Armonavičius, Mantas Stankevičius, Ona Ragažinskienė, Audrius Maruška	
PECULIARITIES OF MOSQUITO LARVAE DISTRIBUTION IN DIFFERENT WATER BODIES ...	369
Kristina Valavičiūtė-Pocienė, Rasa Bernotienė	
RESPONSE OF ENTOMOPATHOGENIC NEMATODE <i>STEINERNEMA FELTIAE</i> TO 1-NONENE, THE VOLATILE OF INSECT CADAVERS.....	370
Deimantė Tiškevičiūtė, Rasa Čepulytė, Vincas Būda	
TRANSCRIPTOMIC AND MUTATIONAL ANALYSIS OF GYNEGOLOGIC CELL LINES AND TUMORS	371
Ieva Vaicekauskaitė, Daiva Dabkevičienė, Julija Šimienė, Diana Žilovič, Rūta Čiurlienė, Sonata Jarmalaitė, and Rasa Sabaliauskaitė	

QUANTITATIVE ANALYSIS OF MICRORNAS IN 4NQO-TREATED LEUKOCYTES OF PATIENTS WITH TYPE 1 DIABETES MELLITUS	372
Bernadeta Kaminskaite, Laura Siaulienė, Zydrune Visockiene, Kristina Daniunaite	
IDENTIFICATION OF CYTOGENETIC POTENTIAL OF THE FISH PATHOGEN SAPROLEGNIA PARASITICA USING ERYTHROCYTIC NUCLEAR ABNORMALITY TEST	373
Eva Kutys, Milda Stankevičiūtė	
IL-1B AND IL-4 CONCENTRATION IN SERA OF PANCREATIC CANCER.....	374
Kornelija Jencevičiūtė, Arenida Bartkevičienė, Aldona Jasukaitienė, Jason Matthews, Antanas Gulbinas, Žilvinas Dambrauskas	
ASSESSMENT OF BREX PROTEINS IN ANTIVIRAL DEFENCE.....	375
Aistė Petrauskaitė, Justė Adomaitytė, Tomas Šinkūnas	
COMPLICATIONS IN LEFT-SIDE COLORECTAL CANCER SURGERY	376
Kornelija Rauduvytė, Agata Mlynska, Žilvinas Gričius, Agnė Šeštokaitė, Simona Rūta Letautienė, Kristina Žukauskaitė, Audrius Dulskas, Rasa Sabaliauskaitė, Augustinas Baušys	
FUNGAL DIVERSITY ON INVASIVE <i>CYTISUS SCOPARIUS</i> L. PLANTS IN LITHUANIA	377
Dovilė Čepukoit, Ieva Rinkevičiūtė, Daiva Burokienė	
STABLE ISOTOPES IN YOUR HAIR CAN TELL WHAT YOU ATE AND HOW YOU LIVED.....	378
Raminta Skipitytė, Andrius Garbaras	
VEGETARIAN OR EATING MEAT? STABLE ISOTOPES REVEAL THE DIETARY HABITS OF MODERN AND ANCIENT HUMANS IN LITHUANIA.....	379
Raminta Skipitytė, Rimantas Jankauskas	
STRUCTURAL ANALYSIS OF <i>SIW14</i>, PROTEIN AFFECTING [PSI+] PRION APPEARANCE IN <i>SACCHAROMYCES CEREVISIAE</i>	380
Gvidas Katauskas, Justina Versockienė, Audrius Gegeckas, Eglė Lastauskienė	
EVALUATION OF SEVERAL <i>IN VITRO</i> RESEARCH METHODOLOGY STEPS FOR NONCODING CIRCULAR RNA QUANTIFICATION	381
Marta Tamošiūnaitė, Rūta Maleckaitė, Kristina Daniūnaitė	
THE EFFECTS OF GRAPHENE OXIDE AND METAL MIXTURES ON FRESHWATER BROWN TROUT (<i>SALMO TRUTTA</i> L.) SWIMMING	382
Tomas Makaras, Sergej Semčuk	
THE PHYSICOCHEMICAL PROPERTIES OF CHITOSAN VARY DEPENDING ON THE LIVING SOURCE AND THE FUNCTIONS PERFORMED.....	383
Aurelija Ramanauskaitė, Vykintas Baublys, Povilas Mulerčikas	
EVALUATION OF THE SALMONID SENSITIVITY TO THE PATHOGENIC OOMYCETES AT THE EARLY DEVELOPMENT STAGE	384
Gabrielė Oželytė, Gintarė Sauliūtė, Arvydas Markuckas, Milda Stankevičiūtė	
EFFECTS OF MICROGRAVITY ON THE PHYSIOLOGY OF MICROORGANISMS AND RESISTANCE TO CHEMICAL AND PHYSICAL	385
Irmantas Arūnas Čiužas, Eglė Lastauskienė, Justina Versockienė, Vitalij Novickij, Gediminas Staigvila	
THE EFFECT OF MATERNAL HIGH-FAT DIET ON OFFSPRING	386
Neda Ieva Biliūtė, Gintarė Urbonaitė, Guoda Laurinavičiūtė, Urtė Neniškytė	
ADHESION OF MAMMALIAN CELL LINES ON POLYCARBONATE.....	387
Paulina Kizinievič, Neringa Bakutė, Arūnas Stirė	
IN VITRO EVALUATION OF STEM CELL DIFFERENTIATION ON 3D BIOPRINTED HYDROGELS FOR URETHRAL TISSUE ENGINEERING	388
Andrius Buivydas, Povilas Barasa, Egidijus Šimoliūnas, Natalija Krestnikova, Virginija Bukelskienė	
INVESTIGATIONS OF THE EFFECTS OF POLYSTYRENE NANOPARTICLES ON ROOT CELLS OF <i>ALLIUM CEPA</i> BY MOLECULAR METHODS	389
Gabija Zinkevičiūtė, Asta Stapulionytė	
RESEARCH OF GENOTOXIC EFFECTS INDUCED BY POLYSTYRENE	390

Agnė Kilnaitė, Asta Stapulionytė

THE EFFECTS OF HUMAN MENSTRUAL BLOOD MESENCHYMAL STEM CELL GROWTH FACTORS ON CHONDROGENESIS IN VITRO	391
Paulina Bialaglovyte, Rokas Miksiunas, Ignas Lebedis, Jolita Pachaleva, Eiva Bernotiene, Almira Ramanaviciene, Giedrius Kvederas, Ilona Uzieliene	
Un-Settling Virome of Saccharomycetales Yeast: Dispersal within Species.....	392
Kristupas Paulius, Aleksandras Konovalovas, Saulius Serva	
EFFECTS OF SURFACE ROUGHNESS ON THE GIANT MAGNETORESISTANCE PERFORMANCE IN MAGNETIC SANDWICHES.....	393
Aleksandre Melikadze, Lali Kalandadze, Nugzar Gomidze	
CHEMOPREVENTIVE ACTIVITY OF LINSEED OIL ETHYL ESTERS FOR GLIOMA TUMOR CELL PANEL TCP-1018™.....	394
Nikola Hauzer, Maciej Janeczek , Tomasz Gębarowski	
ISOLATION OF STEM CELLS OBTAINED FROM HUMAN SUBCUTANEOUS ADIPOSE TISSUE.....	395
Emilia Kamińska, Weronika Gołąbek, Nikola Hauzer, Maciej Janeczek, Tomasz Gębarowski	
DETERMINATION OF INCREASE IN THE DEGREE OF HESPERIDIN DISSOLUTION IN THE COMPOSITION OF A CENTRIFUGALLY FORMED SOLID DISPERSION SYSTEM.....	396
Vadym Lisovyj, Artem Kharchenko, Andriy Goy, Viktoriia Plavan, Volodymyr Bessarabov	
INHIBITION OF NOVOCAINE HYDROLYSIS IN HUMAN SERUM BY HESPERIDIN IN VITRO...	397
Dmytro Oliinyk, Volodymyr Bessarabov, Galyna Kuzmina, Vadym Lisovyj, Anastasiia Behdai, Vladyslav Udovytskyi	
STUDY OF THE KINETICS OF THE RELEASE OF NIMESULIDE FROM A POLYMER SOLID DISPERSION SYSTEM.....	398
Viktoriia Lyzhniuk, Vadym Lisovyj, Volodymyr Bessarabov, Galyna Kuzmina, Viktor Kostyuk, Andriy Goy	
PROOXIDANT PROPERTIES OF LORATADINE AND DESLORATADINE IN THE CHEMICAL SYSTEM OF AUTO-OXIDATION OF ADRENALINE.....	399
Daryna Taran, Volodymyr Bessarabov, Roman Smishko, Vadym Lisovyj, Galyna Kuzmina, Vladyslav Strashnyi	
CONCENTRATIONS OF FIBRINOGEN AND D-DIMER IN BLOOD PLASMA OF DONORS WITH VARIOUS TITERS OF ANTI-SARS-CoV-2 IgG.....	400
Antonina Rachkovska, Daryna Krenytska, Vitaliy Karbovskiy	
CO-PRECIPITATION SYNTHESIS OF SAMARIUM-GADOLINIUM CO-DOPED CERIA THIN FILMS.....	401
Elessar Mhana, Jurgita Čyviėnė, Brigita Abakevičienė	

TRANSIENT ABSORPTION SPECTROSCOPY OF EXCITATION DYNAMICS AND RADICAL FORMATION IN DIFFERENT PHOTOINITIATORS

Marius Navickas¹, Edvinas Skliutas¹, Mangirdas Malinauskas¹, Mikas Vengris¹

¹Vilnius University, Laser Research Center, Sauletekio av. 10, LT-10223, Vilnius, Lithuania
marius.navickas@ff.vu.lt

Photopolymerization has attracted a great scientific and technological interest due to a large number of applications spanning from optoelectronics to medical areas [1, 2]. This process is promoted by photoinitiators which in a very short time scale produce free radicals that trigger the cross-linking reactions [3, 4]. Thus, the photopolymerization initiation becomes a significant process governing the chemical and physical nature of the final product. A large variety of different photoinitiators have been studied by various spectroscopic techniques, however, the excitation mechanisms are not fully understood. In this work, we present a comparative transient absorption (TA) spectroscopy study of photoinitiation behaviour in commercial BAPO, Irgacure 369, Irgacure 651 and TPO photoinitiators dissolved in isopropanol.

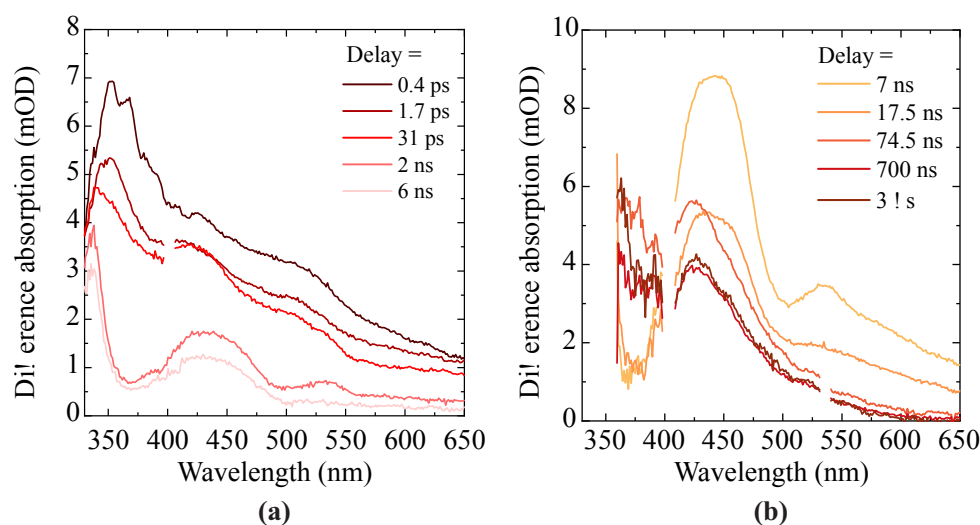


Fig. 1. Transient absorption spectra of BAPO photoinitiator obtained during the (a) pump-probe and (b) laser flash photolysis experiments.

Fig. 1 (a) represents the TA spectra of BAPO photoinitiator recorded during the ultrafast pump-probe experiments. This technique revealed that after one-photon excitation BAPO immediately cleaves into benzoyl, containing methyl groups, and phosphinoyl radicals. In addition, it was observed, that benzoyl radical features a significantly faster relaxation time than phosphinoyl radical. Further, we performed laser flash photolysis experiments to get a deeper knowledge of the radical relaxation timescale and formation mechanisms. The TA spectra observed by means of laser flash photolysis (Fig. 1 (b)) suggest that the latter radical relaxes in several tens of nanoseconds. These results are in a good agreement with the previously discussed photoinitiation mechanism and provide a deeper insight into the primary photoreactions of BAPO.

The TA spectra of Irgacure 369, Irgacure 651 and TPO feature only two broad induced absorption (IA) bands. In case of Irgacure 369, these IA bands span around ca. 350 nm and 470 nm. The presence of transient species was confirmed by the kinetic traces. We found that the IA band of Irgacure 369 grows up in 10 ps and after 100 ps starts to decay, meanwhile the second IA band relaxes after 100 ps. In addition, the laser flash photolysis of argon-saturated Irgacure 369 solution exhibits an increase of initial Irgacure 369 relaxation time, revealing the triplet character of the radical formation.

-
- [1] W. Tomal, J. Ortyl, Water-soluble photoinitiators in biomedical applications, *Polymers* **12**, 1073 (2020).
[2] K. Ikemura, K. Ichizawa, M. Yoshida et. al., UV-VIS spectra and photoinitiation behaviors of acylphosphine oxide and bisacylphosphine, *Dent. Mater. J.* **27**, 765–774 (2008).
[3] C. Decker, The use of UV irradiation in polymerization, *Polym. Int.* **45**, 133–141 (1998).
[4] A. Alberti, M. Benaglia, D. Macciantelli et. al., Further EPR-spin trapping studies of the photoinitiating activity of Irgacure 369, *Eur. Polym. J.* **44**, 3022–3027 (2008).

INVESTIGATION OF NEW TADF MATERIALS DERIVATIVE OF THE 1,3,5-TRIAZINE MOLECULE

Eyad Al Souki,^{1,2} Ikkal Marghad,² Mathieu Sauthier¹

¹ Univ. Lille, CNRS, Centrale Lille, Univ. Artois, UMR 8181, UCCS, Unité de Catalyse et Chimie du Solide, F-59000, Lille, France.

² LABKICOSMOS, École Centrale de Lille, 1 Av. Paul Langevin, 59650 Villeneuve-d'Ascq, France.
eyad.alsouki@univ-lille.fr

Thermally activated delayed fluorescence (TADF) properties, which enable the harvesting of light from both singlet and triplet excitons without the use of any noble heavy metals, are of interest for a wide range of applications. These materials are now considered the third generation of OLED materials [1]. Among such emitters, the 1,3,5-triazine TADF derivatives can be synthesized using the 2,4,6-tris (4-fluorophenyl)-1,3,5-triazine a cost-effective intermediate developed by the company «LABKICOSMOS». Through tri-substitution of the fluoride, the 1,3,5-triazine moiety is decorated with carbazole, phenothiazine, phenoxazine, diphenylamine, and 3-methyl indole donors, yielding donor-acceptor type compounds with the TADF effect [2, 3]. Our second goal was to create a new series of molecules derived from 1,3,5-triazine. To the best of our knowledge, the mono- and di-substitution of the 2,4,6-tris (4-fluorophenyl)-1,3,5-triazine intermediate has never been investigated. This work is focused on a new series of 1,3,5-triazine TADF derivatives through the mono- and di-substitution of our intermediate. The study of the TADF effect and the efficiency of this new series is still in progress. The presentation describes the synthesis of the tri-substituted derivatives as well as the first results concerning the selective synthesis of mono- and di-substituted derivatives.

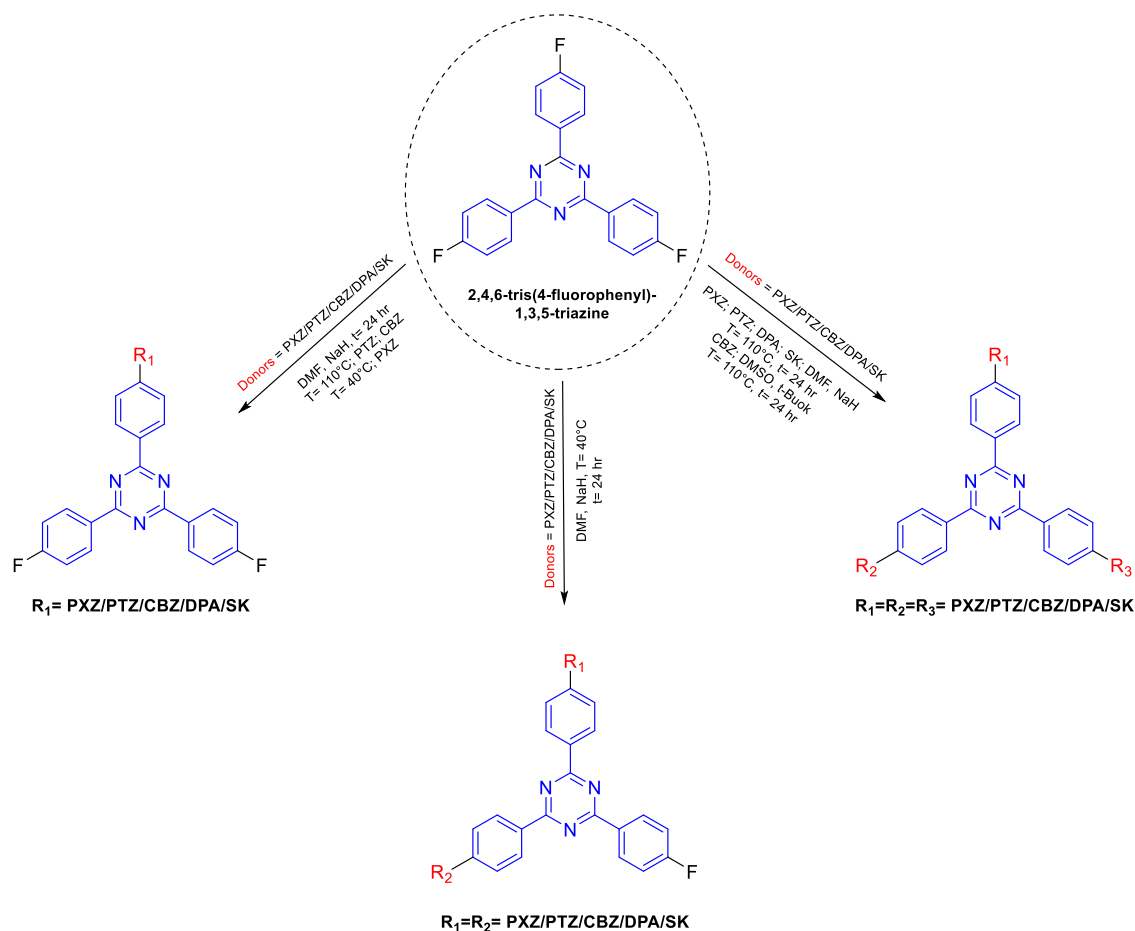


Fig. 1. Synthetic route to new triazine derivatives from the intermediate molecule.

- [1] Uoyama, H., Goushi, K., Shizu, K. *et al.* Highly efficient organic light-emitting diodes from delayed fluorescence. *Nature* **492**, 234–238 (2012).
[2] Marghad, I; Bencheikh, F; Wang, C; Manolikakes, S; Rérat, A; Gosmini, C; Kim, D.H; Ribierre, J-C; Adachi, C. *RSC Adv.*, 2019, **9**, 4336-4343.
[3] Marghad, I; Kim, D. H; Tian, X; Mathevet, F; Gosmini, C; Ribierre, J-C; Adachi, C. *ACS Omega*, 2018, **3**, 2254-2260.

ONE-STEP IMIDAZO[2,1-*b*][1,3]THIAZINE AND IMIDAZO[2,1-*c*][1,4]THIAZEPINE SCAFFOLD SYNTHESIS FROM 2-ALKYNYLTHIOIMIDAZOLES

Indrė Misiūnaitė, Algirdas Brukštus, Ieva Žutautė

Faculty of Chemistry and Geosciences, Vilnius University, Naugarduko g. 24, LT-03225, Vilnius Lithuania
Indre.Misiunaite@chgf.stud.vu.lt

Nitrogen and sulfur-containing heterocyclic compounds have received increased attention in recent years due to their occurrence in a variety of pharmacologically active molecules [1]. Thiazines and thiazepines are no exception. For example, molecules containing imidazo[2,1-*b*][1,3]thiazine framework may exhibit antituberculosis [2], hypocholesterolemic [3], cardiotoxic [4] activity and the [1,4]thiazepine scaffold is present in structure of several medications for the treatment of hypertension [5], angina pectoris [6] and schizophrenia [7]. To the best of our knowledge, no extensive research on synthesis and biological activity has been conducted on various imidazo[2,1-*b*][1,3]thiazines and imidazo[2,1-*c*][1,4]thiazepines. As a result, these heterocycles are appealing in both synthetic and medicinal applications.

In most cases, the formation of [1,3]thiazine and [1,4]thiazepine fragments requires complicated reaction conditions or more than two synthesis steps. One of the new trending pathways to synthesize heterocycles from alkynes is electrophile promoted nucleophilic cyclization reactions [8]. Fascinated by the possibility to investigate synthesis of imidazo[2,1-*b*][1,3]thiazines and imidazo[2,1-*c*][1,4]thiazepines in one reaction step various 2-alkynylthioimidazoles were chosen as starting materials (Fig. 1). To obtain desired scaffolds different electrophiles were tested. Regardless of the electrophile source used, the dominant cyclization reaction pathway was *endo*-dig although *exo*-dig products may form depending on the substituent R in the starting material. During the oral session, the scope and limitations of electrophile promoted nucleophilic cyclization will be discussed.

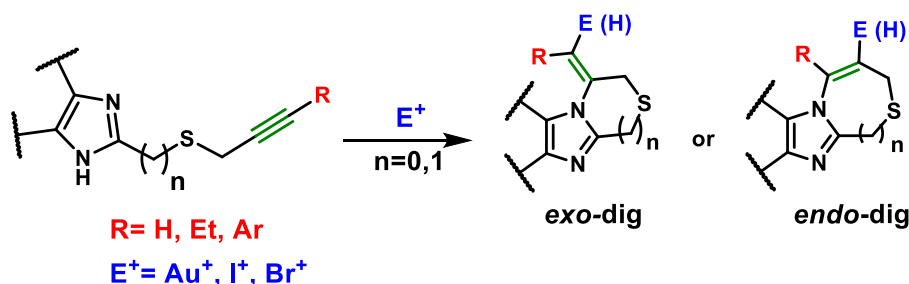


Fig. 1. Synthesis of imidazo[2,1-*b*][1,3]thiazine and imidazo[2,1-*c*][1,4]thiazepine frameworks.

- [1] (a) M. M. Heravi, V. Zadsirjan, Prescribed drugs containing nitrogen heterocycles: an overview, *RSC Adv.*, **2020**, 10, 44, 247. (b) N. Kerru, L. Gummidi, S. Maddila, K. K. Gangu, S. B. Jonnalagadda, A Review on Recent Advances in Nitrogen-Containing Molecules and Their Biological Applications, *Molecules*, **2020**, 25, 1909.
- [2] J.-X. Gong, Y. He, Z.-L. Cui, Y.-W. Guo, Synthesis, Spectral Characterization, and Antituberculosis Activity of Thiazino[3,2-*A*]Benzimidazole Derivatives, *Phosphorus Sulfur Silicon Relat. Elem.* **2016**, 191 (7), 1036–1041.
- [3] E. Abele, R. Abele, P. Arsenyan, S. Belyakov, M. Veveris, E. Lukevics, Phase-Transfer Catalytic Synthesis and Hypocholesterolemic Activity of Thiazino[3,2-*a*]Benzimidazole and Its Silicon Analog, *Chem. Heterocycl. Compd.* **2007**, 43 (2), 220–224.
- [4] V. Garaliene, L. Labanauskas, A. Brukštus, Effect of 1-Acyl-5,6-Dialkoxy-2-Alkylthiobenzod[*d*]Imidazoles on the Action Potential Duration and Isometric Contraction in Guinea Pig Atrium Activated by Carbachol and in Guinea Pig Heart Papillary Muscles. *Arzneimittelforschung* **2006**, 56 (4), 282–287.
- [5] (a) G. M. Pieper, W. Siebeneich, Temocapril, an Angiotensin Converting Enzyme Inhibitor, Protects against Diabetes-Induced Endothelial Dysfunction, *Eur. J. Pharmacol.* **2000**, 403, 129–132. (b) M. Arakawa, M. Sasaki, M. Ohmori, K. Harada, A. Fujimura, Pharmacokinetics and Pharmacodynamics of Temocapril during Repeated Dosing in Elderly Hypertensive Patients, *Eur. J. Clin. Pharmacol.* **2001**, 56 (11), 775–779.
- [6] S. Muthusamy, M. D. S. Kumar, E. Suresh, Synthesis of Indole Annulated [1,3]-Thiazaheterocycles and -Macrocycles via Ring-Closing Metathesis, *ChemistrySelect* **2016**, 1 (11), 2603–2609.
- [7] X. Niu, B. Yang, Y. Li, S. Fang, Z. Huang, C. Xie, C. Ma, A Transition Metal-Free Tandem Process to Pyridazinopyrido[3,2-*f*][1,4]Thiazepine-Diones via Smiles Rearrangement, *Organic & Biomolecular Chemistry* **2013**, 11(24), 4102–4108.
- [8] B. Godoi, R. F. Schumacher, G. Zeni, Synthesis of Heterocycles via Electrophilic Cyclization of Alkynes Containing Heteroatom, *Chem. Rev.* **2011**, 111 (4), 2937–2980.

SYNTHETIC PATHWAY INVESTIGATION OF BENZIMIDAZOLE DERIVATIVES AS POTENTIAL INHIBITORS FOR HSP90

Lukas Neverdauskas, Paulina Kaziukonytė, Algirdas Brukštus

Faculty of Chemistry and Geosciences, Department of Organic chemistry, Vilnius University, Lithuania
lukas.neverdauskas@chgf.stud.vu.lt

Inhibition of Hsp90 (heat shock protein) has been explored as a potential therapeutic strategy for cancer, as many oncogenic client proteins rely on Hsp90 for their stability and activity. Several small-molecule inhibitors of Hsp90 have been developed and are currently being evaluated in clinical trials [1].

Due to the fact that the highest binding constant with the targeted protein is delivered by compounds containing 4-isopropyl-1,3-benzenediol moiety [2], various benzimidazole derivatives were synthesized as potential inhibitors of Hsp90, where 4-isopropyl-1,3-benzenediol moiety was connected by a different number of methylene linkers $n = 0-1$.

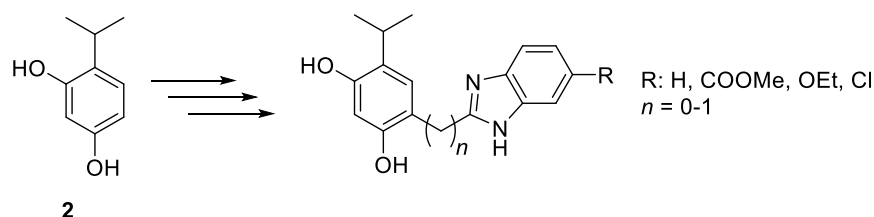


Fig. 1. Previously synthesized benzimidazole derivatives.

To investigate the dependency between methylene groups in synthesized benzimidazoles and the binding constant, we are looking for methods to synthesize benzimidazole derivatives containing double methylene linker ($n = 2$). Furthermore, double methylene linker can be synthesized as ethylene or ethene linker between benzimidazole and 4-isopropyl-1,3-benzenediol moiety by introducing double or triple bonds.

In all cases, the investigation of the synthesis pathways was started with commercially available 1-(2,4-dihydroxyphenyl)ethanone (**1**). Through a multi-step synthesis pathway, the starting material (**1**) was modified to 2,4-dihydroxy-5-isopropylbenzaldehyde (**3**) or ethyl 3-(2,4-dihydroxy-5-isopropylphenyl)propanoate (**4**) as critical starting materials for the investigation of the benzimidazole (**5**) formation (Fig. 2). By changing reaction conditions, the formation of the benzimidazole was investigated.

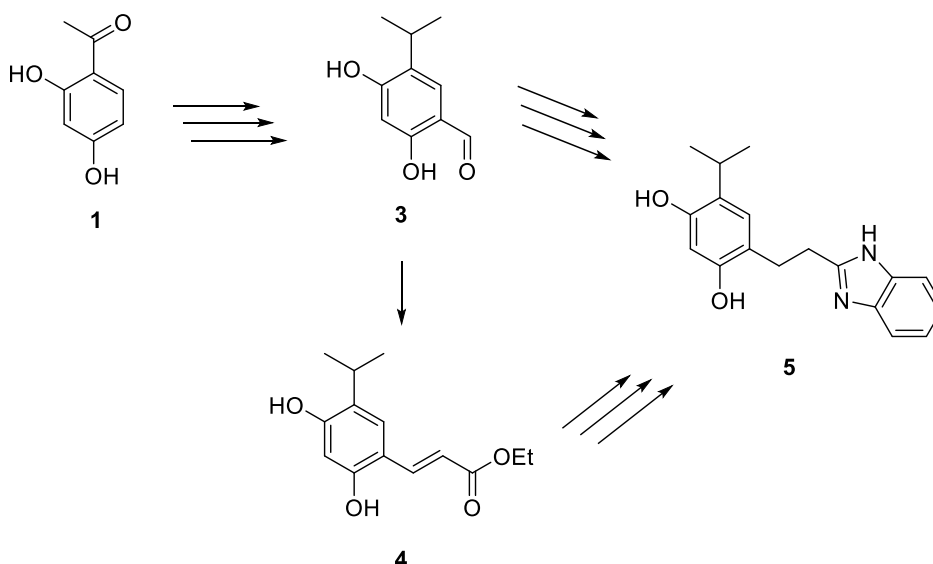


Fig. 2. Synthetic pathway of 4-(2-(1H-benzo[d]imidazol-2-yl)ethyl)-6-isopropylbenzene-1,3-diol.

Final product **5** is yet to be analyzed for inhibition properties for Hsp90.

- [1] L. Neckers. Hsp90 inhibitors as novel cancer chemotherapeutic agents. *Trends Mol. Med.* **2002**, 55–61.
[2] E. Kazlauskas, A. Brukštus, H. Petrikas, et al. Improving the Hsp90 Inhibitors Containing 4-(2,4-Dihydroxyphenyl)-1,2,3-thiadiazole Scaffold: Synthesis, Affinity and Effect on Cancer Cells. *Anticancer. Agents Med. Chem.* **2017**.

FEMTOSECOND LASER WAVELENGTH INFLUENCE ON THE FORMATION OF SINGLE-SHOT GOLD NANOSTRUCTURES

Kernius Vilkevičius, Evaldas Stankevičius

Department of Laser Technologies, Center for Physical Sciences and Technology, Lithuania
Kernius.vilkevicius@ftmc.lt

Using a single pulse of a tightly focused femtosecond laser, the modification without ablation of plastic and highly elastic metals is available with the formation of superficial nanostructures. The stresses induced by a high-intensity pulse produce a momentum normal to the metal surface leading to the delamination of a thin film and the formation of protrusions. The fast heating or even melting of the metal layer and fast resolidification of it lead to energy-dependent morphological shapes of the structures – bumps cones or jets [1].

The periodic arrays of such nanostructures excite hybrid lattice plasmon polariton exhibiting intense and practically applicable plasmon resonance. The narrow peak excitation is due to the interaction of diffracted light with surface lattice plasmons arising from periodically excited localized plasmons in each nanostructure [2]. The periodic gratings can be applied as refractive index sensors, perfect light absorbers, nanolasers, or in Raman spectroscopy [3].

The formation process, size, and shape of the nanostructures depend not only on the pulse energy but also on the laser wavelength. Using the direct laser writing method, the wavelength dependence was investigated by fabricating structures of different morphology using the first (1030 nm), second (515 nm), and third (343 nm) femtosecond laser harmonic. The bump structures remain quite similar, while the cone and jet morphology change significantly. The most prominent difference is seen in the jets (Fig. 1), as the ones fabricated with IR radiation are small and have a thick protrusion, while the ones manufactured with lower wavelengths have a thinner and pointier antenna. Also, using 1030 nm the influence of the polarization on the structure shape symmetry is observed.

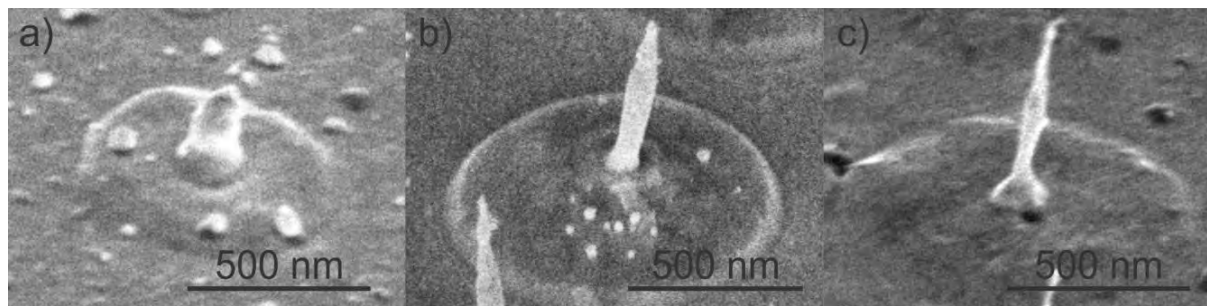


Fig. 1. SEM micrograph of nanoantenna fabricated using 1030 nm (a), 515 nm (b), and 343 nm (c) tilted at a 45° angle.

Furthermore, the laser wavelength influence on the achievable grating period and the nanostructure formation fluence was investigated. Both of these parameters decrease by implementing higher harmonics with shorter wavelengths, leading to a more precise formation of the nanostructures. Also, the thin film stress-induced intrinsic modifications similar to material fatigue were observed as the formation fluence required to obtain specific morphology decreased with higher pulse overlapping at smaller periods.

Finally, the periodic arrays of nanobumps were fabricated using different harmonics and the reflectance spectra were investigated using a spectrophotometer. All gratings exhibit high-quality resonances (Q-factor up to 40) with a marginal influence of the laser wavelength.

-
- [1] D. Pavlov, S. Syubaev, A. Kuchmizhak, S. Gurbatov, O. Vitrik, E. Modin, M. Lapine, Direct laser printing of tunable IR resonant nanoantenna arrays, *Appl. Surf. Sci.* **469**, 514–520 (2019)
- [2] E. Stankevičius, K. Vilkevičius, M. Gedvilas, E. Bužavaitė-Vertelienė, A. Selskis, Z. Balevičius, Direct Laser Writing for the Formation of Large-Scale Gold Microbumps Arrays Generating Hybrid Lattice Plasmon Polaritons in Vis–NIR Range, *Adv. Opt. Mater.* **9**(12), 2100027 (2021).
- [3] K. Yang, X. Yao, B. Liu, B. Ren, Metallic Plasmonic Array Structures: Principles, Fabrications, Properties, and Applications, *Adv. Mater.* **33**, 2007988 (2021).

NITROGEN-MODIFIED REDUCED GRAPHENE OXIDE AS A PLATFORM FOR SENSITIVE AND SELECTIVE ELECTROCHEMICAL DETECTION OF DOPAMINE

Rūta Aukštakojytė¹, Justina Gaidukevič^{1,2}, Rasa Pauliukaitė², Jurgis Barkauskas¹

¹ Institute of Chemistry, Faculty of Chemistry and Geosciences, Vilnius University, Lithuania

² Department of Nanoengineering, Center for Physical Sciences and Technology, Lithuania
ruta.aukstakojyte@chgf.vu.lt

Dopamine (DA) is one of the most important neurotransmitters in the human body, playing a crucial role in motor control, reward and motivation functions, as well as the central nervous and immune systems. Abnormal levels of DA may potentially lead to several neurological diseases such as schizophrenia, depression, attention deficit hyperactivity disorder (ADHD), Parkinson's and Alzheimer's diseases [1]. Therefore, there is an urgent need to develop new platforms for the precise and sensitive determination of DA concentrations in the human body.

In recent years, electrochemical methods have been considered as an efficient tool for DA detection because of their simplicity, cost-effectiveness, fast response time, and reproducibility. Graphene-based derivatives such as graphene oxide (GO) and reduced graphene oxide (rGO) have drawn increasing attention as electrode materials in the development of electrochemical sensors due to the time-efficient and non-expensive synthesis procedure as well as unique chemical, physical, and electronic characteristics. rGO-based materials exhibit a high surface area, chemical stability, electrical conductivity, and the ability to immobilize a variety of different molecules [2]. However, despite these advantages, the development of rGO-based sensors with high sensitivity and rapid response time is still challenging. Therefore, doping with heteroatoms could be a key strategy to tailor structural and electrochemical properties of rGO because the doping process can enhance the charge carrier density, wettability, sensitivity, create new electrocatalytically active sites, and ensure a fast electrochemical response for accurate and sensitive DA detection [2,3].

The aim of this study was to synthesize N-doped reduced graphene oxide (N-rGO) samples and investigate their electrochemical performance in the detection of DA. GO has been prepared using a modified Hummers' method, including the pre-oxidation of natural graphite powder by the mixture of $K_2S_2O_8/P_2O_5/H_2SO_4$ [4]. N-rGO samples have been synthesized by a facile and one-pot hydrothermal treatment of GO in the presence of the organic dye "Bismarck Brown Y" (BB), which has been used as a N source for the rGO modification for the first time. Obtained samples (rGO, rGO_BB20, and rGO_BB50) have been characterized by Brunauer-Emmett-Teller (BET) analysis, scanning electron microscopy (SEM), X-ray photoelectron (XPS), and Raman scattering spectroscopies. The electrical behavior of the prepared materials has also been determined by estimating the dependence between electrical conductivity and bulk density. Electrochemical measurements, including cyclic voltammetry (CV) and chronoamperometry (CA), have been performed to analyse the sensitivity of N-rGO samples toward DA detection. Interference studies have also been carried out to investigate the selectivity of N-rGO samples.

The results of the XPS analysis show that rGO_BB20 and rGO_BB50 consist of 5.3 and 14.2 at% of nitrogen, respectively, indicating a successful rGO modification with N atoms. From the N1s XPS spectra it has been observed that in the rGO_BB20 sample nitrogen occurs mostly in the form of the pyridinic groups (45.0 at%), whereas in the rGO_BB50 sample the pyridinic (40.7 at%) as well as amine groups (35.7 at%) are dominant. I_D/I_G values determined from Raman spectra confirm the increase of structural disorders after the use of the BB additive. The BET analysis shows that the specific surface area decreases with the higher amount of BB used in the hydrothermal synthesis. Electrical conductivity measurements demonstrate that rGO and rGO_BB20 exhibit similar electrical conductivity values, while rGO_BB50 has much lower. From the SEM images, it is found that modification with N atoms leads to corrugation of rGO layers. The CV studies reveal that the rGO_BB20 and rGO_BB50 samples exhibit prospective electrocatalytic activity toward the DA redox peak. The CA studies show that the proposed sensor based on rGO_BB20 demonstrates a relatively high sensitivity of $0.46 \mu A \mu M^{-1} cm^{-2}$ and a low limit of detection (11 nM). Interference analysis in the presence of other electroactive materials such as uric acid, ascorbic acid, citric acid, and H_2O_2 shows the electrochemical response only for dopamine using the rGO_BB20-based electrode, suggesting that it is a promising electrode material for the sensitive and selective determination of DA.

ACKNOWLEDGMENTS. This project has received funding from European Social Fund (project No 09.3.3-LMT-K-712-19-0050) under grant agreement with the Research Council of Lithuania (LMTLT).

[1] R. Franco, I. Reyes-Resina, G. Navarro, Dopamine in health and disease: much more than a neurotransmitter, *Biomedicines* **9**, 109 (2021).

[2] J. Gaidukevic, R. Aukstakojyte, J. Barkauskas, G. Niaura, T. Murauskas, R. Pauliukaite, A novel approach to prepare highly oxidized graphene oxide: structural and electrochemical investigations, *Applied Surface Science* **592**, 153257 (2022).

[3] H. Zhang, S. Liu, Electrochemical sensors based on nitrogen-doped reduced graphene oxide for the simultaneous detection of ascorbic acid, dopamine and uric acid, *Journal of Alloys and Compounds* **842**, 155873 (2020).

[4] X. Yan, J. Chen, J. Yang, Q. Xue, P. Miele, *ACS Appl. Mater. Interfaces*, **2** (2010) 2521–2529.

INVESTIGATION OF THE DEPENDENCE OF LASER PULSE ENERGY ON THE STABILITY OF GOLD, SILVER AND HYBRID NANOPARTICLES GENERATED FROM THIN FILM TARGETS

Vita Petrikaitė¹, Evaldas Stankevičius^{1*}

¹ Department of Laser Technologies, Center for Physical Sciences and Technology, Vilnius, Lithuania
vita.petrikaite@ftmc.lt

The noble metals gold and silver have gained popularity in nanotechnology due to their broad absorption band in the electromagnetic spectrum and the effect known as localized surface plasmon resonance (LSPR), which determines the optical properties of these metal nanoparticles [1]. They have applications in a wide range of technologies, in the electronics industry, medicine, pharmaceuticals, catalysis, optics, spectroscopy, food industry, etc. [2]. Combining gold and silver into a single material - hybrid nanoparticles - could lead to synergistic effects between the two metals and new technological applications. The generation of clean nanoparticles requires suitable nanoparticle starting materials, which must be completely ligand-free to avoid cross-contamination. Nanoparticles produced by pulsed laser ablation in liquid are well suited to these requirements, this process does not require chemical reagents, stabilizers, or additional ligands and therefore avoids the surface contamination of nanoparticles inherent in chemically prepared analogs [3]. Also it is a confirmed method for the generation of hybrid Au-Ag nanoparticles with a homogeneous distribution of elements on a single-particle scale [4]. However, maintaining nanoparticle stability is a difficulty. A good colloidal solution must be stable. The stability of a colloidal system depends on the interaction forces between formed particles. Particles that are not stabilized can aggregate, thereby hindering their further use.

Therefore, this study focused on the stability and how it was affected by the different laser pulse energies (50 μJ to 300 μJ) used. Additionally, thin film evaporation was used to produce hybrid Au-Ag targets (100 nm). Using this method, it was possible to analyze how hybrid nanoparticles are affected when they are made from films with different metal ratios and their order. The nanoparticles were produced in deionized water without the addition of stabilizers. Monometallic and hybrid nanoparticles generated from thin films at laser pulse energies of 50, 150 and 250 μJ are shown in Figure 1. An identical production process was carried out on bulk samples and the characteristics of the colloidal solutions were compared using a spectrophotometer, TEM images, photographs and spectra measurements over a period of 5 weeks. During these weeks, it has become clear that the thin-film approach can produce more stable colloidal solutions, nanoparticles of smaller size and dispersion, and can compare favorably with solutions obtained from a bulk target, as well as what is the most advantageous ratio of metals to form nanoparticles for long-term stability and what pulse energy should be applied.

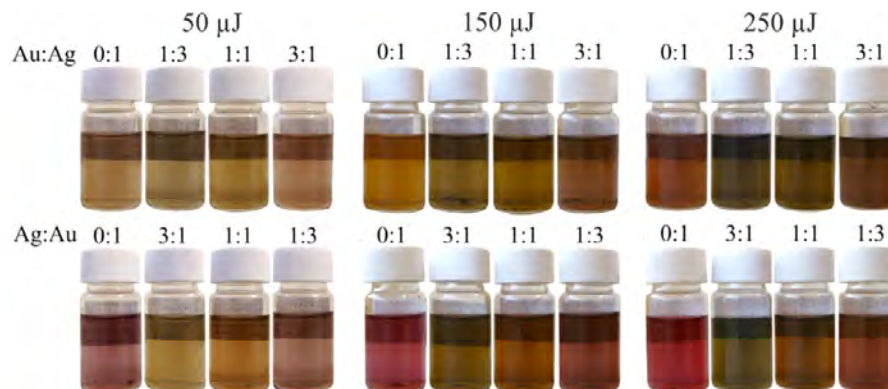


Fig. 1. Photographs of colloidal solutions generated from thin film layers using different laser pulse energies (50 μJ , 150 μJ , 250 μJ). The order of the films is indicated on the left and the ratio of metals above the vials.

[1] E. Petryayeva, U.J. Krull, Localized surface plasmon resonance: Nanostructures, bioassays and biosensing—A review, *Analytica chimica acta*, **706**, 8-24 (2011).

[2] E. Stankevičius, M. Garliauskas, L. Laurinavičius, R. Trusovas, N. Tarasenko, R. Pauliukaitė, Engineering electrochemical sensors using nanosecond laser treatment of thin gold film on ITO glass, *Electrochimica Acta*, **297**, 511-522 (2019).

[3] S. Barcikowski, G. Compagnini, Advanced nanoparticle generation and excitation by lasers in liquids, *Phys. Chem. Chem. Phys.*, **15**, 3022-3026 (2013).

[4] S. Besner, M. Meunier, Femtosecond laser synthesis of AuAg nanoalloys: photoinduced oxidation and ions release, *J. Phys. Chem. C*, **114**, 10403-10409 (2010).

ENHANCED BIOIMAGING PROPERTIES OF NANOSIZED FLUOROAPATITE COMPOSITES, DOPED WITH EUROPIUM(III) IONS VIA INCORPORATION OF RUBIDIUM(I) IONS

Nicole Nowak^{1,2*}, Dominika Czekanowska¹, Tomasz Gebarowski², Rafal J. Wiglusz¹

¹ Institute of Low Temperature and Structure Research, Polish Academy of Sciences, Okolna 2, PL-50-422 Wroclaw, Poland

² Department of Animal Biostructure and Physiology, Wroclaw University of Environmental and Life Sciences, Norwida 25, PL-50-375 Wroclaw, Poland

n.nowak@intibs.pl

Europium is the rarest element among the lanthanides and yet the most reactive one. Europium element has two different oxidation states +2 and +3 with the electronic configuration [Xe]4f⁶ and [Xe]4f⁷, respectively. It is easier to obtain inorganic materials doped with europium with +3 oxidation state than with the oxidation state +2, which relates to reductive synthesis conditions. Despite the high reactivity of europium element, it has also interesting luminescence properties. The Eu³⁺ ions emit strong red-orange visible light exciting in the UV range of energy for the electromagnetic spectrum. [1]. Therefore, this ion can be used as a sensitive luminescence probe. Moreover, many studies confirmed the highly biocompatible properties of inorganic composites based on calcium phosphate compounds doped with Eu³⁺ ions [2].

Synthetic apatites are widely used in biomedical field, as a bone or teeth fillers, due to their highly developed specific surface and ability to develop stable bond with living tissues. Fluorapatites have particular advantage over hydroxyapatites via their structural stability and more resistant for demineralization process that occurs in the bone tissue. Hence, fluorapatites can be more suitable substitution for hydroxyapatite in biomedical uses [3].

Rubidium as a trace element can occur in the low concentration in human teeth. However, it seems to have valuable biological features. Interestingly, many studies confirmed biocompatibility of Rb⁺ ions and their positive effect on osteo- and chondrogenesis. Moreover, by its similarity to lithium ions it also exhibits antidepressant properties [4].

Our research team developed highly stable two series of fluorapatite compounds co-doped with Eu³⁺ ions and various concentration of Rb⁺ ions (1, 3, 5, 7 mol%). Structure and morphology were investigated via X-ray powder diffraction technique (XRPD), infrared spectroscopy (FT-IR) and transmission electron microscopy (TEM). Luminescence properties were evaluated by measuring emission and excitation spectra but also by luminescence kinetics. Finally, to evaluate biological properties obtained nanomaterials were tested toward NHDF. Additionally, immune response was evaluated by testing materials toward THP-1 macrophage cell line.

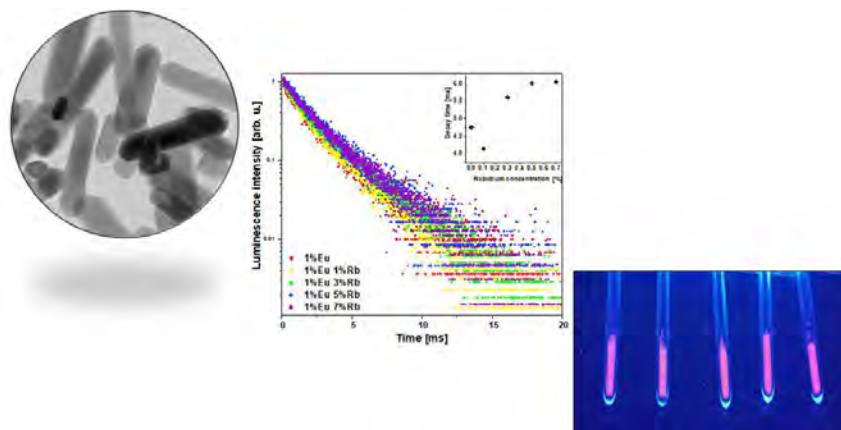


Fig. 1. TEM and life time and image of obtained fluoroapatite based compounds co-doped with Eu³⁺ and Rb⁺ ions.

- [1] Binnemans, K. (2015). Interpretation of europium(III) spectra. *Coordination Chemistry Reviews*, 295, 1–45.
- [2] K. Melcher, L.-M. Ng, E. Zhou et al., A gate-latch-lock mechanism for hormone signaling by abscisic acid receptors, *Nature* **462**, 602–608 (1990).
- Di, W., Li, J., Shirahata, N., Sakka, Y., Willinger, M. G., & Pinna, N. (2011). Photoluminescence, cytotoxicity and in vitro imaging of hexagonal terbium phosphate nanoparticles doped with europium. *Nanoscale*, 3(3), 1263–1269.
- [3] Abou Neel EA; Aljabo A; Strange A; Ibrahim S; Coathup M; Young AM; Bozec L; Mudera V. Demineralization-Remineralization Dynamics in Teeth and Bone. *Int J Nanomedicine* **2016**, 11, 4735–4741
- [4] Nowak, N., Czekanowska, D., Reeks, J. M., & Wiglusz, R. J. (2022). Structural, Spectroscopic, and Biological Characterization of Novel Rubidium(I) and Europium(III) Co-Doped Nano-Hydroxyapatite Materials and Their Potential Use in Regenerative Medicine. *Nanomaterials*, 12(24), 4475.

PROBING METHYL GROUP TUNNELING IN $[(\text{CH}_3)_2\text{NH}_2][\text{Zn}(\text{HCOO})_3]$ HYBRID PEROVSKITE USING Co^{2+} EPR

Gediminas Usevičius¹, Ignas Pocius¹, Vidmantas Kalendra¹, Mirosław Mączka², Jūras Banys¹, Mantas Šimėnas¹

¹ Faculty of Physics, Vilnius University, Sauletekio 3, 10257 Vilnius, Lithuania

² Institute of Low Temperature and Structure Research, Polish Academy of Sciences, Okólna 2, 50-422 Wrocław, Poland
gediminas.usevicius@ff.vu.lt

At high temperature, methyl group exhibits classical reorientation dynamics around its symmetry axis, while at lower temperatures, it acts as a quantum rotor exhibiting rotational quantum tunneling, which is highly sensitive to a local methyl group environment (Fig. 1a). Recently, we observed this effect using pulsed electron paramagnetic resonance (EPR) in two dimethylammonium containing hybrid perovskites doped with paramagnetic Mn^{2+} ions [1].

In this work, we investigate the feasibility of using a fast-relaxing Co^{2+} paramagnetic center to study the methyl group tunneling in dimethylammonium zinc formate $[(\text{CH}_3)_2\text{NH}_2][\text{Zn}(\text{HCOO})_3]$ (Fig. 1b) hybrid perovskite using a multifrequency EPR experiments. Our pulsed EPR experiments reveal magnetic field independent electron spin echo envelope modulation (ESEEM) signals, which are assigned to the methyl group tunneling. The extracted tunnel frequency of 1.84 MHz from the experimental data is used in density operator simulations, which allows us to calculate the rotational barrier of the methyl groups. The comparison of these results [2] with the previously reported Mn^{2+} [1] case shows that our approach can detect very small changes in the local methyl group environment opening pathway for a new spectroscopic tool.

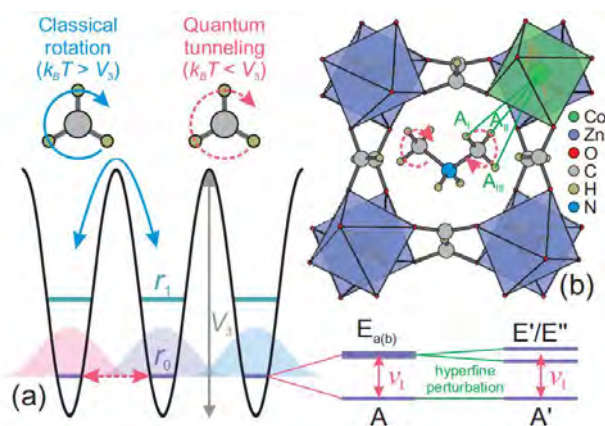


Fig. 1. (a) Schematic energy level diagram of a methyl group rotor with rotational barrier V_3 . At lower temperatures, the group acts as a hindered quantum rotor enabled by the wave-function overlap, which also splits the ro-librational levels by the tunnel splitting ν_t . (b) Low-temperature structure of DMAZn:Co. The hyperfine interactions between the paramagnetic Co^{2+} ion and protons of the nearest methyl group are indicated by green lines.

[1] M. Šimėnas, et al., Magnetic excitation and readout of methyl group tunnel coherence. *Sci. Adv.* 2020, 6, eaba1517.

[2] G. Usevičius, et al. Probing Methyl Group Tunneling in $[(\text{CH}_3)_2\text{NH}_2][\text{Zn}(\text{HCOO})_3]$ Hybrid Perovskite Using Co^{2+} EPR. *Molecules* 2023 28, 979.

INVESTIGATION OF TES-ADT BASED NIR-TO-VIS PHOTON UPCONVERSION SYSTEM

Justas Lekavičius¹, Edvinas Radiunas¹, Karolis Kazlauskas¹

¹Institute of Photonics and Nanotechnology, Faculty of Physics, Vilnius University, Lithuania
justas.lekavicius@ff.stud.vu.lt

Triplet-triplet annihilation based NIR-to-visible photon upconversion (TTA-UC) is a photophysical process used to generate visible photons from low power density incoherent NIR excitation [1]. Due to forementioned qualities, UC could become handy in various practical applications such as harvesting sub-bandgap photons in photovoltaic devices, using UC materials in night vision equipment, photopolymerization and other fields of science and technology [1-3]. Typically, TTA-UC systems are composed of two types of molecular species: sensitizer and emitter. The first one is used for NIR light absorption and triplet generation, whereas emitter is responsible for triplet-triplet annihilation (TTA) and visible light emission. Rubrene molecule is the most popular emitter option in the field, yet due to aggregation it shows poor performance in solid-state [2]. Modified antrathiophene (TES-ADT) could become a suitable replacement for rubrene and other widely used emitters, due to promising solid-state performance [3] and low triplet state energy. Therefore its photophysical properties in various UC systems should be thoroughly studied.

The aim of this research is to investigate liquid TES-ADT based TTA-UC system. To obtain UC the TES-ADT emitter is coupled with palladium phthalocyanine (PdPc) sensitizer. Experimentally, a series of 8 UC samples with constant sensitizer and varying emitter concentration (1 – 200 mM) was made to determine the optimal TES-ADT concentration for the best TTA-UC performance. The performance was evaluated by measuring UC quantum yield (Φ_{UC}) using integrating sphere and comparative methods. The results (see Fig. 2) show that 20 mM emitter solution yields the highest value of around $\Phi_{UC} = (7,7 \pm 2,7)\%$ (Fig. 1-2). Moreover, it is shown that lower emitter concentrations result in poor triplet energy transfer, whereas higher than optimal amount of TES-ADT evoke aggregation indicated by the drop of the fluorescence quantum yield from 100% to 11%. High Φ_{UC} values obtained, motivate further research and possible applications in solid-state.

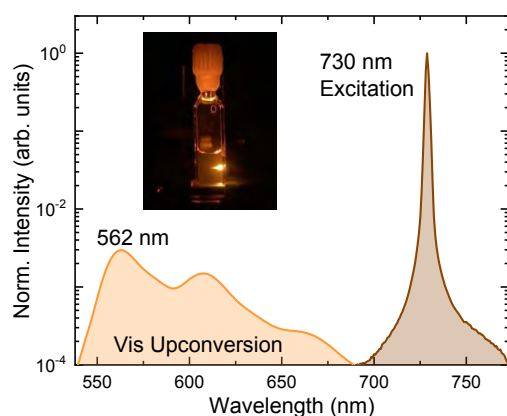


Fig. 1. UC spectrum in Vis region of TES-ADT:PdPc (10 mM:15 μ M) solution under 730 nm CW excitation.

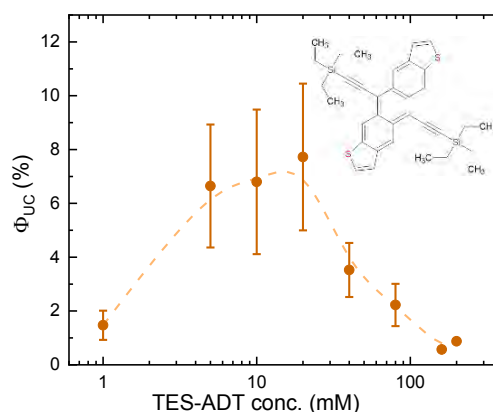


Fig. 2. UC quantum yield of samples with constant PdPc concentration (15 μ M) and variable emitter concentration in toluene.

[1] Murakami, I., Kamada, K., Kinetics of photon upconversion by triplet-triplet annihilation: a comprehensive tutorial. *Phys. Chem. Chem. Phys.* 23, 18268-18282 (2021).

[2] Radiunas, E. et al., Impact of t-butyl substitution in a rubrene emitter for solid state NIR-to-visible photon upconversion. *Phys. Chem. Chem. Phys.* 22, 7392-7403 (2020).

[3] Nishimura, N. et al., Photon upconversion utilizing energy beyond the band gap of crystalline silicon with a hybrid TES-ADT/PbS quantum dots system. *Chem. Sci.* 10, 4750 (2019).

MICROSCOPIC ANALYSIS OF MAGNETISATION PROCESSES USING THE ISING MODEL

Jorūnas Dobilas^{1,2}

¹Faculty of Physics, Vilnius University, Lithuania

²Department of Functional Materials and Electronics, State Research Institute Center for Physical Sciences and Technology, Lithuania

jorunas.dobilas@ff.stud.vu.lt

In many different fields of science, analysis of physical problems using analytical mathematical models can be difficult. Inclusion of every single possible interaction causes mathematical equations to become too complicated, even for the best supercomputers to this day. In spintronics, effects such as magnetoresistance (MR) heavily depend not only on the selection of materials, but also on the magnetisation process [1][2], latter of which can be quite difficult to grasp even utilizing quantum mechanics. To simplify the problem, one way to analyse microscopic magnetisation processes is by using the Ising model [3], where an arbitrary volume is divided into some number of unit cells that have quantized spin (in the most common case, having spin $1/2$ or $-1/2$). These cells then interact with neighbouring cells and depending on the exchange coupling constant, cells either try to orient their spin in one direction or in opposite directions. Such model is usually solved using Monte Carlo methods, where the probability for a cell to change its spin value can be calculated using Boltzmann statistics. With this model one can analyse phase transition and magnetic hysteresis dynamically. The Ising model is also an approximation of the classical Heisenberg model and only one spin projection is considered.

In this work, some common examples are analysed, such as defects in ferromagnets and artificial antiferromagnet configuration using the Ising model (Fig. 1). By changing exchange coupling, interacting neighbour count, volume size and adding macroscopic effects, such as demagnetizing field or anisotropy, changes in phase diagrams and magnetic hystereses are explored.

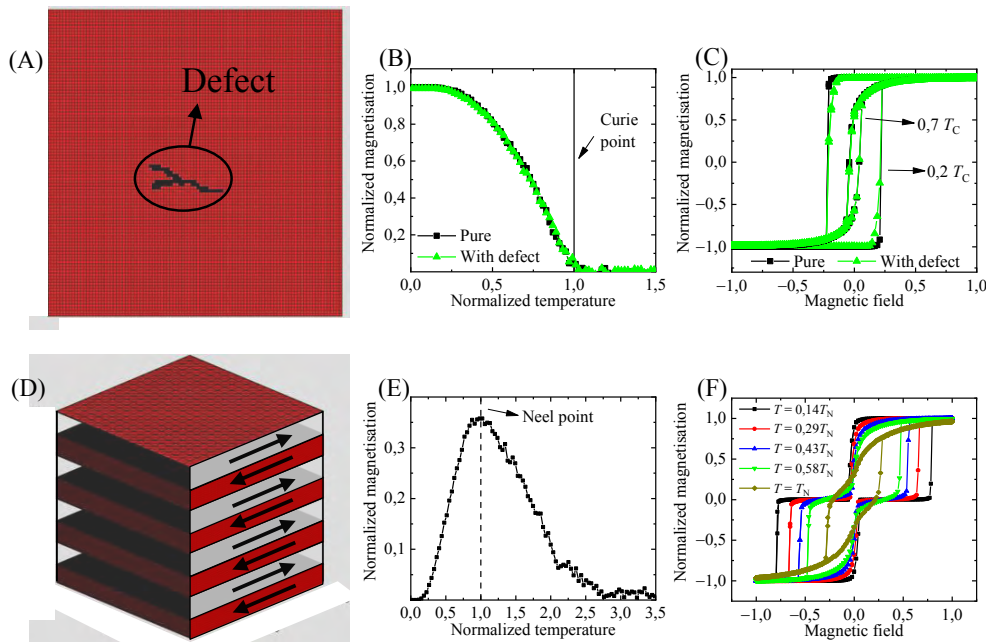


Fig. 1. Ising models for different kinds of magnetic structures. (A) – Ferromagnet with non-magnetic defect (crack). (B) – Normalized magnetisation vs temperature, normalized by Curie temperature, with and without the defect. (C) – Magnetic hystereses with and without the defect at two different temperatures (T_C – Curie temperature). (D) – Alternating magnetisation structure (artificial antiferromagnet), where red layers have 3 times stronger interaction than grey and both layers have antiferromagnetic coupling. (E) – Normalized magnetisation vs temperature, normalized by Neel point temperature. (F) – Magnetic hystereses at different temperatures (T_N – Neel temperature).

[1] Ramirez, A. P. (1997). Colossal magnetoresistance. *Journal of Physics: Condensed Matter*, 9(39), 8171.

[2] Xiao, J. Q., Jiang, J. S., & Chien, C. L. (1992). Giant magnetoresistance in nonmultilayer magnetic systems. *Physical Review Letters*, 68(25), 3749.

[3] Singh, S. (2020). *The Ising Model: Brief Introduction and Its Application*. *Solid State Physics* [Working Title].

MODELLING GLIBENCLAMIDE IN AQUEOUS MIXTURES OF BIOACTIVE IONIC LIQUIDS

Žynginta Einorytė¹, Vytautas Klimavičius¹, Kęstutis Aidas¹

¹ Institute of Chemical Physics, Faculty of Physics, Vilnius University, Lithuania
zynginta.einoryte@ff.vu.lt

Glibenclamide, also known as glyburide, is a sulphonyl urea drug used to treat type 2 diabetes. New ways to use this compound for inhibiting headaches or various inflammations are also being found [1]. Unfortunately, glibenclamide is poorly soluble in water (15-24 $\mu\text{g/mL}$) [2] which makes it harder to find new pharmaceutical applications. To improve solubility of glibenclamide, a biological choline-tryptophanate ionic liquid was added to water, increasing glibenclamide's solubility to 27 mg/mL – by 130-600 times compared to the solubility in pure water [3].

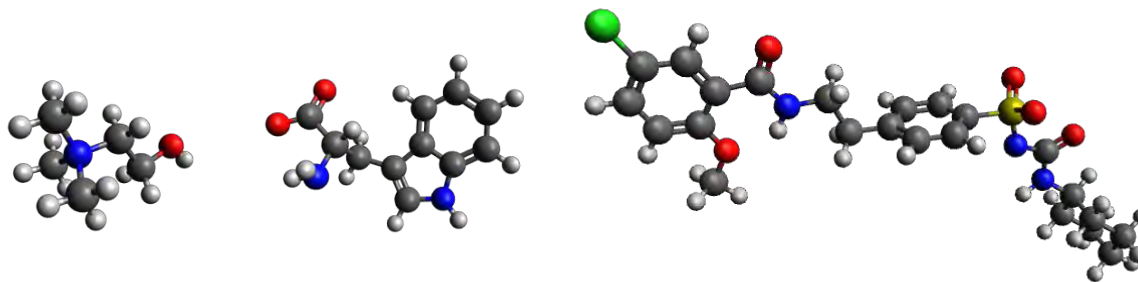


Fig. 1. Optimised structures of choline, tryptophanate and glibenclamide ions.

The main goal of this study was to find out what intermolecular interactions result in the increase of glibenclamide's solubility in aqueous mixtures with ionic liquid by using molecular dynamics (MD) simulations and quantum mechanics/molecular mechanics (QM/MM) methods. One of the main tools for studying intermolecular interactions is nuclear magnetic resonance (NMR) spectroscopy as ¹H NMR chemical shifts depend on the surroundings of the molecule. The NMR parameters of two systems: glibenclamide in aqueous solution (Glb_{aq}) and in ionic liquid mixture with water (Glb_{IL/}aq), as well as additional structural parameters, were computed and investigated. NMR experiments for these systems were also done.

By analysing the dihedral angles between glibenclamide atoms, it was found that there are no significant changes between the conformations of glibenclamide in Glb_{aq} and Glb_{IL/}aq systems. The calculated coordination numbers between the glibenclamide and solvent atoms and the shift of glibenclamide's magnetic shielding constants let us conclude that the increase of solubility of glibenclamide in ionic liquid mixtures with water is impacted by intermolecular interactions between choline and tryptophanate ions and the amide groups, aromatic rings and cyclohexane cycle of glibenclamide.

Acknowledgements: Computations were performed on resources provided by the High Performance Computing Center North (HPC2N) at Umeå University, Sweden and High Performance Computing Center “HPC Saulėtekis” at Vilnius University, Lithuania.

[1] M. Al, M. Al-Karaghali, M. Sode, A. Gozalov, and M. Ashina, The vascular effect of glibenclamide: A systematic review, <https://doi.org/10.1177/2515816319884937>, 2019, 2, 1–13.

[2] A. A. Elkordy, A. Jatto, and E. Essa, In situ controlled crystallization as a tool to improve the dissolution of glibenclamide, *International Journal of Pharmaceutics*, 2012, 428, 118–120.

[3] M. A. Alawi, I. I. Hamdan, A. A. Sallam, and N. A. Heshmeh, Solubility enhancement of glibenclamide in choline-tryptophan ionic liquid: Preparation, characterization and mechanism of solubilization, *Journal of Molecular Liquids*, 2015, 212, 629–634.

SYNTHESIS OF AROMATIC *N*-OXIDES AND EPOXIDES BY BIOCATALYTIC METHODS

Greta Mačiūitytė^{1,2}, Vytautas Petkevičius¹

¹Department of Molecular Microbiology and Biotechnology, Institute of Biochemistry, Life Sciences Center, Vilnius University, Lithuania

²Faculty of Chemistry and Geosciences, Vilnius University, Lithuania
greta.maciuityte@chgf.stud.vu.lt

Oxygenation reactions are widely used in industry, however, organic chemistry methods usually require metal catalysts or peroxides. Therefore, more environmentally friendly methods are needed, and as a result, more attention is shifting to the enzymes that catalyse such reactions - various oxygenases. Non-heme diiron monooxygenase PmlABCDEf possesses a broad substrate specificity and can oxidize different chemical groups, including ring heteroatoms and C=C double bonds [1].

N-oxides can be applied in the agriculture, and pharmacy industries. They have increased reactivity compared to regular *N*-heteroaromatic compounds [2]. Oxiranes, also known as epoxides, are important intermediates in organic chemistry and they bear the capacity of wide-ranging ring-opening reactions, which usually occur with predictable regioselectivity and stereospecificity [3]. However, it is a challenging task to selectively oxidize chemical groups of different reactivity (e. g. *N*-oxidation versus epoxidation) in a single molecule, therefore diverse synthesis strategies are employed with multiple reaction steps [4].

In this work, we investigated the selectivity of PmlABCDEf monooxygenase with substrates bearing two possible reaction sites – terminal C=C double bond and nitrogen atom in the pyridine ring. Hence, alkenyl-substituted pyridine compounds having different lengths of carbon chains were synthesized from 3-pyridinol and appropriate alkenyl bromides. Produced compounds were used in the bioconversion reactions with *Pseudomonas putida* KT2440 producing recombinant PmlABCDEf monooxygenase. Reaction products were identified as *N*-oxides and epoxides (the reaction scheme is shown in Fig. 1). The efficiency of the conversion as well as the ratio of different oxidation products depended on the length of the alkenyl chain.

The reaction products were extracted and purified using column chromatography on a silica gel. The obtained compounds were analysed with nuclear magnetic resonance (NMR), thin-layer chromatography (TLC), and high-performance liquid chromatography – mass spectrometry (HPLC-MS).

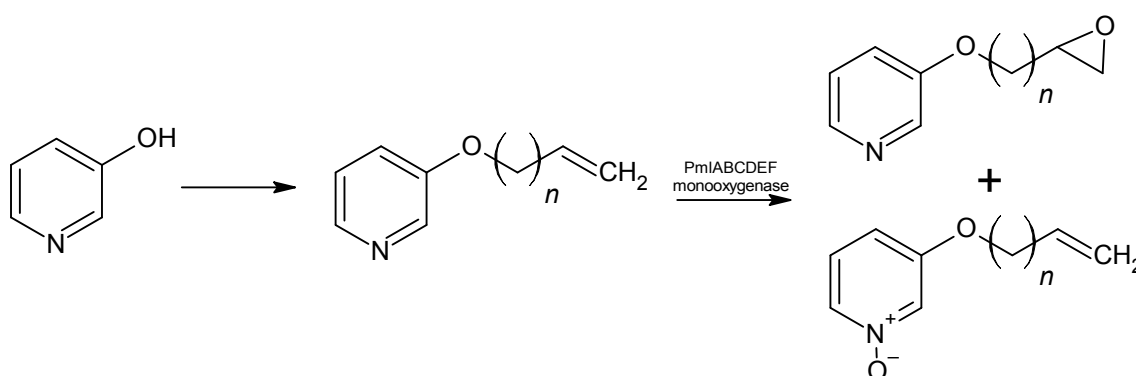


Fig. 1. Substrate synthesis and conversion to oxiranes and *N*-oxides. *n* is 1 – 6

- [1] Petkevičius, V. *et al.* The versatility of non-heme diiron monooxygenase PmlABCDEf: a single biocatalyst for a plethora of oxygenation reactions. *Catal Sci Technol* **12**, 7293–7307 (2022).
- [2] Petkevičius, V., Vaitekūnas, J., Gasparavičiūtė, R., Tauraitė, D. & Meškys, R. An efficient and regioselective biocatalytic synthesis of aromatic *N*-oxides by using a soluble di-iron monooxygenase PmlABCDEf produced in the *Pseudomonas* species. *Microb Biotechnol* **14**, 1771–1783 (2021).
- [3] Hodgson, D. M., Stent, M. A. H., Reilly, M. K. & Gras, E. Oxiranes and Oxirenes: Fused-ring Derivatives. in *Reference Module in Chemistry, Molecular Sciences and Chemical Engineering* (Elsevier, 2014). doi:10.1016/B978-0-12-409547-2.11428-3.
- [4] Kocak, A., Kurbanli, S., & Malkondu S. Synthetic Access to New Pyridone Derivatives through the Alkylation Reactions of Hydroxypyridines with Epoxides, *Synthetic Communications*, 37:21, 3697-3708, (2007).

INSIGHTS INTO THE EFFECT OF BORON DOPING ON THE LUMINESCENCE PROPERTIES OF NOVEL Lu/Gd AND Al/Sc BASED GARNETS FOR SCINTILATION APPLICATION

Greta Inkrataitė¹, Jan-Niklas Keil², Thomas Jüstel², Ramūnas Skaudžius¹

¹ Institute of Chemistry, Faculty of Chemistry and Geosciences, Vilnius University, Vilnius, Lithuania

² Department of Chemical Engineering, Münster University of Applied Sciences, Steinfurt, Germany
greta.inkrataite@chgf.vu.lt

In order to convert high-energy radiation, such as gamma or X-rays, into visible light, special converter materials are needed. Such compounds are usually referred to as scintillators. Over the years many different candidates to fit the requirements were examined. However, compounds with garnet structures have attracted a particularly large amount of attention. Cerium or praseodymium doped lutetium and gadolinium aluminum garnets have high density, high thermal stability, rather efficient luminescence processes, and thus high quantum efficiency which are needed for a good scintillator [1]. However, further optimization and improvement are still required especially w.r.t. a reduced decay time. The duration of the luminescence decay is important because if it is very short then the more signals can be measured within a defined timeframe, resulting in a better resolved and higher quality image, for example in CT devices. One way to improve materials properties is to doping the aforementioned compounds with different elements. As such, by doping we could potentially be able to improve key aforementioned parameters: emission intensity, quantum efficiency and decay times [2,3]. One of these elements is boron. Primarily, it can be used as a flux, and also B^{3+} ion has a suitable neutron capture cross section and can also help absorb gamma radiation [4]. However, garnets can be doped with larger amounts of other elements. In this case, we replaced some of the aluminium with scandium. Lutetium aluminium scandium garnets and gadolinium aluminium scandium garnets doped with Ce^{3+} / Pr^{3+} / B^{3+} were obtained as a result. These garnets are synthesized and studied for the first time.

In the present work, the effect of boron and scandium co-doping on the various characteristic of the LuAG and GAG doped by cerium and praseodymium is investigated. Garnets doped with different amounts of boron and scandium were synthesized by the aqueous sol-gel method. The phase purity of the samples was analyzed by means of X-ray diffraction. The morphology of the compounds was evaluated by using scanning electron microscopy. Photoluminescence properties such as emission and excitation spectra, decay curves, quantum efficiency and temperature dependency of the emission and excitation spectra have been investigated. Radioluminescence was also measured in order to determine the scintillation properties of the samples (Fig.1.). The positive impact of boron addition into the garnet structure on the luminescence properties will be discussed in detail.

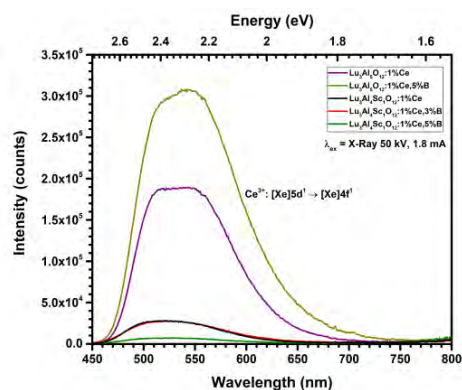


Fig. 1. X-Rays excited emission spectra of 1% cerium and different amounts of boron doped $Lu_3Al_5O_{12}$ and $Lu_3Al_4Sc_1O_{12}$.

ACKNOWLEDGEMENTS:

This research is funded by German Academic Exchange Service (DAAD) scholarship.

- [1] I.P. Machado, V.C. Teixeira, C.C.S. Pedrosa, et. al., X-ray scintillator $Gd_2O_3:Tb^{3+}$ materials obtained by a rapid and cost-effective microwave-assisted solid-state synthesis, *Journal of Alloys and Compounds* **777**, 638 – 645 (2019).
[2] C. Foster, Y. Wu, M. Koschan, et. al., Boron Codoping of Czochralski Grown Lutetium Aluminum Garnet and the Effect on Scintillation Properties, *Journal of Crystal Growth* **486**, 126 – 129 (2018).
[3] D. S. McGregor, Materials for Gamma-Ray Spectrometers: Inorganic Scintillators, *Annual Review of Materials Research* **48**, 254-277 (2018).
[4] G. Inkrataite, M. Kemere, A. Sarakovskis, R. Skaudžius, Influence of boron on the essential properties for new generation scintillators, *Journal of Alloys and Compounds* **875**, 160002 (2021).

ADSORPTION MECHANISM OF METHYLENE BLUE DYE ON POLYMER CLAY NANOCOMPOSITE

Yao Mawuena Tsekpo¹, Augustine Nana Sekyi Appiah², Lucas Nana Wiredu Damoah³, Daniel Amusah³ and Ebenezer Annan³

¹ Faculty of Mechanical Engineering, Silesian University of Technology, Poland

² Laboratory of Materials Research, Faculty of Mechanical Engineering, Silesian University of Technology, Poland

³ Department of Material Science and Engineering, University of Ghana, Ghana
yao.tsekpo@polsl.pl

Dyes are essential chemicals needed in the textile, tanning and printing industries. However, the treatment of dye effluents has been problematic, making it a leading contaminant in wastewater. Many solutions are being proposed and studied for the remediation of dyes, including filtration, ion exchange, coagulation, biological treatment, adsorption and photocatalyst. Adsorption via nanomaterials has been extensively explored for dye removal; however, they still have some drawbacks. The difficulty of collecting them after the adsorption process is notable due to their size.

In this work, the sacrificial template technique was used to prepare a polymer clay nanocomposite to understand the adsorption mechanism of methylene blue dye onto the fabricated composite. The composite was prepared from polydimethylsiloxane (PDMS), nano clay particles (< 50 nm) and magnetite nanoparticles. The PDMS and nano clay were obtained from Sigma Aldrich, whereas the magnetite nanoparticles were synthesised using a green approach. Three samples were used for this study: a control sample with only PDMS; a sample with PDMS and nanoclay (called PB); and a sample with PDMS, nano clay and magnetite nanoparticles (called PBNP). The adsorption test was run by preparing a standard methylene blue dye solution at a concentration of 5 mg/L to mimic the contaminant and expose the adsorbent to it for 5 hours. At the end of the period, the data collected was modelled using the pseudo-first-order, pseudo-second-order, intra-particle diffusion and Boyd kinetic models to understand the kinetics of the process adsorption process. The isothermal behaviour was understood by the Elovich, Harkins-Jura and Dubinin-Radushkevich models.

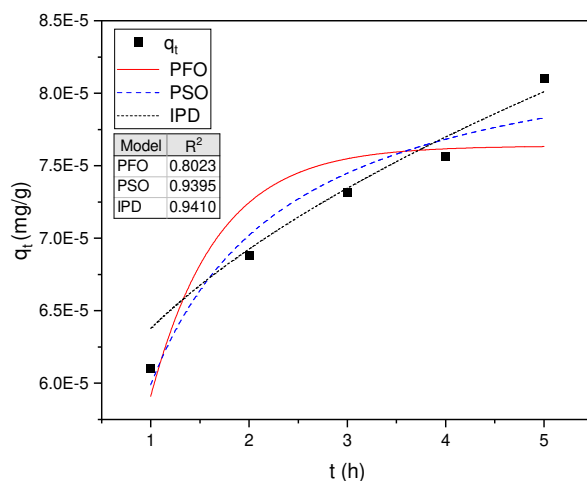


Fig. 1. Kinetic Model description for PBNP adsorbent.

The findings of the study revealed that homogenous dispersion of the nano phase was achieved in the polymer matrix. However, the heterogeneity of the adsorbent's surface influenced the adsorption process. The result from the isothermal modelling revealed the adsorption process for PB and PBNP both fit the Elovich. This is evidence of multilayer formation on the adsorbents surface influenced by chemical reaction. The exponential increase adsorption postulated in this model can be attributed to the varying surface energies caused by the heterogeneity. The kinetic models also go to support his chemical adsorption process with PBNP fit both pseudo second order model and intra-particle diffusion model This points to multi process adsorption as a result of presence of the magnetite and clay nanoparticles and causing surface heterogeneities. The data from the PB sample indicated that the kinetic process indicated a process governed by intra-particle diffusion.

It is seen that the adsorption of methylene blue dye onto the surface of the polymer clay nanocomposite involves varied interactions due to the complexity of the material's surface.

TYROSINE KINASE INHIBITORS COMBINED WITH NANOHYDROXYAPATITE FOR TARGETED THERAPIES - PHYSICOCHEMICAL AND IN VITRO STUDIES

Paulina Sobierajska^{1*}, Anna Serwotka-Suszczak², Sara Targonska¹, Damian Szymanski¹,
Krzysztof Marycz² and Rafal J. Wiglusz¹

¹ Institute of Low Temperature and Structure Research, Polish Academy of Sciences, Okolna 2, 50-422 Wrocław, Poland

² Department of Experimental Biology, Wrocław University of Environmental and Life Sciences, Norwida 27B Street, A7 Building, 50-375 Wrocław, Poland
p.sobierajska@intibs.pl

A promising approach to enhance the effectiveness of anticancer drugs related to reducing their side effects could be an use of nanoparticles for the controlled drug transporting the drugs to tumor sites [1]. Nanohydroxyapatite (nHAp) is a biocompatible material that is very suitable as a drug carrier. The studies have shown that the NI-1 cell line of canine mastocytoma, that has c-Kit tyrosine kinase mutations, is a good model for testing targeted therapeutic agents. There have been used the imatinib and toceranib as protein tyrosine kinase inhibitors (Fig. 1). The effectiveness of the proposed nHAp-drug system was tested *in vitro*. The results have shown the synergistic anti-tumor effect when the drug is delivered with nHAp in comparison to the effect of the drug alone [2,3].

The physicochemical properties of the obtained system were examined using XRPD (X-ray Powder Diffraction), SEM-EDS (Scanning Electron Microscopy-Energy Dispersive X-ray Spectroscopy), FT-IR (Fourier-Transform Infrared Spectroscopy), absorption spectroscopy and DLS (Dynamic Light Scattering) methods. The hydroxyapatite was identified as nanorod-shaped particles with great crystallinity and the amorphous drug was obtained by transforming it from its crystal form. Time-dependent drug release from the nHAp-drug system was carried out.

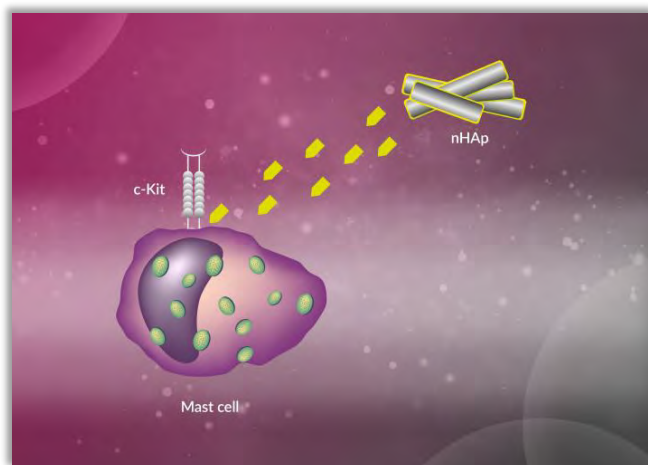


Fig. 1. Schematic of the nHAp-drug delivery system to mastocytoma cells.

-
- [1] I. Brigger, C. Dubernet, P. Couvreur, Nanoparticles in cancer therapy and diagnosis. *Advanced Drug Delivery Reviews* **54** 631–651 (2002)
[2] P. Sobierajska, A. Serwotka-Suszczak, S. Targonska et al., Synergistic Effect of Toceranib and Nanohydroxyapatite as a Drug Delivery Platform—Physicochemical Properties and In Vitro Studies on Mastocytoma Cells, *International Journal of Molecular Sciences* **23**, 1944 (2022)
[3] P. Sobierajska, A. Serwotka-Suszczak, D. Szymanski et al., Nanohydroxyapatite-Mediated Imatinib Delivery for Specific Anticancer Applications, *Molecules* **25**, 4602 (2020)

The authors would like to acknowledge the National Science Centre, Poland (NCN) for their financial support within the project ‘Preparation and investigation of multifunctional biomaterials based on nanoapatites for possible application in bone tumour treatment’ (no. UMO-2017/27/N/ST5/02976). Paulina Sobierajska received financial resources within the confines of financing the ETIUDA doctoral scholarship from the National Science Centre, Poland (NCN) (no. UMO-2018/28/T/ST5/00326). Anna Serwotka-Suszczak obtained funding from the National Science Center, Poland as part of the Miniatura project entitled ‘Initial research is planned as part of the project to assess the impact of including toceranib in the basic structure of Pt-based anti-cancer drugs (cis-platinum, oxaliplatin and transplatin)’ (no. 2019/03/X/NZ5/01138).

MULTI-LEVEL HIERARCHICAL CONSTRUCTION OF NANO- AND MICRO-COMPOSITE PARTICLES SUPPORTED BY MICROFLUIDICAL SYNTHESIS

Raminta Mazetyte¹, Johann Michael Köhler¹

¹Institute for Chemistry and Bioengineering, Group for Physical Chemistry / Microreaction Technology, Technische Universität Ilmenau, 98693 Ilmenau, Germany
raminta.mazetyte@tu-ilmenau.de

Materials with structural hierarchy gained increasing interest in various fields due to their unique and tunable properties. Hierarchically constructed multi-level systems are characterized by a multi-scale organization which can be achieved by assembling nano- and microparticles together in a well-defined manner.

The main advantage of multi-level particles is the ability to integrate multiple components with specific functions into a single system. Additionally, several analytical methods can be combined with great specificity and accuracy. The formation of five-level hierarchical core-shell particles was a model experiment, however, these particles have a great potential for a wide range of applications, including selective sensing, particle-based SERS sensing, catalysis, filtration, as well as various fields in biomedicine and material science.

One of the most important factors for forming multi-level composite particles is controlled assembly of different materials. The controlled assembly needs to be ensured at different levels of organization. In previous works [1,2] the construction principles of a hierarchically structured three and four-level systems were presented in detail. The good reproducibility of the presented four-level composite system allowed the modification of several formation steps in order to increase structural hierarchy. In this way, highly structured five-level systems were formed in a multi-step process. A schematic representation of the design of core-shell composite particles is shown in Fig. 1.

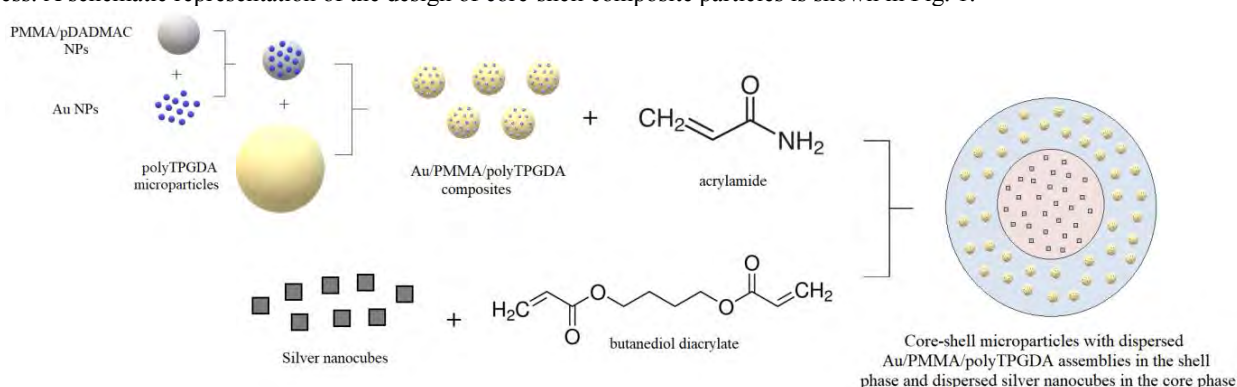


Fig. 1. Schematic representation of the design of the five-level composite system.

First, metal (Au, Ag) and polymer (PMMA, poly-TPGDA) nano- and microparticles were synthesized as individual building blocks. After, Au nanoparticles were electrostatically attached to the surface of PMMA nanoparticles and the Au/PMMA composites were formed. Prepared Au/PMMA composites were mixed with poly-TPGDA microparticles in a batch reaction and incubated at room temperature for 24 h. During incubation time, Au/PMMA composites attached to the microparticle surface and due to electrostatic attraction hierarchically structured Au/PMMA/poly-TPGDA composites were successfully formed. In the next step, core and shell monomer phases were prepared. The Au/PMMA/poly-TPGDA composites were dispersed in the shell monomer phase and Ag nanocubes were dispersed in the core phase. The synthesis of core-shell microparticles containing nested sets of dispersed metal and polymer micro- and nanoparticles was achieved through *in-situ* photopolymerization using a two-co-axial capillary microfluidic device.

The process was optimized by controlling the flow rates of the carrier, shell, and core phases, with the results revealing that an increase in carrier flow rate reduced particle size, while an increase in shell and core flow rate increased particle size. Also, it has been proven that *in-situ* photopolymerized core-shell composite particles are robust, permeable, and potentially applicable for particle-based sensing, for example for SERS applications.

[1] K.P. Kronfeld, R. Mazetyte-Stasinskiene, X. Zheng, J.M. Köhler, Textured and Hierarchically Constructed Polymer Micro- and Nanoparticles, Applied Sciences 2076-3417 (11), 2076-3417 (2021).

[2] R. Mazetyte-Stasinskiene, E. Freiberger, E. Tauscher, J.M. Köhler, Four-Level Structural Hierarchy: Microfluidically Supported Synthesis of Polymer Particle Architectures Incorporating Fluorescence-Labeled Components and Metal Nanoparticles. Langmuir, 38 (29), 8794-8804 (2022).

INVESTIGATION OF FANO RESONANCE NATURE IN SPLIT-RING RESONATOR ARRAY METASURFACE

Darius Urbonis¹, Žilvinas Kancleris¹, Paulius Ragulis¹

¹ Department of Physical Technologies, Center for Physical Sciences and Technology, Saulėtekio av. 3, Vilnius, Lithuania
darius.urbonis@ff.stud.vu.lt

Fano resonance is observed as a closely spaced peak and dip in metasurface transmission or reflection spectra. The excitation of Fano resonance is caused by interference between two resonances of narrow (discrete) and broad (continuum) line shape. The two resonances can be excited due to different physical reasons which determine the nature of Fano resonance. It is observed that interference of resonances such as plasmonic, waveguide and Fabry-Perot can lead to excitation of Fano resonance [1,2]. The issue is that often it is unclear which conditions have to be satisfied for the excitation of Fano resonance. A better understanding of all the necessary conditions would improve the current understanding of Fano resonance in metamaterials and could lead to invention of new devices.

It has been experimentally shown [3] that a metasurface composed of shifted split-ring resonators (SRRs) exhibits multiple Fano resonances, which are excited due to the broken symmetry of the structure. This is achieved by displacing every second column of the SRRs from the symmetry position as is shown in Fig. 1 a). Even a small change of distance Δ between the adjacent SRR causes the appearance of a strong Fano resonance (f_{WM}) (ref. to Fig. 1 b)). The second Fano resonance (f_{BS}) appears when the columns of SRRs are sufficiently close to each other, and becomes progressively stronger with decreasing Δ . Such behavior suggests that the nature of the two Fano resonances is different. It is theorized that the waveguide mode is required for excitation of both resonances. However, the first resonance (f_{WM}) arises purely due to the interference of the waveguide mode (discrete) with plasmonic resonance (continuum), while for the excitation of the second resonance (f_{BS}) the waveguide mode is a necessary but not sufficient condition. The distinction is illustrated in Fig. 1 b), which shows that at large waveguide period (L_x), the frequencies of both Fano resonances coincide with the dielectric waveguide mode (DWM) characteristic frequency, arising in the metasurface due to the diffraction of electromagnetic wave on the periodic structure. As the waveguide period decreases, the frequencies of both Fano resonances diverge, indicating that the approach of the shifted resonator columns to each other affects the frequencies of the Fano resonances differently (ref. to Fig. 1 c)). It should be noted that both frequencies diverge from the DWM line but f_{BS} diverges faster. To elucidate the details of the observed phenomenon, we investigate distributions of electric fields and currents flowing in the SRRs.

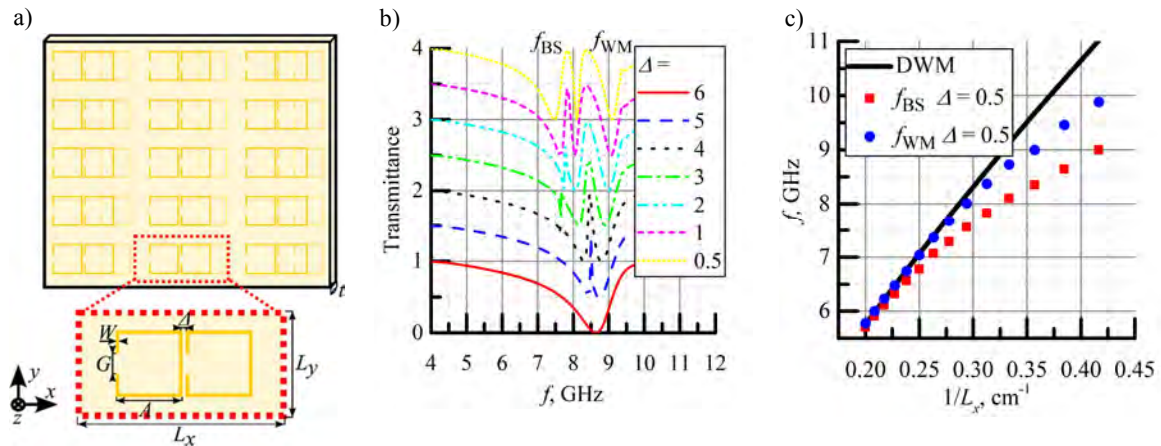


Fig. 1. a) schematic representation of the investigated metasurface, $L_x = 32$, $L_y = 16$, $\Delta = 0.5$, $A = 10$, $W = 0.5$, $G = 3$, $t = 1.5$ (units in mm), relative dielectric constant of substrate $\epsilon = 4.22$. b) calculated transmittance dependence on Δ (units in mm). c) resonance dispersion, f_{BS} – Fano resonance arising due to broken symmetry, f_{WM} – Fano resonance arising due to waveguide mode, DWM – dielectric waveguide mode.

- [1] D. Seliuta et al., Fano resonance arising due to direct interaction of plasmonic and lattice modes in a mirrored array of split ring resonators, Opt. Lett. 44, 759-762, 2019
 [2] Q. Shi et al., Double Fano resonance based on Fabry-Perot mode and asymmetric waveguide mode, Results in Optics, 2021
 [3] D. Urbonis et al., Double Fano resonance in broken symmetry split-ring resonator array metasurface, Advanced Properties and Processes in Optoelectronic Materials and Systems, APROPOS 18, 2022, Vilnius, Lithuania.

BANDGAP MODULATION BY CATIONIC SUBSTITUTION IN QUASI-ONE-DIMENSIONAL SnZrS_3 - SnTiS_3 ALLOY SYSTEM

Rokas Kondrotas^{1*}, Vidas Pakštas¹, Artūras Suchodolskis¹, Katri Muska², Marit Kauk-Kuusik²

¹ Center for Physical Sciences and Technology, Sauletekio Ave. 3, Vilnius 10257, Lithuania

² Department of Materials and Environmental Technology, Tallinn University of Technology, Ehitajate Tee 5 Tallinn 19086, Estonia

rokas.kondrotas@ftmc.lt

Chalcogenides are compounds that are composed of anions from group VI (elements S, Se, Te) and less electronegative cations, e.g. metals. Chalcogenides are widely applicable in various fields from thermoelectrics, infrared sensors to UV-light emitters. One of the advantages of chalcogenides are that they can easily form alloy systems without changing original crystal structure. Due to chemical similarities of sulfur and selenium, substitution one with the other does not induce significant structural changes but enables to modulate bandgap in 0.3 – 0.8 eV range [1]. The same trend applies if substitution is carried out with isovalent cations. ABX_3 where $A=\text{Ca, Sr, Ba, Sn}$, $B=\text{Ti, Zr, Hf}$ and $X=\text{S, Se}$, S is a novel group of chalcogenides poised to have very promising properties for optoelectronic application.

In this work we focus on analyzing SnZrS_3 - SnTiS_3 alloy system with an aim to modulate absorption edge and identify potential application fields. To achieve this goal, a solid state reaction was carried out in 750 – 850 °C temperature range to synthesize $\text{Sn}(\text{Ti}_x\text{Zr}_{1-x})\text{S}_3$ alloys. To facilitate reaction, a transport agent was introduced in the synthesis process. The as-obtained samples were studied using X-ray diffraction method, X-ray energy-dispersive and diffuse reflectance spectroscopies.

Parent structures of SnZrS_3 and SnTiS_3 are not the same. SnZrS_3 crystallizes in orthorhombic crystal structure based on a needle-like phase (prototype structure – RbCdCl_3), whereas SnTiS_3 is found in two phases: more common is misfit compound of $(\text{SnS})_{1.2}\text{TiS}_2$ (monoclinic) [2] and under certain conditions – a needle-like phase with $\text{Sn}_{1.2}\text{Ti}_{0.8}\text{S}_3$ stoichiometry can be obtained [3]. We found that while Ti content was low, i.e. $\text{Ti}/(\text{Ti}+\text{Zr})$ ratio was below 0.5, the major phase was $\text{Sn}(\text{Ti}_x\text{Zr})\text{S}_3$ in needle-like phase with a small contribution of secondary binary phases (Fig. 1). When Ti content was above 0.5, we observed a new phase formed which was most likely related to the misfit compound of $(\text{SnS})_{1.2}(\text{Ti}_x\text{Zr}_{1-x})_2$ nature. Therefore we estimate that a single phase in $\text{Sn}(\text{Ti}_x\text{Zr}_{1-x})\text{S}_3$ can be obtained with x up to 0.5.

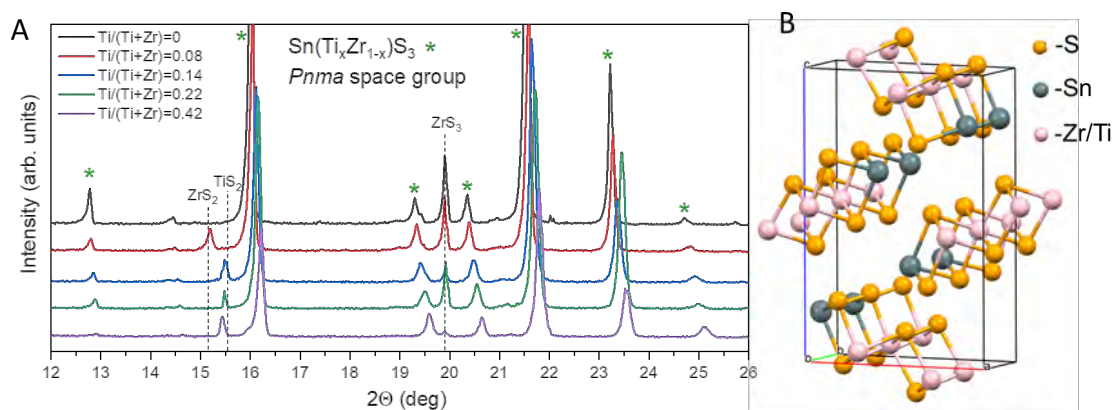


Fig. 1. (A) XRD patterns of $\text{Sn}(\text{Ti}_x\text{Zr}_{1-x})\text{S}_3$ alloys with different Ti content. $\text{Zr}(\text{Ti})\text{S}_2$ and ZrS_3 were found as secondary phases. (B) Schematic representation of quasi-one-dimensional $\text{Sn}(\text{Ti}_x\text{Zr}_{1-x})\text{S}_3$ crystal structure.

Absorption spectra of powder samples were estimated by measuring diffuse reflectance and applying a Kubelka-Munk formulation. We found that absorption edge gradually shifted towards lower energies with the increasing Ti content. Finally, the estimated bandgap varied in 0.8 – 1.4 eV range depending on the Ti concentration. We show that bandgap can be modulated in the wide range depending on the cationic $\text{Ti}/(\text{Zr}+\text{Ti})$ ratio without compromising crystal structure. This demonstrates the potential of $\text{Sn}(\text{Ti}_x\text{Zr}_{1-x})\text{S}_3$ alloy system for optoelectronic application in near infrared and infrared regions.

- [1] H. Neff, O. Lange, M.L. Fearheiley et al., Optical and electrochemical properties of CuInS_2 and CuInS_2 - CuInSe_2 alloys, Applied Physics Letters, **47**, 1089 (1985).
- [2] C. Yin, Q. Hu, G. Wang et al., Intriguing substitution of conducting layer triggered enhancement of thermoelectric performance in misfit-layered $(\text{SnS})_{1.2}(\text{TiS}_2)_2$. Applied Physics Letters, **110**, 043507 (2017).
- [3] K. Suekuni, H. Usui, S. Qiao, K. Hashikuni, et al., Electronic structure and thermoelectric properties of $\text{Sn}_{1.2-x}\text{Nb}_x\text{Ti}_{0.8}\text{S}_3$ with a quasi-one-dimensional structure. Journal of Applied Physics, **125**(17), p.175111 (2019).

NMR CHARACTERIZATION OF NOVEL $Y_{3-x}Na_xAl_{5-y}V_yO_{12}$ GARNETS

Carlos Martin Signes^{1,2}, Diana Vištorskaja³, Aivaras Kareiva³, Vytautas Klimavičius¹

¹ Institute of Chemical Physics, Vilnius University, Lithuania

² Faculty of Science, Physics, University of Granada, Spain

³ Institute of Chemistry, Vilnius University, Lithuania

carlosmsignes@correo.ugr.es

Yttrium Aluminum Garnets ($Y_3Al_5O_{12}$, **YAGs**) are materials with very suitable properties for lightning technologies. Their transparency, and high chemical and heat resistance make them a powerful basis for solid-state lightning applications. To do this, YAGs must be doped with optically-active ions of similar size to replace some of the Yttrium and Aluminum ions. The study of different doping elements and concentrations is of great importance to produce new materials with the desired optical profile, which allows the development of more powerful and precise devices for medicine, technological or lightning applications. Solid-state Nuclear Magnetic Resonance (**NMR**) is a very powerful experimental method for materials research. It provides information on the local structure at molecular level and defects of the material. This information allows to create structure-optical properties relations.

In this work, YAGs doped with different concentrations of ^{23}Na and ^{51}V were analyzed employing ^{27}Al , ^{23}Na and ^{51}V Magic Angle Spinning (**MAS**) NMR experiments. Multiple Quantum MAS technique was used to resolve overlapping signals from different chemical moieties. NMR was found to be very beneficial as crystalline and amorphous moieties formed during the synthesis of these novel garnets were detected. In contrary, XRD (X-ray diffraction) analysis which was performed provided information only on the crystalline phases.

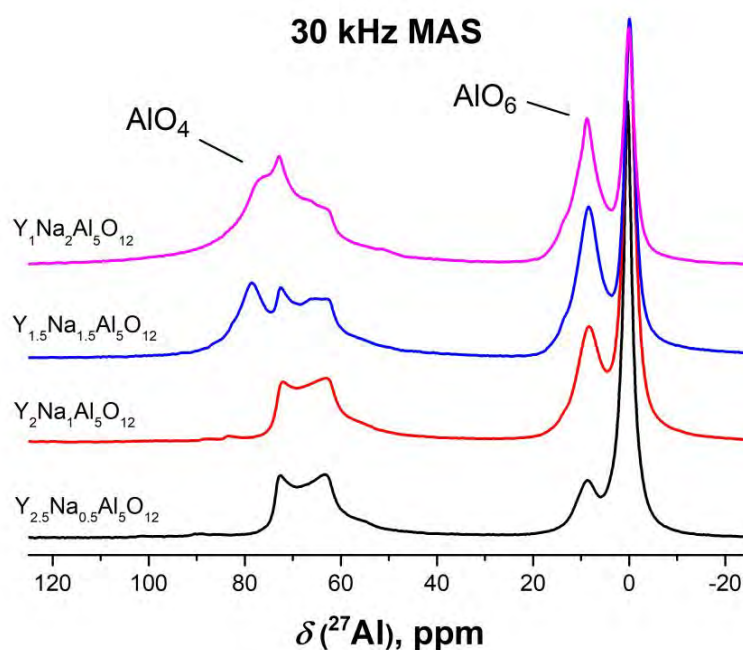


Fig. 1. 30kHz ^{27}Al MAS NMR spectra obtained for studied garnets. More details in the figure.

In Fig. 1, we can observe the ^{27}Al NMR spectra obtained for four YAG samples containing different doping levels of Na. It can be seen that the 4th-coordinated Aluminum peak changes with increasing concentrations of Na; mainly due to the apparition of other phases such as Al_2O_3 , YAP and $YAIO_3$.

A better understanding of the structure and properties of the studied materials will allow for more methodic practical testing in applications; as oftentimes even slight variations in concentration can change the optical properties drastically. Through this research, we aim to produce an NMR characterization of these promising families of YAGs to facilitate the advancement of new technologies.

Funding by Vilnius University Science Promotion Foundation (MSF-JM-5/2022) is acknowledged.

[1] Levitt Malcolm H., Spin Dynamics: Basics of Nuclear Magnetic Resonance, John Wiley & Sons (2001)

PRUSSIAN WHITE AS CATHODE MATERIAL FOR AQUEOUS SODIUM ION BATTERIES

Gintarė Gečė¹, Jurgis Pilipavičius¹, Linas Vilčiauskas¹

¹ Center for Physical Sciences and Technology (FTMC), Saulėtekio al. 3, LT-10257 Vilnius, Lithuania
gintare.pleckaityte@ftmc.lt

Energy has always been a common concern of the world, especially nowadays. Renewable energy sources could solve not only economical but also environmental problems such as pollution. However, the intermittency of energy production is one of the main drawbacks of sustainable electricity and requires efficient, low-cost storage systems. Na-ion rechargeable batteries (SIBs) are expected to be a more preferred choice for large-scale energy storage due to the natural abundance and low cost of sodium in comparison with well-known Li-ion batteries [1].

Variety of Na-based materials belonging to three main families: layered oxides, polyanions, and Prussian blue analogues have been studied as electrode materials for SIBs. Prussian blue analogue (PBA) receive the most extensive attention due to their excellent redox properties and relatively high standard potential. The open three-dimensional cage-like structure exhibits wide channels allowing an insertion of wide range of intercalation ions including sodium. Its preparation is simple, low-cost (e.g. co-precipitation, which is easily scalable) and uses abundant and non-toxic elements. The general chemical formula for PBA can be expressed as $A_xM'[M(CN)_6]_{1-y} \cdot zH_2O$, where A_x is an alkaline metal and M & M' are transition metal cations. Depending on a transitional metal oxidation state, PBA could be divided into three groups: Prussian Green (PG, fully oxidized), Prussian Blue (PB, mixed-state) and Prussian White (PW, fully reduced). PW typically assumes a monoclinic structure in a hydrated form or a rhombohedral structure in an anhydrous state [2-4].

In this investigation, we prepared $Na_{2-x}Fe[Fe(CN)_6] \cdot yH_2O$ in pure monoclinic PW and cubic PB phases via co-precipitation synthesis method by varying the precursors, amounts of them and pH. The structure and morphology of prepared materials were characterized by X-ray diffraction, scanning electron microscopy and thermogravimetric analysis. The electrochemical properties of prepared electrodes were investigated by cyclic voltammetry (Fig. 1) and charge/discharge galvanostatic cycling using different aqueous electrolytes.

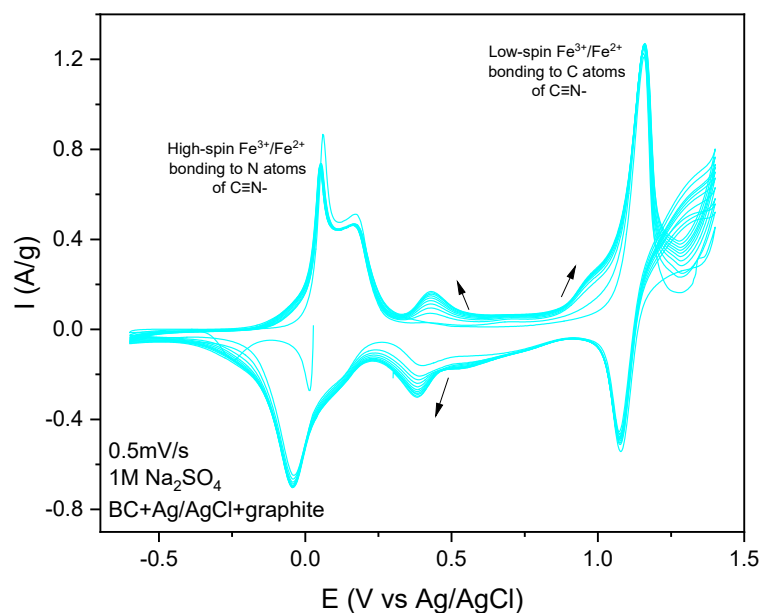


Fig. 1. Cyclic voltammogram of monoclinic $Na_{2-x}Fe[Fe(CN)_6] \cdot yH_2O$ electrode.

Acknowledgements:

This project has received funding from the European Regional Development Fund (Project No. 01.2.2-LMT-K-718-02-0005) under grant agreement with the Research Council of Lithuania (LMTLT).

-
- [1] Delmas, C. Sodium and Sodium-Ion Batteries: 50 Years of Research. *Adv. Energy Mater.* 2018, 8 (17), 170313
[2] Qian, J. et al. Prussian Blue Cathode Materials for Sodium-Ion Batteries and Other Ion Batteries. *Adv. Energy Mater.* 2018 (8) 1702619
[3] Wang, L. et al. Rhombohedral Prussian White as Cathode for Rechargeable Sodium-Ion Batteries. *J. Am. Chem. Soc.* 2015 (137) 2548–2554
[4] Xu, C. et al. Prussian Blue Analogues in Aqueous Batteries and Desalination Batteries. *Nano-Micro Lett.* 2021, 13:166

BEHAVIOUR OF 3D PRINTING FILAMENTS IN ENVIRONMENTS WITH VARIOUS RELATIVE HUMIDITY

Leons Stankevics, Olga Bulderberga, Andrey Aniskevich

University of Latvia, Institute for Mechanics of Materials, Jelgavas Str. 3, Riga, LV-1004, Latvia
leons.stankevics@lu.lv

Frequently, only specialised 3D printing companies closely monitor the storage conditions of unsealed filaments. In most room conditions, filaments are subjected to an atmosphere of 20-50% relative humidity (RH). In such conditions, filaments tend to absorb water from the air, swell, and degrade. The aim of this research was to investigate the water sorption, desorption, and swelling of different polymer filaments used for 3D printing and model these processes.

To prevent filament exposure to humid air, filaments were contained in the producer vacuum package until the beginning of experiments. After unsealing the package, filaments were cut into cylindrical shape samples of length $l = 100$ mm and diameter of $2R = 2.8$ mm. Samples were put into desiccators with constant RH created by silica gel for 12% and saturated aqueous solutions of salts LiCl for 16%, KSCN for 47%, NaCl for 75%, and K_2SO_4 for 97%. Samples were taken out of desiccators every 24 h to weigh them for sorption and measure length for swelling calculations. Mettler Toledo XS205DU balance with precision ± 0.1 mg was used for weighing samples. Mitutoyo Absolute digital micrometre with a precision of ± 0.001 mm was used for sample length measurements. The sorption of filaments was modelled using Eq. (1) which allows calculating sample moisture content Q at time t

$$Q = Q_\infty + \frac{8(Q_0 - Q_\infty)}{\pi^2} \sum_{k=1}^{\infty} \sum_{m=1}^{\infty} \frac{\exp(-\lambda_{k,m}^2 Dt)}{m^2 \gamma_k^2} (1 - (-1)^m)^2, \quad \lambda_{k,m}^2 = \left(\frac{\gamma_k}{R}\right)^2 + \left(\frac{\pi m}{l}\right)^2 \quad (1)$$

where D is the diffusion coefficient, Q_∞ and Q_0 are the equilibrium and starting moisture contents, $\lambda_{m,k}$ is a geometry-based parameter with γ_k being a table constant. Two unknown variables, D and Q_∞ , were found using curve fitting to experimental data. The aim function minimised during the fitting procedure was calculated as average relative deviation. The sorption isotherm indicated the change in equilibrium moisture content at different RH and was approximated by Eq. (2).

$$Q_\infty = a \cdot RH^c + b \quad (2)$$

where a , b , and c are coefficients unique to every material. This approximation was based on the BET theory and Henry's law. Similarly, a relation between equilibrium moisture content and swelling was plotted and modelled as a linear function.

All materials have lost mass in dry environments and gained in humid. Most materials have an equilibrium moisture content of 0.3-0.6% at 97% RH. There are outliers: Koltron has the lowest of 0.1%, and Nylon Transparent has the highest of 8%, followed by ABS-ESD of 3.5%. Examination of diffusion coefficients dependence on RH showed that for PEI, PEKK, PC white, CPE White, Nylon Transparent, and PLA Tough coefficient remained constant; while for PLA LAVA and PET-G White it increased at higher humidity; but for ABS White, ABS ESD, Koltron, and PLA Conductive coefficient at higher humidity decreased. All materials swelled maximally by 0.1-0.45% in the atmosphere 97% RH. Nylon Transparent is an exception that shrunk in the humid environment by 2.43%.

Obtained results demonstrated the specific significance of implementing storage rules for some 3D printing filaments during the work.

Acknowledgement

This research was supported by ERDF Project No. 1.1.1.1/19/A/031 "OPTITOOL, Decision Tool for Optimal Design of Smart Polymer Nanocomposite Structures Produced by 3D Printing".

INVESTIGATIONS OF NONLINEAR ABSORPTANCE AND FATIGUE EFFECT IN HfO₂, ZrO₂, AND Al₂O₃ DIELECTRIC COATINGS

Erikas Atkočaitis¹, Simonas Kičas³, Vaida Grašytė³,
Justinas Galinis², Austėja Aleksiejūtė², Andrius Melninkaitis¹

¹ Laser Research Center, Vilnius University, Saulėtekio al. 10 – LT 10223 Vilnius, Lithuania

² UAB Lidaris, Saulėtekio al. 10 – LT 10223 Vilnius, Lithuania

³ UAB Optomenas, Ukmergės g. 427, Bukiškio k., LT-14185 Vilniaus r, Lithuania
erikas.atkocaitis@ff.vu.lt

The irradiation conditions in the high-power laser systems are extreme for their critical optical elements, thus, often leading to the delayed fatigue effect: a long-term degradation and catastrophic failure [1, 2]. The phenomenon behind the extreme laser light and dielectric optics interaction is typically associated with the nonlinear absorption in optical coatings [2]. The nonlinear response makes these coatings highly optically unstable, however, the knowledge about the nonlinear properties of most dielectric coatings is very limited. Furthermore, multilayer dielectric coatings are even less investigated by the means of nonlinear absorptance. To study these effects at different wavelengths single- and multi-layer HfO₂, ZrO₂, and Al₂O₃ dielectric coatings featuring different process parameters were produced. For the measurements of nonlinear absorption, we combined a high average power laser source, operating at a 1 MHz repetition rate and 10 ps pulse duration, with common-path interferometry (PCI). PCI method is a pump-probe technique [3], where the pumping beam is modulated in time, thus, also producing modulated heating of the coating. Such action subsequently creates a time-varying miniature thermal lens out of the substrate, while the probe beam interrogates the disturbed area. Pump and probe beams are overlapped and crossed at an angle on the target plane. As the probe beam is larger than the pump beam it covers both disturbed and undisturbed regions, thus, producing a high contrast interference modulation in the far field. Such interferometric signal is then directly monitored by using a photodiode. A sample with an identical substrate material and a highly absorbing metallic coating is used to calibrate the system. The results of the nonlinear absorption measurements are then used for the interpretation of the fatigue behaviour in the same type of optical elements. S-on-1 Laser-Induced Damage Threshold (LIDT) testing was conducted in parallel on the same type of samples. An attempt is made to correlate those two types of measurements.

-
- [1] E. Atkočaitis, L. Smalakys, and A. Melninkaitis, “Pulse temporal scaling of LIDT for anti-reflective coatings deposited on lithium triborate crystals”, *Opt. Express* **30**, 28401–28413 (2022).
- [2] L. Smalakys, B. Momgaudis, R. Grigutis, S. Kičas, and A. Melninkaitis, “Contrasted fatigue behavior of laser-induced damage mechanisms in single layer ZrO₂ optical coating”, *Opt. Express* **27**, 26088–26101 (2019).
- [3] A. Alexandrovski, M. Fejer, A. Markosian, and R. Route, “Photothermal common-path interferometry (PCI): new developments,” in *Solid State Lasers XVIII: Technology and Devices*, W. A. Clarkson, N. Hodgson, and R. K. Shori, eds., **7193**, 71930D, International Society for Optics and Photonics, SPIE (2009).

EFFECT OF MICROMACHINING PARAMETERS ON GEOMETRICAL CHARACTERISTICS OF MICRO-HOLES IN FUEL CELL MEMBRANES

Mohamed A. Baba¹, Gazy Rodowan^{1,2}, Brigita Abakevičienė^{1,2},
Sigitas Tamulevičius^{1,2}, Sebastian Molin³, Tomas Tamulevičius^{1,2}

¹ Institute of Materials Science, Kaunas University of Technology, Lithuania

² Department of Physics, Kaunas University of Technology, Lithuania

³ Faculty of Electronics, Telecommunications, and Informatics, Gdansk University of Technology, Poland
mohamed.mahgoub@ktu.lt

Gadolinium doped ceria (GDC) is one of the most broadly adopted materials for the electrolyte layer in Solid oxide fuel cells (SOFCs) due to its high ionic conductivity [1]. These applications require elaborated surface area which can be achieved over micro structuring the Ytria-stabilized zirconia (YSZ) electrolyte surface via plasma micromachining [2,3], Computer Numerical Control (CNC)[4], or laser-based micromachining [5]. The interaction of ultrashort laser pulses with solid-state materials leads to the formation of various surface microstructures. The ablated crater depth, shape, roughness, and taper depend on the laser processing conditions including intensity, wavelength, repetition rate, scanning speed, etc., as well as the material type irradiated [6].

In this work, the impact of 290 fs pulse length Yb:KGW fs-laser Pharos (Light Conversion) processing parameters on the micro-hole morphology in the commercial SOFC cells (400B, Elcogen) was investigated. Firstly, the ablation threshold of the SOFCs was determined by 1030 nm wavelength using 100 kHz repetition frequency. Secondly, three groups of blind microhole arrays were imposed with different laser processing parameters (pulse energy, repeated scanning times, and scanning speed, varied from 3 to 15 μJ , from 2 to 10 times, and 20 to 100 mm/s, respectively). Following ablation, the micro-topography of the blind holes was characterized with a scanning electron microscope (SEM) Quanta 200 FEG (FEI). From the obtained tilted sample SEM micrographs (see Fig. 1) it can be noticed that the depth of the micro holes increases with the increasing pulse energy, decreasing the scanning speed, and increasing the number of scanning times.

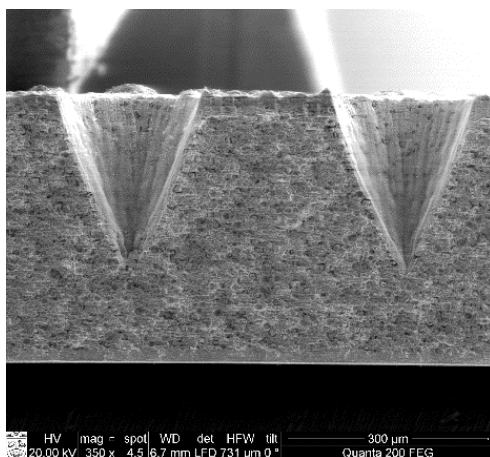


Figure 1. SEM micrographs of the laser-drilled μ -structures obtained in commercial SOFCs.

Acknowledgment

This work was supported by the Research Council of Lithuania (LMT) and Narodowe Centrum Nauki (NCN) DAINA-2, project No P-LL-21-124.

- [1] Zhang, et al. Comparison of solid oxide fuel cell (SOFC) electrolyte materials for operation at 500 C. *Solid State Ionics*, 344, 115138 (2020).
[2] Küngas, R., et al. Evidence of surface-reaction rate limitations in SOFC composite cathodes. *Solid State Ionics*, 225, 146-150 (2012).
[3] Shim, Joon Hyung, et al. "Atomic layer deposition of yttria-stabilized zirconia for solid oxide fuel cells." *Chemistry of materials*:3850-3854 (2007).
[4] Joshi, S. S., and D. Marla. "11.15-Electrochemical Micromachining." *Comprehensive Materials Processing*. Oxford: Elsevier: 373-403 (2014).
[5] Kumar, Vijay, et al. "Recent progresses and applications in laser-based surface texturing systems." *M Today Communications* 26: 101736 (2021).
[6] Nivas, Jijil JJ, and Salvatore Amoruso. "Generation of supra-wavelength grooves in femtosecond laser surface structuring of silicon." *Nanomaterials* 11.1: 174 (2021).

LASER IRRADIATION BY SHORT PULSES FOR WETTABILITY MODIFICATION OF COPPER SURFACE

Saulė Steponavičiūtė¹, Andrius Žemaitis¹, Paulius Gečys¹, Mindaugas Gedvilas¹

¹ Department of Laser Technologies (LTS), Center for Physical Sciences and Technology (FTMC), Savanoriu Ave. 231, 02300 Vilnius, Lithuania.
saulė.steponaviciute@ftmc.lt

Laser processing is an acknowledged technique for the modification of materials' surface properties and therefore has the potential for various applications. The creation of functional surfaces that exhibit various wetting behaviour by laser texturing has been demonstrated numerous times [1]. This work focuses on the control of the wetting properties of copper.

This work aimed to create copper surfaces with different wetting properties (from highly hydrophilic to superhydrophobic). A nanosecond laser was used to process copper samples. The wetting states were determined from static contact angle (CA) measurements, which were performed multiple times during an extended period to track the changes in surface properties over time. A scanning electron microscope (SEM) and 3D optical profiler were used to visualise the surface structures that were formed during laser treatment.

Highly hydrophilic and superhydrophobic surfaces, as well as some states in between, were achieved with different laser texturing parameters (Fig. 1). The CA increased over a longer period of time for almost all different textures regardless of their initial wetting state directly after processing. The influence of surface morphologies on the wetting state was considered and laser processing parameters for the creation of hydrophilic and hydrophobic surfaces were determined.

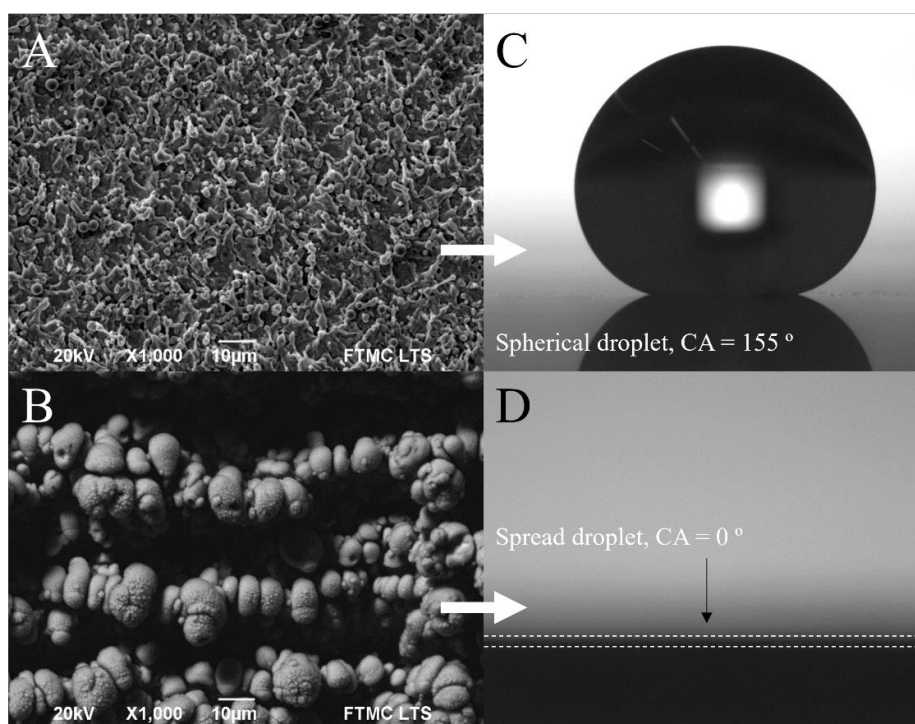


Fig. 1. SEM photographs of the processed surface (A, B) and the corresponding CA measurements for a superhydrophobic (C) and highly hydrophilic (D) surfaces.

Acknowledgement

This project has received funding from European Regional Development Fund (project No. 01.2.2-LMT-K-718-03-0050) under grant agreement with the Research Council of Lithuania (LMTLT).

[1] E. Stratakis, J. Bonse, J. Heitz et al., Laser engineering of biomimetic surfaces. *Materials Science and Engineering: R: Reports* **141**, 100562 (2020).

SUPERCONTINUUM GENERATION IN KGW CRYSTAL AT HIGH REPETITION RATE

Kawthar Reggui, Vaida Marčiulionytė, Gintaras Tamošauskas, Audrius Dubietis

Laser Research Center, Vilnius University, Saulėtekio Avenue 10, LT-10223 Vilnius, Lithuania
kawthar.reggui@ff.stud.vu.lt

Supercontinuum (SC) is an effect that results from femtosecond filamentation, which occurs during the nonlinear propagation of an intense ultrashort laser pulse in a transparent material [1]. Sapphire and YAG are the most reliable and commonly used nonlinear materials for SC generation in the visible and near-infrared spectral range for ultrafast applications [2, 3]. However, the performance can be limited at high laser pulse repetition rates, since the multiple pulse exposure can lead to optical degradation. Their performance can also be limited by the compromise in the pump energy at high laser pulse repetition rates (up to a few MHz). This is particularly crucial in SC-seeded high repetition-rate noncollinear optical parametric amplifiers [4] and optical parametric chirped-pulse amplification systems [5].

These limitations call for nonlinear materials with lower SC generation thresholds. Narrow-bandgap crystals, such as KGW, exhibit high nonlinearity (KGW: $n_2 = 11 * 10^{-16} \text{ cm}^2/\text{W}$ [1]), which results in very low critical power for self-focusing and hence allows SC generation with very small input pulse energies (sub-100 nJ). However, there are only a few studies of SC generation in KGW in general, and no investigations, to our knowledge, at high repetition rates.

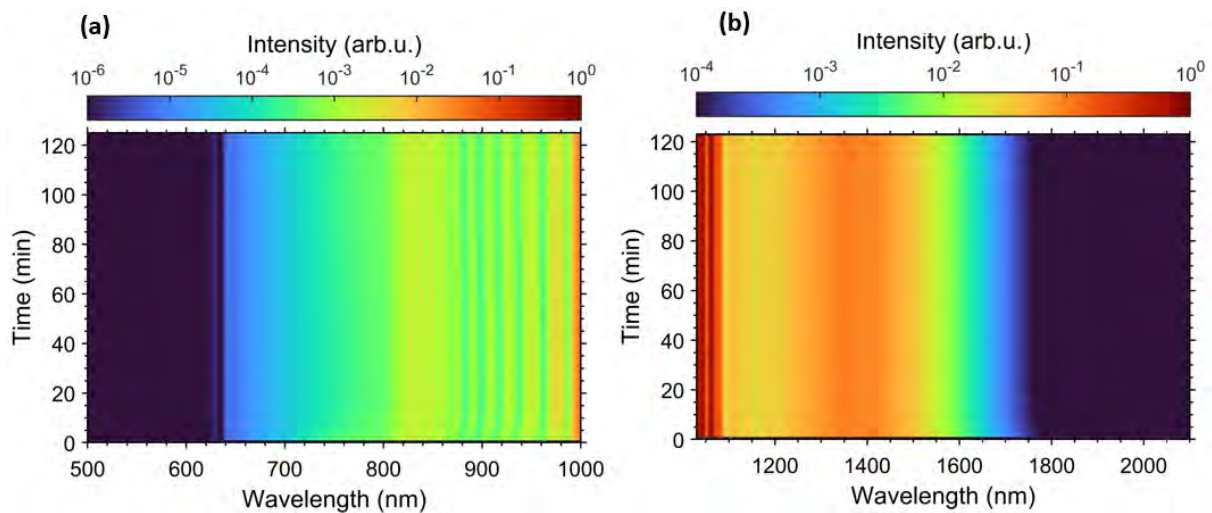


Fig. 1. Time evolution of the SC spectrum in KGW at high repetition rate (2 MHz) and a pump pulse energy of $0.35 \mu\text{J}$ in the visible (a) and NIR range (b). The spectrum is showing a stable performance for 2h of operation.

In this study, the SC generation in sapphire, YAG, and KGW crystals (6 mm length) was investigated with femtosecond Yb:KGW lasers, which deliver 200 fs, 1030 nm pulses at 200 kHz and 2 MHz repetition rate. The SC was generated at lower energies in KGW compared to sapphire and YAG. The largest spectral broadening into the IR region was also obtained in the KGW crystal (up to $\sim 1.8 \mu\text{m}$). The nonlinear transmission was also investigated in the three crystals. For sapphire, the absorbed energy at input energy of $0.75 \mu\text{J}$ was $0.06 \mu\text{J}$, for YAG the absorbed energy was $0.01 \mu\text{J}$ at $0.37 \mu\text{J}$ input energy, and for KGW, it was $0.009 \mu\text{J}$ at $0.14 \mu\text{J}$ input energy. YAG and KGW have the lowest energy absorption, and consequently potentially less heat accumulation, making them suitable for SC generation at very high repetition rates. KGW showed a lower threshold energy for SC generation, making it more suitable for SC generation at very high repetition rates. Therefore, the time evolution of the KGW crystal at 2 MHz was studied and further proved the potential of the crystal in ultrafast applications. As illustrated in Figure 1, the crystal showed a stable performance for 2h with no optical degradation, which opens new possibilities for the use of KGW in new laser systems operating at repetition rates in the MHz range.

- [1] A. Dubietis, G. Tamošauskas, R. Šuminas, V. Jukna and A. Couairon, Ultrafast supercontinuum generation in bulk condensed media, *Lith. J. Phys.* **57**, 113–157 (2017).
- [2] M. Bradler, P. Baum and E. Riedle, Femtosecond continuum generation in bulk laser host materials with sub- μJ pump pulses, *Appl. Phys. B* **97**, 561–574 (2009).
- [3] A. L. Calendron, H. Cankaya, G. Cirmi and F. Kärtner, White-light generation with sub-ps pulses, *Opt. Express* **23**, 13866 (2015).
- [4] M. Bradler and E. Riedle, Sub-20 fs μJ -energy pulses tunable down to the near-UV from a 1MHz Yb-fiber laser system, *Opt. Lett.* **39**, 2588–2591 (2014).
- [5] M. Windeler, K. Mecseki, A. Miahnahri, J. Robinson, J. Fraser, A. Fry and F. Tavella, 100 W high-repetition-rate near-infrared optical parametric chirped pulse amplifier, *Opt. Lett.* **44**, 4287 (2019).

DLC:CU THIN FILM STABILITY TESTING IN CELL CULTURE MEDIUM

Shahd Elkhider¹, Mohamed A. Baba¹, Andrius Vasiliaskas¹, Šarūnas Meškiniš¹, Dainius Zienius², Raimundas Lelešius², Algirdas Šalomskaš², Tomas Tamulevičius^{1,3}

¹Institute of Materials Science, Kaunas University of Technology, Lithuania

²Department of Veterinary Pathobiology, Faculty of Veterinary Medicine Lithuanian University of Health Sciences, Lithuania

³Department of Physics, Kaunas University of Technology, Lithuania

shahd.fateh@ktu.edu

Novel nanoparticles with significant antimicrobial properties are extensively studied in the last two decades due to their different properties from the bulk material in size reduction and high surface area [1, 2]. Copper (Cu) nanoparticles were found to have antiviral properties against a range of viruses [3]. The nanoparticle can increase the drug solubility in water and the drug uptake by the infected cell which can increase the biomedical application in drug delivery systems [4].

In this work, the amorphous diamond-like carbon thin films with Cu nanoparticles (DLC:Cu) were deposited on crystalline silicon substrates by reactive magnetron sputtering of a metal target in an acetylene gas atmosphere. The nanocomposite DLC:Cu films are intended for antiviral effect testing by cell culture method. The DLC:Cu film stability was tested using culture media Dulbecco's Modified Eagle's Medium (DMEM) for a different set of time durations (5 and 10 minutes). The sample changed color from metallic copper to green which was confirmed by the UV-visible spectrophotometry measurements (Fig.1). The initial results suggest that copper nanoparticles are oxidized. Copper oxidation, ion, and nanoparticle release in the medium are important for DLC:Cu application for antimicrobial and antiviral applications.

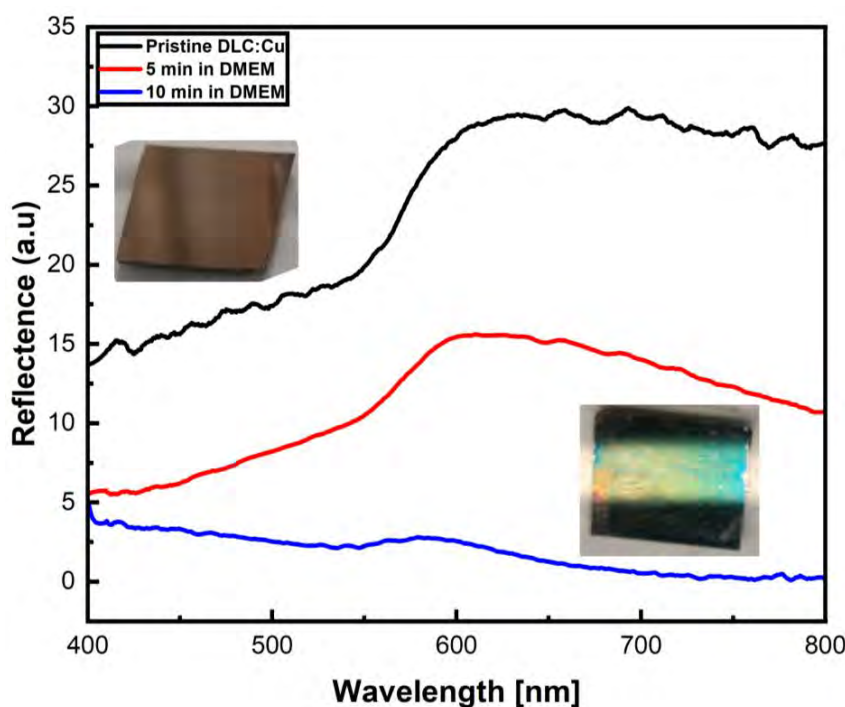


Fig. 1. Effect of the DMEM media on the reflectance of DLC:Cu nanoparticle film after different durations in time. Sample edge length 1 cm.

This work was supported by the European Regional Development Fund, Project No.: 13.1.1-LMT-K-718-05-0018.

[1] Rajesh, K.M., et al., Assisted green synthesis of copper nanoparticles using *Syzygium aromaticum* bud extract: Physical, optical and antimicrobial properties. *Optik*, 2018. 154: p. 593-600.

[2] Salavati-Niasari, M., F. Davar, and N. Mir, Synthesis and characterization of metallic copper nanoparticles via thermal decomposition. *Polyhedron*, 2008. 27(17): p. 3514-3518.

[3] Tavakoli, A. and M.S. Hashemzadeh, Inhibition of herpes simplex virus type 1 by copper oxide nanoparticles. *Journal of virological methods*, 2020. 275: p. 113688.

[4] Tortella, G., et al., Silver, copper and copper oxide nanoparticles in the fight against human viruses: progress and perspectives. *Critical Reviews in Biotechnology*, 2022. 42(3): p. 431-449.

TEMPERATURE DRIVEN PHASE TRANSITIONS IN METASTABLE Sc DOPED HEXAGONAL LuFeO₃

Andrius Pakalniškis¹, Gediminas Niaura², Dmitry Karpinsky³, Guillaume Rogez⁴, Pierre Rabu⁴, Shih-Wen Chen^{5,6}, Thomas Chung-Kuang Yang^{5,6}, Ramūnas Skaudžius¹, Aivaras Kareiva¹

¹Institute of Chemistry, Vilnius University, Naugarduko 24, LT-03225 Vilnius, Lithuania

²Department of Organic Chemistry, Center for Physical Sciences and Technology (FTMC), Sauletekio Ave. 3, LT-10257, Vilnius, Lithuania

³Namangan Engineering-Construction Institute, Dustlik Avenue 4, 160100 Namangan, Uzbekistan.

⁴IPCMS (UMR 7504 CNRS-Université de Strasbourg), Strasbourg, France

⁵Precision Analysis and Materials Research Center, National Taipei University of Technology, Taipei, Taiwan

⁶Department of Chemical Engineering and Biotechnology, National Taipei University of Technology, Taipei Taiwan, andrius.pakalniskis@chgf.vu.lt

The crystal structure and properties of compounds with perovskite structure (nominal chemical formula ABO₃) can be drastically modified by a chemical substitution in A- and/or B- perovskite sublattices. Introduction of elements with different ionic radii leads to a stabilization of structural distortions. The possibility to control physical properties via chemical doping is particularly important when concerning the formation of both electrical and magnetic orderings in the same compounds, which are commonly referred as multiferroics. However, for the most part, due to the conflicting nature of these properties, the coupling between the electrical and magnetic properties is relatively weak. Since magnetic properties usually require the 3d layer to be partially filled by electrons, while electrical properties arise from empty 3d shells. To solve this conundrum, materials with new mechanism for the origin of their ferroelectric properties were discovered, such as lone pair and spin driven mechanisms, that do not require empty electron shells [1]. The second issue that multiferroic compounds suffer from is the fact that most orderings only occur below room temperature. Only few room temperature multiferroics are known, with the main research being focused on BiFeO₃.

Recently a new class of hexagonal rare earth ferrite perovskite compounds has been found to exhibit multiferroic ordering, with a mechanism and structure similar to that of hexagonal manganites, making them a new avenue for potential research. This new family of room temperature multiferroic compounds are based on LuFeO₃ with hexagonal structure (space group *P6₃cm*). It has been discovered that LuFeO₃ in the hexagonal state has both ferroelectric and weak ferromagnetic ordering. Furthermore, it has been reported that the compound in orthorhombic phase (space group *Pnma*) is antiferromagnetic below 620 K, while being in hexagonal structure the magnetic transition shifts down to 440 K while also showing weak ferromagnetism, due to a canting of the magnetic moments towards the c-axis, with the polarization being retained up to 1050 K, at least in the case of thin films [2,3].

It should be noted, that the preparation of hexagonal compounds is quite difficult and the crystal structure can be modified either using the chemical substitution or via preparing the compounds in a form of thin films as the crystal lattice is unstable and tends to form an orthorhombic structure. Due to the unstable nature of the lattice and difficulty of preparation and characterization of the hexagonal variant of LuFeO₃, the main available results have been performed on thin films. However, when analyzing thin films, it is important to take into account the effect of strain and interface interactions as it can significantly affect chemical and physical properties [4].

We provide insights in stabilizing the hexagonal structure in doped LuFeO₃ polycrystalline compounds prepared using aqueous sol-gel synthesis procedure. While also providing further clarification on the concentration ranges of the different structural phases present in the system and analyzed by means of SEM, room temperature X-ray diffraction techniques, and Raman spectroscopy. Furthermore, we also investigate temperature driven polar to non polar phase transitions by means of temperature dependent X-ray diffraction measurements. Lastly, we provide additional insight on the magnetic structure and its changes at low and room temperature.

Acknowledgments: This project has received funding from the European Union's Horizon 2020 research and innovation programme under the Marie Skłodowska-Curie grant agreement No 778070 – TransFerr – H2020-MSCA-RISE-2017.

[1] M. Kumar, et al., Advances and future challenges in multifunctional nanostructures for their role in fast, energy efficient memory devices, *Mater. Lett.* **277**, 128369 (2020).

[2] W. Wang, et al., Room-temperature multiferroic hexagonal LuFeO₃ films, *Phys. Rev. Lett.* **110**, (2013).

[3] S. Cao, et al., On the structural origin of the single-ion magnetic anisotropy in LuFeO₃, *J. Phys. Condens. Matter.* **28**, 156001 (2016).

[4] J. Luxová, P. Šulcová, The effect of partial substitution of Bi on colour properties and thermal stability of Bi_xPr_{1-x}FeO₃ pigments, *J. Therm. Anal. Calorim* **138**, 4303–4312 (2019).

INVESTIGATION OF CHARGE CARRIER DYNAMICS IN Mg DOPED GAN LAYERS BY LIGHT-INDUCED TRANSIENT GRATING TECHNIQUE

Mantas Vaičiulis, Arūnas Kadys, Ramūnas Aleksiejūnas

¹ Institute of Photonics and Nanotechnology, Faculty of Physics, Vilnius University, Saulėtekis Av. 3, LT-10257
Vilnius, Lithuania
mantas.vaiciulis@ff.vu.lt

One of challenges in producing InGaN light emitting structures lies in deposition of p-type GaN contact layer on top of InGaN quantum well (QW) structures, as these two steps require different growth temperatures. For example in MOCVD growth, the InGaN QWs are usually deposited at temperatures below 900°C, while p-GaN contact layers are best grown around 1100°C [1]. As a result, high temperature deposition of p-GaN may lead to degradation of InGaN QW due to diffusion of In atoms into the surrounding layers. Therefore, there is an interest in growing p-type GaN at temperatures as low as feasible.

In this presentation, we investigate the impact of growth conditions – growth temperature and the precursor flow rate – on the doping level and charge carrier transport in GaN layers. For contactless estimation of hole density, we employ measurement of ambipolar diffusion coefficient, D , as a function of carrier density by Light-Induced Transient Grating (LITG) technique [2]. The set of samples consisted of MOCVD-grown uGaN buffer layers, deposited at 1120°C on top of double sided polished c-orientation sapphire substrate followed by cGaN grown at 1100°C. The layers under investigation were grown at temperatures of 950, 920 and 890°C and at each temperature a set of samples were grown using different Mg precursor pressures of 600, 500, 400 and 300 sccm.

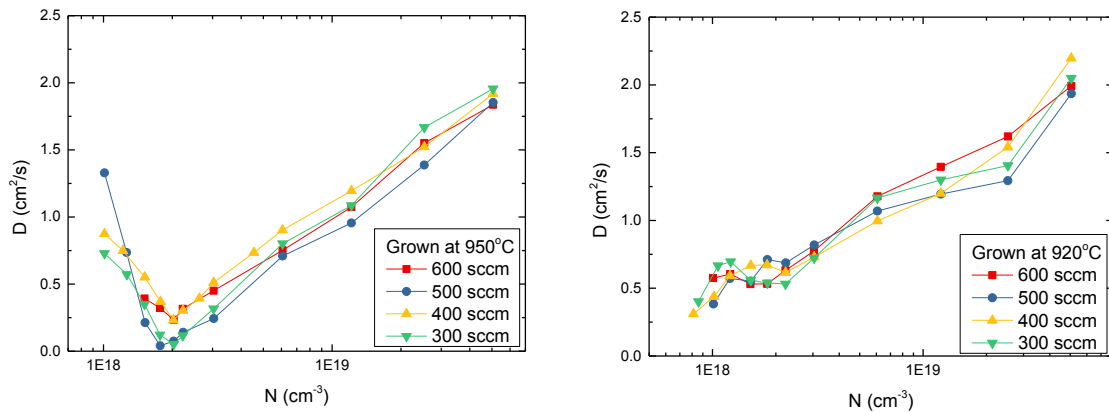


Fig. 1: Dependence of diffusion coefficient on photoexcited carrier density in magnesium doped GaN layers grown at 950 or 920°C temperatures and under Mg precursor flow rates varying from 300 to 600 sccm.

Fig. 1 shows the dependence of ambipolar diffusion coefficient D on photoexcited carrier density N in variously grown GaN layers. The dependence of $D(N)$ in GaN grown at 950°C has a minimum, while in GaN grown at 920°C the diffusivity monotonically increases with excitation. We show by modeling that such a behavior of $D(N)$ can be interpreted in terms of ambipolar diffusion in degenerate electron-hole plasma [3]. The decrease of $D(N)$ at lower densities is a signature of p-type doping and can be used for estimation of equilibrium hole density. The results in Fig. 1 suggest that temperature of 920°C is likely too low for growth of p-type GaN, as the layers are compensated by efficient introduction of n-type impurities. This conclusion is also supported by the dependence of carrier lifetime on growth temperature. The lifetime drops in the samples grown at lower densities, most likely due to higher point defect density in latter samples. In addition, the Mg flow rate seems to affect the mobility of holes as well, which is estimated from D value in the minima of $D(N)$ dependencies.

[1] M. Dmukauskas, Development of MOVPE pulsed growth technique for increased efficiency InGaN/GaN multiple quantum well structures, 2020, DOI:10.15388/vu.thesis.21

[2] H. J. Eichler et al., Laser-Induced Dynamic Gratings, Springer Series in Optical Sciences, 1986, DOI:10.1007/978-3-540-39662-8

[3] S. S. Li et al., Alternative formulation of generalized Einstein relation for degenerate semiconductors, Proceedings of the IEEE, 56(7), 1256–1257, 1968, DOI:10.1109/proc.1968.6561

RESEARCH OF NON-EQUILIBRIUM CHARGE CARRIER DYNAMICS IN GAN FILMS WITH VARYING IMPURITY DENSITIES

Mantas Auruškevičius¹, Kazimieras Nomeika¹

¹Institute of Photonics and Nanotechnology, Vilnius University, Lithuania
mantas.auruskevicius@ff.stud.vu.lt

Gallium nitride (GaN) is a wide bandgap III/V semiconductor, widely used in manufacturing blue light-emitting diodes and high-power electronic components. Its qualities, such as high breakdown electric field, thermal conductivity and electron mobility make it a great material choice for designing small, high power electronic devices [1]. Naturally, further research on this semiconductor might reveal ways to fine-tune the qualities of this material to better suit its uses. This research aims to investigate how equilibrium carrier density, mobility, and certain parameters of GaN film growth affect the dynamics of non-equilibrium charge carriers.

In this research, seven thin GaN films (2,3-2,6 μm thick) were tested using the light-induced transient grating technique (LITG). These films were grown on sapphire using the metalorganic chemical vapor deposition method (MOCVD), but had varying growth parameters, such as the flow of ammonia, temperature, and reaction chamber pressure. Additionally, electron density and mobility were determined in all samples using the Hall effect measurements. All LITG measurements were carried out using a femtosecond laser “PHAROS” (wavelength 1030 nm, pulse duration 250 fs, pulse frequency 30 kHz), an optical parametric system “ORPHEUS” (together with a non-linear crystal for generating the 355 nm pump beam) and a transient grating spectrometer “HARPIA|TG”, made by “Light Conversion”.

The results have shown that the measured diffusion coefficient increases in all samples with the pump beam intensity. This can be linked to the degeneracy of the charge carrier plasma [2]. Additionally, five out of seven samples showed longer charge carrier lifetimes at higher excitation intensities, which could be explained by the saturation of defect states and slower non-radiative recombination [3]. After this, diffusion coefficient, length and charge carrier lifetime values were taken at low (20 $\mu\text{J}/\text{cm}^2$), medium (80 $\mu\text{J}/\text{cm}^2$) and high ($\sim 300 \mu\text{J}/\text{cm}^2$) sample excitation intensities and these values were used to compare the samples. The comparison showed, that higher diffusion coefficients were measured in samples with lower equilibrium electron densities and higher electron mobilities. Lastly, samples grown at higher reactor pressures and higher ammonia flow have shown overall higher measured diffusion coefficients, charge carrier lifetimes and diffusion lengths.

[1] Fornari, Roberto. (2018). Single Crystals of Electronic Materials: Growth and Properties.

[2] Malinauskas, T., Jarasiunas, K., Heuken, M., Scholz, F. and Brückner, P. (2009), Diffusion and recombination of degenerate carrier plasma in GaN. *Phys. Status Solidi (c)*, 6: S743-S746. <https://doi.org/10.1002/pssc.200880856>

[3] Brandt, Wünsche, H.-J., Yang, H., Klann, R., Müllhäuser, J. ., & Ploog, K. . (1998). Recombination dynamics in GaN. *Journal of Crystal Growth*, 189-190, 790–793. [https://doi.org/10.1016/S0022-0248\(98\)00295-4](https://doi.org/10.1016/S0022-0248(98)00295-4)

DEVELOPMENT AND INVESTIGATION OF SUBNANOSECOND PULSE COMBINED OPTICAL PARAMETRIC AMPLIFIER SYSTEM

Augustė Stravinskaitė, Gabrielė Stanionytė, Jonas Banys, Julius Vengelis

Laser Research Center, Faculty of Physics, Vilnius University, Lithuania
auguste.stravinskaite@ff.stud.vu.lt

Nowadays lasers have become necessary optical devices used in many application areas. However, lasers have spectral limitations making wavelength of the lasers extremely hard to change. In order to change the wavelength of laser radiation, parametric light generators (OPGs) are used which have a distinctive flexibility allowing them to tune wavelength of radiation in a broad spectral range. Most of the parametric light generators are within ultrashort (less than 100 ps) and long (more than 1 ns) pulse durations, and, due to certain physical limitations, subnanosecond (300 ps – 1 ns) pulse parametric light generators are very scarce [1-3].

The goal of this research was to construct and investigate combined and optimized subnanosecond optical parametric amplifier system which uses a 15 mm lithium triborate (LBO) crystal as a nonlinear medium, generated signal wave in MgO:PPLM OPG as a seed radiation and 3rd harmonic of Nd:YAG MOPA laser ($\lambda=355$ nm) as pump.

In this work the spectral, energy and temporal characteristics of OPA system were investigated. During optical parametric generation MgO:PPLN optical crystal grating periods were from 27.58 μm to 31.59 μm and signal wavelength range was 1400 nm – 2150 nm. In LBO crystal we achieved signal wave generation via optical parametric amplification of the idler wave (the seed generated in MgO:PPLN OPG). The difference frequency wave (signal wave) range was from 425 nm to 475 nm, which was limited by the tuning limits of the seed radiation spectrum (1400 nm – 2150 nm). The maximum signal power at 475 nm was 24.1 mW which corresponded to maximum conversion efficiency of 37%. Saturation regime of the OPA was achieved with a pump power of 85 mW, which indicated that the device is optimized at current conditions. Furthermore, after the measuring signal pulse duration it was determined, that pulse durations were in the subnanosecond range: from 212 ps to 432 ps.

The results of this work will be used for further development of more effective subnanosecond OPG/OPA systems. This work has received funding from European Regional Development Fund (project No. 01.2.2-LMT-K-718-03-0004) under grant agreement with the Research Council of Lithuania (LMTLT).

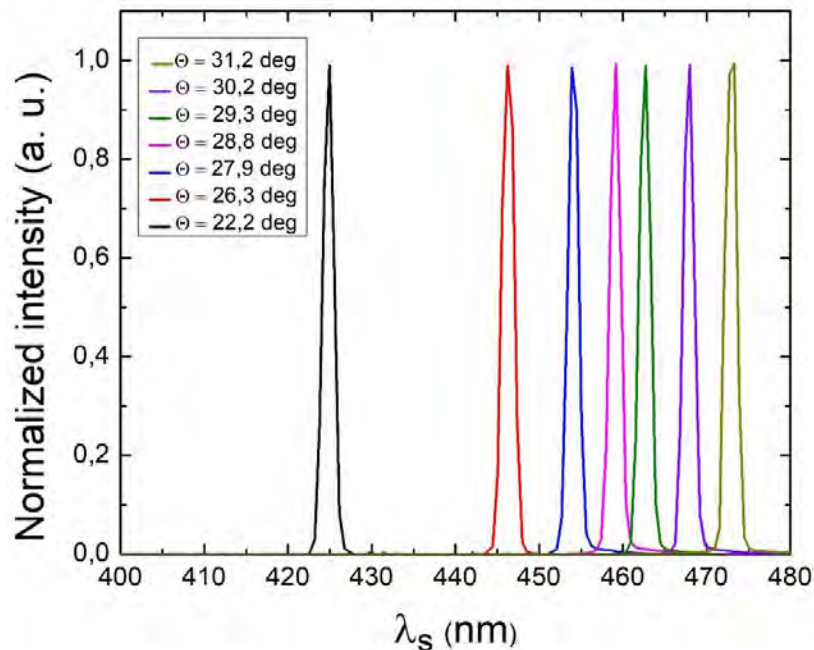


Fig. 1. Spectra of signal wave at different LBO crystal rotation angles.

[1] M. H. Dunn and M. Ebrahimzadeh, Parametric Generation of Tunable Light from Continuous-Wave to Femtosecond Pulses, Science 286, 1513–1518 (1999).

[2] A. Dubietis, Netiesinė optika, (Publisher Vilnius University, Vilnius 2011).

[3] R. W. Boyd, Nonlinear Optics ed. 3 (Academic press, New York 2008).

PHOTOLUMINESCENCE MAPPING OF INGAAS/GAAS MULTI-QUANTUM WELL SYSTEM FOR VECSEL FABRICATION

Andrea Zelioli¹, Arnas Pukinskas¹, Silvija Keraitytė¹, Augustas Vaitkevičius^{1,4}, Sandra Stanionytė², Monika Jokubauskaitė¹, Bronislovas Čechavičius¹, Aurimas Čerškus³, Evelina Dudutienė¹, Renata Butkutė^{1,4}

¹ Department of Optoelectronics, Center for Physical Sciences and Technology, Vilnius, Lithuania

² Department of Characterisation of Materials Structure, Center for Physical Sciences and Technology, Vilnius, Lithuania

³ Laboratory of Electronic Processes, Center for Physical Sciences and Technology, Vilnius, Lithuania

⁴ Institute of Photonics and Nanotechnology, Faculty of Physics, Vilnius University, Vilnius, Lithuania
andrea.zelioli@ftmc.lt

Vertical-external-cavity surface-emitting lasers (VECSEL) also called optically pumped semiconductor lasers (OPSL) or semiconductor disk laser (SDL) belong to relatively new laser family that combines many of the desirable properties.

VECSELS were developed to overcome key problems typical to conventional semiconductor lasers. In comparison to both types of electrically pumped vertical-cavity surface-emitting lasers (VCSELS), which emit circular fundamental transverse mode beam but exhibit low power and edge emitting lasers (Fabry-Perot and DFB) that can reach high output power but an asymmetric beam with strong angular divergence, VECSELS are capable to generate high optical power with circular beam quality [1].

The output power of such structures is proportional to the area of the emitting surface. Thus, it is very important to grow large area samples of the highest optical uniformity [2]. For this reason, it is necessary to achieve high crystalline quality. In homogeneity, sharpness of interfaces, smooth surface and minimum density of both dislocations and non-radiative recombination centers.

In this work InGaAs/GaAs multiple quantum well structures were grown on semi-insulating GaAs substrate using molecular beam epitaxy technique. MQW structures were targeted to 976 nm operation wavelength. To keep strain balance the investigation and optimization was performed by varying the In content and well thickness. The In content in the QW was varied from 18% to 24.5% and the QW thickness was selected from the range of 3.5-7 nm. Two types of MQWs structures were grown: Fig.1(i) to reach target wavelength simple structures of twelve QW with narrow GaAs barriers of 7 nm were fabricated, Fig.1(ii) for detailed investigation MQW structures containing six double-QW (like in (i) type) separated by wider GaAs barriers of order of hundred nanometers (modelled MQW geometry for VECSEL) were grown.. Both types of MQW were studied by HR-XRD to evaluate In content and period of QW and barrier, and to evidence the strain balance. The surface roughness was investigated using AFM. The optical homogeneity of $\frac{1}{4}$ of 2 inches samples was measured by mapping of PL on a single wavelength corresponding to the maximum of the PL intensity. The effect of different quantum wells design, QW thickness and In content in the well was investigated.

This research was supported by Research Council of Lithuania under grant No. S-MIP-22-86 (LMTLT) "A3B5 Nanostructure-Based Near Infrared Lasers".

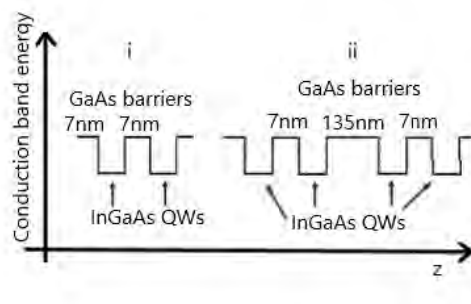


Fig. 1. Two types of quantum well investigated. i) The couple of wells was repeated 6 times to obtain 12 wells in total. ii) This structure was repeated 3 times to obtain 12 wells in total.

[1] Guina, M., A. Rantamäki, and Antti Härkönen. "Optically pumped VECSELS: review of technology and progress." *Journal of Physics D: Applied Physics* 50.38 (2017): 383001.

[2] Seurin, Jean-Francois, et al. "Progress in high-power high-efficiency VCSEL arrays." *Vertical-Cavity Surface-Emitting Lasers XIII*. Vol. 7229. SPIE, 2009.

THE DEPENDANCE OF MAGNETO-OPTICAL SIGNALS ON THE RELATIVE PUMP-PROBE BEAM INTENSITY IN Cs ATOMS FOR ZERO MAGNETIC FIELD DETECTION

A. Nikolajevs¹, A. Mozers¹, L. Busaite¹, D. Osite¹, F. Gahbauer¹, M. Auzinsh¹

¹ Laser Centre, University of Latvia, Raina Boulevard 19, LV-1586 Riga, Latvia
antons.nikolajevs@lu.lv

Magneto-optical signals in a caesium vapour cells can be used for extremely precise magnetic field measurement in 3D [1]. We present experimental results based on angular momentum alignment precession in atomic caesium. The linearly polarized pump beam passing through the cell in the direction \vec{k}_p creates an aligned state in caesium ground state along \vec{E}_p . As an external magnetic field is applied (\vec{B}_x or \vec{B}_y), the distribution of angular momentum precesses about the applied field axis. This change in the distribution of angular momentum can be probed by low-intensity linearly polarized (\vec{E}_x or \vec{E}_y) probe beam with its polarization at a 45 degree angle with respect to the pump beam polarization (\vec{E}_p) and in a plane perpendicular to the applied magnetic field. This pump-probe geometry (see Fig. 1 (a)) is based on [2]. The probe beam transmission signals show strong dispersion-like dependence on the applied magnetic field when the pump beam is on.

The dependence of transmission signals on pump beam intensity and laser frequency as well as beam diameter was studied. We found that the shape of the transmission signal also has strong dependence on the probe beam intensity (see Fig. 1 (b)) as it perturbs the aligned state created by the pump beam. Nevertheless, the experimental results are in agreement with the numerically simulated signals.

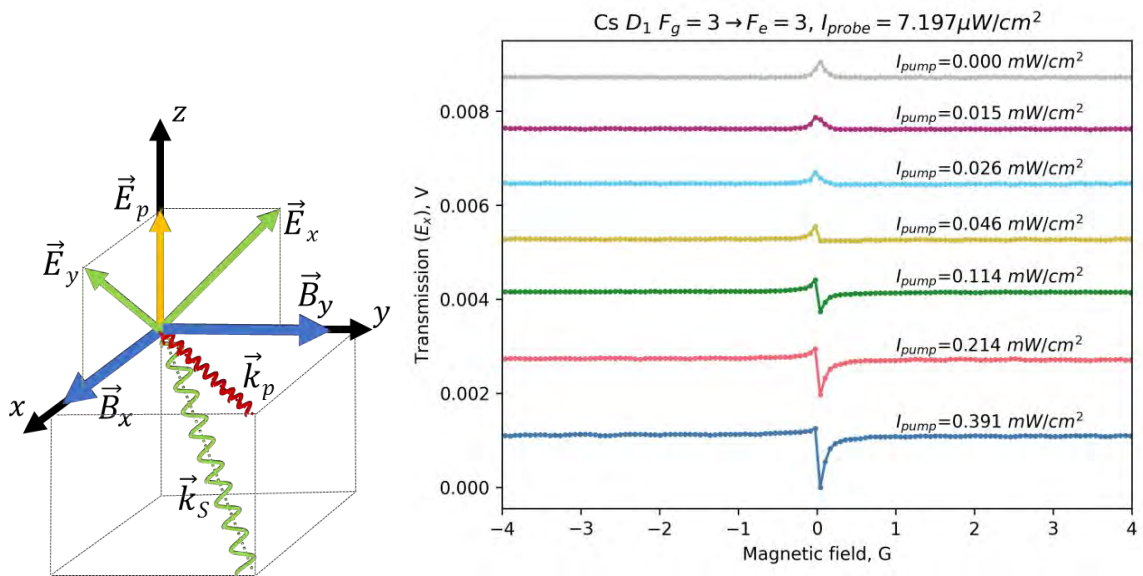


Fig. 1. (a) Pump-probe geometry for obtaining dispersive signals. (b) Signal dependence on the pump beam power with fixed probe beam intensity.

We acknowledge the support from the Latvian Council of Science, project No. lzp-2020/1-0180: “Compact 3-D magnetometry in Cs atomic vapor at room temperature”.

[1] Patton, B., et al. "All-optical vector atomic magnetometer." Physical review letters 113.1 (2014): 013001

[2] G. Le Gal, G. Lieb, F. Beato, T. Jager, H. Gilles, and A. Palacios-Laloy, Phys. Rev. Appl. 12, 064010 (2019)

THIN MICROWAVE ANTENNA DESIGN FOR WIDE FREQUENCY RANGE OPTICALLY DETECTED MAGNETIC RESONANCE MEASUREMENTS

Emils Smits, Reinis Lazda, Florian Gahbauer and Marcis Auzinsh

Laser Centre, University of Latvia, Jelgavas street 3, LV-1004, Riga, Latvia
emils.smits@lu.lv

To use the favorable magnetic field sensing properties of nitrogen-vacancy (NV) centers in diamond the ground state electronic spin energy levels need to be manipulated (with a green laser and electromagnetic radiation in the microwave frequency range), which can be done by using the method of optically detected magnetic resonance (ODMR) [1]. To increase the efficiency of microwave delivery to NV centers in a diamond, a microwave antenna that is capable of creating a region with a uniform magnetic flux density distribution, generating microwaves with a specific polarization, that has a resonant frequency of about 2.87 GHz and also has a wide enough bandwidth for effective operation in dual-resonance magnetometry [2] can be used.

Previously, in most cases, this task was achieved by using a simple coil or wire antenna that could reach varying degrees of efficiency. In recent years, however, there has been an increasing number of studies with more “intelligent” types of antennas for applications in NV center experiments. Using a method from one such study [3] we are designing a new antenna, shown in Fig. 1a, for use in NV center based magnetometry experiments.

In this work, we are using COMSOL multiphysics software to model antenna prototypes and examine the relationships between the geometrical parameters (see Fig. 1b) of the antenna and its electromagnetic properties such as resonant frequency and bandwidth which are seen in expressions (1) and (2) respectively [3]. This knowledge will be essential for creating a new antenna design that meets the desired specifications for microwave polarization, frequency bandwidth and efficiency (see Fig. 2).

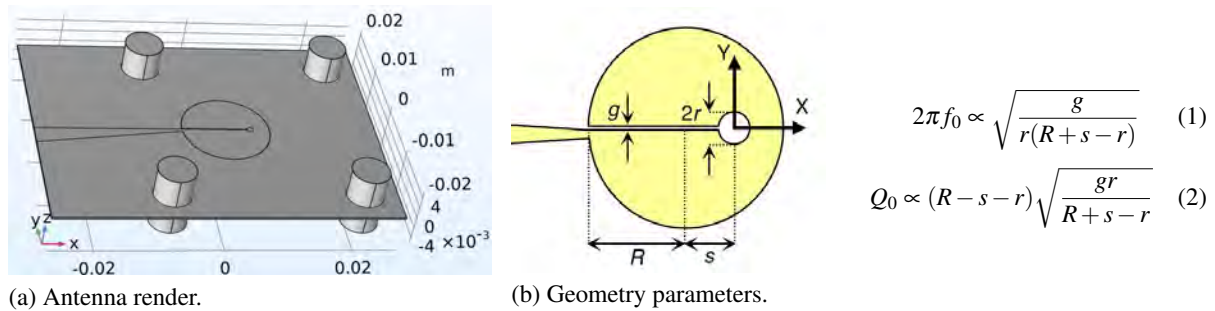


Fig. 1. Antenna design and geometry parameters.

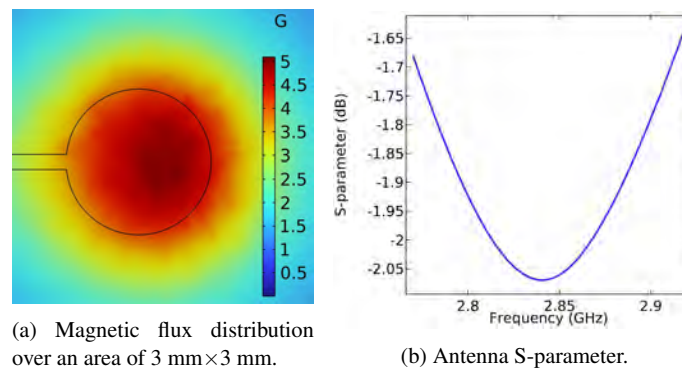


Fig. 2. Microwave antenna simulation results.

We acknowledge the support from the Latvian Council of Science, project No. lzp-2021/1-0379: “A novel solution for high magnetic field and high electric current stabilization using color centers in diamond”.

-
- [1] M. Auzinsh, A. Berzins, D. Budker, L. Busaite, R. Ferber, F. Gahbauer, R. Lazda, A. Wickenbrock, and H. Zheng, 10.1103/PhysRevB.100.075204 (2019).
 [2] Ilja Fescenko, Andrey Jarmola, Igor Savukov, Pauli Kehayias, Janis Smits, Joshua Damron, Nathaniel Ristoff, Nazanin Mosavian, and Victor M. Acosta, doi.org/10.1103/PhysRevResearch.2.023394 (2020).
 [3] K. Sasaki, Y. Monnai, S. Saijo, R. Fujita, H. Watanabe, J. Ishi-Hayase, K.M. Itoh, and E. Abe, 10.1063/1.4952418 (2016).

APPLICATION OF A NV BASED MAGNETOMETER AS A HIGH DC CURRENT SENSOR

Antra Asare, Reinis Lazda, Oskars Rudzitis, Florian Gahbauer, and Marcis Auzinsh

Laser Centre, University of Latvia, Jelgavas street 3, LV-1004, Riga, Latvia
antra.asare@lu.lv

Nitrogen-vacancy (NV) color centers in diamond crystals exhibit unique quantum properties that make them suitable for a wide range of technological applications, including precise measurements of magnetic fields. NV centers have triplet ground and excited states, which undergo Zeeman splitting in a magnetic field and exhibit dynamics that allow the ground state to be polarized to the spin-zero state through optical pumping (Fig. 1. (Left)) [1]. The transition energy of the electron-spin magnetic sublevels can be directly measured using the method of optically detected magnetic resonance [2].

The aim of the work described here is to create a prototype device for high DC current stabilization. The basis of the device is NV magnetometry with a diamond containing NV centers as the probe for a feedback loop for a power supply (Fig. 1. right). This approach is significantly different from existing methods, because it offers a wide dynamic range, high sensitivity and measurement rate (bandwidth) allowing for a compact, energy efficient, lightweight device.

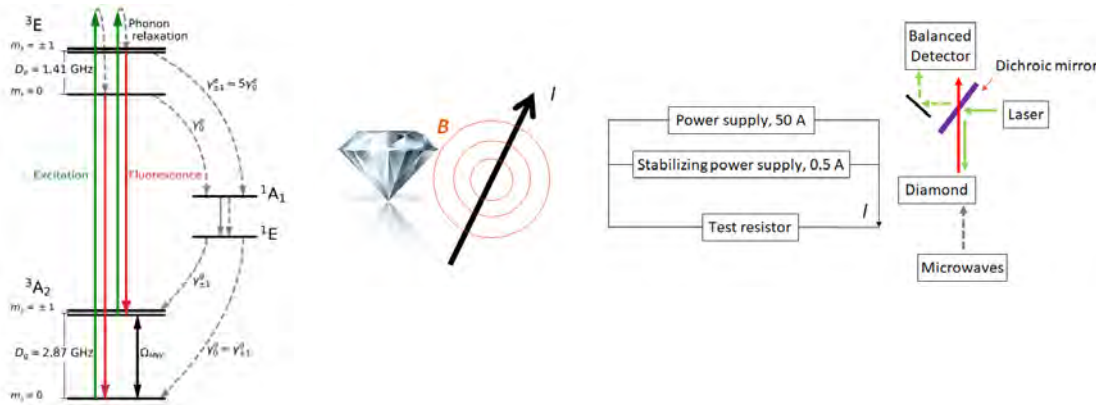


Fig. 1. (Left) Energy level scheme for an NV center in diamond [2] where m_S is the electron spin projection quantum number, D_g and D_e are the ground and excited-state zero-magnetic-field splittings. (Right) Experimental setup.

One of the key challenges for NV based magnetometers is achieving a high enough magnetic field sensitivity, in this case, to measure changes in the current flowing through a wire with a high enough accuracy. Therefore, optimal engineering design and power parameters play a major role in a successful implementation. The magnetic field sensitivity achieved in this work at the moment is $30 \text{ nT/Hz}^{1/2}$ for measurement frequencies above 90 Hz (Fig. 2.), using 110 mW laser power, 100 mW microwave power and a dual-resonance modulation technique [3].

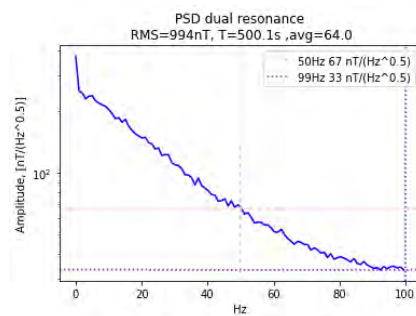


Fig. 2. Magnetic field sensitivity up to 100 Hz of measurement rate.

We acknowledge the support from the Latvian Council of Science, project No. lzp-2021/1-0379: “A novel solution for high magnetic field and high electric current stabilization using color centers in diamond”.

[1] L. Busaite, R. Lazda, A. Berzins, M. Auzinsh, R. Ferber, and F. Gahbauer, doi.org/10.1103/PhysRevB.102.224101 (2020).
 [2] M. Auzinsh, A. Berzins, D. Budker, L. Busaite, R. Ferber, F. Gahbauer, R. Lazda, A. Wickenbrock, H.Zheng, 10.1103/PhysRevB.100.075204 (2019).
 [3] I. Fescenko, A. Jarmola, I. Savukov, P. Kehayias, J. Smits, J. Damron, N. Ristoff, N. Mosavian, and Victor M. Acosta, doi.org/10.1103/PhysRevResearch.2.023394 (2020).

COMPLEX S_3 -SYMMETRIC THREE-HIGGS-DOUBLET MODELS

Anton Kuncinas¹, Odd Magne Øgreid², Per Osland³, Margarida Nesbitt Rebelo¹

¹Centro de Física Teórica de Partículas – CFTP and Dept de Física Instituto Superior Técnico – IST, Universidade de Lisboa, Av. Rovisco Pais, P-1049-001 Lisboa, Portugal

²Western Norway University of Applied Sciences, Postboks 7030, N-5020 Bergen, Norway

³Department of Physics and Technology, University of Bergen, Postboks 7803, N-5020 Bergen, Norway
anton.kuncinas@tecnico.ulisboa.pt

It is by now established that the Standard Model (SM) of Particle Physics cannot be the final theory. In fact, on the one hand the SM leaves several questions open and on the other hand there is already clear evidence for physics beyond the SM. The phenomenon of neutrino oscillations requires the extension of the leptonic sector of the SM. Accounting for the observed baryon asymmetry of the Universe requires new sources of CP violation [1]. Furthermore, there are by now several experimental anomalies in the flavour sector hinting at the existence of new physics [2, 3].

There are strong motivations to consider multi-Higgs extensions of the SM, despite the fact that the properties of the Higgs boson discovered in 2012 are still in experimental agreement with the SM Higgs predictions [4, 5]. Among these motivations are the possibility of having new sources of CP violation. CP violation plays a very important role in nature with implications both for Particle Physics and for Cosmology. Accounting for the observed matter anti-matter asymmetry of the Universe requires the existence of new sources of CP violation beyond the SM. In models with an extended scalar sector CP violation can emerge either explicitly, i.e., at the Lagrangian level, or spontaneously. Spontaneous CP violation occurs in the framework of the electroweak symmetry breaking whenever the Lagrangian conserves CP and the vacuum breaks it. This requires that not all vacuum expectation values be real. In the context of multi-Higgs extensions of the SM imposing the existence of a scalar basis where all couplings are real is a sufficient condition for CP to be explicitly conserved. In the case of spontaneous CP breaking the complex parameters of the Cabibbo–Kobayashi–Maskawa matrix would be generated through phases of the vacuum expectation values of Higgs fields.

Among the simplest extensions of the SM are the so-called two-Higgs-doublet models (2HDM) [6], in which a second SU(2) scalar doublet with the same quantum numbers as the one of the SM is introduced, allowing for explicit CP violation in the scalar sector. The CP properties and cosmological implications of 2HDM have been extensively studied and are still of great interest. Despite the rich phenomenology of 2HDM, models with three Higgs doublets are attracting a lot of interest in the literature. Within three-Higgs-doublet models (3HDM) it is possible to have an additional source of CP violation in the scalar sector while at the same time having natural flavour conservation [7]. The predictability of models with several SU(2) scalar doublets can be quickly lost due to the rapid growth of free parameters as the number of doublets increases. Therefore, it is essential to control the number of free parameters by means of symmetries [8]. It was found that in many cases imposing additional symmetries to multi-Higgs models eliminates the possibility of having CP violation in the Higgs sector.

We study the CP properties of the S_3 -symmetric 3HDM allowing for complex couplings in the potential. The case of real couplings was studied before in Ref. [9]. With real couplings CP is explicitly conserved by the scalar potential and there is only the possibility of having spontaneous CP violation for special vacua. Different vacua correspond to different regions of parameter space which are determined by imposing the minimisation conditions. In the case of complex couplings some of the CP conserving vacua structures of the real potential now correspond to regions of parameter space that allow for explicit CP violation. For instance, CP can be explicitly violated even in the case where the vacuum preserves the S_3 symmetry.

In order to understand what are the possible sources of CP violation in the Yukawa sector we analyse the implications of the different available choices of representations for the quarks under the S_3 group. This classification is based strictly on the exact S_3 -symmetric scalar potential with no soft symmetry breaking terms. The scalar sector of one such model was explored numerically. After applying the theoretical and the most important experimental constraints the available parameter space is shown to be able to give rise to light neutral scalars at the $\mathcal{O}(\text{MeV})$ scale.

-
- [1] M. B. Gavela, P. Hernandez, J. Orloff and O. Pene, *Mod. Phys. Lett. A* **9** (1994), 795-810 doi:10.1142/S0217732394000629 [arXiv:hep-ph/9312215 [hep-ph]].
- [2] E. Graverini [ATLAS, CMS and LHCb], *J. Phys. Conf. Ser.* **1137** (2019) no.1, 012025 doi:10.1088/1742-6596/1137/1/012025 [arXiv:1807.11373 [hep-ex]].
- [3] E. Kou *et al.* [Belle-II], *PTEP* **2019** (2019) no.12, 123C01 [erratum: *PTEP* **2020** (2020) no.2, 029201] doi:10.1093/ptep/ptz106 [arXiv:1808.10567 [hep-ex]].
- [4] [CMS], *Nature* **607** (2022) no.7917, 60-68 doi:10.1038/s41586-022-04892-x [arXiv:2207.00043 [hep-ex]].
- [5] [ATLAS], *Nature* **607** (2022) no.7917, 52-59 [erratum: *Nature* **612** (2022) no.7941, E24] doi:10.1038/s41586-022-04893-w [arXiv:2207.00092 [hep-ex]].
- [6] G. C. Branco, P. M. Ferreira, L. Lavoura, M. N. Rebelo, M. Sher and J. P. Silva, *Phys. Rept.* **516** (2012), 1-102 doi:10.1016/j.physrep.2012.02.002 [arXiv:1106.0034 [hep-ph]].
- [7] S. Weinberg, *Phys. Rev. Lett.* **37** (1976), 657 doi:10.1103/PhysRevLett.37.657
- [8] I. P. Ivanov and E. Vdovin, *Eur. Phys. J. C* **73** (2013) no.2, 2309 doi:10.1140/epjc/s10052-013-2309-x [arXiv:1210.6553 [hep-ph]].
- [9] D. Emmanuel-Costa, O. M. Og Reid, P. Osland and M. N. Rebelo, *JHEP* **02** (2016), 154 [erratum: *JHEP* **08** (2016), 169] doi:10.1007/JHEP08(2016)169 [arXiv:1601.04654 [hep-ph]].

MAGNETIC PROPERTIES OF L₁₀ FENI THIN FILMS WITH SURFACES (010), (111), AND (001): DENSITY FUNCTIONAL THEORY CALCULATIONS

Joanna Marciniak, Mirosław Werwiński

Institute of Molecular Physics, Polish Academy of Sciences, M. Smoluchowskiego 17, 60-179 Poznań, Poland
joanna.marciniak@ifmpan.poznan.pl

The growing demand for strong permanent magnets such as neodymium magnets and the volatile prices of rare earth elements are stimulating the search for new hard magnetic materials that do not contain rare earth elements. At the same time, the increasing miniaturization of electronic circuits, evident in today's processors, is directing researchers' attention to structures on the order of nanometres in size, whose properties can differ significantly from those of bulk macroscopic materials. In this context, many systems are considered, such as Fe_{1-x}Co_x alloys, iron-based L₁₀ phases: FePt and FeNi, or L₁₀ CoPt [1, 2].

Experimental and computational studies of ordered L₁₀ FeNi thin films [3, 4] indicate that the L₁₀ FeNi phase in the form of ultrathin films exhibits magnetic properties that allow potential applications. We decided to take another look at this material, and more specifically, the thin layers made of it with the surfaces (111), (010), and (001). For this purpose, we performed quantum calculations based on the full-potential local-orbital (FPLO) method using the density functional theory (DFT) implemented in the FPLO18 code [5].

Our research allowed us to determine the preferred direction of magnetization easy-axis in the considered systems. We also investigated changes in this direction as a function of film thickness. In the case of the systems with the surface (111), the deflection of the magnetization easy-axis from the [001] direction was observed, depending on the number of monolayers of the tested system. In addition, we determined changes in magnetic moments and energy differences of systems with magnetization consistent with particular crystallographic directions as a function of layer thickness.

The computational results obtained still require experimental confirmation. However, the predicted magnetization configurations, for example, in the direction oblique to the plane of the layer, may find applications in electronic devices.

We acknowledge the financial support of the National Science Centre Poland under DEC-2018/30/E/ST3/00267.

-
- [1] R. Skomski and J. M. D. Coey, *Magnetic anisotropy — How much is enough for a permanent magnet?*, *Scr. Mater.* **112**, 3 (2016)
 - [2] J. Marciniak, W. Marciniak, and M. Werwiński, *DFT calculation of intrinsic properties of magnetically hard phase L₁₀ FePt*, *J. Magn. Magn. Mater.* **556**, 169347 (2022)
 - [3] M. Ogiwara, S. Iihama, T. Seki, T. Kojima, S. Mizukami, M. Mizuguchi, and K. Takanashi, *Magnetization damping of an L₁₀-FeNi thin film with perpendicular magnetic anisotropy*, *Appl. Phys. Lett.* **103**, 242409 (2013)
 - [4] M. Werwiński and W. Marciniak, *Ab initio study of magnetocrystalline anisotropy, magnetostriction, and Fermi surface of L₁₀ FeNi (tetrataenite)*, *J. Phys. D: Appl. Phys.* **50**, 495008 (2017)
 - [5] K. Koepf and H. Eschrig, *Full-potential nonorthogonal local-orbital minimum-basis band-structure scheme*, *Phys. Rev. B* **59**, 1743 (1999)

TOPOLOGICAL CHARGE PUMPING IN SUBWAVELENGTH OPTICAL LATTICES

Domantas Burba¹, Mantas Račiūnas¹, Ian B. Spielman², Gediminas Juzeliūnas¹

¹Institute of Theoretical Physics and Astronomy, Vilnius University, Lithuania

²Joint Quantum Institute, University of Maryland, USA

domantas.burba@ff.vu.lt

Ultracold atoms in optical lattices represent a unique platform for simulating various condensed matter phenomena as well as realizing paradigmatic models. However, conventional optical lattices for ultra-cold atoms rely on the AC Stark shift to produce a potential proportional to the local optical intensity. As a direct result, the lattice period cannot be smaller than half the optical wavelength λ . Recently, two techniques have emerged to create deeply sub-wavelength lattices [1, 2, 3]; both can be understood in terms of “dressed states” created by coupling internal atomic states with one- or two-photon optical fields.

Here we focus on a scheme, relying on sequentially coupling N internal atomic states using two photon Raman transitions. This results in an adiabatic potential for each of the N dressed states, displaced by $\lambda/2N$ from each other. We show that adding temporal modulation to the detuning from Raman resonance can couple the s and p bands of adjacent lattice sites belonging to different dressed states. In the tight-binding limit, this gives rise to a pair of coupled Rice-Mele (RM) chains with new regimes of topological charge pumping. The present study opens new possibilities in studying the topological properties of subwavelength optical lattices induced by periodic driving.

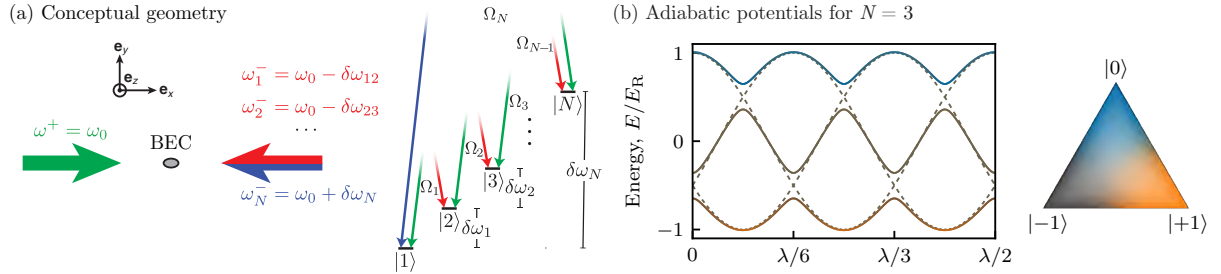


Fig. 1. Lattice concept. (a) Representative experimental geometry with a single frequency Raman beam traveling along \mathbf{e}_x and N beams sharing the same spatial mode traveling along $-\mathbf{e}_x$. The level diagram for cyclic coupling is depicted on the right. (b) Dressed state energies for $N = 3$. The dashed curves are computed for $\Omega_j = E_R$ and the colored curves are computed with a non-zero detuning.

[1] R. P. Anderson, D. Trypogeorgos, A. Valdés-Curiel, Q.-Y. Liang, J. Tao, M. Zhao, T. Andrijauskas, G. Juzeliūnas, and I. B. Spielman, *Phys. Rev. Research* **2**, 013149 (2020).

[2] T.-C. Tsui, Y. Wang, S. Subhankar, J. V. Porto, and S. L. Rolston, *Phys. Rev. A* **101**, 041603 (2020).

[3] Y. Wang, S. Subhankar, P. Bienias, M. Łacki, T.-C. Tsui, M. A. Baranov, A. V. Gorshkov, P. Zoller, J. V. Porto, and S. L. Rolston, *Phys. Rev. Lett.* **120**, 083601 (2018).

EXCITED STATES OF CHLOROPHYLL MOLECULES IN LIGHT-HARVESTING ANTENNA OF PSI

Gabrielė Rankelytė^{1,2}, Jevgenij Chmeliov^{1,2}, Andrius Gelzinis^{1,2}, Leonas Valkunas^{1,2}

¹Institute of Chemical Physics, Faculty of Physics, Vilnius University, Lithuania

²Department of Molecular Compound Physics, Centre for Physical Sciences and Technology, Vilnius, Lithuania
gabriele.rankelyte@ff.stud.vu.lt

Photosynthesis is one of the most important processes on Earth. The most efficient organisms that carry out photosynthesis are land plants or higher plants. In thylakoid membrane of chloroplasts there are two systems that carry out photosynthesis – Photosystem I (PSI) and Photosystem II (PSII), both with their own light harvesting complexes - LHCI and LHCII. PSI is the most efficient light-to-energy conversion apparatus with quantum yield almost equal to 1 [1]. One of the conditions needed for high efficiency is very fast energy transfer between molecules in light harvesting complex. The excitation dynamics in LHCI is highly affected by the charge-transfer (CT) states that occur between two or more pigments (chlorophylls or carotenoids). Some sites in which CT states occur in LHCI are known, however, they do not completely explain the spectral properties of this antenna, such as the red-shifted peak in fluorescence spectrum.

Light-harvesting complex of PSI absorbs and emits light at the longest wavelengths compared to other pigment-protein complexes. In plants light harvesting antenna of PSI is composed of four species of LHCI complexes. They all have very similar structure, however, their spectral properties are different. The most red-shifted peak (at around 733 nm) is observed in the fluorescence spectrum of Lhca4 light harvesting sub-complex [2].

The structure of Lhca4 was obtained as the 4th chain of PSI supercomplex structure, freely accessible on Protein Data Bank (PDB) [3]. In order to find possible locations of the charge-transfer states in Lhca4, we examined chlorophyll dimers that have the shortest (up to 12 Å) Mg-Mg distance. After performing geometry optimization of selected individual chlorophylls, whose phytol tail was removed for computing time saving reasons, they were mapped on the Lhca4 structure to form dimers (as shown in Fig. 1). We then examined the excited states properties of all selected dimers in vacuum. An excited state is considered to be a charge-transfer state if it exhibits relatively small absolute value of transition from the ground to the excited state dipole moment and large static electric dipole moment value. The sum of partial Mulliken charges for a dimer in charge-transfer state is approximately equal to 1 for one pigment and to -1 for another. Therefore, it was also used to indicate the CT states. After analyzing the data of 12 chosen dimers and their 8 lowest excited states, 19 charge-transfer states were located.

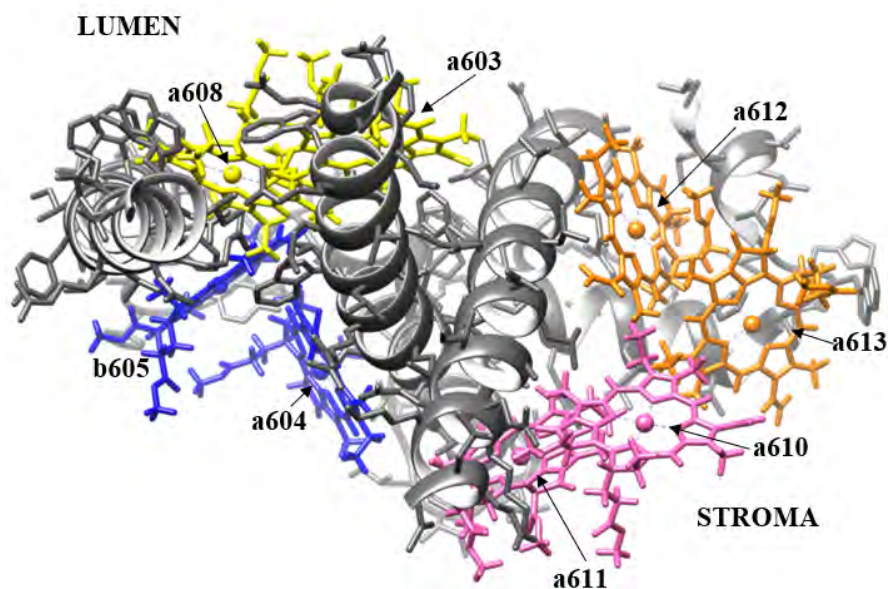


Fig. 1. Lhca4 complex. Amino acids are presented in gray, carotenoids are not in the picture. The four dimers of chlorophylls (without the phytol tail) are indicated in the figure.

[1] R. Croce and H. van Amerongen, Light-harvesting in Photosystem I, *Photosynthesis Research* **116**, 153-166 (2013).

[2] T. Morosinotto et al., Pigment-pigment interactions in Lhca4 antenna complex of higher plants Photosystem I, *Journal of Biological Chemistry* **280**, 20612-20619 (2005).

[3] X. Qin et al., Structural basis for energy transfer pathways in the plant PSI-LHCI supercomplex, *Science* **348**, 989-995 (2015).

KINETICS OF THE CONFORMATIONAL CHANGES OF THE NITROGEN MATRIX ISOLATED DISUBSTITUTED SILACYCLOHEXANES: EXPERIMENT MEETS THEORY AT FINITE TEMPERATURE RANGE

Joanna Stocka¹, Pawel Rodziewicz², Valdas Sablinskas¹, Gamil A. Guirgis³

¹ Institute of Chemical Physics, Vilnius University, Saulėtekio al. 3, 10257 Vilnius, Lithuania

² Institute of Chemistry, Jan Kochanowski University, 15G Świętokrzyska St., 25-406, Kielce, Poland

³ Department of Chemistry and Biochemistry, College of Charleston, Charleston, SC 29424, USA

joana.stocka@gmail.com

Organosilicon compounds find a usage in the field of surface science due to its good surface adhesion properties which are mostly related to a π electron orbital [1]. The substitution of the carbon atom in the ring with a silicon atom enhances adhesion since it acts as hydrolytically sensitive center that can react with inorganic substrates such as glass to form stable covalent bonds [2]. 1-chloromethyl-1-fluorosilacyclohexane and 1-chloro-1-chloromethylsilacyclohexane were newly synthesized molecular compounds with unknown structural parameters and conformational diversity. In our previous works the detailed conformational, structural and spectroscopic analysis of the latter mentioned molecules is presented. [3, 4] The next step is theoretical studies of the dynamical structural changes and lifetime of different conformers at finite temperature with the help of Car-Parrinello molecular dynamics simulations.

Car-Parrinello molecular dynamics simulations have been performed with PBE functionals, DFT (PW), Nosé-Hoover chain thermostats, temperature was set to 20, 50 and 70 K (to mimic experimental conditions), the production run of 200 ps was derived utilizing the CPMD program package.

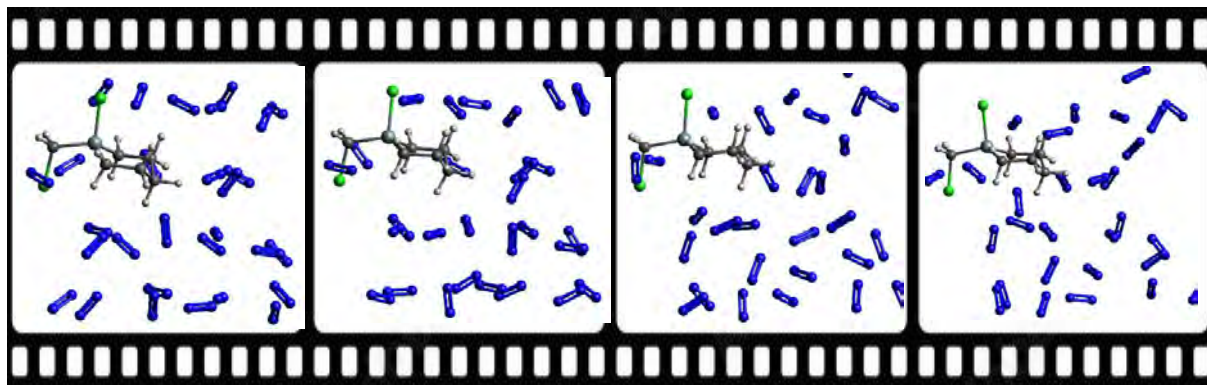


Fig. 1. Snapshots from the CPMD simulations at 20K for 1-Chloro-1-Chloromethyl-1-silacyclohexane.

In the matrix the molecule remains in the global energy minimum structure (chair axial trans), the structural parameters and the interaction with the matrix were traced by Radial Pair Distribution Function and bond distance analysis.

The biggest advantage of the Molecular Dynamics Simulations is that they explicitly describe the experimental conditions, due to the temperature influence. The static calculations in most cases, describe the isolated molecules without taking into account the temperature impact. This is a huge step in the computational description of the experimental conditions. Despite the fact the molecule does not undergo any conformational changes, the molecule – matrix interactions were traced.

[1] H. Butt, K Graf, M. Kappl, *Physics and Chemistry of Interfaces*, Wiley, 2003

[2] J. Ceponkus, V. Sablinskas, V. Aleksa, M. Pucetaite, R. PlatakYTE, C.W. Reed, C. Cotter, G. Guirgis, *Vibrational Spectroscopy*, 81, 136-143, 2015

[3] T.M.C. McFadden, R. PlatakYTE, J. Stocka, J. Ceponkus, V. Aleksa, T. Carrigan-Broda, V. Sablinskas, P. Rodziewicz, G.A. Guirgis, Experimental (Raman and IR) and computational (DFT, MP2) studies of conformational diversity of 1-chloromethyl-1-fluorosilacyclohexane, *Journal of Molecular Structure*, 1221 (2020).

[4] J. Stocka, R. PlatakYTE, T.M.C. McFadden, J. Ceponkus, V. Aleksa, A.G. Hanna, V. Sablinskas, P. Rodziewicz, G.A. Guirgis, Conformational diversity of 1-chloro-1-chloromethylsilacyclohexane with experimental (Raman and IR) and computational (DFT, MP2) methods, *Journal of Molecular Structure*, 1249 (2022).

SOLID STATE NMR SPECTROSCOPY STUDY OF CALCIUM PYROPHOSPHATE ($\text{Ca}_2\text{P}_2\text{O}_7$) POLYMORPHS EXPOSED TO X-RAY RADIATION

Aurimas Dubauskas¹, Diana Griesiūtė², Andris Antuzevics^{2,3}, Aleksej Žarkov², Vytautas Klimavičius¹

¹ Institute of Chemical Physics, Faculty of Physics, Vilnius University, Lithuania

² Institute of Chemistry, Vilnius University, Lithuania

³ Institute of Solid State Physics, University of Latvia, Latvia

aurimas.dubauskas@ff.stud.vu.lt

Calcium phosphates (CaPs) are a versatile family of materials most widely used as bone graft substitutes and for targeted drug delivery in biomedical fields [1], in creation of sensors for direct detection of phosphate in aqueous solutions [2], in water purification for heavy metals [3], etc. CaPs are known for their biocompatibility, they are also easily and inexpensively produced, are safe, and can be relatively easily certified for clinical use. In the medical field, calcium orthophosphates such as hydroxyapatite (HA, $\text{Ca}_{10}(\text{PO}_4)_6(\text{OH})_2$), tricalcium phosphate (TCP, $\text{Ca}_3(\text{PO}_4)_2$), and amorphous calcium phosphate (ACP) are frequently utilized. Recent studies on biomaterials showed the potential of the use of calcium pyrophosphate (CPP, $\text{Ca}_2\text{P}_2\text{O}_7$) for biomedical applications [4]. We studied α -CPP, β -CPP and γ -CPP polymorphs.

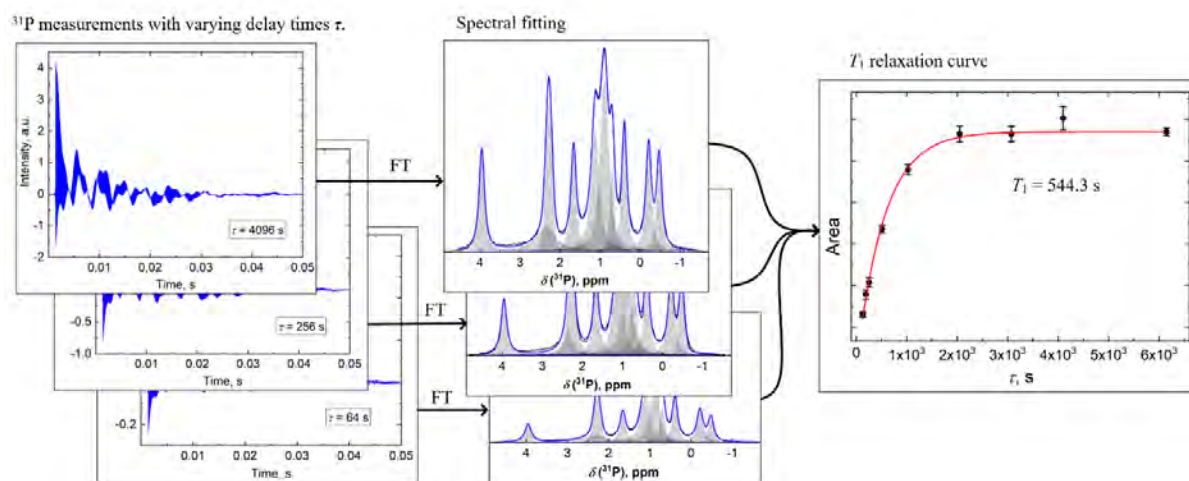


Fig. 1. Visualized procedure of the T_1 relaxation measurement. Left – acquired free induction decays (FID) of the samples. Middle – after Fourier transform (FT) peaks were approximated by theoretical curves. Right – first peak's (3.95 ppm) T_1 relaxation curve and fitting by using Eq. (1) approximation.

$$I(\tau) = I_0 \cdot \exp\left(-\frac{\tau}{T_1}\right) \quad (1)$$

To study CPPs, solid-state nuclear magnetic resonance (NMR) was used. Spin-lattice (T_1) relaxation times were measured using the saturation recovery method. Radiation-exposed CPP samples showed reduced relaxation times. For overlapping peaks spectral fitting using Gauss, Lorentz or Voigt theoretical spectral lines were performed. The overlapping peaks positions were referenced from [5] article. By examining the dependence of relaxation time by exposure time, the structural integrity of CPP polymorphs was evaluated.

[1] Habraken, W., Habibovic, P., Epple, M. & Bohner, M. Calcium phosphates in biomedical applications: Materials for the future? *Mater. Today* 19, 69–87.

[2] Sun, S., Chen, Q., Sheth, S., Ran, G. & Song, Q. Direct electrochemical sensing of phosphate in aqueous solutions based on phase transition of calcium phosphate. *ACS Sensors* 5, 541–548.

[3] Goto, T. & Sasaki, K. Synthesis of morphologically controlled hydroxyapatite from fish bone by urea-assisted hydrothermal treatment and its Sr²⁺ sorption capacity. *Powder Technol.* 292, 314–322.

[4] Kaido Kurrikoff, Birgit Vunk, Ülo Langel. (2021) Status update in the use of cell-penetrating peptides for the delivery of macromolecular therapeutics. *Expert Opinion on Biological Therapy* 21:3, pages 361-370.

[5] Griesiute, D., Garskaite, E., Antuzevics, A. *et al.* Synthesis, structural and luminescent properties of Mn-doped calcium pyrophosphate ($\text{Ca}_2\text{P}_2\text{O}_7$) polymorphs. *Sci Rep* 12, 7116 (2022).

THE MIEYE: BENCH-TOP SUPER-RESOLUTION MICROSCOPE WITH COST-EFFECTIVE EQUIPMENT

Mohammad Nour Alsamsam^{1,2}, Aurimas Kopūstas^{1,2}, Meda Jurevičiūtė², Marijonas Tutkus^{1,2}

¹Department of Molecular Compound Physics, Center for Physical Sciences and Technology, Vilnius, Lithuania.

²Institute of Biotechnology, Life Sciences Center, Vilnius University, Vilnius, Lithuania.

nour.alsamsam@gmail.com

We introduce the miEye platform, a cost-effective microscope with high-resolution wide-field fluorescence imaging capabilities [1]. Advanced super-resolution (SR) imaging devices can be purchased commercially for a high cost. Affordable open-source microscopy systems frequently often support single imaging modularity, fall short of their more high-priced siblings, or lack dedicated software. The miEye design is based on a modular aluminium CNC milled microscope body that can be customized with optomechanical components that are commercially available. The microEye open-source Python package is used for microscope operation, data visualization, and analysis. The microEye utilizes commonly used iCMOS (industrial complementary metal oxide semiconductor) cameras, IR-based automatic focus stabilization, and laser control through an Arduino-based laser relay. The open-source effort seeks to make the super-resolution community's adaption and contribution relatively easy. The system cost can sum up to about 50,000 euros. It features a flexible emission path and two interchangeable excitation regimes (SM-fiber and MM-fiber). The miEye maintains less than 5 nm/min stability of lateral sample drift. After software drift correction, the miEye achieves ~10–40 nm lateral resolution for dSTORM and DNA-PAINT single-molecule localization microscopy (SMLM) experiments. The platform is a versatile and cost-effective addition to the open-source microscopy community that may enable high-quality SR imaging for research groups with limited funding.

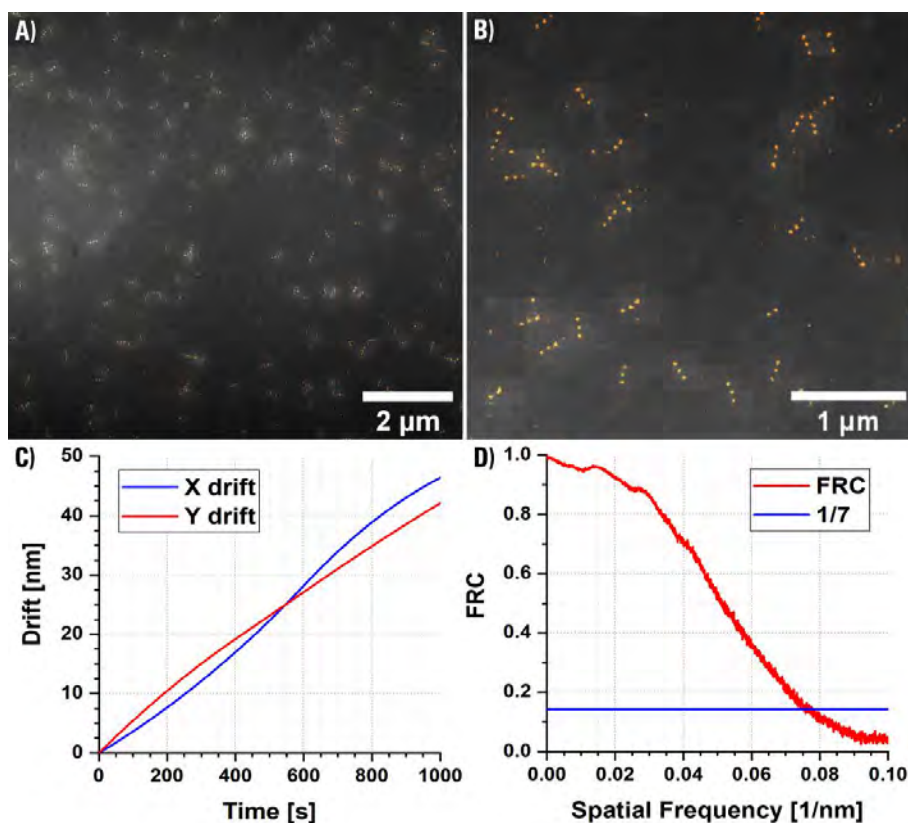


Fig. 1. TIRF microscopy image of sparsely distributed DNA nano-rulers with 80-nm spacing. Three independent imaging experiments under the 638 nm wavelength excitation were done with a similar outcome. A) Larger field-of-view (FOV) conventional TIRF microscopy average stack overlaid with reconstructed super-resolution (SR) image. B) Zoomed image of the larger FOV presented in panel A. C) Graph showing curves of X and Y drift used for drift correction using cross-correlation. D) FRC (Fourier Ring Correlation) curve, which showed a resolution value of 14.3 nm.

[1] M. N. Alsamsam, A. Kopūstas, M. Jurevičiūtė, and M. Tutkus, The miEye: Bench-top super-resolution microscope with cost-effective equipment, *HardwareX*, vol. 12, p. e00368 (Oct. 2022).

ROA-CPL SPECTROSCOPY CAN CLEARLY DISTINGUISH POST-TRANSLATIONAL MODIFICATIONS OF PEPTIDES

Agnieszka Domagała^{1,2}, Grzegorz Zając¹, Małgorzata Barańska^{1,3}

¹ Jagiellonian University, Jagiellonian Centre for Experimental Therapeutics (JCET), Bobrzyńskiego 14, 30-348 Cracow, Poland

² Jagiellonian University, Doctoral School of Exact and Natural Sciences, prof. S. Łojasiewicza 11, 30-348 Cracow, Poland

³ Jagiellonian University, Faculty of Chemistry, Gronostajowa 2, 30-387 Cracow, Poland
domagala.agnieszka@doctoral.uj.edu.pl

Post-translational modifications (PTMs) of proteins are widespread in human organisms and could be the reason for various civilization diseases. Linking the chemical species to the backbone or sidechains of amino acids residues can significantly change the function and dynamic of proteins, and in consequence, lead to health abnormalities. For instance, cardiovascular and neurodegenerative diseases are associated with acetylation, methylation, and glycosylation, and cancers are related to phosphorylation.[1] The study of proteins' PTMs still arouses the interest of researchers looking for new strategies to treat common civilization diseases.

Chiroptical spectroscopy techniques are promising tools to investigate the proteins' PTMs, however, they are rarely used for that aim. Their potential is mainly due to the high sensitivity to even small structural changes in chiral molecules and supramolecular systems (e.g., carotenoid aggregates, protein fibrils), or biological samples (blood serum and plasma). Raman optical activity (ROA), vibrational circular dichroism (VCD), electronic circular dichroism (ECD), and circularly polarized luminescence (CPL) are the most used chiroptical spectroscopies based on different interactions (Raman scattering, absorption, emission) of chiral molecules with the left- and right circularly polarized light.[2]

ROA-CPL spectroscopy is a method that enables the observation of the CPL signal on the ROA spectrum. It uses a lanthanide-based probe due to its unique luminescent properties and abundance of narrow emission bands. The most suitable compounds for that purpose contain europium(III) ion which gives luminescent bands in the ROA/Raman spectrum range (0-2500 cm⁻¹ which equals 532-610 nm). Additionally, the chiral environment of an achiral Eu(III) probe can induce its chirality which manifests as CPL bands of Eu(III) present on the ROA spectrum. Due to the high power of the excitation laser line used in the ROA spectrometer (532 nm), which is matched to the energy of some electronic transitions of Eu(III), the luminescent bands of europium(III) that appeared in the ROA spectrum are strongly enhanced. This approach allows to register the CPL signals which are hard or impossible to measure using a commercial CPL spectrometer.[3]

In this study, we present the first application of ROA-CPL spectroscopy as an excellent tool to distinguish PTMs of glutathione (GSH). The results unambiguously show different CPL patterns for unmodified peptide and for both modification models, even with their small concentrations. It let us expect that ROA-CPL spectroscopy in the use of the Eu(III) probe will be equally effective for the study of more complex protein systems.

This work was supported by National Science Centre in Poland (Grant No. 2019/35/B/ST4/04161 to GZ).

[1] P. Vellosillo, P. Minguez, A global map of associations between types of protein posttranslational modifications and human genetic diseases, *iScience* **24**, 102917 (2021).

[2] L.A. Nafie, Vibrational optical activity: From discovery and development to future challenges, *Chirality* **32**, 667-692 (2020).

[3] T. Wu, A Raman optical activity spectrometer can sensitively detect lanthanide circularly polarized luminescence, *Phys. Chem. Chem. Phys.* **24**, 15672–15686 (2022).

MAPPING VISCOSITIES OF LIPID BILAYERS IN LIVE CELLS AND MODEL MEMBRANES THROUGH FLIM

Artūras Polita¹, Gintaras Valinčius¹

¹ Institute of Biochemistry, Life Sciences Center, Vilnius University, Lithuania
arturas.polita@bchi.stud.vu.lt

Viscosity is the essential physical characteristic of cell membranes – it controls diffusion of lipids and macromolecules, affects the lipid raft formation, and influences the passive transport of solutes across the plasma membrane. Lipid membranes are inherently heterogeneous and are able to phase separate into liquid ordered (Lo) and liquid-disordered (Ld) domains. Viscous Lo phase is of particular biological importance – ordered microdomains of lipids and proteins, so called lipid rafts, play a key role in immune signaling [1,2], host-pathogen interactions [3,4], cardiovascular diseases [5], and cancer [6-8]. Thus, the ability to distinguish Lo and Ld phases and determine their precise viscosity values is of great interest and viscosity-sensitive probes offer a convenient solution for this task.

In this work, we present novel membrane-targeting viscosity probe – BODIPY-PM. Combining the use of BODIPY-PM with Fluorescence Lifetime Imaging Microscopy (FLIM), we demonstrate the ability of BODIPY-PM to recognize Lo and Ld phases in complex biological systems – large unilamellar vesicles (LUVs), tethered bilayer membranes (tBLMs) and live cancer cells (Fig. 1). In addition, we explore the plasma membrane viscosity changes in cells that undergo apoptosis. Importantly, our method allows both imaging and dynamic monitoring of viscosity changes in real time in live cells, as well as model lipid systems.

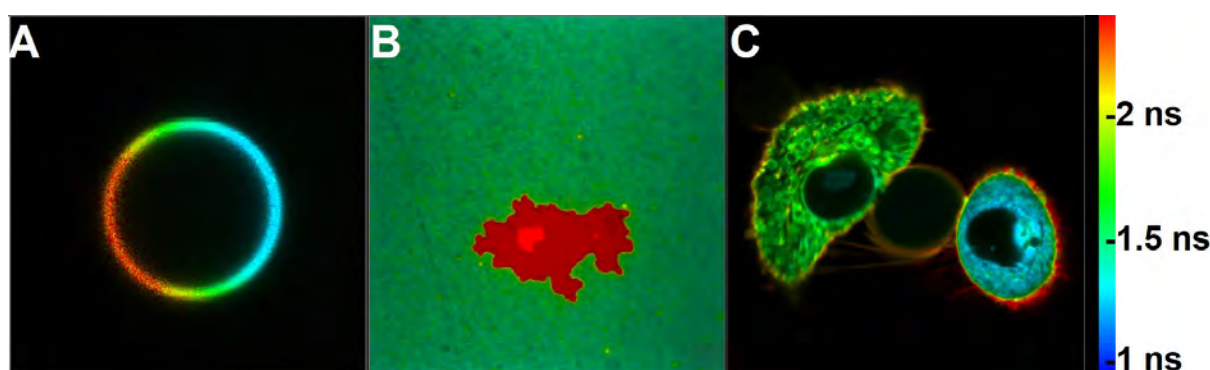


Fig. 1. FLIM images of DOPC/DPPC/Chol LUV showcasing phase separation (A), DOPC/DPPC/Chol tBLM with Lo domain in the center (B), viscosity changes in cancer cells during apoptosis – on the left, and before apoptosis – on the right (C).

- [1] K. A. Field, D. Holowka, B. Baird, Fc epsilon RI-mediated recruitment of p53/56lyn to detergent-resistant membrane domains accompanies cellular signaling, *Proc. Natl Acad. Sci. USA* **92**, 9201-9205 (1995).
- [2] P. Varshney, V. Yadav, N. Saini, Lipid rafts in immune signalling: current progress and future perspective, *Immunology* **149**, 13-24 (2016).
- [3] K. Iwabuchi, Lactosylceramide-enriched Lipid Raft-mediated Infection Immunity, *Front. Biosci.*, **20**, 325-334 (2015).
- [4] E. Teissier, and E. Pecheur, Lipids as modulators of membrane fusion mediated by viral fusion proteins, *Eur. Biophys. J.* **36**, 887-899 (2007).
- [5] F. J. O. Rios, M. Ferracini, M. Pecenin, M. M. Koga, Y. Wang, D. F. J. Ketelhuth, S. Jancar, Uptake of oxLDL and IL-10 Production by Macrophages Requires PAFR and CD36 Recruitment into the Same Lipid Rafts, *PLoS ONE* **8**, e76893 (2013).
- [6] J. B. Larsen, M. B. Jensen, V. K. Bhatia, S. L. Pedersen, T. Bjørnholm, L. Iversen, M. Uline, I. Szleifer, K. J. Jensen, N. S. Hatzakis, and D. Stamou, Membrane Curvature and Lipid Composition Synergize To Regulate N-Ras Anchor Recruitment, *Nat. Chem. Biol.* **11**, 192-194 (2015).
- [7] C. Gajate, and F. Mollinedo, Edelfosine and perifosine induce selective apoptosis in multiple myeloma by recruitment of death receptors and downstream signaling molecules into lipid rafts, *Blood* **109**, 711-719 (2007).
- [8] Á. Cuesta-Marbán, J. Botet, O. Czyz, L. M. Cacharro et al., Drug uptake, lipid rafts, and vesicle trafficking modulate resistance to an anticancer lysophosphatidylcholine analogue in yeast. *Journal of Biological Chemistry*, *J. Biol. Chem.* **11**, 192-194 (2015).

EFFECT OF UV AND IR WAVELENGTHS ON PLASMA CHARACTERISTICS FOR FEMTOSECOND LIBS ON COPPER AND STEEL SAMPLES

Gytis Zaremba¹, Ona Balachninaite¹, Domas Paipulas¹

¹Laser Research Center, Vilnius University, Saulėtekio ave. 10, LT – 10223 Vilnius, Lithuania
gytis.zaremba@ff.vu.lt

Laser induced breakdown spectroscopy (LIBS) is a known method for elemental analysis of various materials, both in-situ and in the laboratory [1]. Using fs pulses for LIBS results in reduced sample damage [2], lower ablation threshold, low continuum emission and better repeatability [3]. An important parameter of LIBS is the wavelength used for plasma generation. The effect of wavelength is thought to be more critical for longer nanosecond pulses, but in the case of fs-LIBS, the laser-matter interaction is different, the pulse duration is much shorter than material heat transfer, plasma forms after the pulse, signifying that there is no shielding of the pulse. However, the dependence on wavelength for fs - LIBS has not been extensively studied.

Femtosecond Yb:KGW laser "Pharos" (Light Conversion Ltd) with pulse duration of 170 fs, 6 kHz repetition rate and up to 6 W of average power was used. Andor Mechelle Spectrograph with an ICCD camera was used to record spectra. The fundamental (1030 nm) and third (343 nm) harmonics were used to determine the effect of source wavelength on LIBS parameters. Energy fluence on the sample was kept constant with both wavelengths. The samples used were O. F. H. C. copper (99.95+% purity) and AISI 301 stainless steel.

Plasma temperature was evaluated at thermal equilibrium using the Boltzmann plot method. 400-800 ns after laser ablation, the plasma temperature was around 9000 K on copper and 8000 K on steel, and there was no difference, within error, between UV and IR wavelengths. Electron density was estimated to be $(1.2 \pm 0.4) \cdot 10^{18} \text{ cm}^{-3}$ on copper sample and $(1.4 \pm 0.4) \cdot 10^{16} \text{ cm}^{-3}$ on steel sample, the use of UV and IR wavelengths resulted in equal densities. Signal-to-noise ratio (SNR) was evaluated for both wavelengths and is shown in Fig. 1. Our experiments showed that fs UV-LIBS in copper and stainless steel samples gives higher SNR than fs IR-LIBS at the same energy fluence.

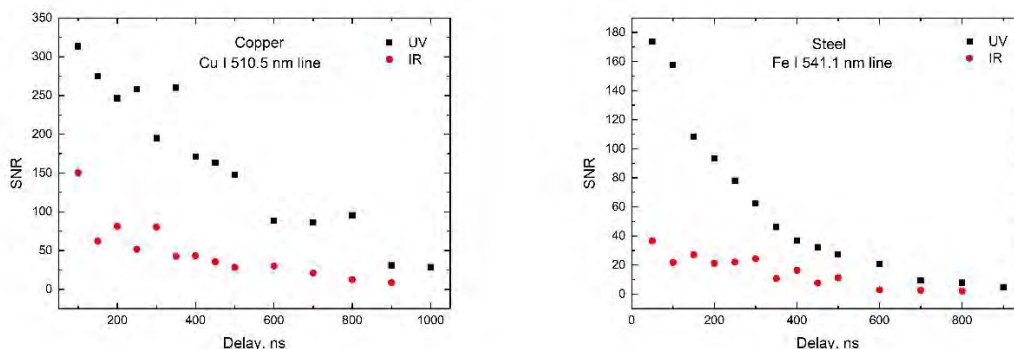


Fig. 1. Comparison of UV and IR LIBS signal to noise ratios of Cu I 510.5 nm (on the left) and Fe I 541.1 nm (on the right) spectral lines.

Acknowledgments

This work has received funding from European Regional Development Fund (project 01.2.2-LMT-K-718-03-0029) under grant agreement with the Research Council of Lithuania (LMTLT).

[1] Santagata, A. et al. fs/ns dual-pulse LIBS analytic survey for copper-based alloys. *Appl. Surf. Sci.* 254, 863–867 (2007).

[2] De Bonis, A. et al. Comparison of the performances of nanosecond and femtosecond Laser Induced Breakdown Spectroscopy for depth profiling of an artificially corroded bronze. *Appl. Surf. Sci.* 302, 275–279 (2014).

[3] Hartig, K. C., Colgan, J., Kilcrease, D. P., Barefield, J. E. Jovanovic, I. Laser-induced breakdown spectroscopy using mid-infrared femtosecond pulses. *J. Appl. Phys.* 118, (2015).

HST APERTURE PHOTOMETRY OF THE STAR CLUSTERS IN M31

Eimantas Kriščiūnas¹, Rima Stonkutė^{1,2}, Vladas Vansevicius^{1,2}

¹ Center for Physical Sciences and Technology, Saulėtekio av. 3, 10257 Vilnius, Lithuania

² Vilnius University Observatory, Saulėtekio av. 3, 10257 Vilnius, Lithuania
eimantas.krisciunas@fmcc.lt

Star clusters are key for studying galaxy formation and evolution. Photometry of a large sample of star clusters in the Andromeda (M31) galaxy by the Hubble Space Telescope (HST) would enable studying star formation processes across the galaxy disk in detail. Observations were performed in the framework of the Panchromatic Andromeda Treasury (PHAT; [1]) survey, which covered a third of the M31 disk, and results for a large number of star clusters are already published [2][3]. These clusters reside in diverse environments, from dense central parts of the galaxy to the sparse outskirts.

The aim of our study is to perform a new multicolour high-accuracy aperture photometry of star clusters by carefully accounting for bright field stars projecting on clusters and to derive cluster parameters. We use a two-aperture method described in [4]: (i) standard aperture photometry to measure ‘total’ (T) magnitudes; (ii) adaptive aperture photometry to measure ‘colour’ (C) magnitudes of clusters’ central parts. We select C apertures to avoid bright field stars, thus ensuring more consistent star cluster colours.

In Fig. 1(a,b) we show two-colour diagrams of 646 star clusters (selected by applying a requirement of photometric accuracy in all three passbands, $\sigma_{F336T,F475T,F814T} < 0.03$) constructed from T (a) and C (b) magnitudes. The main differences arise due to the smaller number of the non-cluster stars residing within apertures used for photometry. Fig. 1b shows more compatible colours of the real clusters and stochastic star cluster models, especially in the sense of artificial excess extinction arising due to red field stars. Thus, Fig. 1 clearly demonstrates validity and quality of the new aperture photometry method.

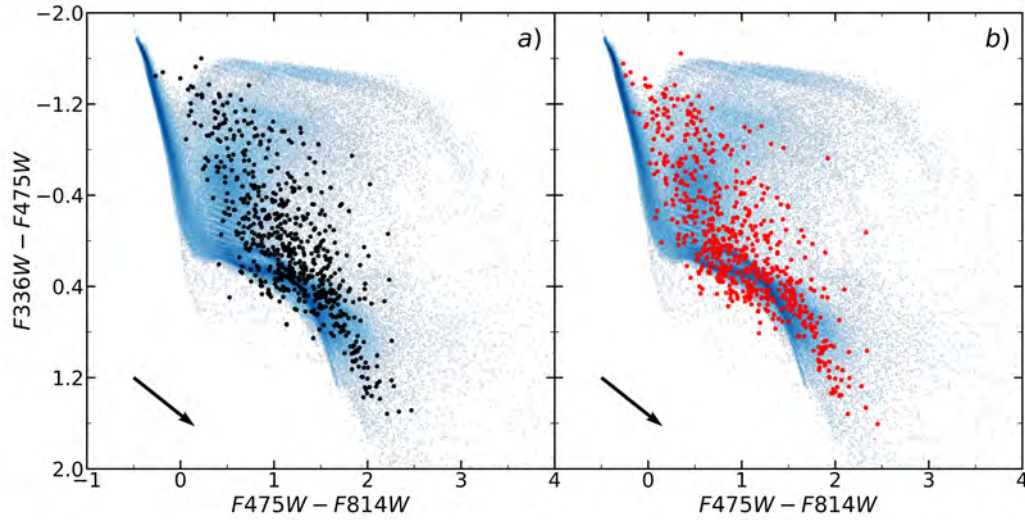


Fig 1. Two-colour diagrams produced by using T (a) and C (b) magnitudes. Star clusters ($N = 646$) of high photometric accuracy ($\sigma_{F336T,F475T,F814T} < 0.03$) are plotted (T – black dots, C – red dots). Stochastic star cluster models are shown in the background (blue dots). Arrows in the lower-left corners indicate the interstellar extinction vectors of $A_V = 1$, assuming standard Milky Way extinction law.

-
- [1] Dalcanton, J. J., Williams, B. F., Lang, D., et al., The Panchromatic Hubble Andromeda Treasury, *The Astrophysical Journal Supplement Series*, 200:18 (37pp), 2012
 - [2] Johnson, L. C., Seth, A. C., Dalcanton, J. J., et al., PHAT Stellar Cluster Survey. I. Year 1 Catalog and Integrated Photometry, *The Astrophysical Journal*, 752:95 (23pp), 2012
 - [3] Johnson, L. C., Seth, A. C., Dalcanton, J. J., et al., PHAT Stellar Cluster Survey. II. Andromeda Project Cluster Catalog, *The Astrophysical Journal*, 802:127 (22pp), 2015
 - [4] Naujalis, R., Stonkutė, R., Vansevicius, V., Deriving physical parameters of unresolved star clusters. VI. Adaptive aperture photometry of the M31 PHAT star clusters, *Astronomy & Astrophysics*, 654, A6 (10pp), 2021

AGN OUTFLOW-INDUCED STAR FORMATION IN GALACTIC DISC

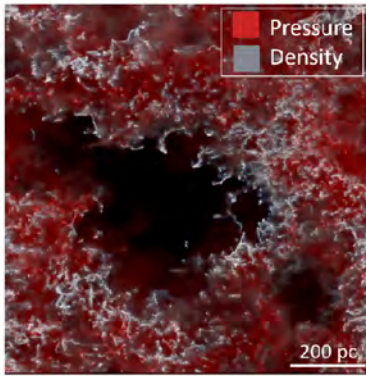
Martynas Laužikas¹, Kastytis Zubovas^{1,2}

¹Astronomical Observatory, Vilnius University, Saulėtekio al. 3, Vilnius LT-10257, Lithuania

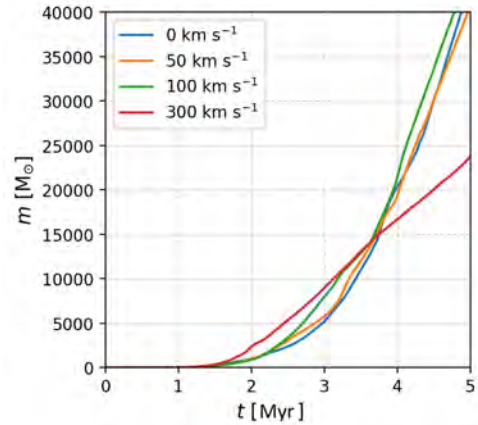
²Centre for Physical Sciences and Technology, Saulėtekio al. 3, Vilnius LT-10257, Lithuania
martynas.lauzikas@ff.stud.vu.lt

It is well established that most massive galaxies host a central supermassive black hole (SMBH). Matter accretion onto the SMBH creates an active galactic nucleus (AGN) - they are the brightest constant sources of light in the Universe. However, the effect of AGN on star formation and evolution of the galaxy is still debated. While the SMBH is massive, its gravitational influence is limited only to the very central parts of the galaxy and radiation poorly couples with diffuse matter and leaves the galaxy mostly unimpeded. But observational data shows a connection between the mass of the SMBH and properties of the galaxy (e.g. $M - \sigma$ relation), suggesting there exists an AGN feedback mechanism. Galactic outflow-induced star formation may hold the key to understanding this connection.

Properties of the galaxy-wide outflows are well reproduced by AGN wind model - central parts of younger galaxies are gas-rich and provide suitable conditions for outflow formation via relativistic particle wind. The wind interacts with the diffuse interstellar medium (ISM) forming fast outflows and either pushes the gas to outer regions or in the case of molecular clouds - ablates and evaporates them. However, further from the AGN, as outflows evolve and cool, they lose their destructive power. Moreover, high gas content of the galactic disk provides an obstacle to the expansion, producing turbulent mixing zones which cool the outflow by removing energy from it. Contrary to fast ones, outflows of hundred km s^{-1} , can produce an over-pressure in the disc, exceeding typical ISM pressure (fig. 1a) and may lead to an outburst of star formation.



(a) Disc pressure-density composition.



(b) Cumulative stellar particle mass.

Fig. 1. (a) Vertical view of disc density and pressure (100 km s^{-1} model after 1.5 Myrs of evolution). Red color indicates regions where ISM pressure is higher than mean disc pressure in quiescent galaxies ($> 10^{-11} \text{ dyn cm}^{-2}$). (b) Total mass of stars formed. Outflows enhances star formation in all models between 1.5-3.7 Myrs.

I use the public smoothed particle dynamics (SPH) code Gadget4 [1] to model a galactic disc cutout - a 1 kpc^3 cube with partial periodic boundary conditions, creating an infinite galactic disc sheet. Outflow compresses the disc at an 55° angle from both sides. I include hydrodynamics, gravity, stellar potential and relevant cooling and heating processes via precomputed cooling tables. For a cooling estimate I used the spectral synthesis code Cloudy [2]. Star formation is approximated by a simple stochastic model where cool dense ($> 10^6 \text{ m}_p \text{ cm}^{-3}$) SPH particles are converted to stars. I model three systems with initial outflow velocities of 50, 100, 300 km s^{-1} and one reference model with stationary ISM.

I find that slow outflows enhance star formation in the densest regions of giant molecular clouds, but the duration is limited to a few Myrs (fig. 1b). Enhancement is significant ($\sim 2\times$) for the system with the fastest outflow, but the long-term effect is star formation quenching. Slower, 50, 100 km s^{-1} outflows, while enhancing star formation for short periods, have a negligible effect on long-term evolution. Further analysis shows a low correlation between average diffuse ISM pressure (atomic and ionized gas) and star formation rate, indicating that the rate is governed by cloud-cloud collisions. The key takeaway is that outflows enhance star formation, but the magnitude of the effect depends on the homogeneity of the outflow and the disc itself.

[1] V. Springel, R. Pakmor, O. Zier, M. Reinecke, Simulating cosmic structure formation with the GADGET-4 code, MNRAS **506**(2), 2871–2949 (2021).

[2] G. J. Ferland, M. Chatzikos, F. Guzmán, et al., The 2017 Release Cloudy, RMxAA, Oct. 2017, **53**, 385–438.

STOCHASTICITY OF STAR CLUSTER PARAMETERS

Karolis Daugevičius¹, Rima Stonkutė^{1,2}, Vladas Vansevicius^{1,2}

¹ Center for Physical Sciences and Technology, Saulėtekio av. 3, LT-10257 Vilnius, Lithuania
² Astronomical Observatory of Vilnius University, Saulėtekio av. 3, LT-10257 Vilnius, Lithuania
karolis.daugevicius@ftmc.lt

Star formation mostly happens in clustered environments, such as star clusters and stellar associations. This makes star clusters an important tool for understanding the formation and evolution of their host galaxies. Cluster parameters are derived using various methods that often employ broad-band photometry results. However, earlier studies have shown that in the cases of young (<1 Gyr) low mass (<10⁴ M_⊙) star clusters, such methods are susceptible to uncertainties introduced by the stochastic nature of bright star distribution inside clusters [1,2].

The aim of this study is to evaluate the effects of bright star distribution and random cluster projection in the plane of the sky on the accuracy of star cluster parameters. We simulated a grid of artificial 3D clusters covering the parameter space of real objects observed in the Andromeda galaxy (M31). Distributions of stellar masses were modelled using the Kroupa initial mass function [3], and spatial distributions of stars were generated according to Elson-Fall-Freeman profile [4]:

$$\rho(R) = \rho_0(1 + R^2/r_0^2)^{-(\gamma+1)/2}, \quad (1)$$

where ρ_0 – central cluster density; R – deprojected (3D) distance from the cluster’s center; γ – power-law slope of the cluster’s radial profile; r_0 – scale factor, related to the cluster’s core radius, r_c , through $r_c = r_0(2^{2/\gamma} - 1)^{1/2}$. The explored parameter ranges of solar metallicity models are: mass – from 10² to 10⁴ M_⊙; age – from 10 Myr to 10 Gyr; r_c – from 0.05 to 0.80 arcsec; γ – from 2.2 to 7.0. At each node of the grid, we simulated 100 different clusters and generated their images to be consistent with real observations of M31 clusters in the PHAT survey [5]. Images were produced using 100 different 2D projections of each model, imitating their observation from 100 different angles. Simulated frames were measured by applying aperture photometry techniques [6].

We have demonstrated that young low-mass clusters without (Group 1) and with (Group 2) post-main-sequence stars photometrically differ significantly (Fig. 1). Clusters of Group 1 occupy a much smaller area in the colour-colour diagram (CCD) compared to the Group 2 objects, which are redder and their colour indices (CIs) cover a broader range (Fig. 1a). In Fig. 1b the corresponding ranges of CIs arising solely due to different viewing angles are much smaller. However, they are larger than photometry errors; thus, they must be considered. We also find that the spread directions of clusters’ CIs closely follow the direction of the extinction vector, suggesting that projection effects imitate those of extinction (Fig. 1c).

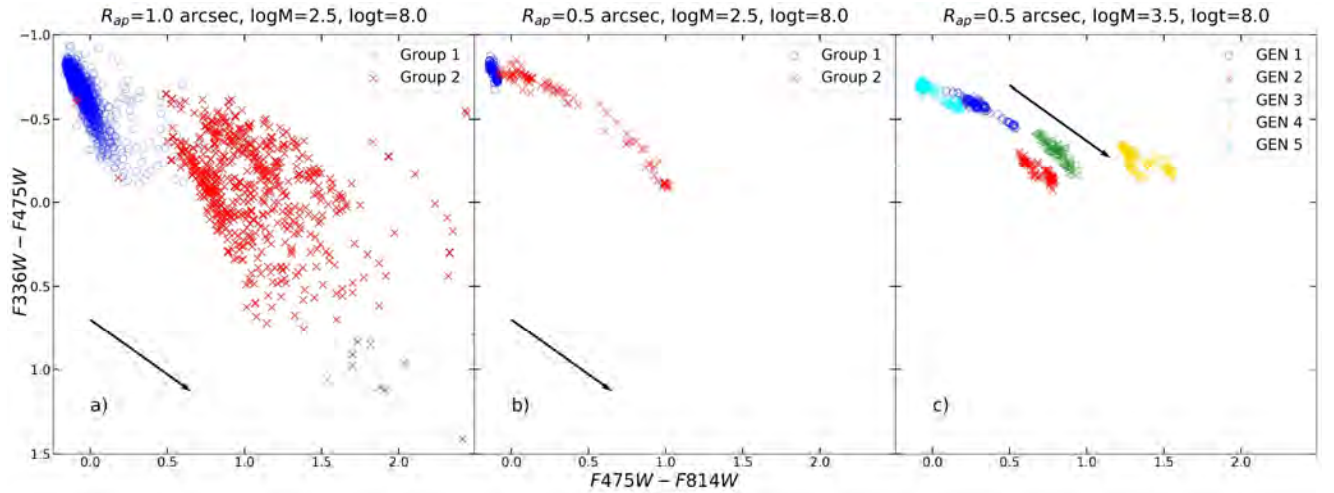


Fig. 1. Panel a) CCD of independently generated 100 clusters (for Group definitions, see text). Panel b) projection (100 viewing angles) effects are shown for one cluster from each Group. Panel c) projection effects imitate interstellar extinction: photometry results for five different clusters and 100 projections for each are shown. In all panels: arrow – extinction vector ($A_V = 1$); aperture radii, mass, and age of clusters are indicated above panels.

-
- [1] M. Fouesneau, A. Lançon, Accounting for stochastic fluctuations when analysing the integrated light of star clusters. I. First systematics, *Astronomy & Astrophysics*, **521**, A22 (2010).
[2] D. Narbutis, D. Semionov, R. Stonkutė et al., Deriving structural parameters of semi-resolved star clusters. FitClust: a program for crowded fields, *Astronomy & Astrophysics*, **569**, A30 (2014).
[3] P. Kroupa, On the variation of the initial mass function, *Monthly Notices of the Royal Astronomical Society*, **322**, 231 (2001).
[4] R. A. W. Elson, S. M. Fall, K. C. Freeman, The structure of young star clusters in the Large Magellanic Cloud, *Astrophysical Journal*, **323**, 54 (1987).
[5] J. J. Dalcanton, B. F. Williams, D. Lang et al., The Panchromatic Hubble Andromeda Treasury, *The Astrophysical Journal Supplement*, **200**, 18 (2012).
[6] R. Naujalis, R. Stonkutė, V. Vansevicius, Deriving physical parameters of unresolved star clusters. VI. Adaptive aperture photometry of the M31 PHAT star clusters, *Astronomy & Astrophysics*, **654**, A6 (2021).

A FAST GRID-BASED FEEDBACK INJECTION METHOD IN NUMERICAL AGN SIMULATIONS

Matas Tartėnas¹, Kastytis Zubovas^{1,2}

¹Department of Fundamental Research, Center for Physical Sciences and Technology, Lithuania

²Astronomical Observatory, Vilnius University, Lithuania

matas.tartenas@gmail.com

An episodic cycle of feeding and feedback (FB) seems to connect large galactic scales to the many orders of magnitude smaller supermassive black hole (SMBH) scales [1]. The ever-increasing amount of observations concerning the interplay between the infalling/outflowing ISM requires increasingly realistic and complex implementations of FB in numerical simulations.

A number of FB injection methods are currently available for use specifically in Smoothed-particle hydrodynamics simulations, which have their advantages and disadvantages. The simplest, spherical energy injection [2], distributes energy over a number of gas particles closest to the SMBH particle, ostensibly isotropically. While effective in many cases, this quick and dirty method is less successful when the small-scale structures in the proximity of the SMBH are of interest or the distribution of said matter is highly nonspherical [3]. On the other end, the virtual particle-based approach [4] allows for a more complex and flexible distribution of FB but is computationally very expensive.

We propose a new method that combines the flexibility of the virtual particle method while having a much lower computational cost. We define a spherical grid on which we propagate accretion disc wind at constant speed $v_{\text{wind}} \sim 0.1c$. Any particle that makes contact with the wind gets a portion of its energy/momentum or other stored quantity proportional to its contribution to the density field in that portion of the grid. Using our approach we are able to vary wind parameters over time and in different directions, for example to follow the variation of the accretion disc plane or to distribute FB in a conical shape.

Currently, the method is implemented in Gadget-3 [5]. Our method compares well to the virtual particle-based approach in test cases (examples in Fig. 1). These are promising results, as our approach produces similar and consistent outcomes at only a fraction of the computation time (about 10 times faster in our current tests).

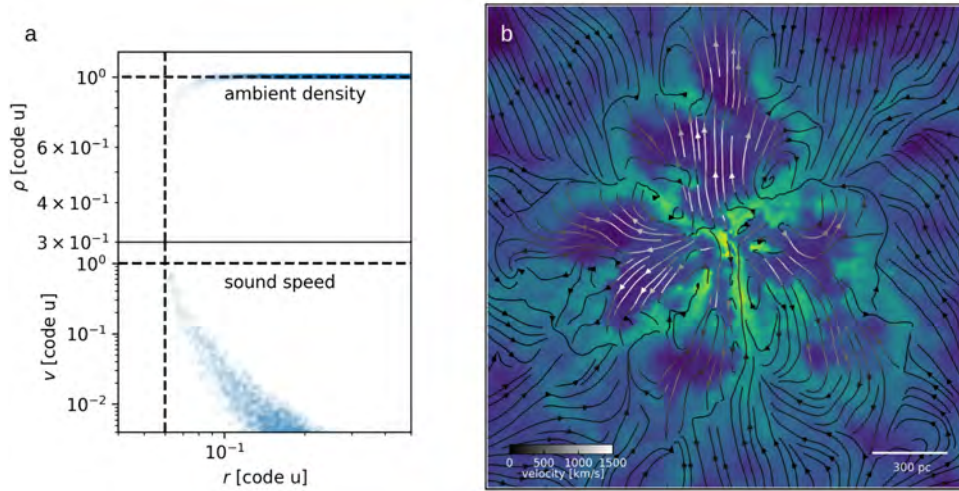


Fig. 1. a - properties of a quasi-steady state system in a periodic box with a low luminosity source. A central cavity of the expected size is opened with random velocity oscillations $\sim c_s$ in a narrow transitional region. b - A simulation of AGN in turbulent isothermal gas distribution. AGN shining at the Eddington limit produces outflows of varied morphology and velocities ~ 1000 km/s, which are typical for galactic-scale outflows - results are generally similar to those using the virtual particle method.

-
- [1] M. Gaspari, F. Tombesi and M. Cappi, Linking macro-, meso- and microscales in multiphase AGN feeding and feedback, *Nature Astronomy*, 4:10–13 (2020)
 - [2] V. Springel, T. Di Matteo and L. Hernquist, Modelling feedback from stars and black holes in galaxy mergers, *Monthly Notices of the Royal Astronomical Society*, 361:776-794 (2005)
 - [3] K. Zubovas, M. A. Bourne and N. Sergei, A simple way to improve AGN feedback prescription in SPH simulations, *Monthly Notices of the Royal Astronomical Society*, 457:496-509 (2016)
 - [4] S. Nayakshin, S. Cha and A. Hobbs, Dynamic Monte Carlo radiation transfer in SPH: radiation pressure force implementation, *Monthly Notices of the Royal Astronomical Society*, 397:1314-1325 (2009)
 - [5] V. Springel, The cosmological simulation code gadget-2, *Monthly Notices of the Royal Astronomical Society*, 364:1105–1134 (2005)

SPATIAL DIVERSITY IN COMPETING DYNAMICS ISING MODEL

Justas Kvedaravicius¹, Aleksejus Kononovicius²

¹Faculty of Physics, Vilnius University, Lithuania

²Institute of Theoretical Physics and Astronomy, Faculty of Physics, Vilnius University, Lithuania
justas.kvedaravicius@ff.stud.vu.lt

The development of sociophysics brought significant attention to opinion dynamics. Recent years have seen new efforts to facilitate comparison of results from temporal opinion models to empirical or experimental data [1, 2]. Such data is usually rich in spatial diversity and accounting for mobility dynamics can bridge the gap of theory and experiment. However there is little investigation on effects of both temporal and spatial dynamics in spin models except for a special case of Ising model [3].

This research analyzes changes in spatial patterns of competing Metropolis (temporal) and Kawasaki (spatial) dynamics in Ising model. Numerical analysis is performed for competing dynamics model with various Metropolis temperatures T_M and dynamics selection parameter p . Four distinct cases of Kawasaki dynamics temperatures T_K are considered - zero ($T_K = 0$), infinite ($T_K = \infty$), critical ($T_K = T_C$) and varying temperatures ($T_K = T_M$).

Spatial patterns are determined by evaluating the proposed diversity index and calculating the fractal dimension by utilizing box-counting method. Both values are obtained through scaling of the model lattice. Diversity index is calculated by changing resolution of lattice just like with renormalization technique. Instead spins of the scaled lattice represent mean values of the spins from the original lattice. For each new scale of lattice relative standard deviation is calculated and a scaling curve is obtained. Usual antiferromagnetic, ferromagnetic and paramagnetic configurations result in unique scaling curves by this procedure and it is used to get diversity index values ranging from -1 (antiferromagnetic configuration) to 1 (ferromagnetic one).

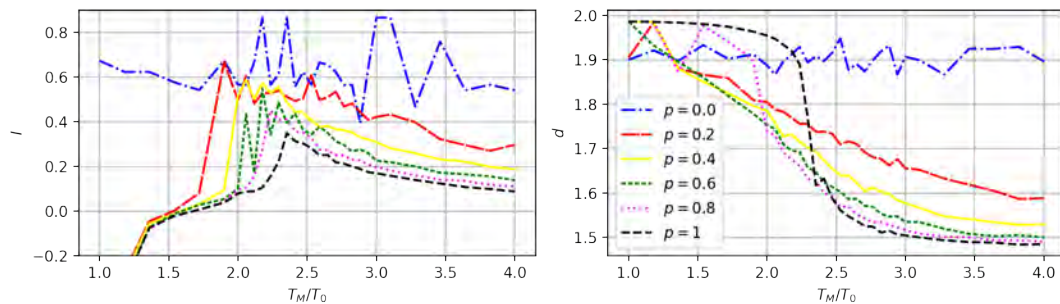


Fig. 1. Diversity index (left) and fractal dimension (right) values for competing Metropolis-Kawasaki dynamics in Ising model. The case of global Kawasaki dynamics with $T_K = 0$ is shown. Different curves account for dynamics selection parameter p values, where $p = 1$ corresponds to pure Metropolis dynamics and $p = 0$ to pure Kawasaki dynamics. Calculations were made for 64×64 lattice with 10^5 MC steps for equilibration, fractal dimension was calculated for boxes covering from 1 up to 16 spins.

Two distinct cases of competing dynamics in ferromagnetic Ising model show profound changes in lattice configurations. Cases for zero and infinite Kawasaki temperatures leads to change of phase transition temperature. Zero temperature Kawasaki dynamics allows only energy reducing Monte Carlo steps and leads to formation of fractal structures in ferromagnetic temperature range as seen in Fig. 1. Whereas infinite temperature Kawasaki allows only energy increasing MC steps and antiferromagnetic ordering emerges for sufficiently small p .

Setting Kawasaki dynamics temperature equal to that of Metropolis results in Metropolis-type spatial patterns. Diversity index in such case reaches its peak value at critical temperature point even though ferromagnetic temperature range should show highest index values. This result is mainly due to inaccuracy of index with order parameter at limit values. Fractal dimension also differs from usual topological dimension at critical point confirming scale invariance. Paramagnetic temperature ranges exhibit non-integer fractal dimension due to the selected small boxes scaling range (see Fig. 1). Critical Kawasaki temperature case only strengthens domain separation at critical temperature value.

In conclusion, the non-trivial results of zero or infinite Kawasaki temperature in competing dynamics match those reviewed in [3] and referenced therein. In terms of spatial diversity, scaling methods prove relevant in capturing spatial patterns and scale invariances so abundant in Ising type models.

[1] J. Fernandez-Gracia, K. Suchecki, J. J. Ramasco, M. Miguel, V. Eguiluz, *Is the voter model a model for voters?*, Physical Review Letters 112, 158701 (2014).

[2] A. Kononovicius, *Compartmental voter model*, Journal of Statistical Mechanics: Theory and Experiment 2019, 103402 (2019).

[3] S. Artz, S. Trimper, *Competing Glauber and Kawasaki Dynamics*. International Journal of Modern Physics B. 23. 10.1142/S0217979298001393, (1998).

SODIUM SILICATE PARTICLE SIZE MEASUREMENTS USING TIME - RESOLVED FLUORESCENCE ANISOTROPY

Daniel Doveiko¹, Simon Stebbing², Yu Chen¹, David J. Birch¹, Vladislav Vyshemirsky³, Olaf Rolinski¹

¹ Photophysics Group, Department of Physics, University of Strathclyde, Scottish Universities Physics Alliance, Glasgow G4 0NG, U.K.

² PQ Silicas UK Limited, Warrington, WA5 1AB, U.K.

³ School of Mathematics and Statistics, University of Glasgow, Glasgow G12 8QQ, U.K.
daniel.doveiko.2018@uni.strath.ac.uk

Sodium silicates are versatile inorganic chemicals produced by combining silica sand and soda ash (sodium carbonate) under high temperature. When in aqueous solution, they are often used in coating and bonding applications. Additionally, they exhibit a range of attractive characteristics, such as being odorless and non-toxic, high strength and rigidity, resistance to high temperatures and low-cost [1].

The important characteristics of silicates are the correlation between the ratio of silica to soda concentrations and the size of the species. Traditionally, the particle sizes of nanoparticles are determined using methods such as Dynamic Light Scattering (DLS) [2], Small-Angle X-Ray Scattering (SAXS) [3], Small Angle Neutron Scattering (SANS) [4] and Transmission Electron Microscopy (TEM) [5]. All these methods are far from ideal and have significant drawbacks: DLS becomes difficult for particles below 10 nm, SAXS and SANS are expensive and complex, and TEM requires complex sample preparations which can lead to alterations of particle sizes [6-8].

Here, we present a new way of determining the particle sizes of sodium silicate liquors at high pH using time-resolved fluorescence anisotropy. Different from previous approach of using a single dye label, two fluorescent labels were used in this work [9,10]. Rotational times of the non-binding rhodamine B and electrostatically binding rhodamine 6G were used to determine the medium microviscosity and the silicate particle radius, respectively. This approach of using two dyes ensures that the microviscosity stays accurate in time, unlike in the case when a single dye was used. Applying this method to samples of various pH (prepared by diluting the stock solution of silicate to the concentrations of NaOH ranging from 0.2M to 2M) and different temperatures (10°C to 55°C), the recovered average particle size was found to have an upper limit of $7.0 \pm 1.2 \text{ \AA}$.

-
- [1] Yang, X., W. Zhu, and Q. Yang, The viscosity properties of sodium silicate solutions. *Journal of Solution Chemistry*, 2008. 37(1): p. 73-83.
- [2] Gratz, H., A. Penzkofer, and P. Weidner, Nanometer particle size, pore size, and specific surface determination of colloidal suspensions and porous glasses by Rayleigh light scattering. *Journal of non-crystalline solids*, 1995. 189(1-2): p. 50-54.
- [3] Paradies, H.H., Particle size distribution and determination of characteristic properties of colloidal bismuth—silica compounds by small-angle x-ray scattering and inelastic light scattering. *Colloids and Surfaces A: Physicochemical and Engineering Aspects*, 1993. 74(1): p. 57-69.
- [4] Winter, R., et al., A SANS study of the effect of catalyst on the growth process of silica gels. *Journal of non-crystalline solids*, 1989. 108(2): p. 137-142.
- [5] Van Blaaderen, A. and A. Kentgens, Particle morphology and chemical microstructure of colloidal silica spheres made from alkoxysilanes. *Journal of Non-Crystalline Solids*, 1992. 149(3): p. 161-178.
- [6] Uskoković, V., Dynamic light scattering based microelectrophoresis: main prospects and limitations. *Journal of dispersion science and technology*, 2012. 33(12): p. 1762-1786.
- [7] Pauw, B.R., Everything SAXS: small-angle scattering pattern collection and correction. *Journal of Physics: Condensed Matter*, 2013. 25(38): p. 383201.
- [8] Williams, D.B. and C.B. Carter, The transmission electron microscope, in *Transmission electron microscopy*. 1996, Springer. p. 3-17.
- [9] Yip, P., et al. (2012). "Fluorescence anisotropy metrology of electrostatically and covalently labelled silica nanoparticles." *Measurement Science and Technology* 23(8): 084003.
- [10] Geddes, C. and D. Birch (2000). "Nanometre resolution of silica hydrogel formation using time-resolved fluorescence anisotropy." *Journal of non-crystalline solids* 270(1-3): 191-204.

DYNAMIC FORCE SPECTROSCOPY OF HEMOGLOBIN–INOSITOL PHOSPHATES INTERACTION SIMULATED BY STEERED MOLECULAR DYNAMICS

Wojciech Marciniak^{1,2}, Joanna Marciniak², Arkadiusz Ptak¹

¹Institute of Physics, Faculty of Materials Engineering and Technical Physics, Poznań University of Technology, Piotrowo 3, 61-139 Poznań, Poland

²Institute of Molecular Physics Polish Academy of Sciences, Smoluchowskiego 17, 60-179 Poznań, Poland
wojciech.robe.marciniak@doctorate.put.poznan.pl

Inositol phosphates fulfill multiple roles in the living cells, most importantly regulatory ones. Lower inositol phosphates consist of a part of the metabolic cycle in legumes, grains, beans, and other plants [1]. Moreover, myo-inositol hexakisphosphate (phytic acid) and myo-inositol trispyrophosphate are considered good allosteric effectors of hemoglobin, stronger than the natural effector of hemoglobin, 1,3-bisphosphoglyceric acid (BPG), which lowers its affinity towards oxygen and promotes more efficient oxygen transport. This activity is promising in treating hypoxia, which can be one of the effects of carcinogenesis [2].

In order to probe the interaction, we applied molecular docking in AutoDock Vina and steered molecular dynamics (SMD) simulations in the Gromacs package. We prepared molecular models of multiple phosphates (mono- to hexakisphosphates) of all inositol conformations. The models were docked to hemoglobin across the pocket containing BPG-binding site. The results reveal five distinct binding sites, one being the exact site binding PBG. We present the results of molecular docking and Gibbs free energy change (ΔG) of the specific bond formed. In order to extract additional information including the kinetics of the bond, we performed multiple SMD simulations according to a procedure presented in Fig 1.

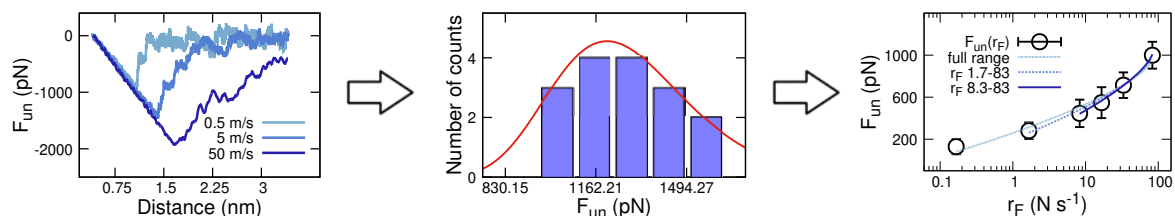


Fig. 1. Force-distance curves for different separation rates (left), log-normal function fitted to the distribution of unbinding forces for an exemplary separation rate (middle), and Dudko-Hummer-Szabo model fit to the extracted most probable unbinding force *versus* the loading rate dependency (right).

For the most promising candidates, we performed multiple SMD simulations of the unbinding process with the separation rate in the range between 0.1 m s⁻¹ and 50 m s⁻¹. In order to extract the specific bond parameters, such as the Gibbs free energy of activation in the absence of the external force (ΔG_β), the dissociation constant (k_{off}^0) and the distance between the bound state minimum and the position of the activation barrier (x_β), the results were analyzed with Dudko-Hummer-Szabo (DHS) model of thermally-activated unbinding under external force, formulated as [3, 4]:

$$F_{un} = \frac{\Delta G_\beta}{v x_\beta} \left\{ 1 - \left[\frac{k_B T}{\Delta G_\beta} \ln \frac{k_{off}^0 k_B T \exp\left(\frac{\Delta G_\beta}{k_B T}\right)}{x_\beta r_F} \right]^v \right\} \quad (1)$$

where F_{un} is the most probable unbinding force, k_B is the Boltzmann constant, v is the barrier shape parameter, and r_F is the loading rate, calculated as the product of systems spring constant and separation rate.

The work has been funded by the Polish Ministry of Education and Science under the grant DI2017/007947 in the Diamond Grant program 2018 edition.

-
- [1] Frank, A. *Chemistry of plant phosphorus compounds*, Elsevier (2013).
 [2] Kieda C., Greferath R., Silva C.C.D., Fylaktakidou K.C., Lehn J.M. and Nicolau C. *Suppression of hypoxia-induced HIF-1 α and of angiogenesis in endothelial cells by myo-inositol trispyrophosphate-treated erythrocytes*, PNAS 103 (42) 15576 (2006). doi:10.1073/pnas.0607109103
 [3] Dabrowski J., Nowak W., Ptak A., *How strong are hydrogen bonds in the peptide model?*, Physical Chemistry Chemical Physics 22, 1392–1399 (2020). doi:10.1039/C9CP05564A
 [4] Dudko O., Hummer G., Szabo A., *Intrinsic Rates and Activation Free Energies from Single-Molecule Pulling Experiments*, Physical Review Letters 96, 108101 (2006). doi:10.1103/PhysRevLett.96.108101

STUDY OF THE ANTIVIRAL PROPERTIES OF SURFACE COATINGS USING THE SERS SPECTROSCOPY TECHNIQUE

Marius Balodis, Sonata Adomavičiūtė-Grabusovė, Valdas Šablinskas

Institute of Chemical Physics, Faculty of Physics, Vilnius University, Saulėtekio al. 3, Vilnius, Lithuania

marius.balodis@ff.stud.vu.lt

With hundreds of deaths and thousands of new infections every day in the US alone, COVID-19 will take time to transition from a pandemic to an endemic. [1] One of the leading means of coronaviruses spreading is through the frequently touched surfaces (FTS) such as door handles or handrails. [2]

These pathogens have an envelope covered by protein spikes responsible for adsorption to surfaces. [3] Presuming we can obtain and cover FTS with coatings that have repelling properties towards the proteins, a restriction of coronaviruses spreading could be ensured.

To become aware of how proteins adsorb to coatings, we detected bovine serum albumin (BSA) adsorption using Surface-enhanced Raman spectroscopy (SERS) method. SERS was chosen as an eligible method with the known general ability to detect small concentrations of the substance (seeking up to 10^{-10} – 10^{-15} mol/l). It currently has a wide field of applications in various studies surrounding biological objects. [4]

Firstly, to optimize experimental conditions, a SERS must-have standard Lee-Meisel colloid [5] was prepared and then concentrated using centrifugation. After this, five clean and differently coated plates were soaked in a BSA solution for 10 minutes, rinsed and left to dry. The following day, a drop of colloid was dried on top of it too and the coating was ready for testing.

FT-Raman spectrometer with an excitation laser of 1064 nm wavelength was used to execute the experiment. Ring vibrations with a 1003 cm^{-1} band were observed at the albumin SERS spectra. While studying a specimen on a reflective aluminum plate surface, this characteristic band was visible even at the albumin solution's concentration as low as 10^{-9} M (fig. 1).

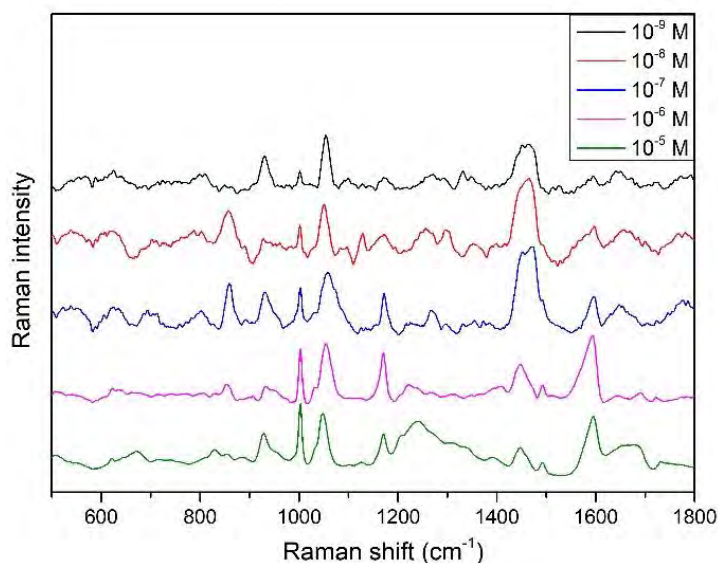


Fig. 1. BSA SERS spectra on an aluminum plate using different initial concentrations of BSA solution.

After further measurement of protein adsorption on five different test coatings, variation of band intensities was observed with the weakest when using coating named *Coating from Cu mixed with SiO₂ + Ag*.

Hence the purpose of our study is to optimize the experimental conditions for protein adsorption detection using SERS method and to test the given plates. Assuming we observe a weak or void characteristic band amongst the test coatings, these could be considered having antiviral properties and suitable for the FTS.

[1] R. H. Shmerling, MD. Is the COVID-19 pandemic over, or not? Harvard Health Publishing. October 26, 2022 (<https://www.health.harvard.edu/blog/is-the-covid-19-pandemic-over-or-not-202210262839>).

[2] D. Dobrynin, I. Polishchuk, L. Portal, I. Zlotver, A. Sosnik, B. Pokroy. Adsorption of SARS CoV-2 spike proteins on various functionalized surfaces correlates with the high transmissibility of Delta and Omicron variants, *Materials Today Bio*, Volume 14, 2022, 100265, ISSN 2590-0064, (<https://doi.org/10.1016/j.mtbio.2022.100265>).

[3] C. Bamford, New coronavirus variant: what is the spike protein and why are mutations on it important? *The conversation*, 2020. (<https://theconversation.com/new-coronavirus-variant-what-is-the-spike-protein-and-why-are-mutations-on-it-important-152463>).

[4] Hering, K., Cialla, D., Ackermann, K. et al. SERS: a versatile tool in chemical and biochemical diagnostics. *Anal Bioanal Chem* 390, 113–124 (2008). (<https://doi.org/10.1007/s00216-007-1667-3>).

[5] P. C. Lee, D. Meisel. Adsorption and Surface-Enhanced Raman of Dyes on Silver and Gold Sols. *J. Phys. Chem.* 1982, 86, 3391–3395.

GAS FLOW DYNAMICS AND PURIFICATION FROM ULTRAFINE PARTICULATE MATTER IN A NEWLY DEVELOPED APPARATUS

Aleksandras Chlebnikovas¹, Artūras Kilikevičius²

^{1,2} Research Institute of Mechanical Science, Vilnius, Lithuania
aleksandras.chlebnikovas@vilniustech.lt

General ecology and environmental protection are among the main priorities at this stage of industrial progress, taking into account sustainable development and reducing the impact on climate change. In general, the level of environmental pollution is increasing, in particular cases, especially in the developed regions of the planet, special measures are effectively applied to improve the environment both in the generation process itself and by reducing emissions in a specific environment. Atmospheric pollution has a special role, as it is the only habitat not only for humans, but also for a large part of wildlife. Changes in air quality due to emitted pollutants impair quality of life, contribute to various injuries and long-term illnesses, depending on the type of pollution. The most common pollution associated with fine and ultra-fine particles hovering in the open air [1]. The sources of this pollution are a large part of industrial production, road transport, energy, as well as various types of work, which inevitably spray or otherwise emit dust. The content of the generic term called particulate matter may vary depending on the type of activity in which they entered the atmosphere and the air stream. Thus, along with the mechanical effect of exposure, particles can also carry chemical components, which further aggravate the negative impact they create on the environment [2]. Most modern technologies quite effectively solve the problem of pollution with large solid particles, i.e., more than 10–15 microns. For such purposes, air flow filtration technologies are used as in air ducts using filters, including bag/cassette, some types of electrostatic precipitators, as well as centrifugal cyclones, sometimes cleaning using a water stream is used [1,3]. Only a part of filters is effective for settling or containment of fine dust, among which most of them require special operating conditions, have a narrow range of effective action, and their use requires special skills and personnel training.

In this paper, we study the apparatus of a new improvement, which in its design has several improved models of treatment technologies. The type of apparatus of each of the technologies is used in individual cases, however, such a solution is not effective and convenient with modern requirements for treatment facilities. The scientific object of this work combines in one building various stages of purification, operating according to different principles of work, but coordinated with each other. Thus, the use of such an apparatus is possible without preliminary primary purification of the gas flow, which makes it possible to effectively use this technology with a wide range of primary flow characteristics.

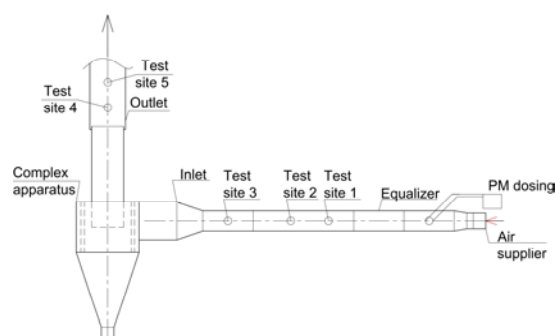


Fig. 1. Experimental stand of complex apparatus for aerodynamic and efficiency testing

The studies described in this paper present experimental results on flow dynamics on a laboratory bench that simulates industrial conditions. The dependences of the gas flow rate in certain sections on the source of the generated flow to the inlet to the cleaning apparatus and the exit from it were studied. The aerodynamic parameters and the dependences of various characteristics on each other were studied at a gas flow rate in the range of 50–300 m³/h. The purification efficiency of the gas stream was investigated using fine and ultra-fine quartz solid particles. The total and fractional concentrations of particles before and after purification were studied for particles 0.3–10 μm in size. The overall efficiency of cleaning the gas stream from solid particles, according to preliminary data, exceeded 80%, and in particular, solid particles ranging in size from 2 μm to 10 μm in most cases were not detected in the stream after cleaning.

Acknowledgments

This project has received funding from the Research Council of Lithuania (LMTLT), agreement No [S-PD-22-31].

- [1] L. Calderón-Garcidueñas and A. Ayala, 'Air Pollution, Ultrafine Particles, and Your Brain: Are Combustion Nanoparticle Emissions and Engineered Nanoparticles Causing Preventable Fatal Neurodegenerative Diseases and Common Neuropsychiatric Outcomes?', *Environ Sci Technol*, vol. 56, no. 11, pp. 6847–6856, Jun. 2022, doi: 10.1021/acs.est.1c04706.
- [2] L. Song et al., 'Airborne pathogenic microorganisms and air cleaning technology development: A review', *J Hazard Mater*, vol. 424, p. 127429, 2022, doi: <https://doi.org/10.1016/j.jhazmat.2021.127429>.
- [3] X. Ji et al., 'Advances in particulate matter filtration: Materials, performance, and application', *Green Energy & Environment*, Apr. 2022, doi: 10.1016/J.GEE.2022.03.012.

CRYO-EM STRUCTURES OF *STREPTOCOCCUS THERMOPHILUS* CAS9 BOUND TO TARGET AND NON-TARGET DNA

Ugne Gaizauskaite^{1*}, Arunas Silanskas¹, Giedrius Sasnauskas¹

¹ Department of Protein-Nucleic Acids Interactions, Vilnius University, Lithuania
ugne.gaizauskaite@gmc.vu.lt

Cas9 is a programmable RNA-guided DNA endonuclease [1; 2]. It recognises a short DNA sequence, known as a protospacer-adjacent motif (PAM), and cleaves DNA at a fixed position in accordance to PAM when there is full complementarity between DNA and RNA strands. This feature has made the Cas9 protein a highly attractive and popular molecular tool for genome editing. Nevertheless, there are still gaps in full understanding of the Cas9 biological role in prokaryotic cells. Cas9 belongs to II-type CRISPR-Cas systems and is essential for all three stages of the CRISPR-Cas mechanism (adaptation, RNA biogenesis and interference). During adaptation, viral DNA is selected, cut and integrated as a spacer into the CRISPR region in a bacterial chromosome. The precise mechanism of adaptation in II-A subtype CRISPR-Cas systems is yet to be determined. It has been shown that during adaptation Cas9 aids in viral DNA selection by recognising the PAM sequence [3]. In some way Cas9 has to convey the information of PAM recognition to macromolecular Cas1-Cas2-Csn2 adaptation complexes, which then finalise the adaptation stage [4]. When viral DNA is inserted into the CRISPR region, it is transcribed by RNA polymerase and processed by Cas9 and RNase III into CRISPR RNA (crRNA), which is hybridized with trans-activating crRNA (tracrRNA) forming a functional guide RNA. In the final interference stage, Cas9 uses guide RNA to find the target DNA molecules and induce DNA double-strand breaks. In this way, CRISPR-Cas system confers hereditary and adaptive immunity against viruses.

Here, we report the structure of *Streptococcus thermophilus* Cas9 in complex with guide RNA and target DNA (interference mode). We also present the structure of *Streptococcus thermophilus* Cas9-RNA bound to non-target DNA, with the PAM-adjacent target DNA strand non-complementary to the guide RNA. We show that Cas9-RNA adopts different conformations, which might be exploited for the distinct roles of Cas9 in adaptation and interference.

-
- [1] G. Gasiunas, R. Barrangou, P. Horvath, V. Siksnys. Cas9-crRNA ribonucleoprotein complex mediates specific DNA cleavage for adaptive immunity in bacteria. *Proc. Natl. Acad. Sci. U.S.A.*, 109, 15539–15540 (2012)
- [2] M. Jinek, K. Chylinski, I. Fonfara et al. A programmable dual-RNA guided DNA endonuclease in adaptive bacterial immunity. *Science* 337, 816–21 (2012)
- [3] R. Heler, P. Samai, J.W. Modell, C. Weiner, G.W. Goldberg, D. Bikard, L.A. Marraffini. Cas9 specifies functional viral targets during CRISPR-Cas adaptation. *Nature* 519, 199–202 (2015)
- [4] M. Wilkinson, G. Drabavicius, A. Silanskas, G. Gasiunas, V. Siksnys, D.B. Wigley. Structure of the DNA-Bound Spacer Capture Complex of a Type II CRISPR-Cas System. *Mol. Cell*, 75, 90–101 (2019)

STRUCTURAL CHARACTERIZATION OF A TYPE II CRISPR-CAS INTEGRASE COMPLEX

Rugilė Ivanickaitė¹, Giedrius Sasnauskas¹

¹ Life Sciences Center, Institute of Biotechnology, Vilnius University, Lithuania
rugile.ivanickaite@gmc.stud.vu.lt

CRISPR-Cas are widespread bacterial and archaeal adaptive immune systems, which protect cells against mobile genetic elements, such as viruses or foreign plasmid DNA. The mechanism of CRISPR-Cas systems comprises three stages, called adaptation, CRISPR RNA maturation and interference, while the CRISPR loci contain inverted sequences (CRISPR repeats), interspaced by short fragments acquired from foreign DNA (spacers). A key component in the adaptation step is the heterohexameric integrase complex composed of a Cas2 dimer sandwiched by two Cas1 dimers. The role of this complex is to capture fragments of foreign DNA (prespacers) and integrate them into the CRISPR locus, leading to formation of new spacers that confer immunity against the corresponding viral DNA. So far, CRISPR-Cas adaptation is best described in systems of subtypes I-E and II-A [1], yet the mechanism of spacer acquisition in subtype II-C systems remains unclear.

In order to better understand the adaptation stage of a subtype II-C CRISPR-Cas system, we purified the Cas1-Cas2 integrase complex and determined its structure using cryo-electron microscopy (Fig. 1), which revealed molecular interactions between the integrase complex and prespacer DNA. According to our structural data, Cas2 dimer plays a major role in maintaining non-specific interactions through its ability to coordinate Mg²⁺ ions, as well as having its α -helices interact with the major grooves of the prespacer DNA. Additionally, the catalytic Cas1 subunits have symmetric Val residues that act as a molecular ruler and ensure the correct prespacer duplex length of 22 bp.

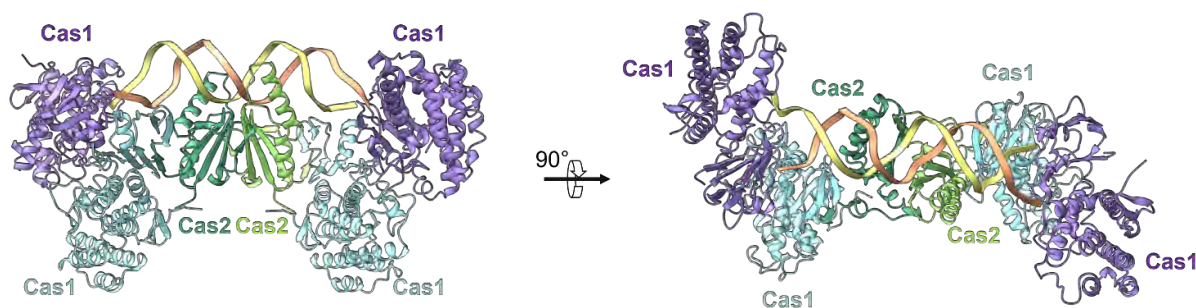


Fig. 1. The structure of subtype II-C Cas1-Cas2 integrase complex.

Our results suggest that the adaptation in a subtype II-C CRISPR-Cas system might be generally similar to other type II systems since our obtained structure is comparable to a subtype II-A integrase structure [2]. However, as it lacks accessory proteins like Csn2 and Cas4 found in subtypes II-A and II-B respectively, the overall adaptation mechanism may differ and further investigation is needed to elucidate it.

[1] Sasnauskas, G., & Siksnys, V. (2020). CRISPR adaptation from a structural perspective. *Current Opinion in Structural Biology*, 65, 17-25.

[2] Xiao, Y. et al. (2017). How type II CRISPR-Cas establish immunity through Cas1-Cas2-mediated spacer integration. *Nature*, 550(7674), 137-141.

PROPIDIUM IODIDE, OLIGO- AND POLYNUCLEOTIDE SIZE INFLUENCE ON CELL ELECTROTRANSFER EFFECTIVENESS

Aras Rafanavičius¹, Rūta Palepšienė¹, Saulius Šatkauskas¹

¹Department of Biochemistry, Faculty of Natural Sciences, Vytautas Magnus University, Lithuania
aras.rafanavicius@vdu.lt

Electroporation (EP) is a method used to permeate cell plasma membrane (PM) by exploiting short electric pulsation to allow movement of extracellular and intracellular molecules across the PM. The technique may be used to deliver molecules such as oligo- and polynucleotides or small hydrophilic compounds into cells, and this is researched for application in cancer electrochemotherapy, gene therapy for treatment of neurological and congenital diseases as well as, in the case of oligonucleotide electrotransfection, development of cancer vaccines [1]. However, it is known that character of electrotransfer is dependent on mass, shape and charge of the compound, and different EP parameters must be used to effectively deliver substances of diverse characteristics [2,3]. Thus, the purpose of this investigation was to identify the nature of electrotransfer of molecules of different size: plasmid DNA (pDNA), oligonucleotides and propidium iodide (PI), in order to evaluate the influence of treatment conditions on electrotransfer efficiency and to conclude the most advantageous electroporation parameters – pulse voltage, duration and number.

Electroporation was performed on Chinese hamster ovary cells. The cells were suspended in low conductivity medium (0,1 S/m) and placed within a 2 mm gap between stainless steel electrodes. Propidium iodide and pDNA electrotransfer was performed by applying either 1, 5 or 10 LV (500 V/cm, 5 ms) pulses or 1 HV (1400 V/cm, 100 μs) pulse, and electrotransfer efficiency was determined via flow cytometry (in the case of pDNA transfection, GFP expression was evaluated 24 h after EP procedure). PI electrotransfer timelapse was further visualised via fluorescence microscopy using copper electrodes in coplanar configuration to deliver pulsation. Oligonucleotide transfection was performed upon the cells by applying a single pulse of varying duration and voltage (1500 V/cm 100 μs, 1200 V/cm 250 μs, 500 V/cm 5 ms), which allowed to identify optimum parameters that were subsequently further analysed by treating the cells with a different number of up to 10 pulses.

The results indicate that electrophoretic force caused by electrical pulses had considerable effect on oligonucleotide electrotransfer but had no significant impact on PI transfer. Conversely, PI electrotransfer appears not to be affected by total pulse duration and continues to occur after the external electric pulsation has ceased, which was not observed for oligo- and polynucleotide electrotransfection. Majority of the cells treated with 10 LV pulses remain permeable 15 minutes after the treatment was conducted, and this diminishes viability of the cells to up to 10 % of control viability. Furthermore, maximum pDNA expression was observed upon applying one HV pulse, whereas longer LV pulses had a negative impact on cell viability and negligible transfection rate. This, compared to oligonucleotide electrotransfer, indicates that the underlying phenomenon behind the uptake of these molecules into electropermeabilized cells is distinct, and additional research is required in order to establish optimum parameters to achieve effective nonconcurrent or simultaneous electrotransfer of nucleotides of varying size.

[1] J. Gehl, Electroporation: theory and methods, perspectives for drug delivery, gene therapy and research, *Acta physiologica Scandinavica* **177**, 437-447 (2003).

[2] H. Wolf, M. P. Rols, E. Boldt, E. Neumann et al., Control by pulse parameters of electric field-mediated gene transfer in mammalian cells, *Biophysical journal* **66**, 524-531 (1994).

[3] S. Sachdev, S. Feijoo Moreira, Y. Keehen et al., DNA-membrane complex formation during electroporation is DNA size-dependent, *Biochimica et biophysica acta – Biomembranes* **1862** 183089 (2020).

THERMODYNAMIC CHARACTERISTICS OF THE SOLID DISPERSION SYSTEM OF DIOSMIN

Artem Kharchenko, Vadym Lisovyi, Volodymyr Bessarabov, Olga Kovalevska,
Andriy Goy, Iryna Povshedna

Department of Industrial Pharmacy, Kyiv National University of Technology and Design, Ukraine
a.kharchenko@kyivpharma.eu

Recently, an important direction of pharmaceutical development is the search for substances effective in the treatment of disorders of the circulatory system. These substances include flavonoids, which can potentially be used to protect the cardiovascular system.

Diosmin is one of the representatives of semi-synthetic flavonoids with a wide spectrum of pharmacological properties [1]. It is used in the treatment of chronic venous insufficiency and hemorrhoidal disease, increases the vasoconstrictor effect of noradrenaline on the venous walls, increasing venous tone [2].

The main disadvantage of using diosmin as an active pharmaceutical substance is its low solubility in water, which causes low bioavailability. Therefore, to increase the degree of solubility of diosmin in water, the technique of forming solid dispersed systems (SDS) is used by the method of co-dissolving diosmin with pharmaceutically acceptable polymers and surfactants with subsequent removal of the solvent by evaporation.

The method of obtaining SDS. In a flask with a capacity of 100 ml, 45 ml of solvent were placed successively; 0.05 g of diosmin; 7.50 g of polyvinylpyrrolidone K-25 and 0.01 g of nonionic surfactant. The process of dissolving the components of the mixture was carried out by heating in a water bath (37 ± 0.5 °C) and intensive stirring for 30.0 ± 0.5 min. Separation of aqueous and solid phases was carried out by centrifugation at 6000 rpm. within 30.0 ± 0.5 min. The aqueous phase (solution) was decanted and placed in a drying chamber. The drying process was carried out at a temperature of 50.0 ± 0.5 °C to a constant mass.

The solubility of diosmin in the composition of SDS was determined spectrophotometrically by the transition of the flavonoid into an aqueous solution at $\lambda=348$ nm.

According to the results of the study, the growth in the coefficient of increase in the solubility of diosmin was determined depending on the temperature. At a temperature of 25°C, this coefficient increases to 3.2 times, a slight increase is noted when the temperature rises from 25°C to 30°C (up to 3.7 times). A further increase in the temperature of the medium to 37°C allows to increase the solubility coefficient by 4.4 times, and the highest value is reached at a temperature of 40°C – 5.8 times ($p < 0.05$).

Also, the stability constant (K_s) of the complexes was determined for SDS. The obtained values of the stability constant are in the range of 197.5-208.2 M^{-1} . This value indicates the favorability of the process of formation of intermolecular complexes, because it is in the optimal range (100 M^{-1} to 1000 M^{-1}).

In the reaction of complex formation, the thermodynamic interaction between the components of the system is a critical factor.

The following thermodynamic parameters were calculated for this reaction of the formation of intermolecular complexes: change in Gibbs free energy (ΔG), change in enthalpy (ΔH) and change in entropy (ΔS).

Table 1. Thermodynamic characteristics of the system

Temperature Parameters	25 °C (298 K)	30 °C (303 K)	37 °C (310 K)	40 °C (313 K)
$\Delta H^0, kJ \times M^{-1}$	-0,0842	-0,0842	-0,0842	-0,0842
$\Delta G^0, kJ \times M^{-1}$	-13,2195	-13,3158	-13,7449	-13,7556
$\Delta S^0, J \times M^{-1}$	44,6435 \pm 0,9322	44,2246 \pm 0,5340	44,6102 \pm 0,7583	44,2169 \pm 0,5745

The obtained data allow us to conclude that the process of formation of intermolecular complexes takes place with a slight release of energy (exothermic), since the enthalpy acquires negative values. Positive entropy values indicate that the formation of complexes between diosmin and auxiliary substances occurs when the aqueous solvate shell of molecules is destroyed. Negative values of the Gibbs free energy change indicate favorable conditions for diosmin solubilization in the presence of the polymer.

Therefore, a study of the effect of temperature on the solubility of diosmin in water as part of polymeric SDS was carried out. The obtained values show that the maximum value of increasing the solubility of diosmin is observed at a temperature of 40 °C. The thermodynamic characteristics of the system were calculated for this SDS, from which it can be seen that the process of formation of complexes is spontaneous and takes place with the release of energy.

[1] L. Pari, S. Srinivasan, Antihyperglycemic effect of diosmin on hepatic key enzymes of carbohydrate metabolism in streptozotocin-nicotinamide-induced diabetic rats, *Biomedicine & pharmacotherapy = Biomedecine & pharmacotherapie* **64(7)**, 477–481 (2010).

[2] S. L. Dholakiya, K. E. Benzeroual, Protective effect of diosmin on LPS-induced apoptosis in PC12 cells and inhibition of TNF- α expression, *Toxicology in vitro : an international journal published in association with BIBRA* **25(5)**, 1039–1044 (2011).

[3] K. A. Connors, *Thermodynamics of Pharmaceutical Systems: An Introduction for Students of Pharmacy*, ISBN:978-0-471-46139-5, 360 (2002).

DECREASE IN P53 FUNCTION IS AN EARLY STEP TOWARDS CHEMORESISTANCE IN COLORECTAL CANCER CELLS

Julius Žukas¹, Nadežda Dreizė¹, Silvija Urnikytė¹, Mantas Špakovas¹

¹Proteomics Centre, Vilnius University Institute of Biochemistry, Vilnius, Lithuania
julius.zukas@bchi.stud.vu.lt

The p53 protein is a transcription factor, often labelled as the “guardian of the genome” due to its role in DNA repair and protection from cell malignant transformation. Depending on the type (chemotherapy, UV radiation, etc.) and extent of damage to the cell, p53 can trigger DNA damage response, senescence, or if the cell is damaged irreparably, apoptosis. Because of its importance, the deregulation of p53 can lead to susceptibility to cancer, or in the case of already malignant cells, to drug resistance. In colorectal cancer (CRC) p53 mutations are found in 43 % of tumours and usually are associated with advanced disease and chemoresistance to 5-fluorouracil, doxorubicin and cisplatin.

Here we show that short exposure to moderate amounts of oxaliplatin (OxaPt) leads to the downregulation of p53 in CRC cell line HCT116 expressing wild-type p53. This downregulation impairs expression of the cell cycle-arresting protein p21 and pro-apoptotic proteins BAX, FAS, DR5, PUMA, therefore rendering cells moderately resistant to OxaPt. After transfection with wild-type inducible p53 the sensitivity to OxaPt is restored. Interestingly, HCT116 cells showing high resistance to OxaPt after prolonged exposure to the drug (HCT-Oxa), harbour p53 mutations and have downregulated pro-apoptotic proteins. However, HCT-Oxa cells show no restoration of sensitivity to OxaPt after the induced expression of wild-type p53. These results suggest that the compromise of p53 function is important for the early steps of drug resistance in CRC, but dispensable for the late stage drug resistance.

THE EFFICACY OF GEMCITABINE ON VIABILITY AND SURVIVAL OF PANCREATIC CANCER CELLS POST AHR GENE SILENCING, IN VITRO

Gabrielė Karvelytė¹, Darius Stukas¹, Aldona Jasukaitienė¹, Jason Matthews², Antanas Gulbinas¹, Žilvinas Dambrauskas¹

¹ Faculty of Medicine, Medical Academy, Lithuanian University of Health Sciences, Lithuania

² University of Oslo, Norway

Gabriele.Karvelyte1@stud.lsmu.lt

Introduction. Pancreatic cancer (PC) is emerging as one of the most lethal types of cancer with only a 10% five-year survival rate [1]. This is attributed to the fact that most incidences of PC are diagnosed in advanced or metastatic stages [2]. In such cases, gemcitabine (GEM) remains one of the first-line drugs used for treatment [2,3] but the efficacy of the treatment can fall short due to PC tumour heterogeneity and its acquired resistance to said chemotherapies [4]. A notable aspect of PC is the remarkable overexpression of aryl hydrocarbon receptor (AhR) mRNA and subsequently AhR itself with mRNA expression increasing on average 27-fold [5]. AhR is a ligand-dependent nuclear receptor which upon ligand binding activates the transcription of several metabolising enzymes which are implicated in tumour initiation and progression [6]. Due to poor future projections, low survival rates, limited treatment options and commonly observed resistance to drugs, it's imperative to discover ways to improve upon currently available treatments by means of modifying the expression of potentially involved genes.

Aim. The aim of this research was to investigate how AhR gene silencing can alter the effect of gemcitabine on cell metabolic activity and long-term colony formation of different PC cell lines.

Methods. PC cell lines BxPC-3 and Su.86.86 were transfected by lipofectamine mediated siAhR for 24 hours. Afterwards the cell lines were treated with IC50 doses of GEM (determined for each cell line separately) for 48 hours. After the treatment, short-term cytotoxic effect of GEM was determined by MTT assay and long-term effect was determined by seeding cells for clonogenic assay and subsequently growing them for 7 days.

Results. Treatment of the modified (siAhR) BxPC-3 cell line with the IC50 dose of GEM resulted in a statistically significant decrease in the short-term metabolic activity to 21,4 +/- 3,9 % in comparison to 50,6 +/- 10 % in unmodified control cells. As for the Su.86.86 cell line, AhR gene silencing had a statistically significant effect on metabolic activity in and of itself while also increasing cell sensitivity to GEM, however these results are inconclusive due to the mentioned responsiveness to silencing itself. In regards to long-term clonogenic assay, the IC50 dose of GEM decreased unmodified BxPC-3 colony formation to 18,3 +/- 7,3 % and Su.86.86 to 30,3 +/- 4,2 % when compared to control cells. Silencing of AhR on its own resulted in a decrease of colony formation in the BxPC-3 line to 19,3 +/- 2,7 % and the Su.86.86 line to 27,7 +/- 4,9 % when compared to control cells. AhR silencing in combination with GEM treatment also caused a decrease in colony formation capabilities compared to control cells: the BxPC-3 line dropping to 3,7 +/- 1,6 % and the Su.86.86 line to 11,3 +/- 3,2 %. Furthermore, the Su.86.86 cell line was observed to be more resistant to GEM in both unmodified and transfected cells.

Conclusion. AhR expression modulation can possibly impact PC cell susceptibility to first-line drugs such as GEM which causes a detrimental effect on cell viability and long-term survival, however different responses of different cell lines show that the effect can vary depending on the profile of the cancer cells, therefore making reliable predictions difficult.

[1] Hu JX, Zhao CF, Chen WB, Liu QC, Li QW, Lin YY, Gao F. Pancreatic cancer: A review of epidemiology, trend, and risk factors. *World journal of gastroenterology*. 2021 Jul 7;27(27):4298.

[2] Kamisawa T, Wood LD, Itoi T, Takaori K. Pancreatic cancer. *The Lancet*. 2016 Jul 2;388(10039):73-85.

[3] Buscail L, Bournet B, Cordelier P. Role of oncogenic KRAS in the diagnosis, prognosis and treatment of pancreatic cancer. *Nat Rev Gastroenterol Hepatol*. 2020 Mar;17(3):153-168. doi: 10.1038/s41575-019-0245-4.

[4] Juiz NA, Iovanna J, Dusetti N. Pancreatic cancer heterogeneity can be explained beyond the genome. *Frontiers in oncology*. 2019 Apr 5;9:246.

[5] Koliopoulos A, Kleeff J, Xiao Y, Safe S, Zimmermann A, Büchler MW, Friess H. Increased arylhydrocarbon receptor expression offers a potential therapeutic target for pancreatic cancer. *Oncogene*. 2002 Sep;21(39):6059-70

[6] Dietrich C, Kaina B. The aryl hydrocarbon receptor (AhR) in the regulation of cell-cell contact and tumor growth. *Carcinogenesis*. 2010 Aug 1;31(8):1319-28.

SIALIDASE GENE EXPRESSION AND ENZYMATIC ACTIVITY ASSESSMENT IN THE DEVELOPING MOUSE HIPPOCAMPUS

Rimas Prokopovicius¹, Ugne Kuliesiute^{1,2}, Urte Neniskyte^{1,2}

¹Institute of Biosciences, Vilnius University, Lithuania

²VU-EMBL Partnership Institute, Vilnius University, Lithuania
rimas.prokopovicius@gmc.stud.vu.lt

Nearly all cells are covered in a carbohydrate-enriched coating called the glycocalyx, which is constructed out of various glycoconjugates and is one of the first barriers in cell-to-cell communication. Sialidases, enzymes also known as neuraminidases, cleave sialic acid from glycoconjugates and play a crucial role in the regulation of neuronal glycocalyx. Structural and chemical changes of the neuronal glycocalyx contribute to neuronal synapse formation and the removal of sialic acid is suggested as one of the mechanisms of synapse pruning, a process required to eliminate unnecessary synapses during brain development leading to healthy neuronal network [1]. There are four main sialidases, named Neu1 – Neu4, which vary in expression during the development of mammalian brain, with *Neu2* being barely expressed [2]. Neuronal sialylation is an essential process for healthy neuron activity [3], however the connection between sialidase activity and synaptic function is poorly understood, and the exact role of sialidases in the process of neuronal network development and maturation remains understudied.

During this study, the expression of sialidases between various age groups (P0 to P90) was quantified by real-time PCR and the ddCT method was used to analyse the collected data. At the same postnatal age points, enzymatic sialidase activity was measured in freshly collected mouse hippocampus tissue samples. Enzymatic activity was normalised to the amount of total protein in the sample. Statistical analysis was performed to determine the differences between age groups and sex effect.

Our results demonstrated that *Neu1* gene had the highest expression and the *Neu2* had the lowest gene expression. *Neu1* gene had the highest expression which remained consistent during the development of hippocampus, there was a slight increase in *Neu2* expression, *Neu3* expression decreased and *Neu4* gene had a tremendous (around 600 times) increase in expression, indicating that *Neu1* and *Neu4* play the primary roles in brain development. As for the enzymatic activity of sialidases, barely any activity was present in the P0 mice hippocampus, suggesting that sialidases do not contribute to the prenatal development of brain. The highest enzymatic activity of sialidases, around double compared to the other age groups, was observed at age P14 with significantly higher activity in male hippocampus compared to female. This discovery suggests that the neuronal desialylation of the hippocampus may differ between male and female mice.

Overall, we showed that *Neu1* gene expression is the highest in mouse hippocampus. However, at the early postnatal age development (P14) of mouse hippocampus an immense increase in the expression of *Neu4* was observed. In line, sialidases demonstrate the highest activity at the age of P14, which corresponds to the timepoint of most active developmental pruning of synapses in the hippocampus. Our findings suggest that sialidases play a key role in the mechanism of synaptic pruning in the developing brain.

[1] Paolicelli, R. C., Bolasco, G., Pagani, F., Maggi, L., Scianni, M., Panzanelli, P., Giustetto, M., Ferreira, T. A., Guiducci, E., Dumas, L., Ragozzino, D., & Gross, C. T. (2011). Synaptic pruning by Microglia Is Necessary for Normal Brain Development. *Science*, 333(6048), 1456-1458.

[2] Pshezhetsky, A. V. & Ashmarina, M. (2018). Keeping it Trim: Roles of Neuraminidases in CNS Function. *Glycoconj J*, 35, 375-386.

[3] Schnaar, R. L., Gerardy-Schahn, R., & Hildebrandt, H. (2014). Sialic Acids in the Brain: Gangliosides and Polysialic Acid in Nervous System Development, Stability, Disease, and Regeneration. *Physiol Rev*, 94, 461-518.

FOLICULOGENESIS-RELATED GENE EXPRESSION IN CHEMOTHERAPY-INDUCED PREMATURE OVARIAN FAILURE MODEL

Indrė Krastinaite¹, Veronika Viktorija Borutinskaitė¹, Rūta Navakauskienė¹

¹ Vilnius University, Life Sciences Center, Vilnius, Lithuania
indre.krastinaite@gmc.stud.vu.lt

Premature ovarian failure (POF) has become one of the main causes of infertility in women of reproductive age and the incidence of POF is increasing year by year, having a substantial impact on the physical and mental health of patients and increasing the economic burden on families and society as a whole. POF is characterized by follicle loss, ovarian dysfunction, decreased estrogen production, and finally resulting in infertility. This reproduction disorder affects 1% of women under the age of 40 and 0.1% of women under the age of 30. However, the etiology and pathogenesis of POF are complex and not very clear at present. Potential causes of POF are genetic, autoimmune disorders, and iatrogenic factors, such as ovarian surgery, radiotherapy, or chemotherapy [1]. In the past decade, stem cell-based therapy, particularly mesenchymal stem cells (MSCs), has emerged as one of the promising alternative treatments for POF. Due to their properties including immunoregulation, anti-inflammation, angiogenesis, anti-apoptosis, and trophicity, MSCs have been used extensively in reproductive medicine [2]. MSCs produce a large variety of bioactive factors that stimulate the survival, proliferation, and differentiation of the cells in the damaged tissue and facilitate its repair [3]. MSCs can be isolated from various adult or embryonic tissues, including bone-marrow, adipose, placenta, and others [4].

In our study, we investigated changes in the expression of genes important for folliculogenesis in a chemotherapy-induced POF mouse model. We observed the decreased expression of *Amh*, *Amhr*, *Fshr*, *Gjal*, *Mvh*, and *Zp1* genes due to chemotherapy. The decreased gene expression correlated with lower levels of Anti-Müllerian Hormone (AMH) in serum which indicated that chemotherapy led to ovarian dysfunction and the successful establishment of the POF model. During the next stage, MSCs were administered to the treated mice and the ovarian function recovery was evaluated at the gene expression level. The increased level of AMH in serum and changes in expression levels of the above-mentioned genes were observed when compared with expression levels after chemotherapy, indicating the healing of ovarian tissue. Additional experiments are required to confirm these findings and investigate the changes in the levels of folliculogenesis-associated protein expression.

[1] Lee, E. h., Han, et al. Establishment of Effective Mouse Model of Premature Ovarian Failure Considering Treatment Duration of Anticancer Drugs and Natural Recovery Time, *Journal of Menopausal Medicine* **24**(3), 196–203 (2018).

[2] Gao, M., Yu, Z., et al. Mesenchymal stem cells therapy: A promising method for the treatment of uterine scars and premature ovarian failure, *Tissue and Cell* **74**, 101676 (2022).

[3] Fu, Y., Karbaat, L., Wu, et al. Trophic Effects of Mesenchymal Stem Cells in Tissue Regeneration, *Tissue Engineering Part B: Reviews* **23**(6), 515–528 (2017).

[4] Mebarki, M., Abadie, C., et al. Human umbilical cord-derived mesenchymal stem/stromal cells: A promising candidate for the development of advanced therapy medicinal products, *Stem Cell Research & Therapy* **12**(1), 152 (2021).

CARBON FROM COCONUT SHELLS FOR EFFICIENT REMOVAL OF NITROBENZENE FROM AQUEOUS SOLUTION

Aleksandar M. Đorđević^{1,2}, Jadranka Milikić³, Aldona Balčiūnaite⁴ and Biljana Šljukić^{3,5}

¹University of Belgrade, Institute of General and Physical Chemistry, Studentski trg 12/V, 11158 Belgrade, Serbia

²University of Belgrade, Faculty of Chemistry, Studentskitrg 12–16, 11158 Belgrade, Serbia

³University of Belgrade, Faculty of Physical Chemistry, Studentski trg 12-16, 11158 Belgrade, Serbia

⁴Center for Physical Sciences and Technology, Saul'etekio ave. 3, Vilnius LT-10257, Lithuania

⁵CeFEMA, Instituto Superior Técnico, Universidade de Lisboa, 1049–001 Lisbon, Portugal

*adjordjevic@iofh.bg.ac.rs

Nitrobenzene (NB) is a common reagent in the industry. It is extensively used in the production of pesticides, dyes, explosives, polyurethane foams, elastomers, and industrial solvent production, and it is contained in industrial waste, thus being air, water, and soil pollutant [1-3]. The contamination of water sources by NB could lead to severe health risks for humans. Due to its poor biodegradability, long-term residues, and accumulation in the environment, many countries have listed NB as a priority pollutant. Therefore, strategies for removing NB from aqueous solutions must be developed [4-5].

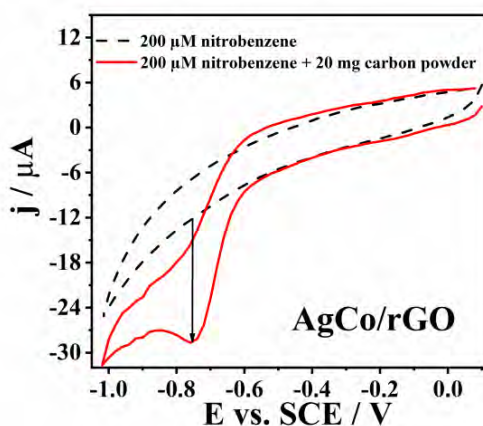


Fig. 1. Cyclic voltammograms of AgCo/rGO electrode in 200 μM nitrobenzene + phosphate buffer without (—) and after mixing with 20 mg of carbon powder (---).

The NB adsorption on the carbon obtained from coconut shells was studied at pH 7. Carbon powder (20 mg) was placed in 50 mL of 200 μM NB solution and mixed for 10 min. The sample was next filtered. Figure 1. shows that the control cyclic voltammogram of AgCo/rGO electrode recorded in solution after treatment with carbon powder does not show peaks in the potential range where the NB reduction reaction is expected, while the cyclic voltammogram recorded in 200 μM NB, before treatment, shows a reduction peak of NB at a potential of about -0.78 V. Result shows that carbon powder obtained from coconut shells can be used for successful adsorption of NB from aqueous solution.

Acknowledgments

The authors would like to thank the Ministry of Education, Science and Technological Development of the Republic of Serbia (contract no. 451-03-68/2022-14/200288, 451-03-68/2022-14/200146 and 451-03-68/2022-14/200168). Fundação para a Ciência e a Tecnologia (FCT, Portugal) is acknowledged for contract no. IST-ID/156-2018 (B. Šljukić).

[1] W. Wei, R. Sun, Z. Jin et al., Hydroxyapatite–Gelatin Nanocomposite as a Novel Adsorbent for Nitrobenzene Removal from Aqueous Solution. *Appl. Surf. Sci.* **292**, 1020–1029 (2014).

[2] Y. Mu, R. A. Rozendal, K. Rabaey, et al., Nitrobenzene Removal in Bioelectrochemical Systems. *Environ. Sci. Technol.*, **43** (22), 8690–8695 (2009).

[3] S.-S. Li, J.-H. Fang, L. Li, et al., An Ultra-Sensitive Electrochemical Sensor of Ni/Fe-LDH toward Nitrobenzene with the Assistance of Surface Functionalization Engineering. *Talanta* **225**, 122087 (2021).

[4] D. Wang, H. Shan, X. Sun, et al., Removal of nitrobenzene from aqueous solution by adsorption onto carbonized sugarcane bagasse. *Adsorption Science & Technology*. **36**(5-6):1366-1385 (2018).

[5] H. Gu, Y. Gao, M. Xiong, et al., Removal of nitrobenzene from aqueous solution by graphene/biochar supported nanoscale zero-valent-iron: Reduction enhancement behavior and mechanism, *Separation and Purification Technology* **275**, 119146 (2021).

ASCORBATE STABILIZED SYNTHESIS OF TIN SULFIDE AND THE APPLICATION FOR SUPERCAPACITORS

Asta Bronusiene¹, Anton Popov², Ieva Barauskiene¹, Ingrida Ancutiene¹

¹ Department of Physical and Inorganic Chemistry, Kaunas University of Technology, Radvilenu str. 19, LT-50254 Kaunas, Lithuania

² NanoTechnas – Center of Nanotechnology and Materials Science, Faculty of Chemistry and Geosciences, Vilnius University, Naugarduko st. 24, LT-03225, Vilnius, Lithuania
astbak@ktu.lt

With the consumption of traditional fossil energy and worsening of the environment, the development and utilization of renewable energy become extremely urgent contemporary [1]. Due to their unstable output of energy, electrochemical energy storage devices are key technologies to adjust and accelerate the effective application of green energy [2]. Supercapacitors, as necessary energy storage devices, have gained progressively more attention due to their excellent properties, such as high power density, long cycle life, fast charge-discharge process, and environmental friendliness [3].

One of the most difficult challenges is the development of thin films based on an inexpensive and simple process using materials of high abundance. It is very important to find cheap, environmentally friendly products that have the possibility of deposition in a large area and that adhere well to the substrate method. The aim of the work was to form environmentally friendly thin tin sulfide films by applying the safety and inexpensive SILAR method and using "green" precursors, aqueous solutions, low deposition temperature, and environmental safety reducing agent. The use of L-ascorbic acid for chemical synthesis is relatively new and less explored. Fluorine-doped Tin Oxide (FTO) glass slides were used as a substrate for the deposition of thin films of SnS.

Two high abundance precursor solutions were used for the deposition: tin(II) chloride and sodium disulfide. The reaction between tin ions complexed by ascorbic acid and sulfide ions resulted in the formation of tin sulfide film. Thin films of tin sulfide had a blackish brown color. The deposited films were uniform, without any slots, pinholes. Thin films adhere to the substrate by Van der Waals forces and based on these forces crystals possess unique physical and chemical properties. These properties, including a large surface area to volume ratio, high tensile strength, and novel electronic band structures that do not have counterparts in traditional systems, have been widely researched.

The composition, optical and electrochemical properties of the deposited films were characterized. Scanning electron microscopy images allowed us to examine the microstructure of the samples. Tin sulfide is formed of irregular morphology nanoparticle clusters, which are densely packed. X-ray diffraction (XRD) patterns show the formation of orthorhombic phases, mainly SnS. The peaks of SnO₂ which are on the top of the substrate were also indicated. To summarize the acquired results, more intensive SnS peaks are observed when using 30 SILAR cycles, and their prolongation is clearly seen with an increase in the amount of L-ascorbic acid. Tin sulfide films deposited on FTO glass slides were found to consist of an average crystallite size of 9 to 10 nm and 11 to 15 nm for films obtained using 20 and 30 SILAR deposition cycles, respectively. The Raman study together with the X-ray diffraction confirms the growth of single-phase SnS films. The band gap of the samples was in the range of 1.1-1.4 eV, and the value clearly depends on the deposition conditions. Electrochemical measurements showed meaningful results. It appears that both the number of cycles and the quantity of ascorbic acid have a certain influence on the performance of films in this potential range. Generally, the higher number of SILAR deposition cycles increases the mass of films and, therefore, the current density is enhanced by the reactions occurring in the deeper layers of the active substance. Taking into account the impact of ascorbic acid, a higher amount has a positive effect when using 20 SILAR cycles. Presumably, this may be due to the higher probability of intercalation of ions and organic fragments between layers during the SILAR synthesis. When 0.8 g of ascorbic acid was used, a significant increase in specific capacity and specific energy was observed due to an increase in the number of SILAR cycles. The tin sulfide film prepared using the lowest amount of ascorbic acid is able to generate the specific capacitance of 6.35 F·g⁻¹ with the best specific energy value of 3.53 Wh·kg⁻¹. These results confirmed that obtained tin sulfide films on FTO glass are a promising material to be used as a supercapacitor.

In this paper, we describe a simple, eco-friendly method for the synthesis of tin sulfide nanoparticles stabilized with L-ascorbic acid. The results obtained showed that SnS thin films demonstrate the possibility of using them in electrochemical capacitors.

[1] Ibrahiem, D. M. & Hanafy, S. A. Dynamic linkages amongst ecological footprints, fossil fuel energy consumption and globalization: an empirical analysis. doi:10.1108/MEQ-02-2020-0029.

[2] Syum, Z. *et al.* Superior lithium-ion storage performance of hierarchical tin disulfide and carbon nanotube-carbon cloth composites. *J Power Sources* **482**, 228923 (2021).

[3] Barik, R., Devi, N., Perla, V. K., Ghosh, S. K. & Mallick, K. Stannous sulfide nanoparticles for supercapacitor application. *Appl Surf Sci* **472**, 112–117 (2019).

PRUSSIAN BLUE – MODIFIED ELECTRODES IN FORMATION OF BIOSENSORS

Gabija Kavaliauskaitė¹, Aušra Valiūnienė¹

¹ Department of Physical Chemistry, Institute of Chemistry, Vilnius University, Lithuania
Gabija.kavaliauskaite@chgf.stid.vu.lt

Iron hexacyanoferrate (Prussian blue (PB)) is an inorganic, electrochromic compound, which is selective for several monovalent ions (Cs^+ , Rb^+ , K^+ and NH_4^+). These ions (Cs^+ , Rb^+ , K^+ and NH_4^+) are incorporated in the crystal lattice of PB when PB is electrochemically reduced in Cs^+ , Rb^+ , K^+ or NH_4^+ ions containing solution [1]. Moreover, the concentration of PB reduction promoting ions (Cs^+ , Rb^+ , K^+ and NH_4^+) affects the reduction potential of PB. For this reason, PB can be used as a signal transducer in optical and electrochemical analytical systems, such as electrochemical ion sensors [2]. Thus, Prussian Blue is often used as a redox mediator and signal transducer in biosensors, for example urea and glucose biosensors [3, 4].

In this research work, Prussian Blue was used in formation of glass/FTO/PB/enzyme type electrodes, for the analysis of glucose and urea (Fig.1). Furthermore, these studies introduce the glass/FTO/PB/GOx electrode for optical glucose sensing and the glass/FTO/PB/urease electrode for electrochemical sensing of urea by using electrochemical impedance spectroscopy.

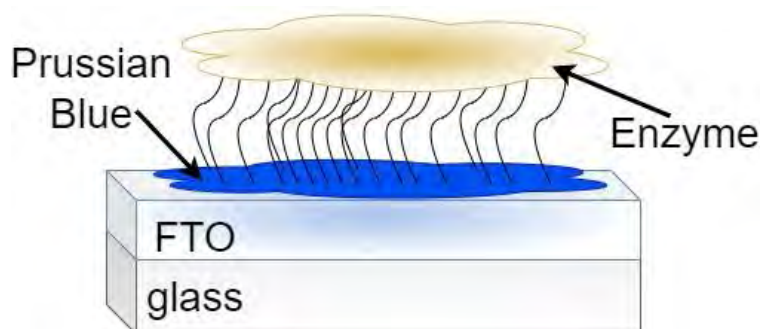


Fig. 1. Scheme of glass/FTO/PB/enzyme type electrode construction.

[1] A.A. Karyakin, E. E. Karyakina, L. Gorton, On the mechanism of H_2O_2 reduction at Prussian Blue modified electrodes, *Electrochemistry Communications* 1, p. 78 – 82 (1999).

[2] A. A. Karyakin, Prussian Blue and Its Analogues: Electrochemistry and Analytical Applications, *Electroanalysis*, No. 10, 13 (2001).

[3] P. Virbickas, A. Valiuniene, G. Kavaliauskaite, A. Ramanavicius, Prussian White-Based Optical Glucose Biosensor, *Journal of The Electrochemical Society*, 166 (12), B927- B932 (2019).

[4] A. Valiuniene, G. Kavaliauskaite, P. Virbickas, A. Ramanavicius, Prussian Blue based impedimetric biosensor, *Journal of Electroanalytical Chemistry*, 895, (2021).

CRYO-FOCUSING IN GC ANALYSIS: A NEW APPROACH FOR MEASURING TERPENES IN *CANNABIS SATIVA*

Audrius Sadaunykas, Audrius Zolumskis, Evaldas Naujalis

Organic Chemistry Department, State Research Institute Center for Physical Sciences and Technology
Saulėtekio al. 3, LT-10257 Vilnius, Lithuania
audrius.sadaunykas@ftmc.lt

Gas chromatography (GC) is an analytical technique that has undergone numerous improvements since its introduction in 1903 [1]. One approach to improving GC is through the use of cryo-focusing or cryo-enrichment [2], which involves cooling down a portion or all of the GC column to enhance various aspects of chromatographic analysis. A new and improved module was developed, featuring a two-stage cryo-cooler and improved temperature control capabilities. The performance of this improved module was evaluated by developing and validating a method for the measurement of α -pinene and β -caryophyllene in *Cannabis Sativa* plants [3]. The aim of this study was to improve upon previous GC cryo-enrichment techniques and apply this improved method to the analysis of these terpene compounds in *Cannabis Sativa* plants.

An in-house GC cryo-enrichment module was developed and constructed. It is an add-on device that can be attached to a standard GC system via a heated transfer line (as shown in Figure 1). The module includes a custom-made aluminum column holder that sits on top of a cryo-cooled aluminum block. The aluminum block is cooled to -60 degrees Celsius using a SP Scientific FC100 Flexi-Cool immersion cooler. The column holder contains a nichrome wire heater and is controlled by a stepper motor that moves the holder between cooling and heating positions. During sample injection, the column holder is pressed down onto the cryo-cooled aluminum block and maintained at -60 degrees Celsius. After multiple injections, the column holder is raised by the stepper motor and heated to 150 degrees Celsius. The GC column is then passed from the GC system through the transfer line, wrapped around the column holder and returned to the GC system via the same transfer line.

To test the performance of the system, method for terpene analysis with GC was created and validated. The method was found to be precise, accurate, sensitive, linear, and have low limits of detection and quantification. The cryo-enrichment module allowed for multiple injections of the sample, resulting in a higher sensitivity and concentration of the analytes in the GC analysis. Overall, the improved cryo-enrichment module and method for measuring α -pinene and β -caryophyllene in *Cannabis Sativa* were proven to be an efficient enhancement over previous cryo-enrichment techniques.

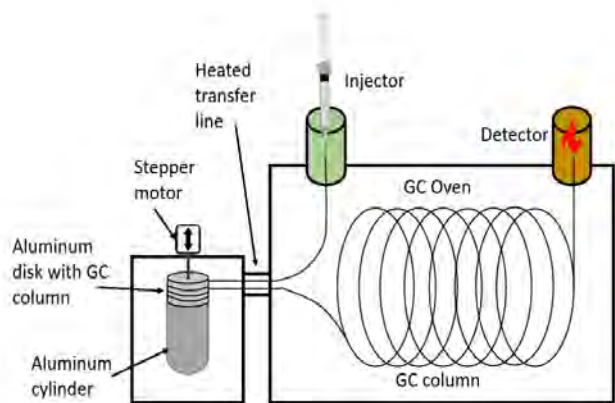


Fig. 1. Gas chromatography system with cryofocusing add-on

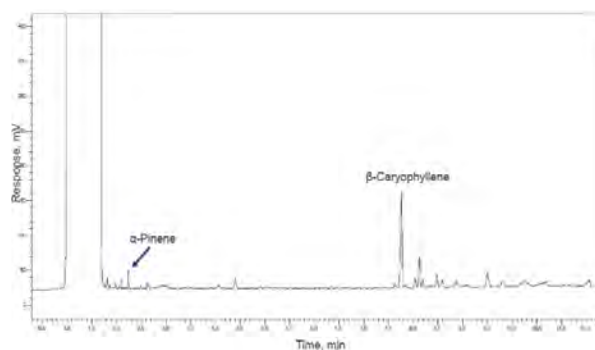


Fig. 2. Chromatogram of *Cannabis sativa* extract

- [1] Bartle, Keith D., and Peter Myers. "History of gas chromatography." *TrAC Trends in Analytical Chemistry* 21.9-10 (2002): 547-557.3. Chin, S.-T., Maikhunthod, B., & Marriott, P. J. *Universal Analytical Chemistry*, 83(17), 6485-6492 (2012).
- [2] Chopra, Miriam D., et al. "Residual solvent analysis with hyper-fast gas chromatography-mass spectrometry and a liquid carbon dioxide cryofocusing in less than 90 s." *Journal of Chromatography A* 1648 (2021): 462179.
- [3] Nuutinen, Tarmo. "Medicinal properties of terpenes found in *Cannabis sativa* and *Humulus lupulus*." *European journal of medicinal chemistry* 157 (2018): 198-228.10. Amaral, Renata G., et al. *Journal of Applied Biomedicine* 14.4 265-272 (2016).
- [4] Sadaunykas A., On-column cryofocusing and analyte enrichment device for gas chromatography systems, *Chemija*, Vol 31, Issue 4, 284-289, (2020)

SYNTHESIS OF CALCIUM CHLORAPATITE THROUGH THE PHASE CONVERSION OF AMORPHOUS CALCIUM PHOSPHATE IN MOLTEN CHLORIDES

Erlandas Kabasinskas¹, Jonas Stadulis¹, Diana Griesiute¹, Dovydas Karoblis¹, Eva Raudonyte-Svirbutaviciene¹, Aleksej Zarkov¹

¹ Institute of Chemistry, Vilnius University, Naugarduko 24, LT-03225 Vilnius, Lithuania
erlandas.kabasinskas@chgf.stud.vu.lt

Calcium phosphates (CPs) are the family of materials, widely used in different areas such as medicine and bone regeneration, catalysis, sensors, removal of heavy metals from water, as host matrices for the development of optical materials, etc. CPs can be classified by many parameters including crystal structure, Ca-to-P ratio, presence of other structural species (e.g. OH⁻, CO₃²⁻, Cl⁻, F⁻). Compositional and structural variety of CPs leads to their different chemical and physical properties. Some CPs can be easily synthesized by direct precipitation from aqueous solutions or solid state reaction. Another approach for the synthesis of CPs considers phase transformation of less stable CPs under specific conditions. [1], [2]

The remarkable member of this family is amorphous calcium phosphate (ACP), which possesses a number of features making it a very special material. Due to the absence of crystalline ordering ACP exhibits very high solubility and reactivity. Moreover, unlike the most crystalline CPs, where Ca-to-P ratio is well-defined, in ACP this ratio can vary in a relatively broad range from 1.2 to 2.2. ACPs can be used as precursors for the preparation of crystalline materials. Phase conversion of ACP to other crystalline CPs can be induced in different ways. In aqueous medium ACP rapidly transforms to apatite-like crystalline material. Another approach is the crystallization of ACP induced by thermal treatment at elevated temperatures. ACP with the Ca-to-P ratio 1.5:1 upon calcination transforms to tricalcium phosphate (TCP, Ca₃(PO₄)₂). This material cannot be precipitated directly from aqueous solution under artificial or physiological conditions, it can be synthesized only through the thermal treatment of other CPs. The α -TCP prepared in such a manner is also called metastable α -TCP, upon heating it transforms to β -TCP at around 950 °C and again to α -TCP at around 1125 °C.[3]

In the present work, we demonstrate the phase transformations of ACP in molten chlorides. LiCl, NaCl, KCl, CaCl₂ and their mixtures were mixed with initial ACP and annealed above their melting point. The obtained results revealed that ACP reacts with molten chlorides resulting in the formation of chlorinated CPs. Under certain conditions ACP can be converted to calcium chlorapatite (Ca₅(PO₄)₃Cl) or CaPO₄Cl. The influence of synthesis conditions such as annealing temperature, time, flux composition and ACP-to-chlorides ratio was investigated in detail.

The phase purity, crystal structure and structural changes were evaluated by powder X-ray diffraction (XRD), Fourier-transform infrared (FTIR) spectroscopy. Scanning electron microscopy (SEM) was used for the characterization of morphological features of products.

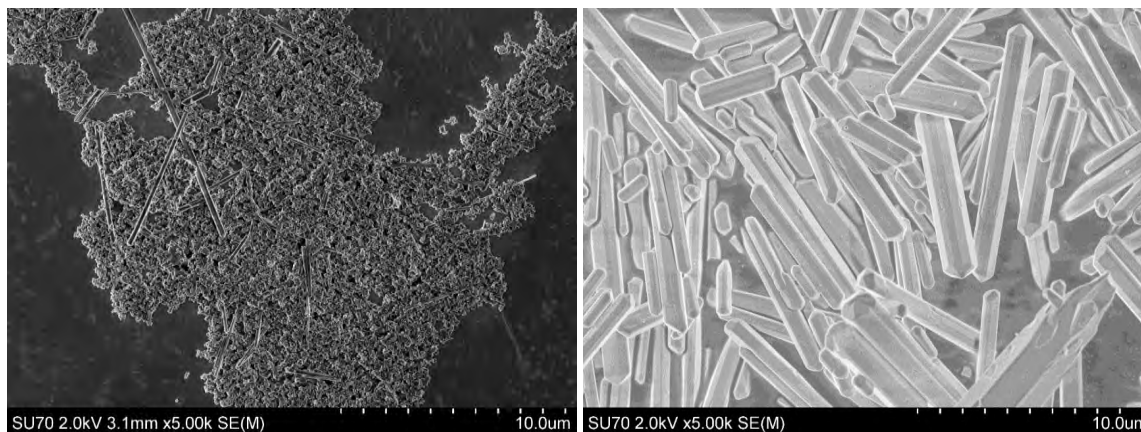


Fig. 1. SEM images of calcium chlorapatite powders obtained under different synthetic conditions.

-
- [1] Z. Zhang, *et al.*, The energy transfer from Eu²⁺ to Tb³⁺ in calcium chlorapatite phosphor and its potential application in LEDs, *Applied Physics B* 91, 529–537 (2008).
[2] D. Huang *et al.*, Remediation of lead-contaminated sediment by biochar-supported nano-chlorapatite: Accompanied with the change of available phosphorus and organic matters, *J Hazard Mater* 348, 109–116 (2018).
[3] S. Dorozhkin, Calcium Orthophosphates in Nature, Biology and Medicine, *Materials* 2009 vol. 2, no. 2, 399–498 (2009).

EVALUATION OF THE INTERACTION BETWEEN SARS-COV-2 SPIKE GLYCOPROTEINS AND THE MOLECULARLY IMPRINTED POLYPYRROLE

Ernestas Brazys¹, Vilma Ratautaitė², Raimonda Boguzaitė², Arūnas Ramanavičius^{1,2}

¹Department of Physical Chemistry, Institute of Chemistry, Faculty of Chemistry and Geosciences, Vilnius University, Naugarduko str. 24, Vilnius LT-03225, Lithuania

²Department of Nanotechnology, State Research Institute Center for Physical Sciences and Technology, Sauletekio av. 3, Vilnius LT-10257, Lithuania
ernestas.brazys@chgf.stud.vu.lt

Severe acute respiratory syndrome coronavirus 2 (SARS-CoV-2) is a virus that causes COVID-19 disease. In this research, SARS-CoV-2 spike glycoprotein was selected as a template for the development of an electrochemical sensor based on the molecularly imprinted polymer.

The general molecular imprinting process consists of chemical or electrochemical polymerization from a mixture containing functional monomers and template molecules. The polymerisation step is then followed by the removal of the template, which generates the binding sites in the structure of the polymer, which are specific or complementary to the template molecules [1]. This characteristic can be used in the development of sensors for detecting both biological and chemical molecules [2].

In this study, the SARS-CoV-2 spike glycoprotein imprinted polypyrrole-based (MIP-Ppy) sensor was developed [3]. The pre-polymeric mixture contained 0.5 M pyrrole as a monomer and 50 µg/mL of SARS-CoV-2 spike glycoprotein as a template in PBS solution, pH 7.4. The polymeric layer was deposited electrochemically onto the surface of a platinum electrode by a sequence of potential pulses. The template molecules were extracted by washing the polymer in 0.05 M H₂SO₄ solution for 10 min. In comparison, an electrode was modified with a non-imprinted polypyrrole layer (NIP-Ppy). The properties of both MIP-Ppy and NIP-Ppy were evaluated by pulsed amperometric detection. The interaction between SARS-CoV-2 spike glycoproteins and MIP-Ppy was assessed by the Anson plot-based calculations.

The obtained results prove that SARS-CoV-2 glycoprotein interaction is stronger with MIP-Ppy film than with NIP-Ppy film.

Acknowledgement: This project has received funding from the Research Council of Lithuania (LMTLT), GILIBERT 2021 program agreement No S-LZ-21-4 and was co-founded by Campus France grant No. 46593RA (PHC GILIBERT 2021).

[1] S. A. Piletsky, A. P. F. Turner. Electrochemical Sensors based on Molecularly Imprinted Polymers. *Electroanalysis*, **14**(5), 317–323 (2002).

[2] J. J. BelBruno. Molecularly Imprinted Polymers. *Chemical Reviews*, **119**(1), 94–119 (2019).

[3] V. Ratautaitė, R. Boguzaitė, E. Brazys, D. Plausinaitis, S. Ramanavičius, U. Samukaite-Bubniene, M. Bechelany, A. Ramanavičius. Evaluation of the interaction between SARS-CoV-2 spike glycoproteins and the molecularly imprinted polypyrrole. *Talanta*, **253** (2023).

INVESTIGATION OF THE CORONAVIRUS SARS-CoV-2 STRUCTURAL PROTEINS AND SPECIFIC ANTIBODIES INTERACTIONS USING OPTICAL AND PIEZOELECTRIC METHODS

Silvija Juciūtė¹, Vincentas M. Mačiulis^{1,2}, Ieva Plikusienė^{1,2}

¹ Nanotechnas, Nanotechnology and Materials Sciences Center, Faculty of Chemistry and Geosciences, Vilnius University, Naugarduko 24, Vilnius, Lithuania;

² State Research Institute Centre for Physical Sciences and Technology, Sauletekio Avenue 3, Vilnius, Lithuania
silvija.juciute@chgf.stud.vu.lt

The SARS-CoV-2 coronavirus caused a pandemic three years ago, and although society became used to the virus, scientists never stopped investigating its interactions with the human body. The development and application of vaccines against this virus helped to control the unwanted reactions caused by Covid-19 disease. As new variants of the SARS-CoV-2 spike protein emerge, it is necessary to find ways to faster virus detection so new outbreaks can be avoided. Biological immunosensors can selectively and effectively detect various antigens or antibodies. Development of immunosensors that are sensitive to the SARS-CoV-2 spike protein could make monitoring of virus spread easier and fatal consequences could be avoided. The SARS-CoV-2 spike protein is one of the main proteins of the virus. The spike protein binds to the ACE2 receptor found on the human cells and triggers further spread of the virus in the body [1]. The immune system must react fast and synthesize specific antibodies to block the spike protein. To get better understanding of immune complex formation different SARS-CoV2 spike protein variants were chosen for our research and interactions with specific antibodies were investigated.

One of the methods used in this investigation was total internal reflection ellipsometry (TIRE). TIRE is an optical method which can be applied to thin layer optical properties' research. During the experiment, changes in the phase Δ and the amplitude Ψ of light wave are measured and the index of refraction and dielectric constant of the material can be calculated. TIRE can be applied to the monitoring as it is very sensitive, non-destructive and label-free method, so biomolecules such as proteins do not lose their structure and activity [2].

Quartz crystal microbalance with dissipation (QCM-D) is a piezoelectric method using which the changes in frequency and dissipation are measured during real time biomolecules layer formation. QCM-D is a noninvasive, label-free method that can be used for measurements in liquids.

The combination of QCM-D with spectroscopic ellipsometry (SE) was applied to study SARS-CoV-2 coronavirus spike proteins and specific antibodies interactions. TIRE was used to find the most effective immobilization conditions for different spike proteins (wild, α and β variants). SARS-CoV-2 spike proteins' interaction with specific antibodies were researched by QCM-D and SE methods combination and thermodynamical parameters of immune complex formation were calculated.

[1] Ramanathan, Muthukumar et al. "SARS-CoV-2 B.1.1.7 and B.1.351 spike variants bind human ACE2 with increased affinity," *Lancet Infect. Dis.*, vol. 21, no. 8, p. 1070, 2021.

[2] I. Plikusienė, V. Mačiulis, A. Ramanaviciene, Z. Balevicius, A. Zvirbliene, and A. Ramanavicius, "Evaluation of kinetics and thermodynamics of interaction between immobilized SARS-CoV-2 nucleoprotein and specific antibodies by total internal reflection ellipsometry," *J. Colloid Interface Sci.*, vol. 594, pp. 195–203, 2021.

ELECTRONIC EXCITED STATES OF CHLOROPHYLLS IN PHOTOSYNTHETIC COMPLEX CP29

Sandra Barysaite^{1,2}, Andrius Gelzinis^{1,2}, Jevgenij Chmeliov^{1,2}, Leonas Valkunas^{1,2}

¹ Faculty of Physics, Vilnius University, Vilnius, Lithuania

² Department of Molecular Compound Physics, Centre for Physical Sciences and Technology, Vilnius, Lithuania
sandra.barysaite@ff.stud.vu.lt

Light harvesting – the first step of photosynthesis – is carried out by photosystems I and II (PSI and PSII) that are located in the thylakoid membrane of chloroplasts. PSII oxidizes water and produces oxygen molecules that can react with the excited triplet state of chlorophyll and generate singlet oxygen which can cause photo-oxidative damage to PSII. For this reason, plants have developed protective mechanisms such as non-photochemical quenching (NPQ) [1]. Quenching sites have been identified in LHCII and CP29 antenna complexes of PSII. NPQ in LHCII is thought to be correlated with Chl–Chl charge-transfer (CT) states [2]; this could also be the case for CP29 because it is positioned between the outer antenna complexes and the reaction center.

In this work, the high resolution crystal structure of spinach photosynthetic complex CP29 [3] was chosen for the identification of Chl–Chl CT states in CP29. CT states can form between strongly interacting chlorophylls, so only those chlorophyll dimers with distances less than 10 Å between chlorophylls were used in calculations. The geometries of chlorophylls forming the dimers were optimized in vacuum using density functional theory (DFT). In all calculations performed in this work, the phytyl group in chlorophyll structure was changed to methyl group. The excited state energy spectra and related parameter values for each dimer were calculated using time-dependent density functional theory (TD-DFT). The values of static and transition dipole moments and the sums of Mulliken charges were taken into consideration to identify CT states in dimers.

Nine CT states were identified in five of the six analyzed chlorophyll dimers and are presented in Table 1 together with the energy values. CT states with the lowest energies could possibly be related to NPQ and other processes in PSII; the lowest energy CT state was identified in dimer *b614–a613*. The results were compared to the experimental data in Ref. [4], where time-resolved fluorescence was measured in CP29 and its knock-out mutants, i.e. CP29 lacking either chlorophyll *a612* or *a603*; these chlorophylls form strongly coupled dimers *a611–a612* and *a603–a609* that were analyzed in this work.

Table 1. Excited states S_n corresponding to the identified CT states in dimers and their energies in ascending order.

Chl–Chl dimer	S_n	Energy, cm^{-1}
<i>b614–a613</i>	S_5	22565
<i>b606–a604</i>	S_5	22780
<i>a611–a612</i>	S_5	23070
<i>a611–a615</i>	S_5	24276
<i>a603–a609</i>	S_5	24417
<i>a603–a609</i>	S_6	24672
<i>a611–a612</i>	S_6	25330
<i>a611–a615</i>	S_6	25394
<i>b606–a604</i>	S_6	25459

[1] P. Müller, X.-P. Li, K. K. Niyogi, Non-photochemical quenching. A response to excess light energy, *Plant Physiology* **125**, 1558–1566 (2001)

[2] Y. Miloslavina, *et al.*, Far-red fluorescence: a direct spectroscopic marker for LHCII oligomer formation in non-photochemical quenching, *FEBS Letters* **582**, 3625–3631 (2008)

[3] X. Pan, *et al.*, Structural insights into energy regulation of light-harvesting complex CP29 from spinach, *Nature Structural & Molecular Biology* **18**, 309–315 (2011)

[4] V. Mascoli, *et al.*, Light-harvesting complexes access analogue emissive states in different environments, *Chemical Science* **11**, 5697–5709 (2020)

OPTIMIZATION OF SOL-GEL SYNTHESIS PROCEDURE FOR DEPOSITION OF BiVO_4 COATINGS

Pamela Rivera¹, Milda Petrulevičienė¹, Irena Savickaja¹, Kamila Turuta², Jurga Juodkazytė¹, Arūnas Ramanavičius¹

¹ Center for Physical Sciences and Technology, Department of chemical engineering and technology
Saulėtekio av. 3, LT-10257 Vilnius

² Institute of Chemistry, Faculty of Chemistry and Geosciences, Naugarduko str. 24, LT-03225 Vilnius University, Lithuania
pamela.rivera@ftmc.lt

The presence of organic pollutants in wastewater negatively impacts people and ecosystems [1]. Among advanced oxidation processes used for wastewater treatment, photocatalytic degradation of pollutants using solar light has been attracting increasing attention recently [2]. Bismuth vanadate (BiVO_4) is a promising semiconductor photocatalyst due to low production cost, low toxicity, high photostability, resistance to photo-corrosion and narrow band gap with a good response to visible-light excitation [3], however BiVO_4 photoanodes have not yet achieved the desired performance to make them suitable for practical applications [4].

In the present work the influence of polyvinyl alcohol (PVA) used in sol-gel process as well as the number of deposition cycles (equivalent to thickness of the layer) on the photoelectrochemical (PEC) activity of BiVO_4 coatings was investigated. BiVO_4 films were deposited on fluorine doped tin oxide (FTO) substrate using dip-coating technique. Crystalline structure and morphology of coatings were analyzed using X-ray diffraction (XRD) analysis and scanning electron microscopy (SEM), respectively. The PEC properties of coatings were evaluated using cyclic voltammetry (CV) and electrochemical impedance spectroscopy (EIS).

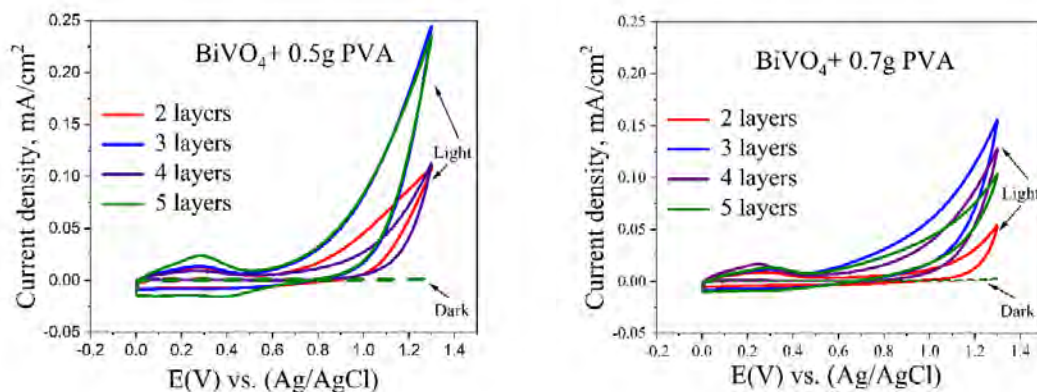


Figure 1. Cyclic voltammograms of BiVO_4 electrodes with different number of layers and PVA amount used in the synthesis. Experiments were performed in 0.5 M Na_2SO_4 solution; Reference electrode: Ag/AgCl; potential scan rate 50 mV/s. Light intensity 100mW/cm².

Obtained results revealed, that amount of PVA used in the sol-gel process has significant influence on PEC performance of the coatings. Smaller amount of PVA (0.5 g instead of 0.7 g) was beneficial for PEC activity and photoanodic current increased with the number of deposition cycles (Fig. 1). The results on PEC production of reactive species in the electrolytes of various composition as well as the efficiency of decomposition of organic compounds will be presented at the conference.

Acknowledgement: This project has received funding from the Research Council of Lithuania (LMTLT), agreement No S-PD-22-2

- [1] Y. Wen, G. Schoups, and N. van de Giesen, "Organic pollution of rivers: Combined threats of urbanization, livestock farming and global climate change," *Sci Rep*, vol. 7, no. 1, p. 43289, Feb. 2017, doi: 10.1038/srep43289.
- [2] S. Bakhtiarnia, S. Sheibani, A. Billard, H. Sun, E. Aubry, and M. A. P. Yazdi, "Enhanced photocatalytic activity of sputter-deposited nanoporous BiVO_4 thin films by controlling film thickness," *J Alloys Compd*, vol. 879, p. 160463, Oct. 2021, doi: 10.1016/j.jallcom.2021.160463.
- [3] M. A., M. J., M. Ashokkumar, and P. Arunachalam, "A review on BiVO_4 photocatalyst: Activity enhancement methods for solar photocatalytic applications," *Appl Catal A Gen*, vol. 555, pp. 47–74, Apr. 2018, doi: 10.1016/j.apcata.2018.02.010.
- [4] L. Xia, J. Li, J. Bai, L. Li, S. Chen, and B. Zhou, " BiVO_4 photoanode with exposed (040) facets for enhanced photoelectrochemical performance," *Nanomicro Lett*, vol. 10, no. 1, 2018, doi: 10.1007/s40820-017-

PHOTOPOLYMERIZATION OF GLYCEROL ACRYLATES AND THEIR MIXTURES WITH VANILLIN STYRENE

Evelina Saunoryte¹, Aukse Navaruckiene¹, Jolita Ostrauskaite¹

¹ Department of Polymer Chemistry and Technology, Kaunas University of Technology, Radvilenu Rd. 19, LT-50254 Kaunas, Lithuania.
evelina.saunoryte@ktu.edu

In recent years, photopolymerization engendered high interest due to the considerable practical and economic benefits. It is characterized by rapid cure, low energy consumption, high efficiency, low volatile organic compound emission, and the large number of applications not only in conventional areas such as coatings, inks, and adhesives, but also in high-tech domains, such as microelectronics, optoelectronics, laser imaging, stereolithography, and nanotechnology [1]. The renewable feedstock use in materials production using photopolymerization processes reveals the great potential of renewable raw molecules and their ability to substitute petrochemical-based materials [2]. Glycerol, the by-product of biodiesel refining is a promising candidate which can be used as monomer in the synthesis of polymers as it is or after chemical modification [3].

In this work, three glycerol acrylates having different number of acryl groups: 2-hydroxy-3-phenoxypropyl acrylate, glycerol 1,3-diglycerolate diacrylate, and glycerol trimethacrylate, have been photopolymerized with addition of vanillin styrene in order to obtain copolymers with improved mechanical and thermal properties. The homopolymers of glycerol acrylates have been synthesized for comparison. Diphenyl(2,4,6-trimethylbenzoyl)phosphine oxide was used as photoinitiator. The chemical structure of monomers is presented in Fig 1.

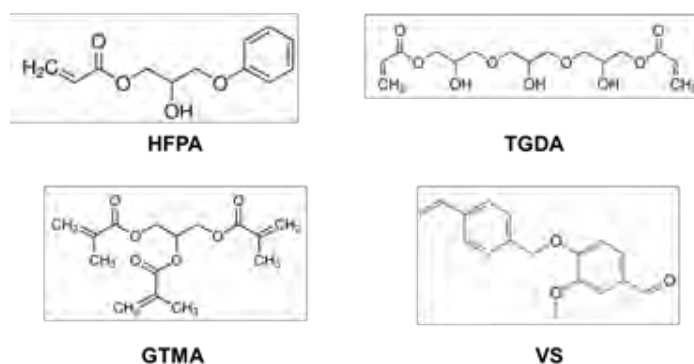


Fig. 1. Chemical structure of 2-hydroxy-3-phenoxypropyl acrylate (HFPA), glycerol 1,3-diglycerolate diacrylate (TGDA), glycerol trimethacrylate (GTMA), and vanillin styrene (VS)

The structure of the homopolymers and copolymer was confirmed by FT-IR spectroscopy, Soxhlet extraction, and swelling test. It was determined that the insoluble fraction of the resulting copolymers depended on the number of functional groups of the glycerol acrylate used and ranged from 93 % to 97 %. The degree of swelling of the copolymers in toluene was very low (0,45-4 %) while that of the homopolymers was a bit higher (0,2-14 %) and depended on the number of functional groups of the monomers used. The copolymers obtained using mono- and difunctional glycerol acrylates had a higher density of cross-links and less swelled than the homopolymers of the corresponding glycerol acrylates. In the case of trifunctional glycerol acrylate, the results were reversed.

- [1] Y. Fuchs, O. Soppera, K. Haupt, Photopolymerization and photostructuring of molecularly imprinted polymers for sensor applications-A review, *Analytica Chimica Acta* **717**, 7-20 (2012).
[2] L. Pierau, C. Elian, J. Akimoto et al., Bio-sourced monomers and cationic photopolymerization-The green combination towards eco-friendly and non-toxic materials, *Progress in Polymer Science* **127**, 1015187 (2022).
[3] Z.Y. Ben, H. Samsudin, M.F. Yhaya, Glycerol: Its properties, polymer synthesis, and applications in starch based films, *European Polymer Journal* **175**, 111377 (2022).

REMOVAL EFFICIENCY AND DISTRIBUTION OF MICROPLASTIC PARTICLES AT WASTEWATER TREATMENT PLANT

Sonata Pleskytė, Ieva Uogintė, Steigvilė Byčenkienė

Department of Environmental Research, Center for Physical Sciences and Technology, Lithuania
sonata.pleskyte@ftmc.lt

Plastics are synthetic or semi-synthetic polymeric materials with a wide range of additives (plasticizers, acid scavengers, pigments, thermal stabilizers). Their unique properties such as lightweight, elasticity, durability, resistance to corrosion and moisture lead to a wide range of application fields. The plastic particles that are larger than 1 nm but smaller than 5 mm in size are defined as microplastic particles (MPs). Many different environments contain MPs including the air, soil, ocean, and even freshwater systems. Moreover, microplastic particles cause an increasing concern as they pose threats to aquatic species as well as human beings. This type of pollutant is ubiquitous on our planet and might cause a global hazard in terms of environmental health.

There are two types of microplastic particles: primary and secondary. Primary MPs can be produced to have a specific small size which is widely used in personal care products, cosmetics, different detergents, and cleaners. For example, researchers have found between 327 and 832 microplastic particles per gram in toothpaste and facial scrubs [1], [2]. Secondary MPs are fragmented from larger-sized pieces of plastics as a result of environmental degradation processes. Either primary or secondary MPs have different sizes, shapes, colors, and chemical compositions. The properties of MPs mentioned above are crucial for removing these particles.

Studies indicated that wastewater treatment plants (WWTPs) play an important role in the microplastic particles removal process. The majority of MPs from industrial and domestic sources are captured in wastewater treatment plants. Modern WWTPs include three main stages of treatment: primary precipitation (sand or other larger debris settling and grease removal), secondary settling (biological treatment), and tertiary treatment (advanced oxidation processes). The removal efficiency of MPs between countries is surprisingly varying from 64% in Southeast Spain to 99% in Finland [3],[4]. However, even advanced wastewater treatment technologies (such as ozonation, chlorination, physical sorption, ultrafiltration, and membrane bioreactors) are unable to completely remove microplastic particles from sewages. According to Murphy (2016), despite a 98% removal rate, over $6.5 \cdot 10^7$ MPs could enter the aquatic environment daily from a WWTP in Scotland [5]. The research on microplastic removal across WWTP might help reach significant changes in environmental improvement.

The aim of this research work is to analyze microplastic particles removal efficiency and distribution at different stages of WWTP in Lithuania. The full characteristics of MPs (size, shape, color, and chemical composition) are also fully evaluated and described.

The new insights into MPs pollution levels in influent and effluent wastewater might help create more efficient wastewater treatment systems and ensure environmental safety.

Acknowledgment: This research is funded by the European Social Fund under the No 09.3.3-LMT-K-712 “Development of Competencies of Scientists, other Researchers, and Students through Practical Research Activities” measure. (Grant No. 09.3.3-LMT-K-712-19-0112).



-
- [1] Bhattacharya, P. (2016). A review on the impacts of microplastic beads used in cosmetics. www.memed.us/journal/abs.
- [2] Madhumitha, C. T., Karmegam, N., Biruntha, M., Arun, A., al Kheraif, A. A., Kim, W., & Kumar, P. (2022). Extraction, identification, and environmental risk assessment of microplastics in commercial toothpaste. *Chemosphere*, 296. <https://doi.org/10.1016/j.chemosphere.2022.133976>.
- [3] Bayo, J., Olmos, S., & López-Castellanos, J. (2021). Assessment of microplastics in a municipal wastewater treatment plant with tertiary treatment: Removal efficiencies and loading per day into the environment. *Water (Switzerland)*, 13(10). <https://doi.org/10.3390/w13101339>.
- [4] Talvitie, J., Mikola, A., Koistinen, A., & Setälä, O. (2017). Solutions to microplastic pollution – Removal of microplastics from wastewater effluent with advanced wastewater treatment technologies. *Water Research*, 123, 401–407. <https://doi.org/10.1016/j.watres.2017.07.005>.
- [5] Murphy, F., Ewins, C., Carbonnier, F., & Quinn, B. (2016). Wastewater Treatment Works (WwTW) as a Source of Microplastics in the Aquatic Environment. *Environmental Science and Technology*, 50(11), 5800–5808. <https://doi.org/10.1021/acs.est.5b05416>.

SYNTHESIS AND ANALYSIS OF GdPO₄·H₂O:Eu FUNCTIONALIZED WOOD

Monika Baublytė¹, Denis Sokol¹, Ramūnas Skaudžius¹

¹Department of Inorganic Chemistry, Faculty of Chemistry, Vilnius University, Naugarduko st. 24, Vilnius, monika.baublyte@mb.vu.lt

The growing demand for multifunctional materials with novel properties has interested studying wood structures doped with gadolinium phosphate (WCC). One of the main characteristics limiting wood's potential is its flammability whereas rapid destruction and collapse of wood structures occur. High weathering and biological resistance of wood is also desirable as wood is the most abundant building material used in residential and non-residential buildings, furniture constructions, and decoration. Therefore, inorganic compounds within the wood matrix impact wood's mechanical properties such as compressive, tensile, bending strengths, and award additional luminescent/magnetic properties [1-4].

This work proposes inorganic GdPO₄·H₂O:Eu compound produced by in situ hydrothermal synthesis as a new alternative method to increase wood chemical resistance and confer new optical properties.

After in situ synthesis, the characteristics of the samples were observed by scanning electron microscopy (SEM) and computed tomography (CT); optical properties were determined by luminescence analysis (Fig.1). Thermogravimetric (TG) analysis was performed to attest the effects of GdPO₄ on the thermal degradation of wood.

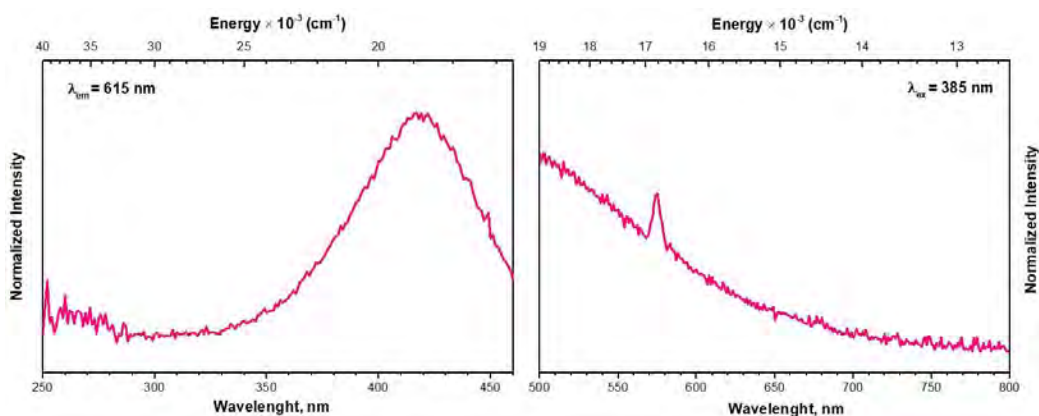


Fig. 1. Excitation and emission spectra of untreated wood.

-
- [1] S. Wu, J. Yin, H. Qu, A. Li, L. Liu, and Y. Shao, Photoluminescence properties of gadolinium phosphate nanoprisms doped with lanthanide ions for multicolor live cell imaging, *J. Mater. Sci. Mater. Electron.* **30**, 11336–11345 (2019).
- [2] N. B. Amar, T. Kallel, T. Koubaa, M. A. Hassairi, M. Dammak, and E. Cavalli, Synthesis, characterization and optical spectroscopy of GdPO₄:Er³⁺, *Luminescence*, **35** (7) 1056–1067 (2020).
- [3] J. S. Fabiyi and A. G. McDonald, Effect of wood species on property and weathering performance of wood plastic composites, *Compos. Part Appl. Sci. Manuf.* **41**, 1434–1440 (2010).
- [4] J. Chen, Z. Zhu, H. Zhang, S. Tian, and S. Fu, Wood-derived nanostructured hybrid for efficient flame retarding and electromagnetic shielding, *Mater. Des.* **204**, 109695 (2021).

STUDY OF EUROPIUM-DOPED SODIUM ALUMINUM GERMANATE

Marius Dzvinka, Martynas Misevičius

Institute of Chemistry, Vilnius University, Lithuania
marius.dzvinka@chgf.stud.vu.lt

Luminescent materials nowadays find use among a variety of different applications, thus attracting a lot of attention for studying such compounds. Many such materials can be obtained by doping a certain matrix with lanthanide ions. This work concentrates on NaAlGeO₄ doped with europium (III) ions, as properties of such compound are relatively unknown.

Samples (Na_{1-x}AlGe_{1-0.5x}O₄Eu_x) were obtained using solid-state synthesis. Stoichiometric amounts of sodium carbonate, aluminum oxide, germanium (IV) oxide and europium (III) oxide were weighed, mixed in agate mortar and sintered in 1000 °C for 6 hours.

The samples were firstly analyzed by X-ray diffractometer. Using the obtained X-ray diffraction results, it was concluded that all of the samples are single-phased. The aforementioned data was also used to refine the existing NaAlGeO₄ unit cell using the Rietveld method. It was determined that the occupancy of europium sites in the crystal cell directly correlates to the bulk concentration of europium during the solid-state synthesis. Also, samples with more europium tended to have a bigger unit cell.

The luminescent properties of the specimens were investigated by photoluminescence spectroscopy. Samples with higher europium concentrations showed strongest emission when excited by light wavelength of 392,5 nm. The highest emission peaks observed were at 610 nm and 702,5 nm.

STUDY OF FORMATION OF 1-ARYL-3*a*,8*b*-DIHYDRO-1*H*-BENZOFURO[2,3-*d*]IMIDAZOLES DURING THE VAN LEUSEN REACTION

Vilius Petraška, Paulina Kaziukonytė, Ieva Žutautė, Algirdas Brukštus

Faculty of Chemistry and Geosciences, Vilnius University, Lithuania
vilius.petraska@chgf.stud.vu.lt

Imidazoles are the 7th most common cyclic structure in pharmaceuticals and can be found in thirty commercially available drugs [1]. Compounds containing an imidazole moiety have been found to exhibit anti-cancer, anti-bacterial, anti-microbial, anti-diabetic, and antioxidant properties [2].

One of the most popular methods of imidazole synthesis is the van Leusen reaction [3]. While synthesizing HSP90 inhibitors using this type of reaction, 1-aryl-3*a*,8*b*-dihydro-1*H*-benzofuro[2,3-*d*]imidazoles were obtained alongside the main products — diarylimidazoles. Compounds containing this new tricyclic moiety have not been reported before.

The 2,3-dihydrofuran moiety is found in many different compounds in nature (e.g., (+)-decursivine, linderol A, caraphenol B and many others [4]) and therefore it is important to find new ways of synthesizing this structure. In nature, the hydrogen atoms of the five-membered ring of dihydrobenzofuran most commonly occur in the *trans* configuration, however, compounds containing the *cis* configuration have also been found. These compounds exhibit anti-HIV, antibacterial, antifungal, antimalarial, anticancer, and anti-inflammatory properties [4].

The objective of this work — to synthesize various 1-aryl-3*a*,8*b*-dihydro-1*H*-benzofuro[2,3-*d*]imidazoles and determine the influence of the substituents on the formation of these compounds.

The starting compounds were prepared from salicylic aldehyde and various anilines. During this work, conditions that would promote the formation of 1-aryl-3*a*,8*b*-dihydro-1*H*-benzofuro[2,3-*d*]imidazoles as the major product of the van Leusen reaction were sought after. Numerous experimental conditions were tested — the reaction was carried out at different temperatures and the influence of various organic as well as inorganic bases and their amounts on the yields of the products, was studied.

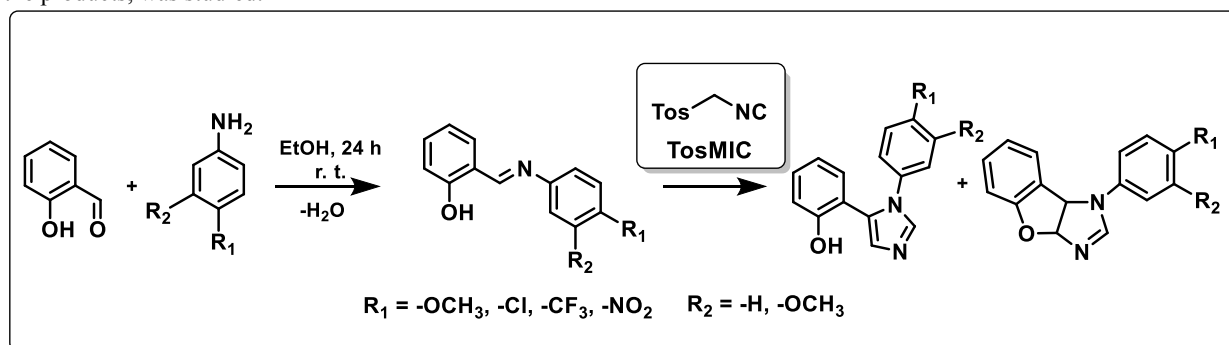


Fig. 1. Condensation of imines as well as the the formation of imidazoles and 1-aryl-3*a*,8*b*-dihydro-1*H*-benzofuro[2,3-*d*]imidazoles in the van Leusen reaction.

The optimal conditions for the formation of 1-aryl-3*a*,8*b*-dihydro-1*H*-benzofuro[2,3-*d*]imidazoles were determined to be MW 40 °C, 5 min and using K₂CO₃ as the base. It was established that the highest yields of 1-aryl-3*a*,8*b*-dihydro-1*H*-benzofuro[2,3-*d*]imidazoles are obtained in aromatic systems with electron withdrawing substituents.

[1] R. D. Taylor, M. Maccoss, A. D. G. Lawson, Rings in drugs, J. Med. Chem. 57, 5845–5859. (2014)

[2] A. Siwach, P. K. Verma, Synthesis and therapeutic potential of imidazole containing compounds, BMC Chem. 15, 1–69 (2021).

[3] A. M. van Leusen, J. Wildeman, O. H. Oldenzel, Base-Induced Cycloaddition of Sulfonylmethyl Isocyanides to C, N Double Bonds. Synthesis of 1, 5-Disubstituted and 1, 4, 5-Trisubstituted Imidazoles from Aldimines and Imidoyl Chlorides, J. Org. Chem. 42, 1153–1159 (1977).

[4] Z. Chen, M. Pitchakuntla, Y. Jia, Synthetic approaches to natural products containing 2,3-dihydrobenzofuran skeleton, Nat. Prod. Rep. 36, 666–690 (2019).

PROGRESS TOWARDS SYNTHESIS OF BICYCLO[3.3.1]NONANE-BASED POLYAROMATIC RECTANGULAR CAVITANDS

Nojus Radzevičius¹, Edvinas Orentas¹

¹ Institute of Chemistry, Faculty of Chemistry and Geosciences, Vilnius University, Naugarduko str. 24, Vilnius, Lithuania
nojus.radzevicius@chgf.stud.vu.lt

Polyaromatic hydrocarbons (PAHs) are abundant in fossil fuels and can also form as unwanted side products during incomplete combustion of organic matter[1]. Due to their lipophilic nature, they are often poorly soluble in water and instead disperse in air or water, adsorb to soil particles, or form sediment layers on various surfaces. Their poor water solubility limits the rate of biological degradation and thus leads to accumulation of PAH particles in the environment[2]. Exposure to PAHs has been proven to cause cancer, cardiovascular diseases, and poor neurological development[3]–[5].

A potential method of managing PAH waste is by exploiting their large aromatic surfaces to bind them to insoluble pi-receptor polymers through noncovalent pi stacking interactions. The main focus of this research has been to synthesize rectangular cyclic tetrameric cavitands with polyaromatic surfaces and easily controllable cavity size, which could possibly be polymerized by further functionalization of the indole N atom.

The initial synthesis strategy proceeded through Fischer indolization of enantiomerically pure bicyclo[3.3.1]nonane-2,6-dione (which can be synthesized readily from low-cost starting materials and enantiomerically enriched with selective oxidation by baker's yeast [6]) and an aromatic, C₂-symmetric di-hydrazine. Initial syntheses with 1,5-naphthalenedihydrazine were unsuccessful due to poor solubility of the indole products. The problem was solved by functionalizing the bicyclo[3.3.1]nonane skeleton with n-butyl groups. However, further attempts of Fischer indolization were not very successful. Indolization with a 1:1 ratio of the dione and dihydrazine gave a poorly-separable mixture of products, most appearing to be various oligomers, but no cyclic tetramer was found. Indolization with an excess of the dione gave the expected diindole (**1**) as the product, however with poor yields (Fig. 1.). Attempts of further serial indolization of the diindole (**1**) were unsuccessful, with the starting material appearing to decompose under reaction conditions.

Further plans include attempts of using alternative cyclocondensation reactions, such as the Friedländer synthesis with respective amino aldehydes to give di-quinoline derivatives.

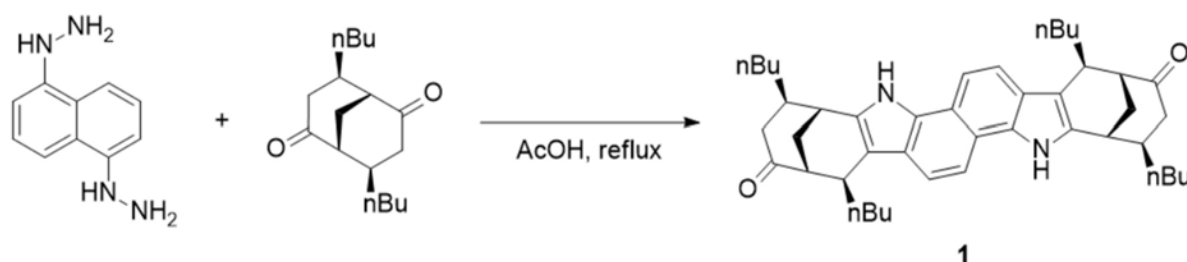


Fig. 1. Fischer indolization of 1,5-naphthalenedihydrazine with an excess of functionalized dione.

Acknowledgement: This research was funded by the Research Council of Lithuania (project no. S-SV-22-135)

- [1] H. I. Abdel-Shafy and M. S. M. Mansour, A review on polycyclic aromatic hydrocarbons: Source, environmental impact, effect on human health and remediation, *Egyptian Journal of Petroleum* **25**(1), 107–123 (2016)
- [2] A. K. Haritash and C. P. Kaushik, Biodegradation aspects of Polycyclic Aromatic Hydrocarbons (PAHs): A review, *J Hazard Mater* **169**(1–3), 1–15 (2009)
- [3] W. M. Baird, L. A. Hooven, and B. Mahadevan, Carcinogenic polycyclic aromatic hydrocarbon-DNA adducts and mechanism of action, *Environ Mol Mutagen* **45**(2–3), 106–114 (2005)
- [4] E. Suades-González, M. Gascon, M. Guxens, and J. Sunyer, Air Pollution and Neuropsychological Development: A Review of the Latest Evidence, *Endocrinology* **156**(10), 3473–3482 (2015)
- [5] H. Korashy and A. El-Kadi, The Role of Aryl Hydrocarbon Receptor in the Pathogenesis of Cardiovascular Diseases, *Drug Metabolism Reviews* **38**(3), 411–450 (2008)
- [6] C. J. Wallentin, E. Orentas, E. Butkus, and K. Wärmarm, Baker's Yeast for Sweet Dough Enables Large-Scale Synthesis of Enantiomerically Pure Bicyclo[3.3.1]nonane-2,6-dione, *Synthesis (Stuttg)* **2009**(05), 864–867 (2009)

PREPARATION OF HEXAGONAL RARE EARTH MANGANITES BY MOLTEN SALT SYNTHESIS

Dovydas Karoblis¹, Aleksej Zarkov¹, Aivaras Kareiva¹

¹Institute of Chemistry, Vilnius University, Lithuania
Dovydas.karoblis@stud.chgf.vu.lt

Hexagonal rare earth manganites are family of compounds with general formula of ReMnO_3 (Re – rare earth element), which demonstrates two ferroic properties in the same phase without any external fields. These compounds are ferroelectrics under high temperature (T_C – 620-1000 K) [1] and display antiferromagnetic ordering at lower temperature (T_N – 57-130 K) [2]. Out of all hexagonal manganites, yttrium manganite (YMnO_3) is the most researched one. This material has multiferroic properties with a low Neel temperature ($T_N \sim 70$ K) and a high Curie temperature ($T_C \sim 900$ K) [3]. This manganite can be prepared via multiple synthetic approaches, with solid-state synthesis being the most common one. Unfortunately, solid-state synthetic technique has some drawbacks, like long reaction times, several reaction stages, low rates of diffusion, formation of impurity phases and high reaction temperature. These disadvantages can be avoided by conducting the synthesis in inorganic salt medium, with temperature slightly beyond the melting point of the salt, so called molten salt synthesis [3].

In this work we prepared several rare earth manganites by using novel molten salt synthesis technique. All the prepared samples were investigated using several characterization techniques, including X-Ray diffraction, FT-IR spectroscopy and scanning electron microscopy (SEM). It was observed that a use of simple inorganic salt mixture led to the formation of phase pure samples at lower temperature. Moreover, this synthetic approach generated hexagonal shape particles with the size varying in micrometer range (Fig. 1).

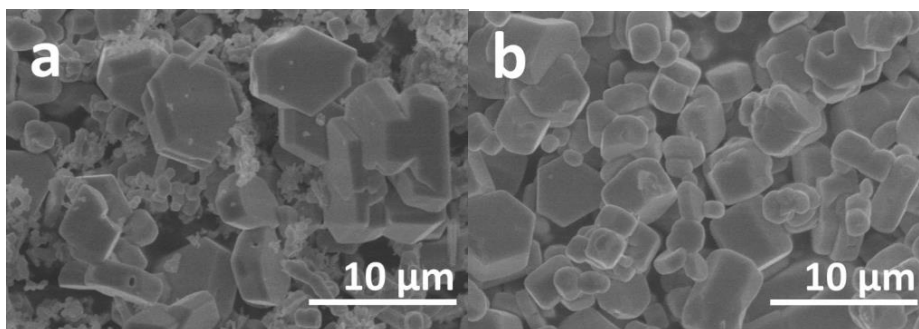


Fig. 1. SEM micrographs of YMnO_3 , prepared at 1000 (a) and 1100 °C (b) temperatures.

-
- [1] B. Lorenz, Hexagonal Manganites—(RMnO_3): Class (I) Multiferroics with Strong Coupling of Magnetism and Ferroelectricity, *International Scholarly Research Notices* **2013**, (2013).
- [2] M. Li, H. Tan, W. Duan, Hexagonal Rare-Earth Manganites and Ferrites: A Review of Improper Ferroelectricity, Magnetoelectric Coupling, and Unusual Domain Walls, *Physical Chemistry Chemical Physics* **22**, 14415-14432 (2020).
- [3] M. Wang et. al., Enhanced Multiferroic Properties of YMnO_3 Ceramics Fabricated by Spark Plasma Sintering along with Low-Temperature Solid-State Reaction **10**, 474 (2017).
- [4] S.K. Gupta, Y. Mao, Recent Developments on Molten Salt Synthesis of Inorganic Nanomaterials: A Review, *The Journal of Physical Chemistry C* **125**, 6508-6533 (2021).

SYNTHESIS AND INVESTIGATION OF ACRYLATED EPOXIDIZED SOYBEAN OIL AND VANILLIN DIMETHACRYLATE BASED PHOTOPOLYMER

Vilte Šereikaite¹, Aukse Navaruckiene¹, Jolita Ostrauskaite¹

¹ Department of Polymer Chemistry and Technology, Kaunas University of Technology, Radvilenu Rd. 19, LT-50254 Kaunas, Lithuania

vilte.sereikaite@ktu.edu

Considering recent challenges related to climate change and the state of the environment, as well as increasing progress of sustainable technologies, it is particularly important to develop new sustainable materials applicable in such technologies [1]. Biobased photopolymers well suit for this, as they can be applied in environmentally friendly light-based film, coating, and additive manufacturing technologies.

In this study, cross-linked polymer (VS) was synthesized by photopolymerization of two biobased acrylic monomers: acrylated epoxidized soybean oil and vanillin dimethacrylate, in the presence of the thiol monomer pentaerythritol-tetra(3-mercaptopropionate) [2]. 2,4,6-Trimethylbenzoyl-diphenylphosphine oxide was used as the photoinitiator and 2,5-bis(5-tert-butylbenzoxazol-2-yl) thiophene was used as a UV blocking agent in the photocurable system. Radical photopolymerization and thiol-acrylate photopolymerization were combined in a dual curing system. The photoresin composition was as follows: 3 mol of AESO / 1 mol of VDM / 0.25 mol of PETMP / 2.5 % of TPO / 0.08 % of UV-blocker. The Helios Italquartz lamp (250-450 nm, 310 mW·cm⁻²) was used for photocuring. The structure of the cross-linked polymer VS was confirmed by FT-IR spectroscopy, Soxhlet extraction, and swelling test. The synthesized polymer VS has a low swelling value of 8-10% in different solvents, mostly due to the high density of cross-links. The yield of the insoluble fraction of the polymer was 95% after Soxhlet extraction with acetone.

The mechanical properties of the cross-linked polymer were investigated by tensile and compression tests. Young's modulus, elongation at break, tensile strength, and compressive modulus have been determined. The values of these mechanical characteristics were compared with those of other polymers with similar composition. It was found that the cross-linked polymer VS has excellent mechanical properties. It is rigid, strong, non-brittle, and its Young's modulus and compressive modulus are higher than those of other polymers with similar composition, especially the compression modulus (Fig.1).

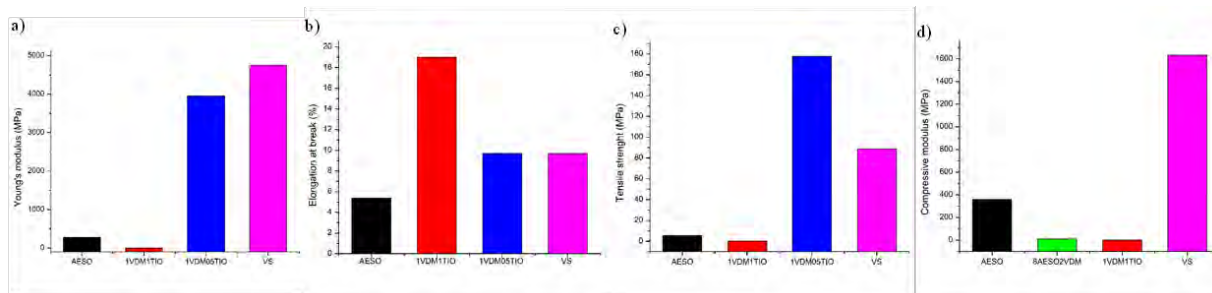


Fig. 1. Comparison of the mechanical characteristics of polymer VS and polymers with similar composition: a – Young's modulus during stretching; b – elongation at break; c – tensile strength; d - compressive modulus

The thermal properties of the polymer VS were investigated by dynamic mechanical thermal analysis and thermogravimetric analysis. The glass transition temperature of the polymer VS is 9 °C. Such a low value of glass transition temperature is characteristic for cross-linked polymers of vegetable oils, due to the long, flexible fatty acid chains. It was found that the synthesized cross-linked polymer VS has high thermal stability. Its destruction temperature at 10% weight loss is 373 °C and is higher than that of the other polymers with similar structure.

[1] Baranwal J, Barse B, Fais A, Delogu GL, Kumar A. Biopolymer: A Sustainable Material for Food and Medical Applications. *Polymers*, 2022, 14, 983. doi: 10.3390/polym14050983.

[2] Sereikaite, V.; Navaruckiene, A.; Jaras, J.; Skliutas, E.; Ladika, D.; Gray, D.; Malinauskas, M.; Talacka, V.; Ostrauskaite, J. Functionalized Soybean Oil- and Vanillin-Based Dual Cure Photopolymerizable System for Light-Based 3D Structuring. *Polymers*, 2022, 14, 5361. <https://doi.org/10.3390/polym14245361>

MOLECULAR DYNAMICS AND RAMAN STUDY FOR LYCOPENE AND CYCLODEXTRIN COMPLEXES

Goda Bankovskaitė¹, Mindaugas Mačernis

¹ Institute of Chemical Physics, Faculty of Physics, Vilnius University, Saulėtekio av. 3, LT-10257 Vilnius, Lithuania
goda.bankovskaite@ff.stud.vu.lt

Carotenoids (Cars) have linear conjugated isoprenoid chain that affords them an intense absorption in the blue-green range, and the colors they confer on fruits, flowers and animals lie at the basis of complex signaling processes. In photosynthetic organisms, they are implicated in the harvesting of solar photons while natural carotenoids display a large structural diversity, and more than one thousand molecular species have been now identified [1]. Typically, Cars are insoluble in water, and the complexation of lycopene with β -cyclodextrin is one of the strategies to resolve the problem [2].

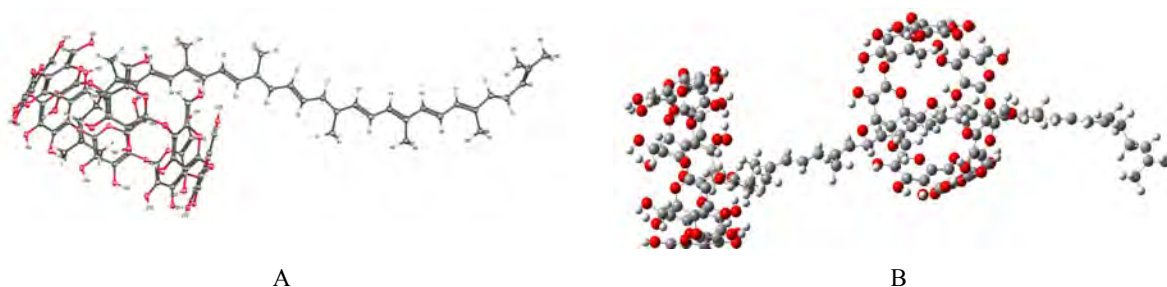


Fig. 1. Complexes of Lycopene and cyclodextrin: A - γ -cyclodextrin and lycopene; B - lycopene with the two β -cyclodextrin molecules.

The Car was chosen lycopene (Fig.1). The complexes between cyclodextrin and lycopene were made artificially. All structures were optimized separately. Careful orbital analysis allowed us to label all calculated excited states. We chose the B3LYP and CAM-B3LYP functionals with cc-pVDZ basis sets for the present study which are available in the Gaussian package. All analyzed complexes were without imaginary frequencies. Study was done using a combination of resonance Raman and absorption spectroscopy and density functional theory (DFT) modelling by using B3LYP methodology, and CAM-B3LYP for AMBER molecular dynamics (MD).

Here we will present MD analysis and computational details for lycopene with several cyclodextrin. This study provides the framework to explain Raman ν_1 changes in the lycopene complexed with β -cyclodextrin and γ -cyclodextrin. This study aims to further our understanding of the sensitivity of Raman ν_1 band to Cars' distortions into its symmetry perturbations and lycopene crystal preparations.

Acknowledgements

Computations were performed on resources at the supercomputer "VU HPC" Saulėtekis of Vilnius University in Faculty of Physics location.

[1] S. Streckaitė, M. Mačernis, et al. Electronic and Vibrational Properties of Allene Carotenoids, *J. Phys. Chem. A* **124**, 2792 (2020).

[2] M. Mačernis, A. Bockuviene, et al. Raman study for β -ring positioning in β -Carotene complexes with Cyclodextrins and Chitoooligosaccharides, *J. Mol. Str.* **1226**, 129362 (2021).

DETERMINATION OF PPY LAYER STABILITY FOR THE DEVELOPMENT OF THE SENSOR

Raimonda Bogužaitė¹, Vilma Ratautaitė¹, Greta Pilvenytė¹, Arūnas Ramanavičius^{1,2}

¹ Department of Nanotechnology, State Research Institute Center for Physical Sciences and Technology, Laboratory of Nanotechnology, Sauletekio av. 3, Vilnius LT-10257, Lithuania

² Faculty of Chemistry and Geosciences, Institute of Chemistry, Vilnius University, Naugarduko str. 24, LT-03225 Vilnius

raimonda.boguzaitė@ftmc.lt

Polypyrrole (Ppy) is one of the conducting polymers that has been used to create various kinds of sensors [1]. Chemical [2], enzymatic [3], electrochemical [4], or other methods are simple ways to synthesize Ppy. In our case, Ppy was used to create coatings on the indium tin oxide (ITO) electrode. The deposition of coatings on an ITO electrode presents many challenges. This study analysed the conditions under which the layer should be prepared and stored. The stability of the layer over time was also observed.

The first and one of the most important steps is proper electrode preparation and washing. Using a specific procedure, the electrode is pre-treated and can be modified later. The modification of the glass/ITO surface with silane could be performed in a 4% (v/v) solution of TEMS in acetone overnight and correspondingly TEMS modified structure (glass/ITO_(TEMS)) could be formed. [5]

The possibility to cover electrodes with layers of conductive polymers and/or their composites with high conductivity is one of the benefits of electrochemical polymerization. By controlling the synthesis conditions, the physical properties of chemically synthesized conductive polymers, such as particle size and shape, can be managed [6]. The thickness can be partially controlled by changing the concentration of the monomer, the number of potential pulses, number of potential cycles. It was observed that the thicker the layer obtained, the more difficult it is to keep it mechanically attached to the electrode surface. Also, the use of heparin in the polymerization mixture improves adhesion to the surface.

This study aimed to evaluate the Ppy layer stability on the electrode when layers were stored in air, Britton-Robinson buffer (pH 3), or water.

In summary, it can be stated that the layer kept in the air, covered with the thinnest possible layer and modified with diverse substances, such as heparin or phenothiazine derivatives, has the best stability properties and can be used for the creation of various sensors.

References

- [1] V. Ratautaitė, R. Bogužaitė, M.B. Mickeviciute, L. Mikoliunaite, U. Samukaite-Bubniene, A. Ramanavicius, A. Ramanaviciene, Evaluation of Electrochromic Properties of Polypyrrole/Poly(Methylene Blue) Layer Doped by Polysaccharides. *Sensors*, 22, 232 (2022).
- [2] K. Leonavicius, A. Ramanaviciene, A. Ramanavicius, Polymerization Model for Hydrogen Peroxide Initiated Synthesis of Polypyrrole Nanoparticles. *Langmuir* 27, 10970–10976 (2011).
- [3] N. German, A. Ramanaviciene, A. Ramanavicius, Formation of polyaniline and polypyrrole nanocomposites with embedded glucose oxidase and gold nanoparticles. *Polymers* 11, 377 (2019).
- [4] D. Plausinaitis, L. Sinkevicius, U. Samukaite-Bubniene, V. Ratautaitė, A. Ramanavicius, Evaluation of Electrochemical Quartz Crystal Microbalance Based Sensor Modified by Uric Acid-imprinted Polypyrrole. *Talanta* 220, 121414 (2020).
- [5] V. Ratautaitė, G. Bagdziunas, A. Ramanavicius, and A. Ramanaviciene, “An Application of Conducting Polymer Polypyrrole for the Design of Electrochromic pH and CO₂ Sensors,” *J. Electrochem. Soc.*, 166, 6, B297–B303 (2019).
- [6] R. Bogužaitė, V. Ratautaitė, L. Mikoliunaite, V. Pudzaitis, A. Ramanaviciene, A. Ramanavicius, Towards analytical application of electrochromic polypyrrole layers modified by phenothiazine derivatives, *Journal of Electroanalytical Chemistry*, 886, 115132 (2021).

FABRICATION OF CoFe, CoFeMn, CoFeMo COATINGS AND THEIR APPLICATION FOR HYDROGEN EVOLUTION REACTION.

Karina Vjūnova^{1,2}, Zita Sukackienė¹, Jūratė Vaičiūnienė¹, Loreta Tamašauskaitė-Tamašiūnaitė¹

¹Center for Physical Sciences and Technology (FTMC), Saulėtekio ave. 3, LT10257 Vilnius, Lithuania

²Vilnius university, Faculty of Chemistry and Geosciences, Naugarduko str. 24, LT03225 Vilnius, Lithuania
karina.vjunova@chgf.stud.vu.lt

Hydrogen has the advantages of high combustion heat, non-toxic, and pollution-free energy conversion process. Progress of cost-effective and efficient non-noble metal catalysts for hydrogen evolution reaction (HER) is a great challenge [1]. In this study, the binary and ternary CoFe, CoFeMn, and CoFeMo coatings with different compositions have been deposited on the nickel foam substrate using the electroless metal deposition method and morpholine borane as the reducing agent. CoFe, CoFeMn and CoFeMo coatings are compact and crack-free, with typical globular morphology. Scanning electron microscopy (SEM) and inductively coupled plasma optical emission spectroscopy (ICP-OES) were used for the characterization of the surface morphology, structure and composition of prepared catalysts. HER was investigated in 1 M KOH solution by linear sweep voltammetry (LSV). It was determined that the CoFeMn and CoFeMo coatings give lower overpotential values of -135.8 and -149.6 mV, respectively, for the HER to obtain a current density of 20 mA cm⁻² as compared with the CoFe coating (-243.9 mV). The obtained catalysts are good candidates to use them as cathode material for HER in alkaline media [2].

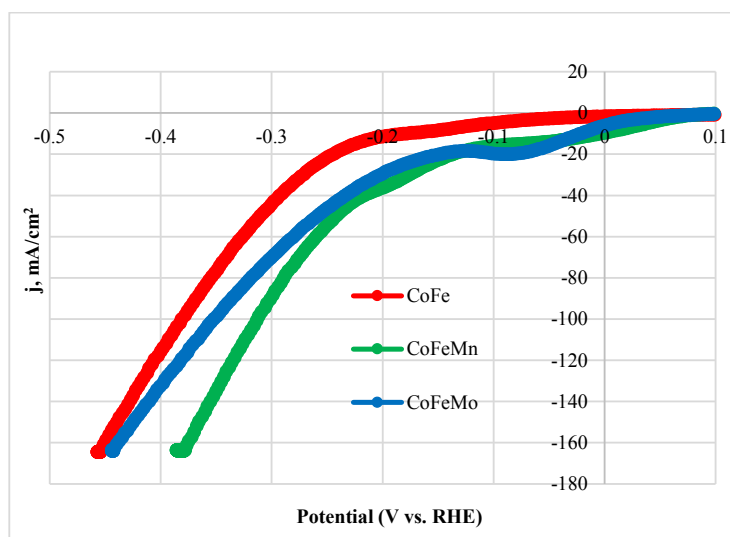


Fig. 1. LSVs of the investigated catalysts recorded in a 1M KOH solution at 5mV/s.

[1] Khalafallah, D., Zhi, M., & Hong, Z. (2019). Recent trends in synthesis and investigation of nickel phosphide compound/hybrid-based electrocatalysts towards hydrogen generation from water electrocatalysis. *Topics in Current Chemistry*, 377, 1-48.

[2] Sukackienė, Z., Balčiūnaitė, A., Kepienienė, V., Vaičiūnienė, J., Stalnionis, G., Pakštas, V., ... & Norkus, E. (2022). Comparison of the Activity of 3D Binary or Ternary Cobalt Coatings for Hydrogen and Oxygen Evolution Reactions. *Batteries*, 8(9), 129.

SYNTHESIS AND CHARACTERIZATION OF CoFe, CoFeMn, CoFeMo COATINGS AND THEIR APPLICATION FOR OXYGEN EVOLUTON REACTION

Huma Amber¹, Zita Sukackienė¹, Jūratė Vaičiūnienė¹, Loreta Tamašauskaitė-Tamašiūnaitė¹

¹ Center for Physical Sciences and Technology (FTMC), Saulėtekio ave. 3, LT10257 Vilnius, Lithuania
huma.amber@ftmc.lt

The oxygen evolution reaction (OER) is a critical half-cell reaction which can be used to produce hydrogen fuel using renewable energies via water electrolysis. Currently, there is tremendous interest in the discovery of low cost and efficient electrocatalysts for the OER. OER electrolysis as an important reaction involved in rechargeable metal-air batteries and has attracted immense attention for clean energy generation and efficient energy storage[1]. In this work, by using the electroless metal deposition method the binary and ternary CoFe, CoFeMn, and CoFeMo coatings with different compositions have been deposited on the nickel foam substrate. The reducing agent was morpholine borane. The surface morphology, structure and composition of prepared catalysts were characterized by scanning electron microscopy (SEM) and inductively coupled plasma optical emission spectroscopy (ICP-OES). OER was investigated in 1 M KOH solution by linear sweep voltammetry (LSV). The deposited catalysts (CoFe, CoFeMn, CoFeMo coatings) provide compact and crack-free layers with typical globular morphology. It was derived that the CoFe coating gives the lowest overpotential of 331.7 mV and the highest mass activity of 81.79 mA mg⁻¹ for the OER to achieve a current density of 40 mA cm⁻² [2].

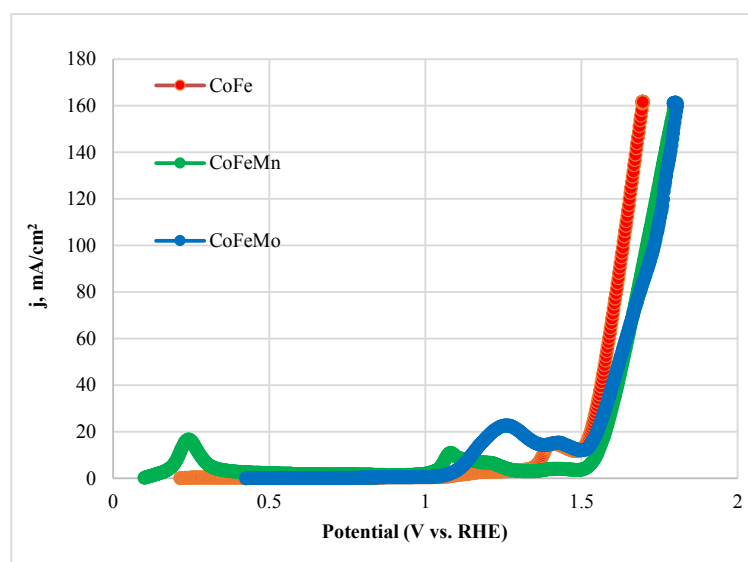


Fig. 1. LSVs of the investigated catalysts recorded in a 1M KOH Solution at 5mV/s.

[1] Zhou, D., Li, P., Lin, X., McKinley, A., Kuang, Y., Liu, W., ... & Duan, X. (2021). Layered double hydroxide-based electrocatalysts for the oxygen evolution reaction: identification and tailoring of active sites, and superaerophobic nanoarray electrode assembly. *Chemical Society Reviews*, 50(15), 8790-8817.

[2] Sukackienė, Z., Balčiūnaitė, A., Kepenienė, V., Vaičiūnienė, J., Stalnionis, G., Pakštas, V., ... & Norkus, E. (2022). Comparison of the Activity of 3D Binary or Ternary Cobalt Coatings for Hydrogen and Oxygen Evolution Reactions. *Batteries*, 8(9), 129.

LUMINESCENCE OF EUROPIUM, DYSPROSIUM AND BISMUTH DOPED NaAlGeO₄

Gabija Janusauskaite¹, Martynas Misevicius^{1,2}

¹Institute of Chemistry, Faculty of Chemistry and Geosciences, Vilnius University, Lithuania

²Institute of Chemical Physics, Faculty of Physics, Vilnius University, Lithuania

gabija.janusauskaite@chgf.stud.vu.lt

Currently, white light-emitting diodes (w-LEDs) are mainly manufactured by coating yellow-emitting YAG:Ce³⁺ phosphors on the blue-emitting InGaN chips. However, this LED due to the lack of red-emitting component exhibits the high correlated color temperature (CCT) and low color rendering index (CRI) [1]. To overcome these drawbacks, there is a need to find a stable, inorganic rare-earth based phosphor with high luminescence efficiency.

Sodium aluminum germanate NaAlGeO₄ has the calcium ferrite structure with space group Pnma and having cell parameters a=8.87, b=2.84, c=10.40 Å and Dx=4.73 g/cm³ [2]. Recently, germanate compounds have been paid more and more attention because of low synthesized temperature and excellent physical/chemical properties. Some germanate-based phosphors with excellent luminescence performance for different practical applications have been developed such as K₂SrGe₈O₁₈:Eu³⁺[3], CaZnGe₂O₆:Bi³⁺[4] and CaMgGe₂O₆:Mn²⁺,Sm³⁺ [5,6]. LiYGeO₄:Bi³⁺[7] is known as persistent luminescent material that can luminescent for hours after removing the excitation source. In this study, NaAlGeO₄ phosphors doped with Eu³⁺, Dy³⁺ and Bi³⁺ can be expected for LEDs application.

During this work, a series of NaAlGeO₄ activated with the different concentration of trivalent Eu, Dy and Bi ions were synthesized using solid-state synthesis method. Obtained samples were characterized by powder X-ray diffraction (XRD) method and photoluminescence (PL) measurements such as excitation and emission spectra, luminescence decay times and quantum efficiencies. XRD analysis revealed that all the samples consist of pure NaAlGeO₄ phase. From the PL measurements we found out, that Eu³⁺-doped samples exhibit red emission at 611 nm with highest intensity peak at 16% sample, while the longest luminescence decay was observed in the Na_{1-x}AlGe_{1-0.5x}O₄:Eu 0.5% sample. The highest Dy³⁺ emission intensities were found to be at 573.5 nm in the Na_{1-x}AlGe_{1-0.5x}O₄:Dy 1% sample and Bi³⁺-doped at 420 nm with the concentration of 0.3%.

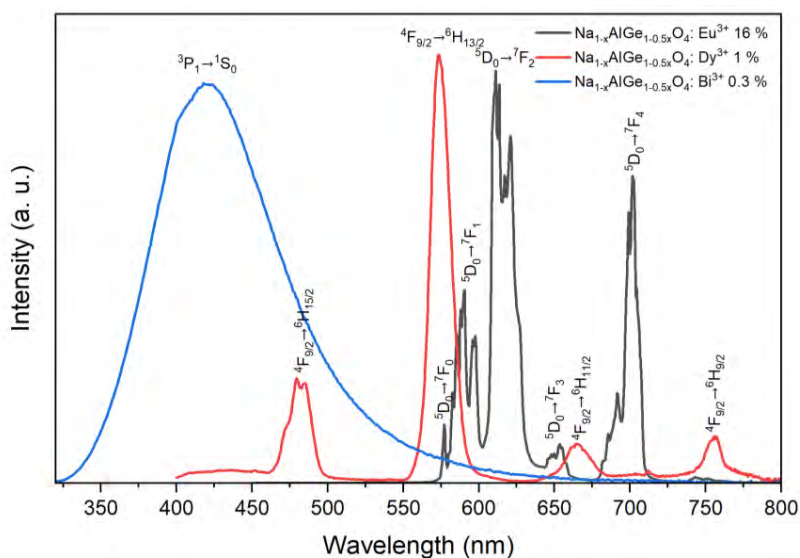


Fig. 1. Photoluminescence emission of Eu³⁺-doped ($\lambda_{\text{ex}} = 393$ nm), Dy³⁺-doped ($\lambda_{\text{ex}} = 348$ nm) and Bi³⁺-doped ($\lambda_{\text{ex}} = 310$ nm) Na_{1-x}AlGe_{1-0.5x}O₄ samples.

- [1] B. Fan, W. Zhou, S. Qi, W. Zhao, Eu³⁺-doped NaYGeO₄: A novel red-emitting phosphors for ultraviolet or blue chips excited white LEDs, *Journal of Solid State Chemistry*, Volume 283 (2020).
- [2] A. F. Reid, A. D. Wadsley, A. E. Ringwood, High pressure NaAlGeO₄, a calcium ferrite isotype and model structure of silicates at depth in the earth's mantle, *Acta Crystallographica*, 23, 736–739 (1967).
- [3] Q. Zhang, X.C. Wang, Y.H. Wang, A novel germanate based red-emitting phosphor with high efficiency, high color purity and thermal stability for white light-emitting diodes and field emission displays, *Inorganic Chemistry Frontiers*, Issue 4, 1034-1045 (2020).
- [4] X.J. Dou, H.W. Xiang, P.L. Wei, S.A. Zhang, G.F. Ju, Z.M. Meng, L. Chen, Y.H. Hu, Y. Li, A novel phosphor CaZnGe₂O₆:Bi³⁺ with persistent luminescence and photostimulated luminescence, *Materials Research Bulletin*, Volume 105, 226-230 (2018).
- [5] Q.F. Ye, Y.H. Wang, H.J. Guo, X.F. Zhou, P. Feng, S.S. Ding, Designing a novel red to near-infrared persistent phosphor CaMgGe₂O₆:Mn²⁺,Sm³⁺ based on a vacuum referred binding energy diagram, *Dalton Transactions*, Issue 29 (2019).
- [6] Han, Y. Chen, B. Liu, J. Zhang, Solid state synthesis and luminescence properties of Eu³⁺ doped NaYGeO₄ phosphors, *Optik*, Volume 242 (2021).
- [7] J. Shi, X. Sun, S. Zheng, X. Fu, Y. Yang, J. Wang, H. Zhang, Super-Long Persistent Luminescence in the Ultraviolet A Region from a Bi³⁺-Doped LiYGeO₄ Phosphor, *Advanced Optical Materials*, Volume 7, Issue 19 (2019).

SYNTHESIS OF NOVEL 6-(5-ARYL-1,2,3-THIADIAZOL-4-YL)-4-ARYLBENZENE-1,3-DIOLS IN SEARCH FOR POTENTIAL HSP90 CHAPERONE INHIBITORS

Urtė Milerytė¹, Algirdas Brukštus², Ieva Žutautė²

¹Faculty of Medicine, Vilnius University, M. K. Čiurlionio g. 21, LT-03101, Vilnius, Lithuania

²Faculty of Chemistry and Geosciences, Vilnius University, Naugarduko g. 24, LT-03225, Vilnius, Lithuania
urte.mileryte@mf.stud.vu.lt

According to the World Health Organization (WHO), cancer is the leading cause of mortality globally. This illness claimed the lives of around 10 million individuals in 2020.[1] Studies on the etiology of cancer indicate that its causes are diverse: they include genetic mutations (e.g., somatic mutations) as well as epimutations (e.g., tumor suppressor gene silencing through hypermethylation).[2] It is important to note that cancer illnesses share one trait in common, despite their diverse etiologies. That trait is oncogenic proteins with brittle and flexible structures. Because these proteins are unstable, they require aid from molecular chaperones for efficient structure maintenance.

One of the most significant chaperones involved in oncogenesis is a heat shock protein 90 (HSP90). Due to this protein's role in the stability of oncoproteins and signaling pathways, malignant cells typically have elevated HSP90 levels in contrast to normal cells. These characteristics have made this heat shock protein an appealing molecular target for cancer treatment, leading to the creation of new inhibitors with an alternative mechanism of action. [3, 4] Novel anticancer agents, HSP90 inhibitors, are classified based on which molecular structure of the chaperone they affect: N-terminal domain, middle domain, or C-terminal domain. As a result, three classes of HSP90 inhibitors exist.

For this research, it was decided to synthesize resorcinol-based inhibitors of the N-domain's nucleotide-binding pocket. The activity of these compounds requires a second aromatic ring with an appropriate spatial configuration, which is provided by the 5-membered heterocyclic ring that connects them. To this day, a variety of HSP90 inhibitory analogs with imidazole and thiaziazole rings have been synthesized, with varying substitutes at the 6-position of the resorcinol fragment and the 4-position of the phenyl group. However, there is not a single compound documented in the literature that has an aryl group connected to the 4-position of the resorcinol structure. Therefore, the purpose of this work is to synthesize novel 6-(5-aryl-1,2,3-thiadiazol-4-yl)-4-arylbenzene-1,3-diols bearing an aryl group at the 4-position of the resorcinol fragment in the hopes of increasing their selectivity for the HSP90 N domain's nucleotide-binding pocket. The overall synthesis consists of 5 stages, which challenges will be discussed during the presentation. More details about HSP90, its involvement in oncogenesis, and inhibitor classes, will also be covered.

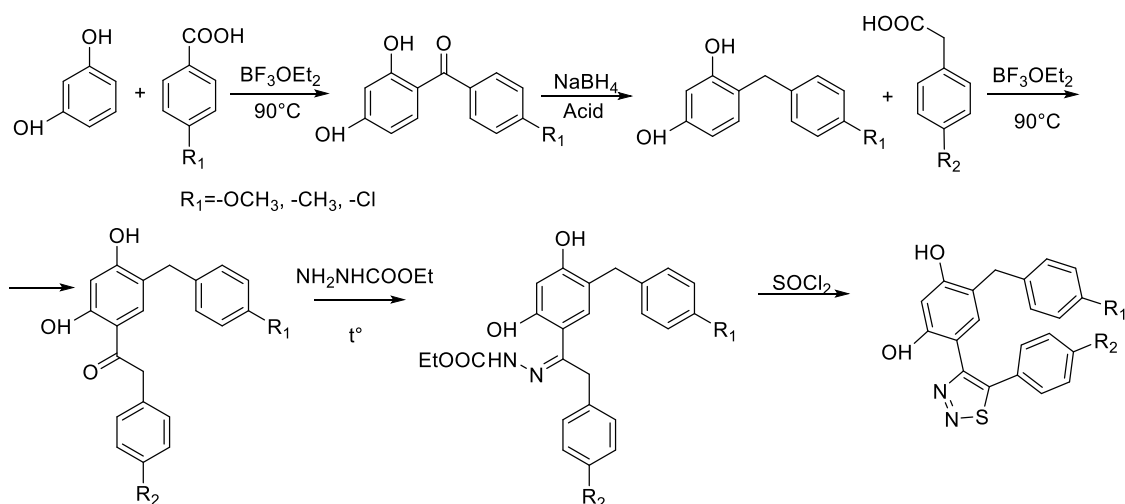


Fig. 1. General scheme of reactions

[1] <https://www.who.int/en/news-room/fact-sheets/detail/cancer>

[2] Diori I.K., Sanlier SH. Reviewing cancer's biology: an eclectic approach. Journal of the Egyptian National Cancer Institute volume 33, Article number: 32 (2021).

[3] Rappa F., Farina F., Zummo G., David S., Campanella C., Carini F., Tomasello G., Damiani P., Cappello F., Conway de Macario E., Macario A. HSP-Molecular Chaperones in Cancer Biogenesis and Tumor Therapy: An Overview. ANTICANCER RESEARCH 32: 5139-5150 (2012).

[4] Birbo B, Madu EE, Madu CO, Jain A, Lu Y. Role of HSP90 in Cancer. Int J Mol Sci. 2021 m. spalio 1 d.;22(19):10317.

FRASS – UNTRADITIONAL RAW MATERIAL FOR PRODUCTION OF FERTILIZERS

Goda Gudinskaitė, Rasa Paleckienė, Rasa Šlinkšienė

Faculty of Chemical Technology, Kaunas University of Technology, Lithuania
goda.gudinskaite@ktu.edu

Humanity cannot abandon economic activity, but the aim is to contribute to its lower negative impact on the environment. The current direction of development is the green course, and its main goal is to create a sustainable, modern economy without harming the environment. In order to avoid the negative effects of intensive farming, various options for sustainable agriculture are often offered, such as partially replacing synthetic fertilizers, replacing chemical plant protection measures with biological ones. Due to the growing world population, the agricultural industry is challenged to produce the required amount of food. This is not possible without the use of fertilizers [1]. The use of chemical fertilizers is one of the most common ways of developing intensive agriculture nowadays [2, 3]. However, the continuous long-term use of chemical fertilizers causes negative effects on the environment, such as soil degradation, pollution of bodies of water. In the fertilizer market, new products, which focus on the processes occurring naturally in the plant and the circular economy, are now appearing next to traditional fertilizers more frequently. Residues from other agricultural branches can be used as an alternative raw material to produce fertilizers. The current trends in insect breeding, which are gaining wider applicability and legalization for use in the food industry, also create prerequisites for the development of possibilities for processing waste products [4].

Under laboratory conditions, studies of frass were carried out (Fig. 1) by the company UAB "Divaks", concerning the suitability for fertilizer production, the chemical composition of frass and the composition of their extracts. Nitrogen, phosphorus and potassium content and properties of samples were determined by using standard techniques [5].

Table 1 shows the concentrations of the major nutrients identified in the Frass samples.



Figure 1. Frass (insect waste)

Table 1. Concentration of major nutrients in Frass samples

Example	N, %	P ₂ O ₅ , %	K ₂ O, %
DF1	20.22	1.10	2.69
DF2	15.89	1.53	2.77

The physical properties of two different frass samples were tested. The pH of the 10% solution of the first sample (DF1) is 5.85, the moisture content is 7.41%, the bulk density is 524.89 kg/m³, the 0.2–0.5 mm fraction is the major part – 93.36%. The pH of the 10% solution of the second sample (DF2) is 5.45, the moisture content is 8.76%, the bulk density is 393.81 kg/m³, the 0.2–0.5 mm fraction is the major part – 95.75%.

Seeing that frass contains a large amount of organic matter, carbon concentration studies were conducted. The possibility of extracting the plant nutrients contained in frass using different solvents was also investigated. The samples of Frass aqueous solutions and extracts in acidic and alkaline media were prepared under different conditions and using different experimental durations. The concentration of the main nutrients (N, P, K) and carbon were determined in the extracts. The concentration of carbon in the extracts depends mostly on the duration of the extraction. It was also found that the carbon concentrations in the potassium hydroxide solutions are close to the carbon levels present in the original samples. Extracts, obtained by using potassium hydroxide, can be used as a fertilizer component to increase the carbon content of the soil.

The use of insects for human and animal foods and fertilizer is expected to continue to grow as it has the potential to help reduce the amount of waste, increase food reserves and yields.

[1] Paleckienė Rasa, Šlinkšienė Rasa. *Trąšos. Gavimas ir analizė. Mokomoji knyga* (2018).

[2] MONREAL, C. M., et al. Nanotechnologies for increasing the crop use efficiency of fertilizer-micronutrients. *Biology and fertility of soils*, 2016, 52.3: 423–437.

[3] Adesemoye, A. O. & Kloepper, J. W. Plant–microbes interactions in enhanced fertilizer-use efficiency. *Applied Microbiology and Biotechnology* 85, 1–12 (2009).

[4] Houben, D., Daoulas, G., Faucon, MP. *et al.* Potential use of mealworm frass as a fertilizer: Impact on crop growth and soil properties. *Sci Rep* 10, 4659 (2020).

[5] Regulation (EC) No 2003/2003 of the European Parliament and of the Council of 13 October 2003 relating to fertilisers. *Official Journal* № 304-1. (2003).

MODIFICATION OF PINE WOOD WITH Mg_2/Al_1-CO_3 AND Zn_2/Al_1-CO_3 LAYERED DOUBLE HYDROXIDE: SYNTHESIS AND ANALYSIS

Neringa Gailiūtė, Denis Sokol

Institute of Chemistry, Faculty of Chemistry and Geosciences, Vilnius University, Naugarduko st. 24, LT-03225
Vilnius
neringa.gailiute@chgf.stud.vu.lt

Wood has been a crucial resource for thousands of years and remains an essential part of various industries, including fuel, construction, furniture, and paper. These products are generally low in CO_2 emissions, easily available from sustainable sources and mechanically durable. Despite its advantages, wood is also vulnerable to moisture, various microorganisms, and ignition [1,2].

To improve the properties of wood and wood-based products, they are commonly treated with chemical preservatives, such as TiO_2 , ZnO , $Al(OH)_3$ and various copper compounds. These treatments provide resistance against insects, fungi, bacteria, fire, weathering, and UV light, while also reducing smoke emission during burning [2,3]. However, the surface impregnation method is often inadequate and impractical.

To address these limitations, a recent study used inorganic Mg_2/Al_1-CO_3 and Zn_2/Al_1-CO_3 based layered double hydroxides (LDHs) to modify pine wood. LDHs are a non-toxic and environmentally friendly alternative to traditional wood preservatives and do not affect the mechanical properties of the wood. Furthermore, CO_3^{2-} intercalated LDHs have endothermic decomposition, which makes them effective as flame retardants and reduces smoke emission during combustion [4].

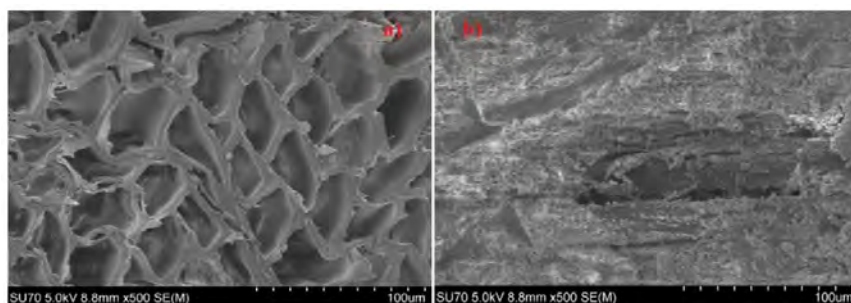


Fig. 1. SEM images of (a) the pristine pine wood surface and b) the surface of wood modified with Zn_2/Al_1-CO_3 LDH.

LDHs also have several advantages as antibacterial materials, including their basic character and strong oxidant species (OH^- ions) [5]. Zn-LDHs have been shown to inhibit the growth of bacteria and have antimicrobial activity against a broad range of bacteria. This effect can be achieved by adhering to bacteria, changing its charge distribution, binding to intracellular DNA or blocking nutrient transport [6,7].

In conclusion, wood and wood-based products are essential resources for various industries and can be improved with treatments such as inorganic LDHs. These treatments not only provide protection against various environmental factors but also potentially can improve the flame retardant and antimicrobial properties of the wood. By using LDHs, the industries can take a step towards a more sustainable and environmentally friendly future.

-
- [1] Anderson, Ingeborga & Andersons, Bruno et al., Handbook of wood chemistry and wood composites, second edition. (2012).
[2] Khademibami, Laya & dos Santos Bobadilha, Gabrielly. (2022). Recent Developments Studies on Wood Protection Research in Academia: A Review. *Frontiers in Forests and Global Change*.
[3] Guo, B., Liu, Y et al., Efficient Flame-Retardant and Smoke-Suppression Properties of Mg–Al-Layered Double-Hydroxide Nanostructures on Wood Substrate. *ACS Applied Materials & Interfaces*, 9(27), 23039–23047. (2017).
[4] Lv, S., Kong, X. et al., Flame-retardant and smoke-suppressing wood obtained by In situ growth of hydrotalcite-like compound on the inner surface of vessels. *New Journal of Chemistry*. (2019)
[5] Lobo, Marta & Nájera-Meléndez, Gisel & Luna, Gilberto & Segura-Pérez, Verónica & Rivera, Johel & Fetter, Geolar. (2018). ZnAl layered double hydroxides impregnated with eucalyptus oil as efficient hybrid materials against multi-resistant bacteria. *Applied Clay Science*. 153. 61-69. 10.1016/j.clay.2017.11.017.
[6] Cheng, H., Gao, X. et al., A novel antimicrobial composite: ZnAl-hydrotalcite with p-hydroxybenzoic acid intercalation and its possible application as food packaging material. *New Journal of Chemistry*. (2019).
[7] Awassa, Jazia & Soulé, Samantha & Cornu, Damien & Ruby, Christian & EL-Kirat-Chatel, Sofiane. (2022). Understanding the Role of Surface Interactions in the Antibacterial Activity of Layered Double Hydroxide Nanoparticles by Atomic Force Microscopy. *Nanoscale*. 14.

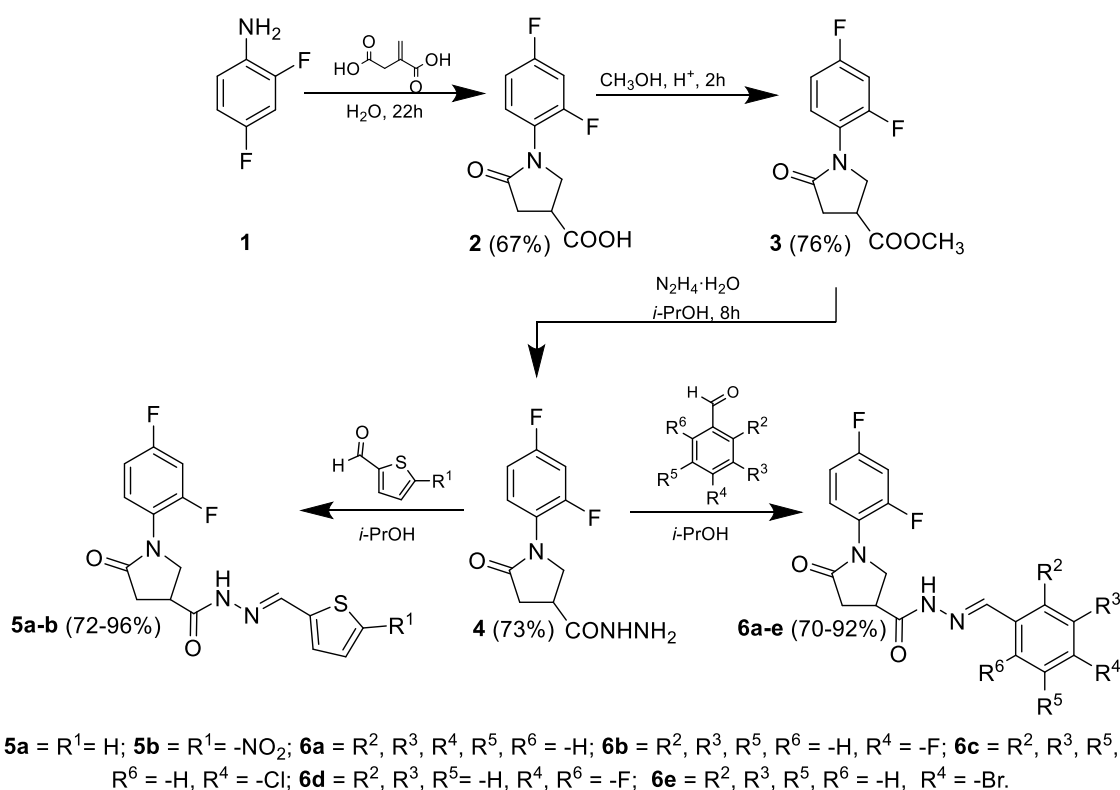
SYNTHESIS AND CHEMICAL PROPERTIES OF 1-(2,4-DIFLUOROPHENYL)-5-OXOPYRROLIDINE-3-CARBOXYLIC ACID

Guoda Pranaitytė, Birutė Grybaitė, Vytautas Mickevičius

Department of Organic Chemistry, Kaunas University of Technology, Lithuania
guoda.pranaityte@ktu.edu

Pyrrolidine fragment is present many biologically important pharmacophores. Pyrrolidine fragments are known for anti-inflammatory, antiviral, antimycobacterial and antitubercular activity in various drug molecules [1]. Recently *N*-substituted pyrrolidine derivatives have been synthesized as anticancer agents [2].

Hydrazone agents are known for antimicrobial, anticonvulsant, analgesic, anti-inflammatory, antiplatelet, antitubercular and antitumoral activities. Hydrazone derivatives are also used for antimalarial, antiviral, analgesic, antidepressant, vasodilator drug synthesis. They work as enzyme inhibitors and receptor agonists or antagonists [3].



Scheme 1. Synthesis of 1-(2,4-difluorophenyl)-5-oxopyrrolidine-3-carboxylic acid derivatives

The starting compound 1-(2,4-difluorophenyl)-5-oxopyrrolidine-3-carboxylic acid **2** was prepared from 2,4-difluoroaniline reaction with itaconic acid in water, at the boiling temperature of the mixture. 4-Acetyl-1-(2,4-difluorophenyl)pyrrolidin-2-one **3** was obtained from the esterification reaction using catalytic amount of sulfuric acid. In order to synthesize a compound with functional group of hydrazide, methyl ester **3** was transformed into the product **4** (1-(2,4-difluorophenyl)-5-oxopyrrolidine-3-carbohydrazide) by reaction with hydrazine monohydrate in refluxing isopropanol. Functional group of hydrazide **4** easily participates in condensation reactions, for this reason interaction of the compound **4** with various aromatic aldehydes were investigated (Scheme 1). The desired products **5a-b** and **6a-e** were obtained by stirring carbohydrazide **4** with corresponding aromatic aldehyde in isopropanol at the boiling temperature. The structure of the compounds has been proven by ¹H NMR, ¹³C NMR, FT-IR spectroscopy and elemental analysis. Further studies of the biological activity of synthesized compounds are planned.

[1] Jeelan Basha, N., Basavarajaiah, S. M., & Shyamsunder, K. (2022). Therapeutic potential of pyrrole and pyrrolidine analogs: an update. *Molecular Diversity* 2022 26:5, 26(5), 2915–2937. <https://doi.org/10.1007/S11030-022-10387-8>

[2] Bhat, A. A., Singh, I., Tandon, N., & Tandon, R. (2023). Structure activity relationship (SAR) and anticancer activity of pyrrolidine derivatives: Recent developments and future prospects (A review). *European Journal of Medicinal Chemistry*, 246, 114954. <https://doi.org/10.1016/J.EJMECH.2022.114954>

[3] Rollas, S., & Güniz Küçükgülzel, Ş. (2007). Biological activities of hydrazone derivatives. *Molecules*, 12(8), 1910-1939.

SYNTHESIS AND CHEMICAL PROPERTIES OF 1-(2-HYDROXY-5-METHYLPHENYL)-5-OXOPYRROLIDINE-3-CARBOXYLIC ACID

Karolis Krikštaponis¹, Birutė Grybaite¹

¹ Department of Organic Chemistry, Kaunas University of Technology, Lithuania
karolis.krikstaponis@ktu.edu

Pyrrolidinone derivatives exhibit various pharmacological properties: antibacterial, antioxidant, anti-cancer, antifungal, antiviral and anticonvulsant [1, 2]. Many examples of drugs such as piracetam, metadoxine, rolipram, raltegravir are known, the active ingredient of which is a pyrrolidinone derivative [3]. Therefore, in this study synthesized novel pyrrolidinone derivatives could be potential bioactive compounds in the discovery of new candidate drugs. To further improve the biological properties, other bioactive moieties were introduced into molecular structures [4]. This includes pyrazole, pyrrole and other heterocyclic scaffolds. The desired compounds were prepared by multi-step synthesis process as shown in figure 1.

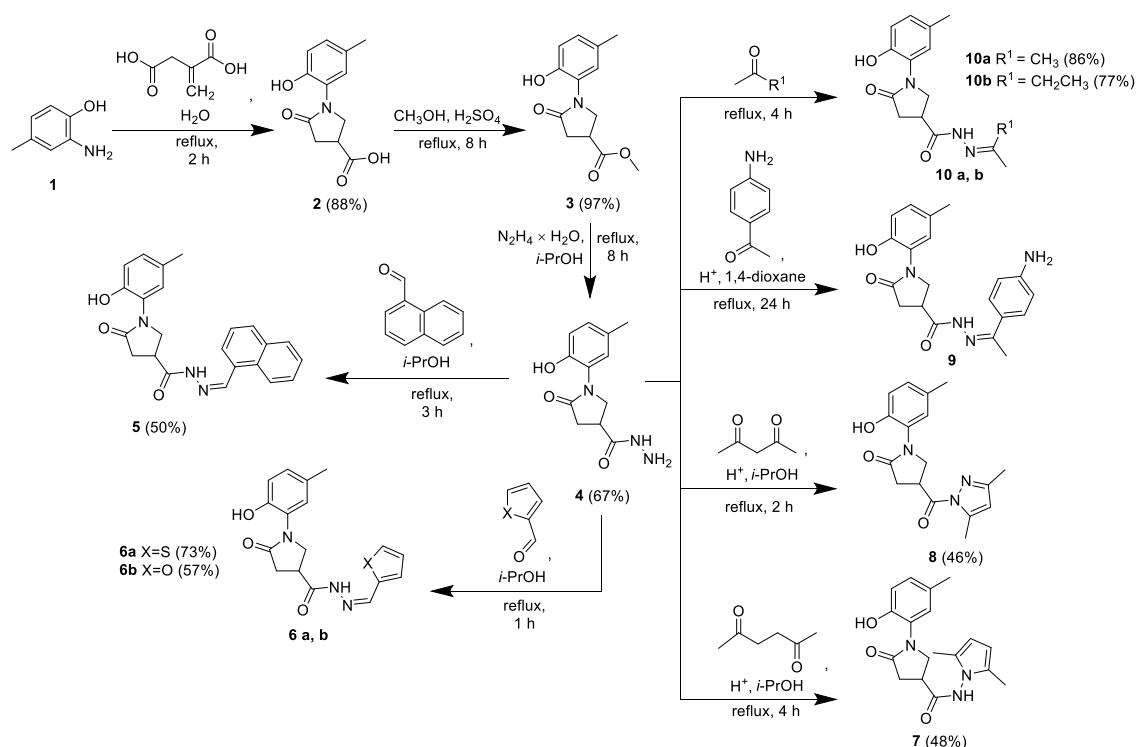


Fig. 1. Synthesis of 1-(2-hydroxy-5-methylphenyl)-5-oxopyrrolidine-3-carboxylic acid and its derivatives

The 1-(2-hydroxy-5-methylphenyl)-5-oxopyrrolidine-3-carboxylic acid (2) obtained from the reaction of the 2-amino-4-methylphenol (1) and itaconic acid in refluxing water solution. The gained crystals were filtered and purified by dissolving them in 5% NaOH solution followed by second filtration. After the procedure the obtained alkaline solution was acidified to pH 2, target compound (2) was isolated. The carboxyl group was esterified using methanol and a catalytic amount of sulfuric acid. Purified methyl ester (3) was further transformed to carbohydrazide by reaction with hydrazine monohydrate in isopropanol solution. Functional group of hydrazide (4) easily participate in condensation reactions. Therefore, interactions of the compound (4) with various aromatic carbaldehydes as well as mono- and diketones were investigated. The following target compounds 5-10 synthesized according to the conditions shown in figure 1. Further studies on the biological activity of all these compounds are planned. The structure of the compounds has been proven by ¹H NMR, ¹³C NMR, FT-IR spectroscopy and elemental analysis.

[1] M. Gagné-Boulet, C. C. Bouzriba, A. C. Alvarez, F. Sébastien, Phenyl 4-(2-oxopyrrolidin-1-yl)benzenesulfonates and phenyl 4-(2-oxopyrrolidin-1-yl)benzenesulfonamides as new antimicrotubule agents targeting the colchicine-binding site, *European Journal of Medicinal Chemistry* **213**, 113136 (2021).

[2] I. Tumosienė, I. Jonuškienė, K. Kantminienė, V. Mickevičius, V. Petrikaitė, Novel *N*-Substituted Amino Acid Hydrazone-Isatin Derivatives: Synthesis, Antioxidant Activity, and Anticancer Activity in 2D and 3D Models *In Vitro*, *International Journal of Molecular Sciences* **22**, 7799 (2021).

[3] Pyrrolidinones, Drugbank.com, Online: <https://go.drugbank.com/categories/DBCAT000973>, [2023-01-29].

[4] M. Maciuszek, A. Ortega-Gomez, S. L. Maas, et. al., Design, synthesis, and biological evaluation of novel pyrrolidinone small-molecule Formyl peptide receptor 2 agonists, *European Journal of Medicinal Chemistry* **226**, 113805 (2021).

STRUCTURAL ANALYSIS OF BIS-2-HYDROXYETHYLENE TEREPHTHALATE OBTAINED FROM DEPOLYMERIZATION OF POLYETHYLENE TEREPHTHALATE

Diana Masiulionytė, Monika Čekavičiūtė, Laura Pečiulytė, Joana Bendoraitienė

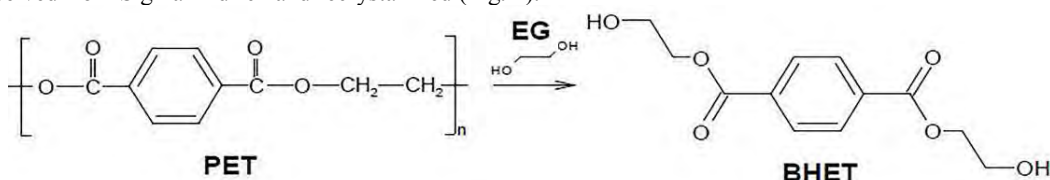
Department of Polymer Chemistry and Technology, Kaunas University of Technology, Lithuania
diana.masiulionyte@ktu.lt

Polyethylene terephthalate (PET) is one of the most utilized plastics for food and beverages packaging. PET does not have side effects in nature. However, there is a huge problem of increasing amount of plastic wastes in the world. Chemical recycling is one of the options to reduce PET wastes.

PET glycolysis, chemical recycling method, is a transesterification reaction. There are four main techniques of glycolysis: (i) catalyzed glycolysis; (ii) solvent-assisted glycolysis; (iii) supercritical glycolysis; (iv) microwave-assisted glycolysis. PET flakes dissolve in ethylene glycol (EG) in the presence of catalyst and causes formation of bis-2-hydroxyethyl terephthalate (BHET) monomer (Scheme 1) [1].

In our research, mayenite ($\text{Ca}_{12}\text{Al}_{14}\text{O}_{33}$) was used as a catalyst for glycolysis reaction. Synthesis and preparation of mayenite have influence for its catalytic activity. The highest surface area (m^2/g) and reducibility ($\text{mmol H}_2/\text{g}$) of mayenite particles, the more active catalysis [2].

BHET synthesis was carried out in three-neck round bottom flask. Mayenite, which calcination temperature was $900\text{ }^\circ\text{C}$, was added to EG solvent, heated until $196\text{ }^\circ\text{C}$, then PET flakes were added and mixture was heated for 2.5 hours. After 2.5 hours, the mixture was cooled in ice-bath; boiling water was poured and heated until $100\text{ }^\circ\text{C}$. Mixture was filtered still hot. The filtrate was reheated until its clear, cooled to $5\text{ }^\circ\text{C}$ and left for 16 h. The obtained crystals were dried at $60\text{ }^\circ\text{C}$. The BHET structure was proved by NMR, FTIR, XRD, TA analysis and compared to reference BHET, which was received from Sigma-Aldrich and recrystallized (Fig. 1).



Scheme 1. Synthesis of BHET

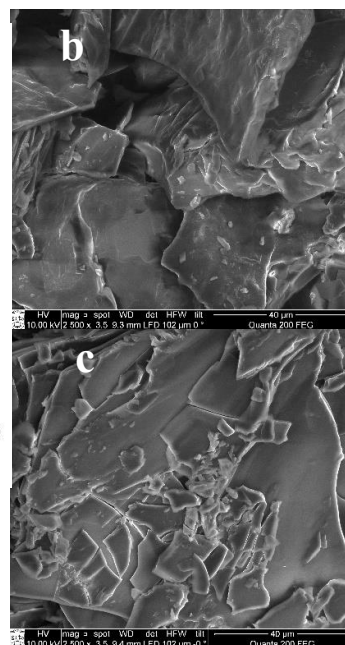
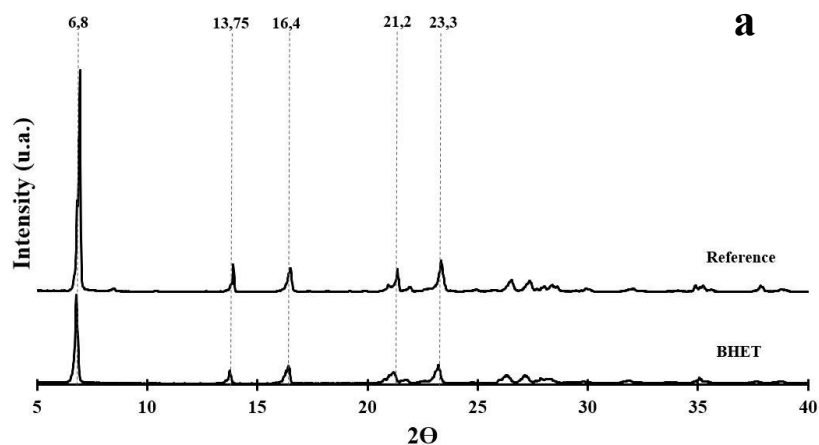


Figure 1. a – XRD spectra of BHET and reference; b and c – SEM images of BHET and reference crystals respectively, magnification 2500x

[1] A. Sheel, D. Pant, 4 - Chemical Depolymerization of PET Bottles via Glycolysis, Recycling of Polyethylene Terephthalate Bottles, ISBN 978-0-12-811361-5, India, 61-84 (2019).

[2] A. Intiso, F. Rossi, A. Proto, R. Cucciniello, The fascinating world of mayenite ($\text{Ca}_{12}\text{Al}_{14}\text{O}_{33}$) and its derivatives, Rendiconti Lincei. Scienze Fisiche e Naturali **32**, 699-708 (2021).

CONFORMATIONAL STUDY OF 1,1-DICHLORGERMACYCLOPENTANE BY MEANS OF VIBRATIONAL SPECTROSCOPY

Tautvydas Taraškevičius¹, Jogilė Mačytė¹, Gamil A. Guirgis², Valdas Šablinskas¹

¹Institute of Chemical Physics, Vilnius University, Saulėtekio av. 3, 10257 Vilnius, Lithuania
²Department of Chemistry and Biochemistry, College of Charleston, Charleston, SC 29424, USA
tautvydas.taraskevicius@ff.stud.vu.lt

Conformational analysis is an important part of the study of organic compounds and their properties. This work concerns on the possible conformations of the molecule 1,1-dichlorgermacyclopentane, a recently synthesized molecular compound. The conformers may differ in their physical properties, reactivity, etc., therefore detailed conformational analysis of the molecule is needed to predict its behavior¹. The aim of our study is to determine the possible stable conformations 1,1-dichlorgermacyclopentane using vibrational spectroscopy and DFT calculations.

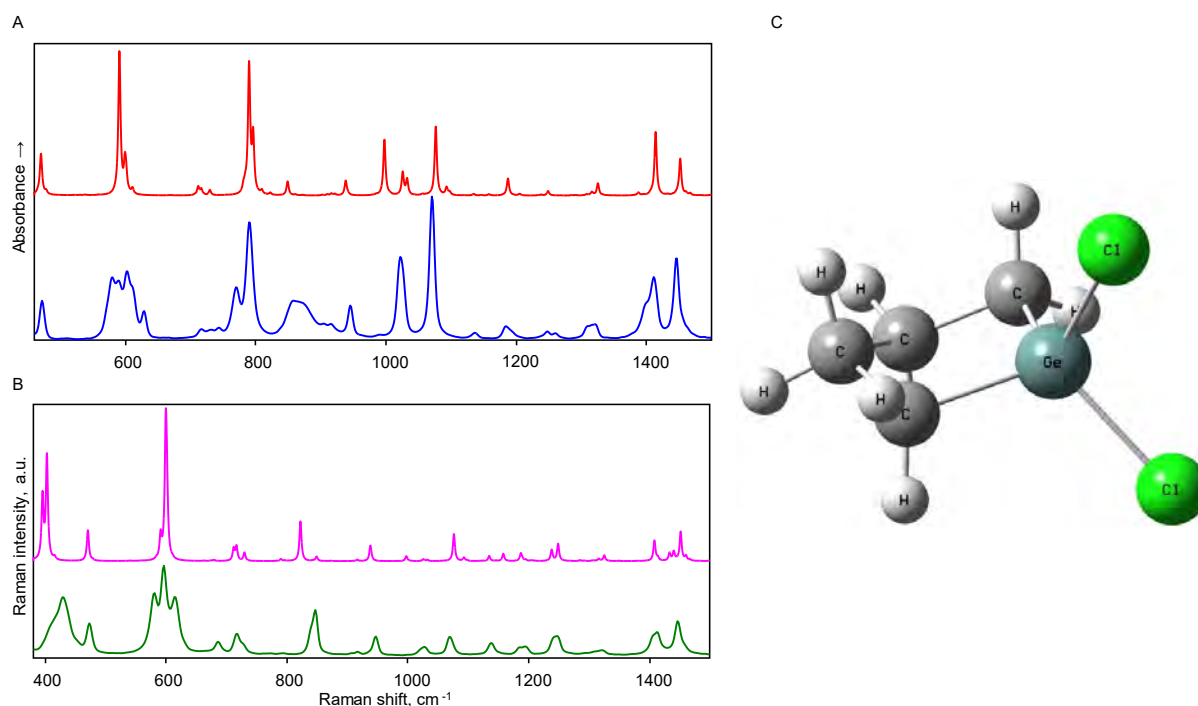


Fig. 1. (A) ATR-FTIR spectrum of 1,1-dichlorgermacyclopentane (blue) together with theoretically calculated IR spectrum (red) conformer; (B) FT-Raman spectrum of 1,1-dichlorgermacyclopentane spectra (green) together with theoretically calculated Raman spectra (pink) conformer; (C) theoretically (B3LYP/cc-pVTZ) calculated *envelope* structure of 1,1-dichlorgermacyclopentane.

Four different techniques of vibrational spectroscopy were employed to study the molecule. Firstly, liquid phase ATR infrared spectra were recorded in order to get the first view of the vibrational spectra of the molecule. To complement these data Raman spectra were recorded as well. Additionally, experiments with polarized Raman scattering were performed in order to facilitate attribution of experimental bands to symmetric and antisymmetric vibrational modes. Finally, in order to investigate further on possible conformational dynamics, gas phase and matrix isolated molecule infrared spectra were recorded. Interpretation of spectroscopic data was performed with the use of DFT calculations.

DFT calculations were performed utilizing B3LYP functional and augmented Dunning correlation-consistent valence double zeta basis set and assessing anharmonicity. The calculations reveal that 1,1-dichlorgermacyclopentane has one stable conformation (see fig.1C) - the envelope conformer. The calculated spectra fit well with the experimental ones (see fig.1A and 1B), confirming that the computed structure is the one is observed in spectroscopic experiments using liquid sample. Complete assignment of experimental spectral bands was performed based on calculation data. Experiments in gas phase as well as the matrix isolation revealed that the molecule is highly unstable in gas phase and defragments rapidly.

[1] Dragojlovic, V. Conformational analysis of cycloalkanes. *ChemTexts* 1, 14 (2015). <https://doi.org/10.1007/s40828-015-0014-0>

EFFICIENT BIMETALLIC NICKEL-MANGANESE/TITANIUM BIFUNCTIONAL ELECTROCATALYST FOR ALKALINE WATER SPLITTING

Sukomol Barua, Aldona Balčiūnaitė, Jūrate Vaičiūnienė, Loreta Tamašauskaitė-Tamašiūnaitė,
Eugenijus Norkus

Department of Catalysis, Center for Physical Sciences and Technology (FTMC), Vilnius, Lithuania
sukomol.barua@ftmc.lt

The fabrication and designing of an active, stable, and cost-effective bifunctional electrocatalyst with high performance for overall water splitting are of utmost importance for renewable energy supply but remain challenging. Herein, we demonstrate the facile synthesis of bimetallic nickel-manganese alloy electrocatalysts supported on a Ti surface ($1 \times 1 \text{ cm}^2$) by electrochemical deposition through a dynamic hydrogen bubble template technique. In this work, we report the outstanding bifunctional electrocatalytic performance of fabricated Ni-Mn alloy catalysts with $\text{Ni}^{2+}/\text{Mn}^{2+}$ molar ratio of 1:3 (denoted as $\text{Ni}_1\text{Mn}_3/\text{Ti}$) and 1:4 (denoted as $\text{Ni}_1\text{Mn}_4/\text{Ti}$) for hydrogen evolution (HER) and oxygen evolution (OER) reactions in alkaline media (1 M KOH). The $\text{Ni}_1\text{Mn}_3/\text{Ti}$ electrocatalyst exhibits overpotential of 170 mV and 245 mV to reach a current density of 10 mA/cm^2 and 20 mA/cm^2 , respectively, for HER, whereas $\text{Ni}_1\text{Mn}_4/\text{Ti}$ catalyst shows excellent HER activity with lower overpotentials of 149 mV and 225 mV at the current density of 10 mA/cm^2 and 20 mA/cm^2 , respectively. Similar results were obtained for OER. The prepared catalysts have shown lower overpotential of 356 mV and 401 mV by $\text{Ni}_1\text{Mn}_3/\text{Ti}$ and 366 mV and 406 mV by $\text{Ni}_1\text{Mn}_4/\text{Ti}$ to drive the current density of 10 mA/cm^2 and 20 mA/cm^2 , respectively. Both catalysts have exhibited excellent long-term durability for 10 h in an alkaline solution highlighting their robustness and higher feasibility of fabricating a number of non-precious Mn-containing active, stable binary, and ternary efficient bifunctional electrocatalysts for overall water splitting.

SYNTHESIS AND CHEMICAL PROPERTIES OF 3-(1-(4-METHOXY-2-NITROPHENYL)THIOUREIDO)PROPANOIC ACID

Roberta Gelminauskaitė¹, Birutė Grybaitė¹, Vytautas Mickevičius¹

¹ Department of Organic Chemistry, Kaunas University of Technology, Kaunas, Lithuania
roberta.gelminauskaite@ktu.edu

Thiazole ring is commonly used as functional group to enhance the bioactivity of related pharmacophores, which mostly emerged as a substructure in a large class of β -lactam antibiotics. Thiazolones, one series of thiazole derivatives, exist widely in bioactive natural compounds and exhibit various biological properties such as antitumor, antibiotic and has been used in a variety of commercially available drugs to treat diseases like inflammation and hypertension. [1-3]

New studies shows that thiazole derivatives, containing differently substituted phenyl ring, can be used as an antidiabetic agent against diabetes mellitus chronic metabolic disease. Pharmaceutically thiazole scaffold derivatives are well known, especially in number of anticancer compounds, displaying activities against a variety of tumor cell lines, including non-small cell lung cancer, human colon cancer and human breast adenocarcinoma. Besides that, they have also been proven to be potent inhibitors of cyclin-dependent kinases targets. These medicinal properties states that thiazole derivatives can be encouraging candidates for further drug development. [4,5]

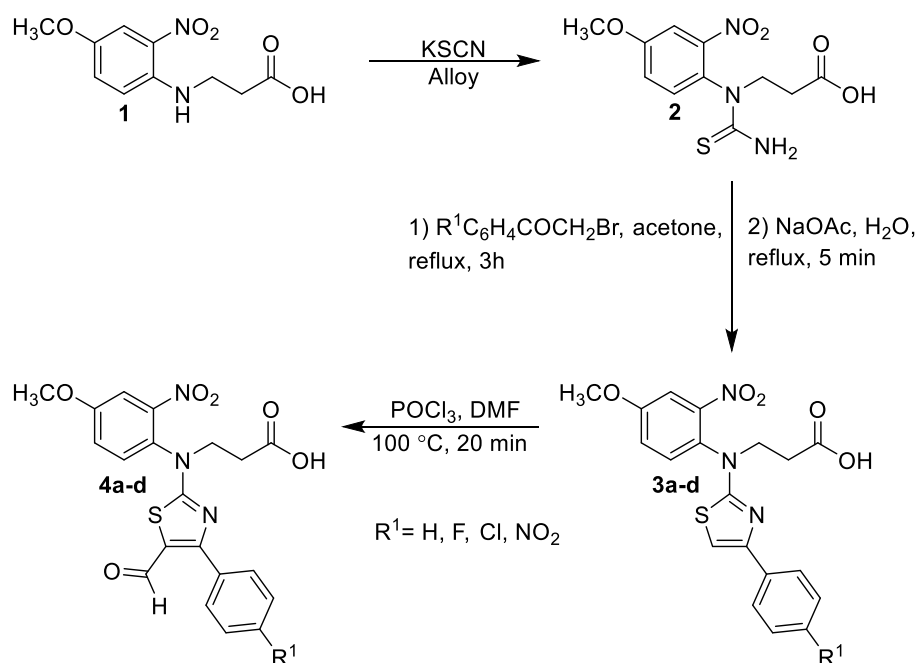


Fig. 1. Synthesis of new aminothiazole derivatives 3,4.

3-[(Carbamothioyl)(4-methoxy-2-nitrophenyl)amino]propanoic acid (**2**) was obtained by the reaction of 3-[(4-methoxy-2-nitrophenyl)amino]propanoic acid (**1**) and potassium thiocyanate when heated at 200 °C. Using the convenient method for the synthesis of thiazoles, i.e. the action of compound **2** with different bromoacetophenones in refluxing acetone, aminothiazole hydrobromides were obtained, which then were transferred into the bases **3a-d** by boiling them in the aqueous sodium acetate. The previously synthesized compounds **3a-d** were used for the preparation of derivatives **4a-d** (Fig. 1). Reaction of thiazoles **3a-d** with Vilsmeier reagent afforded aldehydes **4a-d**. The structure of the compounds has been proven by ¹H NMR, ¹³C NMR, FT-IR spectroscopy and elemental analysis. Further studies of the biological activity of synthesized compounds are planned.

[1] Qing-Song Dai, et al. (2018). Chiral Amine-Catalyzed Stereoselective [4+2] Annulations of Alkenyl Thiazolones and Aliphatic Aldehydes via a Step-Wise Mechanism. *Advanced Synthesis and Catalysis*. Volume 360, Issue 22. 4435-4440. <https://doi.org/10.1002/adsc.201800806>

[2] Yong-Xing Song, Da-Ming Du. (2020). Recent advances in the catalytic asymmetric reactions of thiazolone derivatives. *Organic & Biomolecular Chemistry*. Volume 18, Issue 31, 21 August 2020. 6018-6041. <https://doi.org/10.1039/d0ob01261k>

[3] Min Lu, et al. (2019). Primary amine catalyzed diastereo- and enantioselective Michael reaction of thiazolones and α,β -unsaturated ketones. *Organic & Biomolecular Chemistry*. Issue 42. DOI <https://doi.org/10.1039/C9OB02067E>

[4] HayatUllah, et al. (2022). Synthesis, molecular docking study of thiazole derivatives and exploring their dual inhibitor potentials against α -amylase and α -glucosidase. *Chemical Data Collections*. Volume 41. <https://doi.org/10.1016/j.cdc.2022.100932>

[5] Samukelisiwe PrettyKhathi, et al. (2018). Design and synthesis of novel thiadiazole-thiazolone hybrids as potential inhibitors of the human mitotic kinesin Eg5. *Bioorganic & Medicinal Chemistry Letters*. Volume 28, Issue 17. <https://doi.org/10.1016/j.bmcl.2018.07.007>

INVESTIGATIONS ON APPLICATION OF BiVO₄ PHOTOANODE FOR GLYCEROL DEGRADATION

Rūta Baltaragytė¹, Milda Malakauskaitė-Petrulevičienė², Irena Savickaja², Jurga Juodkazytė², Alvydas Zagorskis¹, Arūnas Ramanavičius²

¹ Department of Environmental Protection and Water Engineering, Vilnius Gediminas technical university, Lithuania

² Department of Chemical Engineering and Technology, Center for Physical Sciences and Technology, Lithuania
ruta.baltaragyte@stud.vilniustech.lt

Photoelectrochemical (PEC) decomposition of organic compounds is attracting great attention from scientists and industry, because it enables to decompose various hazardous organic compounds to more environmentally friendly products. PEC system has many advantages, e.g. sustainability, because it uses sunlight energy, and flexibility - many types of organic compounds can be decomposed, moreover, this process can be coupled with production of hydrogen [1]. PEC decomposition is based on oxidation of organic compounds on the surface of photoanode under light illumination. The most widely studied photocatalysts are TiO₂, ZnO, WO₃, BiVO₄ and Fe₂O₃ [2]. Bismuth vanadate (BiVO₄) is a promising material, because of its ability to absorb visible light, low valence band position (2.4 V) and stability in neutral electrolytes.

In this work bismuth vanadate was used for PEC decomposition of glycerol. BiVO₄ thin films were synthesized using sol-gel route and dip-coating technique. Composition and morphology of electrodes were studied using X-ray diffraction and scanning electron microscopy, respectively. Photoresponse of BiVO₄ photoanode was first evaluated using cyclic voltammetry (CV) in 0.5 M Na₂SO₄ and 0.5 M NaCl electrolytes. Electrochemical impedance spectroscopy (EIS) measurements were performed to evaluation of charge transfer resistance of the films. Next, CV and chronoamperometric (CA) experiments were performed in 0.1 M NaCl solution with 1, 2, 3, 4 and 5 g/L of glycerol under illumination. Certain amount of charge was passed through the cell in CA experiments. After that the amount of glycerol was evaluated using Fourier-transform infrared spectroscopy (FTIR). Results of CV and CA experiments are presented in Fig. 1. It can be seen that photocurrent density was increasing with increase in concentration of glycerol. The efficiency of glycerol decomposition will be discussed at the conference.

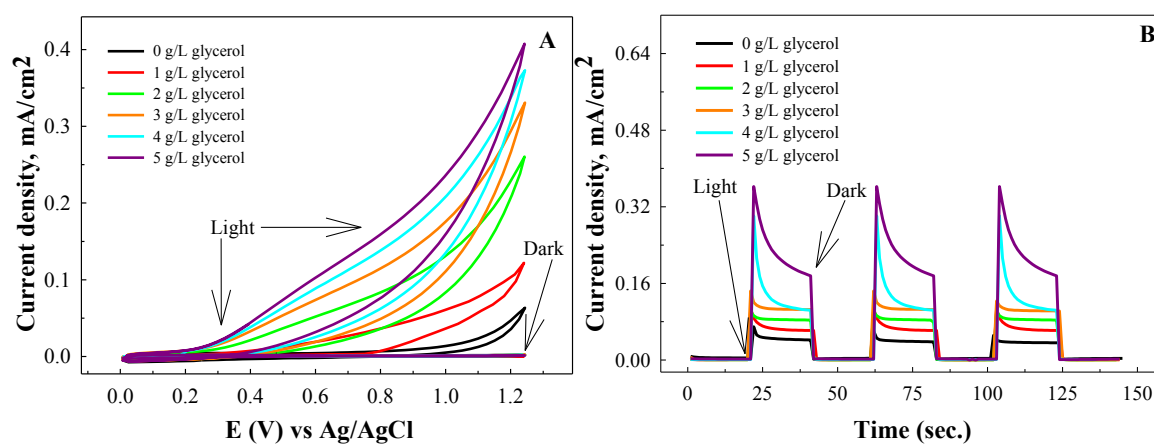


Fig. 1. A) Cyclic voltammograms of BiVO₄ photoanode in 0.1 M NaCl containing various concentrations of glycerol, 50 mV s⁻¹, illumination intensity ~100 mWcm⁻²; B) Chronoamperograms of BiVO₄ photoanode recorded in two electrode cell with Pt cathode under 1.4 V bias under chopped illumination

Acknowledgement: This project has received funding from the Research Council of Lithuania (LMTLT), agreement No S-PD-22-2

- [1] Liu, D., Liu, J. C., Cai, W., Ma, J., Yang, H. B., Xiao, H., ... & Liu, B. (2019). Selective photoelectrochemical oxidation of glycerol to high value-added dihydroxyacetone. *Nature Communications*, 10(1), 1779.
- [2] Li, Z., Luo, W., Zhang, M., Feng, J., & Zou, Z. (2013). Photoelectrochemical cells for solar hydrogen production: current state of promising photoelectrodes, methods to improve their properties, and outlook. *Energy & Environmental Science*, 6(2), 347-370.

INVESTIGATION OF BIOACTIVE FILMS BASED ON NATURAL POLYSACCHARIDES AND PLANT EXTRACTS

Emilija Galkauskaite¹, Ramune Rutkaite¹, Vaida Kitryte-Syrpa², Dovile Liudvinaviciute¹, Michail Syrpas²

¹ Department of Polymer Chemistry and Technology, Kaunas University of Technology, Lithuania

² Department of Food Science and Technology, Kaunas University of Technology, Lithuania

emilija.galkauskaite@ktu.edu

One of the most progressive pathologies in the world is various oral cavity infections. They are associated with the worsening quality of life and increasing health costs [1]. Developing the new ways to treat these diseases are very important. Oral disintegrating films (ODF) are thin, flexible films made of hydrophilic polymers, pharmacologically active substances, plasticizers, flavorings, dyes and sweeteners [2, 3]. There are many reports on films that quickly disintegrate in the oral mucosa and immediately release biologically active components into the systemic circulation. However, self-disintegrating films with prolonged activity are still underexplored and could be effective method for the local treatment of periodontal diseases, caries, stomatitis, and other infections in the oral cavity.

The main goal of this research work was the formation of ODFs from natural polysaccharide derivatives and natural plant extracts and investigation of their properties. Polymeric films of various composition were formed by solvent casting method using natural polysaccharide derivatives - chitosan, hydroxyethylcellulose, hydroxypropylmethylcellulose, plasticizer glycerin and crosslinking agent citric acid, in which the extracts of hop and birch leaves were immobilized.

The mechanical, thermal, hydrophobic and water vapor permeability properties of the various films were evaluated. The solubility in various aqueous solutions was determined. The films of hydroxyethylcellulose were the most elastic and the least rigid. Immobilization of plant extracts reduced the tensile strength and modulus of elasticity of the polymeric films. The water wetting angle of the films of various composition ranged from 42.3 to 86.3 degrees. In films containing plant extracts wetting angle increased from 80 to 86°. The films of natural polysaccharide derivatives formed using citric acid had the lowest solubility in distilled water, with a water solubility being less than 25 percent after 7 days. Films containing birch leaf extract showed higher water vapor sorption, which was equal to 72.5 percent after 72 hours, while the moisture sorption of the films containing hop extract was less than 35 percent. Meanwhile, the solubility of the films containing natural plant extracts in saliva simulant solution after 7 days was less than 32 percent.

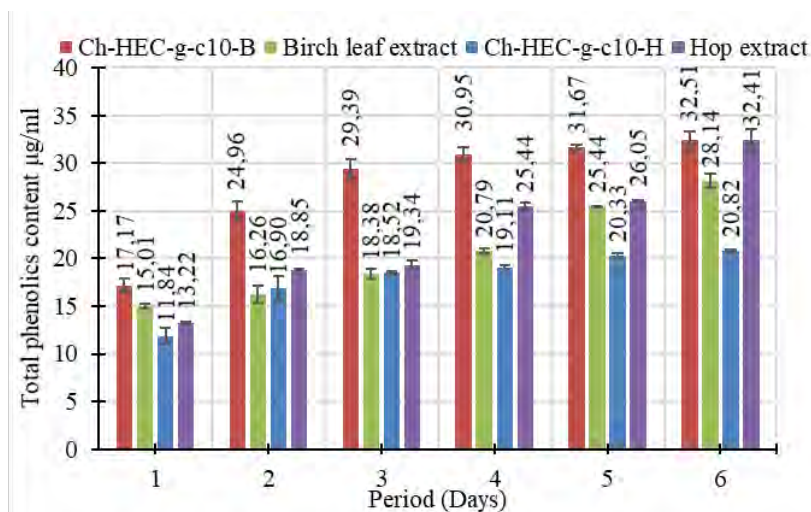


Fig. 1. The amount of total phenolic compounds released from the samples into the saliva model solution dependence of time

The release of bioactive components from polymer films into saliva model solution was investigated by using UV spectroscopy method. Approximately 22.75 percent of hop extract and about 93.9 percent of birch leaf extract were released from the polymeric films into the saliva simulant within 48 hours. The assessment of phenolic compounds release into the saliva simulant (Fig. 1) and antioxidant properties studies by Folin-Ciocalteu, CUPRAC and ABTS assays showed that phenolic compounds were released from the films and they were bioactive.

[1] MENDEZ-VILAS, Antonio. The use of plants against oral pathogens. From: Microbial pathogens and strategies for combating them : science, technology and education. Badajoz: Formatex Research Center, 2013, pp. 1375-1384. ISBN 9788493984397

[2] HEINEMANN, Riana Jordao Barrozo, et al. Characterization of low cost orally disintegrating film (ODF). Polimeros, 2017, 27(1), 48-54. ISSN 0104-1428.

[3] MAZUMDER, Sonal, et al. Quality by Design approach for studying the impact of formulation and process variables on product quality of oral disintegrating films. International Journal of Pharmaceutics, 2017, 527(1-2), 151-160. ISSN 0378-5173.

POLYETHYLENE TEREPHTHALATE GLYCOLYSIS USING MAYENITE AS CATALYST

Klaudija Bojanauskaitė, Diana Masiulionyte, Laura Peciulyte, Joana Bendoraitiene

Department polymer chemistry and technology, Kaunas University of Technology, Lithuania
klaudija.bojanauskaitė@ktu.edu

Polyethylene terephthalate (PET) is a thermoplastic polyester. It is widely used to make films, bottles and textile fibres because of its resistance to water, high strength-to-weight ratio, safety, and availability. However, as the packaging and bottling industries increased their use of plastic, the amount of non-biodegradable plastic waste skyrocketed, becoming a significant global environmental issue. Furthermore, because plastics are long-lasting and cannot be easily broken down by microorganisms in nature, the recycling of PET products is in high demand [1].

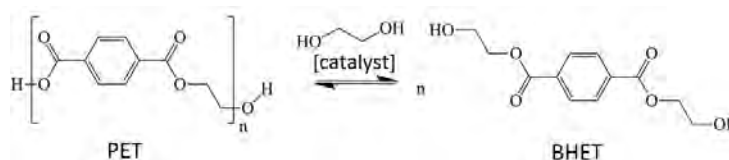


Fig. 1. PET glycolysis reaction

Chemically, the glycolysis reaction is defined as the “molecular degradation” of PET polymer where the ester linkages break and replace with hydroxyl groups. This reaction is a type of solvolysis in which a catalyst and ethylene glycol (EG) are used (Fig. 1.). Factors that have been reported to influence the results of the reaction are temperature, time, solvent, amount of catalyst and particles size of PET. Bis(2-hydroxyethyl) terephthalate (BHET) and oligomers (PET glycolyzates) are the reaction products of EG and PET [2]. In this work, the influence of mayenite ($\text{Ca}_{12}\text{Al}_{14}\text{O}_{33}$) to BHET yield was investigated. Mayenite is a mesoporous calcium aluminium oxide with a distinctive crystalline structure. The framework of mayenite, in contrast to aluminosilicate zeolites, consists of interconnected cages with a positive electric charge per unit cell [3]. The reaction mixture of EG and mayenite were mixed and heated to 196°C, then PET was added, and the glycolysis reaction was set to 2.5 hours. After reaction the mixture immediately was cooled in the ice-bath. Boiling distilled water was added to the cold mixture and heated. When temperature reached 100°C the mixture was filtered. The BHET-containing filtrate was heated until it became clear, and the reaction products were left for 16 hours at 4°C. The cold mixture was filtered once more to obtain BHET crystals. The crystals were dried for 30 hours at 60°C. The synthesis of BHET was carried out using a catalyst content between 3.23 and 12.87 mmol/kg_{PET}. The best results of the PET glycolysis were using mayenite as catalyst and isolated BHET yield was reached up to 69%, when reaction duration was 2 hours at 196 °C with a catalyst amount 4.22 mmol/kg PET.

[1] Lalmangaihzuola, S., Laldinpuii, Z., Lalmuanpuia, C., & Vanlaldinpuia, K. (2020). Glycolysis of Poly(Ethylene Terephthalate) Using Biomass-Waste Derived Recyclable Heterogeneous Catalyst. *Polymers* 2021, Vol. 13, Page 37, 13(1), 37.

[2] Sheel, A., & Pant, D. (2019). Chemical Depolymerization of PET Bottles via Glycolysis. *Recycling of Polyethylene Terephthalate Bottles*, 61–84.

[3] Cucciniello, R., Intiso, A., Castiglione, S., Genga, A., Proto, A., & Rossi, F. (2017). Total oxidation of trichloroethylene over mayenite ($\text{Ca}_{12}\text{Al}_{14}\text{O}_{33}$) catalyst. *Applied Catalysis B: Environmental*, 204, 167–172.

INFLUENCE OF DODECENYLSUCCINATE CONTENT ON PROPERTIES OF ACETYLATED POTATO STARCH DODECENYLSUCCINATE

Jonas Luneckas¹, Laura Peciulyte¹, Joana Bendoraitiene¹, Ramune Rutkaite¹

¹ Department of Polymer Chemistry and Technology, Kaunas University of Technology, Radvilėnų pl. 19, 50254
Kaunas, Lithuania
jonas.luneckas@ktu.edu

The demand for plastics in the world is growing every year, leading to an increased demand for resources required to produce those non-renewable plastics which are depleting at a rapid pace. To address this growing problem, the alternative polymers from renewable sources can be produced and starch is receiving increasing attention. Naturally found starch does not possess thermoplastic properties (has neither melting nor glass transition temperature) and it's of hydrophilic nature. To overcome these disadvantages, the starch could be chemically modified in order to obtain thermally processable materials based on renewable resources.

The aim of this study was to synthesize acetylated potato starch dodecenylsuccinates with varying degree of substitution and determine the influence of dodecenylsuccinate content in those derivatives on their thermal properties.

Potato starch was modified with 2-dodecen-1-yl succinic anhydride and acetic anhydride in an alkaline medium. The starch was modified in two stages. In the first stage, starch dodecenylsuccinate was obtained at room temperature in an alkaline environment, maintaining the pH at 8-8.5 with a goal to get at least three starches with varying degree of substitution to use as a base for the second reaction. Then in the second stage starch dodecenylsuccinates were modified with acetic anhydride at 100-140 °C at different reaction duration. The degree of substitution of dodecenylsuccinate and acetate groups in obtained potato starch esters was determined according to the methodology given in the literature [1]. Moreover, Fourier-transform infrared spectroscopic analysis of the synthesized starch derivatives was performed. In order to assess the changes in the hydrophobicity, the water contact angle of the surface of the compressed acetylated starch dodecenylsuccinate tablets was evaluated. Differential scanning calorimetry analysis demonstrated that glass transition was characteristic of both acetylated starches and acetylated starch dodecenylsuccinates, and depended on the degree of substitution of both acetyl and dodecenylsuccinate groups. Granular structure did not change during modification of starch with dodecenyl succinic anhydride. But scanning electron microscopy shows that destruction of granules occurred during starch dodecenylsuccinate modification with acetic anhydride at higher degree of substitution.

[1] J.F. Zhu, G.H. Zhang, Z.C. Lai, G.H. Zhang Synthesis and Characterization of Maize Starch Acetates and its Biodegradable Film, *Polymer-Plastics Technology and Engineering*, 2007, 46:12, p 1135-1141.

ELECTRONIC EXCITATION DEACTIVATION PATHWAYS OF BODIPY MOLECULAR ROTORS WITH ROTATING HYDROCARBON GROUP

Delianas Palinauskas¹, Stepas Toliautas¹

¹Institute of Chemical Physics, Faculty of Physics, Vilnius University, Sauletekio av. 9-III, 10222 Vilnius (Lithuania)
delianas.palinauskas@ff.stud.vu.lt

Interaction of photoactive compounds with light by absorption involves excitation into higher energy levels. Excitation energy can be either dissipated among vibrational modes of molecule or radiated in the form of photons. Energetically accessible conical intersections (CI) provide funnel between any two (or more) electronic states for non-radiative excitation energy dissipation. Since conical intersections are not single points on potential energy surface, but rather 3N – 8 dimensional seams, configuration space must be thoroughly explored, lowest energy structures and their accessibility must be assessed. Accessibility of these CIs can be related to energy barrier height (TS, Fig. 1), which must be overcome to reach CI. Height of energy barrier determines the rate of non-radiative process. Minimum energy pathways (MEP) from Franck-Condon (FC) region to conical intersection can be used to determine CI accessibility and make predictions about photophysical properties of molecules in study.

Molecules bearing BODIPY fragment are model photoactive compounds with wide applications in fluorescence imaging and biosensing [1, 2]. Accessibility of conical intersection for BODIPY compounds is affected by nature of rotor group at 8 position (Fig. 1) and overall BODIPY fragment substitution [2]. The aim of this study is to determine minimum energy path for different BODIPY compounds and predict their photophysical properties.

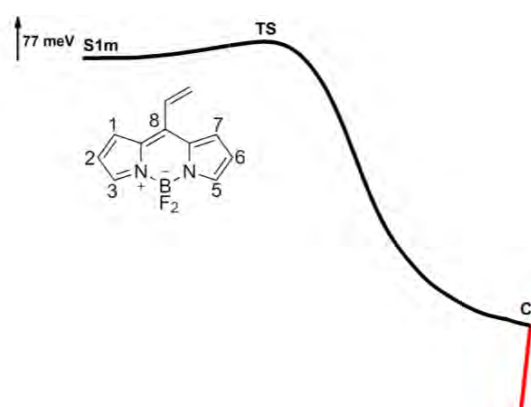


Fig 1. Fragment of MEP and 8-vinyl-BODIPY molecule with numbered positions

In this work, minimum energy pathways from FC region to CI in excited state (S1) and ground state (S0) were calculated for several BODIPY compounds by Nudged Elastic Band (NEB) method implemented in Orca 5.0.3 software. All stationary points on potential energy surface were optimized and NEB calculations were done at (TD-)DFT/PBE0 level of theory using cc-pVDZ basis set. In order to confirm that optimized CIs are involved in non-radiative relaxation of BODIPY, energy barrier heights for transition from excited state minimum (S1m, Fig. 1) to conical intersection were calculated for all molecules. The computed energy barriers qualitatively agree with empirical data i.e. the higher energy barrier the higher experimental quantum efficiency of molecule is. This trend confirms that optimized conical intersection structures were indeed involved in radiationless relaxation. The main findings of this study suggest that despite introduction of bulky phenyl groups at 2, 6 positions at BODIPY fragment and methyl groups at 1, 3, 5, 7 BODIPY fragment positions accessibility to conical intersection was similar for all compounds in study.

- [1] S. Toliautas, J. Dodonova, A. Žvirblis, I. Čiplys, A. Polita, A. Devižis, S. Tumkevičius, J. Šulskus, A. Vyšniauskas, *Chemistry – A European Journal*. 25 (2019) 10342–10349.
[2] S. V. Dzyuba, *Biosensors*. 10 (2020) 192.
[3] A. Prlj, A. Fabrizio, C. Corminboeuf, *Phys. Chem. Chem. Phys.* 18 (2016) 32668–32672.

BIOREFINING OF THREE *VINCETOXICUM* SPECIES INTO VALUABLE COMPONENTS BY DIFFERENT EXTRACTION METHODS

Jovita Jovaišaitė¹, Laura Jūrienė¹, Audrius Pukalskas¹, Petras Rimantas Venskutonis¹

¹ Department of Food Science and Technology, Kaunas University of Technology, Lithuania
jovita.jovaisaite@ktu.edu

Vincetoxicum belongs to the family *Apocynaceae*, the subfamily *Asclepiadoideae* [1]. It is an herbaceous, perennial, climbing plant native to Europe, North America and Asia. In Chinese medicine, the plant has often been used to treat scabies. Additionally, swallow-wort have diuretic and laxative properties and a powder made from the roots is said to accelerate wound healing. It must be stressed that swallow-wort is a poisonous plant, which in large doses can affect the nervous, vascular and cardiac systems [2]. However, there is very little detailed scientific information on the phytochemical composition and properties of these plants.

The aim of this work was to develop technology for producing various fractions rich in bioactives from three *Vincetoxicum* species using biorefining concept and characterize the extracts. *V. hirundinaria*, *V. nigrum* and *V. luteum* were defatted by supercritical fluid extraction with carbon dioxide (SFE-CO₂). The lipophilic extracts were analyzed by different methods. Triacylglycerols (TAGs) were analyzed by ultra-performance liquid chromatography (UPLC), while the total chlorophyll and carotenoid were measured by spectrophotometric method. Defatted leaves were further extracted by the mixture of three different polarity solvents (acetone-methanol-water). Antioxidant activity of non-polar and polar extracts was evaluated by using different *in vitro* antioxidant capacity assays: the DDPH assay and the Oxygen Radical Absorbance Capacity (ORAC) assay. Total phenol content was measured by *Folin-Ciocalteu* method. The phytochemical composition of *V. luteum* extract was analysed by ultra-performance liquid chromatography (UPLC).

The yields of lipophilic fractions recovered by SFE-CO₂ were 1.2-1.5%. Linoleic linolenic, oleic and palmitic acids were major in the extracted triacylglycerols. The concentration of carotenoids and chlorophylls varied between different species. The extracts obtained by different extraction methods were characterized by their antioxidant potential. Thus, all measured values for lipophilic fractions were rather low, while the mixture of different polarity solvents recovered the majority of polar polyphenolic antioxidants. UPLC-MS/MS results indicated that in *V. luteum* extract was identified several phenolic compounds: chlorogenic acid, caffeic acid, isoquercitrin, kaempferol and various flavonoid glycosides. The obtained extracts contain different classes of bioactive compounds. It can be concluded that extraction by supercritical fluid extraction with carbon dioxide and the mixture of different polarity solvents can extract valuable bioactive compounds from leaves of different *Vincetoxicum* species.

[1] ENDRESS, Mary E.; BRUYNS, Peter V. A revised classification of the Apocynaceae sl. *The Botanical Review*, 66.1: 1-56 (2000).

[2] WANG, Li-Qin, et al. A new C21 steroidal glycoside from *Cynanchum inamoenum* (Maxim.) Loes. *Journal of Asian natural products research*, 10.9: 867-871 (2008).

SYNTHESIS AND PROPERTIES OF OCTENYL SUCCINIC ANHYDRIDE MODIFIED DEXTRIN

Emilija Morkvėnaite, Ramune Rutkaite, Vesta Navikaite-Snipaitiene

Department of Polymer Chemistry and Technology, Kaunas University of Technology, Lithuania
emilija.morkvenaite@ktu.edu

Numerous studies have revealed that bioactive substances have drawn significant interest due to their wide array of potential uses in various spheres of life, including food, engineering, and the biomedical sector. However, such bioactive compounds limited practical applicability and decreased bioavailability are caused by their low water solubility, instability under light and heating conditions, and other considerations. Nanocapsules, emulsions, and micelles might enhance the half-life of drugs in vivo and in vitro while overcoming the drawbacks of their instability. Dextrin, a primary degradation product of starch, exhibits non-Newtonian fluid properties in solution and has excellent properties such as water-solubility, emulsibility, dispersibility, adhesion and film-forming properties. Compared to native starch, dextrin can be more easily modified by octenyl succinic anhydride (OSA) due to its low molecular weight. Moreover, it's known that OSA modified dextrin possess excellent emulsifying properties and could be exploited for the immobilisation of bioactive substances [1, 2].

This study aimed to explore preparation of octenyl succinic anhydride modified dextrans and to study their emulsifying properties. OSA modified dextrans were synthesized by esterification of potato dextrin with OSA in aqueous solution (see scheme in Fig. 1). The amount of OSA added was 3, 6, 9 and 12 percent of the weight of dextrin while maintaining the pH at 8 using NaOH solution. By changing the amount of OSA, four different hydrophobically modified dextrin derivatives were prepared.

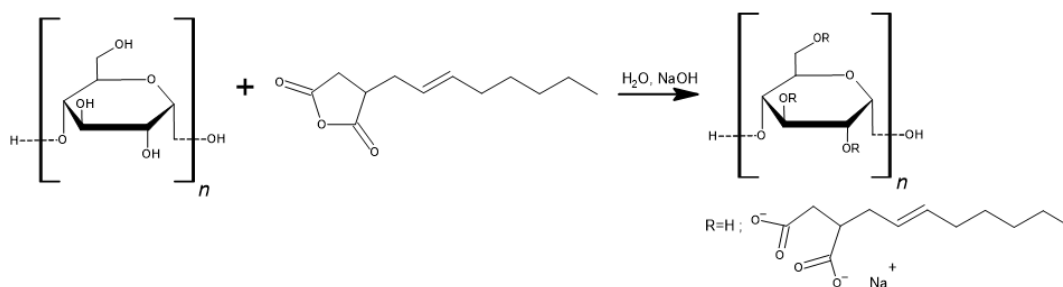


Fig. 1. Scheme of the esterification reaction between dextrin and OSA

The obtained OSA modified dextrans were characterized by FT-IR spectroscopy, thermal analysis and other techniques. Moreover, they were adopted as emulsifiers to stabilize aqueous emulsions of rape seed oil. The emulsions prepared by using various amounts of OSA modified dextrans were prepared and the droplet size, zeta potential, emulsifying stability, storage stability characteristics were investigated.

[1] Y. Pan, Z. Wu, B. Zhang et al., Preparation and characterization of emulsion stabilized by octenyl succinic anhydride-modified dextrin for improving storage stability and curcumin encapsulation, *Food Chemistry* 294, 326 (2019).

[2] J.A. Han, H. J. Chung, S.T. Lim, Physical and emulsifying properties of OSA-corn dextrin with various manufacturing methods, *Food Hydrocolloids* 89, 563 (2019).

BIOREFINING OF TAGETES PATULA BY INNOVATIVE EXTRACTION METHODS

Laura Jūrienė¹, Audrius Pukalskas¹, Petras Rimantas Venskutonis¹

¹ Department of Food Science and Technology, Kaunas University of Technology, Lithuania
laura.tamkute@gmail.com

Tagetes patula belongs to the family *Asteraceae* and is widely recognized for its phytochemical and therapeutic properties. Traditionally, the plant is used to treat many symptoms and diseases such as colic, diarrhea, rheumatism, eye problems, cough and constipation. Previous studies have shown that these flowers are rich source of carotenoids, flavonoids, steroids, thiophenes and monoterpenoids. The essential oil is well characterized of these plants, but still there is a lack of information about the composition of other components obtained by innovative extraction methods. In recent years such innovative methods as supercritical fluid extraction with carbon dioxide (SFE-CO₂) and pressurized liquid extraction (PLE) has gain the popularity in isolating bioactive compounds from various plants.

The aim of this work was to develop separation technology for producing various nutrients (products rich in bioactive components) from *Tagetes patula* flowers using biorefining and green extraction concepts, as well as characterization of obtained extracts. Flowers first of all was defatted by supercritical fluid extraction with carbon dioxide (SFE-CO₂) using 45 MPa pressure and 50°C temperature. Triacylglycerols (TAGs), sterols and tocopherols content were analysed by ultraperformance liquid chromatography (UPLC), while fatty acids composition was determined by gas chromatography (GC). Total carotenoids content was measured by spectrophotometric method. Defatted flowers were further extracted by pressurized liquid extraction (PLE) sequently with ethanol and water. Antioxidant activity of different fractions (lipophilic and polar extracts) was evaluated by using different *in vitro* antioxidant capacity assays: the ABTS assay, which measures the relative ability of antioxidants to scavenge the ABTS, as compared with a Trolox standard; the Oxygen Radical Absorbance Capacity (ORAC) assay, which measures a fluorescent signal from a probe that is quenched in the presence of Reactive Oxygen Species (ROS) and added antioxidant absorbs the generated ROS. Total phenol content (TPC) was measured by *Folin-Ciocalteu* method.

The yield of lipophilic fraction recovered by SFE-CO₂ was 1.5%. Highly unsaturated TAGs were majorly found in the extract: LLLn, OLnL, LLnLn and OLL. Four tocopherols (sometimes also called E-vitamins) and 4 phytosterols were preliminarily quantified by their peak areas in the extract. α -tocopherol was dominating in *Tagetes patula* oil, while the content of β -sitosterol was many times higher than the content of other detected sterols. Lipid fraction recovered by supercritical CO₂ extraction was composed of linoleic, oleic and linolenic acids. Deffated *Tagetes patula* flowers further were sequentially extracted with ethanol and water by PLE. The yield of ethanol extract was 34%, while water additionally recovered 17% of extract. The antioxidant capacity of extracts measured by different methods increased with increasing solvent polarity. It may be concluded that the lipophilic and hydrophilic extracts isolated from *Tagetes patula* flowers by supercritical CO₂ and pressurized liquid extractions are a good source of bioactive compounds, which might find applications in the formulation of cosmetics and nutraceuticals.

ENHANCING SCOTS PINE WOOD WITH CALCIUM PHOSPHATE BIOCERAMICS SYNTHESIZED FROM EGGSHELLS FOR IMPROVED STRENGTH AND FIRE RESISTANCE

Gabija Navašinskaitė, Denis Sokol

Institute of Chemistry, Faculty of Chemistry and Geosciences, Vilnius University, Naugarduko st. 24, LT – 30225,
Vilnius, Lithuania

gabija.navasinskaite@chgf.stud.vu.lt

Wood has been used in construction and other applications for centuries due to its unique properties. It is a natural composite material made up of various components, with the structural components of the wood cell wall mainly composed of cellulose, hemicelluloses, and lignin. These components contribute to the unique properties of wood, such as its strength, durability, and ability to absorb and release moisture. One of the most significant advantages of wood is the diverse possibilities for its modification due to its chemical composition and hierarchical porous structure. Despite all mentioned wood advantages enhancing the physicochemical properties of wood products and extending their useful life is crucial to sustainable production and consumption. Improvements are needed in properties such as photodegradation protection, thermal stability or fire retardancy, mechanical strength, resistance to biological degradation, and more [1-5].

In this work, the goal is to improve the physical and chemical properties of wood by using eggshells as a source of calcium carbonate to create bioceramic-reinforced wood materials. Since eggshells are considered waste material and are rich in calcite, which is a source of calcium, they can be used to create a biocompatible ceramic material called carbonated hydroxyapatite. This process leads to the mineralization of wood, making it stronger and more fire-resistant. Additionally, incorporating calcite within the wood matrix can result in a CO₂ storing hybrid wood material, which can help fight climate change by reducing emissions. The main focus of the work is to reinforce locally produced pine wood with biocompatible calcium phosphate-based ceramics to improve mechanical strength and fire-retardancy.

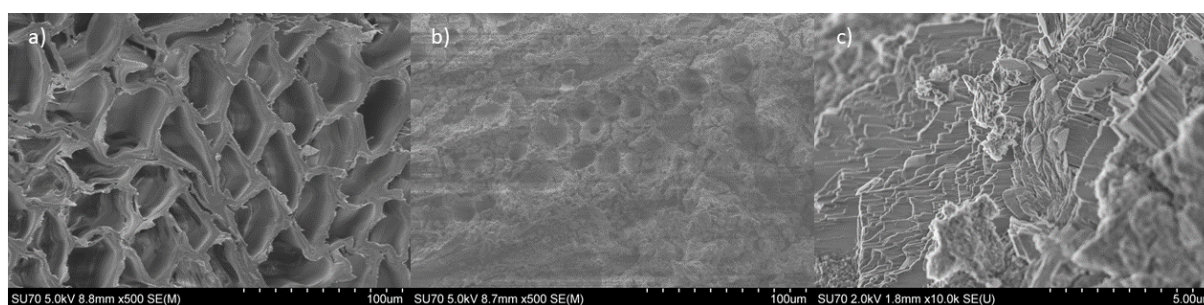


Fig. 1 SEM micrographs of untreated Scots pine (a), HAP treated Scots pine (b) and HAP powder from self-made calcium acetate.

-
- [1] Kuzman, Manja & Grošelj, Petra. (2012). Wood as a construction material: Comparison of different construction types for residential building using the analytic hierarchy process. *Wood Research*, 57, 591-600.
 - [2] Upton, B., Miner, R., Spinney, M., & Heath, L. S. (2008). The greenhouse gas and energy impacts of using wood instead of alternatives in residential construction in the United States. *Biomass and Bioenergy*, 32(1), 1–10.
 - [3] Rowell, R.M. *Handbook of Wood Chemistry and Wood Composites*, 2nd ed.; CRC Press, Taylor and Francis Group: Boca Raton, FL, USA, 2012.
 - [4] Hill Callum A. S. 2006. *Wood Modification: Chemical Thermal and Other Processes*. Chichester England: John Wiley & Sons.
 - [5] K. Ronan and M. B. Kannan, *ACS Sustain Chem. Eng.*, 2017, 5, 2237.

STATISTICAL ANALYSIS OF BODIPY DERIVATIVES ROTATIONAL ENERGY TRANSITIONS AND GEOMETRY

Rokas Garbačauskas, Stepas Toliautas

¹Institute of Chemical Physics, Physics Faculty, Vilnius university, Lithuania
rokas.garbacauskas@ff.stud.vu.lt

Quantum chemistry modelling is a valuable tool for comparing, explaining and predicting various chemical phenomena. On the other hand, the results are very sensitive to chosen initial conditions and used parameter sets. The idea behind our research is to ride the wave of recent developments in data science and machine learning to cope with large amounts of synthesized molecular modelling data. The aforementioned techniques can be used to distill various degrees of freedom into compound class specific or general meta parameters that could help navigate the potential energy surfaces to find less local energy minima and/or help the current mainstream algorithms to converge faster. Our goal currently is the statistical analysis of a particular class of chemical compounds, namely boron-dipyrromethene (BODIPY) and its various derivatives, that are known for their usage as fluorescent dyes [1] and markers in biological research [2] or for viscosity measurements [3]. Our current focus of investigation is the creation of suitable tools for statistical analysis of Phenyl-BODIPY molecule and its rotational conformer models, generated with Gaussian software, geometry. The designed tools are still to be applied to a wider range of BODIPY derivatives.

[1] B., Noël and L., Volker and D., Wim, Fluorescent indicators based on BODIPY, *Chem. Soc. Rev.* **2012**, 41, 3, 1130-1172.

[2] O. S. Vodyanova, B. A. Kochergin, et al. BODIPY dyes in bio environment: Spectral characteristics and possibilities for practical application, *Journal of Photochemistry and Photobiology A: Chemistry.* **2018**, 350, 44-51.

[3] S. Toliautas, J. Dodonova, et al., Enhancing the Viscosity-Sensitive Range of a BODIPY Molecular Rotor by Two Orders of Magnitude, *Chem. Eur. J.* **2019**, 25, 10342.

STUDY OF VISCOSITY AND FRICTION OF POLYURETHANE ADHESIVES

Paulina Nemaniūtė¹, Dalia Bražinskienė¹, Tadas Matijošius¹, Svajus Asadauskas¹

¹ Department of Chemical Engineering and Technology, Center for Physical Sciences and Technology
paulina.nemaniute@ftmc.lt

Polyurethane (PUR) adhesives are widely used in various industries for their high performance and versatility. PUR are composed of soft segment (a polyether or polyester polyol) and hard segment (diisocyanate and chain extender). The soft segment provides elasticity, whereas the hard segment increases strength and rigidity through physical cross-linking points [1]. One of the key factors affecting the performance and processing characteristics of PUR adhesives is viscosity during the reaction. Processing parameters like mixing, spreading, and application as well as final properties like gel time, adhesion strength, and tensile strength are all impacted by viscosity during the reaction. The Coefficient of Friction (COF) is also investigated in certain applications such as in automotive and industrial machinery, where the adhesive bond must be able to withstand high loads and maintain its strength [2].

In this study polydiethylene glycoladipate (PDEA of 2700 g/mol) was reacted with trifunctional adduct hexamethylene -1,6- diisocyanate (HDI3) in 1,4 mol excess. In order to reduce initial viscosity of PUR, PDEA was diluted with polyethylene glycol (PEG of 200 g/mol (PEG200) or 400 g/mol (PEG400)). Three mixtures were investigated:

- “PDEA+HDI3” (containing 83,25% wt. and PDEA 16,75% wt. HDI3)
- “PDEA+PEG200+HDI3” (containing 48,46% wt. PDEA, 12,12% wt. and PEG200 39,42% wt. HDI3)
- “PDEA+PEG400+HDI3” (containing 41,42% wt. PDEA, 22,30% wt. PEG400 and 36,28% wt. HDI3)

Viscosity during the reaction of polyurethane formation was measured using Anton Paar MCR302 rheometer at 50°C with concentric cylinder system. The procedures were described previously in detail [3]. Later fully reacted PUR sheet was formed with a thickness of 0,5 mm. The COF of fully reacted PUR was measured using Anton Paar tribometer (Switzerland) in ball on plate linearly reciprocal configuration. As a stationary part, 6 mm diameter corundum ball of 99.8% purity from Ceratec (Belgium) was held constant against the PUR sheet, mounted on a pre-installed tribometer module under 1 N load. Linear reciprocal motion of 2 mm amplitude was maintained resulting in a track length of 4 mm and a total distance of 8 mm for one reciprocal friction cycle. To ensure good reproducibility, each sample was tested two times at given conditions and the most representative runs were selected for the comparison between samples. The results are shown in Fig. 1.

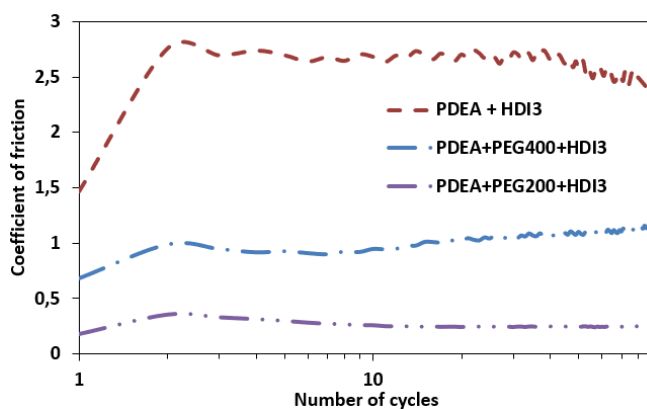


Fig. 1. Influence of different PUR mixtures on friction tendencies. Tribotests against the corundum ball.

Adding lower molecular weight and short chain polymer PEG not only reduced initial viscosity but also affected final mechanical properties of formed polyurethane. In this case, PEG200 or PEG400 reduced COF at least two times of the formed PUR sheet. More experiments are needed to investigate the effects of different PUR mixtures.

Acknowledgements. This study was carried out under project TERMINUS, funded by the European Union under Horizon 2020. Call: H2020-MBP-ST-IND-2018. Grant Agreement: 814400.



[1] J. Datta and P. Kasprzyk, Polym Eng Sci, pg 824-830, 2018, doi:10.1002/pen.24633

[2] Song, H.-J., Zhang, Z.-Z., Men, X.-H., Luo, Z.-Z., Wear, pg 79-85, 2010, doi: 10.1016/j.wear.2010.03.011

[3] P. Nemaniūtė, M. Jurkūnas, D. Bražinskienė, S. J. Asadauskas. Proc. 65th Int. Conf “Open Readings 2022”, Vilnius, Lithuania, 2022, pg. 400. doi:10.5281/zenodo.635969

COVALENT RADII DERIVATION FROM OPEN CRYSTALLOGRAPHIC DATA

Eglė Šidlauskaitė¹, Andrius Merkys², Antanas Vaitkus²

¹ Faculty of Medicine, Vilnius University, Vilnius, Lithuania

² Sector of Crystallography and Chemical Informatics, Institute of Biotechnology, Life Sciences Center, Vilnius University, Lithuania
egle.sidlauskaitė@mf.stud.vu.lt

Crystallography allows to determine the exact positions of atoms that constitute crystal structures, [1] however, it is unable to capture chemical bonding. In practice, two atoms are considered to be connected by a covalent bond if the calculated distance between them does not exceed the sum of their covalent radii. Therefore, covalent radii tables, created by statistically analysing lengths of observed chemical bonds, are often used to determine chemical bonding.

The most popular covalent radii tables [2][3][4] are derived using data from the Cambridge Structural Database [5] which is distributed under a proprietary license and restricts the usage and spread of such derivative datasets. Thus there is a clear need to develop a completely independent workflow that allows covalent radii tables to be automatically calculated using open crystallographic datasets. In this research, methodology based on the determination of the van der Waals gap is used to determine covalent radii in structures deposited to the Crystallography Open Database [6].

The van der Waals gap is an interval within the interatomic distance distribution that corresponds to the lowest density region [7] and separates peaks formed by covalent interactions from those formed mainly by van der Waals interactions. In order to identify the lowest density region, a Gaussian distribution mixture model is applied to the histogram of interatomic distances. Covalent radii are derived using the weighted least squares method.

The methodology used in this research is sensitive to structures with abnormal interatomic distance observations. To address this, suitable crystallographic structures were identified based on a set of quality criteria such as compatibility between the declared and calculated properties, use of standard experimental environment conditions, reasonable crystal structure density, etc. Currently applied filters determine about 70% of data structures published in the COD to be suitable for covalent radii derivation calculations. Further development and refinement of these criteria is part of an ongoing investigation.

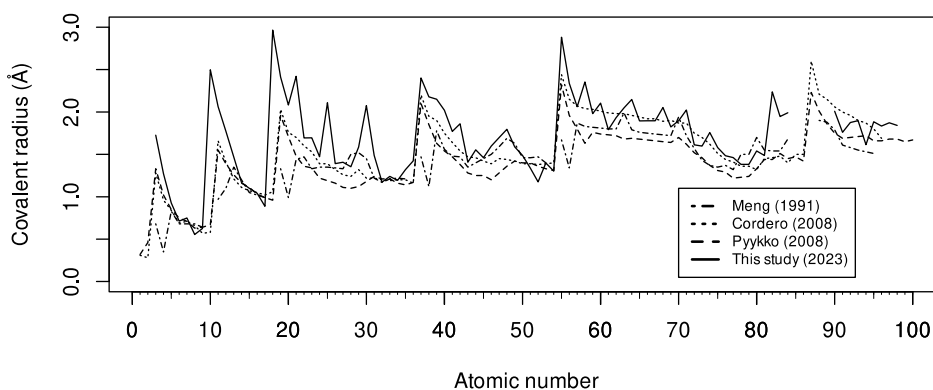


Fig. 1. Comparison of covalent radii in selected covalent radii tables.

The comparison of derived results with selected published covalent radii tables is displayed in Figure 1. Review of the derived results, comparison between radii in published tables and visualisation of covalent bond length determination for pair of chemical elements are available online [8]. Furthermore, a tool for structure validation using derived covalent radii is accessible online [9].

[1] S. Gražulis et al., Computing stoichiometric molecular composition from crystal structures, *J Appl Crystallogr* 48(1), 85-91 (2015).

[2] E. C. Meng, R. A. Lewis, Determination of molecular topology and atomic hybridization states from heavy atom coordinates, *J Comput Chem* 12(7), 891-898 (1991).

[3] B. Cordero et al., Covalent radii revisited, *Dalton Trans* (21), 2832-2838 (2008).

[4] P. Pyykkö, M. Atsumi, Molecular Single-Bond Covalent Radii for Elements 1–118, *Chemistry*, 15(1), 186-197 (2008).

[5] C. R. Groom, I. J. Bruno, M. P. Lightfoot et al., The Cambridge Structural Database, *Acta Crystallogr B Struct Sci Cryst Eng Mater* 72(2), 171-179 (2016).

[6] S. Gražulis et al., Crystallography Open Database (COD): an open-access collection of crystal structures and platform for world-wide collaboration, *Nucleic Acids Res* 40, D420-D427 (2012).

[7] S. Alvarez, A cartography of the van der Waals territories, *Dalton Trans* 42(24), 8617-8636 (2013).

[8] E. Šidlauskaitė (2023). Covalent radii table. [online] Available at: http://databases.crystallography.lt:8080/contacts/website/cgi-bin/cov_radii_table.pl [Accessed 1 Feb. 2023].

[9] A. Merkys (2023). Inter-atom contact checker. [online] Available at: http://databases.crystallography.lt:8080/contacts/website/cgi-bin/check_contacts.pl [Accessed 1 Feb. 2023].

PHASE TRANSITION STUDIES OF CALCIUM-SUBSTITUTED $\text{La}_2\text{Mo}_2\text{O}_9$ CERAMIC PREPARED BY AN AQUEOUS SOL-GEL METHOD

Giedrė Gaidamavičienė, Artūras Žalga

Faculty of Chemistry and Geosciences, Institute of Chemistry, Vilnius University, Naugarduko str. 24, LT-03225 Vilnius, Lithuania
giedre.prievelyte@chf.vu.lt

In recent years, solid oxide fuel cells (SOFCs) have played an important role in green energy generation. This technology features low maintenance, high impurity tolerance, wide fuel flexibility, and low pollutant emission, which has proven to be the most efficient and environmentally friendly. An electrolyte is considered as a core component in SOFCs because it determines the fuel cell's operating temperature. Also, there are some requirements that SOFC electrolytes should meet: chemical and physical stability under oxidizing and reducing atmospheres and compatibility with other cell components, high oxygen-ion conductivity and negligible electronic conductivity, similar thermal expansion to avoid cracking during the cell operation, dense ceramic to prevent gas mixing and other [1, 2]. These days, many electrolytes are known such as perovskites (e.g., doped LaGaO_3), fluorite structured oxides (e.g., CeO_2), and yttria-stabilized zirconia (YSZ), which is commonly used in SOFCs as an electrolyte material. However, YSZ operates at a high temperature (1000 °C), which shortens the lifetime of the fuel cell [3].

LAMOX-type conductors have tremendous potential to become solid electrolytes in SOFC and can operate in intermediate temperatures. At room temperature, lanthanum molybdate exists in low-symmetry monoclinic α -phase, which, above 580 °C of temperature, turns into cubic β -phase and this transition effect increases an oxygen-ion conductivity almost by two orders of magnitude. To stabilize cubic β -phase, lanthanum, and molybdenum sites could be substituted by different cations such as K^+ , Ba^{2+} , Bi^{3+} , V^{5+} , S^{6+} , W^{6+} . Lanthanum substitution by alkaline earth metals not only could reduce a phase transition, but also could increase oxygen vacancies that lead to higher anionic conductivity of the corresponding ceramic mixture [4, 5].

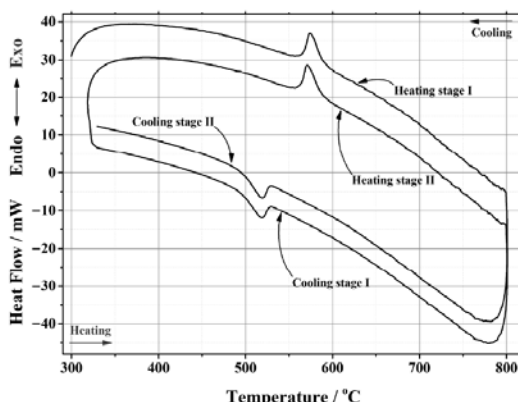


Fig. 1. DSC curve of the phase transition cycles for $\text{La}_{1.95}\text{Ca}_{0.05}\text{Mo}_2\text{O}_{8.975}$ ceramic heat-treated at 1000 °C [6].

In this work, the $\text{La}_{2-x}\text{Ca}_x\text{Mo}_2\text{O}_{9-\delta}$ ($x=0.001-0.3$) ceramic was prepared by an aqueous sol-gel synthesis method using tartaric acid as a complexing agent. The phase transition dependency from the substitution degree by calcium in $\text{La}_{2-x}\text{Ca}_x\text{Mo}_2\text{O}_{9-\delta}$ ceramic was investigated by differential scanning calorimetry (DSC). The obtained results showed that the substitution effect reduces the phase transition from cubic β -phase to monoclinic α -phase and vice versa. Furthermore, the influence of sample annealing temperature and sample preparation method on the phase transition are discussed. X-ray diffraction (XRD) analysis was performed to determine the crystal structure and impurity phases of the heat-treated ceramic materials. It was found that homogenous substitution of lanthanum by calcium ions takes place up to $x=0.05$. Moreover, to analyze the density and surface morphology of the synthesized ceramics heat-treated at 1200 °C, scanning electron microscopy (SEM) analysis was performed.

- [1] A. Boudghene Stambouli, E. Traversa, Solid oxide fuel cells (SOFCs): a review of an environmentally clean and efficient source of energy, *Renewable and Sustainable Energy Reviews* **6**, 433-455 (2002).
- [2] S. P. S. Badwal, K. Foger, Solid oxide electrolyte fuel cell review, *Ceramics International* **22**, 257-265 (1996).
- [3] A. Das, Lakhanlal, I. Shajahan, et al., Dilatometer studies on LAMOX based electrolyte materials for solid oxide fuel cells, *Materials Chemistry and Physics* **258**, 123958 (2021).
- [4] C. Tealdi, G. Chiodelli, et al., Effect of alkaline-doping on the properties of $\text{La}_2\text{Mo}_2\text{O}_9$ fast oxygen ion conductor, *Journal of Materials Chemistry*, **14**, 3553-3557 (2004).
- [5] D. Zhang, Z. Zhuang, et al., Electrical properties and microstructure of nanocrystalline $\text{La}_{2-x}\text{A}_x\text{Mo}_2\text{O}_{9-\delta}$ ($\text{A} = \text{Ca}, \text{Sr}, \text{Ba}, \text{K}$) films, **181**, 1510-1515 (2010).
- [6] A. Žalga, G. Gaidamavičienė, Thermoanalytical and X-ray Diffraction Studies on the Phase Transition of the Calcium-Substituted $\text{La}_2\text{Mo}_2\text{O}_9$ System, *Materials* **16**(2), 813 (2023).

ESTIMATION OF CARBONACEOUS AEROSOL PARTICLE SOURCES AT TWO LOCATIONS IN METRO MANILA, PHILIPPINES

Touqeer Gill¹, Simonas Kecorius^{1,2}, Kamilė Kandrotaitė¹, Vadimas Dudoitis¹, Leizel Madueno³, Alfred Wiedensohler³, Steigvilė Byčenkienė¹ and Kristina Plauškaitė¹

¹ Center for Physical Sciences and Technology (FTMC), Vilnius, Lithuania

² Helmholtz Zentrum München – German Research Center for Environmental Health, Neuherberg, Germany

³ Leibniz-Institute for Tropospheric Research (TROPOS), Leipzig, Germany

touqeer.gill@ftmc.lt

According to the report of World Health Organization (WHO, 2021), 99% of the global population breathes air that exceeds WHO guideline limits and contains high levels of pollutants [1]. In urban environment, carbonaceous aerosol particles are the major component of fine particulate matter (PM_{2.5}) [2]. Formed during the combustion process (e.g. biomass burning, emissions of internal combustion engines), Black Carbon (BC) particles are known to be especially harmful to human health. A better understanding about the sources of BC particles, its magnitude, and source specific concentrations, especially in economically developing countries is mandatory for the improvement of air quality and well-being. Raising the awareness about the prevailing environmental crisis is one of the first steps towards sustainable development.



Fig. 1. Map of Metro Manila with the approximate locations of the measurement sites.

To raise the awareness about poor air quality due to unsustainable development, intensive field campaign focusing on BC, was conducted in Metro Manila, Philippines (as a part of project “A Transdisciplinary Approach to Mitigate Emissions of Black Carbon” (TAME-BC)). Equivalent black carbon (eBC) mass concentration was measured using 7-wavelength Aethalometer (AE-31) during a period of 3 months (December 2019 to February 2020) in urban environments of Metro Manila: Quezon City’s East Avenue roadside (QCG site) and Manila’s North Port (Port site) (Fig. 1). To investigate the magnitude of air pollution in Metro Manila, the focus was set on the sources of eBC, as well as mass concentration variation. Wavelength dependent absorption coefficient analysis revealed that at Port site transport (eBC_{TR}) and biomass burning (eBC_{BB}) related eBC contribute approximately 82% and 18% to the total eBC mass, respectively. In the case of Quezon City, this contribution is 76% and 24%, respectively (Fig. 2a, 2b). The diurnal trend of eBC_{TR} at both sites (QCG and Port site) indicated a higher mass concentration during the morning hours (6-8 h) and a lower mass concentration during the midday (11-13 h). Both sites (QCG and Port) showed a similar trend for eBC_{BB} mass concentration, which reached a maximum between 6-8 hours and minimum between 11-13 hours.

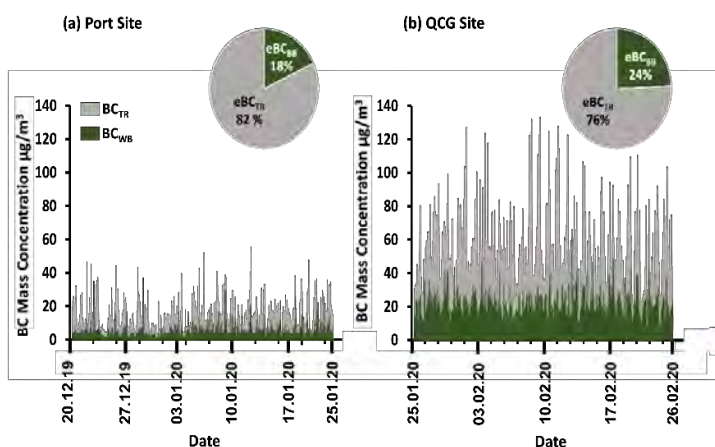


Fig. 2. Time series and contributions of eBC_{TR} and eBC_{BB} to the total eBC at port site (a) and QCG site (b).

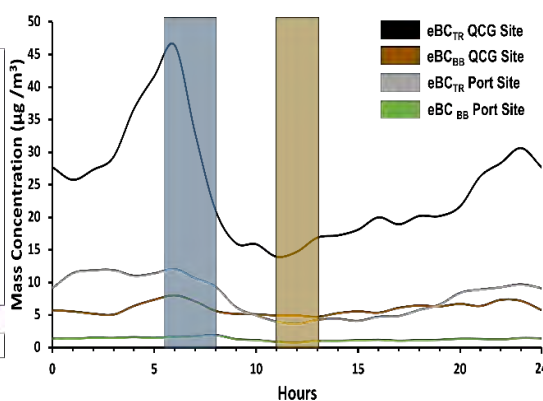


Fig. 3. eBC_{TR} and eBC_{BB} diurnal trend at Manila Port site and QCG site.

[1] WHO Global Air Quality Guidelines. *Coast. Estuar. Process.* 2021, 1–360

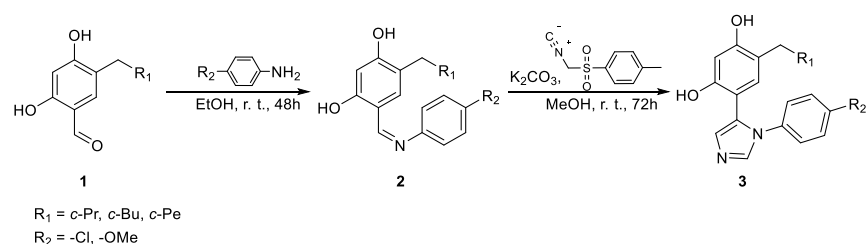
[2] Oh, H.J.; Ma, Y.; Kim, J. Human Inhalation Exposure to Aerosol and Health Effect: Aerosol Monitoring and Modelling Regional Deposited Doses. *Int. J. Environ. Res. Public Health*, 17, 1–2, (2020).

SYNTHESIS OF POTENTIAL HSP90 INHIBITORS 4-(CYCLOALKYL)-6-(1-(4-SUBSTITUTED)-1H-IMIDAZOL-5-YL OR -1,2,3-THIADIAZOL)BENZENE-1,3-DIOLS

Kamilė Venskūnaitė, Algirdas Brukštus

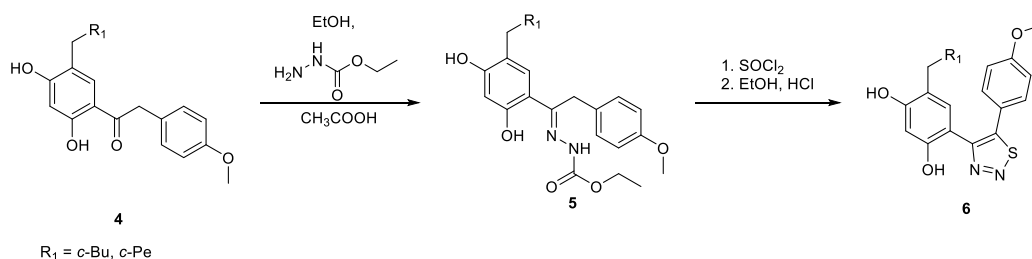
Department of Chemistry and Geosciences, Vilnius University, Lithuania
kamile.venskunaite@chgf.stud.vu.lt

Heat shock protein Hsp90 is a molecular chaperone which is found in all living organisms, except archaea. Hsp90 stabilizes and folds proteins that are under stress conditions therefore, controls cell survival [1]. Molecular chaperone has hundreds protein substrates and is involved in a lot of cellular processes besides protein folding. For example, DNA repair, immune system response and treatment of neurodegenerative diseases, cancer [2]. Furthermore, there are ongoing researches on parasitic diseases treatment using Hsp90 [3]. Therefore, the main aim of this scientific work is to synthesize new compounds which could be potential Hsp90 inhibitors.



Scheme 1. Synthesis of 4-(cycloalkyl)-6-(1-(4-substituted)-1H-imidazol-5-yl)benzene-1,3-diols (3).

The reaction between aldehyde 1 and 4-substituted aniline yielded imines 2. After, cyclization reaction was done using toluenesulfonylmethyl isocyanide (TosMIC) and previously synthesized imines 2 resulted in formation of final products 3.



Scheme 2. Synthesis of 4-(cycloalkyl)-6-(5-(4-methoxyphenyl)-1,2,3-thiadiazol-4-yl)benzene-1,3-diols (6).

Compound 5 was obtained after compound 4 was submitted into reaction in ethanol with ethyl hydrazinecarboxylate. The cyclization was done by using thionyl chloride and yielded final products 6. The synthesized compounds are currently in biological research.

[1] Somogyvari, M.; Khatatneh, S.; Soti, C. Hsp90: From Cellular to Organismal Proteostasis. *Proteostasis. Cells* **2022**, *11*, 2479.

[2] Schopf, F. H.; Biebl, M. M.; Buchner, J. The HSP90 chaperone machinery. *Nat Rev Mol Cell Biol* **2017**, *18*(6), 345–360.

[3] Faya, N.; Penkler, D. L.; Bishop, Ö. T. Human, vector and parasite Hsp90 proteins: A comparative bioinformatics analysis. *FEBS Open Bio* **2015**, *5*, 916-927.

CONTROLLED CARBON COATING OF ANODE MATERIALS THROUGH IN-SITU POLYMERIZATION

Nadežda Traškina¹, Jurgis Pilipavičius¹, Jurga Juodkazytė¹, Linas Vilčiauskas¹

¹ Center for Physical Sciences and Technology (FTMC), Department of Chemical Engineering and Technology, Saulėtekio al. 3, LT-10257 Vilnius, Lithuania
nadezda.traskina@ftmc.lt

In the last decades, environmental awareness has induced the interest towards the development of novel renewable and clean energy storage devices. The market is currently dominated by lithium ion batteries, which, despite their obvious advantages, suffer from precursor's high cost and lack of environmental benignity. [1] As a result, sodium ion batteries, especially their aqueous modifications, have been pathing their way as an alternative to LIBs owing to sodium's high abundance in nature and elimination of highly toxic and flammable organic electrolytes. [2] NASICON-structured $\text{NaTi}_2(\text{PO}_4)_3$ (NTP) is the most promising and studied aqueous Na-ion battery anode material owing to its high theoretical capacity, good thermal stability and environmental compatibility. Despite possessing a great ionic mobility, NTP suffers from inherently low electron conductivity. Moreover, active material dissolution and degradation into aqueous electrolyte results in inferior cycle life stability [4]. Conventional particle carbon coating by pyrolyzing glucose or citric acid does not ensure an even and controllable active material encapsulation. Growing a polymer e.g. polydopamine shell on the surface of active material is a promising route to obtain a controllable surface carbon layer, which is both protective and conductive [5].

The aim of this work was to investigate the dependency of electrode electrochemical performance on the precursor of carbon layer. The anode materials were prepared by varying the amount of citric acid and dopamine hydrochloride in the carbon-coating stage. The electrochemical properties of NTP electrodes were investigated by charge/discharge galvanostatic cycling and cycling voltammetry. The structural characterization was carried out via thermogravimetric analysis and Brunauer-Emmett-Teller (BET) surface area analysis.

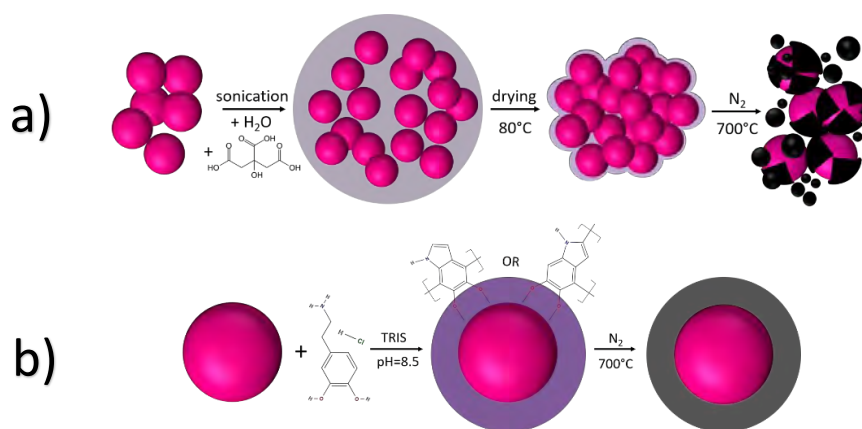


Fig. 1. Preparation of carbon-coated NTP particles with a)CA and b)PDA as carbon source scheme

Acknowledgements:

This project has received funding from the European Regional Development Fund (Project No. 01.2.2-LMT-K-718-02-0005) under grant agreement with the Research Council of Lithuania (LMTLT).

[1] Wu, M., et al., NASICON-Structured $\text{NaTi}_2(\text{PO}_4)_3$ for Sustainable Energy Storage. *Nano-Micro Letters* **11**, 44 (2019).

[2] Bin, D., et al., Progress in Aqueous Rechargeable Sodium-Ion Batteries. *Advanced Energy Materials*, **8**, 1703008 (2018).

[3] Plečkaitytė et al. Understanding and mitigation of $\text{NaTi}_2(\text{PO}_4)_3$ degradation in aqueous Na-ion batteries. *Journal of Materials Chemistry A* **9** p. 12670-12683

[4] Chi et al. Optimizing the carbon coating on LiFePO_4 for improved battery performance. *RSC Advances* **4** p. 7795-7798 (2014)

SYNTHESIS AND CHARACTERIZATION OF IRON DOPED CALCIUM PHOSPHATE WITH WHITLOCKITE STRUCTURE

Diana Griesiute^{1, *}, Jonas Stadulis¹, Aleksej Zarkov¹

¹ Institute of Chemistry, Vilnius University, Naugarduko g. 24, LT-03225, Vilnius, Lithuania
[*diana.griesiute@chgf.vu.lt](mailto:diana.griesiute@chgf.vu.lt)

Calcium phosphates (CaP) are the family of materials, which are widely used in regenerative medicine due to their excellent biocompatibility and osteoconductivity [1]. There is a variety of applications of different CaP phases including medical, environmental, optical etc. Human hard tissues mostly consist of calcium hydroxyapatite (HAp) which is the most stable CaP phase around neutral pH [2]. The second most abundant CaP phase in human body is whitlockite. Magnesium whitlockite is a member of CaPs family, where part of calcium ions are substituted by smaller magnesium ions, chemical formula of magnesium whitlockite is $\text{Ca}_{18}\text{Mg}_2(\text{HPO}_4)_2(\text{PO}_4)_{12}$ [3].

Doping of CaPs with other metal ions may result in the appearance of new physical and biological properties, which can be used for wider application. Iron is an essential microelement in bones and teeth, it is a micronutrient essential for various biological processes and an important component of several metalloproteins [4]. It is known that Fe-doped HAp not only demonstrates antibacterial properties, but also exhibits strong ferromagnetic properties, whereas undoped HAp is diamagnetic [5]. Due to these properties, this material can be applicable in medicine, drug delivery or in bone transplantation. The main aim of this work was to synthesize and characterize phase-pure Fe^{2+} -doped CaP with whitlockite structure.

The results of powder X-ray diffraction analysis (XRD), Fourier-transform infrared spectroscopy (FTIR) and Raman spectroscopy confirmed that synthesized Fe-doped CaP has whitlockite structure. It was demonstrated that optimal reaction temperature is 230 °C, at this temperature single-phase whitlockite powder can be obtained. Optimal pH range was determined to be from 6.1 to 6.3. Neighboring crystalline phases were observed at lower temperatures and higher/lower pH of the reaction medium. Also, it was found that optimal reaction time is only about 1 hour. Investigation of magnetic properties showed that synthesized material is paramagnetic in the temperature range from 5 to 300 K. Thermal stability studies revealed that iron whitlockite is thermally unstable and decomposes upon a heat treatment.

Acknowledgements

This research was funded by a grant WHITCERAM (No. S-LJB-22-1) from the research Council of Lithuania.

-
- [1] W. Habraken, P. Habibovic, M. Epple, & M. Bohner, Calcium phosphates in biomedical applications: Materials for the future? *Materials Today*, **19** (2016) 69–87. <https://doi.org/10.1016/j.mattod.2015.10.008>.
 - [2] H. L. Jang, H. K. Lee, K. Jin, H. Y. Ahn, H. E. Lee, & K. T. Nam, Phase transformation from hydroxyapatite to the secondary bone mineral, whitlockite. *Journal of Materials Chemistry B*, **3** (2015) 1342–1349. <https://doi.org/10.1039/c4tb01793e>.
 - [3] H. Cheng, R. Chabok, X. Guan, A. Chawla, Y. Li, A. Khademhosseini, & H. L. Jang, Synergistic interplay between the two major bone minerals, hydroxyapatite and whitlockite nanoparticles, for osteogenic differentiation of mesenchymal stem cells. *Acta Biomaterialia*, **69** (2018) 342–351. <https://doi.org/10.1016/j.actbio.2018.01.016>.
 - [4] S. Gomes, A. Kaur, J. M. Grenèche, J. M. Nedelec, & G. Renaudin, Atomic scale modeling of iron-doped biphasic calcium phosphate bioceramics. *Acta Biomaterialia*, **50** (2017) 78–88. <https://doi.org/10.1016/j.actbio.2016.12.011>.
 - [5] V. Sarath Chandra, G. Baskar, R. V. Suganthi, K. Elayaraja, M. I. Ahymah Joshy, W. Sofi Beaula, R. Mythili, G. Venkatraman, & S. Narayana Kalkura, Blood compatibility of iron-doped nanosize hydroxyapatite and its drug release. *ACS Applied Materials and Interfaces*, **4** (2012) 1200–1210.

NEUTRALIZATION OF THE SIMULANTS OF VESICANT/BLISTER CHEMICAL AGENTS IN THE PRESENCE OF MONTMORILLONITE

Drizhd Varvara¹, Vakhitov Ramil²

¹ Department of Nucleophilic Reactions Research, L. M. Litvinenko Institute of Physical-Organic and Coal Chemistry of the National Academy of Sciences of Ukraine, Ukraine

² Department of Chemical Technology and Resource Saving, Kyiv National University of Technology and Design, Ukraine

varvara.drizhd@gmail.com

Studies of the oxidation of methyl phenyl sulfide (MFS) by hydrogen peroxide (H₂O₂) and urea peroxysolvate (CO(NH₂)₂·H₂O₂), catalyzed by organomodified montmorillonite (Claytone HY – montmorillonite modified with a tall alkonium cation) were performed. The kinetics of MFS oxidation were studied in the following decontamination environments: 1 – water; 2 – iso-propyl alcohol (i-PrOH)/water mixture; 3 – ethanol (EtOH); 4 – micellar solution of cetyltrimethylammonium bromide (CTABr); "oil-in-water" type microemulsion, containing either cationic CTABr (5), neutral Triton X-100 (6), or SDS – anionic sodium dodecyl sulfate (7) as a detergent. Claytone HY nanoclay was introduced into the decontamination systems in the amount of 1%. The choice of specific components and composition of reaction media is not random and was based on the results of previous research [1,2].

The selectivity of oxidation under the conditions used in measuring the speed of the processes ([MFS]₀=2,0·10⁻³, [H₂O₂]₀=[CO(NH₂)₂·H₂O₂]₀ = 0,1–1,0 M⁻¹) was confirmed using gas chromatography. It was established that oxidation mainly results in the formation of methylphenylsulfoxide:



Further oxidation of sulfoxide to toxic sulfone does not occur within at least 24 hours from the starting point of MFS oxidation. It should be emphasized that uncatalyzed processes of oxidation by hydrogen peroxide are characterized by extremely low reaction rates and are not of practical interest. The present study is aimed at demonstrating the catalytic effect of layered silicate in reaction (1). Table below contains the values of the rate constants (k₂, M⁻¹·s⁻¹) for second-order reactions of MFS consumption in reaction medias 1–7, in the presence and absence of Claytone HY nanoclay. Numerical values of the catalytic effect (CE), which is calculated as the ratio of the corresponding k₂ values for catalytic and non-catalytic oxidation, are also provided in the Table.

Table. MFS oxidation rate constants

Decontamination system	k ₂ , M ⁻¹ ·s ⁻¹ ·10 ⁴					
	H ₂ O ₂			CO(NH ₂) ₂ ·H ₂ O ₂		
	–	Claytone HY	CE	–	Claytone HY	CE
1	15,1	34,5	2,3	20,6	38,4	1,9
2	6,12	21,3	3,5	8,04	22,4	2,8
3	2,45	12,4	5,1	3,43	18,9	5,5
4	0,42	1,89	4,5	0,89	3,23	3,6
5	1,01	3,21	3,2	2,12	8,32	3,9
6	2,3	8,94	3,9	3,67	15,3	4,2

Kinetic data allow us to state that a slight acceleration of the oxidation rate occurs when a solid source of hydrogen peroxide – CO(NH₂)₂·H₂O₂ urea complex, is used. An increase in the rate of MFS decomposition is also observed in systems containing nanoclay. The scope of the experiment does not make it possible to establish the exact reason for this acceleration of the reaction in the presence of montmorillonite clay. The main hypothesis is based on the assumption that the catalytic effect of clays is largely due to molecular interactions of active centers of montmorillonite (Brønsted-Lewis centers) leading to the formation of H-bonds and stabilization of transition states of intermediates (characteristical for the S_N2 mechanism). Claytone HY montmorillonite clay with its large surface area is also likely to act as a strong acid due to its interlayer cations and surface protons. Either acid-base interaction, or the formation of hydrogen bonds between the silicon atom in clay and hydrogen peroxide molecules, shall increase the electrophilicity and reactivity of the intermediate hydroperoxide compound compared to inactivated H₂O₂. These hypotheses require further study and development. The established effect of accelerating the process of decomposition of organophosphorus substrates in a micellar medium by montmorillonite derivatives can be used in designing the fast-acting eco-friendly chemical warfare agents' neutralization systems.

[1] L. Vakhitova, V. Bessarabov et al., Decontamination of methylparathion in activated nucleophilic systems based on carbamide peroxysolvate, Eastern-European Journal of Enterprise technologies, **90**, 31–37 (2017).

[2] L.N. Vakhitova, N.V. Lahtarenko et al., Kinetics of the Oxidation of Methyl Phenyl Sulfide by Peroxoborate Anions, Theoretical and Experimental Chemistry, **51**, 297-302 (2015).

DESIGN AND SYNTHESIS OF STRUCTURALLY SIMPLE SUPRAMOLECULAR CAPSULE

Domantas Valčekas¹, Edvinas Orentas¹

¹ Department of Organic Chemistry, Vilnius University, Naugarduko 24, LT-03225, Vilnius, Lithuania
domantas.valceckas@chgf.stud.vu.lt

The molecular recognition utilizing well-defined tubular molecular constructs lies at the heart of supramolecular chemistry. The molecular capsules, typically assembled using coordination or hydrogen bonds (H-bonds), are extremely well suited to interrogate the complexation phenomena and gain fundamental insights into the nature of non-covalent interactions [1]. In order to unambiguously drive the formation of the capsular aggregates, large degree of preorganization of the recognition elements is required. In most approaches, the latter is ensured by the cost of chemical synthesis by which, geometrically fixed molecular scaffold is constructed. In this way, the formation of the desired aggregate is facilitated by reducing the entropic penalty. On the other hand, the formation of molecular capsules from highly flexible building blocks, possessing large degree of conformational freedom is rarely used despite their much simpler synthesis. In our report, we present a new approach toward molecular capsules using simple tripoidal monomer, containing three ureidopyrimidinone (UPy) 4H-bonding units connected to a central trimesic acid core (Fig. 1). We have shown that such monomer quantitatively forms dimeric molecular capsules via H-bonding. Moreover, the stabilization of the capsule is ensured by the secondary H-bonding of the amide bonds with UPy carbonyl group. The presented monomer represents one of the simplest capsule-forming building blocks reported in literature to date.

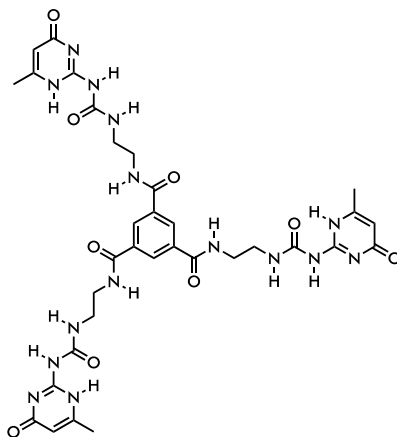


Fig. 1. Chemical structure of the supramolecular monomer.

[1] A. Morgan Conn and J. Rebek, Self-assembling Capsules. *Chem. Rev.*, **97**, 1647-1668 (1997).

SYNTHESIS AND PROPERTIES OF TRIPHENYLETHYLENE DERIVATIVES AS HOLES TRANSPORTING MATERIALS

Julius Petrulevičius¹, Marytė Daškevičienė¹, Egidijus Kamaraukas², Kristijonas Genevičius², Vy gintas Jankauskas², Vytautas Getautis¹

¹ Department of Organic Chemistry, Kaunas University of Technology, Lithuania

² Institute of Chemical Physics, Vilnius University, Lithuania

julius.petrulevicius@ktu.lt

As a result of increasing global warming, renewable energy sources are gaining more interest as an alternative to fossil fuels. One of these alternatives is that the Sun is an infinite resource of energy. Solar cells (SC), also known as photovoltaic devices, are used for the conversion of solar energy into electricity. Nowadays, silicon solar cells (first-generation photovoltaic technology) still dominate the photovoltaic market due to high efficiency and high device stability, despite having disadvantages such as high cost, inflexibility, and opacity, which limit their future development prospects. Fortunately, perovskite solar cells (PSCs) have undoubtedly become the super star in the photovoltaic field, and now the certified power conversion efficiency (PCE) has reached a very high level of 25.7%, which is comparable to that of crystalline silicon solar cells [1].

Holes transporting material (HTM) is one of the main factors of a perovskite solar cell, which determines the cost, energy conversion effectiveness and continuity of the device. However, most HTMs have many disadvantages, including complicated and expensive synthesis, the tendency of self-aggregation, which degrades the quality of the hole transport layer and reduces device stability and efficiency. Therefore, considerable and continuous efforts are made to develop more ideal HTMs, which should exhibit the following advantages: matching well with the valence band and conduction band of the perovskite to enable hole extraction and electron blocking, minimal absorption in the visible and NIR regions of the solar spectrum, sufficient hole mobility, excellent thermal and photochemical stability, high processability, and low cost.

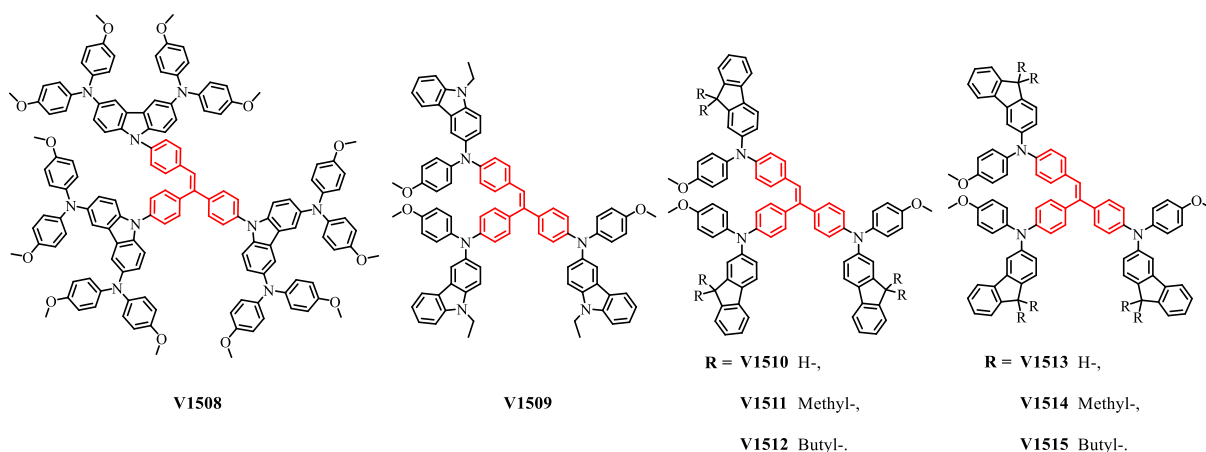


Fig. 1. The structures of triphenylethylene-based HTMs.

In this work, eight asymmetric 3D HTMs (labeled **V1508-V1515**) comprising a triphenylethylene core and various side arms were smoothly synthesized. All HTMs were obtained from facile preparation procedures and simple purification techniques. The structures of the synthesized new compounds **V1508-V1515** were confirmed by ¹H and ¹³C NMR, IR spectroscopy, mass spectrometry and elemental analysis data. These compounds are amorphous, which is an advantage for the formation of homogenous films, as well as eliminate the possibility for films to crystallize during operation of the devices. The solid-state ionization potentials (I_p) of HTMs were determined using electron photoemission spectroscopy in air (PESA) of the thin films to assess the HOMO energy levels [2]. I_p values of novel HTMs were found to be lower than 5.7 eV (4.99 – 5.34 eV), which equals to the valence band (VB) energy of the triple cation-based perovskite, therefore efficient hole transfer from perovskite to the cathode should be ensured. Additionally, xerographic time of flight (XTOF) measurements [3] were used to determine the charge mobility of the V-series layers. As a result, the hole mobility of **V1508-V1515** was found to be $2.1 \cdot 10^{-6} - 4.6 \cdot 10^{-5} \text{ cm}^2/\text{Vs}$ at the zero-electric field, which is comparable to that of the reference standard spiro-OMeTAD ($4.1 \cdot 10^{-5} \text{ cm}^2/\text{Vs}$) under identical conditions.

[1] National Renewable Energy Laboratory: best research-cell efficiencies chart. Available at <https://www.nrel.gov/pv/cell-efficiency.html>

[2] E. Miyamoto, Y. Yamaguchi, M. Masaaki, Ionization potential of organic pigment film by atmospheric photoelectron emission analysis. *Electrophotography*, **28**, 364-370, (1989).

[3] E. Montrimas, V. Gaidelis, A. Pazera, The discharge kinetics of negatively charged Se electrophotographic layers. *Lith. J. Phys.* **6**, 569-578, (1966).

THE PSEUDO-POLY (AMINO ACIDS) AS COMPONENTS OF PERFUMERY-COSMETIC TOOLS

Daria Botsula¹, Roman Taras², Natalia Bukartyk², Valeriia Shabikova²

¹ Department of Computer Chemical Engineering, Lviv Polytechnic National University, Ukraine

² Department of Organic Chemistry, Lviv Polytechnic National University, Ukraine

daria.botsula.mnkhtm.2021@lpnu.ua

Highly concentrated, time-stable emulsions of vegetable fats and essential oils constitute a significant interest for the pharmaceutical, perfume and food industries. There are severe requirements for the stabilizers of these emulsions as far as it may contact human epithelium more or less. The use of synthetic ionic and combined stabilizers encounters certain concerns, due to their toxicity and capacity for accumulation in the body.

Therefore, developing of a similar emulsion based on pseudopolyaminoacids -amphiphilic polymers from the natural origin is of great interest. They constitute non-ionic surface-active compounds with a non-toxic tendency and inability to be deposited in interior or exterior organs due to their biodegradability. We used N-derivative of dicarboxylic α -amino acids, polyols and glycerine of different nature for their preparation. The preparation was carried out by using a Steglich reaction with N,N'-dicyclohexylcarbodiimide activator (DCC) in the catalyst of dimethylaminopyridine (DMAP). Branched pseudopolyamino acids as well as dispersed media on this basis have been synthesized from natural dicarboxylic amino acids and polyoxyalkylenediols, using glycerol as a trifunctional hydroxyl-containing comonomer that ensures the shaping a desired structure.

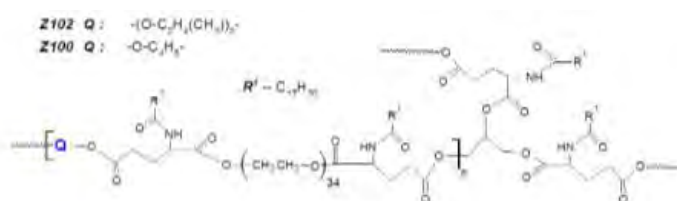


Fig. 1. The structure of the branched polyester.

Above-mentioned stabilisers lead to formation a stable emulsions with 80% concentration of lavender oil. The size of the dispersed phase in the obtained emulsions was 3 μ m. Figure 2 represents the procedure of exact lavender oil emulsion creation via applying described natural amphiphilic polymers as stabilisers.

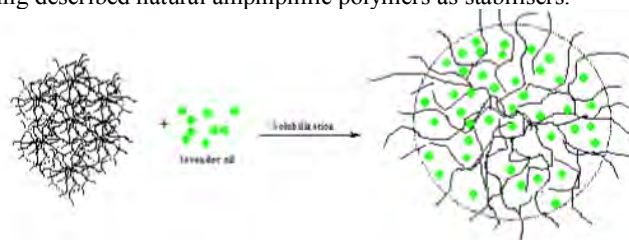


Fig. 2. Stabilization process of lavender oil.

According to this scheme, the emulsion is generated due to solubilization or swelling of pseudopolyamino acid particles with a branched structure. The hydrophilic fragments (polyoxyethylene chains) are oriented at the interface due to which the oil in water is stabilized by the mechanism of a structural-mechanical barrier. The solubilizers (Fig. 3.b) remained stable during the study period (6 months). According to the thermogravimetric analysis, the solubilization of essential oil in the particles of the synthesized copolyester decelerates their evaporation compared to pure essential oils.

As all the above points have demonstrated, new pseudo-polyamino acids of a branched structure simultaneously act as stabilizers, solubilizers and aroma fixatives that allows to use it for developing high-quality water-based perfume compositions in cosmetics and perfumery.



Fig. 3. a – Micrograph of lavender oil solubilized with a pseudopolyamino acid dispersion, b – photo of samples of the polymer-stabilized m/w emulsion.

CASCADE CYCLISATION OF PYRAZOLE-4-CARBALDEHYDES AND PHENYLENDIAMINES: ACCESS TO NOVEL PYRAZOLOOXAZEPANES

Agnė Užupytė^{1*}, Gabrielė Antulytė², Eglė Arbačiauskienė³, Algirdas Šačkus⁴

¹Kaunas University of Technology, Kaunas, Lithuania,

* agne.uzupyte@ktu.edu

Cascade reactions are described as multiple organic transformations happening one after the other without changing the reaction conditions in a single flask. [1] These reactions fall into the category of 'green' or sustainable chemistry as they are known for their atom economy, as well as show economies of time, labor, resource management and waste generation [2,3]. The successful application of cascade reactions has led to the efficient synthesis of various complex natural products and organic scaffolds [4].

Fused pyrazole-based heterocyclic compounds are integrated into everyday life, including pharmaceuticals [5], agrochemicals [6], various functional materials [7]. These compounds exhibit wide spectrum of biological properties, including antioxidant, antimicrobial, and antiproliferative activities [8].

In this work, we present a cascade synthesis approach to obtain novel benzo[4,5]imidazo[1,2-*d*]pyrazolo[4,3-*f*][1,4]oxazepines starting from easily accessible pyrazole-4-carbaldehydes and phenyldiamines. A one-pot two-step process was found to be highly atom economical, simply and enabled the generation of novel polycyclic system in good yield.

The structures of novel fused heterocyclic compounds were confirmed by ¹H, ¹³C, and ¹⁵N-NMR spectroscopy.

[1] T. J. J. Müller *Angew. Chem., Int. Ed.*, **2007**, (46), p. 2977.

[2] B. M. Trost *Angew. Chem.*, **1995**, (107), p. 285.

[3] L. F. Tietze. *Chem. Rev.*, **1996**, (96), p. 115.

[4] Shivam, Geetika Tiwari. *Org. Biomol. Chem.*, **2022**, (20), p. 3653.

[5] R. D. Taylor, M. MacCoss, A. D. G. Lawson. *Journal of Medicinal Chemistry*, **2014** (57), p. 5845.

[6] X.-H. Liu, et al. *Journal of Agricultural and Food Chemistry*, **2020** (68), p. 7324.

[7] M. Mindt, et al. *Microbial Cell Factories*, **2022** (21), p. 45.

[8] K. Karrouchi, et al. *Molecules*, **2018** (23), p. 134.

DESIGN AND SYNTHESIS OF PHOTOCLEAVABLE RESIN FOR PREPARATION OF OBOC DNA-ENCODED CHEMICAL LIBRARIES

Alberta Jankūnaitė¹, Edvinas Orentas¹

¹Department of Organic Chemistry, Faculty of Chemistry and Geosciences, Vilnius University, Lithuania
alberta.jankunaite@chgf.vu.lt

DNA-encoded chemical libraries (DELs) – platform used in medicinal chemistry to synthesize and screen considerable collections of small molecule compounds. Each compound is covalently linked to a DNA fragment that encodes information about the structural peculiarity of each library member. Combinatorial solid-phase synthesis method produces resin-bound libraries in the one-bead-one-compound (OBOC) format, where each bead carries multiple copies of a single compound encoded with a unique DNA sequence [1].

Herein we present synthesis of photocleavable resin which will be used to prepare primary OBOC libraries of the main protease of the coronavirus (SARS-CoV-2 MPro) inhibitors.

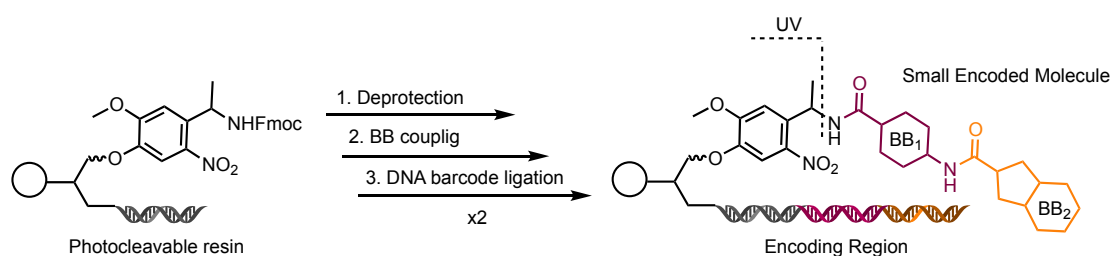


Fig. 1. Schematic representation of photocleavable resin and further proceeding of solid-phase synthesis.

[1] Wesley G. Cochrane, Marie L. Malone, Vuong Q. Dang, Valerie Cavett, Alexander L. Satz, Brian M. Paegel, Activity-Based DNA-Encoded Library Screening, *ACS Comb. Sci.* **2019**, *21*, 5, 425-435.

CONTINUOUS FLOW SYNTHESIS OF SILICON DIOXIDE MICROSPHERES

Lukas Šerpytis¹, Matas Damonskis², Lukas Taujenis^{1,2}, Simas Šakirzanovas¹

¹Institute of Chemistry, Faculty of Chemistry and Geosciences, Vilnius University, Lithuania

²Thermo Fisher Scientific Baltics, UAB Vilnius, Lithuania

lukas.serpytis@chgf.stud.vu.lt

Base catalysed polymerized silica sol-gel can be used to form variety of end products such as film, particles coating, wet gel or polymeric colloidal silica particles [1]. Methods to synthesise mesoporous silica microspheres using organotrialkoxysilanes and tetraalkoxysilanes is well described in multiple literature sources [2,3]. Nevertheless, reproducible synthesis of well-defined particles is a challenging task due to kinetic and thermodynamic factors.

Continuous flow systems could produce narrower particle size distributions compared to batch reactors in the Stöber synthesis of silica particles using the same reactant compositions and experimental conditions. According to literature the use of continuous flow led to lower polydispersity, higher inter-run reproducibility and lower synthesis times, compared to the batch system. These results can be explained on the basis of a better mixing and a higher surface to volume ratio in the tube reactor system, leading to shorter nucleation times and to a higher homogeneity (composition, temperature) in the reaction mixture [4].

This investigation is focused on base catalysed silica microspheres synthesis using continuous flow synthesis method. To achieve the goal reactors multiple designs were investigated to synthesize silicon dioxide microspheres. Silicon dioxide microspheres were synthesized using Stöber process [5]. In this work several designs of reactors were compared against clogging, residence time, flow speed and reactor length. Clogging was analysed visually; particles size distribution was analysed using laser particle sizer and morphology were analysed using scanning electron microscope.

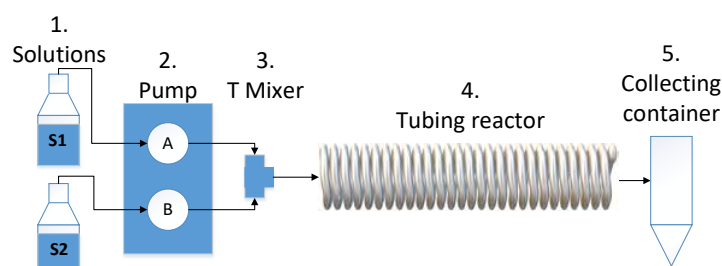


Fig. 1. Simplified tube reactor scheme.

-
- [1] T. W. Zerda, I. Artaki, and J. Jonas, "Study of polymerization processes in acid and base catalyzed silica sol-gels," *J. Non. Cryst. Solids*, vol. 81, no. 3, pp. 365–379, 1986.
- [2] Lee, I., Yoo, Y., Cheng, Z., & Jeong, H. K. (2008). Generation of monodisperse mesoporous silica microspheres with controllable size and surface morphology in a microfluidic device. *Advanced Functional Materials*, 18(24), 4014–4021. <https://doi.org/10.1002/adfm.200801093>
- [3] Ma, Y., Qi, L., Ma, J., Wu, Y., Liu, O., & Cheng, H. (2003). Large-pore mesoporous silica spheres: Synthesis and application in HPLC. *Colloids and Surfaces A: Physicochemical and Engineering Aspects*, 229(1–3), 1–8. <https://doi.org/10.1016/j.colsurfa.2003.08.010>
- [4] Gutierrez, L., Gomez, L., Irusta, S., Arruebo, M., & Santamaria, J. (2011). Comparative study of the synthesis of silica nanoparticles in micromixer-microreactor and batch reactor systems. *Chemical Engineering Journal*, 171(2), 674–683.
- [5] P. P. Ghimire and M. Jaroniec, "Renaissance of Stöber method for synthesis of colloidal particles: New developments and opportunities," *J. Colloid Interface Sci.*, vol. 584, pp. 838–865, 2021.

FORMATION OF MACROPOROUS HYDROGEL MATERIAL FOR MEDICAL PURPOSES BASED ON SODIUM ALGINATE

Valeriia Shabikova¹, Iryna Dron¹, Daria Botsula², Zoriana Nadashkevych¹, Volodymyr Samaryk¹

¹ Department of Organic Chemistry, Lviv Polytechnic National University, Ukraine

² Department of Computer Chemical Engineering, Lviv Polytechnic National University, Ukraine

valeriia.shabikova.mkhtkhd.2021@lpnu.ua

Hydrogel materials are becoming increasingly common in medicine. Current development in this field shows a trend towards creating hydrogel materials based on natural polymers. The advancement is explained by the fact that natural polymers are tolerant to the human body. The newest and latest implementation way of hydrogel foam-based material relies on a producing intra-abdominal dressing by unique conception that promotes hemostasis and prevents the infection of a wound. A significant number of deaths from penetrating wounds of the abdominal cavity are associated with internal bleeding and wound infection. In non-hospital conditions, the situation becomes critical quickly or even ends fatally. Applying macroporous hemostatic remedy features stops internal bleeding, prevents sepsis and preserves the damaged internals for safe transportation of injured body.

The regularities of forming alginate macroporous hydrogel materials for invasive medical purposes based on experimental data have been studied in this work. The macroporous material was formed by a chemical method based on two major processes in parallel, namely the liquid foam formation and liquid foam templating. Foaming occurs due to the interaction between sodium bicarbonate and the carboxyl groups of sodium alginate and polyacrylic acid. The way alginate macromolecules are structured by calcium ions implemented into polyacrylic acid proceeds the gelation of liquid foam simultaneously. It leads to the formation a highly porous hydrogel which must be considered a foam. The composition contains 3% water solution of sodium alginate with added sodium bicarbonate powder and a calcium salt of polyacrylic acid with plasticizers and surfactant. Figure 1 represents the micro photo of the xerogel material obtained under the research.

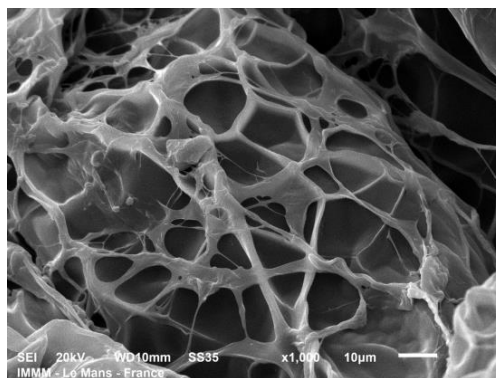


Fig. 1. SEM image of sodium alginate xerogel porous structure.

In particular, the issues of generating macroporous structures due to coordination of the gelation kinetics and the rate of release of the foaming gas were considered. The challenge of optimal surfactant selection for dispersion adjusting of the product was investigated with increased focus. Cocamide Monoethanolamine, commonly known as Cocamide MEA, as a highly prevalent surfactant and foaming agent, triggers a significant surface tension decrease as the graph implies, even with a compound content within (0.5% - 1%).

Additional research has been conducted to determine the release kinetics of selected drug compounds such as antimicrobials and analgesics from the elaborated foam material. The compositions developed during the work are the basis for the formation of abdominal foam dressings with hemostatic and antiseptic properties or xerogel porous surgical dressings.

ESSENTIAL PREPARATIONS FOR THE DELIVERY OF TRACE ELEMENTS BASED ON N-DERIVATIVES OF GLUTAMIC ACID WITH A HYDROPHILIC SUBSTITUENT

Alona Sachuk, Viktoriia Oleksa, Serhii Varvarenko, Roman Matiishyn

Department of Organic Chemistry, Lviv Polytechnic National University, Ukraine
alona.sachuk.mkhtkhd.2022@lpnu.ua

At this stage, essential supplements of trace elements of mineral origin are widely used to correct the diet of both humans and animals. The problem with using such supplements is their low efficiency. It is known that only about 10% of their total amount is absorbed, and the rest passes through the body in transit. As a result, the body either does not create the amount of trace elements necessary for its normal functioning, or it has to be introduced into the diet in amounts significantly higher than necessary. Neither the first nor the second option can be considered optimal. In the first case, the diet is not corrected to the required extent. In the second, there may be problems of body toxicity, especially when correcting the diet of baby food. In addition, it has been observed that poor absorption of essential additives, in the case of intensive livestock farming, leads to their accumulation in manure. The use of such manure as an organic fertilizer leads to an imbalance in the ratio of trace elements in the soil, with the corresponding environmental problems.

The absorption efficiency of new generation essential supplements, in which the trace element ion is in chelated form in combination with an organic ligand, is much higher. But in this case, questions arise about the metabolism of the compounds used as a ligand and their toxicity. At the same time, the search for a non-toxic organic ligand with a high ability to transport a trace element ion into the cell is the most relevant way to create highly effective forms of essential trace element supplements.

This report presents the results of a study of the method for the preparation of glutamic acid derivatives with hydrophilic polyoxyethylene substituents in the N-position and the preparation of complex salts with divalent iron, copper, zinc, and manganese on their basis. The general structural formula of the obtained complex salts of these metals can be shown in the following scheme (Fig 1.):

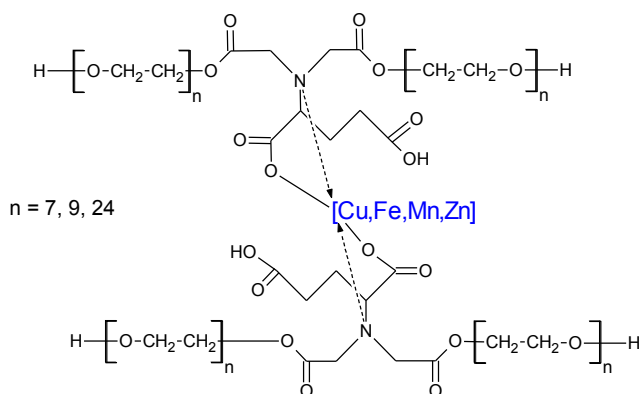


Fig. 1. General structure of the complex salts

A polyoxyethylene derivative of glutamic acid was prepared by N-alkylation of glutamic acid. The paper presents studies on the optimization of the alkylation process and PMR spectroscopy data confirming the structure of the obtained product. In addition, the work describes studies on the preparation of complex salts based on synthesized derivatives of glutamic acid with confirmation of the process of complex formation by the method of electron spectroscopy.

In addition, the results of studies of the cytotoxicity of the synthesized compounds and the efficiency of energy processes in the cell in the presence of the obtained salts are presented. These studies, which were carried out using live bull sperm cells, showed that the amounts less than two orders of magnitude of the amounts of traditional forms of essential additives ensure the normal course of energy processes in the cell. At the same time, no toxic effects of the used complex salts were detected.

STUDY OF THE PROCESS OF OBTAINING CROSS-LINKED POLYACRYLAMIDE MESH REINFORCED WITH MODIFIED POLYPROPYLENE FIBER

Solomiia Kapatsila, Olena Bordeniuk, Alona Sachuk, Nataliia Nosova

Department of Organic Chemistry, Lviv Polytechnic National University, Ukraine
solomiia.kapatsila.mnkhtm.2022@lpnu.ua

The research is devoted to the development of technology for producing hydrogel therapeutic agents with high physical and mechanical properties on the basis of acrylamide copolymers. An increase in the physico-mechanical properties of polyacrylamide hydrogels is achieved by covalent grafting of the gel-forming polymer to the polypropylene surface. Hydrogel structure provides biocompatibility with tissues of living organism, the ability to adsorb and release drugs, atraumatic technique; the reinforcing polymer material provides necessary mechanical strength during the technological operations in the production and application of this hydrogel material. A peculiarity proposed in this work is the covalent attachment of the gel-forming polymer to the polypropylene surface allowing the resulting material to be integrated in a coherent structure and thus obtaining the characteristics of a composite.

In this paper presents the experimental results regarding the comonomers radical copolymerization, which is simultaneously initiated by two peroxide initiators. One of the initiator is localized in the reaction volume, and the second one is covalently grafted to the polymer surface. The following items are discussed in this section: the dynamics of the of acrylamide polymerization process; copolymerization of acrylamide, N,N-methylenebisacrylamide and potassium acrylate; the formation of polymer network points; the effect of process conditions and reaction mixture composition on the time and conversion of gelation. The comparison of the formation rates of the gel-forming polymer macromolecules, which were initiated from the reaction volume and from the surface of the reinforcing material, was of special attention. It is shown that the consistency of mentioned two processes is the basis for hydrogel grafting to the surface.

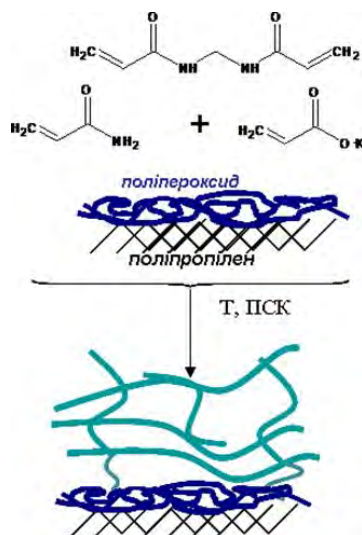


Fig. 1. The general scheme of the formation of a reinforced hydrogel with a gel-forming polymer grafted to the surface of polypropylene nets by the radical mechanism.

A mathematical model for the formation of polymer network of acrylamide, N,N-methylenebisacrylamide and potassium acrylate copolymer was obtained using statistical methods. The model well describes the experimental data and explains the nature of the main factors effect on the time and conversion of gelation, as well as the ratio between sol- and gel-fractions during the whole hydrogel formation process.

Based on the experimental results and predictive data generated by the mathematical model, the basic regularities of the formation of a three-dimensional hydrogel network (formation of polymer molecules, cross-linking) before the system gelation (conversion > 5-7%) and after it till deep stages of copolymerization (conversion > 75-85%) were examined. Dependences of the basic parameters of the hydrogel formation (rate, copolymer composition, average degree of polymerization, density of cross-linking, ratio between sol and gel fractions) on the process conditions were obtained. This allowed to demonstrate that the grafting to the surface is realized after the gel point and the majority of covalent bonds that provide the grafting of the gel-forming polymer to the surface is formed in deep stages (conversion > 75-85%).

BISMUTH SULFIDE STUDY USING X-RAY DIFFRACTION ANALYSIS

Aistis Melnikas¹, Skirma Žalėnė¹

¹ Department of Physical and Inorganic Chemistry of Kaunas University of Technology, Lithuania
aistis.melnikas@ktu.edu

Bismuth sulfide is a non-toxic, *n* type semiconductor popular for its use in photoconductive appliances. It has a band gap energy value of 1.3 eV. Bismuth sulfide is a good light absorber, because its coefficient of absorption is high (about 10^4 – 10^5 cm⁻¹). It has good electrical and optoelectronic properties, which is why it is suitable for use in solar cells, photo optic appliances and many more [1].

In this research, we determine the optimal bismuth sulfide synthesis conditions. Distilled water and analytically pure reagents were used to prepare reaction solutions. The temperature for each one of these reactions was 80 °C:

- 1) 0.1 mol·dm⁻³ Bi(NO₃)₃·5H₂O mixed with 1 mol·dm⁻³ SC(NH₂)₂;
- 2) 0.1 mol·dm⁻³ Bi(NO₃)₃·5H₂O mixed with 1 mol·dm⁻³ SC(NH₂)₂ with an added oxidizing agent (NH₄)₂S₂O₈;
- 3) 0.1 mol·dm⁻³ Bi(NO₃)₃·5H₂O mixed with 1 mol·dm⁻³ SC(NH₂)₂ with added basic buffer solution;
- 4) 0.1 mol·dm⁻³ Bi(NO₃)₃·5H₂O mixed with 1 mol·dm⁻³ SC(NH₂)₂ with an added oxidizing agent (NH₄)₂S₂O₈ and a basic buffer solution.

Black precipitate of bismuth sulfide was present after every reaction and washed with acetone and distilled water.

All samples were analyzed by X-ray diffraction analysis on the Bruker D8 Advance diffractometer. Precipitate was scanned over the range $2\theta = 3$ – 70° at a scanning speed of 1° min⁻¹ using a coupled two theta/theta scan type. This test determined structural characterization of the obtained materials. After an XRD analysis, it was clear that the most precise match with Bi₂S₃ standard structure was obtained from the first reaction with no oxidizing agent and no basic buffer solution, hence the deposition on FTO glass was made using the first solution and its precipitate.

[1] Timothy O. Ajiboye, Damian C. Onwudiwe, Bismuth sulfide based compounds: Properties, synthesis and applications, Results in Chemistry **3**, 100151 (2021).

THE INVESTIGATION OF FLUORINATED SECONDARY BENZENSULFONAMIDES BINDING MECHANISM AND STRUCTURE FOR CARBONIC ANHYDRASES

Aivaras Vaškevičius¹, Denis Baronas¹, Virginija Dudutienė¹, Vaida Paketurytė¹, Visvaldas Kairys², Alexey Smirnov¹, Vaida Juozapaitienė¹, Elena Manakova³, Saulius Gražulis³, Asta Zubrienė¹, Daumantas Matulis¹

¹Department of Biothermodynamics and Drug Design, Institute of Biotechnology, Life Sciences Center, Vilnius University, Lithuania

²Department of Bioinformatics, Institute of Biotechnology, Life Sciences Center, Vilnius University, Lithuania

³Department of Protein-DNA Interactions, Institute of Biotechnology, Life Sciences Center, Vilnius University, Lithuania

aivaras.vaskevicius@gmc.vu.lt

Carbonic anhydrases (CA) are zinc metalloenzymes that catalyzes reversible CO₂ hydration reaction at astonishing rates ($k_{cat} = 1 \cdot 10^5 - 1 \cdot 10^6 \text{ s}^{-1}$) [1]. Although these enzymes are responsible for important processes such as respiratory, pH regulation and bone resorption, some isoforms are associated with various diseases such as glaucoma, epilepsy, obesity, cancer and etc. [2]. One of the treatment of these diseases are selective CA isoform inhibition. To this day the most prominent class of CA inhibitors are primary sulfonamides. These inhibitors are capable of binding to CA up to picomolar affinity [3], yet analogous secondary sulfonamides affinity for CA is dramatically lower [4].

In order to explain this phenomena we synthesized a series of fluorinated sulfonamides together with their secondary/tertiary counterparts as well as determined their affinities for 12 catalytically active human CAs by fluorescent thermal shift assay, isothermal titration calorimetry and stopped-flow assay. In some cases, secondary fluorinated sulfonamides showed dissociation constants (K_d) which were lower more than 10 000 fold compared to their primary analogues [5]. Substituted sulfonamides demonstrated similar U-shaped K_d correlation with pH which indicated that structure-thermodynamics analysis is required. After calculating and comparing primary and secondary sulfonamide *intrinsic* Gibbs energies we hypothesised that large differences in energy values may be related to conformational changes or solvation/desolvation of compounds and enzymes. Thus, few crystal structures of CA II in complex with secondary sulfonamides were solved and compared to crystal structure of CA II in complex with primary sulfonamide (fig. 1). Furthermore, additional computational modeling gave insight into sulfonamides interactions with amino acids at the enzyme active center as well as explained stronger primary sulfonamides binding with CA.

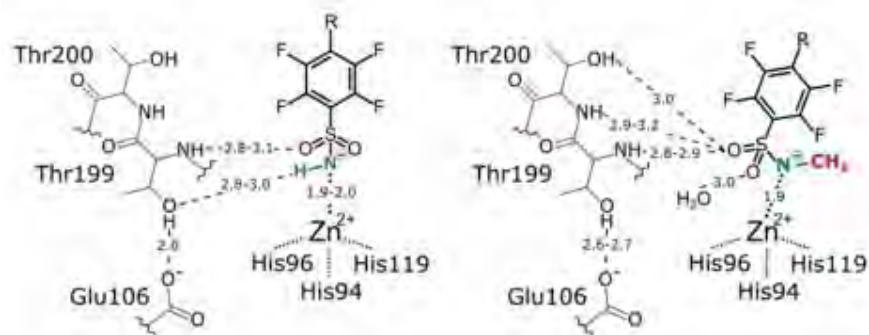


Fig. 1. Primary and secondary fluorinated benzensulfonamide interactions with amino acids in CA II active site [5].

[1] S. Lindskog, J. E. Coleman, The catalytic mechanism of carbonic anhydrase, Proceedings of The National Academy of Sciences **70**(9), 2505-2508 (1973).

[2] C. T. Supuran, Carbonic anhydrases as drug targets - an overview, Current Topics in Medicinal Chemistry **7**, 825-833 (2007).

[3] V. Dudutienė, J. Matulienė, A. Smirnov et al., Discovery and characterization of novel selective inhibitors of carbonic anhydrase IX, Journal of Medicinal Chemistry **57**, 22, 9435-9446 (2014).

[4] H. A. Krebs, Inhibition of carbonic anhydrase by sulphonamides, Biochemical Journal **43**(4), 525-8 (1948).

[5] D. Baronas, V. Dudutienė, D. Matulis et al., Structure and mechanism of secondary sulfonamide binding to carbonic anhydrases, European Biophysics Journal **50**, 993-1011 (2021).

DIBLOCK COPOLYMERS WITH GRADIENT DISTRIBUTION OF ZWITTERIONIC AND BRUSH FRAGMENTS, AND CONTAINING CATECHOL MOIETIES FOR SURFACE MODIFICATION

Marijus Jurkūnas, Vaidas Klimkevičius, Ričardas Makuška

Faculty of Chemistry and Geoscience, Vilnius University, Lithuania
marijus.jurkunas@chgf.vu.lt

Poly(2-methacryloyloxyethyl phosphorylcholine) (pMPC) is known as a hydrophilic polymer with unique properties – antifouling effect, penetration across cell plasma, fluid lubrication, etc. [1]. Due to structural and characteristic similarities to phospholipids, zwitterionic block brush copolymers p(MPC-*block*-PEO₁₉MEMA) have promising potential for biomedical applications. Supposedly, they can be used as lubricants for joint cartilages. The effect of lubrication could be increased if such copolymers possess additional moiety capable of sticking to the surface of cartilages. It is well known that the polymers containing catechol side groups possess surface adhesive properties [2].

In the present study, we developed a strategy to synthesize the copolymers containing copolymeric block p(MPC-*co*-PEO₁₉MEMA) responsible for lubrication, and the block of poly(dopamine methacrylamide) (pDOPMA) responsible for the attachment of the copolymers to various surfaces. For the synthesis of the copolymers pDOPMA-*block*-p(MPC-*co*-PEO₁₉MEMA), acetonide-protected DOPMA (ADOPMA) was polymerized first using 4-((butylthio)carbonothioyl)thio-4-cyanopentanoic acid as a RAFT chain transfer agent (CTA), ACVA as an initiator, and DMF as a solvent. pADOPMA was precipitated, purified and dried, giving macroCTA. The second block of p(MPC-*co*-PEO₁₉MEMA) was synthesized by RAFT copolymerization of MPC and PEO₁₉MEMA at the same conditions and in the presence of the macroCTA pADOPMA. Protective acetonide functional groups of the pADOPMA blocks were removed by trifluoroacetic acid. In order to evaluate the effect of PEO₁₉MEMA units on the properties of the copolymers, PEG-free block copolymers pDOPMA-*block*-pMPC were synthesized as well. The copolymers were studied by size exclusion chromatography, ¹H NMR and FT-IR spectroscopy.

As it was shown in our previous study [3], RAFT copolymerization of MPC and PEO₁₉MEMA leads to the copolymers with strongly expressed gradient microstructure. Thus, the terpolymers pDOPMA-*block*-p(MPC-*co*-PEO₁₉MEMA) should possess unique structure combining hydrophilic block with gradient distribution of zwitterionic and brush fragments and relatively hydrophobic block responsible for adhesion. pADOPMA as the first block (DP close to 20) was obtained with rather low dispersity (Đ below 1.2). Unfortunately, we had no possibility to study the copolymers pADOPMA-*block*-p(MPC-*co*-PEO₁₉MEMA) by SEC because of the absence of an eluent dissolving both blocks of a very different nature. The only common solvent for both hydrophilic p(MPC-*co*-PEO₁₉MEMA) block and hydrophobic pADOPMA block was methanol which is not compatible with the known SEC columns. Composition of the copolymers as well as DP of the second block was calculated by studying ¹H NMR spectra of the copolymers in MeOD-*d*₆. We succeeded to synthesize diblock brush copolymers in which DP of the second block was from 40 to 80. Moreover, ¹H NMR spectra confirmed the complete removal of the acetonide protective groups (Fig. 1).

A study of surface activity and lubrication properties of the synthesized zwitterionic diblock brush copolymers pDOPMA-*block*-(MPC-*co*-PEO₁₉MEMA) is in progress.

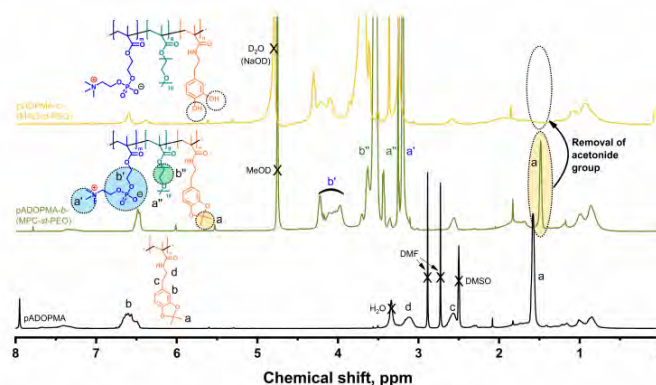


Fig. 1. ¹H NMR spectra of the copolymers: pADOPMA, pADOPMA-*block*-(MPC-*co*-PEO₁₉MEMA) and deprotected pDOPMA-*block*-(MPC-*co*-PEO₁₉MEMA).

[1] I. Yasuhiko, K. Ishihara, Cell membrane-inspired phospholipid polymers for developing medical devices with excellent biointerfaces, *Science and Technology of Advanced Materials* **13**, 064101 (2012).

[2] M. Steponavičiūtė, V. Klimkevičius, R. Makuška, Synthesis and stability against oxidation of random brush copolymers carrying PEO side chains and catechol moieties, *Materials Today Communications* **25**, 101262 (2020).

[3] M. Jurkunas, V. Klimkevičius, A. Uscilaite, R. Makuška, Synthesis of superhydrophilic gradient-like copolymers: Kinetics of the RAFT copolymerization of methacryloyloxyethyl phosphorylcholine with PEO methacrylate. *European Polymer Journal* **183**, 111764 (2023).

TIME-RESOLVED SPECTROSCOPIC CHARACTERIZATION OF THE PORPHYRIN-CONTAINING MOLECULAR DIMERS

Ivan Halimski¹, Vidmantas Jašinaskas¹, Ally Aukauloo², Renata Karpicz¹, Jevgenij Chmeliov^{1,3}, Vidmantas Gulbinas^{1,3}

¹ Department of Molecular Compound Physics, Center for Physical Sciences and Technology, Lithuania

² Institut de Chimie Moleculaire et des Materiaux d'Orsay, Paris-Saclay University, France.

³ Institute of Chemical Physics, Faculty of Physics, Vilnius University, Lithuania
ivan.halimski@ftmc.lt

Nowadays mankind is in need of green energy sources. Photocatalytic processes could help us to get energy in ecologically-friendly ways (for example, photosynthesis is photocatalytic process). Moreover, photocatalytic processes not only involve chemical reactions between the molecules being in the ground state, but also depend on their electronic excited states. That is the reason of studying charge separation processes in complex systems, such as photosynthetic complexes. But for the beginning simpler systems are worth studying.

In this work two different dimeric Porphyrin systems are studied, namely TPP-Ur-TPP (P₂Ur) and TPP-Ur-F₆ (P₂UaS), both solubilized in either DCM or DMSO. The difference between them is that P₂Ur (Fig. 1a) has symmetrical structure of the molecule and P₂UaS has an asymmetrical structure. In order to characterize the excited states of these molecules and also to study the formation of intra-molecular charge transfer states, we performed a set of the stationary and time-resolved spectroscopic measurements: transmission, fluorescence, and transient absorption (TA). The later are shown in Fig. 1b and c.

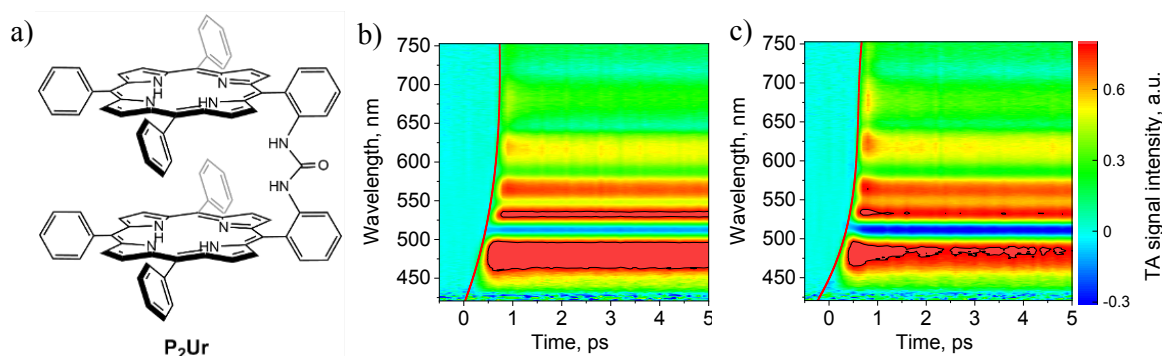


Figure 1. a) Chemical structure of the studied dimeric molecular system P₂Ur. b) TA spectrum of P₂Ur in DCM (thickness of the cuvette with solution is 1 mm, excitation wavelength $\lambda=410$ nm). c) TA spectrum of P₂UaS in DCM (thickness of the cuvette with solution is 1 mm, excitation wavelength $\lambda=430$ nm).

TA spectra in combination with global analysis techniques provide detailed information about the ultrafast transitions between electronic states of the studied molecules. More details about the samples as well as the obtained spectral characteristics of their excited states and the light-induced excitation dynamics will be presented at the conference.

SYNTHESIS OF THE ROD-SHAPE CARBAZOLE-BASED PHOSPHONIC ACID

Kotryna Gumauskaitė, Aida Drevilkauskaitė, Vytautas Getautis, Artiom Magomedov

Department of Organic chemistry, Kaunas University of Technology, Lithuania
kotryna.gumauskaite@ktu.edu

For the last decade, perovskite solar cell technology gained significant popularity due to the promise of low-cost fabrication and high efficiency. On the way to successful commercialization, each component needs to be optimized, independent, and in full stack. In particular, hole-selective contact is commonly mentioned as one of the weaker links. And this is the case where molecular design can be particularly useful.

In the last years, material [2-(9H-Carbazol-9-yl)ethyl]phosphonic acid, better known as 2PACz became a popular choice for the fabrication of perovskite solar cells. Originally used in tandem devices,[1] due to the simplicity of the layer formation, very low material consumption, and superior performance, this and related materials (MeO-2PACz and Me-4PACz) are becoming a “standard” option.

Layer formation of the 2PACz is based on the (self)-assembly of the phosphonic acid functional group on the surface of indium tin oxide (ITO), thus leading to the functional layer with the thickness of the single molecule. 2PACz molecule has a T-shape, where the phosphonic acid functional group and linker are perpendicular to the carbazole molecule (attached to the nitrogen atom). In this work, we are exploring an alternative design, in which carbazole chromophore would be in the same line as the linker and anchoring group, proposedly having a “rod” – type shape. It is expected that this could lead to denser packing, avoiding “voids” between the molecules. As a consequence, due to the higher concentration of the carbazole chromophore higher efficiency and stability are anticipated.

To achieve that, we are using the reactive -OH group in the second position of the carbazole for further functionalization. Starting with the 2-methoxy-9-methylcarbazole, the methoxy group was hydrolyzed with BBr₃, and further functionalized with a phosphonic acid group through the three-stage synthesis, including alkylation, Arbuzov reaction, and nucleophilic ester cleavage. The structure of the target material was confirmed by means of ¹H and ¹³C NMR spectroscopy. Synthesized materials will be further used for the fabrications of the perovskite solar cells and the performance will be compared to that of the state-of-the-art phosphonic acid-based selective materials.

[1] A. Al-Ashouri, A. Magomedov, M. Roß et al., Conformal monolayer contacts with lossless interfaces for perovskite single junction and monolithic tandem solar cells, *Energy Environ. Sci.*, **12**, 3356-3369 (2019).

STUDY OF CHEMICAL AND ELECTROCHEMICAL DEGRADATION OF VANADIUM-BASED PHOSPHATE FRAMEWORKS AS AQUEOUS NA-ION BATTERY CATHODES

Davit Tediashvili,^{1,2} Linas Vilčiauskas²

¹ Institute of Chemistry, Faculty of Chemistry and Geosciences, Vilnius University, Lithuania

² Center for Physical Sciences and Technology, Sauletekio al. 3, LT-10257 Vilnius, Lithuania

Davit.Tediashvili@ftmc.lt

Rechargeable Li-ion batteries, employing organic electrolytes are considered one of the main electrochemical energy storage devices, due to their high efficiency, energy density, and stability. However, for large-scale stationary applications, all these attractive properties are overshadowed by price and safety of operation, which are of paramount importance. Aqueous Na-ion batteries are deemed as one of the main alternatives, satisfying both of the conditions by employing sodium and aqueous solutions as a charge carrier and electrolyte, respectively. Despite the development of novel electrolyte systems, suppressing gas evolutions, and expanding operating window [1], the absence of high potential and stable cathode materials remains a bottleneck for fully utilizing and deploying this technology.

For Li-ion batteries, Co and Ni-based materials are the most successfully utilized due to their high operating voltage and stability. However, in recent years, considerable effort has been made to develop rare-earth-metal free systems based on Mn, Fe and V. Mn offers the highest operating voltage however, unfavorable aqueous chemistry limits its application [2,3]. Vanadium offers 2nd best alternative in terms of operating voltage as well as relatively high stability.

Here we report a chemical and electrochemical degradation study of $\text{Na}_3\text{V}_2(\text{PO}_4)_3$ (NVP) and $\text{Na}_3\text{V}_2(\text{PO}_4)_2\text{F}_3$ (NVPF). Electrodes were prepared by a conventional slurry-casting method. The electrochemical activity of cathodes was characterized by galvanostatic charge-discharge cycling (GCD) and cyclic voltammetry (CV). Degradation was assessed by (XRD), ICP-OES, SEM/EDX, rotating ring-disc electrode (RRDE), and double redox titration of the electrolyte after measurement. Results show poor chemical stability of NVP in aqueous media, as well as rapid electrochemical degradation. RRDE study gave insight into the mechanism of degradation during operation. The introduction of fluoride in the lattice seems to relatively stabilize the structure, and suppress most of the chemical dissolution, however, electrochemical degradation remains significant.

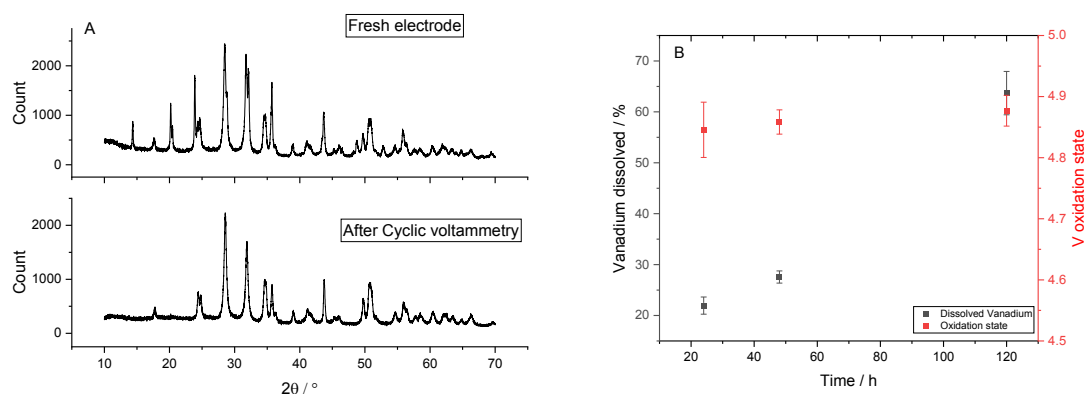


Figure 1. Degradation study of prepared electrode. A – XRD spectra before and after electrochemical degradation. B – Dissolved vanadium and its oxidation state during chemical dissolution for variable time.

Acknowledgements:

This project has received funding from the European Regional Development Fund (Project No. 01.2.2-LMT-K-718-02-0005) under grant agreement with the Research Council of Lithuania (LMTLT)

[1] L. Suo et al., “Water-in-salt” electrolyte enables high-voltage aqueous lithium-ion chemistries, *Science* **350**, 938-943 (2015).

[2] Thackeray, M. M. et al. The quest for manganese-rich electrodes for lithium batteries: Strategic design and electrochemical behavior. *Sustain. Energy Fuels* **2**, 1375–1397 (2018).

[3] Bin, D. et al. Progress in Aqueous Rechargeable Sodium-Ion Batteries. *Advanced Energy Materials* **8**, 1–31 (2018).

SYNTHESIS AND INVESTIGATION OF TETRAHYDROFURFURYL ACRYLATE-BASED PHOTOCROSS-LINKED POLYMERS

Justinas Jaras¹, Aukse Navaruckiene², Jolita Ostrauskaite^{2*}

¹ Department of Polymer Chemistry and Technology, Kaunas University of Technology, Radvilenu Rd. 19, LT-50254
justinas.jaras@ktu.edu

The depletion of fossil fuels and the increase in their price accelerate the society to use greener materials for their necessities. Research on biobased plastics has increased dramatically in the past 30 years while exceedingly large implications for oil-based plastics begin to unfold [1]. One way to address this issue is to use polymers derived from natural sources, such as plants. In this work, two biobased monomers: tetrahydrofurfuryl acrylate derived from hemicellulose and tridecyl methacrylate derived from natural oils, were chosen for photocross-linked polymer synthesis. A dual-curing process allowing to combine two polymerization mechanisms and thus achieve greater properties compared to separate parts [2] was used in this work. Stimuli-responsive materials, also known as shape-memory materials, have attracted researchers and industry due to their unique ability to change and maintain shape in response to external stimuli. Shape-memory polymers have a great potential to be applied in biomedicine, electronics, optics, robotics, etc. [for example, 3]. However, only a few shape-memory polymers have been synthesized by using an environmentally friendly UV-induced dual-curing method.

The aim of this work was to investigate the influence of the amount of the biobased monomer tetrahydrofurfuryl acrylate on the photocuring kinetics, mechanical and thermal characteristics, and shape-memory properties of the resulting polymers. Ethyl(2,4,6-trimethylbenzoyl)phenylphosphinate was used as a photoinitiator. The chemical structure of the used compounds is presented in Figure 1.

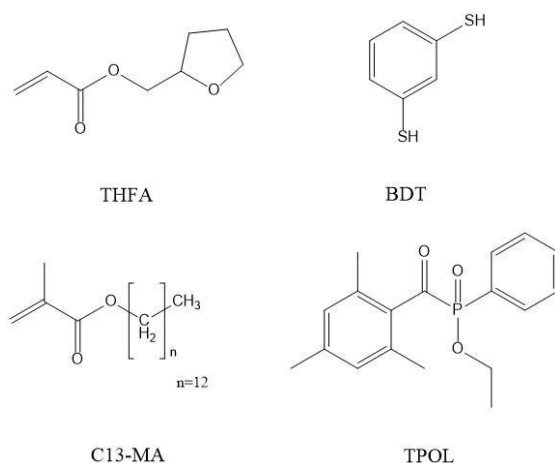


Fig. 1. Chemical structures of tetrahydrofurfuryl acrylate (THFA), 1,3-benzenedithiol (BDT), tridecyl methacrylate (C13-MA), and ethyl(2,4,6-trimethylbenzoyl)phenylphosphinate (TPOL).

Photocuring kinetics was monitored by the real-time photorheometry which provides a wide-range information on typical rheological properties such as storage and loss modulus while a material is irradiated with UV/vis light. The chemical structure of the cross-linked polymers was confirmed by FT-IR spectroscopy, Soxhlet extraction, which shows which part of the polymer is cross-linked, and determination of the swelling value. Mechanical characteristics were determined by tensile and compressive tests. The thermal properties were investigated by dynamic mechanical thermal analysis and thermogravimetric analysis. Shape-memory properties were investigated by deformation of polymer samples and maintaining them at a temperature below and above their glass transition temperature.

It was determined that the rheological, thermal, mechanical, and shape-memory properties are highly dependent on the amount of biobased monomer tetrahydrofurfuryl acrylate fragments in the resulting polymers.

Acknowledgement. This research was funded by the Research Council of Lithuania under the measure "Student research during semesters" (project No. S-ST-22-10).

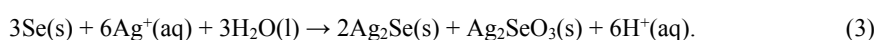
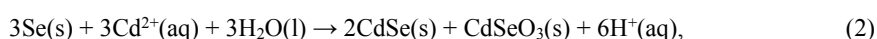
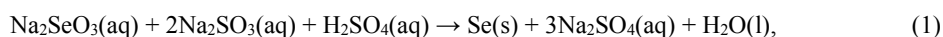
-
- [1] G. Friso Versteeg et al., RAFT Polymerization of a Biorenewable/Sustainable Monomer via a Green Process, *Macromolecular Rapid Communications*, **43**, 1-7 (2022).
[2] X. Ramis et al., *Click-Based Dual-Curing Thermosets and Their Applications*, *Thermosets: Structure, Properties, and Applications: Second Edition*, (2018).
[3] J. Delaey et al., Shape-Memory Polymers for Biomedical Applications, *Advanced Functional Materials*, **30**, (2020).

DEPOSITION AND INVESTIGATION OF SELENIDES THIN FILMS ON POLYAMIDE FOR OPTOELECTRONIC APPLICATIONS

Emilija Skuodaite¹, Henrieta Markevičiūtė¹, Valentina Krylova¹

¹Department of Physical and Inorganic Chemistry, Kaunas University of Technology, Lithuania
emilija.skuodaite@ktu.edu

Ordered nanoscale sized a-Se, CdSe and Ag₂Se films on the polymers are the promising compounds for various applications because of its potential physicochemical and optoelectronic properties such as conductivity, wide energy band gap and high absorbance coefficient [1, 2]. The chemical synthesis methods based on solution-phase procedures provide an excellent route to fabricate nano-selenium and nano-selenides. This work aims to synthesize and characterize a-Se/PA, Cd-Se/PA and Ag-Cd-Se/PA composites. These composites obtained applying different chemical synthesis methods: the a-Se/PA via chemical bath deposition at room temperature, the Cd-Se/PA by successive ionic layer adsorption and reaction at 80 °C, and the Ag-Cd-Se/PA by cation exchange at room temperature, according to the following reactions (Eq. 1-3):



In order to have a deep understanding of the relationship between the composition and the end-use properties of obtained composites, we mainly focused on the description of the microstructure, morphology and optical properties. The X-Ray Diffraction (XRD) analysis of the samples were performed on the Bruker Advance D8 diffractometer. Scanning Electron Microscopy/Energy-Dispersive X-Ray Spectroscopy (SEM/EDS) measurements were performed by using a Hitachi S-3400N microscope equipped with the Bruker Quad 5040 EDS system. Atomic force microscopy (AFM) imaging were carried out using a NanoWizard 3 NanoScience microscope. The ultraviolet-visible (UV-Vis) spectrum were recorded using a Spectronic Genesys 8 UV/Visible spectrophotometer.

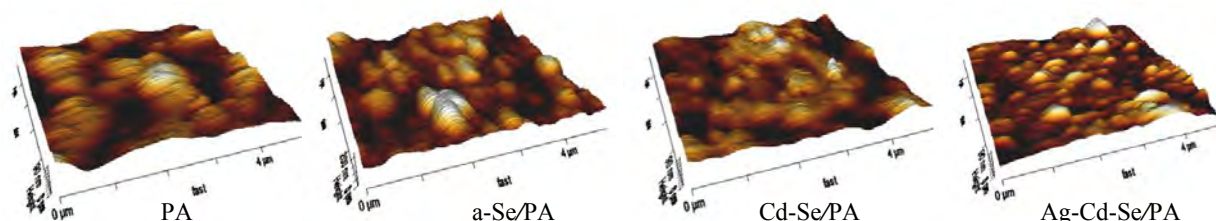


Fig. 1. Three-dimensional AFM topographical images of obtained composites.

Investigation of the surface morphology using AFM (Fig. 1) and SEM corroborates the change in morphology depending on chemical composition deposited films. In a-Se/PA composite selenium was amorphous (a-Se). In Cd-Se/PA composite the diffraction peaks indexed as hexagonal CdSe and monoclinic Se₈ which occur after a-Se crystallization at higher temperature. Ag-Cd-Se/PA composite XRD patterns showed crystalline composition with hexagonal CdSe, orthorhombic Ag₂Se, metallic Ag and monoclinic Se₈.

Table 1. The fundamental absorption edge (λ_g), optical band gap ($E_{op.g.}$), Urbach energy (E_U) and steepness parameter (σ) of studied composite materials

Polymer/Composite	λ_g , nm	$E_{op.g.}$, eV	E_U , eV	σ
PA	278	4.46	1.32	0.0195
a-Se/PA	555	2.23	0.094	0.237
Cd-Se/PA	606	2.05	0.397	0.0646
Ag-Cd-Se/PA	757	1.64	0.695	0.0369

Relatively high Urbach energy values indicate the formation of disordered structures, which correlates with heterogeneous surface morphology and composition. The optical properties of the obtained composites indicate a shift in the energy band gap from 2.23 eV to 1.64 eV with a stepwise incorporation of Cd²⁺ and Ag⁺ (Table 1). The energy band gap is suitably located in the visible solar energy region, which make these composites ideal for solar energy harvesting.

[1] M. Afzaal, P. O'Brien, Recent developments in II–VI and III–VI semiconductors and their applications in solar cells, *J. Mater. Chem.* **16**, 1597–1602 (2006).

[2] Q. Gao, W. Wang, Y. Lu, et al., High power factor Ag/Ag₂Se composite films for flexible thermoelectric generators, *ACS Appl. Mater. Interfaces* **13**, 14327–14333 (2021).

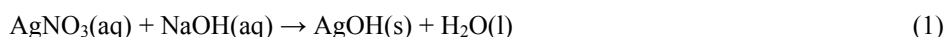
DEPOSITION AND INVESTIGATION OF SILVER OXIDE THIN FILMS ON POLYVINYLCHLORIDE TEXTILE SURFACE

Emilija Skuodaitė¹, Valentina Krylova¹

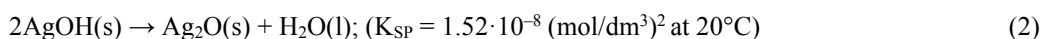
¹Department of Physical and Inorganic Chemistry, Kaunas University of Technology, Lithuania
emilija.skuodaite@ktu.edu

Textile-based solar thermal energy collectors (TSTEC) are one form of novel flexible solar thermal harvesting product, and one that can widely be applied to building roofs and facades [1]. Thin film metal oxides are superior solar light absorbers. Many of the metal oxides are n-type semiconductors. Known p-type oxides include silver (I) oxide. They can be combined into a functional material when deposited on polymeric substrates. The optical band gap for Ag₂O ranges from 1.2 eV [2] to 3.4 eV [3] depending on the stoichiometry, structure and physical properties that result from the deposition method.

In this study, silver oxide films were synthesised on a polyvinylchloride textile (PVC), and an investigation was carried out into the structural and optical properties of the treated fabric. The chemical deposition method was used to modify the PVC textile surface. Ag₂O can be prepared by combining aqueous solutions of AgNO₃ and NaOH:



This reaction does not provide appreciable amounts of silver hydroxide due to the favourable energetics for the following reaction:



With suitably controlled conditions, this reaction can be used to prepare Ag₂O with properties which are suitable for several uses, including as a fine-grained conductive thin films.



Fig. 1. Photographs of the reaction container with samples.

Prior to the process of depositing the materials, the mechanically roughened surface was pre-treated with hot alkali solution [4]. Then pre-treated samples were inserted vertically along the reactor wall with a 0.1M AgNO₃ solution and were left undisturbed for six hours (Fig. 1). At the end of the exposure time, the samples were taken out, washed with distilled water, and then exposed to freshly prepared 0.35M NaOH solution at room temperature for six hours. Sample immersion in AgNO₃ and subsequent immersion in the NaOH solution formed one Ag₂O preparation cycle. In summary, six cycles were employed. The obtained samples were cleaned, dried, and then characterized.

An X-ray diffraction (XRD) analysis was carried out to provide a level of understanding in regard to the formation of the silver oxide phase and its crystalline structure of the prepared samples. The XRD analysis revealed that deposited films exist as polycrystalline mixed-phase material, which is composed of Ag₂O, AgO, and metallic Ag. Ultraviolet-visible (UV-Vis) diffuse reflectance spectra were recorded to study the optical properties of deposited films. It was found that Ag-O/PVC composites are direct band gap semiconductors; the optical band gap is 0.89±0.02eV.

[1] W. D. Abdul Jalil, Smart textiles for the architectural façade, IOP Conf. Ser.: Mater. Sci. Eng. **737**, 012078 (2020).

[2] E. Fortiu, F. L. Weichman, Photoconductivity in Ag₂O, Phys. Stat. Sol. B, **5** 515-524 (1964).

[3] E. Lund, A. Galeckas, A. Azarov, et al., Photoluminescence of reactively sputtered Ag₂O films, Thin Solid Films, **536**, 156-159 (2013).

[4] V. Krylova, N. Dukštienė, M. Lelis, et al., PES/PVC textile surface modification by thermo-chemical treatment for improving its hydrophilicity, Surf. Interfaces, **25**, 101184 (2021).

MIXED Zn-Co OXIDE (Zn:Co 1.25:1) LAYERS FOR PHOTOCATALYTIC APPLICATIONS

Agnietė Juciūtė¹, Dovilė Sinkevičiūtė¹, Nerita Žmuidzinavičienė¹, Agnė Šulčiūtė^{1*}

¹ Department of Physical and Inorganic Chemistry, Kaunas University of Technology, Lithuania
agne.sulciute@ktu.lt

In recent years, a considerable interest has been focused on fabrication of heterojunctions, which are able to provide better photocatalytic activity, especially p- and n-type semiconductors, when in contact, form a junction with a space-charge region at their interfaces [1].

Our goal was to synthesize environmentally friendly double p–n heterostructure of spinel type mixed Zn-Co coatings to investigate the photoelectrochemical properties and to test as prospective materials to catalyze oxygen evolving reaction (OER).

Mixed Zn-Co oxide layers (Zn:Co 1,25:1) were formed using two-step synthesis: chemical precipitation and thermal treatment (400 – 600 °C). Firstly, 0.5 M zinc nitrate and 0.5 M cobalt nitrate solutions were mixed by adding slowly 200 mL of 1 M NaOH and under continuous stirring (Fig. 1). Precipitates were annealed at 400 – 600 °C for 2 h in air atmosphere.

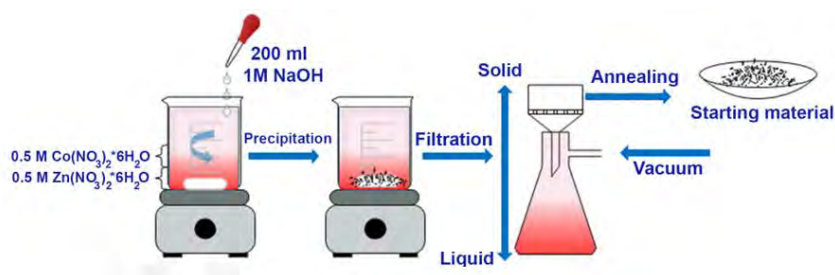


Fig. 1. Synthesis of mixed Zn-Co oxides

Photoelectrochemical activity of prepared mixed Zn- Co oxide layers were explored in a quartz cell in phosphate-bufer solution (pH 7) using the General Electric F8W/BLB lamp, which $\lambda_{\max}=366$ nm and average power density is 1.8 mW cm^{-2} , as a source of UV radiation. UV source was placed 2 cm from working electrode. IPCE value of a photoelectrode was calculated using the following equation [3].

$$IPCE(\%) = 100 \frac{1240 \cdot j_{ph}}{\lambda \cdot P} \quad (1)$$

Where j_{ph} is photocurrent density in mA cm^{-2} , λ is a wavelength of incident light in nanometers (here 366 nm), P is incident light intensity in mW cm^{-2} .

Applied bias photon-to-current efficiency (ABPE) calculations were used in order to characterize photo-response efficiency of photoelectrode material under applied voltage according to the following equation [2]:

$$ABPE(\%) = 100 \frac{|j_{ph}| \cdot (1.23 - |V_{appl}|)}{I_0} \quad (2)$$

Here j_{ph} is photocurrent density (mA cm^{-2}), I_0 is input intensity of incident light falling on a surface of photoelectrode (1.8 mW cm^{-2}) and V_{appl} is applied potential, which is calculated according to the equation [1]:

$$V_{appl} = V_{mea} - V_{oc} \quad (3)$$

Here V_{mea} is working electrode potential at which photocurrent was measured under illumination and V_{oc} is working electrode potential at open circuit condition under similar conditions.

-
- [1] A. Simanaitienė, A., I. Barauskienė, Š. Varnagiris, et al., Mixed zinc–cobalt oxide coatings for photocatalytic applications, *Applied Physics A* **126**, 695 (2020).
 [2] Q. Liu, Q. Chen, J., Bai, et al., Enhanced photoelectrocatalytic performance of nanoporous WO_3 photoanode by modification of cobalt–phosphate (Co–Pi) catalyst. *Journal of Solid State Electrochemistry* **18**, 157–161 (2014).
 [3] J. Georgieva, S. Armyanov, E. Valova, et.al, Photoelectrocatalytic Activity of Electrosynthesised Tungsten Trioxide- Titanium Dioxide Bi-Layer Coatings for the Photooxidation of Organics, *Journal of Advanced Oxidation Technologies* **11**, 300–307 (2008).

FERROELECTRIC, PIEZOELECTRIC, AND BROADBAND DIELECTRIC STUDIES OF LEAD-FREE $x(\text{Bi}(\text{Zn}_{2/3}\text{Nb}_{1/3})\text{O}_3)-(1-x)\text{BaTiO}_3$ SOLID SOLUTIONS

Žygimantas Logminas¹, Artyom Plyushch¹, Jessica Marshall², David Walker², Pam Thomas², Jūras Banys¹

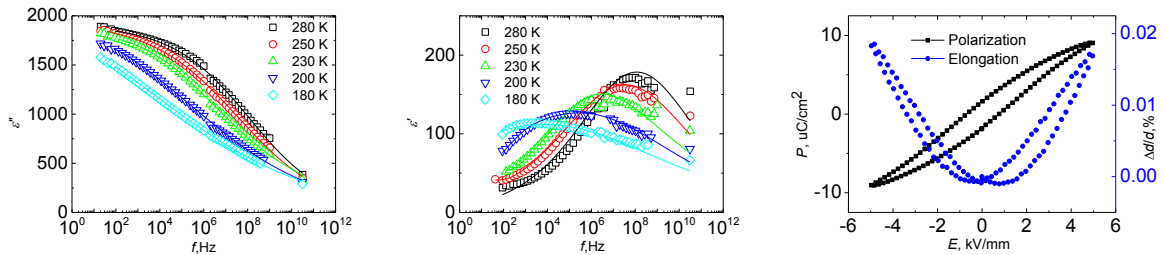
¹Faculty of Physics, Vilnius University, Sauletekio 9, LT-10222 Vilnius, Lithuania

²Department of Physics, University of Warwick, Gibbet Hill Road, Coventry, CV4 7AL, UK

zygimantas.logminas@ff.stud.vu.lt

Relaxors are a type of materials, that exhibit high dielectric constant and slim polarization hysteresis curves. For these reasons, they are widely used in capacitors [1] and RAM microchips [2]. Some of examples of such materials are lead magnesium niobate or lead scandium niobate. Such materials contain lead, which, when disposed inappropriately, can cause severe damage to the ecosystem and human health. One possible alternative to replace aforementioned composites are barium titanate-based compositions. In this report the $x(\text{Bi}(\text{Zn}_{2/3}\text{Nb}_{1/3})\text{O}_3)(1-x)\text{BaTiO}_3$, $x=3.6-7.0\%$ solid solution was studied. It was previously reported that the composition undergoes a ferroelectric-relaxor structural phase transition in the concentration range of $4.0\% < x < 5.0\%$ [3]. However, there is still uncertainty regarding the phase composition around the boundary. Additionally, the dielectric properties were reported only for low frequency range.

The aim of present research is to investigate the dielectric properties of the samples by means of the dielectric spectroscopy methods in wide frequency (20 Hz – 40 GHz) and temperature (100 – 500 K) ranges. Ferroelectric and piezoelectric properties were studied using 100 Hz, 50 kV/cm alternating electric field in temperature range from 233 K to 423 K.



Figures 1. Frequency dependence of the dielectric permittivity of the sample with $x=7\%$ real part (left) and imaginary part (middle). Symbols denote experimental data; lines are the best fits with Cole-Cole law (1). Polarization loop and relative elongation due to electrostriction of the same sample 283 K (right).

All samples demonstrate phase transition-related anomalies in the behavior of the dielectric constant. The spectra of dielectric permittivity demonstrate pronounced relaxation behaviour (see Figure 1). The imaginary part shows that maximum shifts towards lower frequencies as the temperature increases. The dependencies follow the Cole-Cole law:

$$\epsilon^* = \epsilon_s + \frac{\epsilon_s - \epsilon_\infty}{1 + (i\omega\tau)^{1-\alpha}} \quad (1)$$

here ϵ_s and ϵ_∞ are static and infinite frequency dielectric constants, ω is the angular frequency, τ is relaxation time and α is an empirical parameter describing spectral shape. The hysteresis loops thinners gradually with the concentration of BZN. Depending on BZN concentration, the shape of elongation curves switches between piezoeffect to electrostriction. (see Figure 1 right).

[1] ZHANG, Lei; PU, Yongping; CHEN, Min. Ultra-high energy storage performance under low electric fields in Na_{0.5}Bi_{0.5}TiO₃-based relaxor ferroelectrics for pulse capacitor applications. *Ceramics International*, 2020, 46.1: 98-105

[2] GRANZOW, Th, et al. Polarization-based adjustable memory behavior in relaxor ferroelectrics. *Physical review letters*, 2002, 89.12: 127601

[3] Marshall, Jessica, David Walker, and Pam Thomas. "Bismuth zinc niobate: BZN-BT, a new lead-free BaTiO₃-based ferroelectric relaxor?." *Journal of Advanced Dielectrics* 10.06 (2020): 2050033.

SYNTHESIS OF THERMORESPONSIVE COPOLYMERS BASED ON CHITOSAN AND N-ISOPROPYLACRYLAMIDE

Vesta Navikaite-Snipaitiene¹, Arminta Kairyte¹, Migle Babelyte¹, Ramune Rutkaite¹, Laura Peciulyte¹, Volodymyr Samaryk²

¹ Department of Polymer Chemistry and Technology, Kaunas University of Technology, Lithuania

² Department of Organic Chemistry, Lviv Polytechnic National University, Ukraine

vesta.navikaite@ktu.lt

Thermo-responsive polymers are considered to be a “smart” class of materials that can be used in tissue engineering, wound dressings and drug delivery systems. Polysaccharides such as chitosan represent an ideal matrix for preparing of biocompatible copolymers with improved biodegradability properties compared to those of synthetic thermoresponsive materials. Furthermore, chitosan is highly appreciated for the production of multi-response copolymers due to high reactivity of functional groups and pH-responsivity [1, 2].

The aim of this work was to obtain chitosan-graft-poly(N-isopropylacrylamide) copolymers using different molar ratios of medium molecular weight chitosan (CH) and N-isopropylacrylamide (NIPAA), and investigate thermo-responsive properties of prepared copolymers in aqueous medium. The synthesis of copolymers was carried out in aqueous solution using potassium persulfate (PPS) as an initiator (Fig.1).

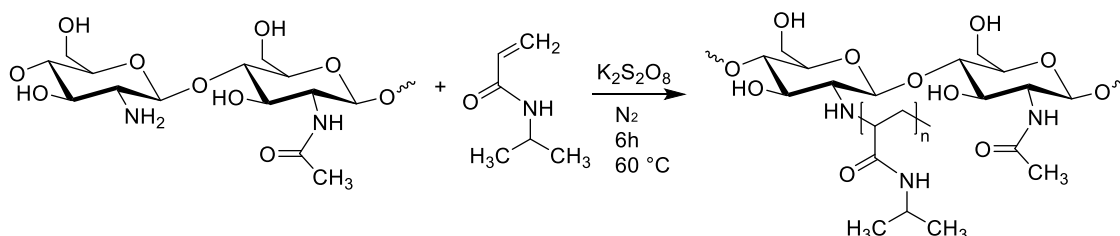


Fig. 1. Synthesis scheme of chitosan-graft-poly(N-isopropylacrylamide) copolymers.

The free-radical polymerization was carried out for 6 hours at $60\text{ }^\circ\text{C}$ temperature under a nitrogen atmosphere. After the reaction, the products were precipitated into acetone and obtained copolymers were purified by using methanol. The molar ratio of CH to NIPAA in the polymerization mixture was changed from 1:0.25 to 1:10. The obtained chitosan-graft-poly(N-isopropylacrylamide) copolymers with different fractions of CH and NIPAA of comonomers were characterized by using various techniques such as $^1\text{H-NMR}$, FT-IR, thermal analysis and etc. The lower critical solution temperature behavior of prepared copolymers in water was assessed by dynamic light scattering and turbidimetric methods.

Acknowledgements. The financial support of the Research Council of Lithuania for the project No. S-LU-22-11 in the frame of Lithuanian–Ukrainian Cooperation Programme in the Fields of Research and Technologies is highly acknowledged.

[1] X. Xu, Y. Liu, W. Fu et al., Poly(N-isopropylacrylamide)-Based Thermoresponsive Composite Hydrogels for Biomedical Applications, *Polymers* **12**, 508 (2020).

[2] L. Marsili, M. D. Bo, F. Berti et al., Chitosan-Based Biocompatible Copolymers for Thermoresponsive Drug Delivery Systems: On the Development of a Standardization System, *Pharmaceutics* **13**, 1876 (2021).

SYNTHESIS AND APPLICATION OF TiO₂ NANOTUBE ARRAYS FOR WASTEWATER TREATMENT

Maria-Anthoniette Onoriode-Afunzie^{1*}, Agne Sulciute¹, Vytautas Abromaitis²

¹Department of Physical and Inorganic Chemistry, Faculty of Chemical Technology, Kaunas University of Technology, Kaunas, Lithuania

²Department of Environmental Engineering, Faculty of Chemical Technology, Kaunas University of Technology, Kaunas, Lithuania
maria.onoriode@ktu.edu

Environmental problems are major worldwide issues. Various companies produce a lot of effluent because of the expansion of the industrial sector, which is characterized by high levels of suspended particles, a high Chemical Oxygen Demand (COD), changing pH, high temperatures, and dye mixtures [1]. TiO₂ has been thoroughly investigated as a catalyst to break down dyes and other dangerous substances in wastewater. TiO₂ nanoparticles are substances that may be used since they are affordable, eco-friendly, and very sensitive to ultraviolet light. [2] [3]

MATERIALS AND METHODS

Grade 2 TiO₂ was used for this experiment. It was prepared by cutting it into a circle with a handle, drilling holes, roughening the surface with 220grit sandpaper, and finishing with 800 grit sandpaper. To rinse the surface, tap water and demineralized water were used. Afterwards, it was put into a petri dish for 1 minute with HF, HNO₃, and H₂O solutions poured on top. After washing with tap and demineralized water, it was placed in an ultrasonic bath for ten minutes before getting rinsed. A mixture of 1L of 5.5g/L NH₄F and 132g/L NH₄SO₄ with demineralized water was electrolyzed for 2 hours at 20V. Then 10mg/l concentration of methylene blue mixed in a 1L flask was degraded using UV light. Ozone was also bubbled into a methylene blue solution with the catalyst.

RESULTS AND DISCUSSION

The removal of methylene blue revealed that using UV alone is ineffective, as over 80% of the methylene blue was still present in the solution after 120 minutes. The degradation of methylene blue by UV and catalyst yielded better results, with the concentration after 120 minutes being 1.76mg/l. UV photodegradation with TiO₂ catalyst and Ozone yielded the best results in the shortest time frame. After 20 minutes, the methylene blue concentration was 0.472mg/l. According to figure 1, the degradation of methylene blue with the catalyst, UV, and Ozone was 5.4 times faster than with just UV or UV and catalyst. This supports the theory that adding ozone to water treatment improves efficiency and shortens the time required for treatment. The results of this experiment show higher performance than would have been obtained if only pure TiO₂ had been used. This improvement is due to increased photocatalytic activity, which has been enhanced by catalyst doping. The reaction constant values show that UV with Ozone and TiO₂ catalyst has the quickest degradation.

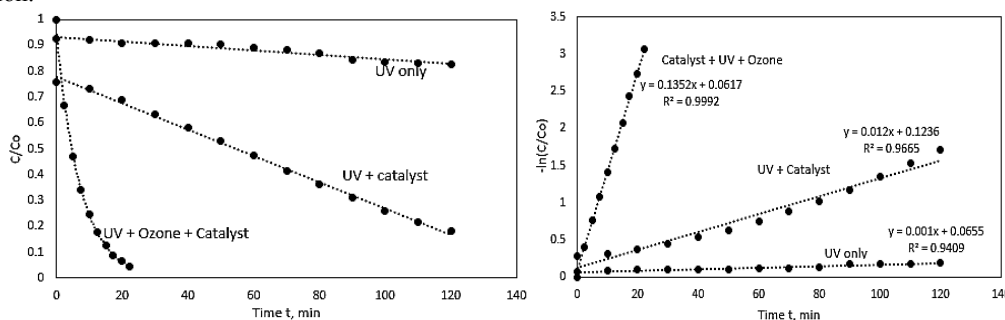


Figure 1. Methylene blue degradation (left) and pseudo-second-order reaction kinetics (right) versus time.

- [1] Tim Robinson, "Remediation of dyes in textile effluent: a critical review on current treatment technologies with a proposed alternative," *Bioresource Technology*, pp. 247-255, 2001.
- [2] YuLin Min, "Doping nitrogen anion enhanced photocatalytic activity on Titanium dioxide hybridized with graphene composite under solar light," *Separation and Purification Technology (Vol 106)*, pp. 97-104, 2013.
- [3] Akira Fujishima, "Titanium dioxide photocatalysis and related surface phenomena," *Surface Science Report (Vol 63), (Issue 12)*, pp. 515-582, 2008.

MIXED Zn-Co OXIDE LAYERS FORMATION AND THEIR ELECTROCHEMICAL PROPERTIES

Vasaris Statkevičius¹, Dovilė Sinkevičiūtė¹, Agnė Šulčiūtė¹, Nerita Žmuidzinavičienė^{1*}

¹ Department of Physical and Inorganic Chemistry, Kaunas University of Technology, Lithuania
nerita.zmuidzinaviciene@ktu.lt

In recent years, much interest has been focused on the fabrication of heterojunctions capable of providing improved photocatalytic activity, in particular for p- and n-type semiconductors, which form a junction with a space charge region at their interfaces. [1].

Our aim was to synthesize environmentally friendly spinel-type mixed Zn-Co coatings with a double p-n heterostructure, to investigate the photoelectrochemical properties and to test them as promising materials for catalyzing the oxygen evolution reaction (OER).

Mixed Zn-Co oxide layers (Zn:Co 1:1,25) were formed by a two-step synthesis: chemical precipitation and heat treatment (400-600 C). First, solutions of 0,5 M cobalt nitrate and 0,5 M zinc nitrate were mixed by the slow addition of 200 ml of 1 M NaOH with continuous stirring (Figure 1). The precipitates were heated at 400-600 C for 2 hours in an air atmosphere.

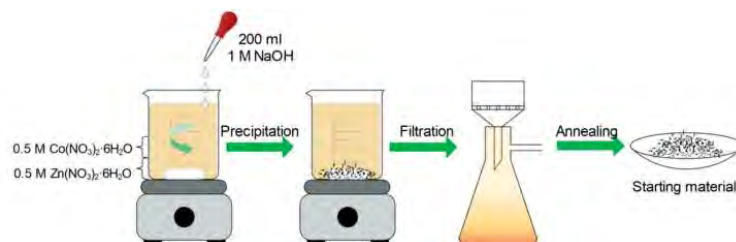


Fig. 1. Synthesis of mixed Zn-Co oxides[1]

The photoelectrochemical activity of the prepared mixed Zn-Co oxide layers was investigated in a quartz cell in phosphate-buffered saline (pH 7), using a General Electric F8W/BLB lamp with $\lambda_{\max}=366$ nm and an average power density of $1,8 \text{ mW cm}^{-2}$ as a UV source. The UV source was located at a distance of 2 cm from the working electrode. The IPCE value of the photoelectrode was calculated using the following equation [3].

$$IPCE(\%) = 100 \frac{1240 \cdot j_{ph}}{\lambda \cdot P} \quad (1)$$

Where j_{ph} is the photocurrent density in mA cm^{-2} , λ is the wavelength of the incident light in nanometres (in this case 366 nm), P is the intensity of the incident light in mW cm^{-2} .

In order to characterise the photoresponse efficiency of the photoelectrode material at the applied voltage, the photon-current efficiency (ABPE) calculations were carried out according to the following equation [2]:

$$ABPE(\%) = 100 \frac{|j_{ph}| \cdot (1,23 - |V_{appl}|)}{I_0} \quad (2)$$

Here j_{ph} is the photocurrent density (mA cm^{-2}), I_0 is the input intensity of the light incident on the surface of the photoelectrode ($1,8 \text{ mW cm}^{-2}$), and V_{appl} is the applied potential, which is calculated according to equation [1]:

$$[1]: V_{appl} = V_{mea} - V_{oc} \quad (3)$$

Here V_{mea} is the potential of the working electrode at which the photocurrent was measured under illumination and V_{oc} is the potential of the working electrode in an open circuit under similar conditions.

[1] A. Simanaitienė, A., I. Barauskienė, Š. Varnagiris, et al., Mixed zinc-cobalt oxide coatings for photocatalytic applications, Applied Physics A **126**, 695 (2020).

[2] Q. Liu, Q. Chen, J., Bai, et al., Enhanced photoelectrocatalytic performance of nanoporous WO_3 photoanode by modification of cobalt-phosphate (Co-Pi) catalyst. Journal of Solid State Electrochemistry **18**, 157–161 (2014).

[3] J. Georgieva, S. Armanyanov, E. Valova, et al., Photoelectrocatalytic Activity of Electrosynthesised Tungsten Trioxide- Titanium Dioxide Bi-Layer Coatings for the Photooxidation of Organics, Journal of Advanced Oxidation Technologies **11**, 300–307 (2008).

DETERMINATION OF MAGNESIUM WHITLOCKITE STRUCTURAL PROPERTIES: RIETVELD MODELING

Agnė Kizalaite, Jonas Stadulis, Aleksej Žarkov

Institute of Chemistry, Vilnius University, Lithuania
agne.kizalaite@chgf.vu.lt

One of the major minerals in human body is magnesium whitlockite ($\text{Ca}_{18}\text{Mg}_2\text{H}_2(\text{PO}_4)_{14}$). This compound is one of the main components of the human hard tissue, constituting to approximately 20–35 wt%, and plays an important role in various bone formation processes [1]. Magnesium whitlockite is known for its excellent osteogenic capability as well as having an active role in natural bone healing processes, therefore it is a promising candidate for application in bone regenerative medicine and tissue engineering [2]. In recent years this compound has attracted a lot of attention and the scientific community however it is not yet widely researched.

In the present work, whitlockite powders were synthesised using hydrothermal synthesis method while using calcium hydrogen phosphate dihydrate and magnesium acetate tetrahydrate as starting materials. Synthesis was performed at a temperature of 160 °C for 3 h under hydrothermal conditions. Synthesized compounds were analyzed by X-ray diffraction (XRD) and the obtained data was used for Rietveld refinement. Whitlockite structure was modeled taking large number of crystallographic positions available for substitution into account. The simulation of the XRD data showed clear differences due to the presence of Mg^{2+} ions in crystalline structure. It also allowed us to obtain data about preferential sites of $\text{Ca}^{2+}/\text{Mg}^{2+}$ substitutions.

Acknowledgements

This research was funded by a grant WHITCERAM (No. S-LJB-22-1) from the Research Council of Lithuania.

-
- [1] H. Cheng, R. Chabok et al. Synergistic interplay between the two major bone minerals, hydroxyapatite and whitlockite nanoparticles, for osteogenic differentiation of mesenchymal stem cells, *Acta Biomaterialia* **69**, 342-351 (2018).
[2] H. L. Jang, G. Bin Zheng et al. s, In Vitro and In Vivo Evaluation of Whitlockite Biocompatibility: Comparative Study with Hydroxyapatite and β -Tricalcium Phosphate, *Advanced Healthcare Material* **5**, 128–136 (2015).

CYANO-SUBSTITUTED 1,2-DIPHENYLBENZOIMIDAZOLE DERIVATIVES AS HOSTS FOR OLED APPLICATIONS

Simas Macionis¹, Murad Najafov¹, Jurate Simokaitiene¹, Juozas V. Grazulevicius¹, Jiun-Haw Lee², Chia-Hsun Chen², Bo-Yen Lin³, Tien-Lung Chiu⁴

¹ Department of Polymer Chemistry and Technology, Kaunas University of Technology, Radvilenu pl. 19, LT-50254, Kaunas, Lithuania

² Graduate Institute of Photonics and Optoelectronics and Department of Electrical Engineering, Material Science and Engineering, and Physics, National Taiwan University, Taipei 10617, Taiwan

³ Department of Opto-Electronic Engineering, National Dong Hwa University, Shoufeng, Hualien 974301, Taiwan.

⁴ Department of Electrical Engineering, Yuan Ze University, Taiwan
simas.macionis@ktu.edu

OLED technology has come far since the first reported successful demonstration in the late 80s by Van Slyke and Tang [1]. It has, since then, found its way into mainstream technology and remains a competitive research topic in both industry and academia [2]. Thanks to the discovery of thermally activated delayed fluorescence (TADF) [3] OLED technology has received a much needed influx of research worldwide. Today, OLED technology is evolving at a rapid pace yet development of stable, high emission color purity and efficient materials remains center most focus. One of the key components in majority of OLEDs are host materials of emissive layers, due to their ability to prevent excitons from self-quenching via triplet-triplet annihilation, which furthermore improves electroluminescence efficiency [4]. Yi-Mei Huang et al. recently reported a series of di-carbazolyl substituted 1,2-diphenylbenzoimidazole derivatives as hosts for multi colored OLEDs (red, green, blue) with external quantum efficiency up to 31% [5].

In this work we propose two new cyano-substituted 1,2-diphenylbenzoimidazoles with di-*tert*-butylcarbazole moieties as hosts for OLEDs. The proposed materials were synthesized in a simple two-step, noble metal-free synthesis method. The electrochemical, thermal and photophysical properties will be reported as well as characteristics of OLEDs. External quantum efficiency values ranging from 10% to 13% for green and sky-blue emitting devices were observed.

[1] Tang and S.A. Van Slyke Appl. Phys. Lett. 51, 913 (1987)

[2] D'Andrade, B. . and Forrest, S., White Organic Light-Emitting Devices for Solid-State Lighting. Adv. Mater. (2004)

[3] Q. Zhang, B. Li, S. Huang, et al. Efficient blue organic light-emitting diodes employing thermally activated delayed fluorescence. Nature Photon 8, 326–332 (2014).

[4] M. A. Baldo, C. Adachi and S. R. Forrest, Phys. Rev. B: Condens. Matter Mater. Phys, 62, 10967, (2000)

[5] Y.M. Huang, T.Y. Chen, et al. Why triage materials with low luminescence quantum efficiency: the use of 35Czbz4BzCN as a universal host for organic light emitting diodes through effective triplet energy transfer. J. Mater. Chem. C, 9, 2381-2391, (2021)

INVESTIGATION OF THERMAL PROPERTIES OF DIFFERENT COMPOSITION CAFFEIC ACID AND CHITOSAN COMPLEXES

Dovilė Liudvinavičiūtė, Vesta Navikaitė-Šnipaitienė, Ramunė Rutkaitė, Joana Bendoraitienė

Department of Polymer Chemistry and Technology, Kaunas University of Technology, Lithuania
dovile.liudvinaviciute@ktu.lt

Bioactive compounds, among them and caffeic acid (CA), are becoming the focus of attention given their benefits to human health and their relative abundance in vegetables [1]. Presence of unsaturated bonds makes CA vulnerable to heat, oxygen and moisture, and influences instability especially at higher temperatures. In recent years delivery systems based on complexes formed by electrostatic interactions between polysaccharides and low molecular weight compounds gained a lot of interest [2] and chitosan (CHT) is one of biopolymers that can be ionized and possess positive surface charges. Investigation of thermal properties of complexes formed between CHT and CA are important for the pharmaceutical and food industries, as their concentration in complexes can change significantly during heat treatment. Such investigation can provide the information about the optimal temperature range during processing and storage [3]. Thermogravimetric (TG) analysis method has been used to evaluate complex formation between chitosan and other compounds.

The aim of the present work was to investigate thermal properties of CA and CHT complexes of different composition (further referred as CA-CHT) using TG analysis method. CA-CHT with the molar ratio of CA to CHT equal to 0.23/1 and 0.72/1 were obtained by using multistep adsorption process. TG analysis of CHT and CA-CHT was performed with a Perkin-Elmer (TGA 400, USA) instrument. Measurements were carried out at heating rates of 2.5 °C/min, 5 °C/min, 10 °C/min and 20 °C/min under nitrogen (air in some experiments) atmosphere. About 10 mg of air-dried sample was used. Apparent activation energy (E_a) was determined according to Flynn-Wall-Ozawa (FWO) method [4] in the temperature interval of 200–400 °C.

TG curves of CHT and CA-CHT (0.23 mol/mol) in nitrogen and air atmospheres are presented in Fig. 1. Thermal decomposition of CA-CHT (0.23 mol/mol) in nitrogen atmosphere and in air proceeded in two and three stages, contrary to CHT which decomposed in one and two stages, respectively. An extra step in the temperature range of 150 °C–200 °C in TG curves of CA-CHT (0.23 mol/mol) in both atmospheres occurred due to decarboxylation of adsorbed CA.

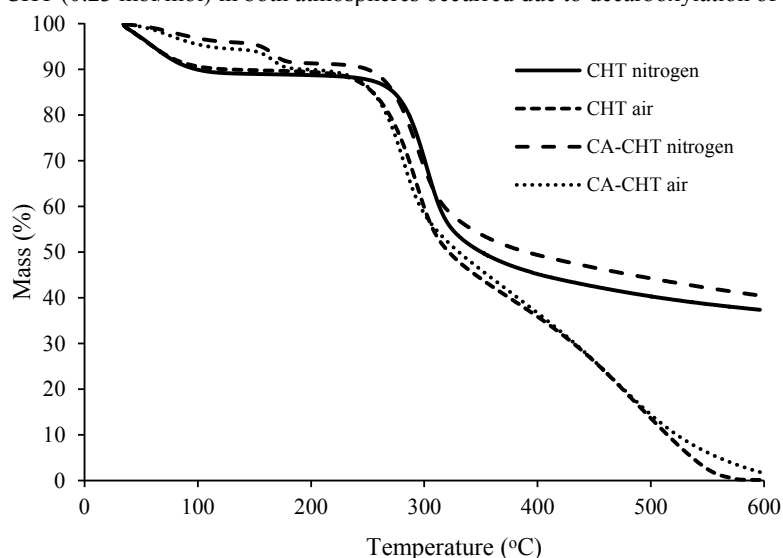


Fig. 1. TG curves of CHT and CA-CHT (0.23 mol/mol) in air and nitrogen atmosphere at heating rate of 10 °C/min.

Values of E_a related to the second stage of thermal decomposition of CA-CHT at conversion values (α) from 0.1 to 0.8 were determined by Flynn-Wall-Ozawa method. The dependence of CA-CHT between E_a and α was very similar to that of CHT.

- [1] P. Kaushik, I. Andujar, S. Vilanova et al., Breeding vegetables with increased content in bioactive phenolic acids, *Molecules* **20**, 18464–18481 (2015).
- [2] T.A. Debele, S.L. Mekuria, & H.-C. Tsai, Polysaccharide based nanogels in drug delivery systems: Application as carrier of pharmaceutical agents, *Materials Science and Engineering C* **68**, 964–981 (2016).
- [3] S.F. Hosseini, M. Zandi, M. Rezaei & F. Farahmandghavi, Two-step method for encapsulation of oregano essential oil in chitosan nanoparticles: Preparation, characterization and in vitro release study, *Carbohydrate Polymers* **95**, 50–56 (2013).
- [4] T. Ozawa, A new method of analysing thermogravimetric data, *Bulletin of the Chemical Society of Japan* **38**, 1881–1886 (1965).

SYNTHESIS AND CHARACTERIZATION OF ACENAPHTHYLENE LABELLED CHITOSAN-GRAFT-POLY(N-ISOPROPYLACRYLAMIDE) COPOLYMERS

Migle Babelyte^{1*}, Ramune Rutkaite¹, Dovile Liudvinaviciute¹, Vesta Navikaite-Snipaitiene¹, Volodymyr Samaryk²

¹Department of Polymer Chemistry and Technology, Kaunas University of Technology, Lithuania

²Department of Organic Chemistry, Lviv Polytechnic National University, Ukraine

migle.babelyte@ktu.edu

Chitosan (CS) is non-toxic, biodegradable, biocompatible, pH-sensitive, inexpensive natural biopolymer. It can be also easily modified *via* grafting reactions. One of the most attractive compounds which can be used for grafting of chitosan is N-isopropylacrylamide (NIPAAm). Poly(N-isopropylacrylamide) (PNIPAAm) is highly thermo-sensitive polymer which shows sharp solubility changes in aqueous solutions around a lower critical solution temperature (LCST). PNIPAAm undergoes a sharp transition from coil to globule in water at 32 °C, changing from a hydrophilic state below this temperature to a hydrophobic state above it. Beyond 32 °C PNIPAAm turns into precipitate and could be dissolved again by lowering the solution temperature. Moreover, acenaphthylene (ACE) could be also introduced into PNIPAAm grafts and serve as a fluorescent marker for more detailed investigation of thermoresponsive behavior of synthesized copolymers.

In this study, ACE labelled chitosan-*graft*-poly(*N*-isopropylacrylamide) (CS-*g*-PNIPAAm-ACE) copolymers were synthesized by free-radical polymerization of CS, NIPAAm and ACE in aqueous solution using potassium persulfate (PPS) as an initiator and thermoresponsive properties of the prepared copolymers were investigated. CS-*g*-PNIPAAm-ACE copolymers were synthesized as shown in the scheme (Fig. 1). By changing the molar ratio of the reagents two ACE labelled graft copolymers of different composition were prepared. The reaction conditions and feed molar ratio of the reagents are presented in the Table 1.

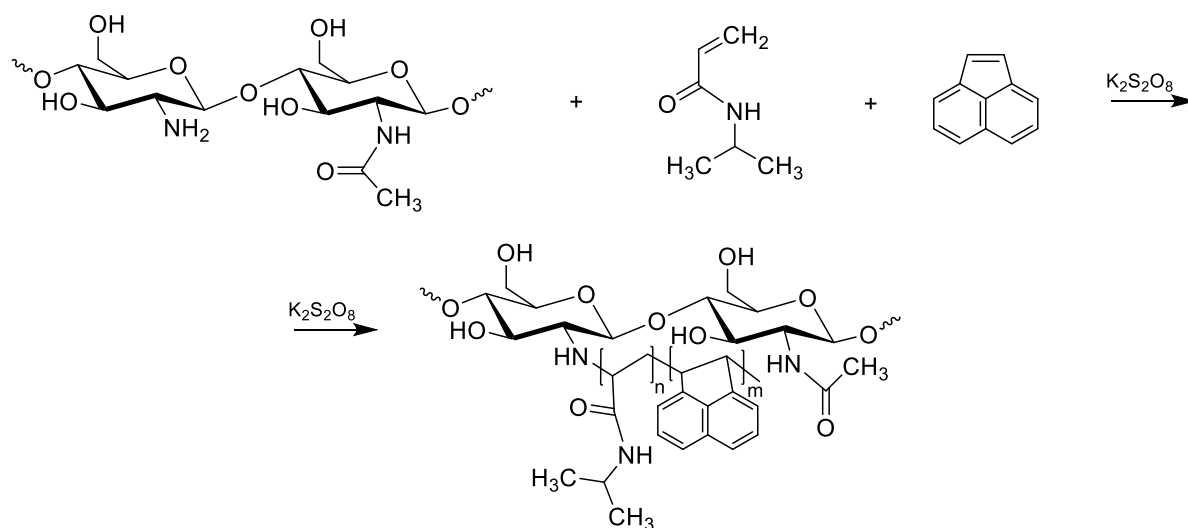


Fig. 1. Synthesis scheme of acenaphthylene labelled chitosan-*graft*-poly(*N*-isopropylacrylamide) copolymer

Table 1. Polymerisation mixture composition and reaction conditions

Copolymer sample	Molar ratio of reagents				Reaction temperature, °C	Reaction time, h	Reaction yield, %
	CS	NIPAAm	PPS	ACE			
CS- <i>g</i> -PNIPAAm-2-ACE	1	0.5	0.16	0.015	60	6	59.8
CS- <i>g</i> -PNIPAAm-6-ACE	1	5	0.16	0.06			63.6

The obtained CS-*g*-PNIPAAm-ACE copolymers were characterized by ¹H-NMR, FT-IR spectroscopy and other techniques. The thermoresponsive behavior of synthesized copolymers in aqueous solutions was determined by differential scanning calorimetry, cloud point, particle size and fluorescence spectroscopy analysis.

Acknowledgment. The financial support of the Research Council of Lithuania for the project No. S-LU-22-11 in the frame of Lithuanian–Ukrainian Cooperation Programme in the Fields of Research and Technologies is highly acknowledged.

ULTRAVIOLET-C PERSISTENT LUMINESCENCE OF $\text{Sr}_2\text{MgSi}_2\text{O}_7:\text{Pr}^{3+}$

Dace Nilova, Andris Antuzevics, Guna Doke, Guna Krieke, Pavels Rodionovs, Jekabs Cirulis, Andris Fedotovs, Uldis Rogulis

Institute of Solid State Physics, University of Latvia, Latvia

dace.nilova@cfi.lu.lv

Persistent luminescence (PersL) is a broad field of research and PersL materials are widely used in various applications. In recent years, new PersL materials with emission outside the visible range have been intensively investigated. Some potential applications require emission of high-energy radiation that can be observed in shortwave ultraviolet (UV-C) range, but suitable materials are limited.

In this study, a novel UV-C persistent phosphor shown in Figure 1 – $\text{Sr}_2\text{MgSi}_2\text{O}_7:\text{Pr}^{3+}$ – was developed. The solubility of Pr^{3+} ions in the matrix was analyzed by X-ray diffraction and the optimal concentration for efficient PersL was determined. Using photoluminescence, thermally stimulated luminescence and electron paramagnetic resonance spectroscopy methods, the optical and structural properties of this material were characterized. By summarizing the obtained results, the knowledge base on the mechanisms of PersL is expanded.

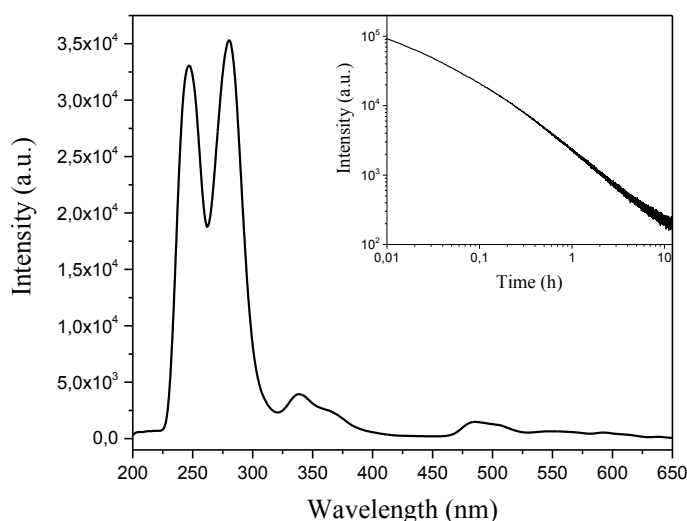


Figure 1. PersL spectra of the $\text{Sr}_2\text{MgSi}_2\text{O}_7:0.7\%\text{Pr}^{3+}$ sample irradiated for 10 min with 232 nm; inset: UV-C PersL decay kinetics of the same sample.

Latvian Council of Science, project “Defect engineering of novel UV-C persistent phosphor materials”, project No. LZP-2021/1-0118 is gratefully acknowledged.

SOLID DISPERSION SYSTEMS AS THE BASIS OF A SUCCESSFUL STRATEGY FOR IMPROVING THE BIOPHARMACEUTICAL PROPERTIES OF ACTIVE PHARMACEUTICAL INGREDIENTS

Volodymyr Yaremenko^{1,2}, Olena Ishchenko¹, Viktoriia Plavan¹

¹ Department of chemical technology and resource saving, Kyiv National University of Technologies and Design, Ukraine

² JSC Farmak, Ukraine

yaremenko.vv@knuutd.edu.ua

One of the most promising directions for optimizing the biopharmaceutical properties of drugs is the method of obtaining solid dispersion systems (SDS). SDS are bi- or multi-component systems consisting of an active pharmaceutical ingredient (API) and a carrier, and represent a highly dispersed solid phase of the API or solid solutions that form complexes with the carrier material.

The low solubility of many APIs in the aqueous environment has become one of the main challenges of pharmaceutical science, especially when it comes to oral solid dosage forms.

The solubility of API in the aqueous environment determines the possibility of effective introduction of the drug into the human body, and the solubility in non-polar solvents - the ability to pass through the lipid barrier of biological membranes. Thus, the factor of solubility in polar and non-polar environments affects the processes of introduction, subsequent transmembrane transfer of API and its overall therapeutic effectiveness [1].

Therefore, increasing the oral bioavailability of poorly water-soluble APIs is an urgent task in the development of original and generic drugs.

Currently, polymer-based SDS are considered one of the main achievements in the field of overcoming the problems of limited solubility and permeability of API.

The purpose of this review is to analyze current approaches to the creation and commercialization of solid dispersion systems and to assess the prospects for the pharmaceutical industry.

In addition to increasing API dissolution, the use of SDS allows solving a number of other applied problems in the creation of drugs:

- release modification;
- increase in chemical and physical stability;
- required pharmaco-technological properties;
- elimination of undesirable properties (side reactions, unpleasant organoleptic properties);
- the ability to bypass patent restrictions on formulation, particle size or polymorphic modifications to create generic drugs [2].

SDS can be defined as a system consisting of a hydrophobic or sparingly soluble API dispersed in a hydrophilic carrier medium. The role of the carrier is usually performed by pharmaceutically acceptable water-soluble or hydrophilic polymers (polyethylene glycol, polyvinylpyrrolidone, cellulose derivatives, and others). Optionally, surfactants can be included in these systems [3].

Industrial technologies on the basis of which solid dispersed systems can be obtained - hot melt extrusion, dissolution and solvent removal, solvent removal by spray drying, production of systems in a fluidized bed, production of systems by high shear granulation, high energy mixing (KinetiSol[®]).

Currently, there are more than 30 drugs using SDS based on pharmaceutically acceptable polymers, which are available on the market and are approved by the US Food and Drug Administration (FDA). Although the first drugs using SDS were commercialized in the 70s of the last century, by 2010 only about 10 such drugs were known, and in recent years there has been a significant increase in the number of such products [4]. In view of the significant scientific capacity and complexity in terms of technological, physico-chemical and regulatory aspects of implementation, the lion's share of commercialized SDS is represented by the flagship companies of the pharmaceutical market (Pfizer, Merck, Janssen, Bayer, Novartis), which definitely confirms the prospects for the development of this direction [5].

Use of SDS is relevant for pharmaceutical science and practice. The implementation of such an approach in the creation of drugs provides opportunities for improving their biopharmaceutical properties and significantly expands opportunities and competitiveness.

[1] Xingwang Z., Huijie X., Yue Z., Zhiguo M. Pharmaceutical Dispersion Techniques for Dissolution and Bioavailability Enhancement of Poorly Water-Soluble. *Pharmaceutics* **10**(3), 74 (2018).

[2] Vasconcelos T., Marques S., das Neves J., Sarmiento B. Amorphous solid dispersions: Rational selection of a manufacturing process. *Adv. Drug Deliv. Rev.* **100**, 85 – 101 (2016).

[3] Smruti P. C., Rohit P. D. Application of surfactants in solid dispersion technology for improving solubility of poorly water soluble drugs. *Vol. 41*, 68-77 (2017).

[4] Zhan J., Han R., Chen W., Zhang W. Analysis of the Literature and Patents on Solid Dispersions from 1980 to 2015. *12*, **23** (7) (2018).

[5] Deck K. T., Daniel A. D. Jr., 2 Dave A. M. (2020). Innovations in Thermal Processing: Hot-Melt Extrusion and KinetiSol[®] Dispersing. *AAPS PharmSciTech*, **21** (8), 312 (2020).

ELECTROSPINNING POSSIBILITIES OF KERATIN MODIFIED WITH HERBAL EXTRACTS AND SILVER NANOPARTICLES

Ugnė Zasčiurinskaitė¹, Akvilė Andziukevičiūtė-Jankūnienė¹, Aistė Balčiūnaitienė², Jonas Viškelis², Erika Adomavičiūtė¹, Virgilijus Valeika³, Virginija Jankauskaitė¹

¹Kaunas University of Technology, Studentu st 56, Kaunas 51424, Lithuania, ugne.zaschiurinskaite@ktu.edu

²Lithuanian Research Centre for Agriculture and Forestry, Institute of Horticulture, 54333 Babtai, Lithuania

³Kaunas University of Technology, Radvilenu st.t 19, Kaunas 51424, Lithuania

The function of the skin is to provide a protective barrier against mechanical, thermal and physical injury, and hazardous substances. Different types of medical dressings are used to facilitate and accelerate wound healing. Bioactive dressings are mainly made from natural or artificial biomaterials (collagen, keratin, etc.) and ensure biocompatibility and non-toxicity. Bioactive dressings initiate the synthesis of fibroblasts, accelerate endothelial migration, and determine more rapid wound healing. Their effectiveness can be enhanced by biologically active additives such as extracts of various medicinal plants. Frequently, herbal extracts alone do not have sufficient antibacterial activity. Their effect on wound healing can be enhanced by addition of silver nanoparticles synthesized using such herbal extracts [1]. For wound healing suitable high surface porosity nonwoven fabric, which ensures moisture and air perviousness, can be obtained by electrospinning. Due to its high specific surface area, electrospun nonwoven fabric can absorb a large amount of wound secreted exudate and protect wound from dehydration [2,3].

The aim of this research was to study the structure and antibacterial activity of electrospun keratin based nonwoven materials modified with biosynthesized silver nanoparticles.

Polyethylene oxide (PEO) and the powder of hydrolyzed keratin (KH) were used to prepare water-based compositions for electrospinning. “Green” silver nanoparticles (AgNPs), synthesized using *Calendula officinalis* and *Matricaria chamomilla* blossoms extracts were chosen. Herbal extracts alone showed slight antibacterial activity against Gram-positive bacteria (tested Gram-negative bacteria were resistant to used herbal extracts), while, biosynthesized AgNPs had a pronounced antibacterial effect against tested pathogenic bacteria strains. A small amount of biosynthesized AgNPs dispersion (5 %) only slightly decreases the viscosity of the keratin hydrolysate, but higher amount of dispersion ($c=15\%$) markedly reduces hydrolysate viscosity (down to 43 %) and conductivity (down to 3.5 %). These parameters affect the diameter of the electrospun keratin nano-microfibers (Fig. 1).

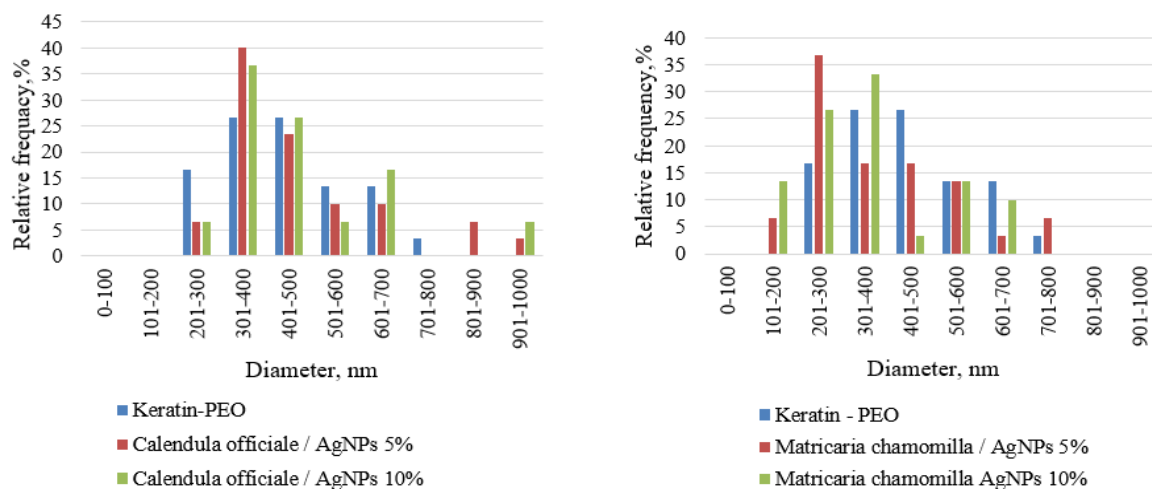


Fig. 1. Polymer composition influence on micro/nanofibers diameter distribution

Nano-microfibers diameter and its distribution depend on the amount of herbal extract additives. While 5-10 % of biosynthesized AgNPs have no significant effect on the morphology of the nonwoven material, 15 % additives significantly reduce the viscosity of the composition and make it unsuitable for the electrospinning of nano-microfibres. Thus, keratin solution with a viscosity greater than 170 mPa·s should be used for mats electrospinning.

Acknowledgments. This work was supported by the Research Council of Lithuania [grant number P-SV-22-73].

[1] Niculescu, A.-G.; Grumezescu, A.M. (2022). An up-to-date review of biomaterials application in wound management. *Polymers*, 14(3), 421.

[2] KONOP, Marek; RYBKA, Mateusz; DRAPAŁA, Adrian. Keratin biomaterials in skin wound healing, an old player in modern medicine: a mini review. *Pharmaceutics*, 2021, 13.12: 2029.

[3] Buivydiene, D. (2020). Formation of fibrous materials for air filtration applications via melt electrospinning. PhD dissertation (Kauno technologijos universitetas), 3-4.

EXPLORING THE STRUCTURE AND DYNAMICS OF CAVITAND – ALKANE COMPLEXES USING QM AND MD METHODS

Benjamins Malmiga¹, Kęstutis Aidas²

¹Faculty of Chemistry and Geosciences, Vilnius University, Lithuania

²Institute of Chemical Physics, Faculty of Physics, Vilnius University, Lithuania

benjamins.malmiga@chgf.stud.vu.lt

Cavitands are container-shaped molecules that are a big part of supramolecular chemistry and are a point of interest particularly for their host-guest interactions. The formations of these host-guest complexes are determined by non-covalent interactions and thus bear a resemblance to biological structures such as enzymes where the binding sites utilize said interactions to confine and orient molecules for reactions that are unfeasible in standard conditions [1]. Such is also the case with cavitands – the container-like structures allow for the orientation of reagents, the host molecule can separate the guest molecule from the surrounding solvent, for example, resorcinarene cavitands form capsule-like dimer structures and the resulting capsule itself acts as a solvent thus influencing the solubility of the reagent [2][3]. These interactions make cavitands relevant in drug delivery systems, chemical synthesis, etc.

The cavitand introduced by de Mendoza is a cup-shaped molecule that contains four 2-benzimidazolone (cyclic carbamide) bridges that enable the cavitand to form dimers via hydrogen bonding [4]. The base of the “cup” is composed of four benzene rings, connected together by alkane bridges, which (in the work by Zhang et. al.) have pyridine “feet” attached to them [5]. This particular cavitand containing pyridine feet demonstrates good solubility in water making it useful for manipulating hydrophobic compounds in water solutions. Furthermore, NMR spectra done by Zhang et. al., indicate that alkanes take up a bent “U” or “J” conformation. Also, the cavitand has been shown to form complexes with drugs and bind to ghrelin.

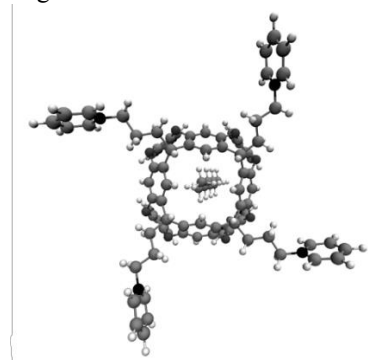


Fig. 1. Complex viewed from below, visible C_{4v} symmetry and n-octane.

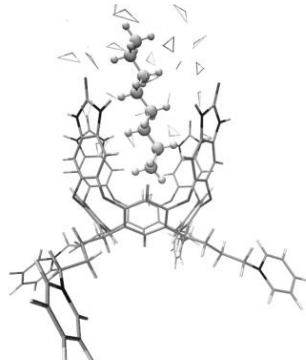


Fig. 2. Complex in water box, the first step of equilibration at 30K, water molecules observed inside of the cavitand.

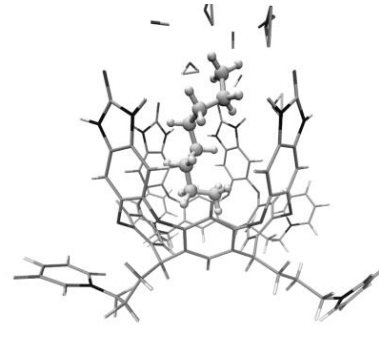


Fig. 3. Complex after equilibration, during simulation, no water observed molecules inside the “cup”.

In this work, classical MD simulations of the octane molecule confined within the supramolecular cavitand were performed aiming to evaluate the intermolecular structure of the complex in aqueous solution. The initial geometry of the cavitand monomer was created and optimized using Gaussian, utilizing the HF/6-31+G* basis set and achieving C_{4v} symmetry followed by analogous construction of the octane molecule, creating a host-guest complex where the guest is a straight n-octane (C_s symmetry) (Fig. 1 & 2). The complex was placed in a periodic box of water molecules and the subsequent steps of energy minimization and equilibration were achieved using AMBER. The equilibration was done under constant pressure, raising the temperature to 298K, achieving standard conditions. The equilibration steps as well as a longer simulation has demonstrated the ability of the host to separate the water molecules from the hydrophobic guest and allow slight conformational changes (Fig. 3). Our MD simulations show the formation of a stable complex between the octane and cavitand molecules. A linear all-trans conformation of octane was observed in the cavitand complex.

Acknowledgement. Computations have been performed on the resources provided by the high-performance computing center “HPC Saulėtekis” of Vilnius University.

[1] Moran et. al., Cavitands: Synthetic Molecular Vessels, *Journal of the American Chemical Society* 104 (21), 5826-5828 (1982)

[2] Ajami et. al., Social Isomers of Picolines in a Small Space, *Chemistry* vol. 19,50 (2013).

[3] Tzeli et. al., Theoretical Study of Hydrogen Bonding in Homodimers and Heterodimers of Amide, Boronic Acid, and Carboxylic Acid, Free and in Encapsulation Complexes, *Journal of the American Chemical Society* vol. 133, no 42, pp. 16977-16985 (2011).

[4] Ebbing et. al., Resorcinarenes with 2-Benzimidazolone Bridges: Self-aggregation, Self-Assembled Dimeric Capsules, and Guest Encapsulation, *Proceedings of the National Academy of Sciences*, vol. 99, no. 8, pp. 4962-4966 (2002).

[5] Zhang et al., Complexation of Alkyl Groups and Ghrelin in a Deep, Water-Soluble Cavitand, *Chem. Commun.*, vol. 50, no. 38, pp. 4895-4897 (2014)

IMPACT OF MICROSECOND PULSED ELECTRIC FIELDS ON ENDOPLASMIC RETICULUM MEMBRANE PERMEABILIZATION

Virginija Siaurusevičiūtė¹, Viktorija Juščenko¹, Gintarė Dalmantaitė¹, Aušra Baradoke², Arūnas Stirke¹

¹ Laboratory of Bioelectrics, State Research Institute Center for Physical Sciences and Technology, Lithuania

² State Research Institute Center for Physical Sciences and Technology, Lithuania

virginija.siauruseviciute@gmail.com

Nanosecond pulses have traditionally been employed for the permeabilization of intercellular organelle membranes, however, the application of this technique can be challenging. An alternative approach is the use of microsecond pulsed electric fields (μ sPEF) which provide the capability to regulate cytosolic signaling molecules such as calcium (Ca^{2+}) concentrations. The increase in cytosolic Ca^{2+} has been shown to alter gene expression through the activation of Ca^{2+} -responsive transcription factors [1]. Thus, μ sPEF may serve as an external gene expression inducer in gene therapy by inducing Ca^{2+} influx.

In this study, we aimed to achieve ion influx through electropermeabilization of the endoplasmic reticulum (ER). Previous literature has indicated that the ER can be permeabilized by 100 μ s PEF without adverse effects on cell viability [2]. To facilitate electropermeabilization, the extracellular conductivity was altered by modifying the extracellular medium composition. 100 μ s and 1 Hz electric pulses were generated to disrupt intracellular organelle membranes. Cytosolic Ca^{2+} concentration changes were used as a marker for ER permeabilization. The increase in cytosolic Ca^{2+} concentration was observed in the HEK 293 cell line using fluorescence microscopy with the fluorescent calcium detection reagent Fluo-4. Furthermore, live cell impermeant SYTOXTM Green, a fluorescent nucleic acid stain, indicated that 0.6 kV/cm μ sPEF caused plasma membrane damage.

Our results demonstrate that μ sPEF treatment leads to an increase in cytosolic Ca^{2+} concentration, however, further studies are required to confirm the source of this increase by blocking specific Ca^{2+} transport system components. This study highlights the potential of easily applied microsecond pulses as a modulator of signaling molecule concentrations in gene therapy.

[1] Thiel G, Schmidt T, Rössler OG. Ca^{2+} Microdomains, Calcineurin and the Regulation of Gene Transcription. *Cells*. 2021 Apr 12;10(4):875.

[2] Hanna, H., Denzi, A., Liberti, M. *et al.* Electropermeabilization of Inner and Outer Cell Membranes with Microsecond Pulsed Electric Fields: Quantitative Study with Calcium Ions. *Sci Rep* 7, 13079 (2017).

Overview of the first LHCb Open Data Release

Mindaugas Šarpis¹

¹University of Bonn, Germany
mindaugas.sarpis@cern.ch

LHCb collaboration is releasing research-quality data to the public for the very first time. A data sample amounting to 200TB has been obtained in 2011 and 2012 during the Run I of the Large Hadron Collider. The data is acquired by the LHCb detector by recording the information of proton collisions in the LHC.

The data has undergone a preprocessing step where physics objects, such as the trajectories of charged particles, were reconstructed from the raw information delivered by the complex detector system. The data is filtered and classified according to 300 physical processes and decays. The data is made available in the same format as is used internally by the LHCb physicists and is accompanied by extensive metadata and documentation, as well as a Glossary explaining several hundred special terms used in the preprocessing. The data can be analyzed using dedicated LHCb software, which is open-source.

In this talk, the overview of LHCb detector as well as released data will be given.

PERSONAL EXPOSURE AND DEPOSITION OF BLACK CARBON ON HUMAN LUNGS IN VILNIUS, LITHUANIA

Abdullah Khan, Lina Davulienė, Sergej Šemčuk, Kamilė Kandrotaitė, Agnė Minderytė, Mehri Davtalab, Ieva Uogintė, Martynas Skapas, Vadimas Dudoitis, Julija Pauraitė, Inga Garbarienė, and Steigvilė Byčenkienė

¹ SRI Centre for Physical sciences and technology, Saulėtekio Ave. 3, Vilnius, Lithuania

² Faculty of Physics, Vilnius University, Universiteto str. 3, LT-01513 Vilnius, Lithuania
abdullah.khan@ftmc.lt

The black carbon (BC) mass concentration values for urban areas are not available from standard air quality monitoring networks in many countries because BC is not currently regulated by the EU Air Quality Directive or WHO [1][2]. The urban environments are very complex due to the different emission sources and their emission activities; therefore, a combination of mobile and stationary measurements allows for a better understanding of the dynamics of BC, whose spatial variation is larger than that of PM_{2.5}—the EU air quality standard. In this study, real-time measurements of BC mass concentrations were performed in an office and on a daily commute to assess work-related personal exposure to BC deposition in the lungs of a participant. The study was conducted in Vilnius, Lithuania, in the spring of 2022. Mobile measurements at the street level showed that the BC mass concentrations were the highest during peak hours, reaching up to 7.14 μg/m³ at hotspots. The hourly mean of the BC mass concentration in March 2022 at the urban background station ranged from 0.30 to 9.01 μg/m³, with traffic-related BC (BC_{tr}) accounting for 66% of the total BC mass concentration.

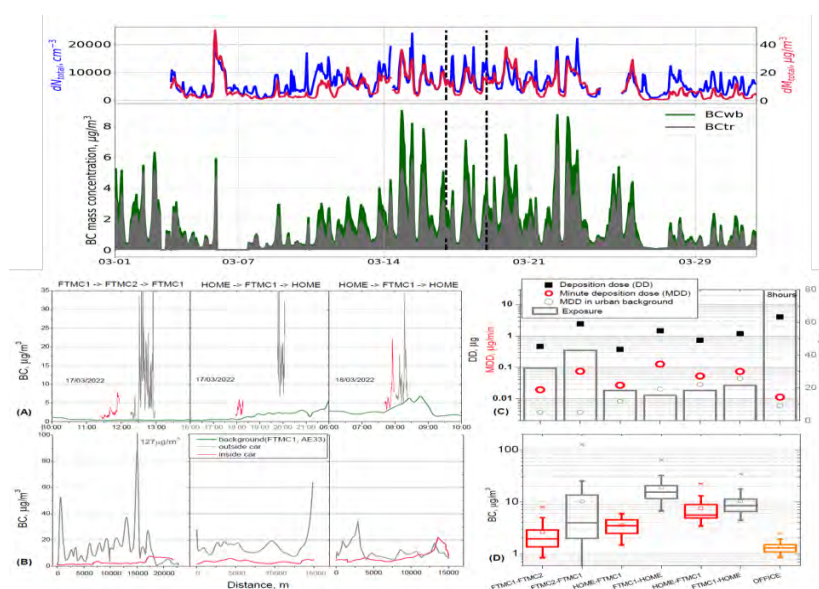


Fig. 1 Time series of total particle number (Ntotal) and mass concentrations (Mtotal) of 10–430 nm aerosol particles from SMPS measurements at the urban background site (FTMC1) in March 2022, (b) deposition dose during commuting and inside the office.

The results of the multi-path particle dosimetry model show that the minute deposition dose of BC (MDD_{BC}) during the working day (including during commuting and office hours) was the highest in the morning rush hour at 52 ng/min and in the evening at 26 ng/min, demonstrating the influence of traffic exhaust emissions on aerosol particles, especially on fine particles. Significant differences were found between the MDD_{BC} in the office and a vehicle. The deposition dose indicates that daily BC exposure in vehicles during commuting could account for up to one-third (2.5) of the work-related exposure of office workers, depending on how much time they spend commuting to work. The distribution of the MDD_{BC} in the human respiratory tract had a maximum in the pulmonary region ranging from 5.1 ng/min in the office to 19.9 ng/min in the car during the morning drive.

Acknowledgment: This research was funded by a grant (No. S-MIP-20-28) from the Research Council of Lithuania.

[1] Viana, Mar, et al. "Particle number (PNC) and black carbon (BC) in European urban air quality networks." ETC/ACM Technical Paper 6 (2012).
 [2] Burki, Talha. "WHO introduces ambitious new air quality guidelines" The Lancet 398.10306 (2021): 1117.

MOLECULARLY IMPRINTED POLYMER-BASED BIOSENSORS FOR THE DETECTION OF ALZHEIMER'S DISEASE BIOMARKERS

Greta Pilvenytė¹, Raimonda Bogužaitė¹, Vilma Ratautaitė^{1,2}, Arūnas Ramanavičius^{1,2}

¹ Laboratory of Nanotechnology, State Research Institute Center for Physical Sciences and Technology, Sauletekio av. 3, Vilnius LT-10257, Lithuania.

² Department of Physical Chemistry, Institute of Chemistry, Faculty of Chemistry and Geosciences, Vilnius University, Naugarduko str. 24, Vilnius LT-03225 Lithuania
greta.pilvenyte@ftmc.lt

According to the World Health Organization, neurodegenerative diseases such as Alzheimer's disease, Parkinson's disease, and other neurological disorders will become the second leading cause of death by 2040 [1]. Early detection and treatment may improve symptoms, relieve pain, and increase mobility, and quality of life. Proteins such as amyloid- β peptides, and phosphorylated-Tau are biomarkers of Alzheimer's disease can be used for the detection of this disease at an early stage of pathogenesis.

The accurate diagnosis of Alzheimer's disease is complicated and routinely performed by invasive, time-consuming, and expensive analysis like cerebrospinal fluid analysis or neuroimaging techniques. However, obvious limitations, such as the need for trained personnel, expensive instruments, complicated procedures, and long detection times, prevent the widespread use of these methods.

Therefore, new detection techniques such as MIP-based electrochemical sensors are being developed, providing a wide range of possibilities for the development of biosensors. MIP-based electrochemical biosensors are devices built with a transducer and recognition element with an imprinted polymer to determine the presence of an analyte. The main advantages of MIP-based electrochemical sensors are low-cost, easy preparation, advanced storage stability, and quick read-out time [2]. The ability to imprint template molecules at room temperature without denaturation or conformational changes is a major feature of MIP-based sensors [3]. Electrochemical biosensors also offer the advantage of detecting various biomarkers in complex biological fluids such as blood, saliva, and urine [2, 4-8].

To improve the selectivity and sensitivity of biosensors, various semiconductor structures such as copper oxide [6], multi-walled carbon nanotubes, delaminated titanium carbide MXenes [7] are being developed, but conducting polymers are most commonly used [3-4, 7]. Among the many conducting polymers, such as polyaniline, polythiophene, and poly(3,4- ethylenedioxythiophene), polypyrrole is one of the most suitable for molecular imprinting [2, 3].

This presentation reviews recent advances in the design of MIP-based biosensors for the detection of Alzheimer's disease biomarkers such as amyloid- β peptides [4, 7] and phosphorylated-Tau protein [8].

[1] K. Gammon, Neurodegenerative disease: Brain windfall, *Nature* 515(7526) (2014) 299-300. <https://doi.org/10.1038/nj7526-299a>.

[2] S. Ramanavicius, A. Jagminas, A. Ramanavicius. Advances in Molecularly Imprinted Polymers Based Affinity Sensors (Review). *Polymers* 13, 974 (2021). <https://doi.org/10.3390/polym13060974>.

[3] D. Plausinaitis, L. Sinkevicius, U. Samukaite-bubniene, V. Ratautaitė, Evaluation of electrochemical quartz crystal microbalance based sensor modified by uric acid-imprinted polypyrrole, *Talanta*. 220 (2020) 121414. <https://doi.org/10.1016/j.talanta.2020.121414>.

[4] S. Ramanavicius, U. Samukaite-Bubniene, V. Ratautaitė, M. Bechelany, A. Ramanavicius. Electrochemical molecularly imprinted polymer based sensors for pharmaceutical and biomedical applications (review). *J. Pharm. Biomed. Anal.*, 215, 114739 (2022). <https://doi.org/10.1016/j.jpba.2022.114739>.

[5] S. Zukauskas, A. Rucinskiene, V. Ratautaitė, A. Ramanaviciene, G. Pilvenyte, M. Bechelany, A. Ramanavicius. Electrochemical Biosensor for the Determination of Specific Antibodies against SARS-CoV-2 Spike Protein. *Int. J. Mol. Sci.* 2023, 24, 718. <https://doi.org/10.3390/ijms24010718>.

[6] F.T.C. Moreira, B.A.G. Rodriguez, R.A.F. Dutra, M.G.F. Sales, Redox probe-free readings of a β -amyloid-42 plastic antibody sensory material assembled on copper@carbon nanotubes, *Sens. Actuat. B-Chem.*, 264 (2018) 1-9. <https://doi.org/10.1016/j.snb.2018.02.166>.

[7] N. Özcan, H. Medetalibeyoglu, O. Akyıldırım, N. Atar, M.L. Yola, Electrochemical detection of amyloid- β protein by delaminated titanium carbide MXene/multi-walled carbon nanotubes composite with molecularly imprinted polymer, *Materials Today Communications*, 23 (2020) 101097. <https://doi.org/10.1016/j.mtcomm.2020.101097>.

[8] A. Ben Hassine, N. Raouafi, F.T.C. Moreira, Novel Electrochemical Molecularly Imprinted Polymer-Based Biosensor for Tau Protein Detection, *Chemosensors*, 9 (2021) 238. <https://doi.org/10.3390/chemosensors9090238>.

MODELING CAROTENOID-CHLOROPHYLL COMPLEXES WITH MOLECULAR DYNAMICS

Justyna Kalaševska¹, Mindaugas Macernis¹

¹Vilnius University, Faculty of Physics, Institute of Chemical Physics, Saulėtekio al. 3, LT-10257 Vilnius
justyna.kalasevska@ff.stud.vu.lt

Photosynthetic antenna complexes gather solar energy in the form of molecular excitations. Photosynthetic systems based on molecular structures and understanding their functions remains a grand challenge. It is important to study dynamic properties of the excited states of carotenoids and chlorophylls for understanding the mechanism of photosynthesis and it could be done by using molecular dynamics [1,2]. Thus, it is important to study such molecular systems by using molecular dynamics (MD) approaches.

The main challenge in MD is to solve the parameterization problem for Magnesium ion which is located in chlorophyll. Other problems are with preparation PDB files for MD packages. Finally in order to perform computations it isn't trivial task.

For this study it was used AMBER20 (a suite of programs for biomolecular modeling) environment, GaussView tool, WebMO environment, Swiss-Pdb program, the MCPB.py (Metal Center Parameter Builder) script was used for Mg parameterization, visualization with the VMD (Visual Molecular Dynamics) environment. Parameterization was done for geometrically optimized structures with DFT methodologies: B3LYP/cc-pVDZ and CAM-B3LYP/cc-pVDZ. The structures were taken from PDB (Protein Data Bank) database with ID 6A2W [3].

The two selected pigments - carotenoid and chlorophyll - were geometrically optimized using the GaussView tool, then parameterization of the newly created PDB files was performed in the AMBER environment, and separate attention was paid to the parameterization of the metal ion in the AMBER environment. With the help of the Swiss-Pdb program, PDB files were extracted from the calculated optimized value files, which correspond to the PDB format files accepted in the AMBER environment. Pigments parameterization, energy minimization and molecular dynamics were performed for both carotenoid and chlorophyll using the AMBER package environment. In the case of chlorophyll, the MCPB.py (Metal Center Parameter Builder) script was used for Mg²⁺ parameterization. From the molecular dynamics file of chlorophyll visualized in the VMD environment (Fig. 1), it can be seen that in the AMBER environment, using the MCPB.py method, the molecular dynamics works, but the Mg ion is completely separated from the rest of the atoms.

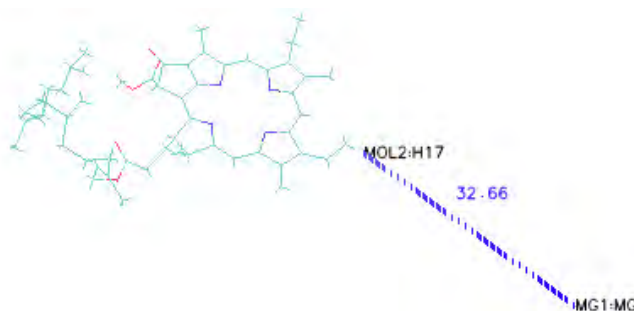


Fig. 1. Chlorophyll structure after MD simulations where it can be seen that molecular structure is not valid.

The AMBER environment only accepts PDB files of a specific format, so you need to know all AMBER requirements for PDB files to properly parameterize molecules. The AMBER environment is not designed to handle metal ions directly, so all molecules containing metal ions must be divided into separate files, parameterized separately in appropriate ways, and finally combined to perform minimization and molecular dynamics. Visualizing these files shows that in MD calculations the metal ion is separated from the chlorophyll molecule and does not come back, it is concluded that although successful managed to run MD. The main result that the AMBER MD successfully performs pure computations, but selected parametrization parameters are not accurate enough as final MD molecular structures are not valid.

Acknowledgements

Computations were performed on resources at the supercomputer "VU HPC" Saulėtekis of Vilnius University in Faculty of Physics location.

[1] K. Zakutauskaitė, M. Macernis, et al., Extracting the excitonic Hamiltonian of a chlorophyll dimer from broadband two-dimensional electronic spectroscopy. *J. Chem. Phys.* **158**(1), 015103 (2023).

[2] A. Mikalčiūtė, A. Gelzinis, et al., Structure-based model of fucoxanthin–chlorophyll protein complex: Calculations of chlorophyll electronic couplings. *J. Chem. Phys.* **156**(23), 234101 (2022).

[3] W. Wang, L.-J. YU et al., Structural basis for blue-green light harvesting and energy dissipation in diatoms. *Science* **363**(6427), eaav0365 (2019).

SYNTHESIS OF 4-AMINO-1,2,4-TRIAZOLE-3-THIONES BEARING 2-PYRIDINYLAMINO MOIETY

Aida Šermukšnytė¹, Kristina Kantminienė², Zigmuntas Jonas Beresnevičius¹, Ingrida Tumosienė¹

¹ Department of Organic Chemistry, Kaunas University of Technology, Lithuania

² Department of Physical and Inorganic Chemistry, Kaunas University of Technology, Lithuania

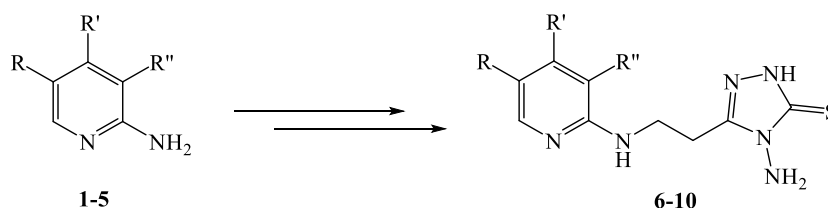
aida.sermuksnyte@ktu.edu

Heterocyclic compounds, cyclic organic compounds containing at least one heteroatom, are considered to be one of the most significant classes of organic compounds that are used in many biological fields due to their diverse activity. Nitrogen, oxygen, and sulphur are the most common heteroatoms in heterocyclic compounds. These ring systems are found as major skeletons in many natural biological molecules such as hemoglobin, DNA, RNA, vitamins, hormones, etc. Heterocyclic pharmacophores constitute the biologically active fragments of many drugs used in the treatment of different diseases. Furthermore, *N*-heterocyclic compounds exhibit a variety of biological activities such as antifungal, antibacterial, anti-inflammatory, antioxidant, anticancer, anticonvulsant, etc. [1].

The 1,2,4-triazole ring is a structural core of compounds that exhibit multidirectional biological activity and possess a variety of biological features, including anticancer action, making it one of the most important nitrogen-containing scaffolds in medicinal chemistry [2,3].

In pharmaceutical targets, pyridine and its precursor molecule dihydropyridine are among the most prevalent structural units. In plants, they are mostly found in alkaloids. Pyridine- and dihydropyridine-containing drugs constitute nearly 14% and 4% of *N*-heterocyclic drugs approved by the US Food and Drug Administration (FDA). The major therapeutic areas of focus of 18% of these drugs are infectious diseases, inflammation, the nervous system, and oncology [4]. Pyridine derivatives exhibit a variety of important pharmacological activities such as antimicrobial, antimalarial, antidiabetic, and anti-inflammatory activities [5].

This work's objective was to synthesize biologically active hybrid compounds bearing 1,2,4-triazole-3-thione and substituted pyridine moieties (Scheme 1):



R/N ^o	1, 6	2, 7	3, 8	4, 9	5, 10
R	H	H	Br	Br	Cl
R'	H	H	H	H	H
R''	H	Br	H	Br	H

Scheme 1. Synthesis of the compounds **6-10**

The target compounds **6-10** were synthesized via a two-step synthesis procedure. In the first step, the corresponding carboxylic acids were synthesized. The starting 2-aminopyridines **1-5** bearing none, one or two halogen substituents dissolved in toluene reacted with acrylic acid under reflux for 17-24 hours. The obtained carboxylic acids were melted with hydrazine hydrate at 185 °C for 5 hours to form the target 4-amino-1,2,4-triazole-3-thiones **6-10**. The structures of the synthesized molecules were proven by the data of the ¹H, ¹³C NMR, and HRMS spectra.

[1] Mermer A., Keles T. and Sirin Y. Recent studies of nitrogen containing heterocyclic compounds as novel antiviral agents: A review, *Bioorganic Chemistry*, **114** (2021).

[2] Strzelecka M. and Świątek P. 1,2,4-Triazoles as Important Antibacterial Agents, *Pharmaceuticals*, **14**(3), 224 (2021).

[3] Šermukšnytė A., Kantminienė K., Jonuškienė I., Tumosienė I., and Petrikaitė V. The Effect of 1,2,4-Triazole-3-thiol Derivatives Bearing Hydrazone Moiety on Cancer Cell Migration and Growth of Melanoma, Breast, and Pancreatic Cancer Spheroids, *Pharmaceuticals*, **15**(8), 1026 (2022).

[4] Ling Y., et al. The Expanding Role of Pyridine and Dihydropyridine Scaffolds in Drug Design, *Drug Design, Development and Therapy*, **15**, 4289–4338 (2021).

[5] Abu-Taweel G., et al. Medicinal Importance and Chemosensing Applications of Pyridine Derivatives: A Review, *Critical Reviews in Analytical Chemistry* (2022), DOI: 10.1080/10408347.2022.2089839.

DONOR-ACCEPTOR-DONOR TYPE ENAMINES FOR PEROVSKITE SOLAR CELLS

Šarūnė Daškevičiūtė-Gegužienė¹, Yi Zhang², Kasparas Rakštys¹, Marytė Daškevičienė¹, Vygintas Jankauskas³, Mohammad Khaja Nazeeruddin², Vytautas Getautis¹

¹ Department of Organic Chemistry, Kaunas University of Technology, Lithuania

² Group for Molecular Engineering of Functional Material, École Polytechnique Fédérale de Lausanne, Switzerland

³ Institute of Chemical Physics, Vilnius University, Lithuania
sarune.daskeviciute@ktu.lt

Over the recent years, organic-inorganic hybrid perovskite solar cells (PSCs) have been attracting a massive worldwide attention due to their low cost and facile fabrication. HTM is one of the quintessential components required for the efficient and stable PSC devices. The hunt is now on for new organic semiconductors that are prepared by simple, cost-effective, and green chemistry without sacrificing the efficiency [1].

In this study, a series of donor-acceptor-donor (D-A-D) type small molecules based on the fluorene and diphenylethenyl enamine units, which are distinguished by different acceptors, as hole transporting materials (HTMs) for perovskite solar cells is presented. The incorporation of the malononitrile acceptor units is found to be beneficial for not only carrier transportation but also defects passivation via Pb-N interactions.

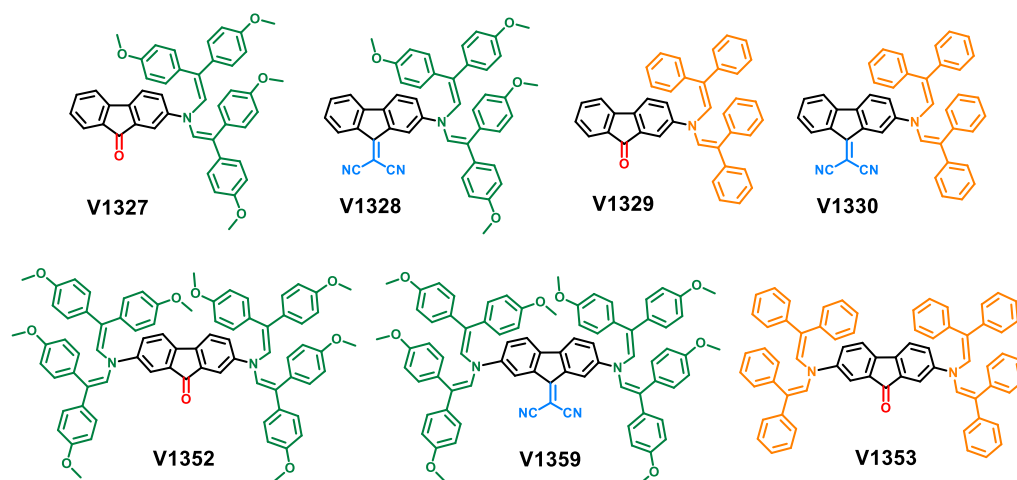


Fig. 1. Reaction scheme of fluorenone/dicianofluorenylidene enamine HTMs and their molecular structures.

The highest power conversion efficiency of over 22% is achieved on cells based on V1359, which is higher than that of spiro-OMeTAD under identical conditions. In addition, we fabricated perovskite solar mini-modules (6.5×7 cm) exhibiting efficiency of 18.6%. This shows that HTMs prepared via simplified synthetic routes are not only a low-cost alternative to spiro-OMeTAD but also outperform in efficiency and stability state-of-art materials obtained via expensive cross-coupling methods.

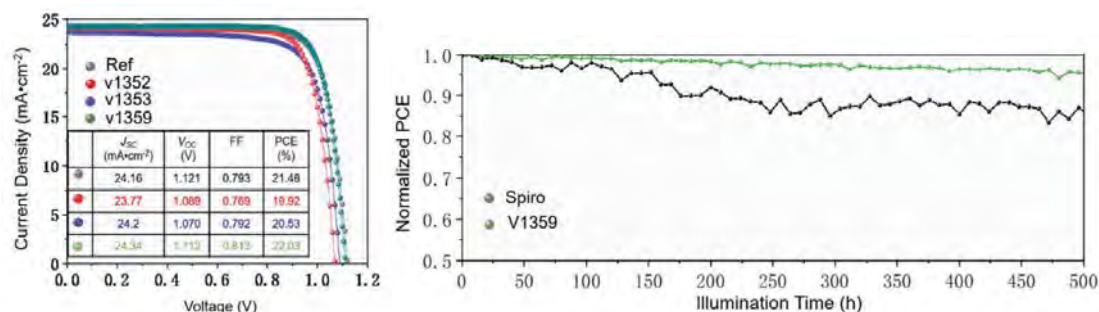


Fig. 2. J - V curves (reverse-scan) of the PSCs based on V352, V1353 and V1359 as HTMs and spiro-OMeTAD and long-term stability study shows in situ measured PCEs of the unsealed solar modules over 500 h under Ar.

[1] M. L. Petrus, A. Music, A. C. Closs, J. C. Bijleveld, M. T. Sirtl, Y. Hu, T. J. Dingemans, T. Bein and P. Docampo, *J. Mater. Chem. A*, **5** (2017) 25200–25210.

MOLECULAR DYNAMICS SIMULATIONS OF BIOMOLECULES ENCAPSULATED IN MACROMOLECULAR MATRICES

Mykolas Jerutis, Einaras Sipavičius, Kęstutis Aidas

Institute of Chemical Physics, Faculty of Physics, Vilnius University, Lithuania
mykolas.jerutis@chgf.stud.vu.lt

Macromolecular matrices are a variety of compounds that form cavities capable of complexing small molecules - these large compounds are also called cavitands. Such complexes can be used in a wide range of applications: catalysing difficult reactions, binding proteins for structural analysis, detecting various compounds, increasing the solubility of compounds. Also, molecules complexed in cavitand exhibit different properties than the ones that are not bound in this complex: these molecules can be stabilized in conformations that do not normally occur, and can participate in exotic chemical reactions. One of the molecules that can be complexed is O-(n-octanoyl)-L-serine (Fig. 1. A.), one of the amino acids in the naturally occurring hormone ghrelin. This molecule is thought to insert its aliphatic chain into the cavitand to form a stable complex. We aim to investigate the intermolecular structure of this complex, as well as the conformational equilibrium of O-(n-octanoyl)-L-serine in different media.

Experiment methods have already been carried out to analyse the complex of O-(n-octanoyl)-L-serine with cavitand (Fig. 1. C.), and hypotheses have been put forward on the structure of this complex [1]. In order to better interpret the experimental data that can be obtained while working with these compounds, it is worthwhile to use molecular dynamics simulations (MDS). This method provides information at the molecular level that is unavailable experimentally. MDS in this situation provide a significant amount of structural information in a relatively simple model. MDS were therefore carried out for two systems: one with 3000 water molecules, one molecule of O-(n-octanoyl)-L-serine and one chloride ion, and the other with 4000 water molecules, a complex of O-(n-octanoyl)-L-serine and a cavitand and five chloride ions. Structure of the cavitand and of the O-(n-octanoyl)-L-serine are shown in Figure 1. (Fig. 1. A. and B.).

The molecular dynamics simulations under NPT and NVT ensembles were followed by calculation of the radial distribution functions as well as other structural parameters. From the radial distribution functions, coordination numbers for atoms that can form hydrogen bonds have been calculated and a distinct cavitand steric effect has been observed. It was also found that the conformational changes of the aliphatic chain of the O-(n-octanoyl)-L-serine molecule are slower when it is in complex with a cavitand. Analysis of the distance between the bottom of the hydrophobic pocket of the cavitand and the last methyl of the O-(n-octanoyl)-L-serine molecule aliphatic chain confirmed the stability of the complex.

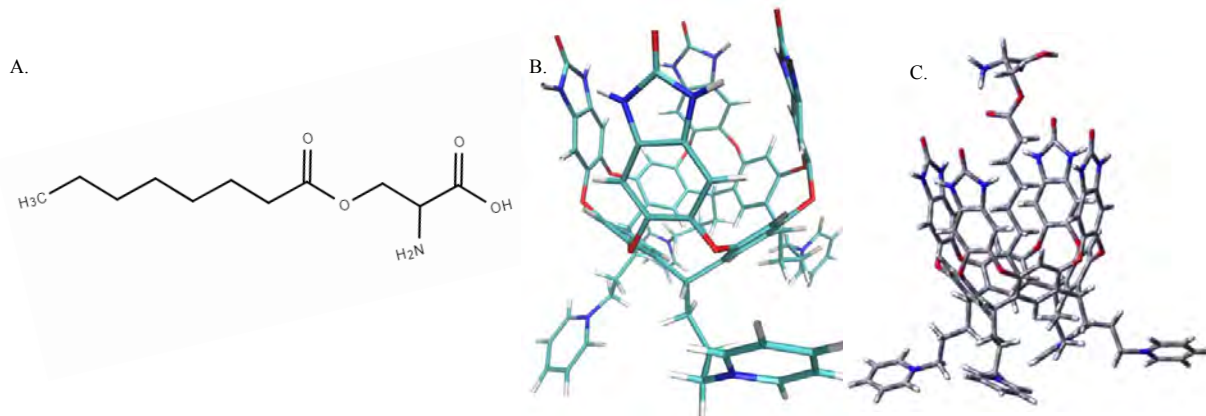


Fig. 1. Molecular structures of: A. O-(n-octanoyl)-L-serine; B. Cavitand; C. Complex of O-(n-octanoyl)-L-serine and cavitand.

Acknowledgment. Computations have been performed on the resources provided by the high-performance computing center „HPC Saulėtekis“ of Vilnius University.

[1] Zhang, K.-D., Ajami, D., Gavette, J. V., & Rebek, J. (2014). Complexation of alkyl groups and ghrelin in a deep, water-soluble cavitand. *Chem. Commun.*, 50(38), 4895–4897.

SYNTHESIS AND INVESTIGATION OF VITRIMERS FROM RENEWABLE RESOURCES

Sigita Grauželiene, Marius Kastanauskas, Jolita Ostrauskaitė

Department of Polymer Chemistry and Technology, Kaunas University of Technology, Lithuania
sigita.grauzeliene@ktu.lt

Vitrimeres are a class of polymers between thermosets and thermoplastics and therefore change their topology through a dynamic bond exchange that results in their self-healing and reprocessability [1]. This can solve the worldwide expanded manufacturing of thermosets and the fast use of fossil-based feedstocks and contribute to environmental protection. Vitrimeres with dynamic covalent bonds that have undergone the most recent research are epoxy or acryl-based and rely on reversible transesterification reactions [2,3]. Over the past five years, there has been an increase in scientific publications involving biobased vitrimeres. This draws attention from vitrimer researchers to the need to develop new biobased monomers for the synthesis of high-performance and sustainable materials. As monomers for various vitrimer synthesis reactions, functionalized triglycerides, lignin, vanillin, tannin, polysaccharides, and furan derivatives have already been used [4]. Glycerol, the main biodiesel by-product of the production from vegetable oil and animal fats, is appealing for vitrimer synthesis of vitrimeres since it has properties such as low volatility, hygroscopicity, plasticization effect, high miscibility, compatibility with a variety of materials, stability, high viscosity, and nontoxicity [5].

The aim of this research was to synthesize sustainable materials for an environmentally friendly strategy by combining the characteristics of renewable resources, glycerol, and vitrimeres. Consequently, functionalized soybean oil, glycerol, and tetrahydrofurfuryl methacrylate (Fig. 1a) in different ratios were chosen for the preparation of UV-curable resins. The conversion of acrylate double bonds was estimated by FTIR on a Bruker Vertex 70 spectrometer and the highest value was (83.8 ± 3.3) % (Fig. 1b). Stress relaxation experiments performed on an Anton Paar MCR302 rheometer revealed that after UV curing, the dynamic networks were able to rapidly undergo thermoactivated network topology rearrangements. The rigidity of the vitrimeres decreased slightly, the viscosity of the resin was reduced, and double bond conversion increased with increasing the amount of tetrahydrofurfuryl methacrylate. The synthesized vitrimeres showed reprocessability, shape memory, and self-healing properties.

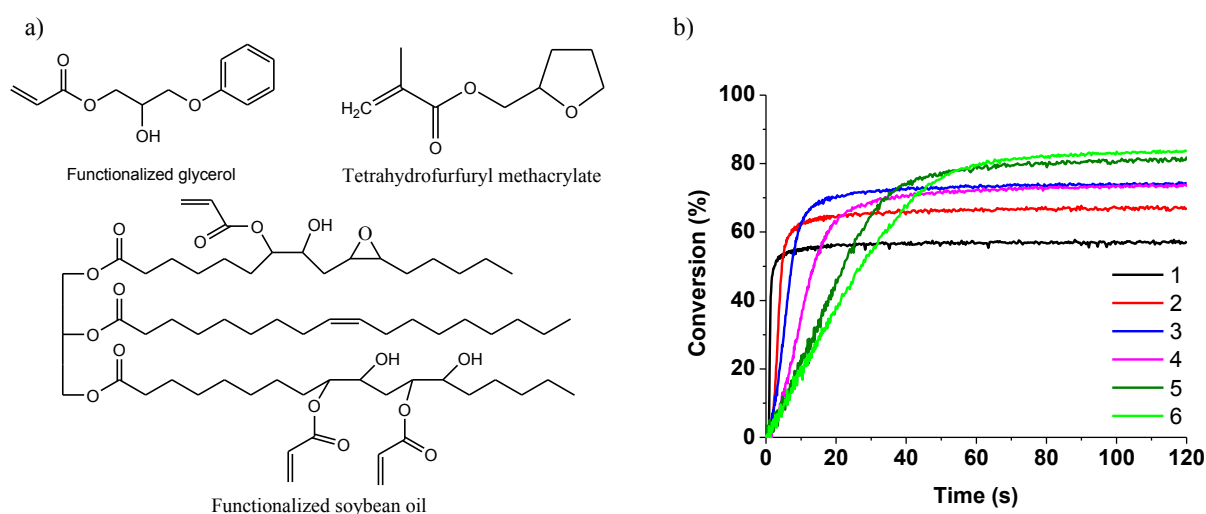


Fig. 1. Chemical structures of functionalized glycerol, soybean oil, and tetrahydrofurfuryl methacrylate (a), the conversion of acrylate double bonds (b).

Acknowledgement. This project has received funding from European Social Fund (project No. 09.9.9-LMT-K-712-23-0088) under a grant agreement with the Research Council of Lithuania (LMTLT).

- [1] W. Post, A. Susa, R. Blaauw et al., A Review on the Potential and Limitations of Recyclable Thermosets for Structural Applications, *Polymer Reviews* **60**, 359-388 (2020).
- [2] H. Memon, Y. Wei, C. Zhu, Recyclable and reformable epoxy resins based on dynamic covalent bonds—Present, past, and future, *Polymer Testing* **105**, 107420 (2022).
- [3] H. Zhang, J. Cui, G. Hu, B. Zhang, Recycling strategies for vitrimeres, *International Journal of Smart and Nano Materials* **13**(3), 367-390 (2022).
- [4] M. A. Lucherelli, A. Duval, L. Avérous, Biobased vitrimeres: towards sustainable and adaptable performing polymer materials, *Progress in Polymer Science* **127**, 101515 (2022).
- [5] M. R. Monteiro, C. L. Kugelmeier, R. S. Pinheiro, M. O. Batalha, A. da Silva César, Glycerol from biodiesel production: Technological paths for sustainability, *Renewable and Sustainable Energy Reviews* **88**, 109-122 (2018).

DYNAMIC HOT EMBOSsing PROCESS OF MICROSTRUCTURES FORMATION

Justas Ciganas¹, Giedrius Janušas¹

¹ Department of Mechanical Engineering, Kaunas University of Technology, Lithuania
justas.ciganas@ktu.lt

Hot embossing molding technology is widely used in the plastic molding process. Thermoplastic polymers are heated to the glass transition temperature and the mold starts the embossing process, then the matrix is cooled, and the demolding procedure is performed [1]. By including dynamic (vibration-assisted) conditions in the forming process, a viscoelastic material with multiple relaxations can be obtained [2]. Vibrations could also improve the flow of plastic into the mold.

To form a dynamic hot embossing forming environment, it should have three main components: a heating element, a pressure element, and a vibration element [3]. In this experiment, heating and vibration were created by using a magnetostrictive device, the technological part is patented by the European patent K158-89 EP and the Lithuanian patent K158-89. The tensile "Tinius Olsen" test machine was used to create the pressure force. Polyvinyl chloride (PVC) plastic was chosen for molding process. Using vibration-assisted hot embossing molding technology, a microstructure was obtained on a 4 mm thick sheet. Various molding parameters that may affect the molding process were tested: temperature, load, vibration frequency and amplitude. The quality of the resulting structure was analyzed using the diffraction method. After being illuminated with green (525 nm) laser light, the light was split into diffraction maxima. The data are arranged in order and presented in Figure 1.

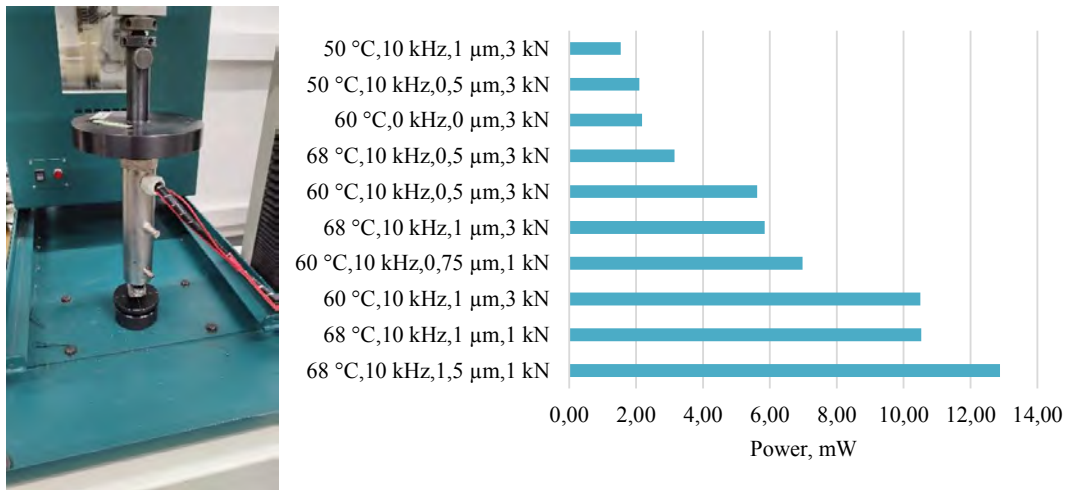


Fig. 1. Magnetrostriktorius įstatytas į "Tinius Olsen" test machine and diffraction efficiency measurement results

During the research, the most approximate conditions for the formation of microstructures were determined. Also, it was found that using hot embossing technology without vibrations, a lower quality microstructure was obtained, comparing vibration-assisted hot embossing molding technology.

[1] B. Saha, W. Quan Toh, E. Liu et. al., A review on the importance of surface coating of micro/nano-mold in micro/nano-molding processes, Journal of Micromechanics and Microengineering, 26-1 (2015).
[2] R. Šakalys, G. Janušas, A. Palevičius et. al., Microstructures replication using high frequency excitation, Microsystem Technologies 22, 1831-1843 (2016).
[3] L. Nguyen, Ultrasonic Vibration-Assisted Hot Glass Embossing Process (Noise and Vibration Control - From Theory to Practice, 2019).

TRIPHENYLETHENE-CARBAZOLE DERIVATIVES FOR AGGREGATION-INDUCED EMISSION IN OLEDs

Gintare Krucaite², Cheng-Yung Ho^{1,3}, Raminta Beresnevičiute², Dovydas Blazevičius², Wei-Han Lin¹, Jhao-Cheng Lu¹, Chang-Yu Lin³, Saulius Grigalevičius², Chih-Hao Chang¹, Ernestas Zaleckas⁴

¹Department of Electrical Engineering, Yuan Ze University, Chung-Li, 32003 Taiwan.

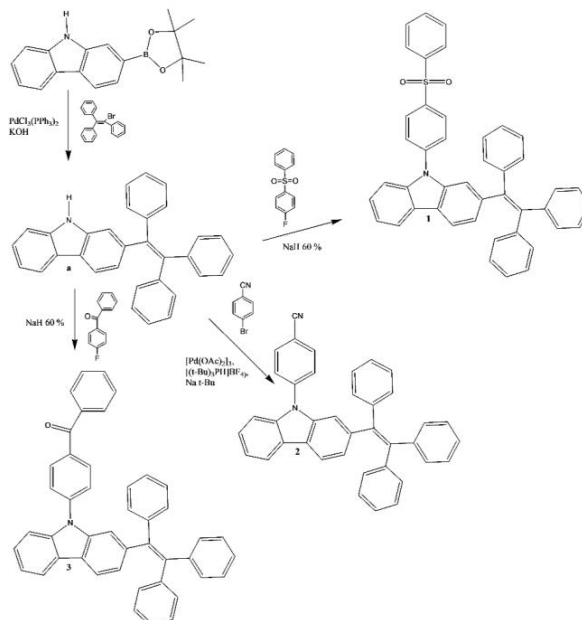
²Department of Polymer Chemistry and Technology, Kaunas University of Technology, Lithuania.

³Department of Mechanical Engineering, Chung Yuan Christian University, Chung-Li, 32023 Taiwan.

⁴Vytautas Magnus University, Agriculture Academy, Department of Agricultural Engineering and Safety, Lithuania. gintare.krucaite@ktu.lt

Organic light-emitting diodes (OLEDs) are becoming increasingly popular for use in display or phototherapy lighting applications due to their various advantages such as high-quality color, low energy cost, light weight, and flexibility. Among the potential molecular structures in blue-emitting aggregation-induced emission (AIE) compounds, tetraphenylethene has been shown to be an effective core molecule for generating excellent AIE [1-3].

Synthesis of compounds **1-3** with different substitutions are shown in Scheme 1. The photophysical, thermal, and electroluminescence characteristics of the designed emitters were investigated to clarify the molecular structure-property-performance relationship.



Scheme 1. Synthesis of the triphenylethylene based compounds.

The doped blue-emitting OLED with compound **2** exhibited satisfactory peak efficiency of 8.7 cd/A and high maximum luminance of 18474 cd/m². The fabricated white-emitting OLEDs with **2** achieved a maximum efficiency of 5.6% (8.0 cd/A and 7.5 lm/W). These results indicate that the triphenylethene-carbazole structure designs for AIE molecules could simultaneously harvest wide energy bandgap and high luminance, demonstrating their high potential for EL applications.

Acknowledgements. This work was supported by project funded by the Research Council of Lithuania (grant No. S-MIP-22-84).

References

- [1] Z. Zhao, J.W.Y. Lam, B.Z Tang, *Tetraphenylethene: a versatile AIE building block for the construction of efficient luminescent materials for organic light-emitting diodes*, *J Mater Chem* **22**, 23726-23740 (2012).
- [2] J. Huang, N. Sun, Y.Dong et al., *Similar or Totally Different: The Control of Conjugation Degree through Minor Structural Modifications, and Deep-Blue Aggregation-Induced Emission Luminogens for Non-Doped OLEDs*, *Adv Funct Mater* **23**, 2329-2337 (2013).
- [3] C.Y.K. Chan, J.W.Y. Lam, Z. Zhao et al., *Aggregation-induced emission, mechanochromism and blue electroluminescence of carbazole and triphenylamine-substituted ethenes*, *J Mater Chem C* **2**, 4320-4327 (2014).

MULTIFUNCTIONAL BICARBAZOLE-BASED TWISTED D-A-D DERIVATIVES FOR BLUE AND GREEN OLEDs

Dovydas Blaževičius¹, Gintarė Kručaitė¹, Daiva Tavgenienė¹, Saulius Grigalevičius¹, Prakalp Gautam², Shahnawaz Shahnawaz², Iram Siddiqui², Jwo-Huei Jou²

¹ Department of Polymer Chemistry and Technology, Kaunas University of Technology, Lithuania

² Department of Materials Science and Engineering, National Tsing Hua University, Taiwan

dovydas.blazevicius@ktu.lt

Organic light-emitting diodes (OLEDs) technology has outperformed other technologies in recent decades [1]. OLEDs are the ultimate technology for display and are stepping rapidly into lighting. At present, there is an intensive need for high-performance deep-blue emitters in full-color display and solid-state lighting [2]. However, as the emission peaks shift towards the deep-blue region, the nonradiative transition rate of metal d-orbitals tends to increase, making it difficult to achieve a high efficiency altogether [3]. To solve the problem, small-molecules fluorescent materials have re-gained attention due to their high color purity and low cost [4]. The synthesis of bicarbazole-based host materials was carried out by the three-step synthetic route as shown in Figure 1. Herein, we introduce a series of donor-acceptor-donor (D-A-D) twisted derivatives based on carbazole-benzophenone moieties.

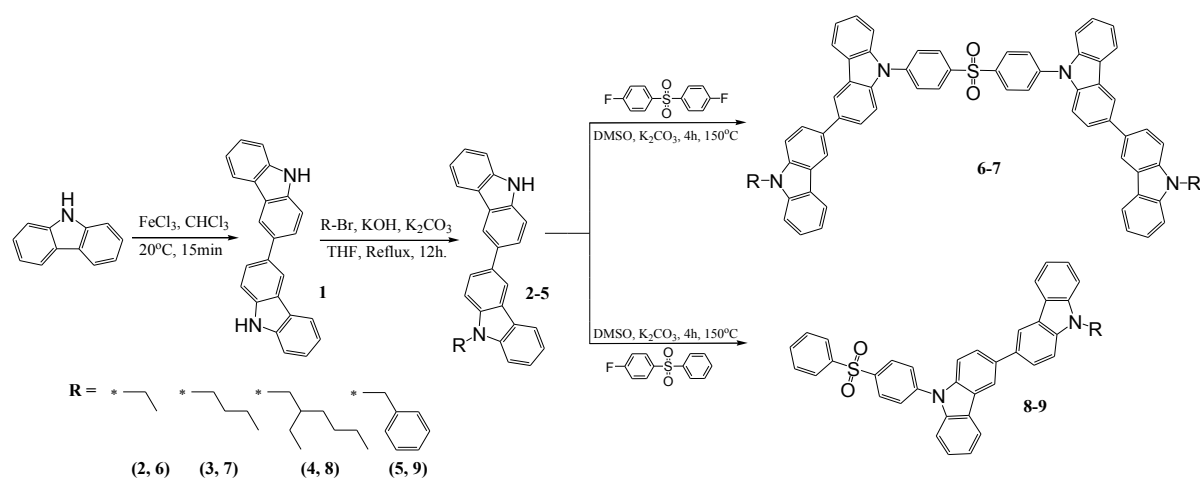


Fig. 1. Synthetic pathway of bicarbazole-based materials.

We have designed three-step synthesized carbazole-benzophenone-based twisted D-A-D derivatives, namely **6**, **7**, **8**, and **9**, as bi-functional materials. These materials possess high decomposition temperatures (>360°C) and glass transition temperature (~125°C), high photoluminescence quantum yield (>60%), wide bandgap (>3.2 eV), and a short decay time (ns). Owing to their properties, the materials were utilized as blue emitters and host materials for deep-blue and green OLEDs, respectively. In terms of the blue OLEDs, the emitter **7**-based device has outperformed others by showing a high maximum EQE of 4.0%, close to the theoretical limit of fluorescent materials, for a deep-blue emission (CIEy=0.09). Whilst the same material also displayed a maximum power efficacy of 45 lm/W as a host material doped with a phosphorescent emitter (Ir(ppy)₃). Furthermore, the materials were also utilized as a host with TADF green emitter (4CzIPN). Due to the high quantum yield of 69%, the host **9**-based green device has displayed a maximum EQE of 11%. Therefore, the bi-functional materials are easily synthesized, economical, possess excellent characteristics and are expected to be useful in a variety of cost-effective and high-performance OLED applications.

Acknowledgements

We acknowledge support from the Research Council of Lithuania (grant No. S-MIP-22-84).

- [1] C.-Y. Chan, L.-S. Cui, J. Kim, H. Nakanotani, C. Adachi, C. Chan, L. Cui, J.U. Kim. Rational Molecular Design for Deep-Blue Thermally Activated Delayed Fluorescence Emitters, *Advanced Functional Materials* **28**, 1706023 (2018).
- [2] Y. Tao, Q. Wang, C. Yang, C. Zhong, J. Qin, D. Ma. Multifunctional Triphenylamine/Oxadiazole Hybrid as Host and Exciton-Blocking Material: High Efficiency Green Phosphorescent OLEDs Using Easily Available and Common Materials. *Advanced Functional Materials* **20**, 2923–2929 (2010).
- [3] J.H. Lee, C.H. Chen, P.H. Lee, H.Y. Lin, M.K. Leung, T.L. Chiu, C.F. Lin. Blue Organic Light-Emitting Diodes: Current Status, Challenges, and Future Outlook. *Journal of Materials Chemistry C* **7**, 5874–5888 (2019).
- [4] Z. Wang, T. Yang, S. Dong, Z. Wen, H. Xu, Y. Miao, H. Wang, J. Yu. Anthracene and Carbazole Based Asymmetric Fluorescent Materials for High-Efficiency Deep-Blue Non-Doped Organic Light Emitting Devices with CIEy=0.06. *Dyes and Pigments* **199**, 110047 (2022).

INDUCED ENERGY BAND BENDING OF PTAA BY USING SELF-ASSEMBLED MOLECULES FOR WIDE BANDGAP LEAD PEROVSKITE SOLAR CELLS WITH INVERTED STRUCTURE

Raminta Beresnevičiūtė¹, Huan Bi², Jiaqi Liu², Gaurav Kapil², Daiva Tavgenienė¹, Beata Achramovic¹, Zheng Zhang², Liang Wang², Chao Ding², Shahrir Razey Sahamir², Yoshitaka Sanehira², Ajay Kumar Baranwal², Kitamura Takeshi², Dandan Wang², Yuyao Wei², Yongge Yang², Dong-Won Kang³, Saulius Grigalevicius¹, Qing Shen², Shuzi Hayase²

¹ Department of Polymers Chemistry and Technology, Kaunas University of Technology, Lithuania

² i-Powered Energy System Research Center (i-PERC), The University of Electro-Communications, Japan

³ School of Energy Systems Engineering, Chung-Ang University, Republic of Korea

raminta.beresnevičiūtė@ktu.lt

Recent years have reached intense research and development efforts of perovskite solar cells (PSCs), due to their growing efficiency [1]. Self-assembled mono-molecular layers have been proven to be useful as the HTL for high-efficiency Pb-PVK PSCs.[2] The molecules for these monolayers have p-type group/linker group/anchor groups. The molecules with phosphonic acids as the anchor group (PACz) are widely used in PSCs.

Poly[bis(4-phenyl) (2,4,6-trimethylphenyl) amine] (PTAA) is commonly employed as a hole transporting layer for FA_{0.8}CS_{0.2}PbI_{1.8}Br_{1.2}. However, since the hydrophobic surface sometimes suppressed the crystal growth of the FA_{0.8}CS_{0.2}PbI_{1.8}Br_{1.2} layer and the Fermi level of PTAA is not well matched with that of perovskite film, the efficiency of the WBG Pb-PVK PSCs consisting of PTAA was not high.

In this study, a series of PACz-based SAMs with different functional groups (**I-3PACz**, **9p-3PACz**, **2M3P-3PACz**) were synthesized to modify the interface between PTAA and perovskite film. The structures of compounds are shown in Figure 1.

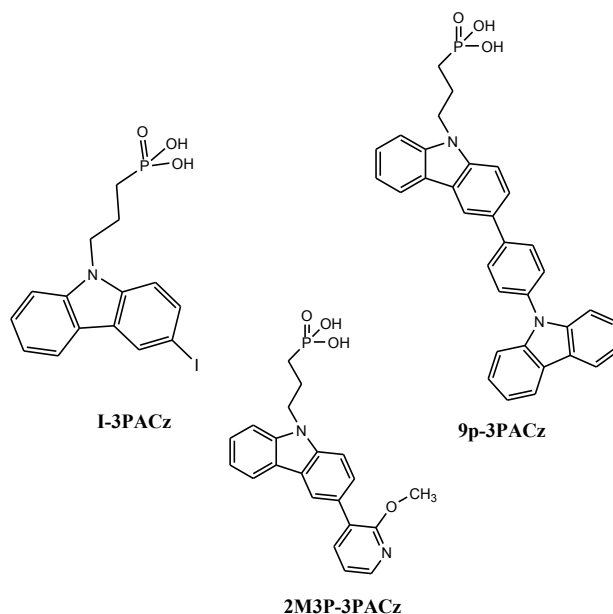


Fig. 1. Structures of compounds **I-3PACz**, **9p-3PACz** and **2M3P-3PACz**

The experimental results showed that molecules with more bulky substituted groups (**9p-3PACz**) achieved the best results. After the 9p-3PACz modification, not only the crystallization of the perovskite thin film improved but also the defect density of the perovskite film reduced. The energy-band bending due to SAMs molecular polarity also reduces the carrier transport and extraction resistance. Also, PTAA/9p-3PACz-based PSCs achieved a high PCE of 16.52 % with a bandgap of 1.77 eV.

Acknowledgements. This research was conducted in the frame of the project with support grant S-LJB-22-2 from Research Council of Lithuania.

[1] P. Yan, D. Yang, H. Wang, S. Yang, Z. Ge. Recent advantages in dopant-free organic hole-transporting materials for efficient, stable and low-cost perovskite solar cells, *Energy Environ. Sci.*, **15**, 3630-3669 (2022).

[2] F. Ali, C. Roldan-Carmona, M. Sohail, M.K. Nazeeruddin. Applications of self-assembled monolayers for perovskite solar cells interface engineering to address efficiency and stability, *Advanced Energy Materials*, **10**, (2020).

DIELECTRIC PROPERTIES OF $[\text{NH}_4][\text{Zn}(\text{HCOO})_3]$ METAL FORMATE FRAMEWORK DOPED WITH ALKALI METALS

Barbora Škėlaite¹, Sergejus Balčiūnas¹, Mantas Šimėnas¹, Mirosław Mączka², Juras Banys¹

¹ Faculty of Physics, Vilnius University, Saulėtekio al. 3, LT-10257, Vilnius, Lithuania

² Institute of Low Temperature and Structure Research, Polish Academy of Sciences, P.O. Box-1410, PL-50-950 Wrocław 2, Poland

barbora.skelaite@ff.stud.vu.lt

Over the years the dielectric properties of $[\text{NH}_4][\text{Zn}(\text{HCOO})_3]$ formate metal framework has been investigated by academic community. Guan-Cheng Xu et al. in their research reported that paraelectric – ferroelectric phase transition for metal organic framework was at 191 K [1]. However, our initial investigation showed that added potassium dopants diffuse into the $[\text{NH}_4][\text{Zn}(\text{HCOO})_3]$ structure, that lead to temperature drop for the paraelectric – ferroelectric phase transition and increase in activation energies.

In this presentation dielectric properties of ammonium zinc formate samples were being investigated. For pure and potassium doped $[\text{NH}_4][\text{Zn}(\text{HCOO})_3]$ frameworks dielectric permittivity dependence on temperature (100 – 300K) were measured, using flat capacitor method in the 10^2 - 10^6 Hz frequency range which was illustrated in figure 1. At significantly high temperatures dielectric permittivity is dependent on frequency, which can be related to Maxwell – Wagner relaxation. Moreover, relaxations near phase transition temperatures can be linked to the motion of domain walls. We present inverse temperature dependence of logarithm of relaxation time, which was obtained by approximating frequency dependencies of dielectric permittivity, using the superposition of several Cole – Cole functions. Furthermore, the activation energies for relaxation for organic metal frameworks both pure ($E_A = 0.15\text{V}$) and doped with potassium ($E_A = 0.34\text{V}$) were approximated following Arrhenius law. Increase in activation energies with K 5% impurities could have happen due to domain wall fixing to point defects, caused by potassium, which hinders its motion.

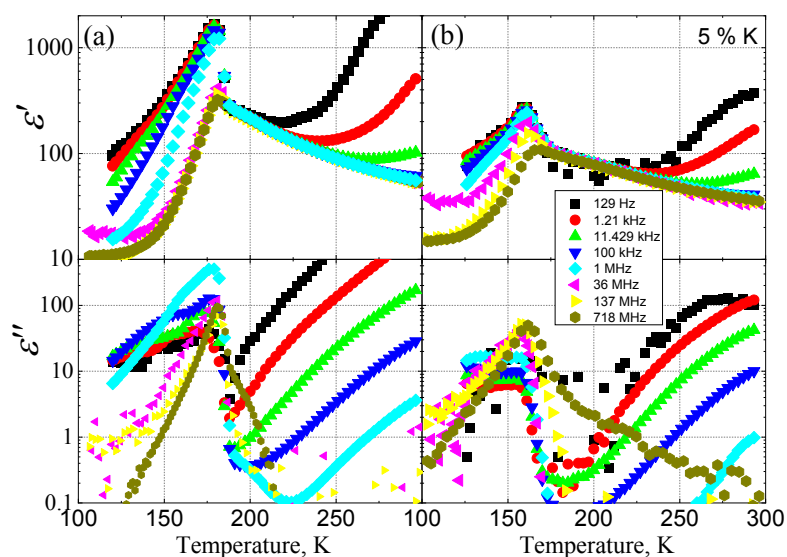


Fig. 1. Temperature dependence of the real (top) and imaginary (bottom) parts of dielectric permittivity of $[\text{NH}_4][\text{Zn}(\text{HCOO})_3]$ crystal along c – axis. (a) pure (b) with 5% K.

[1] Xu, Guan-Cheng, et al. "Disorder – order ferroelectric transition in the metal formate framework of $[\text{NH}_4][\text{Zn}(\text{HCOO})_3]$." Journal of the American Chemical Society 132.28 (2010): 9588-9590

DIELECTRIC AND PIEZOELECTRIC PROPERTIES IN (1 - x)Na_{0,5}Bi_{0,5}TiO₃-xCdTiO₃ SOLID SOLUTIONS

Eglė Martinaitytė^{1,*}, Eriks Birks², Šarūnas Svirskas¹

¹ Faculty of Physics, Vilnius University, Vilnius, Lithuania

² Institute of Solid State Physics, University of Latvia, Kengaraga 8, Riga, Latvia
egle.martinaityte@ff.stud.vu.lt

There is a plethora of piezoelectric ceramics' applications in electronics, telecommunications and medicine. Ceramics containing lead were the most widely used, as they seemed to have the best ferroelectric properties [1]. The problem with lead containing materials is that lead is toxic, which causes the search for lead-free ceramics. One of the most promising lead-free piezoelectric materials is Na_{0,5}Bi_{0,5}TiO₃ (NBT). Pure NBT ceramics with their ferroelectric properties hardly reach lead-based materials and are therefore doped with other materials. In this work - cadmium titanate (CdTiO₃).

Materials under test with different concentrations of CdTiO₃ were prepared by solid state reaction from chemical-grade oxides [2]. We examined samples containing 10 %, 20 %, 35 %, 40 % and 45 % of CdTiO₃. Dielectric properties were obtained by cooling samples in a temperature range from 500 K to 100 K with a HP4284A LCR meter. A temperature change rate was approximately 1 K/min. Polarization hysteresis and electromechanical properties were measured with AixacCT TF 2000 analyzer applying 4 kV external field. Samples were cooled down to 200 K.

Temperature dependences of dielectric permittivity (Fig. 1) shows that increasing CdTiO₃ concentration gives higher dielectric constant values. Comparing it to pure NBT ceramics maximum of dielectric permittivity can be obtained at lower temperatures. Typical ferroelectric properties are only observed for a composition $x = 0.45$ (Fig. 2). Same results can be seen for sample where x is equal to 0.35 but only at lower temperatures. Behavior of sample with 10 % of CdTiO₃ is very similar to linear dielectric and stays the same over the whole temperature range.

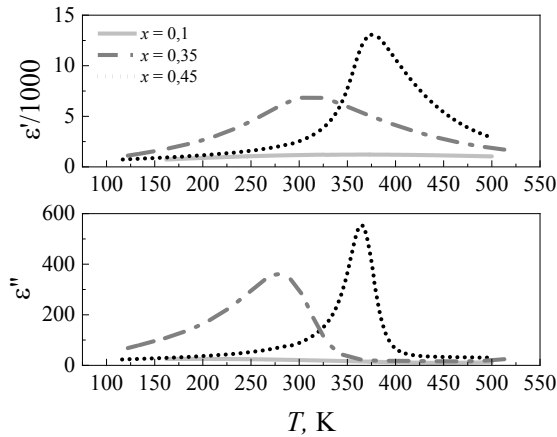


Fig. 1. Temperature dependences of complex dielectric permittivity.

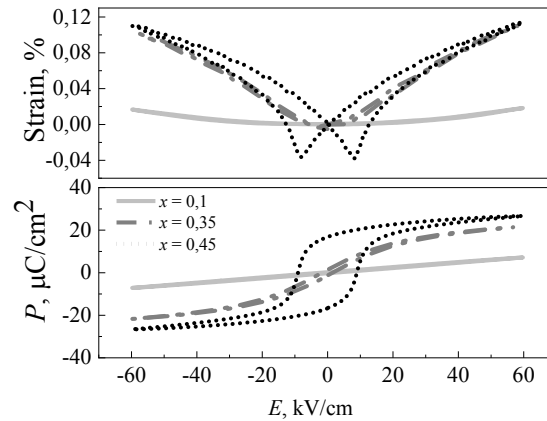


Fig. 2. Electric field dependence of strain and polarization at room temperature.

-
- [1] X. Wang, Y. Huan, S. Ji, Y. Zhu, T. Wei, and Z. Cheng, Ultra-high piezoelectric performance by rational tuning of heterovalent-ion doping in lead-free piezoelectric ceramics, *Nano Energy* **101**, (2022).
[2] M. Duce, E. Birks, M. Antonova, V. Zauls, M. Kundzinsh, and A. Fuih, Structure and physical properties of Na_{1/2}Bi_{1/2}TiO₃-CdTiO₃ solid solutions, *Ferroelectrics* **417**, (2011).

NUMERICAL CALCULATIONS OF THE HEAT CONDUCTIVITY OF SiO₂ GLASS SUBJECTED TO ULTRA-HIGH PRESSURE USING MOLECULAR DYNAMICS

Adam Puchalski¹, Mateusz Ślusarczyk¹, Paweł Keblinski², Tomasz K. Pietrzak¹

¹Faculty of Physics, Warsaw University of Technology, Poland

²Department of Materials Science and Engineering, Rensselaer Polytechnic Institute, USA
adam.puchalski.stud@pw.edu.pl

Silica is a common material with a wide range of commercial applications – including the production of glass, concrete and semiconductors. This makes accurately modelling its properties using molecular dynamics particularly important. Furthermore, procedures for calculating the physical properties of silica can be often generalized for other oxide materials [1].

Recently, a new interbody potential for modelling silicon dioxide interactions has been developed. It has been shown that this potential allows for accurate prediction of the physical properties of amorphous silica even under high pressures with decreased intermolecular distance [1]. Our recent research has shown, that the value of the heat conductivity coefficient can vary substantially depending on the method used. This study attempts to develop an accurate method for calculating heat conductivity of silica using the equilibrium Green-Kubo [2] method and non-equilibrium Müller-Plathe method [3].

Obtaining accurate results turned out to be non-trivial, particularly using the Green-Kubo method. Molecular dynamics simulations in the LAMMPS [4] environment have been conducted in order to compare the results across the two methods and different procedures for obtaining the final heat conductivity value. The aim is to evaluate the results obtained from those methods by comparing them with each other and the known experimental values. The relationship between the heat conductivity coefficient and pressure can also be determined and can serve as another way to evaluate the results.

-
- [1] S. Sundararaman, L. Huang, S. Ispas, and W. Kob, "New optimization scheme to obtain interaction potentials for oxide glasses," *The Journal of Chemical Physics*, vol. 148, no. 19, p. 194504, 2018.
- [2] R. Kubo, M. Yokota, and S. Nakajima, "Statistical-Mechanical Theory of Irreversible Processes. II. Response to Thermal Disturbance," *Journal of the Physical Society of Japan*, vol. 12, no. 11, pp. 1203–1211, 1957.
- [3] F. Müller-Plathe, "A simple nonequilibrium molecular dynamics method for calculating the thermal conductivity," *The Journal of Chemical Physics*, vol. 106, no. 14, pp. 6082–6085, 1997.
- [4] A. P. Thompson, H. M. Aktulga, R. Berger, D. S. Bolintineanu, W. M. Brown, P. S. Crozier, P. J. in 't Veld, A. Kohlmeyer, S. G. Moore, T. D. Nguyen, R. Shan, M. J. Stevens, J. Tranchida, C. Trott, and S. J. Plimpton, "Lammps - a flexible simulation tool for particle-based materials modeling at the atomic, meso, and continuum scales," *Computer Physics Communications*, vol. 271, p. 108171, 2022.

SIMULATING MICROWAVE FIELD DISTRIBUTION IN A NOVEL SUPERCONDUCTING EPR MICRORESONATOR

Ignas Pocius¹, Paulina Verbaitytė¹, Jūras Banys¹, Mantas Šimėnas¹

¹Faculty of Physics, Vilnius University, Lithuania
ignas.pocius@ff.stud.vu.lt

Electron paramagnetic resonance (EPR) is a technique used to study and manipulate electron spins in various functional materials. Recently, major advances in EPR sensitivity were achieved using planar superconducting microresonators [1,2]. However, microresonators fabricated from conventional superconductors have severe limitations for conventional EPR due to their low temperature of operation and susceptibility to the magnetic field. For this reason, microresonators fabricated from high- T_c superconductors are gaining attention [3].

Here, we explore a novel planar “airplane” microresonator geometry coupled to a co-planar waveguide (Fig. 1) using the CST Microwave Studio computational electromagnetics tool. We analyze the distribution and homogeneity of the microwave magnetic field produced by the microresonator. Our results show that the highest magnetic field density is concentrated on the inductor region, although the undesirable contribution from the capacitor is also significant. We discuss ways to further improve the resonator design.

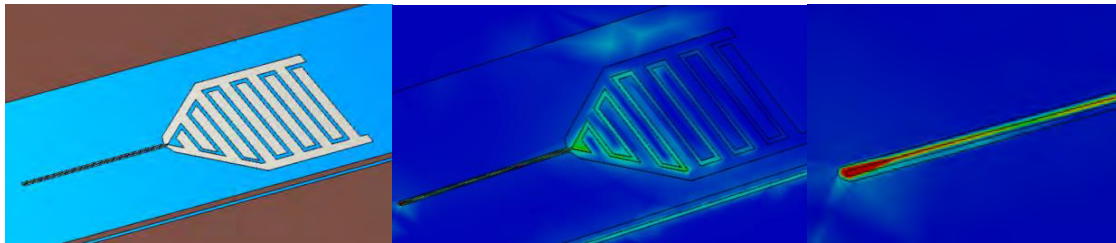


Fig. 1. Model of an “airplane” type resonator on a co-planar waveguide. Colour coding represents the intensity of the microwave magnetic field of the microresonator. The inductor region is emphasized in the enlarged figure.

-
- [1] A. Bienfait, et al., Reaching the quantum limit of sensitivity in electron spin resonance, *Nat. Nanotechnol.* **11**, 253-257 (2016).
[2] J.J.L. Morton, P. Bertet, Storing quantum information in spins and high-sensitivity ESR, *J. Magn. Reson.* **287**, 128-139 (2018).
[3] Ghirri, A. et al. $\text{YBa}_2\text{Cu}_3\text{O}_7$ microwave resonators for strong collective coupling with spin ensembles, *Appl. Phys. Lett.* **106**, 184101 (2015).

SECOND-HARMONIC GENERATION IN A PERIODICAL POLARITY GaN

Ustas Petrusevičius,¹ M. Kolenda,¹ D. Kezys,² T. Grinys,¹ A. Vaitkevičius,¹ A. Kadys,¹
I. Reklaitis,¹ V. Vaičaitis,³ R. Petruškevičius,² R. Tomašiūnas¹

1) Institute of Photonics and Nanotechnology, Vilnius University, Saulėtekio ave. 3, LT-10257 Vilnius, Lithuania

2) State research institute Center for Physical Sciences and Technology, Savanorių ave. 231, LT-02300, Vilnius, Lithuania

3) Laser Research Center, Vilnius University, Saulėtekio ave. 10, LT-10223 Vilnius, Lithuania

The expectations for the use of GaN material for UV-blue light are still very high due to the great demand for lighting sources of high efficiency for various applications, such as automotive manufacturing, water cleaning, and communication technologies. Such high demand encourages extensive search for material improvements, for example, an extension of the spectral range of operation. The most used switching method for spectral range extension is optical harmonic generation. Conventional birefringent materials have got competing methods of satisfying the phase matching condition such as quasi-phase matching (QPM) [1] and modal phase matching (MPM).

In this work, we demonstrate a broadband second harmonic generator for green spectra, that is based on QPM structure - a GaN sample of periodical polarity grown via metalorganic chemical vapor deposition (MOCVD) using Aixtron CCS 3x2" reactor. A periodical polarity GaN (PPO-GaN) structure was fabricated with an alternating periodicity of $4 \mu\text{m}$ and thickness of $1.2 \mu\text{m}$. From the measured second harmonic (SH) in the wavelength range of 500-550 nm, the evaluated SH ($\lambda_{SH} = 512 \text{ nm}$) conversion efficiency was $0.79 \cdot 10^{-5} \% \cdot W^{-1}$ for the pump peak power of 44 kW.

The optical system used to observe and measure the second harmonic signal consisted of a 1kHz repetition rate femtosecond Ti:sapphire chirped pulse amplification laser system, providing 35-40 fs pulses centered at 790 nm with maximal pulse energy of 5 mJ, which was used to pump OPA in order to tune the wavelength between 950 and 1150 nm. The duration of a single OPA pulse energy was about 45 fs and 0.1-0.2 mJ.

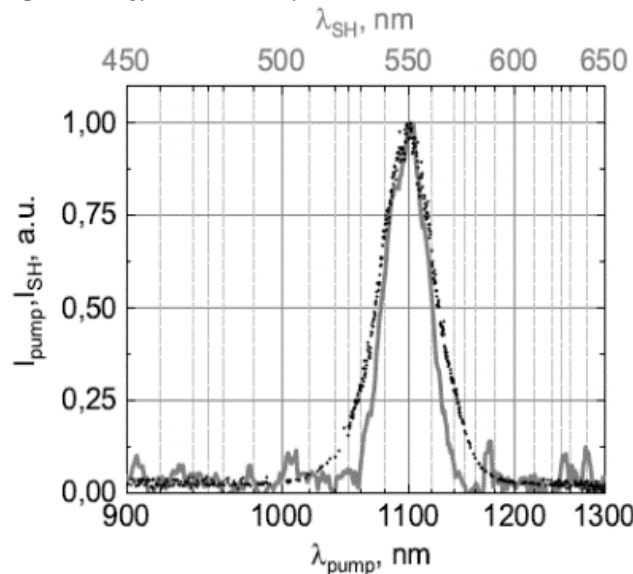


Fig. 1 The experimental pump (black points, bottom scale) and SH (light grey line, upper scale) peak intensity of the PPO-GaN sample.

In Figure 1 we present the measured wavelength spectra of the 1100 nm pump and generated second harmonic (SH) pulse. The temporal and spectral characteristics of the pump pulse are defining the $\sim 50 \text{ nm}$ FWHM of the SH pulse spectra. There is a slight difference in the SH pulse compared to the pump pulse, which can be attributed to some incoherence of the pump at the slopes of the spectra.

[1] D. H. Hahn, G. T. Kiehne, J. B. Ketterson, G. K. L. Wong, P. Kung, A. Saxler, and M. Razeghi, J. Appl. Phys. 85, 2497 (1999).

EMOTION RECOGNITION USING A GENERAL-PURPOSE OBJECT DETECTION ALGORITHM

Arvydas Lozys¹, Ema Spiliauskaite¹, Migle Skystimaite¹, Daichi Tsujimoto¹,
Antanas Zinovicius¹, Vytautas Bucinskas¹

¹ Vilnius Gediminas Technical University, Faculty of Mechanics, Plytines g. 25, 10105 Vilnius, Lithuania
antanas.zinovicius@vilniustech.lt

Emotions are complex psychological states that involve subjective feelings, physiological changes, and behavioural responses to stimuli. They are important because they play a crucial role in how we perceive, interpret, and respond to the world around us [1]. Emotions help us to communicate with others, make decisions, and motivate us to take action. It is important to detect emotions for the reason that they can help us understand and respond appropriately to the needs of others. Detecting emotions can also help us regulate our own emotions, which can improve our relationships and overall well-being. Besides, being able to accurately detect emotions is important in many fields, including psychology, counselling, education, and business [1].

Identifying emotions can sometimes be challenging, so there are technologies that help us to understand what people are feeling. It is possible to train artificial intelligence (AI) systems to recognise people's emotions based on facial expressions, text, gesticulations, and verbal expressions. When it detects a certain emotion, the AI can adjust its behaviour to better suit the specific ongoing situation. People are better at recognizing different emotions, but AI has ability to analyse large amounts of data using computer vision and deep learning algorithms and other techniques [2].

The algorithm we chose for our emotion detection project was YOLOv5 (You Only Look Once) by Ultralytics [3]. Even though this AI algorithm is intended to locate instances of objects in images or real-time video feed, meaning that it is not designed to detect and recognize emotions like other machine learning algorithms. Before the model could be trained, we gathered synthetic data, data from an open-source database and our custom data which was then combined to produce a database made up of 1400 images [4]. The dataset was prepared to train a model which could detect and recognize 3 emotions (happy, neutral, sad) given that we have appropriate camera lighting and positioning.

Our trained model can detect and correctly identify an emotion in real-time from a computer camera with an accuracy of 80%. There is a lot of room for improvement since we used a general-purpose object detection algorithm. In the future we intend to build an algorithm that is created specifically for extracting facial features which will help to increase the accuracy and reliability of the model.

-
- [1] M. Garcia-Garcia, "IMPLICATIONS FOR BRAND SUCCESS AUDIENCESCENCE 2020 The Advertising Research Foundation Global Lead of Neuroscience Global Science Organization, Ipsos," 2020.
- [2] A. McStay, "Emotional AI, soft biometrics and the surveillance of emotional life: An unusual consensus on privacy," *Big Data Soc*, vol. 7, no. 1, p. 205395172090438, Jan. 2020, Doi: 10.1177/2053951720904386.
- [3] Zhang, Z., Lin, P., Ma, S., & Xu, T. (2022). An Improved Yolov5s Algorithm for Emotion Detection. 2022 5th International Conference on Pattern Recognition and Artificial Intelligence, PRAI 2022, 1002–1006. <https://doi.org/10.1109/PRAI55851.2022.9904113>
- [4] IGOR. (2022). emotions dataset Dataset [Open-Source Dataset]. In Roboflow Universe. Roboflow. <https://universe.roboflow.com/igor-dwg3d/emotions-dataset-o>

ANNEALING EFFECTS ON IMPLANTED SILICON FOR SPIN-BASED QUANTUM TECHNOLOGIES

Justinas Turčak¹, Jūras Banys¹, Mantas Šimėnas¹

¹ Faculty of Physics, Vilnius University, Sauletekio 9, LT-10222 Vilnius, Lithuania
justinas.turcak@ff.vu.lt

One of the most important requirements for a spin-based quantum computer [1] is a long spin coherence time in comparison to time necessary for computations. To prolong the quantum superposition, the spin must be isolated from its environment, however this is done at the expense of ability to control the system. Donors implanted in silicon have been demonstrated to offer a solution for easy qubit manipulation [2,3], with coherence times of several seconds [4]. This is typically achieved in doped bulk crystals of silicon. On the other hand, implanting donors very close to the surface (at the depth of hundreds of nanometres) is highly attractive for functional quantum technologies. However, structural defects arising during implantation may limit the number of active spins and shorten their coherence time. Some structural damage could be repaired during annealing [5], but essential parameters for this process are not well studied.

Here, we search for optimal annealing parameters of tellurium donors at the silicon surface. We test samples of different implantation depth by measuring their coherence times and active spin concentrations using electron spin resonance. We base our donor spin concentration estimates on reference sample of silicon doped with phosphorus.

[1] D. P. DiVincenzo, The Physical Implementation of Quantum Computation, *Fortschritte der Physik*, **48**, 771-783 (2000).

[2] B. E. Kane, A silicon-based nuclear spin quantum computer, *Nature*, **393**, 133-137 (1998)

[3] A. Morello et al., Single-shot readout of an electron spin in silicon, *Nature*, **467**, 687-691 (2010).

[4] G. Wolfowicz et al., Atomic clock transitions in silicon-based spin qubits, *Nature technology*, **8**, 561-564 (2013).

[5] M. Šimėnas et al., Near-surface ¹²⁵Te⁺ Spins with Millisecond Coherence Lifetime, *Phys. Rev. Lett.*, **129**, 117701 (2022).

ENHANCING MECHANICAL PROPERTIES OF ALSI10MG ALLOY VIA EQUAL CHANNEL ANGULAR PRESSING POST-PROCESSING

Augustine Nana Sekyi Appiah^{1*}, Przemysław Snopiński¹, Marcin Adamiak¹

¹ Materials Research Laboratory, Faculty of Mechanical Engineering, Silesian University of Technology, 18A Konarskiego Street, 44-100 Gliwice, Poland
augustine.appiah@polsl.pl

The AlSi10Mg alloy is frequently subjected to post-processing after Selective Laser Melting (SLM) in order to enhance its mechanical performance. Hot isostatic pressing is the most commonly used method for plastic deformation processes[1], however, this approach results in a notable decline in strength. To enhance the mechanical properties of various metals, Equal Channel Angular Pressing (ECAP) or Equal Channel Angular Extrusion (ECAE) are often employed as they result in refined microstructure and higher dislocation density[2].

The objective of this study is to enhance the mechanical properties of AlSi10Mg alloy produced by Selective Laser Melting (SLM) by undergoing post-processing using Equal Channel Angular Pressing (ECAP). The research evaluated two post-processing approaches: low-temperature annealing (LTA) followed by ECAP treatment at 150°C and ECAP treatment without heat treatment at various temperatures of 350°C, 400°C and 450°C.

The microstructure and mechanical properties of the alloy were analyzed after each post-treatment stage. The results from metallographic observations, Scanning Electron Microscopy (SEM) and Electron Backscattered Diffraction (EBSD) showed that SLM-produced alloys have a unique cellular microstructure composed of Si networks surrounding an Al-based matrix phase.

LTA followed by ECAP treatment promoted the microstructural development of the alloy, leading to the partial breakup of the Si network and the nucleation of β -Si precipitates throughout the Al matrix. This resulted in a Vickers microhardness of 153 HV and a yield strength of 415 MPa (shown in Fig. 1). These values are among the highest reported in literature for this alloy. The findings indicate that post-processing of SLM-produced AlSi10Mg alloys using ECAP has a significant impact on the microstructural evolution and mechanical properties of the alloy.

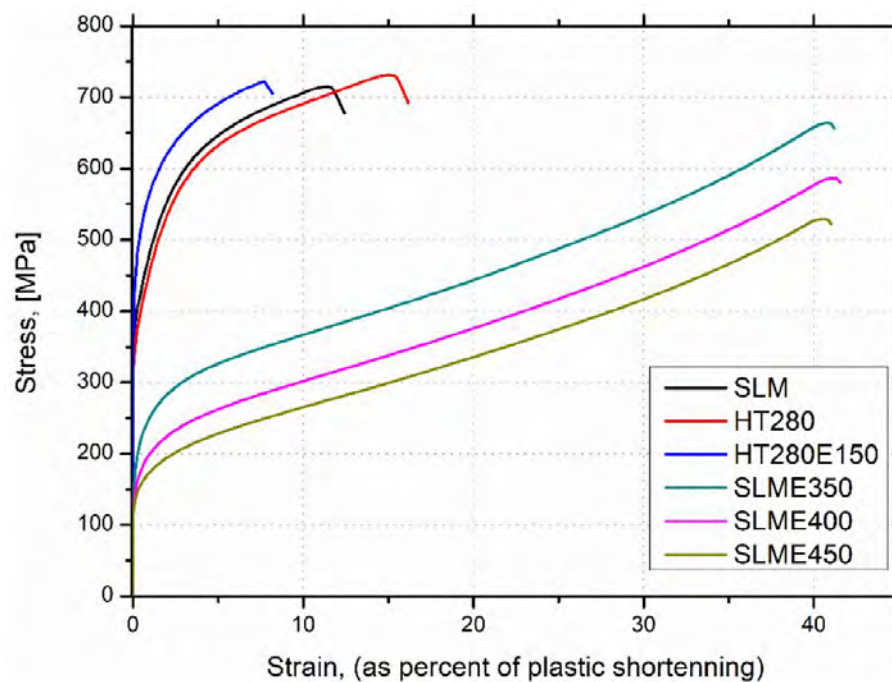


Fig. 1. Compressive test plots of investigated samples.

[1] R. Ma et al., Enhanced strength of the selective laser melted Al-Mg-Sc-Zr alloy by cold rolling, *Materials Science and Engineering A* 775, 138975 (2020).

[2] P. Snopiński, K. Matus, F. Tatiček, S. Ruzs et al., Overcoming the strength-ductility trade-off in additively manufactured AlSi10Mg alloy by ECAP processing, *Journal of Alloys and Compounds*, 165817 (2022).

INDOOR RADIO FREQUENCY ENERGY HARVESTING

Justina Žemgulytė¹, Paulius Ragulis¹, Gediminas Šlekas¹, Romualdas Trusovas², Karolis Ratautas², Rimantas Simniškis¹, Žilvinas Kancleris¹, Gediminas Račiukaitis²

¹Department of Physical Technologies, Center for Physical Sciences and Technology, Lithuania

²Department of Laser Technologies, Center for Physical Sciences and Technology, Lithuania
justina.zemgulyte@fmfc.lt

Due to the vast growth of radio and telecommunication networks, devices that can harvest energy in radio and microwave frequency bands have recently been gaining much attention [1, 2]. One benefit of such devices is that as radio power sources get denser and more of their energy is wasted, it might be possible to further Europe's green deal plan by gathering that energy and using it to power low-current electronics. In addition, because solar panels and wind turbines can't be utilized indoors and there are not so many locations without a WiFi router, radio energy harvesters provide another less well-known benefit.

In this work we investigate the possibility of harvesting energy from a standard WiFi router. For this purpose radio frequency (RF) energy harvesting system is developed. It is made using several high gain antennas, full wave voltage rectifiers with impedance matching networks and a power managing module (BQ25570). The proposed system is developed to work in 2.45 GHz frequency band (8-th channel of WiFi2.4). The reason for using more than one antenna is that power density decreases as $1/R^2$, where R is the distance between the source and the harvester's antenna. Therefore, utilizing more antennas makes it feasible to have a larger surface area, which increases the power that can be harvested. Manufactured slot antennas gain dependence on frequency is shown in Fig. 1. A few different antenna manufacturing methods are investigated: lithography and selective surface activation induced by laser (SSAIL) [3]. From the figure, we observe that at 2.45 GHz antenna manufactured using SSAIL has a higher gain than the one manufactured using lithography. One of the most important elements in such small power energy harvesting systems is the impedance matching circuit. We modeled and manufactured an impedance-matching network for our rectifier. Fig. 2 shows rectifier's rectification voltage when the RF input power from the antenna to the rectifier is 1 mW. When impedance is matched, it is possible to get almost 2.6 more voltage compared to the unmatched rectifier.

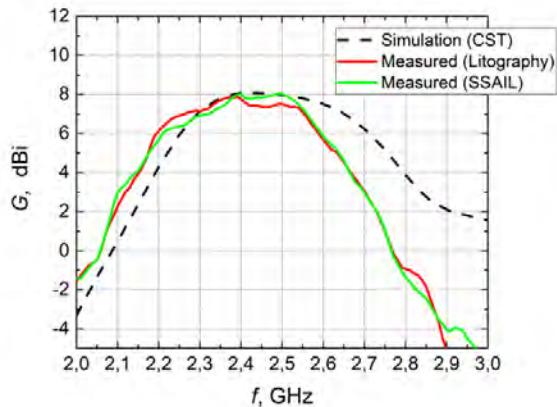


Fig. 1. Slot antenna gain

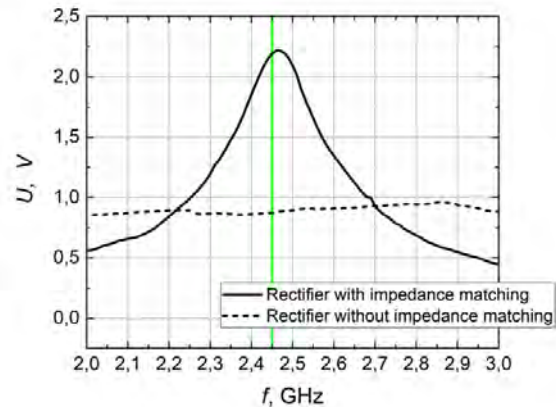


Fig. 2. Full wave voltage rectifier with and without impedance matching network (input power 1 mW)

Manufacturing a rectifier and antenna on a single substrate is our way to improve the overall system's performance by reducing its dimensions and minimising losses due to connectors. This is achieved by applying a novel SSAIL technique, which allows us to grow metallization on planar or 3D structures made of different materials, starting from standard dielectrics and soft or hard ceramics to flexible polymers.

Our goal is to prove that it can collect enough energy to consistently or periodically power a low-power sensor or microcontroller. Such systems can be used in various fields where low-power sensors or sensor networks need to be powered for extended periods of time. This would lessen the demand for batteries and contribute to environmental improvement.

[1] H. D. Do, D. E. Kim, M. B. Lam, and W. Y. Chung, "Self-Powered Food Assessment System Using LSTM Network and 915 MHz RF Energy Harvesting," *IEEE Access*, vol. 9, pp. 97444–97456, 2021, doi: 10.1109/ACCESS.2021.3095271.

[2] R. Berges, L. Fadel, L. Oyhenart, V. Vigneras, and T. Taris, "Conformable dual-band wireless energy harvester dedicated to the urban environment," *Microw. Opt. Technol. Lett.*, vol. 62, no. 11, pp. 3391–3400, Nov. 2020, doi: 10.1002/mop.32461.

[3] Ratautas, K., Norkus, E., Jagminienė, A., Račiukaitis, G., & Stankevičienė, I. (2018). Laser Assisted Selective Metallization of Polymers; Laser Assisted Selective Metallization of Polymers. In 2018 13th International Congress Molded Interconnect Devices (MID).

This project has received funding from European Regional Development Fund (project No 01.2.2-LMT-K-718-03-0038) under a grant agreement with the Research Council of Lithuania (LMTLT)

SIMULATION OF DIFFRACTIVE OPTICS INTEGRATION IN A THZ BOWTIE DETECTOR

Karolis Redeckas¹, Linas Minkevičius¹, Vytautas Jakštas², Ignas Grigelionis¹

¹ Department of Optoelectronics, Center for Physical Sciences and Technology, Saulėtekio al. 3, Vilnius, Lithuania

² Department of Physical Technologies, Center for Physical Sciences and Technology, Saulėtekio al. 3, Vilnius, Lithuania

karolis.redeckas@ff.stud.vu.lt

The goal of reducing the dimensions of THz imaging systems is crucial to make them more versatile and practical for various applications such as security or material science [1]. By utilizing wave optics the diffractive optics approach provides a solution to small size, low weight challenge by enabling precise control of phase shifts and constructive interference. The significance of designing diffractive optical elements has grown in recent years as THz beam-forming [2], imaging [3], have become essential in the development of THz technology. By using diffractive optics, it is possible to achieve similar performance to conventional lenses and design elements with a shorter focal length.

The aim of this work is to increase the efficiency of the THz detector by developing design of the radiation coupling optics that maintains the small dimensions of the whole system offering an "on-chip" solution. At the same time, the developed design simplifies the manufacturing technology of the system by bypassing the problem of conform to the planes on both sides of the InP wafer [4].

In this work, models of diffraction optics (zone plates) with InP wafers systems are created using only a computer program CST MW Studio. Various combination of InP wafer thickness and zone plate focal length were virtually created and tested. The best optical part model was integrated with a bowtie THz detector in order to improve the coupling of radiation into the detector. Numerical simulations of terahertz radiation propagation are performed using the same computer program to evaluate the detection system model.

Best performance was demonstrated by 335 μm thickness InP wafer and $F = 645 \mu\text{m}$ zone plate. The obtained results [Fig. 1(b)] shows that bow-tie detector can effectively concentrate electric field by itself. Adding contacts and zone plate around it [Fig. 1(a)] increases electric field 6 times.

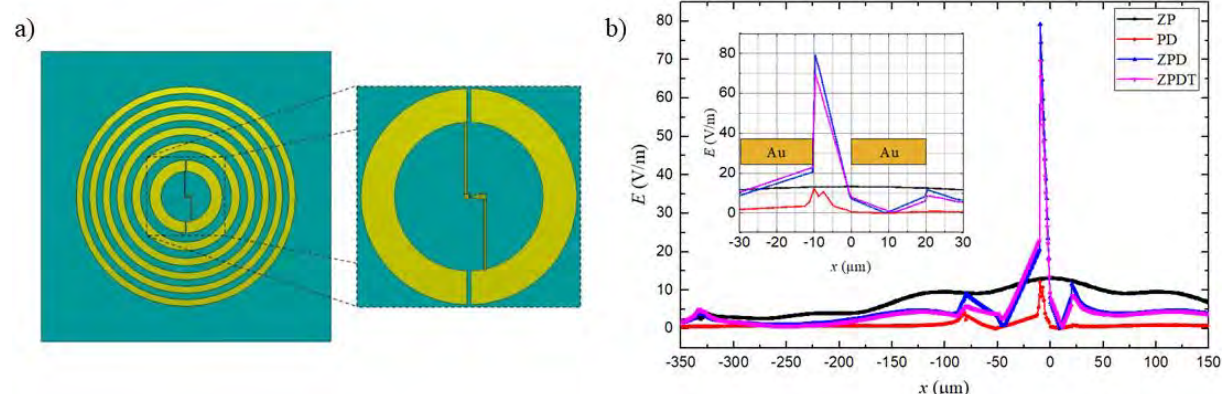


Fig. 1. Panel a): simulated model of the bowtie detector with zone plate and contact tracks. Inset depicts an enlarged view of the bowtie detector. Panel b): cut of the electric field at $z = -0.5 \mu\text{m}$ for different configurations. ZP – zone plate only; PD – bowtie detector only; ZPD – zone plate and bowtie detector; ZPDT – zone plate, bowtie detector, and contact tracks.

This research has received funding from the Research Council of Lithuania (LMTLT), agreement No [S-MIP-22-76]

[1] Tadao Nagatsuma, Terahertz technologies: present and future, IEICE Electronics Express, 2011, Volume 8, Issue 14, Pages 1127-1142, Released on J-STAGE July 25, 2011, Online ISSN 1349-2543, <https://doi.org/10.1587/elex.8.1127>

[2] Daniel Headland, Yasuaki Monnai, Derek Abbott, Christophe Fumeaux, and Withawat Withayachumnankul. Tutorial: Terahertz beamforming, from concepts to realizations. APL Photonics, 3(5):051101, 2018.

[3] Daniel M Mittleman. Twenty years of terahertz imaging. Optics express, 26(8):9417-9431, 2018.

[4] Minkevičius, L., Tamošiūnas, V., Madeikis, K., Voisiat, B., Kašalynas, I. and Valušis, G. (2014), On-chip integration of laser-ablated zone plates for detection enhancement of InGaAs bow-tie terahertz detectors. Electron. Lett., 50: 1367-1369. <https://doi.org/10.1049/el.2014.1893>

THE INFLUENCE OF SYNTHESIS CONDITIONS ON LITHIUM-COBALT BORATE STRUCTURAL PROPERTIES

Alicja Kadziela¹, Przemysław Piotr Michalski¹

¹Faculty of Physics, Warsaw University of Technology, Koszykowa 75, 00-662 Warsaw, Poland
alicja.kadziela.stud@pw.edu.pl

Lithium-cobalt borate is a candidate for a cathode for lithium-ion batteries, commonly used for electricity storage. This material is distinguished from other polyanionic compounds by its higher operating voltage (4 V) and theoretical power density (860 Wh/kg) [1] as well as greater theoretical gravimetric capacity (215 mAh/g). Electrochemical properties of LiCoBO₃ can depend on the method of synthesis and resulting morphology of material.

The main objective of this work was to synthesize lithium-cobalt borate using two methods and to compare the differences in structural properties. The synthesis was carried out using the citrate and modified Pechini methods, belonging to the group of sol-gel methods. Differential thermal analysis was used to determine the temperature ranges for the annealing process. The results of X-ray diffraction measurements provided data on the phases present in the materials and made it possible to define the best calcination conditions. Determination of unit cell parameters and grain size was performed by Rietveld refinement. Scanning electron microscope images were also taken. Raman spectroscopy was used to analyze the chemical bonds in the structure and to check the presence of carbon.

The attempt to obtain pure LiCoBO₃ was unsuccessful, although the content of foreign phases such as Co₃O₄ or CoO in the optimized material is small. The best calcination conditions are 725°C/8 h. Figure 1 shows the XRD data for the best specimens obtained from both methods. It can be seen that the peak positions and intensities of LiCoBO₃ phase correspond to those from the reference pattern. Two reflections from Co₃O₄ in the diffractogram of the sample obtained by the modified Pechini method are marked with stars. A small peak resulting from the presence of CoO in the spectrum of the sample synthesized by the citrate method was distinguished with the heart.

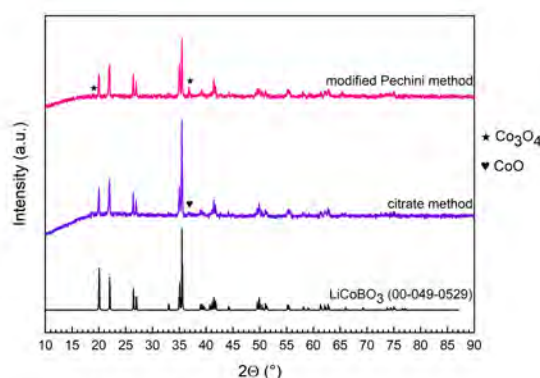


Fig. 1. Diffractograms of the best samples obtained by the citrate and modified Pechini methods. The reference XRD pattern of LiCoBO₃ phase is shown below.

Materials gained from both methods do not contain carbon. This outcome is successful. The resulting gel contained a lot of organic substances which, after thermal decomposition in an argon atmosphere, may have remained in the sample in the form of carbon. An increased relative amount of this element may have a negative effect on the electrochemical properties of the sample. The following cell parameters were determined from the Rietveld refinement: $a = 5.1335(2)$ Å, $b = 8.8431(3)$ Å, $c = 10.1047(2)$ Å, $\beta = 91.377(4)^\circ$, $V = 458.58(2)$ Å³ for the sample synthesized by the citrate method, and $a = 5.1358(2)$ Å, $b = 8.8545(3)$ Å, $c = 10.1131(3)$ Å, $\beta = 91.378(4)^\circ$, $V = 459.76(2)$ Å³ for the material obtained using the modified Pechini method. The specimen obtained by the citrate method had a slightly smaller unit cell and smaller grain size (23 nm) in comparison to that gained from the modified Pechini method (75 nm). As the sample obtained by the citrate method has a smaller grain size, it is likely to have a higher gravimetric capacity.

Further research needs to be conducted to determine the electrochemical properties of those two samples and to prove the influence of morphology and structural properties.

[1] Barpanda, P., Dwibedi, D., Ghosh, S., Kee, Y., and Okada, S. (2015). Lithium metal borate (LiMBO₃) family of insertion materials for Li-ion batteries: a sneak peak. In *Ionics* (Vol. 21, Issue 7, pp. 1801-1812). Springer Science and Business Media LLC.

THE DEVELOPMENT OF TECHNOLOGY OF A NEW GENERATION IDENTIFICATION ELEMENT

Erika Rajackaitė¹, Andrius Žutautas^{1,2}, Rasa Žostautienė¹, Pranas Narmontas¹

¹Institute of Materials Science, Kaunas University of Technology, Lithuania

²Department of Physics, Kaunas University of Technology, Lithuania
erika.rajackaite@ktu.lt

Trends in the promotion of efficiency in the market, implementation of circular economy, strengthening of data, copyright protection create the need to develop a new generation, anti-forgery authentication-identification element integrated into advanced product packaging or labels [1-5]. The aim of this work is to create a new generation security system and element (Fig. 1) with unique properties capable of replacing existing product control, scanning and security systems, and to create a new product design concept by applying holographic technologies. These elements with an integrated active optical protection coding system are automatically identified and authorized at an expert level. The created innovative compositions that protect the environment have exceptional properties – they are resistant to the external environmental impact, are of high strength, and low mass. The created ecological composite materials are characterized by exceptional physico-chemical properties, increased resistance to counterfeiting. Their production has a positive impact on the environment, as the consumption of chemical solvents is reduced, the materials are durable and reliable.

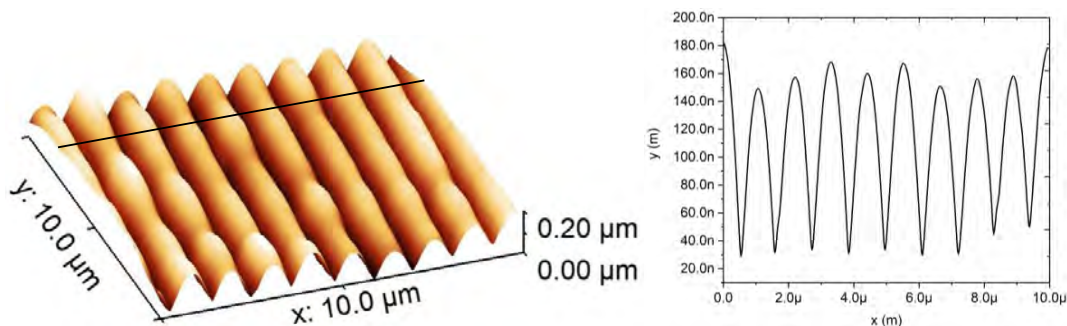


Fig. 1. After optimizing the parameters of the replication technological process during pressing, a periodic structure was formed in the PLEXIGLAS® XT polymer plate. From the atomic force microscopy 3D image and profile, it can be seen that the constant of the formed diffraction grating corresponds to the characteristics set during the designing.

The newly developed complex technology allows to reset the relation between the manufacturer and the consumer, provides protection against counterfeiting, and creates the possibility of automating trade and logistics systems.

-
- [1] Kumar Sharma Amit, Prashant Chauhan, D. Varshney Anshu, Concealing information in security hologram using interferometry, *Optica Applicata* **52**, 385-394 (2022).
- [2] Sanggyun Jung, Jiseok Lee, Holographic Anti-Counterfeiting Solutions Using Photocurable Polymers, *ECHE_Conference Papers* (2022).
- [3] Arvind Mukundan, Hsiang-Chen Wang et al., A Novel Multipurpose Snapshot Hyperspectral Imager used to Verify Security Hologram, 2022 International Conference on Engineering and Emerging Technologies (ICEET), Kuala Lumpur, Malaysia, 22512528 (2022).
- [4] Jiahao Miao, Xinghuo Ding, Shengjun Zhou, Chengqun Gui, Fabrication of Dynamic Holograms on Polymer Surface by Direct Laser Writing for High-Security Anti-Counterfeit Applications, *IEEE Access* **7**, 142926-142933 (2019).
- [5] Hui Gao, Xuhao Fan, Wei Xiong, Minghui Hong, Recent advances in optical dynamic metaholography, *Opto-Electronic Advances* **4**, 210030 (2021).

SELECTIVE FORMATION OF METALLIC MICROSTRUCTURES ON THE SURFACE OF POLYTETRAFLUOROETHYLENE USING LASER AND CHEMICAL TECHNOLOGIES

Šarūnas Mickus¹, Vytautas Vosylius¹, Evaldas Kvietkauskas¹, Viktorija Vrubliauskaitė¹, Karolis Ratautas¹

¹Department of Laser Technologies, State research institute Center for Physical Sciences and Technology, Vilnius, Lithuania
sarunas.mickus@ftmc.lt

Our daily lives are packed with many integrated, functional, and miniaturized devices. The amount of these devices is increasing therefore high demand for fast and cheap manufacturing methods arises. One of the newer methods for molded interconnect devices (MID)[1] production is Selective Surface Activation Induced by Laser (SSAIL)[2], [3]. Technology copes with complex 3D surfaces and allows different materials' metallization by electroless metal plating. However, several challenges related to the selection of optimal surface modification parameters for different surfaces and copper adhesion strength are yet to overcome.

The work is focused on the SSAIL process application on high-performance polytetrafluoroethylene (PTFE) polymer as well as dimensional and electrical properties evaluation of produced electrically conductive copper micro tracks. In this work, two different laser setups with Gaussian and Bessel beams were employed to form conductive microstructures on the Teflon surface. To clarify the best laser modification parameters with a Gaussian beam and the best chemical process steps surface roughness properties including root mean square height (S_q) and core void volume (V_{vc}) parameters were researched before and after the chemical etching step. After additional sheet resistance measurements, a clear successful metallization window was observed between two threshold values of the irradiation dose (13 and 24 J/cm²) and the highest conductivity was demonstrated for the chemically unetched sample. After the formation of micro tracks with the Bessel beam, it was noticed that metallized micro track's width, formed on the PTFE surface, increases as the scanning speed decreases. Finally, the minimal achievable width of copper-plated conductive micro tracks was evaluated.

The SSAIL method is successfully applied on the PTFE surface and selective metallized microstructures are formed (Fig. 1). Laser surface modification parameters such as pulse repetition rate and pulse pitch have a huge impact on process selectivity and final conductive track width. Although working sample electrical circuits and conductive micro tracks were experimentally demonstrated, further research on their successful application for conventional electronics is needed.

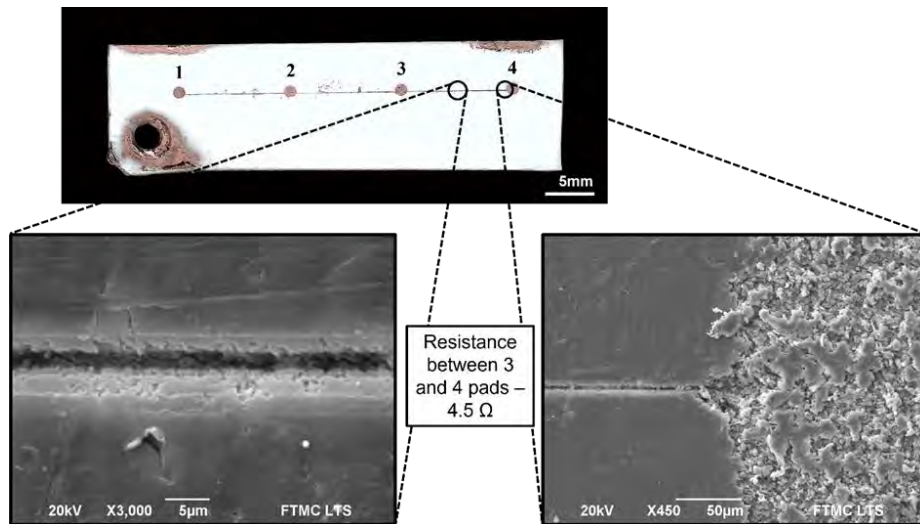


Fig. 1. At the top – scanned image of PTFE sample with copper coated tracks and contact pads. SEM image on the left shows morphology of the line and image on the right shows line connection with contact pad before metallization.

- [1] A. Islam, H. N. Hansen, and N. Giannakas, "Quality investigation of miniaturized Moulded Interconnect Devices (MIDs) for hearing aid applications," *CIRP Ann.*, vol. 64, no. 1, pp. 539–544, 2015.
- [2] K. Ratautas, V. Vosylius, A. Jagminienė, I. Stankevičienė, E. Norkus, and G. Račiukaitis, "Laser-induced selective electroless plating on pc/abs polymer: Minimisation of thermal effects for supreme processing speed," *Polymers (Basel)*, vol. 12, no. 10, pp. 1–16, 2020.
- [3] K. Ratautas, A. Jagminienė, I. Stankevičienė, E. Norkus, and G. Račiukaitis, "Laser assisted fabrication of copper traces on dielectrics by electroless plating," *Procedia CIRP*, vol. 74, pp. 367–370, 2018.

BIOCOMPATIBLE HYDROXYAPATITES CO-DOPED WITH TERBIUM(III) AND RUBIDIUM(I) IONS AS HIGHLY FUNCTIONAL MATERIALS FOR BIOMEDICAL APPLICATIONS

Dominika Czekanowska^{1,2,3*}, Nicole Nowak^{1,4} and Rafal Wiglusz^{1*}

¹ Institute of Low Temperature and Structure Research, Polish Academy of Sciences, Okolna St. 2, PL 50-422 Wroclaw, Poland

² Wroclaw University of Science and Technology, Wyb. Wyspianskiego 27, 50-370, Wroclaw, Poland

³ Refectio Students' Scientific Society, Department of Biostructure and Animal Physiology, Wroclaw University of Environmental and Life Sciences, Kożuchowska 1/3, 51-631 Wroclaw, Poland

⁴ Department of Department of Biostructure and Animal Physiology, Wroclaw University of Environmental and Life Sciences, Norwida St. 31 PL 50-375 Wroclaw, Poland

d.czekanowska@intibs.pl; r.wiglusz@intibs.pl

Recent successes in nanotechnology are reported about diversity of nanomaterials that can be successfully used in the various fields of biology and nanomedicine. Multifunctional nanomaterials may become especially desirable in tissue engineering field as factors leading to increased regeneration of fractured tissues, and as luminescent nanoprobes in bioimaging or bio-detection. One of the materials opening above possibilities are the basic elements of bone and dentin, the hydroxyapatites ($\text{Ca}_{10}(\text{PO}_4)_6(\text{OH})_2$ – HAp), characterized by exceptional biocompatibility, bioactivity, and mechanical properties.

The replacement of calcium ions in the crystal lattice of hydroxyapatite with lanthanide ions, e.g., terbium(III) ions that due to the small differences in ionic radius between Tb(III) ($r_{\text{ion}} = 0.923 \text{ \AA}$) and Ca(II) ($r_{\text{ion}} = 1.10 \text{ \AA}$) ions, can be successfully incorporated, results in enhanced luminescence properties in this material [1,2]. Rubidium(I) ions due to their large ionic radius ($r_{\text{ion}} = 1.51 \text{ \AA}$) in relation to Ca(II) ions, are also readily incorporated into the HAp matrix and show its enhanced bioactivity with maintaining full biocompatibility. In addition, rubidium(I) ions are like well-known lithium(I) ions influence on human bone development and cell proliferation which becomes promising for biomedical applications juxtaposed with the characteristics and functionalities of hydroxyapatite [3,4,5].

In our research, the basic structural, physical, and biological properties of hydrothermally synthesized hydroxyapatites co-doped with terbium(III) and rubidium(I) ions were thoroughly investigated. The X-ray powder diffraction (XRPD), Fourier transform infrared spectroscopy (FT-IR), transmission electron microscopy (TEM) techniques were used in our study to determine the structural characteristics and morphology of the obtained nanocomposites. By measuring excitation spectra, emission spectra and fluorescence lifetime, luminescence in the green visible light range from terbium(III) ions was evaluated. The *in vitro* studies on selected cell lines (L929 mouse fibroblasts, 3T3 mouse fibroblasts, 7F2 mouse osteoblasts) confirmed the high biocompatibility of the resulting nanopowders and the positive effect on cell growth stimulation. In addition, investigations using the human monocyte THP-1 cell line showed that our compounds do not induce stimulatory immune response to the tested cells. In conclusion, obtained hydroxyapatite-based nanocomposites can be successfully used in biomedicine, both as a bio-labelling material and as a potential material for use in treatments involving regenerative medicine and tissue engineering.

[1] Neacsu IA, Stoica AE, Vasile BS, Andronesu E. Luminescent Hydroxyapatite Doped with Rare Earth Elements for Biomedical Applications. *Nanomaterials* (Basel). 2019 Feb 10;9(2):239. doi: 10.3390/nano9020239.

[2] Deshmukh K, Shaik MM, Ramanan SR, Kowshik M. Self-Activated Fluorescent Hydroxyapatite Nanoparticles: A Promising Agent for Bioimaging and Biolabeling. *ACS Biomater Sci Eng*. 2016 Aug 8;2(8):1257-1264. doi: 10.1021/acsbiomaterials.6b00169.

[3] Yan-ni Tan, Wen-juan Chen, Wei Wei, Qian-li Huang, Xiang He. Rubidium-modified bioactive glass-ceramics with hydroxyapatite crystals for bone regeneration. *Transactions of Nonferrous Metals Society of China*. 2021;31(2):521-523. doi: 10.1016/S1003-6326(21)65514-0.

[4] Yanjun Liu, Yanni Tan, Jiangsong Wu. Rubidium doped nano-hydroxyapatite with cytocompatibility and antibacterial. *Journal of Asian Ceramic Societies*. 2021;9(1):323-333. doi: 10.1080/21870764.2020.1865861.

[5] Sobierajska, P. Wiglusz, R.J. Influence of Li⁺ ions on the physicochemical properties of nanocrystalline calcium–strontium hydroxyapatite doped with Eu³⁺ ions. *New Journal of Chemistry*. 2019;43:14908-14916. doi: 10.1039/C9NJ03003D

STUDY OF THE EFFECT OF VIBRATION ON FLUID FLOW IN ALUMINUM OXIDE NANOPORES

Urte Cigane, Arvydas Palevicius

Faculty of Mechanical Engineering and Design, Kaunas University of Technology, Lithuania
urte.cigane@ktu.lt

Looking at modern technologies and their development, miniaturization is integral, and research related to micro- and nano-sized elements is important in different fields such as electrotherapy and drug delivery [1], sensors [2], etc. Expanding and promising areas of technology encourage the study of micro- and nano-sized channels. Since the flow regimes in small fluid volumes are often laminar, fluid heat exchange is limited [3]. Acoustofluidic physics can be used to achieve an efficient mixing process for fluid flow in straight nanopores [4, 5].

In terms of anodic aluminum oxide (AAO) pore geometry, AAO pores can be characterized by a width-to-length ratio. The pore diameter of AAO membranes can be from tens to several hundreds of nanometers, and the length can be several tens of micrometers [6]. It results in limited liquid renewal at the bottom of the pore during the two-step anodization process. Therefore, the application of acoustofluidics to fabricate porous AAO membranes during the anodization process can be used to overcome the limitation. Furthermore, the effect of the vibrations used during the anodization process on the pore geometry is still in its early stages.

Thus, a study of the mixing process of fluid flow in a nano-diameter pore using vibration is presented. After performing theoretical calculations, the change in acoustic pressure, acoustic velocity, and velocity magnitude along the entire length of the pore was determined. The fluid flow velocity contour is presented in Fig. 1. Moreover, comparative curves of different frequencies are shown in Fig. 2.

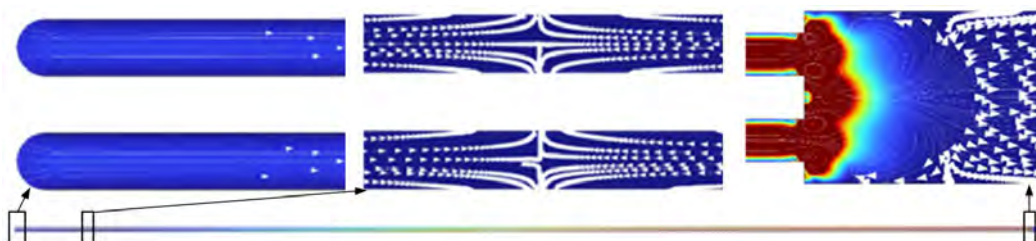


Fig. 1. Fluid flow velocity contour at resonant frequency excitation of 40 kHz when the pore depth is 55 μm .

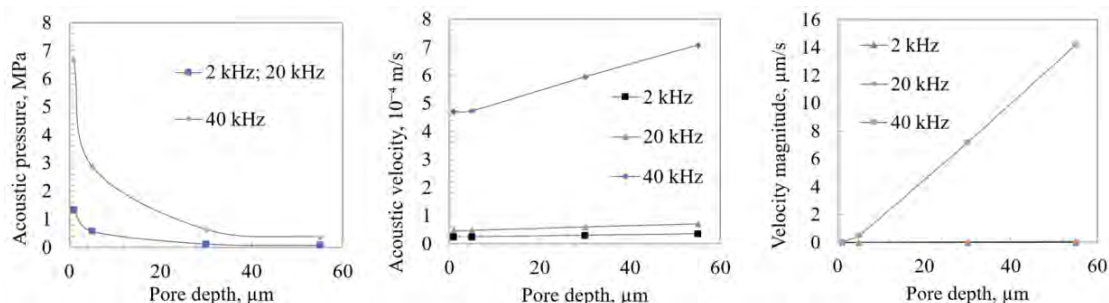


Fig. 2. Comparative curves of acoustic pressure, acoustic velocity, and velocity magnitude of different frequencies.

The results of the numerical simulation showed that the mixing process of the fluid flow in the pore was ensured by using vibrations. Therefore, the electrolyte concentration in the pores was also updated during the mixing process. It can be assumed that vibrations during the anodization process could ensure a more uniform distribution of the electrolyte temperature and pH values along the entire length of the pores.

- [1] Y. Huang, H. Li, T. Hu, et al., Implantable Electronic Medicine Enabled by Bioresorbable Microneedles for Wireless Electrotherapy and Drug Delivery, *Nano Lett.* **22**, 5944-5953 (2022). <https://doi.org/10.1021/acs.nanolett.2c01997>
- [2] M. Farrokhi, S.P. Manavi, F. Taheri, Non-invasive monitoring of pH and oxygen using miniaturized electrochemical sensors, *J Transl Med* **19**, 252 (2021). <https://doi.org/10.1186/s12967-021-02923-1>
- [3] S. Li, H. Zhang, J. Cheng, et al., A Numerical Study on Heat Transfer Performance in a Straight Microchannel Heat Sink with Standing Surface Acoustic Waves, *Heat Transfer Engineering* **43**, 371-387 (2021). <https://doi.org/10.1080/01457632.2021.1874670>
- [4] J.C. Hsu, C.Y. Chang, Enhanced acoustofluidic mixing in a semicircular microchannel using plate mode coupling in a surface acoustic wave device, *Sensors and Actuators A: Physical* **336**, 113401 (2022). <https://doi.org/10.1016/j.sna.2022.113401>
- [5] S. Maramizonouz, C. Jia, M. Rahmati, et al., Acoustofluidic Patterning inside Capillary Tubes Using Standing Surface Acoustic Waves, *International Journal of Mechanical Sciences* **214**, 106893 (2022). <https://doi.org/10.1016/j.ijmecsci.2021.106893>
- [6] A. Ruiz-Clavijo, O. Caballero-Calero, M. Martín-González, Revisiting anodic alumina templates: from fabrication to applications, *Nanoscale* **13**, 2227-2265 (2021). <https://doi.org/10.1039/D0NR07582E>

MULTIFUNCTIONAL NANOSYSTEMS: ASSESSMENT OF UPCONVERTING NANOPARTICLES FOR BIOIMAGING, TEMPERATURE SENSING, AND MRI

Egle Ezerskyte^{1*}, Augustas Morkvenas^{2,3}, Arturas Katelnikovas¹, Vitalijus Karabanovas^{2,3} and Vaidas Klimkevicius¹

¹ Institute of Chemistry, Vilnius University, Lithuania

² Biomedical Physics Laboratory, National Cancer Institute, Lithuania

³ Department of Chemistry and Bioengineering, Vilnius Gediminas Technical University, Lithuania

egle.ezerskyte@chgf.stud.vu.lt

There is an undeniable demand for the development of multifunctional materials that can be used for both bioimaging and drug delivery. Rare-earth doped upconverting nanoparticles (UCNPs) have shown great promise due to their unique optical properties, such as the absence of blinking, excitation with low energy radiation, and high emission signal-to-noise ratio [1]. However, there are several issues that need to be addressed before these materials can be widely used for theranostics. One issue is the extensive heating of samples using 980 nm lasers. To address this issue, researchers have developed approaches to shift the near-infrared (NIR) excitation to 808 nm by co-doping the UCNPs matrix with Yb³⁺ and Nd³⁺ pair [2]. This is beneficial because the 808 nm wavelength falls within the first biological window, where water absorbance is approximately 90-95% lower; therefore, 808 nm laser radiation can penetrate deeper into biological tissues compared to the commonly used 980 nm wavelength laser radiation [3].

In this study, we describe the synthesis of well-defined UCNPs with a complex core-shell composition that can be excited using both 808 and 980 nm laser radiation. Optical and temperature-sensing properties of these UCNPs are evaluated in detail. In addition, we investigate the colloidal stability of the UCNPs in aqueous and biological media, as well as the viability of human kidney cells (HEK 293t) after exposure to UCNPs' solutions of different concentrations. The potential use of these materials as MRI contrast agents is explored as well.

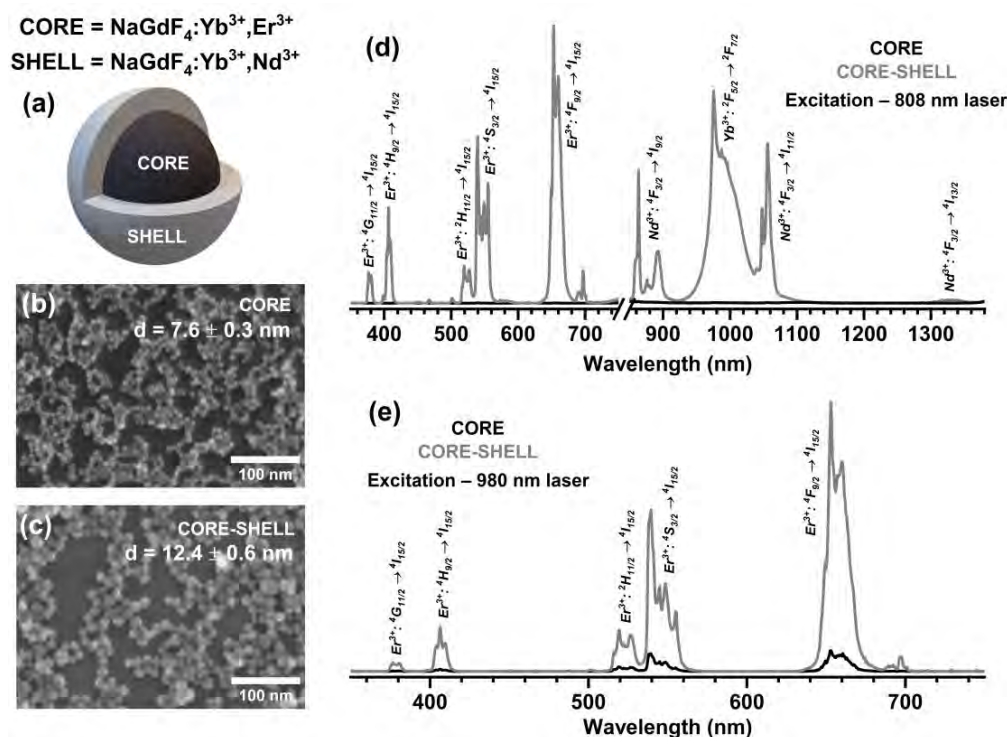


Fig. 1. Schematic representation of studied UCNPs (a); SEM images of NaGdF₄:Yb³⁺,Er³⁺ (b) and NaGdF₄:Yb³⁺,Er³⁺@NaGdF₄:Yb³⁺,Nd³⁺ (c) UCNPs; emission spectra of core and core-shell UCNPs under 808 nm (d) and 980 nm (e) laser excitation.

[1] M. Haase, H. Schäfer, Upconverting nanoparticles, *Angewandte Chemie International Edition*, 50 (2011) 5808-5829.

[2] T. Jia, G. Chen, Lanthanide nanoparticles for near-infrared II theranostics, *Coord. Chem. Rev.*, 471 (2022) 214724.

[3] Z. Yu, C. Eich, L.J. Cruz, Recent advances in rare-earth-doped nanoparticles for NIR-II imaging and cancer theranostics, *Frontiers in Chemistry*, 8 (2020) 496.

INVESTIGATION OF THERANOSTIC PROPERTIES OF SILICATE-SUBSTITUTED HYDROXYAPATITE CO-DOPED WITH Eu^{3+} Gd^{3+} AND Li^+ IONS

Natalia Charczuk^{1*}, Sara Targońska¹ and Rafal J. Wiglusz^{1*}

¹Institute of Low Temperature and Structure Research, Polish Academy of Sciences, Wroclaw, 50-422 Poland

*n.charczuk@intibs.pl, and r.wiglusz@intibs.pl

Searching for multifunctional biocompatible materials is of fundamental importance for theragnostic and bioimaging development. Although, hydroxyapatite's (HAp) usefulness in bone repair and tissue medicine is well known, still its potential as a drug delivery agent has been hardly investigated. Mesoporous HAp materials not only have high specific surface areas but also have OH^- groups that react with appropriate drug functional groups [1]. Because of that HAp-based materials are suitable carriers for loading and releasing drug molecules. What is more, doping the material with rare earth ions (RE^{3+}) results in highly promising materials applied in disease diagnosis and therapy [2].

Herein, novel silicate-substituted hydroxyapatites (Si-HAp), co-doped with rare earth ions (e.g. Eu^{3+} and Gd^{3+} ions) and alkaline metal ions (e.g. Li^+ ion) were obtained *via* short hydrothermal synthesis. Co-doping with both Eu^{3+} and Gd^{3+} ions results in obtaining materials showing simultaneously photoluminescent and magnetic properties. Likewise, the addition of Li^+ ion and silicate group (SiO_4^{4-}) increases nerve and bone regeneration processes [3,4].

To characterize the physicochemical properties of obtained nSi-HAps, the XRPD (X-ray Powder Diffraction), SEM-EDS (Scanning Electron Microscopy-Energy-Dispersive Spectrometry), TEM (Transmission Electron Microscopy), FT-IR (Fourier Transform Infrared) spectroscopy and ICP-OES (Inductively Coupled Plasma - Optical Emission Spectrometry) techniques were used. In further steps photoluminescence (PL) spectra of obtained materials were studied to determine the optimal dopants concentration for novel drug carriers. The effect of alkaline metal ions on the spectroscopic properties of Eu^{3+} and Gd^{3+} ions was thoroughly studied. In the final step, screening *in vitro* assays were used for the determination of biomaterials cytocompatibility.

In the results new nSi-HAp/ Li^+ / Eu^{3+} , Gd^{3+} compounds with the hexagonal structure of hydroxyapatite ($P6_3/m$ group) were synthesized and analyzed. Overall, the presented materials show promising physicochemical properties for potential theranostics applications and are expected to be evaluated in future investigations as potential drug carriers.

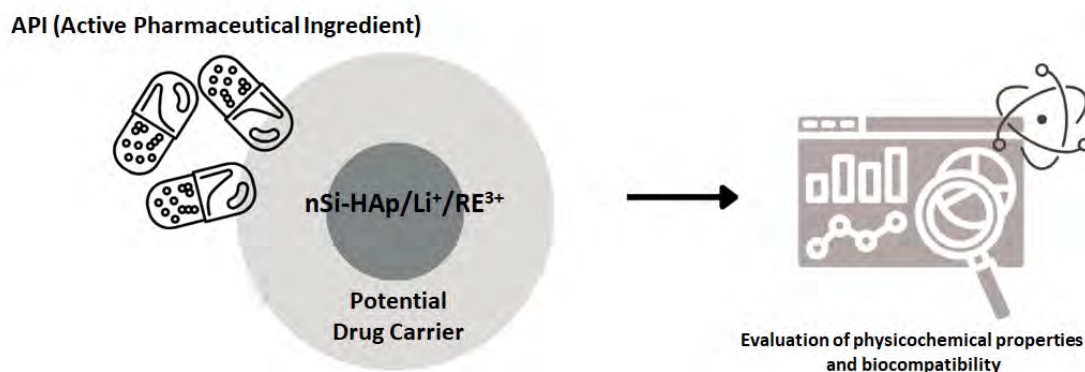


Fig. 1. Outline of our research on new HAp-based drug nanocarriers.

[1] V. Paterlini, M. Bettinelli, et al., Characterization and Luminescence of Eu^{3+} - and Gd^{3+} -Doped Hydroxyapatite $\text{Ca}_{10}(\text{PO}_4)_6(\text{OH})_2$. *Crystals*, **10**, 806 (2020).

[2] S. Targońska, R.J. Wiglusz, Investigation of Physicochemical Properties of the Structurally Modified Nanosized Silicate-Substituted Hydroxyapatite Co-Doped with Eu^{3+} and Sr^{2+} Ions, *Nanomaterials* **11**, 27 (2021).

[3] ZY. Qiu, IS. Noh, SM. Zhang, Silicate-doped hydroxyapatite and its promotive effect on bone mineralization. *Front. Mater. Sci.* **7**, 40 (2013).

[4] K. Marycz, P. Sobierajska, A. Smieszek, M. Marekziak, K. Wiglusz, R.J. Wiglusz, Li^+ activated nanohydroxyapatite doped with Eu^{3+} ions enhances proliferative activity and viability of human stem progenitor cells of adipose tissue and olfactory ensheathing cells. Further perspective of nHAP: Li^+ , Eu^{3+} application in theranostics, *Materials Science and Engineering: C*, **78**, 151 (2017).

TITANIUM ADHESION LAYER INFLUENCE ON LASER DIRECT WRITING FOR THE FORMATION OF GOLD MICROBUMPS ARRAYS

Rodrigas Liudvinavičius, Evaldas Stankevičius

Department of Laser Technologies, Center for Physical Sciences and Technology, Lithuania
rodrigas.liudvinavičius@ftmc.lt

Periodically arranged micro-particles and their structures are found in many applications. Such use is based on a plasmonic effect resulting from light interaction with metal structures. Plasmonics holds huge interest as it is considered a promising effect in terms of utilization in the field of new optical devices, where it is based on surface lattice resonances (SLRs). SLRs are collective charge oscillations coupled to an external electromagnetic field that propagates between metal and a dielectric interface. However, more investigations must be done to improve quality and expand the field of use.

In this work, the SLRs effect is achieved with diffraction phenomena [1], where arranged microparticles of gold act as diffractive grating, demonstrating plasmonic resonances for incidence light. When a plasmon is successfully excited by a photon, the light particle is absorbed, which is reflected in the reflection graph. Such use of a diffraction grating is conditioned by SLR theory, as direct incident light on a flat metal surface can not excite a plasmon due to a momentum mismatch, as a free-space photon has less momentum (wavevector is smaller) than a localized plasmon.

In this study, periodic arrays of microbumps formation were produced on a thin 50 nm gold layer with different titanium adhesion layer thickness (from 0 to 10 nm), using laser direct writing technique (LDW) and forming gold microbumps by a 0.4 nJ single laser pulse. Formed structures were analyzed with a spectrophotometer and a scanning electron microscope (SEM).

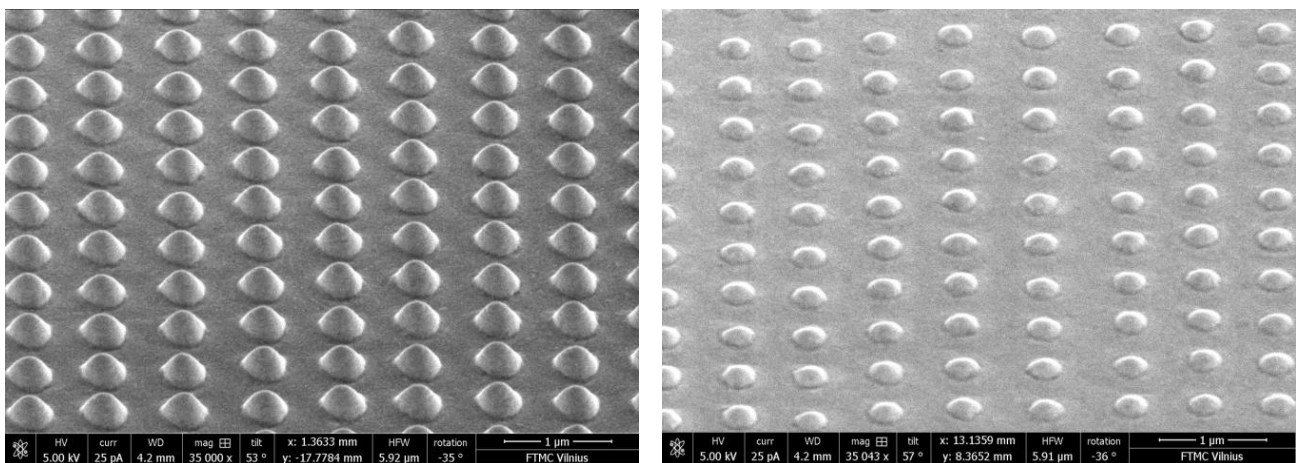


Fig. 1. SEM micrograph of fabricated bumps array in a thin gold film (50 nm): on the left without an adhesion layer and on the right with a 10 nm titanium adhesion layer. Micrographs were taken at a sample tilt angle of 52°. Samples were made using a single-shot laser pulse with 0.4 nJ energy.

The results demonstrate that SLRs besides the main dependencies on the period of the fabricated arrays, light polarization, incident angle of light, and the sample orientation, also show a strong dependency on the adhesion layer, as with an additional titanium layer between the substrate and gold film, better results were achieved. Such experimental results were confirmed by a “basic” tape test, where adhesion was tested by a peeling/removing test and evaluating it by an adhesion rating scale.

The influence of the adhesion layer was compared by measuring spectrophotometer graphs by evaluating the parameters of peaks: depth, full width at half maximum (FWHM), Q factor, and MQ factor.

[1] V. G. Kravets, F. Schedin, A. N. Grigorenko, Extremely Narrow Plasmon Resonances Based on Diffraction Coupling of Localized Plasmons in Arrays of Metallic Nanoparticles, Phys. Rev. Lett. 101, 087403, 2008.

SYNTHESIS OF SILVER NANOWIRES

Gytautė Sirgėdaitė¹, Lina Mikoliūnaitė^{1,2}

¹ Department of Organic Chemistry, Center for Physical Sciences and Technology, Lithuania

² Institute of Chemistry, Faculty of Chemistry and Geosciences, Vilnius University, Lithuania
gytaute.sirgedaite@ftmc.lt

One-dimensional (1D) metal nanoparticles attracted widespread research interest due to their unique electrical, magnetic, optical, thermal, and catalytic properties [1]. Silver nanowires (AgNW) have been one of the main mostly studied NW because of their high electrical conductivity (6.39 S/m) and excellent thermal conductivity (429 W/(m·K)), transparency, physiochemical, optical, and mechanical properties [2,3]. The diameter of Ag nanowires is typically 10-200 nm, and length 5-100 μm [2,4]. AgNW are mainly used in thin-film solar cells, biosensors, organic light-emitting diodes (OLEDs), photoluminescence, surface-enhanced Raman scattering [1,2,5,6].

Among noble metals, Ag nanomaterials are widely studied and used as SERS-active substrate due to their surface plasmon resonance properties. 1D silver NW can provide better insight in investigation the dependence of plasmon-plasmon interaction and electromagnetic scattering due to their panning from nanometer to micrometer scale in length region [7].

Through the years, many synthesis methods were proposed to obtain Ag nanowires. The polyol method to obtain silver NW has gathered much attention since it is facile, scalable, provides good control over nanowire morphology, low production cost [1]. In this work we compare obtained AgNW based on Qian et. al. introduced method. Round-bottom flask with 100 mL of ethylene glycol (EG) containing NaCl, polyvinylpyrrolidone (PVP), AgNO₃, and CuCl₂ were preheated at 185 °C temperature. Subsequently, 30 mL of freshly prepared AgNO₃ in EG was added dropwise with vigorous stirring. After the reaction was completed, the flask cooled down to room temperature. As prepared Ag NWs in EG suspension appeared to be shiny, silky white. The solution in EG was firstly washed repeatedly with water to transfer all the AgNWs/NPs into an aqueous stock solution. Then acetone was added to the stock solution, causing AgNW to precipitate selectively, while the AgNPs remained in the supernatant. After discarding the supernatant and redispersing the pellet in water, the nanowires were significantly enriched and purified [8]. To improve AgNW in length the temperature and heating time was changed. Obtained AgNW were investigated using scanning electron microscopy (SEM), UV-Vis and Raman spectroscopies.

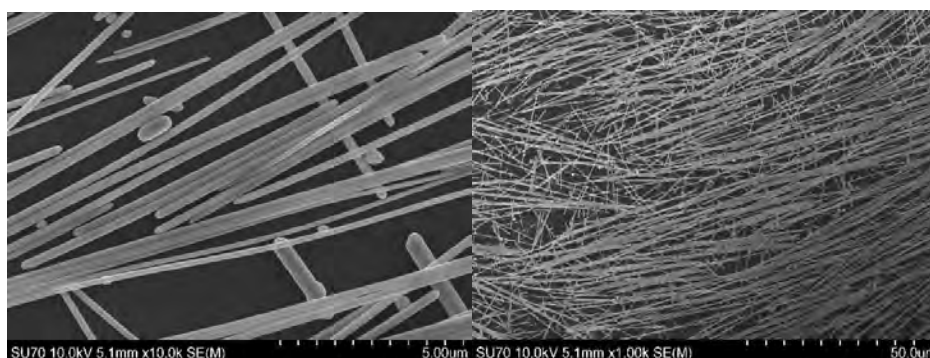


Fig. 1. SEM image of silver nanowires

[1] Kumar, A., Shaikh, M. O., and Chuang, C. H., *Nanomaterials* **11**(3), 693 (2021).

[2] Ha, H., et al., *Colloid and Interface Science Communications* **50**, 100663 (2022).

[3] Tan, D., et al., *J Mater Sci: Mater Electron* **31**, 15669-15696 (2020).

[4] Zhang, P., et al., *Materials Science and Engineering: B* **223**, 1-23 (2017).

[5] Sim, H., et al., *Nanoscale* **10**, 12087 (2018).

[6] Melendrez, M. F., et al., *Nanoscale Res Lett* **10**, 48 (2015).

[7] Zhang, L., et al. *Spectrochimica Acta Part A: Molecular and Biomolecular Spectroscopy* **133**, 411-416 (2014).

[8] Qian et. al., *Nano Lett* **17**, 7171-7176 (2017).

PHOTOCHEMICAL SYNTHESIS OF SILVER NANOPARTICLES AND STUDY OF THEIR STRUCTURAL PROPERTIES

Mindaugas Ilickas¹, Asta Guobienė¹, Brigita Abakevičienė¹

¹Kaunas University of Technology, Institute of Materials Science, Lithuania
mindaugas.ilickas@ktu.lt

The use of silver nanoparticles (AgNPs) has been proposed as a novel strategy for combating bacterial and viral strains with high resistance. AgNPs, which are well-known nanoparticles, have been widely utilized in the identification, treatment, and neutralization of viral infections [1]. For particles with at least two dimensions under 100 nm, it is crucial to examine their acceptable toxicity. Silver nanoparticles have recently garnered significant attention as potential antibacterial agents among nanoparticles [2]. This has resulted in silver-based biocides becoming increasingly prevalent. The synthesis of AgNPs can be achieved through a variety of methods, including physical, chemical, and biological approaches.

In this work, a UV-mediated photochemical synthesis method was employed to prepare coatings on quartz glass substrates using the doctor blade coating technique. Silver nitrate (AgNO₃) was utilized as the precursor, and the solution of AgNO₃ was incorporated into a polyvinyl butyral (PVB) matrix. The experiments were conducted under ambient temperature and pressure conditions using a dual-wavelength UV-Vis source (Desaga Heidelberg 220V, 75W) with wavelengths of 254 nm (1.64 mW/cm² intensity) and 366 nm (0.80 mW/cm² intensity). The structural properties of the coatings were characterized using various techniques such as atomic force microscopy (AFM), UV-Vis's spectroscopy, X-ray diffractometry (XRD), and water contact angle (WCA) measurements.

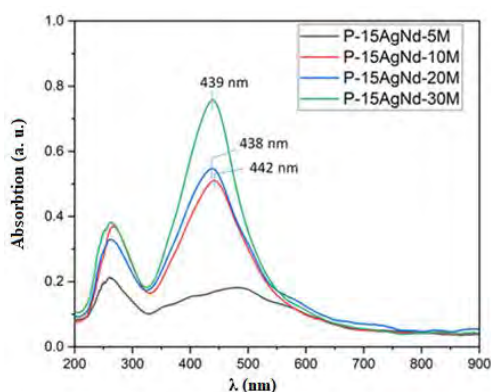


Fig. 1. Absorption spectra of Ag-PVB nanocomposite coatings on glass surface.

The AgNPs-PVB nanocomposite material was characterized through various techniques. The results of these analyses revealed a well-ordered distribution of AgNPs within the polymer matrix of PVB. As the duration of UV irradiation exposure increased, a decrease in the diameter of the AgNPs from 120 to 20 nm was observed, along with a slight change in elasticity (7.6 ± 0.6 N/m) and significant variations in adhesion force. These findings demonstrate that the size and adhesion strength of the NPs can be controlled through adjustments in the UV exposure time. The absorption spectra of the AgNPs-PVB nanocomposite films were recorded and analysed in the wavelength range of 200-900 nm after removal of the PVB polymer on the glass substrate. The UV-Vis spectra showed maxima of Ag peaks at the wavelengths of 438 nm, 439 nm, 442 nm, and 499 nm, indicating the formation of AgNPs with different geometric dimensions in the PVB polymer network. As the exposure time increased from 5 to 30 minutes, the size of the AgNPs decreased. Additionally, the wetting angle of the formed PVB coating on the glass was found to be low at 87.1° . As the duration of exposure to UV irradiation increased and the diameter of AgNPs decreased, the wetting angles of the inserted AgNPs into the PVB polymer network also decreased. Further research could focus on investigating the antiviral properties of the AgNPs-PVB coating and its potential applications in healthcare and food packaging.

[1] K. Khoshnevisan, et al., Nanobiocide Based-Silver Nanomaterials Upon Coronaviruses: Approaches for Preventing Viral Infections, *Nanoscale Research Letters* **16**(1) (2021).

[2] M. Hemmati, et al., Investigation of acute dermal irritation/corrosion, acute inhalation toxicity and cytotoxicity tests for Nanobiocide®, *Nanomedicine Research Journal* **1**(1), 23-29 (2016).

METAL OXIDE NANOSTRUCTURES IN CHEMICAL SENSORS AND BIOSENSORS

Vincentas Mačiulis¹, Almira Ramanavičienė², Miglė Stančiauskaitė², Ieva Plikusienė²

¹Department of Nanotechnology, Center for Physical Sciences and Technology, Lithuania

²NanoTechnas - Nanotechnology and Materials Science Center, Institute of Chemistry, Vilnius University, Lithuania
vincentas.maciulis@ftmc.lt

Metal oxide nanostructures have proven effective in the development of chemical and biosensors due to their unique optical, electrical, and physical properties. Recent advancements in synthesis technologies have allowed for more control over nanostructure production, resulting in increased sensor performance and reliability. Applications include detection of environmental pollutants and biological materials. The use of metal oxide nanostructures in chemical sensors and biosensors is a rapidly growing field with great potential for practical impact in a variety of industries and research areas [1].

Metal oxide nanostructures can be fabricated by a simple chemical precipitation reaction. However, using wet chemical processes alone can make it challenging to acquire accurate dimensions and innovative form of nanostructures. As a result, the use of templates, external energy (thermal or electrical), and pressure can result in more control and variety in the morphology of metal oxide nanostructures produced. A variety of methods for fabricating metal oxide nanostructures are being investigated: synthesis in reverse microemulsions, dendrimer templating, chemical bath deposition, electrodeposition, chemical vapor deposition, and atomic layer deposition [2], [3].

Biosensing and chemical sensing have gained interest in the last decade and are used in many fields: food, environment and healthcare. Both applications rely on an interaction of the analyte with a surface-bound material or chemical interface. Biosensors are typically classified according to the type of bioreceptor (enzyme, antibody, DNA, cells, biomimetic) and signal transmission (optical, calorimetric, piezoelectric, electrochemical). Chemical sensors, on the other hand, are classified by their transmission method (optical, electrical, and mechanical) and by the structure/composition of the chemical interface (metal, metal oxide, and metal-semiconductor). Therefore, in both sensor applications, metal oxide nanostructures can be used to modify/amplify the signal transduction [4], [5].

-
- [1] V. Mačiulis, A. Ramanavičienė, and I. Plikusienė, "Recent Advances in Synthesis and Application of Metal Oxide Nanostructures in Chemical Sensors and Biosensors," *Nanomaterials*, vol. 12, no. 24, 2022, doi: 10.3390/nano12244413.
 - [2] V. Mačiulis *et al.*, "Porous aluminium oxide coating for the development of spectroscopic ellipsometry based biosensor: Evaluation of human serum albumin adsorption," *Coatings*, vol. 10, no. 11, 2020, doi: 10.3390/coatings10111018.
 - [3] I. Plikusienė *et al.*, "Total internal reflection ellipsometry for kinetics-based assessment of bovine serum albumin immobilization on ZnO nanowires," *J. Mater. Chem. C*, vol. 9, no. 4, pp. 1345–1352, 2021, doi: 10.1039/d0tc05193d.
 - [4] A. Ramanavičienė *et al.*, "Magneto-Immunoassay for the Detection and Quantification of Human Growth Hormone," *Biosensors*, vol. 12, no. 2, 2022, doi: 10.3390/bios12020065.
 - [5] L. Sakalauskienė, A. Popov, A. Kausaitė-Minkstimiene, A. Ramanavicius, and A. Ramanavičienė, "The Impact of Glucose Oxidase Immobilization on Dendritic Gold Nanostructures on the Performance of Glucose Biosensors," *Biosensors*, vol. 12, no. 5, p. 320, 2022, doi: 10.3390/bios12050320.

ELECTROCHEMISTRY-DRIVEN AFFINITY SENSOR FOR THE DETECTION OF ANTIBODIES AGAINST SARS-COV-2

Maryia Drobysh¹, Viktorija Liustrovaite², Alma Rucinskiene³, Ausra Baradoke¹, Almira Ramanaviciene², Ieva Plikusiene^{1,2}, Urte Samukaite-Bubniene^{1,2}, Roman Viter⁴, Chien-Fu Chen⁵, Arunas Ramanavicius^{1,2}

¹Department of Nanotechnology, State Research Institute Center for Physical Sciences and Technology, Lithuania

²Department of Physical Chemistry, Faculty of Chemistry and Geosciences, Vilnius University, Lithuania

³Department of Electrochemical Materials Science, State Research Institute Center for Physical Sciences and Technology, Lithuania

⁴Institute of Atomic Physics and Spectroscopy, University of Latvia, Latvia

⁵Institute of Applied Mechanics, National Taiwan University, Taiwan

maryia.drobysh@ftmc.lt

Herein, we reported the study on the use of electrochemical techniques for the detection of antibodies against severe acute respiratory syndrome coronavirus 2 (SARS-CoV-2). The objective was to determine optimal experimental conditions using a variety of substrates, electrochemical methods and immobilisation techniques. In our experiments, we tested the electrochemical detection of antibodies against SARS-CoV-2 (from the real serum sample) by affinity interaction with recombinant Spike protein (rSpike) immobilised on the working electrode surface.

In our earliest work [1], the rSpike was immobilised on the working electrode using a mixture of self-assembled monolayers (SAM): 1-mercaptopundecanoic acid (for protein binding) and 6-mercapto-1-hexanol (as a spacer). We utilised Au-sputtered microscopic glass as the working electrode. Hereafter, the sequential incubation in the antibodies (anti-rS) concentrations range was carried out. The electrochemical methods of cyclic voltammetry (CV) and electrochemical impedance spectroscopy (EIS) were employed for the detection of affinity interaction in phosphate-buffered saline (PBS) pH 7.4 in the presence of 2 mM of $[\text{Fe}(\text{CN})_6]^{3-/4-}$. The limits of detection (LOD) for CV and EIS were 2.53 nM and 1.99 nM, correspondingly [1].

Another experiment [2] was based on the application of screen-printed carbon electrodes (SPCE) with Au nanostructures (AuNS) electrodeposited on the working electrode surface. In this case, L-cysteine was used as SAM for rSpike immobilisation and CV and differential pulse voltammetry (DPV) were applied for electrochemical observation in PBS/ $[\text{Fe}(\text{CN})_6]^{3-/4-}$ medium. The resulting LOD values were 0.27 nM for CV and 0.14 nM for DPV [2].

In our recent study [3], we reported an EIS-based affinity sensor. The rSpike was immobilised on the phytic acid doped polyaniline films (PANI-PA) directly covering SPCE. Electrochemical measurements were performed in PBS without adding $[\text{Fe}(\text{CN})_6]^{3-/4-}$. The calculated LOD value for this sensor was 8.00 nM [3].

We can assume that the system based on the AuNS-modified SPCE is more sensitive toward anti-rSpike detection by comparing LODs for the CV method in the two first tests. Moreover, it is notable that employing SPCE enhanced the reproducibility of the sensor. Among all the electrochemical methods used, it is possible to single out DPV as the fastest one and with the lowest LOD value. However, despite the high LOD value relative to other experiments, the PANI-based sensor had the advantage of label-free detection.

Acknowledgements: These researches were conducted under the Lithuania–Latvia–China (Taiwan) project, and it has received funding according to agreement No S-LLT-21-3 with the Research Council of Lithuania (LMTLT) (No. 110-2923-E-002-004-MY3 for Taiwan).

[1] V. Liustrovaite, M. Drobysh, A. Rucinskiene et al., Towards an Electrochemical Immunosensor for the Detection of Antibodies against SARS-CoV-2 Spike Protein, *Journal of The Electrochemical Society* **169**(3), 037523 (2022).

[2] M. Drobysh, V. Liustrovaite, A. Baradoke et al., Determination of rSpike Protein by Specific Antibodies with Screen-Printed Carbon Electrode Modified by Electrodeposited Gold Nanostructures, *Biosensors* **12**(8), 593 (2022).

[3] M. Drobysh, A. Ramanavicius, A. Baradoke, Polyaniline-based electrochemical immunosensor for the determination of antibodies against SARS-CoV-2 spike protein, *Science of The Total Environment* **862**, 160700 (2023).

POLYANILINE AND POLYPYRROLE NANOCOMPOSITES WITH EMBEDDED GLUCOSE OXIDASE AND GOLD NANOPARTICLES

Natalija German¹, Anton Popov¹, Almira Ramanaviciene¹, Arunas Ramanavicius²

¹ Division of Immunology, State Research Institute Center for Innovative Medicine, Vilnius, Lithuania

² Department of Physical Chemistry, Faculty of Chemistry and Geosciences, Vilnius University, Vilnius, Lithuania

natalija.german@imcentras.lt

Intensive studies and the application of π - π conducting polymers such as polyaniline (PANI) and polypyrrole (Ppy) has been developed extensively during the last few decades [1]. Conducting polymers are used for immobilization strategies and biosensors development [2]. In the process of the enzyme-assisted synthesis of polymers, the suitable monomer is attacked by a radical cation induced by H_2O_2 [3]. Gold nanoparticles (AuNPs) able speed-up the polymerization of monomers [4]. Polymeric nanocomposites based on noble metal nanoparticles embedded within polymers are characterized by unique properties, electrical conductivity, high surface area and flexibility [5].

The main aim of this research was to evaluate the morphology, hydrodynamic diameter and the electrochemical characteristics of enzyme-assisted polymeric nanocomposites (Fig.1). For this purpose polyaniline and polypyrrole nanocomposites with embedded glucose oxidase (GOx) and gold nanoparticles were formed by enzymatic polymerization of corresponding monomers in the presence of 0.46×10^{16} particles L^{-1} 6 nm diameter colloidal gold nanoparticles ($\text{AuNPs}_{(6\text{ nm})}$) or 0.6 mmol L^{-1} solution of tetrachlorauric acid. Enzymatically formed Ppy- and PANI-based nanocomposites were of spherical and lamellar forms and are attractive for the use. It was investigated by dynamic light scattering method, that by an increase of polymerization time until 4.5 days the hydrodynamic diameter of PANI/ $\text{AuNPs}_{(6\text{ nm})}$ -GOx, PANI/ $\text{AuNPs}_{(\text{AuCl}_4^-)}$ -GOx, Ppy/ $\text{AuNPs}_{(6\text{ nm})}$ -GOx and Ppy/ $\text{AuNPs}_{(\text{AuCl}_4^-)}$ -GOx nanocomposites grew up to 1128, 659, 594 and 388 nm [6]. The measurements performed using cyclic voltammetry confirmed high charge transfer ability of synthesized polymeric nanocomposites. It was investigated, that during enzyme-assisted polymerization the conversion of PANI leucoemeraldine form to emeraldine salt took place; the transition of cation-polaron into cation-bipolaron-based state of Ppy is ongoing.



Fig.1. Schematic representation of polymeric nanocomposites synthesis and investigation

Characterized by good yield of polymerization reaction and high purity from surfactants developed nanocomposites can be applied in the future for wide range of applications including various biomedical fields, development of biosensors and biofuel cells.

Acknowledgments. This research was funded by a grant (No. S-MIP-20-18) from the Research Council of Lithuania.

[1] S.C. Luo, Conducting polymers as biointerfaces and biomaterials: a perspective for a special issue of polymer reviews, *Polymer Reviews* **53**, 303-310 (2013).

[2] R. Batool, A. Rhouti, M.H. Nawaz, A. Hayat, J.L. Marty, A review of the construction of nano-hybrids for electrochemical biosensing of glucose, *Biosensors* **9**, 1–19 (2019).

[3] N. German, A. Popov, A. Ramanaviciene, A. Ramanavicius, Evaluation of enzymatic formation of polyaniline nanoparticles, *Polymer* **115**, 211–216 (2017).

[4] M. Ilčíková, J. Filip, M. Mrlík, T. Plachý, J. Tkáč, P. Kasák. Polypyrrole nanotubes decorated with gold particles applied for construction of enzymatic bioanodes and biocathodes, *International Journal of Electrochemical Science* **10**, 6558-6571 (2015).

[5] P.M.A. Poletti, F.R. Caetano, M.F. Bergamini, L.H. Marcolino-Junior, Facile synthesis of a silver nanoparticles/polypyrrole nanocomposite for non-enzymatic glucose determination, *Materials Science & Engineering C* **75**, 88-94 (2017).

[6] N. German, A. Popov, A. Ramanaviciene, A. Ramanavicius, Formation and electrochemical characterisation of enzyme-assisted formation of polypyrrole and polyaniline nanocomposites with embedded glucose oxidase and gold nanoparticles, *Journal of The Electrochemical Society* **167**, 165501 (2020).

RESISTIVITY AND LOW-FREQUENCY NOISE CHARACTERISTICS OF HYBRID COMPOSITES WITH CARBON NANOTUBES AND GRAPHENE

Frydrichas Mireckas¹

¹Institute of Applied Electronics and Telecommunications, Vilnius University, Sauletekio 3, 10257, Vilnius, Lithuania
frydrichas.mireckas@ff.stud.vu.lt

Carbon nanoparticles have garnered a notable amount of attention from the scientific community for their properties, such as excellent electric and thermal conductivity, mechanical stability and the possibility to develop structures that either reflect or transmit light incredibly effectively [1]. Effective practical applications of carbon nanoparticles generally necessitate the formation of various hybrid materials, which stabilises the nanoparticles and enables their use on meso- and macro- levels [2]. One such category of hybrid materials is carbon nanoparticle composites, consisting of carbon nanoparticles distributed in a polymer matrix [3]. These composites are considered to be disordered materials, and their electric properties are dependent on their structure and carbon nanoparticle filler concentration. Therefore, such materials warrant investigation to identify considerations for potential applications.

Low-frequency noise measurements are an effective method for investigation of conduction mechanisms in disordered materials. Of particular note is low-frequency noise that exhibits a spectral density which is inversely proportional to the frequency, also known as $1/f$ noise, the level of which determines the sensitivity limits of sensors [4].

The resistivity and low-frequency noise characteristics of hybrid composites with carbon nanotubes (CNT) and graphene (GR) were investigated. Samples were prepared via melt processing of the polymer *Peran STC* and different concentrations of CNT and GR. Measurements of resistance and low-frequency (10 Hz – 20 kHz) noise characteristics were carried out in a temperature range of (75–365) K. Dominant conduction mechanisms and their dependence on the filler densities were investigated.

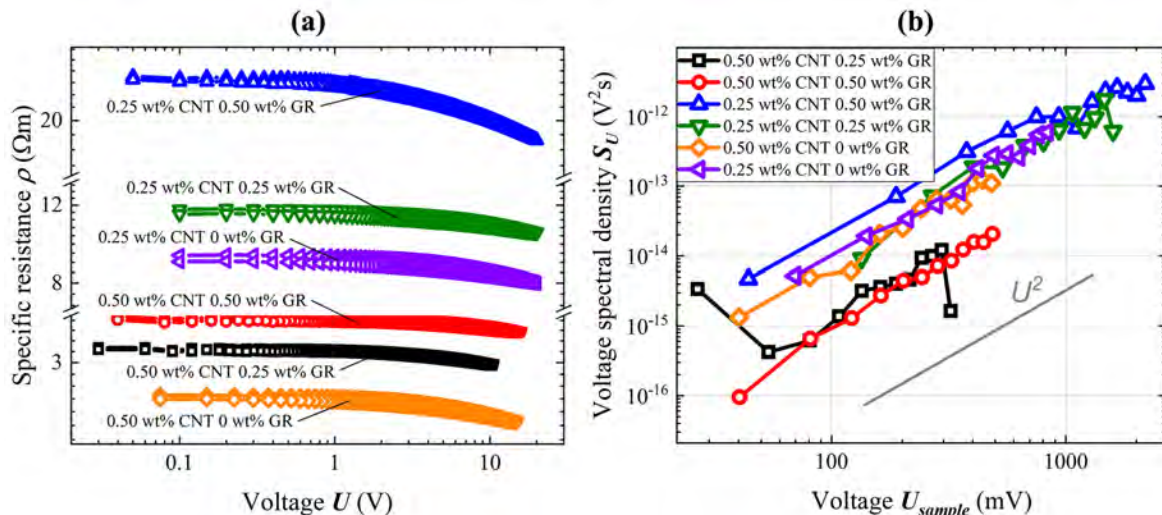


Fig. 1. Specific resistivity dependence on voltage (a) and voltage noise spectra dependence on voltage in room temperature at 86 Hz (b).

The specific resistance of the CNT and GR composites depends more strongly on the concentration of CNT (Fig. 1(a)). In samples with identical CNT concentrations, the samples with lower GR content exhibit lower specific resistance. At temperatures above 323 K, the specific resistance of the composites irreversibly decreases due to the decrease of the specific resistance of the polymer matrix.

At low temperatures ((75–245) K), the temperature dependence of specific resistance is well-fitted by Mott's law, and the dominant charge transfer mechanism in this temperature region is said to be Mott's variable-range hopping.

The resultant low-frequency voltage noise spectra of the investigated carbon nanocomposites consists of $1/f^\alpha$ type noise and impulse noise. The low-frequency voltage noise spectra is proportional to the voltage square U^2 (Fig. 1(b)), and the intensity of the noise is proportional to the specific resistance of the composite.

- [1] Baughman, R. H. (2002). Carbon Nanotubes--the Route Toward Applications. *Science*, 297(5582), 787–792. doi:10.1126/science.1060928
 [2] Spitalsky, Z., Tasis, D., Papagelis, K., & Galiotis, C. (2010). Carbon nanotube–polymer composites: Chemistry, processing, mechanical and electrical properties. *Progress in Polymer Science*, 35(3), 357–401. doi:10.1016/j.progpolymsci.2009
 [3] Khan, W., Sharma, R., & Saini, P. (2016). Carbon Nanotube-Based Polymer Composites: Synthesis, Properties and Applications. *Carbon Nanotubes - Current Progress of Their Polymer Composites*. doi:10.5772/62497
 [4] Tretjak, M., Pralgauskaitė, S., Matukas, J., Macutkevič, J., Banys, J., Shenderova, O. (2019). Low Frequency Noise and Resistivity Characteristics of Hybrid Composites with Onion-Like Carbon and Multi-Walled Carbon Nanotubes. *Fluctuation and Noise Letters*, 18

Investigation of crystals growth in ZnO thin films made by Sol-Gel technique

Deividas Vainauskas, Vidas Pakštas, Arnas Naujokaitis, Rokas Kondrotas

Department of Characterisation of Materials Structure, State research institute Center for Physical Sciences and Technology, Lithuania

deividas.vainauskas@ftmc.lt

Metal oxide semiconductor films have been widely studied and have received considerable attention in recent years due to their optical and electrical properties. Among them, ZnO is one of the metal oxide semiconductors suitable for use in optoelectric devices. It is an alternative material to tin oxide and indium oxide, which have been most used to date [1]. ZnO is extensively studied because of its potential applications in various fields, such as gas sensor, solar cells, photo-detectors, light emitting diodes (LEDs) and laser systems [2].

ZnO films are grown by many different methods such as pulsed laser deposition (PLD), magnetron sputtering, MOCVD, spray pyrolysis and sol-gel process [3]. The properties of ZnO thin films are much influenced by not only the growth methods but also the heat treatment parameters, especially the thermal annealing [4].

In our work we prepared thin-films by sol-gel route, spin-coating method and investigated how layer structure, layer thickness, surface and volume morphology, electrical and optical properties depends on solution concentrations, drying and annealing temperatures.

ZnO thin films were deposited on fluorine-doped tin oxide (FTO) coated glass substrates by spin-coating method. For solution preparation, zinc acetate dihydrate ($\text{Zn}(\text{CH}_3\text{COO})_2 \cdot 2\text{H}_2\text{O}$) was used as a starting material, 2-methoxyethanol and monoethanolamine (MEA) were used as a solvent and stabilizer respectively. Zinc acetate dihydrate was first dissolved in 2-methoxyethanol and then MEA were added. The molar ratio of MEA to zinc acetate dihydrate was maintained at 1.0 and the concentration of zinc acetate dihydrate was 0,3 M; 0,5 M; 0,7 M. The solutions were stirred at 60°C for 2 hours, thus obtained clear solution. After the filtration coating was made. The solution spin-coated at rotation speeds from 0 rpm to 3000 rpm with an acceleration of 200 rpm/s in 15 s, finally reaching 3000 rpm and then additionally rotated at 3000 rpm for 45 sec thus the coating process has been taken 60 s overall. After deposition, the films were dried at 300 °C for 10 min on opened hot plate to evaporate the solvent. The process was repeated to obtain the desirable thickness of the film. Thus obtained multilayer films were covered and annealed on hot plate at various temperatures (300 °C- 550 °C) to achieve crystalline structures.

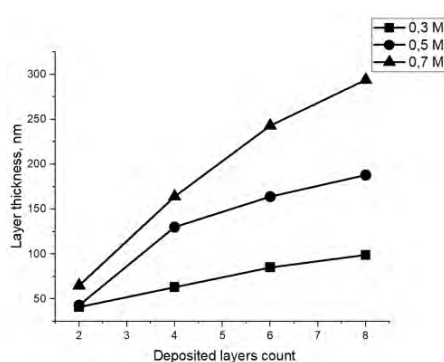


Fig. 1. Layer thickness dependance on concentrations and deposition count.

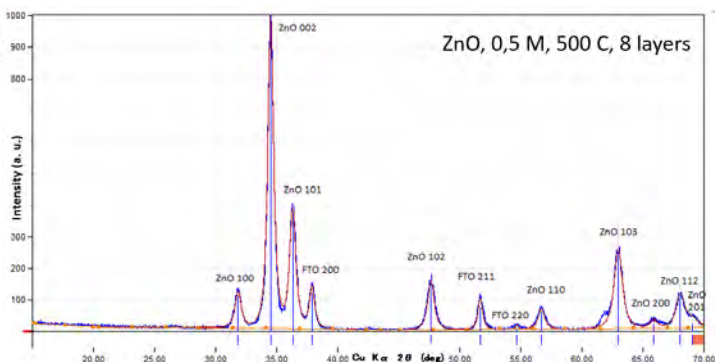


Fig. 2. XRD pattern of ZnO thin-films on FTO substrate.

We found out that ZnO thickness depended proportionally on number of cycles and solution concentration (Fig. 1). The higher concentration of solution, the higher increase in thickness was observed. In addition, it was noticed that more concentrated solutions lead to the formation of more porous films. Therefore for more precise control of the ZnO thickness and more density packed morphology, lower concentration is preferable.

XRD analysis showed that deposited thin films started to crystallize already at 300 °C. In the entire studied annealing range (300-550 °C), a single hexagonal phase of ZnO was formed (JCPDS 36-1451) and showed a preferred (002) grain orientation (Fig. 2).

- [1] C. D. Bojorge, H. R. Canepa, D. Silva, R. E. Marotti, Synthesis and optical characterization of ZnO and ZnO:Al nanocrystalline films obtained by the sol-gel dip-coating process, *J. Mater. Sci. Mater. Electron.* **18**, 1119 (2007).
- [2] S.A. Kamaruddin, M.Z. Sahdan, K.-Y. Chan, M. Rusop, H. Saim, Influence of post-annealing temperature on the material properties of zinc oxide nanorod. *J. Nanosci. Nanotechnol.* **10** (10), 6419 (2010)
- [3] J.Y. Lao, J.G. Wen, Z.F. Ren, Hierarchical ZnO nanostructures. *Nano Lett.* **2**, 1287 (2002).
- [4] M. Puricaa, E. Budianua, E. Rusub, M. Danilaa, R. Gavrilaa, Optical and structural investigation of ZnO thin films prepared by chemical vapor deposition (CVD). *Thin Solid Films.* **403–404**, 485 (2002).

IRON AND COPPER NANOPARTICLES DEPOSITED ON REDUCED GRAPHENE OXIDE FOR OXYGEN EVOLUTION REACTION

Jadranka Milikić^{1*}, Ana Nastasić¹, Kristina Radinović¹, Aldona Balčiūnaitė² and Biljana Šljukić^{1,3}

¹ University of Belgrade, Faculty of Physical Chemistry, Studentski trg 12-16, 11158 Belgrade, Serbia

² Center for Physical Sciences and Technology, Saulėtekio ave. 3, Vilnius LT-10257, Lithuania

³ CeFEMA, Instituto Superior Técnico, Universidade de Lisboa, 1049-001 Lisbon, Portugal

*jadranka@ffh.bg.ac.rs

The global energy crisis leads to an increasing investigation of renewable and green energy sources. Pure energy can be produced by electrochemical water splitting where the main reactions are hydrogen evolution reaction (HER) as the cathodic reaction and oxygen evolution reaction (OER) as the anodic reaction. The main drawbacks of OER are high overpotential needed for the reaction to start and slow kinetics [1]. Benchmark OER electrocatalysts are iridium and ruthenium oxide (RuO₂ and IrO₂) but they are scarce, with a high price and low stability [1]. It is important to find an appropriate OER electrocatalyst that could be easily and inexpensively synthesized. Herein, synthesized iron and copper nanoparticles that are deposited on reduced graphene oxide (Fe/rGO and FeCu/rGO) are investigated for OER in alkaline media.

Scanning electron microscopy with energy dispersive X-ray spectroscopy (SEM-EDS) was used for the physicochemical characterization of Fe/rGO and FeCu/rGO electrocatalysts where the uniform disposition of metal nanoparticles onto reduced graphene oxide (rGO) is seen. The electrochemical testing of Fe/rGO and FeCu/rGO electrocatalysts for OER was done by linear voltammetry in 0.1 M KOH solution at a scan rate of 5 mV s⁻¹.

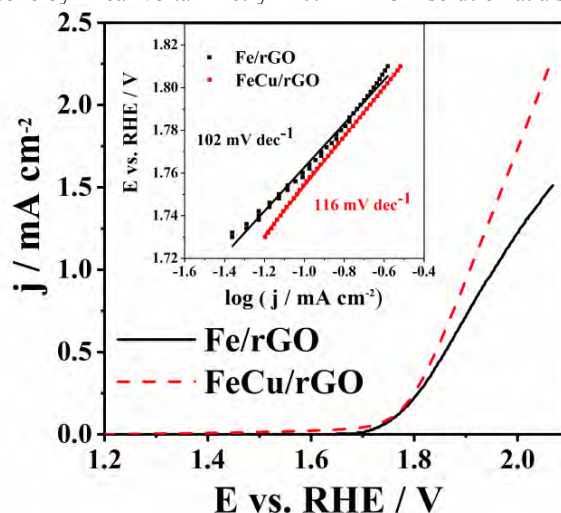


Fig. 1. Polarisation curves of Fe/rGO and FeCu/rGO electrocatalysts in 0.1 M KOH solution at a scan rate of 5 mV s⁻¹.

Polarisation curves of Fe/rGO and FeCu/rGO electrocatalysts under OER conditions were presented in **Fig. 1**. FeCu/rGO showed somewhat higher catalytic activity. The OER current densities were found to be 2.3 and 1.5 mA cm⁻² at 2.1 V for FeCu/rGO and Fe/rGO electrocatalysts, respectively. Approximate values of Tafel slopes of 102 and 116 mV dec⁻¹ were obtained for OER at Fe/rGO and FeCu/rGO electrocatalysts, respectively. Madakanu et al. obtained Tafel slopes with significantly higher values from 153 to 353 mV dec⁻¹ for OER at iron oxide materials deposited on rGO [2]. Next, the stability of the prepared catalysts will be evaluated as another feature essential for use of a novel material in industrial water electrolysis cells.

Acknowledgments

The authors would like to thank the Ministry of Education, Science and Technological Development of the Republic of Serbia (contract no. 451-03-68/2022-14/200146). Fundação para a Ciência e a Tecnologia (FCT, Portugal) is acknowledged for contract no. IST-ID/156-2018 (B. Šljukić).

[1] S.S. Sankar, A. Rathishkumar, K. Geetha, et al., Electrospinning as a tool in fabricating hydrated porous cobalt phosphate fibrous network as high rate OER electrocatalysts in alkaline and neutral media, *Int. J. Hydrogen Energy*. 46, 10366–10376 (2021).

[2] I. Madakannu, I. Patil, B.A. Kakade, et al., Boosting oxygen evolution reaction performance by nickel substituted cobalt-iron oxide nanoparticles embedded over reduced graphene oxide, *Mater. Chem. Phys.* 252, 123238 (2020).

IRON AND COPPER NANOPARTICLES DEPOSITED ON REDUCED GRAPHENE OXIDE FOR ORR IN ALKALINE MEDIA

Ana Nastasić^{1*}, Jadranka Milikić¹, Kristina Radinović¹, Aldona Balčiūnaitė² and Biljana Šljukić^{1,3}

¹ University of Belgrade, Faculty of Physical Chemistry, Studentski trg 12-16, 11158 Belgrade, Serbia

² Center for Physical Sciences and Technology, Saulėtekio ave. 3, Vilnius LT-10257, Lithuania

³ CeFEMA, Instituto Superior Técnico, Universidade de Lisboa, 1049-001 Lisbon, Portugal

*ana.nastasic8@gmail.com

Fossil fuel reserves decrease exponentially due to increasing energy demand. Hereby, as well as because of their negative impact on the environment, an important part of research in the area of electrochemistry is the development of environmentally acceptable sources of energy, such as fuel cells. Alkaline fuel cells (AFCs) convert chemical energy of a fuel into electrical energy in an eco-friendly and efficient way.

The oxygen reduction reaction (ORR) is the most common cathode reaction in fuel cells and thus it is essential for the operation and development of AFCs. The ORR as the cathodic reaction in alkaline media follows either a four-electron mechanism with water as product or the alternative two-electron mechanism with hydrogen peroxide as the product. Platinum group metals (PGMs) are key components in the production of most electrocatalysts used for electrocatalysis of the ORR [1]. However, although they are currently considered the best catalysts for the ORR [2], PGMs are extremely scarce and expensive, and therefore they prevent the full commercialization of fuel cells. Efforts have been made to develop alternative non-PGMs electrocatalysts based on transition metals, which have high catalytic activity, stability, and low cost.

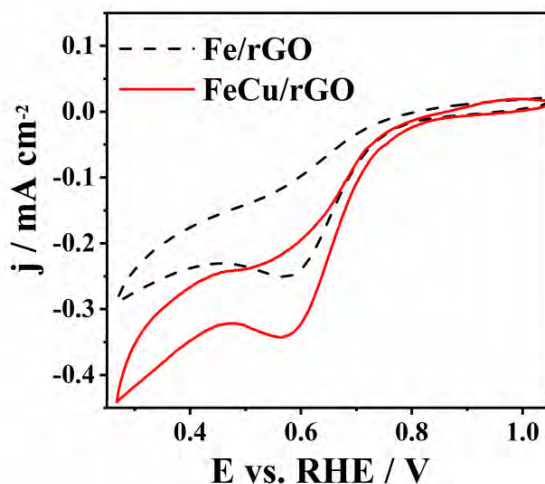


Fig. 1. Cyclic voltammograms of Fe/rGO and FeCu/rGO electrocatalysts in O₂-saturated 0.1 M KOH solution at scan rate of 5 mV s⁻¹.

Herein, iron and iron-copper nanoparticles were deposited on reduced graphene oxide (Fe/rGO and FeCu/rGO), characterised by transmission electron microscopy (TEM) analysis, and examined as electrocatalysts for ORR in alkaline media. TEM images showed nanosized metal particles homogenously deposited on rGO. Subsequently, Fe/rGO and FeCu/rGO were examined in O₂-saturated 0.1 M KOH solution (Fig. 1) by cyclic voltammetry. Characteristic ORR peak was obtained at 0.59 V for both Fe/rGO and FeCu/rGO electrocatalysts with current densities of -0.25 and -0.35 mA cm⁻², respectively. These peaks clearly showed that both electrocatalysts are active for ORR with FeCu/rGO showing somewhat higher electrocatalytic activity under the same conditions. These nanostructured Fe/rGO and FeCu/rGO electrocatalysts could be a potentially good replacement for costly PGMs-based electrocatalysts for ORR because of their easy, fast, and low-cost synthesis.

Acknowledgments

The authors would like to thank the Ministry of Education, Science and Technological Development of the Republic of Serbia (contract no. 451-03-68/2022-14/200146). Fundação para a Ciência e a Tecnologia (FCT, Portugal) is acknowledged for contract no. IST-ID/156-2018 (B. Šljukić).

[1] L. S. Bezerra and G. Maia, Developing efficient catalysts for the OER and ORR using a combination of Co, Ni, and Pt oxides along with graphene nanoribbons and NiCo₂O₄, *J. Mater. Chem. A*, **8**, 17691–17705 (2020).

[2] X. Xu, C. Tan, H. Liu, et al., “Carbon black supported ultra-high loading silver nanoparticle catalyst and its enhanced electrocatalytic activity towards oxygen reduction reaction in alkaline medium,” *J. Electroanal. Chem.*, **696**, 9–14 (2013).

INVESTIGATION OF STABILITY OF SILVER NANOPARTICLES UNDER DIFFERENT STORAGE CONDITIONS

Mantas Mikalkevičius¹, Nadzeya Khinevich¹, Tomas Tamulevičius^{1,2}, Asta Tamulevičiėnė^{1,2}

¹Institute of Materials Science of Kaunas University of Technology, K. Baršausko Str. 59, LT-51423, Kaunas, Lithuania

²Department of Physics of Kaunas University of Technology, Studentų Str. 50, LT-51368, Kaunas, Lithuania
mantas.mikalkevicius@ktu.lt

Nanoparticles are gaining attention due to their wide range of applications such as drug delivery, wound dressing, bio-sensing, household appliances, electronics, water purification, cosmetics, catalysis, etc. Noble metal nanoparticles, especially Ag and Au, have been investigated as the most efficient materials in visible range for sensing, especially for Surface Enhanced Raman Scattering sensors. One of the issues in this application is the particle stability as for assembly of SERS substrate one need only small amount of nanoparticles, whereas the volume of solution varies from few millilitres up to hundreds of millilitres. In such conditions, it is very important to know the shelf life or stability of the colloids as it predetermines the experiment duration. The term “nanoparticle stability” is widely used to describe the preservation of a nanostructure property ranging from aggregation, composition, crystallinity, shape, size, and surface morphology [1].

In the present study, we have analysed the shelf life of the silver nanoparticles that were synthesised using seed mediated growth approach in aqueous medium by reduction of silver nitrate with trisodium citrate and tannic acid [2]. The keeping conditions were selected as the conventional in the laboratory environment: daylight at room temperature; kept in dark at room/+4°C temperature. The stability of colloids was tested for concentrated after the synthesis and diluted to a 1:3 ratio with distilled water. Such dilution level was selected, as it was the optimal ratio for UV-VIS measurements. The absorption spectra were measured of each sample every 2 weeks using an UV-VIS spectrometer.

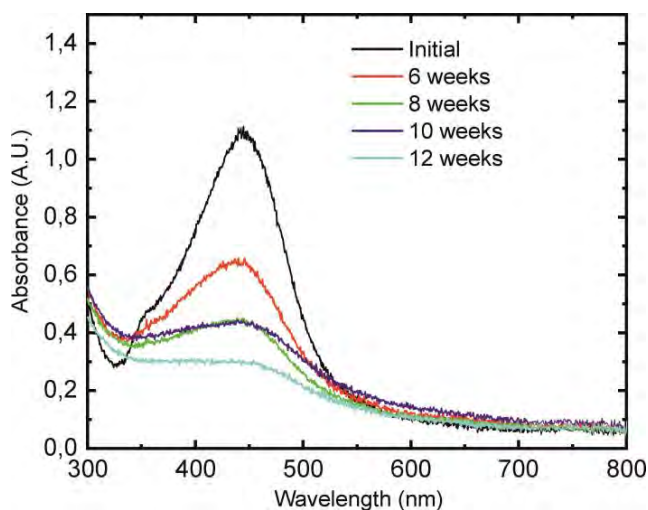


Fig. 1. Absorption spectra of colloid, that was kept diluted (1:3 ratio) in daylight at room temperature up to 12 weeks

Measurements of absorbance spectra (Fig. 1) show that peak intensity decreases almost two times after 6 weeks and almost disappears after 12 weeks when the colloid was diluted and kept in daylight at room temperature. However, concentrated colloid kept in a room temperature behaves oppositely. The peak intensity increased by 12 % after 12 weeks. Concentrated colloid kept in a +4°C and dark environment for several months has almost identical optical properties as right after the synthesis. The observation shows that the optimal conditions for silver colloid are at +4°C in dark. In order to preserve optical properties of the colloid one should dilute colloid only at the time when it is intended for application or testing.

[1] Ullah, S. et al. (2020) “Investigation of stability and rheological properties of silver nanoparticles stabilized by Polyethylene Glycol,” *Journal of Materials Science: Materials in Electronics*, 31(13), pp. 10470–10477. Available at: <https://doi.org/10.1007/s10854-020-03595-1>.

[2] Bastús, N.G. et al. (2014) “Synthesis of highly monodisperse citrate-stabilized silver nanoparticles of up to 200 nm: Kinetic control and catalytic properties,” *Chemistry of Materials*, 26(9), pp. 2836–2846. Available at: <https://doi.org/10.1021/cm500316k>.

THE IMPACT OF DIFFERENT GOLD NANOSTRUCTURES ON THE PERFORMANCE OF ELECTROCHEMICAL IMMUNOSENSORS

Katazyna Blazevic¹, Kristina Sobol¹, Benediktas Brasiunas¹, Almira Ramanaviciene¹

¹ NanoTechnas – Center of Nanotechnology and Materials Science, Institute of Chemistry, Faculty of Chemistry and Geosciences, Vilnius University, Naugarduko st. 24, LT-03225, Vilnius, Lithuania.
katazyna.blazevic@chgf.stud.vu.lt

Nanomaterials are widely used in many fields including medicine, material sciences, electronics, etc. Nanostructures can range in size from 1 to 100 nm and can be classified as nanotubes, nanowires, or nanoparticles [1]. Because of their small size and high surface-to-volume ratio, these materials can be used for their unique physical and chemical properties. Nowadays the application of nanomaterials in biosensing is emerging due to the improvements it brings for qualitative and quantitative detection. Due to unique electrical, optical, and magnetic properties, nanomaterials can be used to improve the analytical parameters of biosensors. The use of nanostructures in electrochemical immunosensors enhances the analytical signal and reduces the limit of analyte detection because of the increased surface area and improved electron transfer kinetics. [2]. Compared to traditional immunoassays, nanoparticle-based immunosensors are more sensitive, specific, and stable allowing the detection of lower concentrations of the analyte [3].

Bovine serum albumin (BSA) is a protein, commonly used by researchers in various ways. BSA could be used in enzyme-linked immunosorbent assays (ELISA) as a protein coating for plates in order to prevent non-specific binding of other biomolecules. In addition, BSA can be employed as a protein standard in various assays. It is considered a fairly non-reactive protein, which can help to reduce background noise. Additionally, BSA and anti-BSA could be used as a model system for the development of new immunosensors [4]. Gold nanostructures (AuNS) are one of the most commonly used materials for the modification of electrochemical immunosensors. The aim of this research was to assess the impact of various AuNS on immunosensor development. This study reviews different electrochemical AuNS deposition methods on graphite electrode using a three-electrode system. The use of AuNS significantly increased registered oxidation-reduction currents of the redox probe after the BSA immobilization and interaction with specific antibodies (anti-BSA). This principle of antibody determination can be applied to the determination of other analytes, e.g. antibody to SARS-CoV-2 proteins.

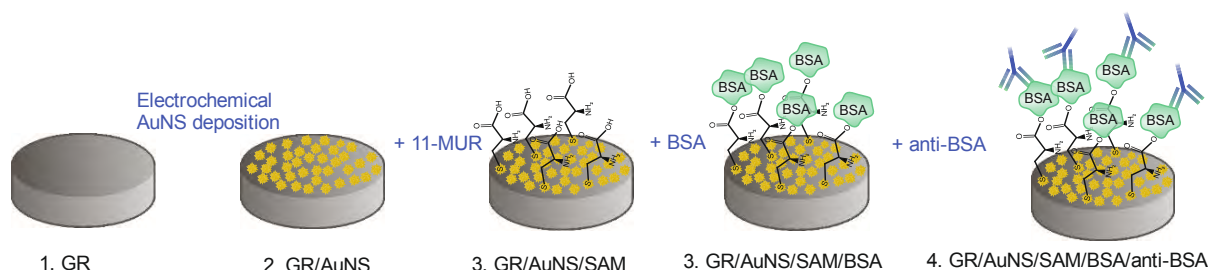


Fig. 1 Schematic representation of experimental stages occurring on the working graphite rod (GR) electrode.

Acknowledgment

This research was funded by a grant (No. S-MIP-22-46) from the Research Council of Lithuania.

- [1] A. Ramanaviciene *et al.*, "Magneto-Immunoassay for the Detection and Quantification of Human Growth Hormone," (2022).
- [2] A. Popov, B. Brasiunas, A. Kausaite-Minkstimiene, and A. Ramanaviciene, "Metal nanoparticle and quantum dot tags for signal amplification in electrochemical immunosensors for biomarker detection," *Chemosensors*, vol. 9, no. 4, 1–23, (2021).
- [3] M. Drobysh *et al.*, "Biosensors for the Determination of SARS-CoV-2 Virus and Diagnosis of COVID-19 Infection," *Int. J. Mol. Sci.*, vol. 23, no. 2, (2022).
- [4] A. Ramanaviciene, A. Kausaite-Minkstimiene, A. Popov, B. Brasiunas, and A. Ramanavicius, "Design of immunosensors for rapid and sensitive detection of biomarkers," S. A. Ozkan, N. K. Bakirhan, and F. B. T.-T. D. of B. Mollarasouli, Eds. Academic Press, 303–333, (2022).

HARNESSING THE POWER OF GOLD NANORODS: A JOURNEY THROUGH SYNTHESIS AND CHARACTERIZATION

Viktorija Lisyte, Anton Popov, Almira Ramanaviciene

NanoTechnas – Center of Nanotechnology and Materials Science, Faculty of Chemistry and Geosciences, Vilnius University, Vilnius, Lithuania
viktorija.lisyte@chgf.vu.lt

Nanomaterials have become increasingly popular and crucial in various industries today, growing in importance every year [1]. Gold nanoparticles (AuNPs) have a rich history in the field of chemistry, dating back to ancient Rome where they were used to enhance the appearance of glasses through staining. The unique physical and chemical properties of AuNPs can be altered by adjusting their structural size through various fabrication techniques. Due to this versatility, AuNPs are a promising option for applications such as colorimetric analysis, biosensors, photothermal transducers, and imaging [2]. Various sized and shaped AuNPs can be synthesized, such as Au nanospheres, nanocages, nanoshells, and nanorods, all of which exhibit surface plasmon resonance [3].

In recent years, gold nanorods (AuNRs), which are rod-shaped AuNPs, have been found to possess distinct physical, optical, and chemical properties that make them suitable for various biomedical uses, such as drug/gene delivery, photothermal/photodynamic therapy, and theranostics [4]. The optical properties of these small nanostructures are related to longitudinal surface plasmon resonance (LSPR), which is a remarkable optical characteristic of metal nanoparticles that arises from the interaction of an incoming electromagnetic wave at a specific wavelength with the electrons, leading to their collective oscillation [5]. The anisotropic structure of GNRs displays two surface plasmon bands in the UV-Vis spectrum, corresponding to surface electron oscillation on the transverse and longitudinal sides of the particle [6]. There are various methods for synthesizing AuNRs, but the seed-mediated growth approach has garnered the most attention due to its simplicity, high production of nanorods, and ability to easily regulate the aspect ratio [7].

The primary objective of the study was to fabricate AuNRs of varying lengths using the seed-mediated method. The characterization of the AuNRs was carried out through the use of SEM, DLS and UV-VIS techniques. These techniques allowed for the detailed examination of the structural and optical properties of the AuNRs and provided valuable insight into the effectiveness of the synthesis method. The results of the characterization were crucial in determining the success of the synthesis process and in further understanding the potential applications of AuNRs in various fields.



Fig. 1. AuNRs of varying lengths were produced using the seed-mediated method.

-
- [1] Brasiunas, B. et al. Gold nanoparticle based colorimetric sensing strategy for the determination of reducing sugars. *Food Chemistry*, 2021, 351:129238.
- [2] Hassan, H. et al. Gold nanomaterials – The golden approach from synthesis to applications. *Materials Science for Energy Technologies*, 2022.
- [3] Dheyab, M. et al. Gold Nanoparticles-Based Photothermal Therapy for Breast Cancer. *Photodiagnosis and Photodynamic Therapy*, 2023, 103312.
- [4] Jahangiri-manesh, A. et al. Gold nanorods for drug and gene Delivery: An overview of recent advancements. *Pharmaceutics*, 2022, 14.3: 664.
- [5] Cao, J. et al. Gold nanorod-based localized surface plasmon resonance biosensors: A review. *Sensors and actuators B: Chemical*, 2014, 195: 332-351.
- [6] Wu, H.Y. et al. Seed-mediated synthesis of high aspect ratio gold nanorods with nitric acid. *Chemistry of materials*, 2005, 17.25: 6447-6451.
- [7] Khan, N. U. et al. Synthesis of gold nanorods and their performance in the field of cancer cell imaging and photothermal therapy. *Cancer Nanotechnology*, 2021, 12:1.

EXPERIMENTAL STUDY ON ACOUSTIC AGGLOMERATION OF ULTRAFINE ASH PARTICULATE MATTER UNDER VARIOUS ENVIRONMENTAL CONDITIONS

Kristina Kilikevičienė¹, Aleksandras Chlebnikovas¹, Artūras Kilikevičius¹

¹ Research Institute of Mechanical Science, Vilnius, Lithuania
kristina.kilikevičienė@vilniustech.lt

Climate change and environmental pollution are closely linked and have recently become a major challenge not only for Lithuania but also for societies around the world. Currently, the most promising technology for removing ultrafine particulate matter (UFPM) from the exhaust gas of stationary fossil fuel and biomass combustion boilers is electrostatic precipitators, which effectively trap UFPM larger than 2.0 μm in diameter, while the removal efficiency for smaller particles is very low [1]. Acoustic agglomeration is the agglomeration and growth of fine particulate matter in exhaust gas into larger particles by sound waves of high intensity and frequency [2, 3]. UFPM penetrate deep into the human respiratory tract and can therefore have significant effects on human health. The efficiency of conventional devices in removing UFPM is quite low. Therefore, it is crucial to develop technologies for primary removal of UFPM before the electrostatic precipitator (ESP).

This paper was aimed at investigating the effects of a newly developed acoustic flow generator for the acoustic agglomeration of particles, which incorporates a number of improvements in its design, on the effect of grazing waves on the agglomeration of ash particulate matter. The use of an acoustic flow generator in combination with the ESP increases the separation efficiency of UFPM. A schematic representation of the developed stand with views is shown in Fig. 1. The results of the UFPM concentration research are shown in Fig. 2.

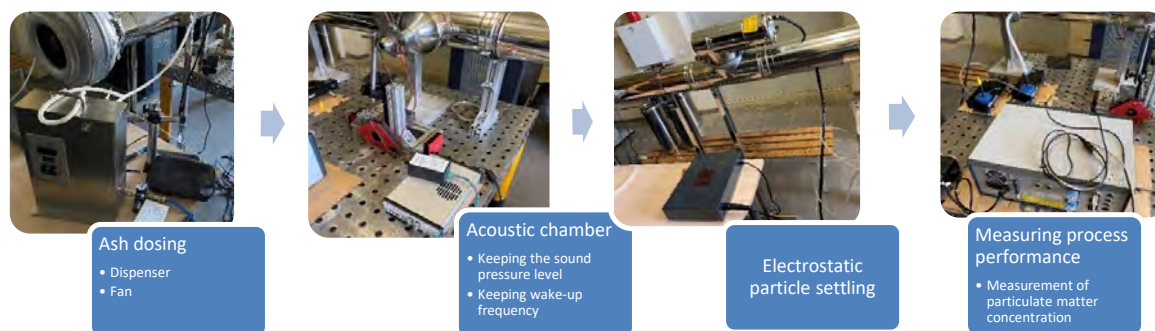


Fig. 1. Schematic diagram and images of an ultrafine particulate matter removal system (consisting of a doser, an acoustic chamber, ESP and measurement equipment of particulate matter concentration)

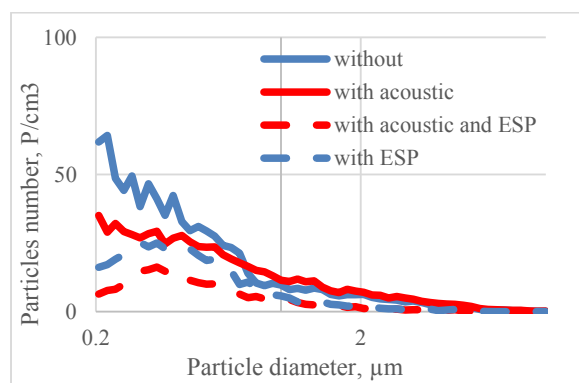


Fig. 2. Results of the ultra fine dust concentration measurements

Acknowledgment

This research has received funding from the European Social Fund (project No. 09.3.3-LMT-K-712-19-0026) under a grant agreement with the Lithuanian Research Council (LMTLT).

- [1] Garbarienė, I., Dudoitis, et al., Application of Acoustic Agglomeration Technology to Improve the Removal of Submicron Particles from Vehicle Exhaust, *Symmetry*, 13(7). (2021).
 [2] Maknickas, A., Markauskas, D., Kačianauskas, R., Discrete element simulating the hydrodynamic effects in acoustic agglomeration of micron-sized particles, *Particulate Science and Technology* 34, 453–460. (2016).
 [3] Kilikevičienė, K., Kačianauskas, R., et al., Experimental investigation of acoustic agglomeration of diesel engine exhaust particles using new created acoustic chamber. *Powder Technology*, 360, 421–429. (2020)

THERMAL ANALYSIS OF GRAPHENE/n-SI(100) DIODE, FORMED USING TRANSFER-LESS METHOD

Šarūnas Jankauskas¹, Rimantas Gudaitis¹, Šarūnas Meškinis¹

¹Institute of Materials Science of Kaunas University of Technology, K. Baršausko st. 59, LT-51423, Kaunas, Lithuania
sarunas.jankauskas@ktu.lt

One of the most prominent materials to date, graphene has captured attention of the scientific world with its unmatched mechanical, optical and electronic properties. Its use as a substitute for metals in Si Schottky junction devices is prospective, especially in solar cell field. Today, the highest power conversion efficiency (PCE) reported for Gr/Si solar cells is 16.61% [1]. Regardless, transfer method from Cu foil to Si substrates is still used as the main graphene synthesis method for graphene based electronics, which is not ideal for mass production. It was shown that microwave plasma enhanced chemical vapor deposition (MW-PECVD) is a viable alternative for direct graphene growth on various dielectric and semiconductor substrates, eliminating the sample contaminations which occur during the transfer process. However, PECVD increases defectiveness and self-doping of graphene, compared to transferred graphene counterparts. This, in turn, decreases graphene/Si solar cell efficiency by affecting charge transport at graphene/Si interface. To understand such changes, thorough studies of current-voltage (I-V) characteristics are needed. Herein, we studied charge transport mechanisms at different operating temperature regimes of transfer-less graphene/n-Si(100) diodes, to understand such drop in performance.

In this work, graphene was grown on the Si(100) substrates by using MW-PECVD system (IPLAS Innovative Plasma Systems GmbH). Diodes were fabricated by growing Al back contact (on Si side) and forming cylindrical Cr/Cu electrodes on top of graphene. The characterization of samples was carried out using Raman scattering spectroscopy (Renishaw inVia, 532 nm) prior to diode formation as well as evaluating fabricated photovoltaic device I-V characteristics (Keithley 6487 picoampere meter/voltage source) with thermal operational conditions being changed (from -20 °C to 40 °C) by a custom-made Peltier element configuration.

Raman spectra appeared to be typical for PECVD graphene grown on Si. Measured I-V characteristics showed an increase of current (from 0.026 mA to 0.067 mA at 1 V) with temperature increase (from -20 °C to 40 °C) (Fig. 1). By analysing charge transport mechanisms, it was evident that graphene exhibits tunnelling at low temperatures and combined tunnelling with thermionic emission mechanism, when temperatures are higher.

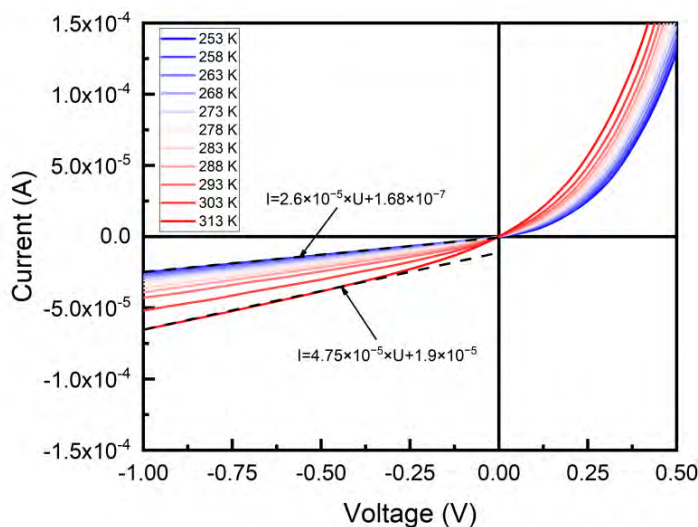


Fig. 1. I-V characteristics of graphene/n-Si(100) diode, measured at different operating temperatures.

[1] H. S. Dong, Y. K. Gyea, et al., Remarkable enhancement of stability in high-efficiency Si-quantum-dot heterojunction solar cells by employing bis(trifluoromethanesulfonyl)-amide as a dopant for graphene transparent conductive electrodes, *Journal of Alloys and Compounds*, **773**, 913-918 (2019).

STUDY OF RECOMBINATION AND ELECTRICAL CHARACTERISTICS IN HIGH ENERGY RADIATION Si SENSORS

Rytis Markevičius, Tomas Čeponis, Laimonas Deveikis, Eugenijus Gaubas, Jevgenij Pavlov,
Vytautas Rumbauskas

Institute of Photonics and Nanotechnology, Vilnius University, Saulėtekio al. 3, Vilnius, Lithuania
rytis.markevicius@ff.stud.vu.lt

Si sensors are widely used in CERN experiments for particle tracking [1-4]. However, high energy radiation creates defects that determine the formation of energy levels within the band gap and affect the sensors' operational characteristics [1, 5]. Therefore, new radiation tolerant sensor structures for future experiments are highly desirable. Currently, sensors of *pin* structure and different types (trip, pixel) are widely employed. However, sensors of *pin* structure suffer from a decrease in charge collection efficiency. Sensors with internal gain layer (*Low Gain Avalanche Detectors - LGADs*) [3, 6] appeared to be a promising alternative over sensors of *pin* structure due to carrier multiplication governed by impact ionization [7] which can compensate the signal drop determined by radiation defects [3]. LGADs are currently being studied within the CERN RD50 program in order to evaluate the changes in sensor parameters after irradiations with high fluences.

This study aimed to examine the recombination and electrostatic characteristics of silicon wafers and junction structures both non-irradiated and irradiated with reactor neutrons and protons of different energies. Microwave probed photoconductivity (MW-PC) transient technique, current-voltage (I-V), and capacitance-voltage (C-V) methods were employed to thoroughly carry out the research.

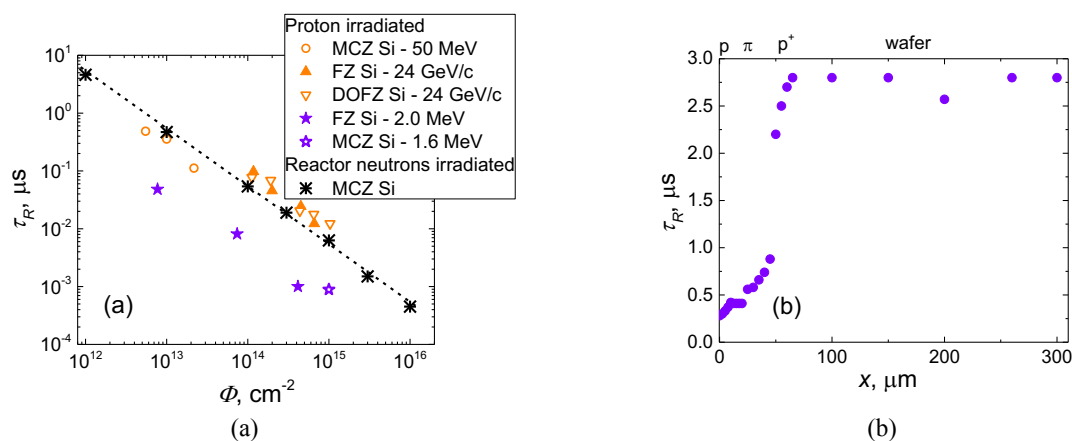


Fig. 1. (a) - Fluence dependent carrier lifetime variations in reactor neutrons and different energy protons irradiated Si wafers. (b) - Carrier lifetime distribution profile measured in non-irradiated *LGAD* structure.

It was determined that carrier lifetime is inversely proportional to fluence due to the increased density of radiation defects in all the investigated samples (Fig. 1(a)). However, carrier lifetime is about an order of magnitude shorter in Si irradiated by stopped protons due to more efficient production of radiation defects at particle penetration depth. The carrier lifetime profiling by edge scanning of microwave-probed photoconductivity transients allowed us to determine the penetration depth of low energy particles. The measurements and analysis of C-V characteristics were used to evaluate the change in the effective density of dopants caused by radiation defects and to determine the penetration depth of the particles stopped within junction structures. Finally, it was shown, that edge scanning of the LGAD sensor structures using a needle-tip microwave antenna and measuring MW-PC transients allows for estimating the charge carrier lifetime τ_R within individual layers of the structure (Fig. 1(b)).

-
- [1] S. N. Ahmed, *Physics and Engineering of Radiation Detection* (Elsevier, Great Britain, 2007).
 [2] G. Lutz, *Semiconductor Radiation Detectors - Device Physics* (Springer, New York, 2007).
 [3] G. Pellegrini, P. Fernández-Martínez, M. Baselga, *et al.*, Technology developments and first measurements of Low Gain Avalanche Detectors (LGAD) for high energy physics applications, *Nucl Instrum Methods Phys Res A* **765**, 12–16 (2014).
 [4] H. Spieler, *Semiconductor Detector Systems* (Oxford University Press, New York, 2005).
 [5] C. Claeys, E. Simoen, *Radiation Effects in Advanced Semiconductor Materials and Devices* (Springer, Germany, 2002).
 [6] J. Lange, M. Carulla, E. Cavallaro, *et al.*, Gain and time resolution of 45 μm thin Low Gain Avalanche Detectors before and after irradiation up to a fluence of $10^{15} \text{ n}_{\text{eq}}/\text{cm}^2$, *Journal of Instrumentation* **12**, P05003 (2017).
 [7] S. M. Sze, K. K. NG, *Physics of Semiconductor Devices* (John Wiley & Sons, USA, 2007).

THERMODYNAMIC ANALYSIS OF NITROGEN DOPED GALLIUM OXIDE - COMPARATIVE STUDY

Ana Kurtanidze¹, Tamar Tchelidze²

^{1,2} Department of Physics, Ivane Javakishvili Tbilisi State University, Georgia
Ana.Kurtanidze854@ens.tsu.edu.ge

Gallium oxide Ga_2O_3 has gained much attention because of its unique properties such as ultra-wide bandgap (4.56eV), and high breakdown field which makes it very promising for application in certain classes of Opto- and power electronics, solar-blind UV photodetectors, solar cells, etc. It is usually reported that there are five different polymorphs of Ga_2O_3 , namely, the monoclinic (β - Ga_2O_3), rhombohedral (α), defective spinel (γ), cubic (δ), or orthorhombic (ϵ) structures. Because of these, the β -polymorph is the stable form under normal conditions and has been the most widely studied and utilized.

However, in gallium oxide, like other semiconductor oxides, obtaining low ohmic hole conductivity is still challenging. The difficulty is connected to low hole mobility caused by the big effective mass of holes, high ionization energies of native and impurity acceptors, compensation processes (appearance of hole killer defects) stipulated by high band-gap, and low lying valence band. After N impurity in β - Ga_2O_3 , the N atom would substitute the site of O atom because it is closest to O in terms of the atomic size and electronic structure. And it is expected to lead to p-type conductivity.

We fulfilled the thermodynamic analysis of the concentration equilibrium for nitrogen doped gallium oxide using the Kroger method of quasi-chemical reactions, which gives one possibility to find the dependence of concentrations of defects and free carriers on growth/processing parameters and impurity concentration, and correspondingly to find their optimal values. Furthermore, the quasi-chemical solution model has a better treatment of configurational entropy which accounts for a non-random distribution of atoms. The analysis was carried out for the system Ga_2O_3 doped samples – vapor of components. According to the analysis, the hole concentration increases with increasing oxygen pressure, and at some critical value holes and substitutional nitrogen become dominant species (for $T=900$ °C, $P=1$ atm). Also further increase of oxygen pressure effects on hole concentration. We took into account the formation of the nitrogen molecule, which is expected to reduce the effect of doping. The formation energy of nitrogen molecules is quite high – 9.756 eV. In Gallium oxide taking into account dielectric screening with local field correction, dissociation energy turned out to be approximately 3 eV. Based on the results one can conclude, that for N doping of gallium oxide, the native donors - oxygen vacancy or Gallium interstitial are responsible for p-conductivity compensation; On the other hand, if we take into account the formation of the nitrogen molecule, then we will not get p-type conductivity.

RELATION BETWEEN DESIGN OF GaAsBi PARABOLIC QUANTUM WELLS AND OPTICAL PROPERTIES

Monika Jokubauskaitė¹, Evelina Dudutienė¹, Bronislovas Čechavičius¹, Arnas Pukinskas¹, Simona Pūkienė¹, Sandra Stanionytė², Martynas Skapas², Renata Butkutė¹

¹ Department of Optoelectronics, Center for Physical Sciences and Technology, Lithuania

² Department of Characterisation of Materials Structure, Center for Physical Sciences and Technology, Lithuania
monika.jokubauskaite@ftmc.lt

Only a few percent of bismuth incorporated in GaAs lattice significantly reduces the band gap of the material. Due to attractive properties like large bowing and energy band gap, less sensitive to temperature, bismides are potential material for the applications of optoelectronic devices operating in infrared range such as light-emitting diodes [1], photodetectors [2], solar cells [3] *etc.* Nevertheless, it is crucial to continue study of GaAsBi and investigate the influence of different designs of quantum structures on the optical properties so that the optimization of future optoelectronic devices could be achieved.

Recently our group [4] developed quantum structure design consisting of GaAsBi quantum wells (QWs) with parabolically graded barriers (PGBs) and a boost in photoluminescence (PL) at room temperature was observed for these structures with 50 times higher PL intensity when compared to conventional rectangular quantum wells. This consequence could be explained by more efficient carrier trapping into the GaAsBi quantum wells and stronger effect of carrier localization. It is important to mention, that enhanced PL intensity is reproducible over the growth conditions in parabolic quantum wells (PQWs).

To find a relation between a design of quantum structure and optical properties that they exhibit more comprehensive study of GaAsBi PQWs grown by molecular beam epitaxy (MBE) was conducted. Different designs of two separate parabolic quantum wells (2PQW), two quantum wells embedded together in parabolic barriers (2in1PQW) and three quantum wells embedded together in parabolic barriers (3in1PQW) were investigated and the latest results will be presented in this work. To explore optical properties a widely used technique of photoluminescence was used. The room temperature PL results are presented in Fig. 1 (a). Also, it was shown that thermal annealing could contribute to structural change of a sample. PL spectra of *in situ* annealed 2PQW structure is redshifted (Fig. 1 (a) red line) at room temperature. In addition, the cross-section transmission electron microscopy (STEM) images (Fig. 1 (b)) revealed the formation of Bi nanocrystals during annealing, and increased distortion of the GaAsBi QW layer. Consequently, the PL band of annealed 2PQW structure was assigned to emission from Bi nanocrystals rather than to GaAsBi QW.

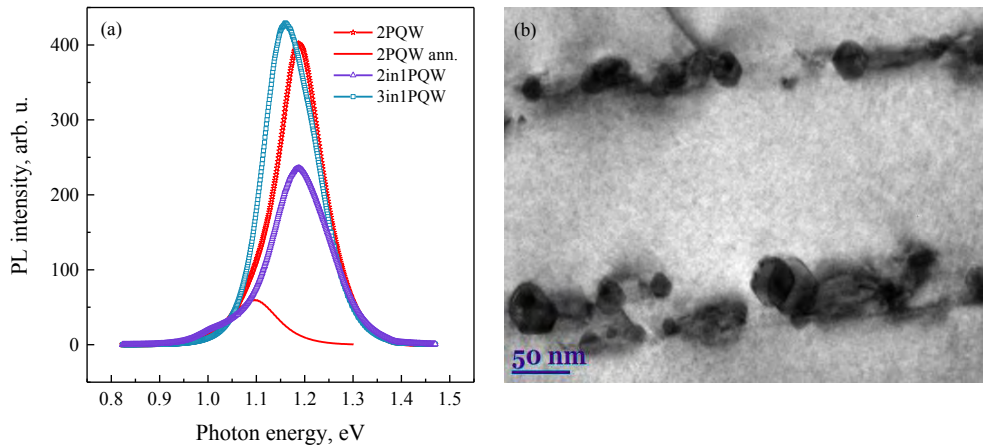


Fig. 1. (a) Room temperature PL spectra of investigated GaAsBi PQW structures of different designs. (b) Cross-section transmission electron microscopy image of formed Bi nanocrystals in 2PQW annealed structure.

Acknowledgement

This research was supported by Research Council of Lithuania under the grant No. S-MIP-22-86 (LMTLT).

-
- [1] P.K. Patil, E. Luna, T. Matsuda, K. Yamada, K. Kamiya, F. Ishikawa, and S. Shimomura, GaAsBi/GaAs multi-quantum well LED grown by molecular beam epitaxy using a two-substrate-temperature technique, *Nanotechnology* **28**, 105702 (2017).
[2] C. J. Hunter, F. Bastiman, A. R. Mohamad, R. Richards, J. S. Ng, S. J. Sweeney, and J. P. R. David, Absorption characteristics of GaAs_{1-x}Bi_x/GaAs diodes in the near-infrared, *IEEE Photonics Technol. Lett.* **24**, 2191–2194 (2012).
[3] R. N. Kini, L. Bhusal, A. J. Ptak, R. France, and A. Mascarenhas, Electron Hall mobility in GaAsBi, *J. Appl. Phys.* **106**, 043705 (2009).
[4] S. Pūkienė, M. Karaliūnas, A. Jasinskas, E. Dudutienė, B. Čechavičius, J. Devenson, R. Butkutė, A. Udal, and G. Valušis, Enhancement of photoluminescence of GaAsBi quantum wells by parabolic design of AlGaAs barriers, *Nanotechnology* **30**, (2019).

STUDY OF ELECTRICAL CHARACTERISTICS IN SILICON PARTICLE SENSORS IRRADIATED WITH PROTONS OF DIFFERENT FLUENCES

Margarita Biveinytė, Tomas Čeponis, Laimonas Deveikis, Eugenijus Gaubas

Institute of Photonics and Nanotechnology, Vilnius University, Saulėtekio av. 3, LT-10257, Vilnius, Lithuania
margarita.biveinyte@ff.stud.vu.lt

Silicon is one of the most widely used semiconductors in micro- and nano-electronics applications. Silicon based particle sensors are widely employed in high energy and nuclear physics experiments for registering of ionizing radiation. One of the most prominent examples is the Large Hadron Collider (LHC) at CERN, where silicon based sensors are employed for particle tracking applications. However, high-energy radiation creates electrically active defects within the bandgap of the material, which determine the deterioration of sensor functional characteristics, e.g., increase of leakage current, decrease of charge collection efficiency, etc. [1]. On the other hand, measurements and analysis of changes of sensor functional characteristics can find beneficial applications, such as dosimetry [2]. Therefore, it is important to characterise the devices before and after irradiation in order to predict the variations of sensor parameters under impact of ionizing radiation, to determine the radiation hardness, to develop new structures and to search for alternative applications.

In this work, a set of Si sensors of CERN standard, irradiated by penetrative protons with fluences in the range of $\Phi = 10^{12}$ - 10^{16} p/cm² were investigated. Current-voltage (I-V) and capacitance-voltage (C-V) characteristics were measured and analysed.

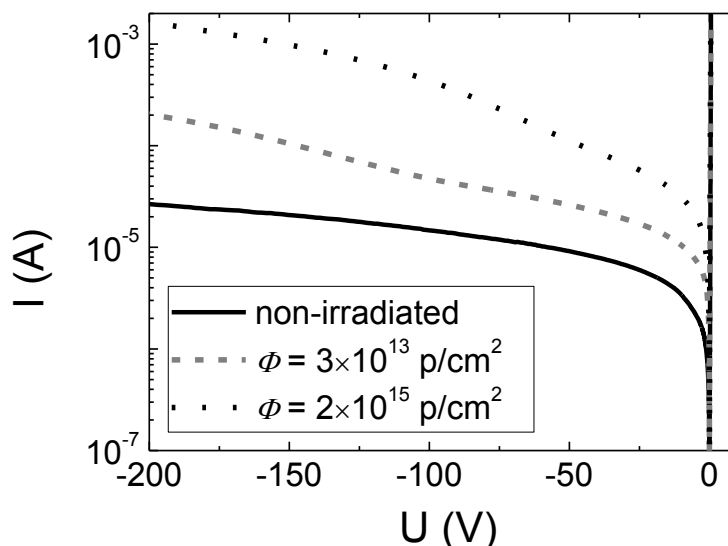


Fig. 1. I-V characteristics of Si particle sensors irradiated with protons of different fluences.

It was found that leakage current (Fig. 1) in sensors increases with irradiation fluence. This phenomenon can be explained by increased density of radiation defects, which act as generation centres. Analysis of C-V characteristics showed variations of effective dopants density in irradiated samples. However, C-V technique could not be applied in heavily irradiated samples due to increased leakage currents. The variations of electrical characteristics and their correlations with proton fluences will be presented and discussed.

[1] H. Spieler, *Semiconductor Detector Systems*, (Oxford University Press, New York, 2005).

[2] S. N. Ahmed, *Physics and Engineering of Radiation Detection* (Elsevier, Great Britain, 2007).

RELATIONSHIP BETWEEN CARRIER LIFETIME AND CATHODOLUMINESCENCE WAVELENGTH IN InGaN COMPOUNDS

Viktorija Mickūnaitė¹, dr. Žydrūnas Podlipskas², Mantas Migauskas³

^{1,2,3}Institute of Photonics and Nanotechnology, Vilnius University, Lithuania
viktorija.mickunaite@ff.stud.vu.lt

Ternary III - nitride alloys such as InGaN allows bandgap tuning by changing molar ratios of the binary constituents. This opens up the possibility of covering the full visible spectrum by changing In content in InGaN compounds which could be applied in developing optoelectronic devices. Growing In content or QW (quantum well) width promotes several problems such as electron hole separation due to internal electric fields, formation of point defects and dislocations, which affect carrier lifetime of the alloy. The aim of this work is to determine the relationship between carrier lifetime and cathodoluminescence wavelength in high (long carrier lifetime) and low (short carrier lifetime) quality InGaN samples.

In this work combination technique of scanning electron microscopy and cathodoluminescence in pulsed mode is used. This method enables determination of carrier lifetimes at all radiative recombination processes by analysing streak camera images of the sample at different sample points.

The results show that for short carrier lifetime InGaN samples carrier lifetime peak is red shifted in relation to cathodoluminescence intensity due to variations in both the local In composition and the QW width related to carrier localization effect in InGaN QW regions and energy band fluctuations. For bulk InGaN samples such dependency is not observed due to higher probability of nonradiative recombination at point defects and dislocations.

For long carrier lifetime InGaN samples few carrier lifetime maxima are observed which could be the result of radiation from different energy levels of QW.

Given results could be used to further analyse radiative and nonradiative mechanisms and causes at various parts of InGaN samples.

EXTENDED DEFECT RELATED LEAKAGE CURRENT IN InGaN LIGHT EMITTING DIODE

Kristupas Karčėmarskas¹, Žydrūnas Podlipskas¹, Virginijus Bukauskas², Tomas Grinys¹

¹Institute of Photonics and Nanotechnology, Vilnius University, Saulėtekio av. 3, LT-10257 Vilnius, Lithuania

²Department of Physical Technologies, Center for Physical Sciences and Technology, Saulėtekio av. 3, LT-10257 Vilnius, Lithuania

kristupas.karcemarskas@ff.stud.vu.lt

Extended defects such as threading dislocations reduces the quantum efficiency of InGaN light-emitting diodes (LEDs). There are a number of point defects around the threading dislocation sites resulting in a deep level states within the band gap. Charge carriers can tunnel through those states inducing a leakage current in the device [2]. The tunneling mechanism in LED device is only qualitatively described in a major of works. An analytical model is still missing. In this work, we measured the reverse leakage current- voltage dependences of an InGaN LED above room temperature in the range of 293-523K. The phonon- assisted tunneling model developed by P. Pipinys et al. [1] was used to analyze the experimental data. The applied model showed good agreement with the current-voltage measurements, especially at high bias voltages (4-10V). We extracted two independent parameters from the model: the height of potential barrier and the density of states. The threading dislocations are non-radiative centers in an LED device. Therefore, it is possible to evaluate the density of such defects by performing scanning electron microscope (SEM) cathodoluminescence measurements. We systematically analyzed the SEM images and found out the threading dislocation density. The number of dislocations extracted from SEM showed good agreement with density of states evaluated from leakage current measurements. This result confirms that number of extended defects inside the device induce a leakage current that can be qualitatively estimated using phonon-assisted tunneling model.

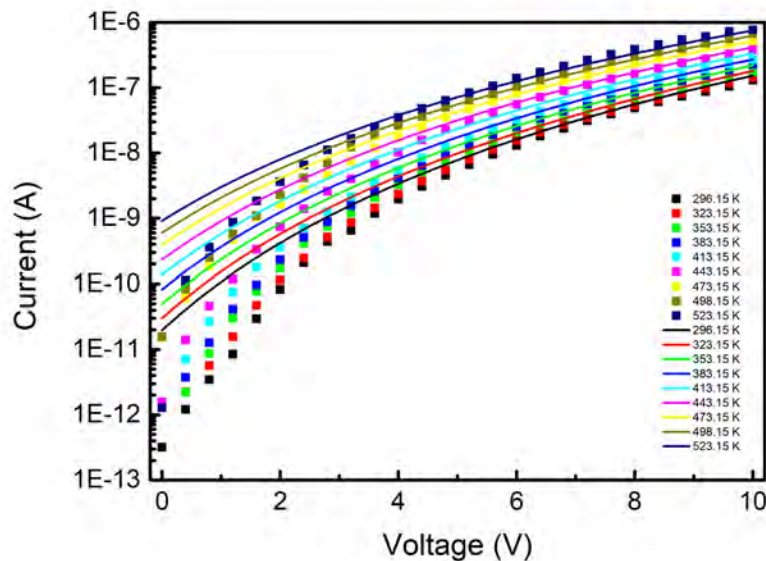


Fig. 1. Theoretical and experimental current-voltage characteristics of an InGaN LED

[1] Lee, M., Lee, H., Song, K.M. *et al.* Significant improvement of reverse leakage current characteristics of Si-based homoepitaxial InGaN/GaN blue light emitting diodes. *Sci Rep* **9**, 970 (2019).

[2] P. Pipinys and V. Lapeika, Temperature dependence of reverse-bias leakage current in GaN Schottky diodes as a consequence of phonon-assisted tunneling, *Journal of Applied Physics* **99**, 093709 (2006).

HIGH-DIMENSIONAL TOPOLOGICAL PUMPING IN TIME-SPACE CRYSTALLINE STRUCTURES

Yakov Braver¹, Egidijus Anisimovas¹, Krzysztof Sacha²

¹Institute of Theoretical Physics and Astronomy, Vilnius University, Vilnius, Lithuania

²Instytut Fizyki Teoretycznej, Uniwersytet Jagielloński, Kraków, Poland
jakov.braver@ff.vu.lt

The motion of a resonantly driven particle in a quantum well can be interpreted as that of a particle in a crystal-like structure, with the time playing the role of a synthetic dimension [1]. Such an analogy lends itself to the introduction of the notion of *time crystals*, originally proposed by Wilczek in the context of spontaneous breaking of time-translation symmetry [2]. Time crystals provide a convenient platform for studying condensed matter phenomena, which have been reproduced in the temporal dimension both theoretically and experimentally [3]. Another possibility opened up by such an approach is that of constructing and studying high-dimensional physical system. This has been considered recently [4] by engineering a time-space crystalline structure, resulting in an up to six-dimensional system.

In the present work, we study topological pumping of particles [5] in systems of two to six dimensions, constructed based on time-space crystals. To this end we change the sinusoidal spatial potential considered previously [6] to a Dirac comb with modulated on-site energies. Starting with a system of a single spatial dimension, we analyse simultaneous pumping in time and space and obtain a gapped quasienergy spectrum (see Fig. 1). The second Chern numbers associated with the gaps are non-vanishing, indicating the topological nature of the pumping [7]. Considering one or two more spatial dimensions results in a four- or six-dimensional time-space crystalline structures, whose quasienergy spectra may remain gapped if parameters are chosen suitably.

To demonstrate the potential usefulness of the obtained results, we cast the spatio-temporal description of the system to an equivalent but conceptually simpler tight-binding form representing hopping of particles in a high-dimensional lattice. This shows that high-dimensional systems that can be conveniently described by a tight-binding Hamiltonian may be realised experimentally with the help of time-space crystalline structures.

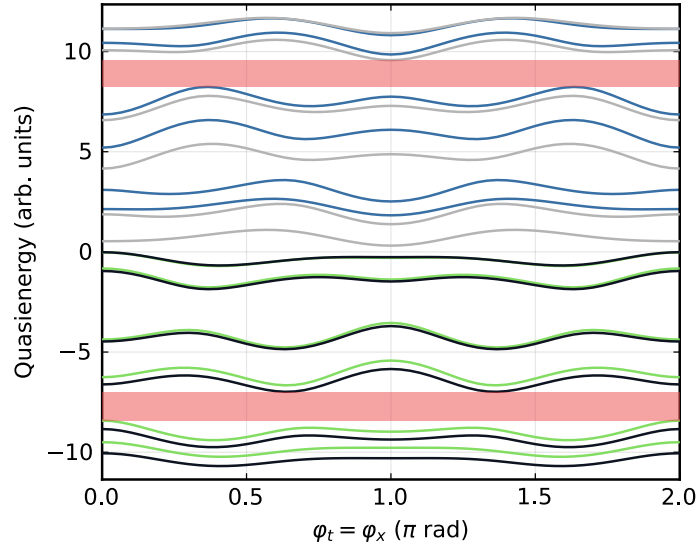


Fig. 1. Quasienergy spectrum [8] of a time-space system versus the pumping phase φ (we consider simultaneous time-space pumping along the trajectory $\varphi_t = \varphi_x$). The plot can be interpreted as the Minkowski sum of two energy spectra: one corresponding to a two-cell spatial lattice with a three-point basis, and one corresponding to a two-cell temporal lattice with a two-point basis. The red-shaded regions indicate gaps, which have non-vanishing second Chern numbers associated with them.

-
- [1] K. Sacha, *Time Crystals* (Springer International Publishing, 2020).
[2] F. Wilczek, Quantum time crystals, *Phys. Rev. Lett.* **109**, 160401 (2012).
[3] L. Guo, P. Liang, Condensed matter physics in time crystals, *New J. Phys.* **22**, 075003 (2020).
[4] G. Żlabys *et al.*, Six-dimensional time-space crystals, *Phys. Rev. B* **103**, L100301 (2021).
[5] S. Nakajima *et al.*, Topological Thouless pumping of ultracold fermions, *Nat. Phys.* **12**, 296 (2016).
[6] Y. Braver *et al.*, Two-dimensional Thouless pumping in time-space crystalline structures, *Phys. Rev. B* **106**, 144301 (2022).
[7] O. Zilberberg *et al.*, Photonic topological boundary pumping as a probe of 4D quantum Hall physics, *Nature* **553**, 59 (2018).
[8] M. Grifoni, P. Hänggi, Driven quantum tunneling, *Phys. Rep.* **304**, 229–354 (1998).

GaN/Graphene STRUCTURES THROUGH A LENS OF SEM-CL MICROSCOPE

Mantas Migauskas¹, Viktorija Mickūnaitė¹, Žydrūnas Podlipskas¹

¹ Institute of Photonics and Nanotechnology, Vilnius University, Lithuania
mantas.migauskas@ff.stud.vu.lt

Recently GaN layers grown on graphene have been getting a lot of attention due to potentially being high quality while lowering manufacturing costs and complexity. Here, we analyze said structures using combined scanning electron (SEM) and cathodoluminescence (CL) microscopies and compare them to GaN layers grown without the graphene interlayer.

In this work, we focus on two samples, both having GaN/graphene and reference GaN/sapphire areas, grown identically using MOCVD process, with one key difference: final GaN layer in one sample was grown for 1800 s (resulting in non-uniform GaN layer, made of semi fused islands), while the other – 4000 s (resulting in homogenous GaN layer). The use of hybrid SEM-CL microscopy lets us see direct correlation between the topography of a given sample and CL signal in the same area.

We analyze the difference in CL spectra between GaN/graphene and reference GaN structures, showing no immediate differences in near band edge (NBE) peak CL luminescence signal despite the presence or absence of graphene layer. However, we observed a small (up to 3 nm) CL peak wavelength blueshift, appearing at dislocations seen in CL pictures. Also, yellow band region CL intensity differs when comparing both structures, most likely due to change in point defect density depending on existence of graphene layer.

Another key characteristic of GaN is its high defect density. Having calculated it in both samples, we demonstrate that CL intensity is inversely proportional to the defect density of examined samples, with higher defect density areas having lower average CL intensity, although this dependence is minimal. More substantial dependence was found in fully grown GaN/graphene layer, where lower amount of point defects resulted in CL intensity roughly 4 times larger than reference GaN.

LUMINESCENCE CHARACTERISTICS IN MOCVD GaN STRUCTURES WITH A CHEMICALLY ETCHED SURFACE

Gertrūda Pociūtė, Tomas Čeponis, Jevgenij Pavlov

Institute of Photonics and Nanotechnology, Vilnius University, Saulėtekio av. 3, LT-10257, Vilnius, Lithuania

gertruda.pociute@ff.stud.vu.lt

Gallium nitride (GaN) is a binary wide-gap (3.4 eV) and direct-gap semiconductor prospective for formation of modern optoelectronic devices, such as light-emitting diodes, lasers as well as radiation detectors [1,2]. Metalorganic Chemical Vapor Deposition (MOCVD) is commonly used method for growing of crystalline layers of GaN, where the density of dislocations in such layers can reach 10^{10} cm^{-2} [3]. These dislocations, being charged and surrounded by space charge region, act as non-radiative recombination centers and also affect the mobility of carriers [4]. The luminescence signals are ascribed to electronic transitions within point defect complexes and depend on the quality of the crystals [5]. The mentioned luminescence bands, ascribed to the point defects, are strongly dependent on temperature, when intensity of scintillation usually increases with cooling of the sample. Manifestation of the luminescence ascribed to electronic transitions within point defect level structure is strongly influenced by dislocations, those density is rather high in MOCVD GaN materials. The wet chemical etching procedures significantly modify the structure of dislocations and their occupied areas and might be the reason of the increase of intensity of scintillation signals in MOCVD GaN based sensors [6]. This work is addressed to consideration of the mentioned phenomena in order to find means for increasing of the MOCVD GaN scintillation signals after modification of dislocations by wet chemical etching.

In this work, the time-integrated (TI) and time-resolved (TR) photoluminescence (PL) characteristics were measured in the 20-300 K temperature range in MOCVD GaN samples chemically etched in orthophosphoric acid (85% H_3PO_4) with exposure duration of 200 s for each step. Microwave probed photoconductivity (MW-PC) transients were measured for examination of non-radiative recombination characteristics after each etching step.

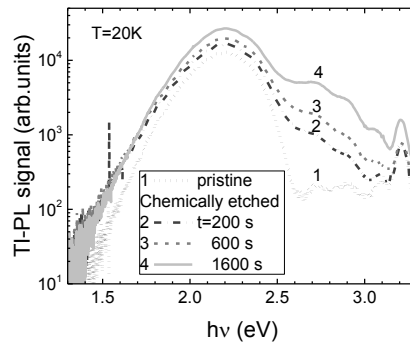


Fig. 1. The TI-PL spectra measured in MOCVD GaN at 20 K after several steps of chemical etching.

An increase of intensity of the yellow luminescence band (Fig. 1) by a factor of two was observed after modification of MOCVD Ga sample surface by etching with orthophosphoric acid. Additionally, the blue luminescence band appeared within the PL spectra measured at temperatures $T < 200$ K in etched GaN samples. The variations of intensity of PL bands might be related to modification of space charge region, surrounding the dislocation cores and acting as non-radiative recombination centers. The variations of PL and MW-PC characteristics in chemically etched MOCVD GaN will be presented and discussed.

-
- [1] W. G. Scheibenzuber, *GaN-Based Laser Diodes* (Springer-Verlag, Heidelberg, Berlin, 2012).
 - [2] S. J. Pearton, B. S. Kang, S. Kim et al., GaN-based diodes and transistors for chemical, gas, biological and pressure sensing, *J. Phys. Condens. Matter*, **16**, R961–94 (2004).
 - [3] O. A. Soltanovich, E. B. Yakimov, N. M. Shmidt et al., Correlation of diffusion length and trap concentration with dislocation density in MOCVD-grown GaN, *Physica B* **340–342**, 479–483 (2003).
 - [4] E. B. Yakimov, A. Y. Polyakov, I-H. Lee et al., Recombination properties of dislocations in GaN, *J. Appl. Phys.* **123**, 161543 (2018).
 - [5] E. Gaubas, T. Ceponis, A. Jasiunas et al., Correlative analysis of the in situ changes of carrier decay and proton induced photoluminescence characteristics in chemical vapour deposition grown GaN, *Appl. Phys. Lett.* **104**, 062104 (2014).
 - [6] Y. Yao, Y. Ishikawa, Y. Sugawara, Revelation of dislocations in HVPE GaN single crystal by KOH etching with Na_2O_2 additive and cathodoluminescence mapping, *Superlattice Microst.* **99**, 83-87 (2016).

INVESTIGATING THE QUALITY OF PHOTOVOLTAIC PANELS BY MEANS OF AN ELECTROLUMINESCENCE CONTROL SYSTEM

Adomas Vasiliauskas, Artūras Jukna, Gražina Grigaliūnaitė-Vonsevičienė

Department of Physics, Vilnius Gediminas Technical University, Lithuania
adomas.vasiliauskas@stud.vilniustech.lt

The efficiency of conversion of light energy into electrical energy of photovoltaic (PV) panels decreases with time. Efficiency is susceptible to defects originating from various factors related to solar cell and/or PV panel manufacturing or handling/shipping, as well as PV panel inaccurate installation processes or extreme weather conditions that can limit not only conversion efficiency but also can cause early device failure. Physical defects such as broken front glass, cells' cracked cells, busbar contact defects, missing or broken snail trails, cracked back-sheets of panels *etc.* have a prominent impact on long-term PV panel efficiency.^[1]

The defects that are invisible to the human eye (*i.e.*, microcracks, soldering defects, *p-n* junction failure *etc.*) detects electroluminescence (EL) control system, which makes the current distribution in the panel visible and helps to identify defect location in the panel.^[2] Electroluminescence is a process of electrical power conversion into light that leads to the generation of photons as a result of the radiative recombination of holes and electrons during the passage of an electric current through a material. This system consists of a source of electrical current to power a solar panel and a CCD camera to capture the light emitted by the panel in response to the passage of an electrical current. A captured image is analysed by a software which compares the contrast in different places of captured image (Fig. 1).

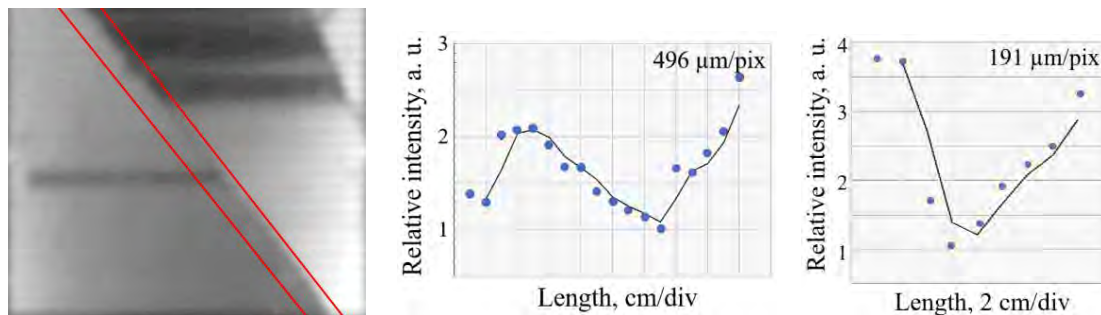


Fig. 1. Defects in a solar cell of a panel identified by means of an EL control system (*on the left*). Dark parts shown in the photo are defected areas of the cell. The results of the contrast of light emission measurements along the defect of the solar cell are marked in the image shown on the left using the EL system at lower and higher resolutions of 496 and 191 $\mu\text{m}/\text{pix}$, respectively. In the graphs, the relative intensities shown by closed symbols and the trendline of chosen points, shown by solid lines. All measurements are completed when the panel is biased at an 8 A current.

The resolution limit of the contrast depends on the distance between the CCD camera and the PV panel as well as the quality of the image captured by the CCD camera. Current work proposes a new approach for increasing a resolution limit of the EL system by means of moving the object closer to the CCD camera and in such a way increasing the resolution of captured image. By increasing the resolution of the EL control system and quality of the captured image, one can more accurately determine the type of observed defects and guess the origin of these defects appearance in the solar cell/panel, the potential of expansion of observed defected area with time depending on ambient temperature and humidity variations, and the defect effect on efficiency of light conversion into electrical energy and lifetime of the entire solar cell or PV module operating in a power plant.

[1] Soomar, A. M., Hakeem, A., Messaoudi, M., Musznicki, P., Iqbal, A., & Czapp, S. (2022). Solar Photovoltaic Energy Optimization and challenges. *Frontiers in energy Research*, 10. doi:10.3389/fenrg.2022.879985

[2] Chubb, D. L. (2007). *Fundamentals of thermophotovoltaic energy conversion*. Elsevier Science Limited.

LUMINESCENCE PROPERTIES OF CERIUM DOPED GARNET EPITAXIAL SCINTILLATORS CODOPED WITH MAGNESIUM

Mikas Iršėnas¹, Augustas Vaitkevičius¹, Saulius Nargėlas¹, Žydrūnas Podlipskas¹, Pavel Bohacek², Martin Nikl², Gintautas Tamulaitis¹

¹Institute of Photonics and Nanotechnology, Vilnius University, Lithuania

²Institute of Physics of the Czech Academy of Sciences, Prague, Czechia

mikas.irsenas@ff.stud.vu.lt

Scintillators are materials that absorb and convert ionizing radiation into UV - Vis light [1]. Cerium-doped, multi-component garnet-structured scintillators show high light yield and resistance to ionizing radiation. They have applications in high-energy particle and nuclear physics experiments, medical diagnostics and radiation safety [2]. However, these crystals are prone to the formation of substitution-type defects, this degrades the scintillation time parameters that are important for the application of these garnets in detectors [3].

One solution to this problem is to grow scintillators by liquid-phase epitaxy, which, due to the lower material processing temperature, reduces the likelihood of the formation of defects and provides a lower cost of production and lower amount of initial material inputs when compared to the conventional, Czochralski, method [4]. Another solution is the use of Mg²⁺ ions, which creates fast recombination pathways but reduces the light yield.

In this work the magnesium concentration dependence of the photoluminescence parameters of cerium-doped lutetium gadolinium aluminum gallium garnet (LuGAGG:Ce) codoped with magnesium, grown by liquid-phase epitaxy, using different measurement techniques was measured and evaluated. Six samples with magnesium concentrations ranging from 0 to 0,6 % were analyzed. The distributions of the surface photoluminescence parameters were measured with a confocal scanning microscope system, the absorption spectra were measured with a UV-Vis spectrophotometer, the scintillation quenching times were obtained with a cathodoluminescence scanning electron microscope operating in pulsed mode.

The analysis of the measurement results showed that with increasing magnesium concentration the photoluminescence intensity decreases, the absorption in the UV region increases, the scintillation quenching time decreases and the quantum yield decreases (Fig 1.). These results are possibly related to the stabilization of Ce ions in the quaternary state, due to the effect of Mg²⁺ on the crystal's ionic charge balance. These cerium ions better compete with other electron capture centers for excited electrons, leading to shorter scintillation quenching times, but creating non-radial recombination pathways leading to lower light yields [2,3].

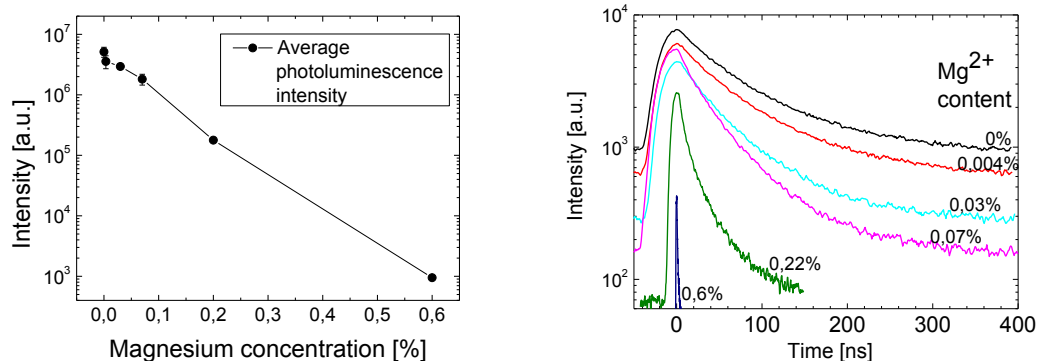


Fig 1. (a) Intensity dependence on magnesium concentration and (b) scintillation decay time dependence on magnesium concentration.

[1] M. Nikl & A. Yoshikawa, Recent R&D Trends in Inorganic Single-Crystal Scintillator Materials for Radiation Detection. *Advanced Optical Materials* 3, (2015).

[2] O. Lalinsky, P. Schauer, & M. Kucera, Influence of Mg-to-Ce Concentration Ratio on Cathodoluminescence in LuAG and LuGAGG Single-Crystalline Films. *physica status solidi (a)* 216, 1801016 (2019).

[3] P. Průša et al. Garnet Scintillators of Superior Timing Characteristics: Material, Engineering by Liquid Phase Epitaxy. *Advanced Optical Materials* 5, 1600875 (2017).

[4] E. Kuphal, Liquid phase epitaxy. *Appl. Phys. A* 52, 380–409 (1991).

[5] V. Babin et al., Effect of Mg²⁺ co-doping on the photo- and thermally stimulated luminescence of the (Lu,Gd)₃(Ga,Al)₅O₁₂:Ce epitaxial films. *Journal of Luminescence* 215, 116608 (2019).

OPTICAL PROPERTIES OF InGaAs/GaAs MULTIPLE QUANTUM WELLS FOR NEAR-INFRARED LASERS

Patricija Šleiniūtė¹, Monika Jokubauskaitė¹, Andrea Zelioli¹, Bronislovas Čechavičius¹, Sandra Stanionytė², Evelina Dudutienė¹, Renata Butkutė¹

¹ Department of Optoelectronics, SRI Center for Physical Sciences and Technology, Lithuania

² Department of Characterisation of Materials Structure, SRI Center for Physical Sciences and Technology, Lithuania
patricija.sleiniute@ftmc.lt

Near infrared (NIR) range is important since it covers laser applications in medicine [1], sensing [2], telecommunications [3] etc. Today, different applications require different laser parameters. Preference is given to lasers that are compatible with other components, not only in terms of dimensions, but also in terms of power, beam geometry, wavelength stability etc. Optical properties of InGaAs quantum well (QW) structures are intensively studied, and it is shown they are suitable for gain media in NIR lasers [4]. However, the growth of InGaAs multiple-quantum wells (MQW) lasers with desired specifications still requires precise optimization in order to find proper growth conditions and design of quantum structure to achieve specific optical properties.

Comprehensive optical study of molecular beam epitaxy grown InGaAs multiple-quantum wells is presented in this work. All investigated structures consisted of twelve InGaAs/GaAs QW. The indium content within QW layer together with thickness of QW were varied in order to obtain emission wavelength at 976 nm. Temperature-dependent photoluminescence (PL) and photoreflectance (PR) spectroscopy techniques were used to probe interband optical transitions over the temperature range of 3 – 300 K (see Fig. 1). PL and PR features positions versus temperature were analysed using Varshni equation [5]. Moreover, activation energies evaluated from PL measurements provided insight into thermal quenching processes of luminescence. Finally, numerical calculations were performed using nextnano software [6] to interpret the observed optical features.

This research was supported by Research Council of Lithuania under grant No. S-MIP-22-86 (LMTLT) “A3B5 Nanostructure-Based Near Infrared Lasers”.

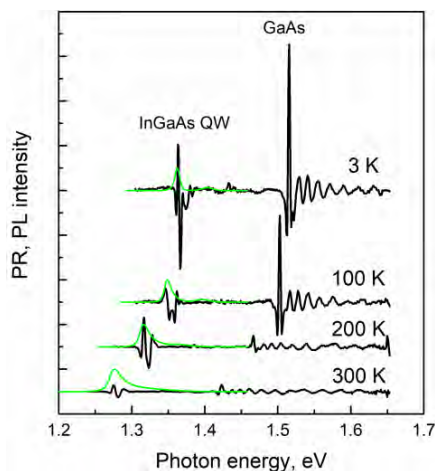


Fig. 1. Temperature-dependent PR and PL spectra of In_{0.22}Ga_{0.78}As/GaAs MQW structure.

-
- [1] V. V. Tuchin, E. A. Genina, A. N. Bashkatov, G. V. Simonenko, O. D. Odoevskaya, G. B. Altshuler, A pilot study of ICG laser therapy of acne vulgaris: photodynamic and photothermolysis treatment, *Lasers in Surgery and Medicine: The Official Journal of the American Society for Laser Medicine and Surgery*, **33**(5), 296-310 (2003).
- [2] P. A. Martin, Near-infrared diode laser spectroscopy in chemical process and environmental air monitoring, *Chemical Society Reviews* **31**(4), 201-210 (2002).
- [3] H. Nasim, J. Yasir, Diode lasers: From laboratory to industry, *Optics & Laser Technology* **56**, 211-222 (2014).
- [4] N. Tansu, J. Y. Yeh, L. J. Mawst, Extremely low threshold-current-density InGaAs quantum-well lasers with emission wavelength of 1215–1233 nm, *Applied Physics Letters* **82**(23), 4038-4040 (2003).
- [5] Y. P. Varshni, Temperature dependence of the energy gap in semiconductors, *Physica* **34**(1), 149-154 (1967).
- [6] See <http://www.nextnano.de/nextnano3> for nextnano3, next generation 3D nanodevice simulator.

MANY BODY LOCALIZATION PHASE TRANSITION, MOBILITY EDGE AND UNIVERSALITY OF SPECTRAL FORM FACTOR IN QUANTUM SUN MODEL

Konrad Pawlik¹, Piotr Sierant², Jakub Zakrzewski^{1,3}

¹ Institute of Theoretical Physics, Faculty of Physics, Astronomy and Applied Computer Science, Jagiellonian University, Łojasiewicza 11, 30-348 Kraków, Poland

² ICFO-Institut de Ciències Fotòniques, The Barcelona Institute of Science and Technology, Av. Carl Friedrich Gauss 3, 08860 Castelldefels (Barcelona), Spain

³ Mark Kac Complex Systems Research Center, Jagiellonian University, 30-348 Kraków, Poland.
konrad.pawlik@student.uj.edu.pl

It is currently of great scientific interest to study generic toy models of ergodicity breaking transition, in search for many-body localized (MBL) phase that survives in the thermodynamic limit [1]. Quantum sun model [2], which describes ergodic quantum dot coupled to particles with spin-1/2, is example of such toy model. Numerical simulations reveal that this model exhibits transition between ergodic and MBL phase and exactly at the transition properties of the system do not depend on the system size, suggesting stability of this transition in the thermodynamic limit.

We extend analysis of [2] by considering a variant of this model with a conserved projection of the total spin \hat{S}_{tot}^z and analysing the biggest symmetry sector. This makes the model more feasible for an experimental implementation using cold-atom platforms, as \hat{S}_{tot}^z corresponds then to the particle number. We find that all hallmarks of the original model, like a universal shape of the spectral form factor independent of system size, are preserved in this variant with conservation up to systems with 24 spins. The biggest studied system sizes are calculated using Polynomially Filtered Exact Diagonalization (POLFED) algorithm [3]. Moreover, model with conservation exhibits the presence of the mobility edge (i.e. a boundary between localized and extended states in the spectrum) in the ergodic phase, which is observed by calculating energy spacing ratio r_n :

$$H|\psi_n\rangle = E_n|\psi_n\rangle, \quad \delta E_n = E_{n+1} - E_n, \quad r_n = \min\left\{\frac{\delta E_n}{\delta E_{n-1}}, \frac{\delta E_{n-1}}{\delta E_n}\right\} = \frac{\min\{\delta E_n, \delta E_{n-1}\}}{\max\{\delta E_n, \delta E_{n-1}\}} \quad (1)$$

and averaging it over many disorder realisations in different energy windows around rescaled energy $\varepsilon = (E - E_{\text{min}})/(E_{\text{max}} - E_{\text{min}})$, as depicted on Fig. 1.

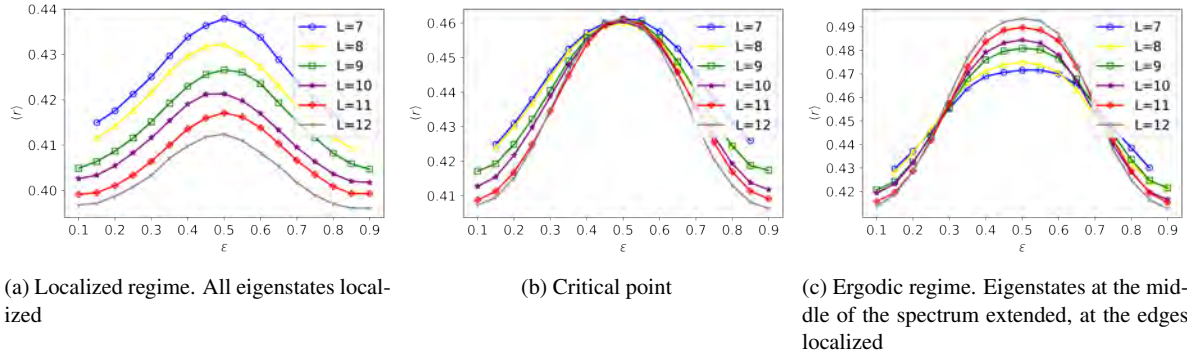


Fig. 1. Average value of spacing ratio $\langle r \rangle$ as a function of position in the spectrum ε , in model with conservation. Data obtained for quantum dot containing $N = 3$ spins and L spins coupled to the dot. Mobility edge in ergodic regime can be observed.

Acknowledgements: The support of PL-Grid Infrastructure is acknowledged. This research has been funded by National Science Centre (Poland) under projects 2019/35/B/ST2/00034 (KP) and 2021/43/I/ST3/01142 (JZ). The support from the Priority Research Area DigiWorld under the Strategic Programme Excellence Initiative at Jagiellonian University is also acknowledged.

-
- [1] Sierant, P., & Zakrzewski, J. (2022). Challenges to observe many-body localization. *Physical Review B*, **105**, 224203.
[2] Šuntajs, J., & Vidmar, L. (2022). Ergodicity breaking transition in zero dimensions. *Physical Review Letters*, **129**(6), 060602.
[3] Sierant, P., Lewenstein, M., & Zakrzewski, J. (2020). Polynomially filtered exact diagonalization approach to many-body localization. *Physical Review Letters*, **125**(15), 156601.

ANNEALING EFFECT ON QUANTUM DOTS FORMATION IN MBE

Arnas Pukinskas^{1,4}, Kipras Mažeika², Augustas Vaitkevičius^{1,2}, Aivaras Špokas^{1,2}, Arnas Naujokaitis³, Martynas Skapas³, Bronislovas Čechavičius¹, Monika Jokubauskaitė¹, Evelina Dudutienė¹, and Renata Butkutė^{1,2}

¹ Department of Optoelectronics, Centre for Physical Sciences and Technology, Saulėtekio av. 3, Vilnius, Lithuania

² Institute of Photonics and Nanotechnology, Faculty of Physics, Vilnius University, Saulėtekio av. 3, Vilnius, Lithuania

³ Department of Characterization of Materials Structure, Centre for Physical Sciences and Technology, Saulėtekio av. 3, Vilnius, Lithuania

⁴ Optogama Ltd., Mokslininkų st. 6B, Vilnius, Lithuania
arnas.pukinskas@ftmc.lt

Several last decades scientists are focused into the miniaturization of the active media of devices thus proceeding to quantum structures like quantum dots, quantum wells, quantum wires and others. These kind of quantum structures tend to be more stable and intensive compared to bulk structures. Moreover, new technique performances allow to manipulate by characteristic parameters of devices applying various technological protocols – different designs of quantum well geometry, interruptions in processes for atom diffusion, *ex-situ* or *in-situ* annealing by applying segregation effect, smoothing boundaries of the layers and enhancement of fundamental properties.

AIII-BV-Bi compounds, namely bismides, are relatively new and not fully explored yet. Bismides are one of the most perspective compounds because of their unique properties: fast reduction of energy band gap replacing As by Bi atoms, and low energy band gap dependance on temperature [1]. Although theoretically bismides is looking like very attractive material for NIR applications it has some technological holdbacks. Low epitaxy temperature and close to 1 arsenic and gallium ratio effect leads to poor crystalline quality and weak luminescent properties. Also, bismuth due to large radius tends to segregate to surface even at low growth temperatures.

Our microscopical studies of post-annealing treatment demonstrated the formation of Bi nanoparticles emitting in the range of 1000 nm – 1300 nm [2]. The main goal of this work was to study the difference between *ex-situ* and *in-situ* annealing for samples grown in Molecular Beam Epitaxy (MBE) reactor. To explore surface and inner layers boundaries differences using atomic force microscopy (AFM) and transmission electron microscopy (TEM) images. Two types of structures with GaAs and AlGaAs barriers were grown. TEM investigation of first type heterostructures showed Bi atoms segregation straight to the surface. To overcome this problem additional ultrathin AlAs barriers were inserted, as Bi atoms blocking layer (see Fig. 1.) It worth noting, that thicker than 1 nm AlAs barriers diminished photoluminescence (PL) intensity. Since these structures will be used for laser source applications, the minimal possible AlAs thickness must be found.

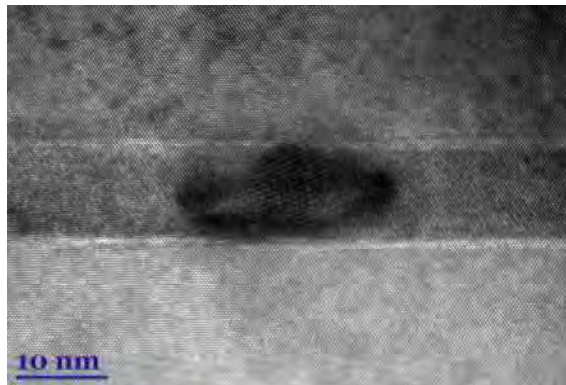


Fig. 1. HR-TEM picture of disc-shaped Bi QDs squeezed between blocking AlAs barriers.

[1] Francoeur, S. et al. (2003). *Band gap of GaAs_{1-x}Bi_x*, Appl. Phys. Lett. 82, 3874.

[2] Butkutė, R. et al. (2017). *Nanoscale research letters* 12 (1), 136, 3.

EXTREMELY NARROW, SHARP-PEAKED RESONANCES AT THE EDGE OF THE CONTINUUM

Ignas Lukosiunas¹, Lina Grineviciute², Julianija Nikitina¹, Darius Gailevicius¹, Kestutis Staliunas^{1,3,4}

¹Vilnius University, Faculty of Physics, Laser Research Center, Sauletekio Ave. 10, Vilnius, Lithuania

²Center for Physical Sciences and Technology, Savanoriu Ave. 231, LT-02300 Vilnius, Lithuania

³ICREA, Passeig Lluís Companys 23, 08010, Barcelona, Spain

⁴UPC, Dep. de Física, Rambla Sant Nebridi 22, 08222, Terrassa (Barcelona) Spain

ignas.lukosiunas@ff.vu.lt

In this work, we primarily focus on the classical phenomenon of resonance shape, its origins, and its behavior in the thin dielectric films that exhibit transverse periodicity. The resonance itself forms whenever the incident light wave excites transverse propagating modes inside the device, which back-scatters it as a consequence. The reflection, induced by the device, corresponds to certain resonant modes which are quantified in the semi-analytical model borrowed from linear quantum mechanics: an asymmetrical quantum potential well in which the wave (i.e., propagating mode) could be localized. The schematic is shown in fig. (a,b), whereas the numerical results are shown in fig. 1 (c,d).

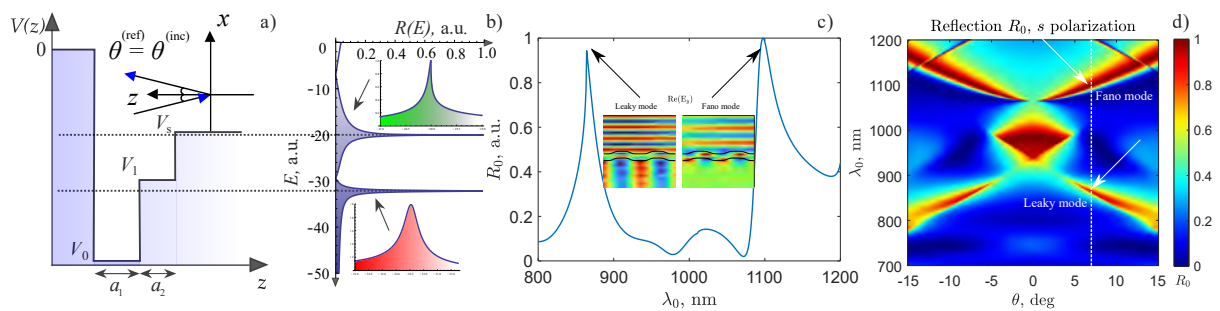


Fig. 1. Conceptual schematics of potential well (a), its resonant reflections (b), numerically calculated reflection coefficients at 6 deg (c) and their corresponding fields, as well as its reflection angular spectrum (d).

The idea of the analytical model is to define the shape of the resonance which is at the top edge (i.e. substrate) of the potential well, thus bringing forth the asymmetrical shape and leaky field behavior. Such an effect is achieved once the right parameters, such as the width, depth, and coupling coefficients of the well are properly tuned to match the resonance for desired wavelengths of the beam propagating perpendicularly about the well. The same effects are achieved for a light wave traveling across the periodic thin dielectric film device which, due to the quantum mechanism analog, couples the incident wave with a reflected one via excited wave-guide mode. Such behavior is thoroughly analyzed with Rigorous Coupled Wave Analysis [1] method and is experimentally realized via the Ion Beam Sputtering method, thus matching the simulated result. Practical applications of such resonances involve - sharp, narrow spectral beam filters, spatial light filters, polarizers, and light couplers [2-5].

- [1] M. G. Moharam, Drew A. Pommet, Eric B. Grann, and T. K. Gaylord, "Stable implementation of the rigorous coupled-wave analysis for surface-relief gratings: enhanced transmittance matrix approach." J. Opt. Soc. Am. A 12, 1077-1086 (1995).
- [2] L. Grineviciute, J. Nikitina, C. Babayigit, and K. Staliunas. "Fano-like resonances in nanostructured thin films for spatial filtering". Applied Physics Letters. 118. 131114. 10.1063/5.0044032 (2021).
- [3] L. Grineviciute, C. Babayigit, D. Gailevicius, M. Peckus, M. Turdnev, T. Tolenis, M. Vengris, H. Kurt, and K. Staliunas. "Nanostructured Multilayer Coatings for Spatial Filtering". Advanced Optical Materials. 10.1002/adom.202001730 (2021).
- [4] I. Lukosiunas, L. Grineviciute, J. Nikitina, D. Gailevicius, and K. Staliunas. "Extremely Narrow, Sharp-Peaked Resonances at the Edge of the Continuum" (2022). Submitted, <https://doi.org/10.48550/arXiv.2211.01997>.
- [5] R. Magnusson, "Flat-top resonant reflectors with sharply delimited angular spectra: an application of the Rayleigh anomaly," Opt. Lett. 38, 989-991 (2013).

MEASUREMENT OF NONLINEAR REFRACTIVE INDEX DISPERSION IN PHOTONIC CRYSTAL FIBER

Jokūbas Pimpė¹, Miglė Kuliešaitė¹, Vygandas Jarutis¹, Julius Vengelis¹

¹ Laser Research Center, Faculty of Physics, Vilnius University, Lithuania
jokubas.pimpe@ff.vu.lt

Photonic crystal fibers (PCFs) are a special type of optical fibers with a unique periodic microstructure area, consisting of air holes running along the entire length of the PCF. Such structure allows to enhance some of the fiber's main optical characteristics and most importantly: nonlinear response [1–2]. Material nonlinear response will determine the efficiency of nonlinear effects caused by third order nonlinear optical susceptibility $\chi^{(3)}$, which can be evaluated by using a parameter called nonlinear refractive index n_2 . The latter parameter is mainly affiliated with the optical Kerr effect, which can be used to describe nonlinear processes such as self-phase modulation (SPM), cross-phase modulation (XPM), four-wave mixing (FWM) and even stimulated Raman scattering. Nonlinear processes appearing in PCF can be qualitatively evaluated only if material's nonlinear refractive index and its dependency on pump wavelengths, i.e., n_2 dispersion, is known [3–5]. Several traditional nonlinear refractive index measurement techniques already exist, although, due to the waveguiding effect, they are not applicable to fibers. Therefore, for fibers, methods based on nonlinear processes are used, but usually they are suited to measure n_2 only for wavelengths close to the zero dispersion wavelength (ZDW) [6-7].

In this work we present a novel PCF nonlinear refractive index measurement method which works in a broad spectral range. The method combines a measurement of spectrally broadened pulse spectrum (due to self-phase modulation) dependency on pump pulse power at different pump wavelengths, which are obtained by using tunable frequency femtosecond pulse oscillator, together with theoretical modeling. The result (PCF nonlinear refractive index dispersion) is obtained when numerical simulation and experiment results are in good agreement. Tunable frequency pulses were obtained by constructing synchronously pumped optical parametric oscillator (644 nm - 1030 nm), which was pumped with amplified pulses, generated from Yb:KGW laser oscillator operating at 76 MHz repetition rate.

The obtained photonic crystal fiber's nonlinear refractive index at various pump pulse wavelengths is depicted in Fig. 1: $n_2 = 3 \cdot 10^{-20} \text{ m}^2/\text{W}$ (646 nm); $n_2 = 2.8 \cdot 10^{-20} \text{ m}^2/\text{W}$ (756 nm); $n_2 = 2.5 \cdot 10^{-20} \text{ m}^2/\text{W}$ (866 nm); $n_2 = 1.6 \cdot 10^{-20} \text{ m}^2/\text{W}$ (955 nm); $n_2 = 2 \cdot 10^{-20} \text{ m}^2/\text{W}$ (1006 nm). From obtained results a significant dispersion of nonlinear refractive index can be observed. We also investigated pulse spectral broadening in the PCF: theoretical modeling enabled to estimate not only PCF nonlinear refractive index dispersion, but also pulse spectrum broadening dynamics. Using tunable frequency femtosecond pulses, it was confirmed, that the pulse broadening in normal dispersion regime is mainly influenced by nonlinear effect, known as self-phase modulation and also PCF's dispersion value.

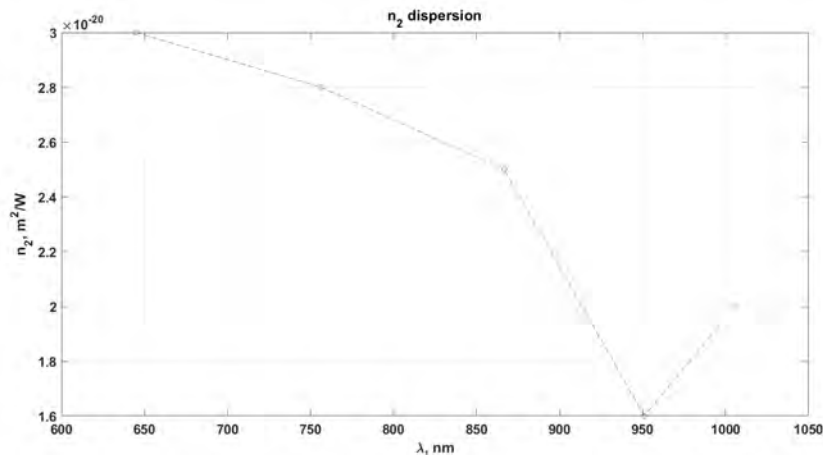


Fig. 1. Nonlinear refractive index values of the investigated photonic crystal fiber obtained from theoretical modeling using tunable frequency laser pulses.

-
- [1] R. Buczyński, Photonic crystal fibers, *Acta Physica Polonica Series A* **106**(2), 141–168 (2004).
 - [2] P. Russell, Photonic crystal fibers, *science* **299**(5605), 358–362 (2003).
 - [3] A. Dubietis, *Netiesinė optika* (Vilniaus universiteto leidykla, 2011).
 - [4] R. W. Boyd, *Nonlinear Optics, Third Edition* (Academic Press, Inc., USA, 2008), 3rd edition.
 - [5] A. P. Stabinis, G. Valiulis, *Ultratrumpųjų šviesos impulsų netiesinė optika* (Vilniaus Universitetas, 2008).
 - [6] L. P'alfalvi, B. Tóth, G. Alm'asi, J. Fülöp, J. Hebling, A general z-scan theory, *Applied Physics B* **97**(3), 679–685 (2009).
 - [7] M. Artiglia, R. Caponi, F. Cisternino, C. Naddeo, D. Roccatò, A new method for the measurement of the nonlinear refractive index of optical fiber, *Optical Fiber Technology* **2**(1), 75–79 (1996).

LOW-FREQUENCY NOISE SPECTROSCOPY OF GaAsBi-BASED QUANTUM WELL LASER DIODES

Richard Pinkrah, Sandra Pralgauskaitė

Institute of Applied Electrodynamics and Telecommunications, Vilnius University, Vilnius, Lithuania
richard.pinkrah@ff.stud.vu.lt

Laser diodes (LDs) are widely used in communication, scientific and medicine applications, sensors and other systems as an effective light source. Infrared lasers are based on double separate confinement heterostructures with one or several quantum wells (QWs) in the active region. This enables a more advanced solution for achieving higher output power, lower threshold current. New solutions to improve LD characteristics and to increase their reliability are constantly being looked for. Therefore, new materials and new active region designs are investigated.

Diluting bismuth with group 3 to 5 semiconductor compounds to produce lasers has become very popular in many scientific researches. Bi modifies GaAs bandgap causing suppression of the non-radiative Auger recombination and significant reduction of the bandgap [1,2].

A detailed study of GaAsBi laser diodes with quantum wells between parabolic barriers grown with MBE technique using low frequency (10 Hz – 20 kHz) noise spectroscopy at temperature ranges from 88 K to 293K is presented.

Current-voltage characteristics of the investigated laser diodes show domination of the diffusion current. Low-frequency electrical noise spectra comprise from $1/f$ and Lorentzian noise components (Fig. 1), what is a result of superposition of charge carrier generation and recombination (GR) processes through different defects, dislocations and imperfections formed charge carrier trapping centers.

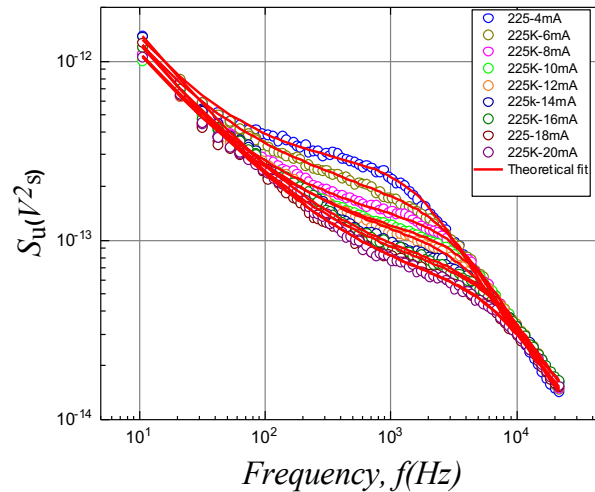


Fig. 1. Noise spectral density dependencies on frequency at fixed temperature and different current (dots – experimental data, solid lines – fitting by eq. (1)).

Noise spectra are well approximated by $1/f$, $1/f^\alpha$ and two GR noise components:

$$S_{el\ sum}(f) = \frac{A_{1/f}}{f} + \frac{A_{1/f^\alpha}}{f^\alpha} + \frac{A_{gr1} \tau_1}{1+(2\pi f \tau_1)^2} + \frac{A_{gr2} \tau_2}{1+(2\pi f \tau_2)^2}, \quad (1)$$

here $A_{1/f}$, A_{1/f^α} , A_{gr} are, respectively, intensities of $1/f$, $1/f^\alpha$ and GR noise components, f is frequency, and τ is characteristic time of the GR process. Lorentzian type components in noise spectra enabled evaluation of the activation energy of the observed active trapping centers responsible for the carrier capture and emission; it was found to be 16.0 meV and 20.4 meV.

[1] S. Pūkienė, M. Karaliūnas, A. Jasinskis, et al., Enhancement of photoluminescence of GaAsBi quantum wells by parabolic design of AlGaAs barriers, *Nanotechnology* **30**, 455001 (2019).

[2] J. Glemža, V. Palenskis, A. Geizutis, et al., Low-Frequency Noise Investigation of 1.09 μm GaAsBi Laser Diodes, *Materials* **12**, 673 (2019).

OPTICAL RESPONSE OF THE HYBRID TAMM-SURFACE PLASMON POLARITON MODES ON THE SURFACE LATTICE ARRAY OF GOLD NANO-BUMBS

Justina Anulytė¹, Ernesta Bužavaitė-Vertelienė¹, Vilius Vertelis¹, Evaldas Stankevičius¹, Kernius Vilkevičius¹, Zigmas Balevičius^{1,2}

¹ Plasmonics and nanophotonics lab., Department of Laser Technology, State research Institute Center for Physical Sciences and Technology, Saulėtekio ave. 3, LT-10257, Vilnius, Lithuania

² Department of Computer Science and Communications Technologies, Faculty of Electronics, VilniusTech, Sauletekio ave. 11, LT-10223, Vilnius, Lithuania

Justina.anulyte@ftmc.lt

Metallic nanostructures arranged in a periodic manner (grating arrays) have recently been used to reduce the losses in metal. Compared with the surface plasmon resonances or local surface plasmons in the randomly distributed metal nanoparticles, the metal nanoparticle lattices have a narrower plasmonic resonance [1]. Such periodic structures based nanophotonic – plasmonic devices have drawn attention to them due to various potential uses, such as plasmonic lasing [2] or enhanced bio-sensing [3], that may sustain prolonged coherence characteristics under the strong coupling. In this research two photonic-plasmonic structures (Fig. 1) that consist of 1D PC and either a thin gold layer (Fig. 1 b) or lattice of gold nano-bump (Fig. 1 c), supporting SPP and TPP modes, were investigated and compared. The strong coupling between the TPP and SPP were measured using the total internal reflection ellipsometry (TIRE) method.

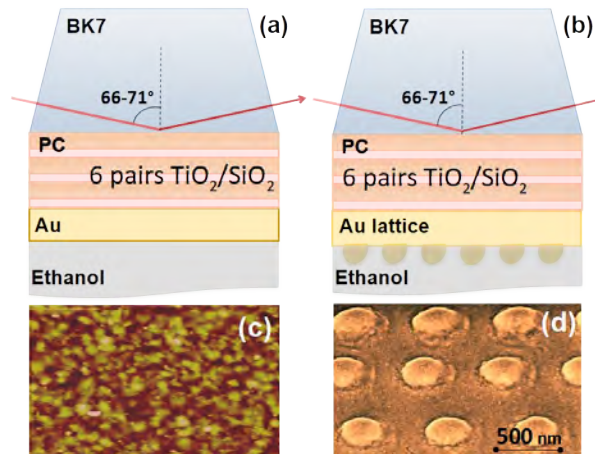


Fig. 1. The investigate structure of PC/Au film (a) and PC/Au array (b) optical configuration and SEM micrograph of (c) a uniform (50 nm) Au layer and (d) a nano-bumps lattice array on the same thin gold layer [4].

According to recent research, the lattice of gold nano-bumps caused the development of an extra Bragg mode associated to the lattice period that was not strongly coupled to the hybrid TPP-SPP polaritonic mode. Despite this, the surface lattice-induced disturbance of the TPP and SPP components propagation length was discovered. Detailed study revealed that while the propagation length of the TPP reduced as a result of the emergence of an extra Bragg mode, the SPP's propagation length increased. The characteristics of 1D PC's optical dispersion and propagation with uniform gold layer and lattice of gold nano-bumps were evaluated by using a two linked oscillator's model and comparing broadening of the wave-vector vs. energy, allowing to indicate the degree of plasmonic modes field localization. The assessed propagation lengths for SPP and TPP components in hybrid polaritonic mode for nanostructures with homogeneous gold layers were $\delta_{SPP}=5.5-6.5 \mu\text{m}$ and $\delta_{TPP}=6.5-9.5 \mu\text{m}$, respectively. In the meantime, the periodic gold surface lattice changes cause the propagation length of the SPP component (SPP_{lattice}) to increase $\delta_{SPP_{\text{lattice}}}\approx 7-10.5 \mu\text{m}$ while the length of the TPP component (TPP_{lattice}) decreases $\delta_{TPP_{\text{lattice}}}\approx 5.5-8.5 \mu\text{m}$. The application of surface lattice resonances together with strong coupling regime leads to decreasing losses, resulting in the increasing propagation length and better coherence properties of such plasmonic resonances, which in turn promises advanced properties for threshold less plasmonic based coherent emission nano-sources [4].

-
- [1] Auguie B., Barnes W. L., Diffractive coupling in gold nanoparticle arrays and the effect of disorder. *Opt Lett* 2009, **34**(4), 401.
 [2] Hakala T. K., Moilanen A. J., Väkeväinen et.al. Bose–Einstein condensation in a plasmonic lattice. *Nat Phys* 2018, **14**(7), 739–744.
 [3] Paulauskas A., Tumenas S., Selskis A., et. al. Hybrid Tamm-surface plasmon polaritons mode for detection of mercury adsorption on 1D photonic crystal/gold nanostructures by total internal reflection ellipsometry. *Opt Express* 2018, **26**(23), 30400.
 [4] Anulyte J., Bužavaitė-Vertelienė E., Vertelis V. et. al. Influence of gold nano-bumps surface lattice array to the propagation length of strongly coupled Tamm and surface plasmon polariton, *J. Mater. Chem. C*, 2022, **10**, 13234-13241.

HIGH-ENERGY 90 PS PULSES FROM PERFLUOROCTANE SBS-COMPRESSOR

Auguste Cerneckyte, Paulius Mackonis, Aleksej M. Rodin

Solid State Laser Laboratory, Center for Physical Sciences and Technology,
231 Savanoriu Ave, 02300 Vilnius, Lithuania
auguste.cerneckyte@ftmc.lt

Pulse compression based on stimulated Brillouin scattering (SBS) in counterpropagating ns pump pulses [1] makes it possible to achieve a pulse width of ~ 110 ps in liquids such as perfluorooctane C_8F_{18} [2] and carbon tetrachloride CCl_4 [3], as well as ~ 180 ps in fused quartz [4]. The most studied CCl_4 is toxic for use in medical lasers, is not suitable for phase conjugation in two-pass amplifiers as it is prone to optical breakdown and has a low reflectivity $\sim 40\%$ of the SBS-mirror. In contrast, the safety of C_8F_{18} has been proven by its use as a coolant, tamponade in eye surgery and even as a breathable fluid. The high breakdown threshold and reflectance above 90% allow it to be used in high-energy >200 mJ two-pass phase-conjugated amplifiers [2]. Self-seeding of the SBS-compressor with CCl_4 allows to improve energy stability, reduce jitter, and achieve shorter pulses [3], albeit with an energy limited to ~ 1 mJ. The goal of this study was to compare different designs of self-seeded SBS-compressors with C_8F_{18} to ensure ~ 90 ps high-energy pulses with a smooth beam suitable for laser dermatology and interference patterning.

Three different self-seeding SBS-compression configurations were experimentally studied (Fig. 1): with a focusing lens (F3) and a flat mirror (PM) returning the pump radiation passed through the SBS-cell (Fig. 1a), with variable splitting of the pulse into seed and pump, followed by their spatial overlap in the SBS-cell and tuning of the relative delay (Fig. 1b) and with a spherical mirror (SM) returning the pump radiation passed through the SBS-cell (Fig. 1c). Input pulses: ~ 2 mJ, ~ 1.1 ns at 10 Hz of TEM₀₀ SLM Nd:YAG laser were used.

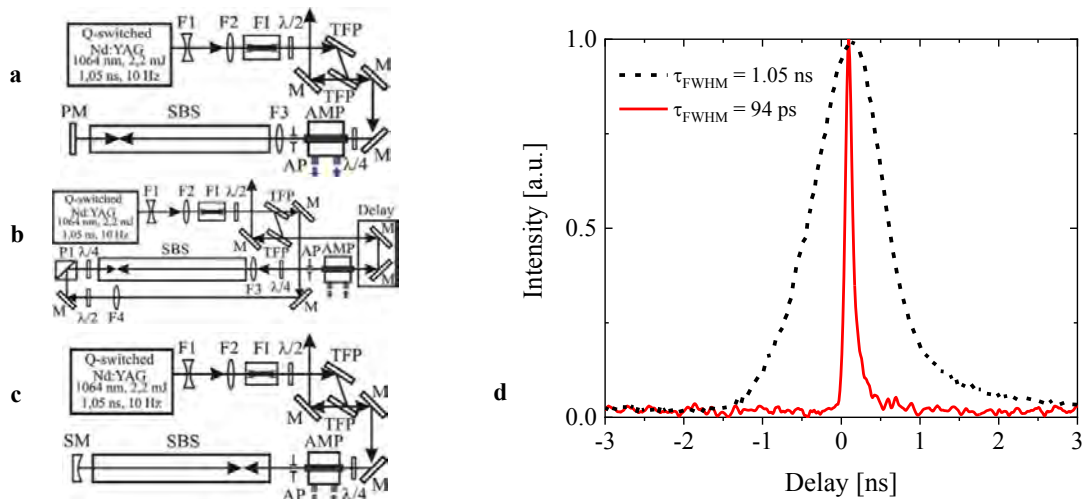


Fig. 1. SBS-compression schemes a – c: FI – Faraday isolator, F1,2 – beam expanding telescope, $\lambda/2$ and $\lambda/4$ – half-wave and quarter-wave retardation plates, TFP – double thin-film polarizer, AMP – double-pass side diode-pumped phase-conjugated Nd:YAG amplifier, AP – aperture. Temporal shapes of the SBS-compressed and incident pulse – d.

In any of the studied SBS-compression configurations, self-seeding reduced the SBS threshold and improved the reflectivity. Despite the expectations associated with more complex seed injection schemes (Fig. 1b, c) and in contrast to [3], the shortest pulse width of ~ 94 ps and the highest energy ~ 9 mJ of compressed Stokes pulses were obtained (Fig. 1d) in the simplest scheme with a return flat mirror (Fig. 1a). When using two consecutive phase-conjugated Nd:YAG amplifier modules, the output energy of compressed pulses can reach ~ 50 mJ at a pulse width of ~ 100 ps.

The developed layout will later be used for high-throughput interference patterning of the metal surface in order to impart water-repellent properties. This project received partial funding from the Research Council of Lithuania, agreement S-LU-22-3 and 01.2.1-MITA-T-852-01-0174.

- [1] C. Cao, Y. Wang, Z. Ba, Y. Li, Y. Yu and Z. Lu, “Developments of Picosecond Lasers Based on Stimulated Brillouin Scattering Pulse Compression,” *Front. Phys.* 9, 747272 (2021).
 [2] N.F. Andreev, E.A. Grishin, O. Kulagin, A. Rodin, “Picosecond Lasers with Brillouin and Raman Pulse Compression,” *Proc. of International Conference on High Power Laser Beams (HPLB-2006)*, Nizhny Novgorod, Russia (2006).
 [3] A.S. Dement'ev, I. Demin, E. Murauskas and S. Slavinskis, “Compression of Pulses During their Amplification in the Field of a Focused Counterpropagating Pump Pulse of the Same Frequency and Width in Media with Electrostriction Nonlinearity,” *Quantum Electron.* 41(2), 153-159 (2011).
 [4] G. Marcus, S. Pearl, G. Pasmanik, “Stimulated Brillouin Scattering Pulse Compression to 175 ps in a Fused Quartz at 1064 nm,” *J Appl Phys* 103(10), 103105 (2008).

STRONG COUPLING BETWEEN SURFACE PLASMON RESONANCE AND EXCITON OF LABELED PROTEIN-DYE COMPLEX FOR IMMUNOSENSING APPLICATIONS

Povilas Jurkšaitis^{1*}, Ernesta Bužavaitė-Vertelienė¹, Zigmas Balevičius^{1,2}

¹ Plasmonics and Nanophotonics Laboratory, Department of Laser Technologies, Center for Physical Sciences and Technology, Sauletekio Ave. 3, LT-10257 Vilnius, Lithuania

² Department of Computer Science and Communications Technologies, Faculty of Electronics, VilniusTech, Sauletekio Ave. 11, LT-10223 Vilnius, Lithuania
povilas.jurksaitis@ftmc.com

Current research on cancer [1], cardiovascular diseases [2], and other health related issues [3] often employ biosensing technology as a tool for detection of various analytes. Biosensing based on biomarker exhibit low detection limit [3]. However one of the main disadvantages using biomarkers for sensing applications is the emergence of photobleaching, which reduces fluorescence lifetime, and as a result, reduces the signal intensity, making the detection of analytes complicated. Light-matter interaction in strong coupling regime provide a method of minimizing the effects of photobleaching due to the formation of new polaritonic states which alter chemical reaction rates [4]. Theoretical modelling of strong coupling has been performed between molecular excitons induced in labeled antibodies and surface plasmon polaritons (SPP) induced in gold [5].

Investigation of a model consisted of thin gold (45 nm) film and Human Serum Albumin (HSA) layer (11 nm) sandwiched between BK7 glass on one side and water on the other was used. AlexaFluor™ 633 was used as protein dye. Optical response of the model was calculated for different concentrations of labeled antibodies in total internal reflection (TIR) configuration. Dispersions in strong coupling regime show the emergence of Rabi energy gap and the formation of upper and lower polariton branches at the anti-crossing point, where dashed lines indicate dispersions of uncoupled system (Fig. 1a). Analysis of Rabi gap dependence for different concentrations of labeled antibody, demonstrate parabolic relation, indicating the relation between adsorbed protein mass to the gold surface and Rabi energy gap (Fig. 1b).

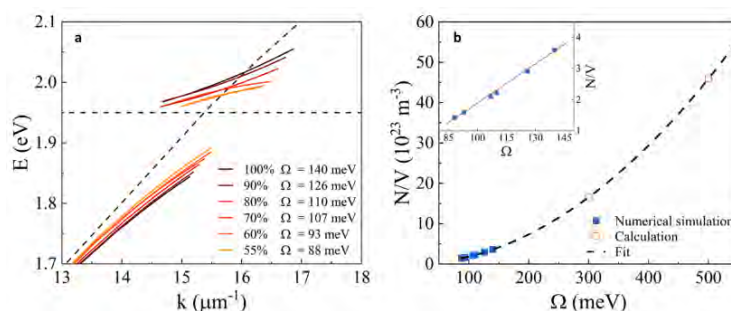


Fig. 1. SPP – exciton dispersion lines in the strong coupling regime for different concentrations of AlexaFluor™ 633 dye (55-100%). Dashed lines indicate uncoupled SPP and exciton dispersion lines (a). Adsorbed protein concentration as a function of Rabi energy gap (b).

The coupling strength between labeled protein and SPP varies from 88 meV to 140 meV and is dependent on the relative concentration of Alexa633 protein dye. Direct relationship between Rabi gap and number of particles participating in strong coupling can be evaluated from equation [4] which describes proportionality of Rabi energy as a square root of density of states. Number of particles in strong coupling regime is around $1 - 4 \times 10^{23}$ and can be linearly approximated due to minor changes in modelled Rabi energy gap (Fig. 1b (inset)).

It was shown that Rabi gap had parabolic dependence on the number of labeled antibodies attached to the gold surface, however the dependence can be linearly approximated for low number of particles participating. The study presents strong coupling regime as a tool to minimize photobleaching effect and paves the alternative way for detection and monitoring of the protein on the metal surface.

- [1] K. R. Spencer, J. Wang, A. W. Silk, S. Ganesan, H. L. Kaufman, and J. M. Mehnert, 'Biomarkers for Immunotherapy: Current Developments and Challenges', *Am. Soc. Clin. Oncol. Educ. Book*, no. 36, pp. e493–e503, May 2016, doi: 10.1200/EDBK_160766.
- [2] S. Guo *et al.*, 'High-performance detection of an abdominal aortic aneurysm biomarker by immunosensing', *Biotechnol. Appl. Biochem.*, p. bab.1877, Jan. 2020, doi: 10.1002/bab.1877.
- [3] B. Li *et al.*, 'Clinical detection of neurodegenerative blood biomarkers using graphene immunosensor', *Carbon*, vol. 168, pp. 144–162, Oct. 2020, doi: 10.1016/j.carbon.2020.06.048.
- [4] P. Törmä and W. L. Barnes, 'Strong coupling between surface plasmon polaritons and emitters: a review', *Rep. Prog. Phys.*, vol. 78, no. 1, p. 013901, Jan. 2015, doi: 10.1088/0034-4885/78/1/013901.
- [5] P. Jurkšaitis, E. Bužavaitė-Vertelienė, and Z. Balevičius, 'Strong Coupling between Surface Plasmon Resonance and Exciton of Labeled Protein–Dye Complex for Immunosensing Applications', *Int. J. Mol. Sci.*, vol. 24, no. 3, p. 2029, Jan. 2023, doi: 10.3390/ijms24032029.

INVESTIGATION OF THZ IMAGING WITH STRUCTURED BEAMS IN A DIGITAL EXPERIMENT

Karolis Mundrys^{1,2}, Paulius Kizevičius², Sergejus Orlovas²

¹ Department of Physics, Vilnius University, Lithuania
² Center for Physical Sciences and Technology, Lithuania
Karolis.mundrys@ff.stud.vu.lt

Electromagnetic THz radiation sources have attracted a lot of attention in the last decade due to their wide applications: from non-invasive spectroscopy [1] to non-ionizing sample imaging methods [2]. One of the more important areas of special applications of optics is the imaging of objects, their recognition and inspection of samples. Due to the complicated detection, Thz imaging is usually implemented by using one pixel method (see Fig. 1) i.e., by changing the position of the sample in the transverse plane. We tried to find the best resolution by changing the distances z_1 , z_2 and by trying different configurations of the illuminating and light collecting elements (to reduce the degree of freedom, distance z_3 was picked equal to 11.5mm and z_1 was picked corresponding to the highest intensity of the beam). Four diffractive masks were investigated: zone plate, axicon, cubic (Airy) and Fibonacci lens. Resolution was defined by spatial frequency (measured in line pairs per millimeter) when the image contrast drops below 20%.

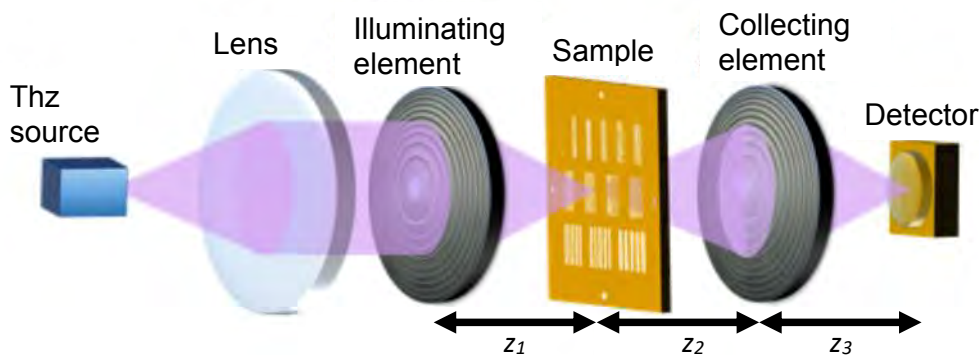


Fig. 1. Single-pixel Thz imaging experiment scheme.

We found that some configurations (cubic mask – axicon, zone plate – axicon, cubic mask – cubic mask, where the first element is the illuminating element and the second is the collecting element) give broad zones of high resolutions while other configuration (Fibonacci lens – Fibonacci lens, Fibonacci lens – cubic mask) give very narrow zones of very high resolution, see Fig. 2. Hence the preference of one configuration over the other heavily depends on the context of the application. This work allows researchers to decide which single pixel Thz imaging configuration is most suitable for their research.

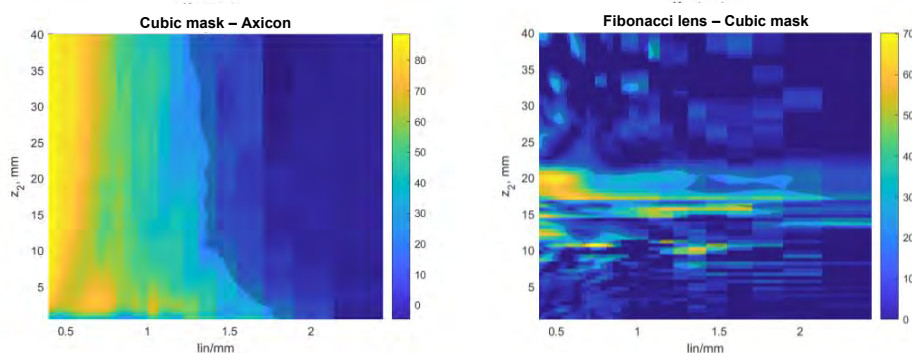


Fig. 2. Image contrast dependance on the distance z_2 and spatial resolution (lin/mm) for cubic mask – axicon (left) and Fibonacci lens – cubic mask (right) configurations.

- [1] Borovkova, M., Khodzitsky, M., Demchenko, P., Cherkasova, O., Popov, A., & Meglinski, I. (2018). Terahertz time-domain spectroscopy for non-invasive assessment of water content in biological samples. *Biomedical optics express*, 9(5), 2266-2276.
[2] Kundu, B. K. (2022). THz Image Processing and Its Applications. *Generation, Detection and Processing of Terahertz Signals*, 123-137.

INVESTIGATION OF OPTICAL PARAMETRIC GENERATOR PUMPED WITH SUBNANOSECOND PULSES BASED ON FAN-OUT GRATING DESIGN MgO:PPLN CRYSTAL

Simona Armalytė¹, Jonas Banys¹, Julius Vengelis¹

¹ Laser Research Center, Faculty of Physics, Vilnius University, Saulėtekio av. 10, Vilnius, Lithuania
simona.armalyte@ff.stud.vu.lt

Optical parametric generators (OPGs) are convenient and easy devices to obtain a wide laser radiation spectrum tuning in the IR region, so they are widely used in fields such as spectroscopy, gas detectors, etc [1,2]. Some applications require subnanosecond (300 ps – 1 ns) duration tunable frequency laser radiation, but such OPGs are difficult to realize, due to laser induced damage threshold (LIDT) of the nonlinear medium, which for subnanosecond pulses in some materials is lower than parametric generation threshold. Due to high nonlinearity, OPGs are often realized with periodically poled crystals where quasi-phase matching is used. In a fan-out grating design, the effective grating period (and quasi-phase matching conditions) changes continuously with the crystal width, allowing a continuous spectrum tuning simply by translating (laterally displacing) the crystal. This tuning is more convenient, faster and more stable than temperature tuning.

In this report we investigate a subnanosecond optical parametric generator with a fan-out grating design in 2.5 cm length 5% magnesium-oxide-doped periodically poled lithium niobate (MgO:PPLN) crystal, which grating period changes continuously from 27.5 μm to 31.6 μm . OPG was pumped by a passively Q-switched Nd:YAG microlaser that generates 1064 nm 520 ps pulses with power up to 1 W and a repetition rate of 1 kHz. With such grating periods in the fan-out design, we achieved continuous spectral tuning for signal from 1420 nm to 2128 nm when the crystal temperature was 200 $^{\circ}\text{C}$ (Fig. 1 (a)). The maximum conversion efficiency of 48.6% was achieved in the degenerate regime (Fig. 1 (b)). The influence of pump focusing conditions for signal energy and spectral characteristics was determined. We also showed that with a fan-out grating design, it is possible to change the central wavelength and spectral width of the generated radiation by rotating the crystal with respect to the incident pump beam.

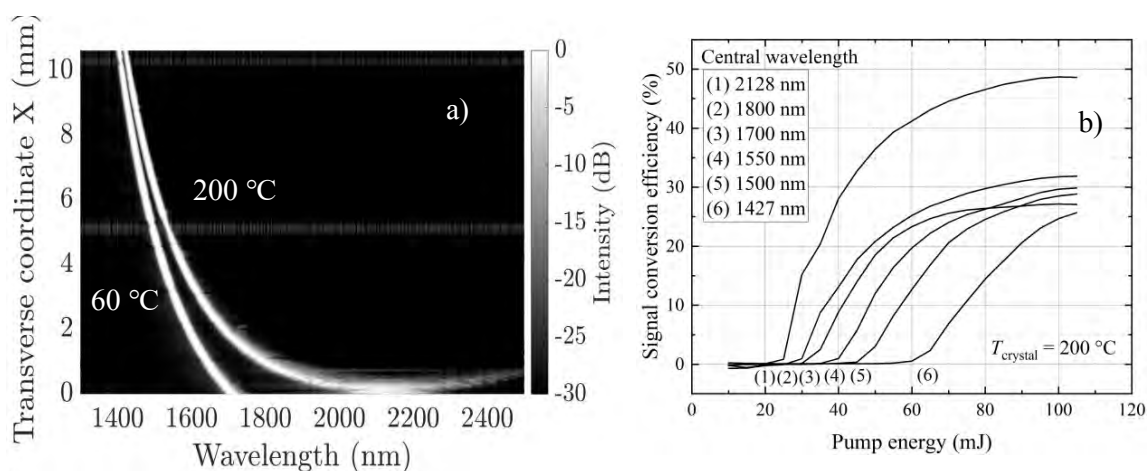


Fig. 1. OPG wavelength tuning range for two fixed temperatures (a) and signal conversion efficiency dependence on pump energy for six different central wavelengths (b).

This work has received funding from European Regional Development Fund (project No. 01.2.2-LMT-K-718-03-0004) under grant agreement with the Research Council of Lithuania (LMTLT).

[1] G. Baxter, M. Payne, B. Austin, C. Halloway, J. Haub, Y. He, A. Milce, J. Nibler, B. Orr, Spectroscopic diagnostics of chemical processes: Applications of tunable optical parametric oscillators, *Appl. Phys. B* **71**(5), 651-663 (2000).

[2] S. Lambert-Girard, M. Allard, M. Piché et F. Babin, Broadband and tunable optical parametric generator for remote detection of gas molecules in the short and mid-infrared, *Appl. Opt.* **54**, 2594-2605 (2015).

MODULATION OF PHASE MAP SEGMENTS TO FORM HOMOGENOUS ILLUMINATION

Mateusz Surma^{1*}, Mateusz Kałuża¹, Paweł Komorowski², Agnieszka Siemion¹

¹Department of Physics, Warsaw University of Technology, Poland

²Institute of Microelectronics and Optoelectronics, Warsaw University of Technology, Poland
mateusz.surma.dokt@pw.edu.pl

Homogenous or uniform illumination finds application in many areas of research and industry. In laboratories, it is often used for imaging purposes to illuminate the object. Different industries apply uniform illumination in processes requiring curing by light, such as 3D printing or photolithography. As one of the developing areas, the terahertz band requires development in this direction.

There exists numerous solutions for obtaining homogenous illumination. Some of them require the application of active elements [1]. Other make use of constant input intensity distributions to realize homogenization passively. Such passive structures can be realized in one of three types of systems: refractive [2], reflective [3], and diffractive. Reflective systems tend to be bulky. Refractive, conversely, may result in thick optical elements and thus call for selection of weakly absorbing optical materials. In the terahertz range, such materials tend to be difficult to find. A solution for this is provided by diffractive elements, which produce similar results to the refractive counterparts but are characterized by smaller thickness. This reduction of thickness comes with a cost of reduction to narrowband applications.

This study explores diffractive and holographic design method to create uniform illumination of terahertz radiation which is realized by division of phase delay map in segments and optimizing the phase modulation of resulting diffractive structure. A number of diffractive structures have been simulated, designed, fabricated, and experimentally verified. Each structure was divided into some number of segments. All segments realized the same functionality: homogenous illumination of a square shape at a defined distance. Segments differed slightly at reconstruction distance. Different structures have been obtained by segment orientations and assembly methods. Examples of two such structures with reconstructions are shown in Fig. 1. The experimental evaluation shows improvement of standard deviation from 0.21 for reference structure to 0.18 and 0.16 for structure 1 and 2, accordingly.

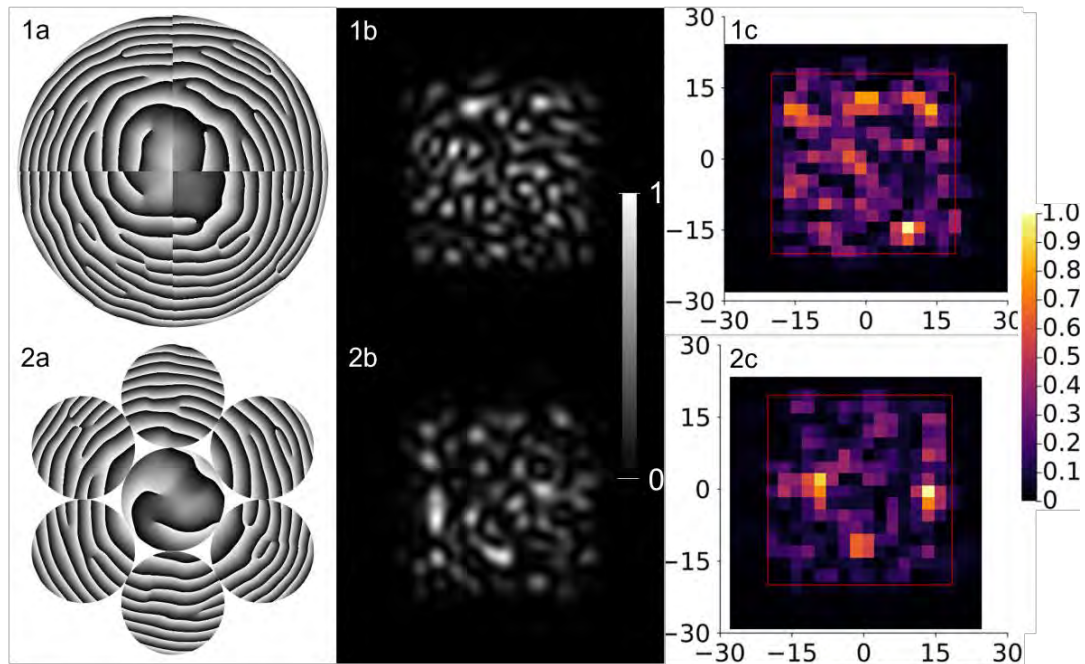


Fig. 1. Examples of two designed structures with a) phase modulation map introduced by the structure, b) intensity distribution resulting from simulation (normalized), and c) experimental reconstruction (normalized).

[1] N. Oda, I. Hosako, T. Ishi et al., The need of terahertz cameras for standardizing sensitivity measurements, *Journal of Infrared, Millimeter, and Terahertz Waves* **35**(8), 671-685 (2014).

[2] R. Zatta, D. Headland, E. Ashna et al., Silicon Lens Optimization to Create Diffuse, Uniform Illumination from Incoherent THz Source Arrays, *Journal of Infrared, Millimeter, and Terahertz Waves* **42**(9), 947-959 (2021)

[3] H. Ries, Laser beam shaping by double tailoring, *Laser Beam Shaping VI* **5876**, 587607 (2005).

LASER 3D PRINTING OF INORGANIC AND OPTICALLY ACTIVE WHISPERING GALLERY MODE MICRO-RESONATOR

Giedrius Balčas¹, Maria Androulidaki^{2,3}, Dimitra Ladika^{2,3}, Vasileia Melissinaki²,
Darius Gailevičius¹, Maria Farsari², Mangirdas Malinauskas¹

¹Laser Research Center, Faculty of Physics, Vilnius University, Vilnius LT-10223, Lithuania

²IESL-FORTH, N. Plastira 100, 70013, Heraklion, Greece

³Department of Materials Science and Technology, 70013, University of Crete, Greece
giedrius.balcas@ff.stud.vu.lt

The utilization of Multi-Photon Lithography (MPL) as a fabrication technique for three-dimensional (3D) micro-optics with free-form shapes has become increasingly prevalent [1]. Its capability to produce intricate and complex structures with high precision and accuracy makes it a suitable option for various applications, including optical communication, sensing, and bio-medical imaging. To further enhance the properties of MPL-fabricated elements, calcination as a post-treatment method has been shown to produce purely inorganic structures [2]. These inorganic structures possess advantageous characteristics for optical applications, such as high thermal and mechanical stability, low absorption losses, and, as demonstrated in this study, exceptional potential for the creation of optically active inorganic structures doped with rare-earth elements [3, 4].

This study describes the fabrication of a notched Whispering Gallery Mode Resonator (WGMR) utilizing MPL and calcination at 1100 °C post-treatment on SZ2080TM organic-inorganic photo-resist doped with Eu³⁺ elements. The combination of MPL and calcination techniques provides control over optical and material properties, resulting in the creation of a non-trivial geometry active resonator. The device design was optimized for high fluorescence emission directionality using a Finite Difference Time Domain numerical model, resulting in an elliptical-shaped WGMR with a sub-wavelength size notch serving as a scattering point (Fig. 1 a)). The fabricated devices were tested using a UV-VIS spectrophotometer system with varying pump power and a central wavelength of 325 nm CW laser. A distinct emission peak at 587 nm was observed, coinciding with the resonator's TM_{57,1} mode, and with a measured quality factor Q higher than 1000 (Fig. 1 b)).

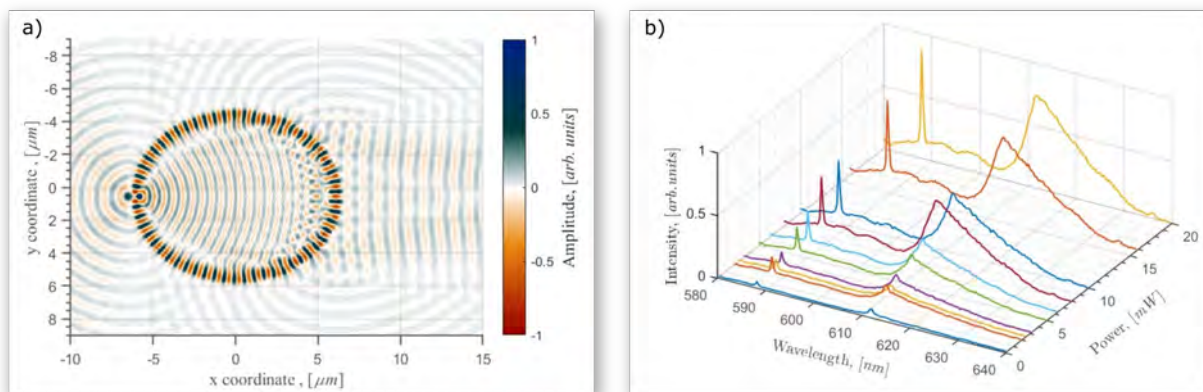


Fig. 1. Results of numerical simulation and experimental analysis of micro-disc resonators. Electric field amplitude distribution of whispering gallery mode TM_{57,1} - a), fabricated structure fluorescence spectra dependence on used pump power - b).

The results of our initial experiments demonstrate the feasibility of utilizing calcinated hybrid organic-inorganic photoresist SZ2080TM as a suitable host matrix for active lanthanide group element fluorescence. This advanced additive manufacturing technique presents a promising platform for a broad spectrum of micro-photonics applications, particularly in cases requiring complex geometries or multi-element systems.

-
- [1] Skliutas, Edvinas, et al. "Polymerization mechanisms initiated by spatio-temporally confined light." *Nanophotonics* 10.4 (2021): 1211-1242.
[2] Gonzalez-Hernandez, Diana, et al. "Laser 3D printing of inorganic free-form micro-optics." *Photonics*. Vol. 8. No. 12. Multidisciplinary Digital Publishing Institute, 2021.
[3] Cooperstein, Ido, et al. "3D printing of micrometer-sized transparent ceramics with on-demand optical-gain properties." *Advanced Materials* 32.28 (2020): 2001675.
[4] Wen, Xiewen, et al. "3D-printed silica with nanoscale resolution." *Nature Materials* 20.11 (2021): 1506-1511.

RAPID LASER MICROMACHINING OF SILICON DIFFRACTIVE OPTICAL ELEMENTS DESIGNED FOR TERAHERTZ IMAGING

Ernestas Nacius^{1,2}, Justinas Minkevičius¹, Orestas Ulčinas², Sergej Orlov¹, Vytautas Jukna^{1,3}

¹ Department of Fundamental Research, Center for Physical Sciences and Technology, 10257 Vilnius, Lithuania

² Workshop of Photonics, 08412, Vilnius, Lithuania

³ Laser Research Center, Vilnius University, 10223, Vilnius, Lithuania

ernestas.nacius@ftmc.lt

Terahertz (THz) optical imaging is an emerging technology from a wide THz applications research field. From optical communications, spectroscopy to optical imaging through various opaque materials without destruction, it can have possible new concepts and applications as a low-cost platform. Borrowing the conceptual ideas from visible light imaging, the THz imaging can be manipulated and improved by making various diffractive elements that can shape the waves [1]. As the THz radiation wavelength is in the millimeter range, ultrashort pulse laser microfabrication technology can be implemented for the manufacturing of custom diffractive elements on various materials. Using the laser ablation process we can structure the surface of a substrate to control the phase of the incoming THz wave [2].

In this work, we aim for optimized laser ablation process parameters to rapidly manufacture silicon diffractive elements suitable for at least 0.1-0.3 THz range. The aim is to find an applicable processing window that maintains good fabrication quality, avoiding oxidation of silicon and keeping low roughness of the ablated area. Additionally, a comparison of different ablating beam shapes of transformed Gaussian beams using geometric phase optical elements will be conducted to find the best cases for possible microfabrication improvements [3, 4]. In this way, the transformation of the Gaussian beam at the focal zone to a flat-top or C-shaped intensity distribution beam can have a positive impact on the process, such as a reduced heat-affected zone or increased ablation rate.

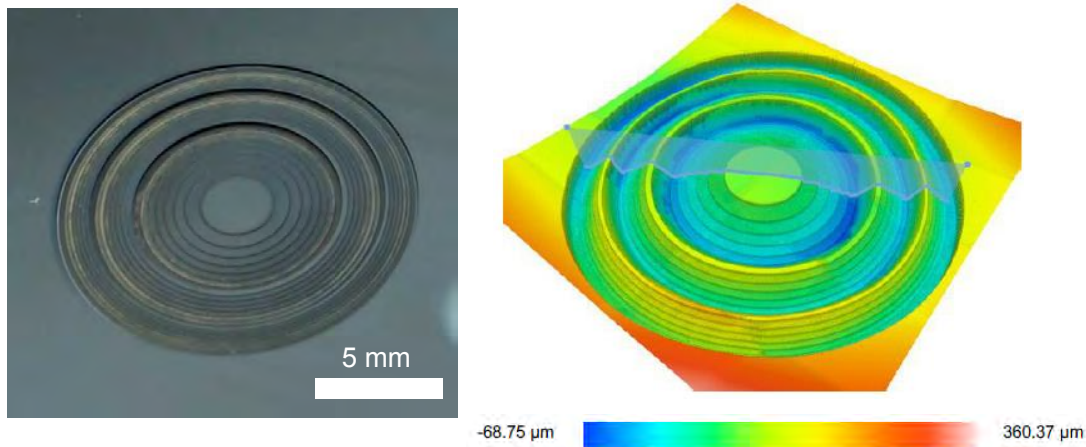


Fig. 1. Diffraction profile of a Fresnel lens inscribed on silicon substrate surface designed for 100 GHz frequency optical imaging. The photograph of manufactured elements is on the left-hand side, while the measured profile is on the right picture.

-
- [1] R. Ivaškevičiūtė-Povilauskienė, P. Kizevičius, E. Nacius, et al. Terahertz structured light: nonparaxial Airy imaging using silicon diffractive optics. *Light Sci Appl* 11, 326 (2022).
- [2] L. Minkevičius, D. Jokubauskis, I. Kašalynas, et al. Bessel terahertz imaging with enhanced contrast realized by silicon multi-phase diffractive optics. *Opt. Express* 27, 36358-36367 (2019).
- [3] M. Beresna, M. Gecevičius, P.G. Kazansky, and T. Gertus, "Radially polarized optical vortex converter created by femtosecond laser nanostructuring of glass", *Appl. Phys. Lett.* 98, 201101 (2011).
- [4] E. Nacius, P. Gotovski, O. Ulčinas, S. Orlov, A. Urbas, V. Jukna, Spatially displaced and superposed Bessel beams for transparent material laser microprocessing, *J. Opt. Soc. Am. B* 38, 3886-3895, (2021).

SURFACE HARDNESS MEASUREMENTS OF STEEL SAMPLES USING FEMTOSECOND LASER INDUCED BREAKDOWN SPECTROSCOPY, COMPARISON OF ULTRAVIOLET AND INFRARED IRRADIATION

Aušrys Vaitiekūnas¹, Ona Balachninaite²

¹Laser Research Center, Faculty of Physics, Vilnius University, Lithuania

ausrys.vaitiekunas@ff.stud.vu.lt

Successful application of femtosecond laser breakdown spectroscopy (fs-LIBS) in surface hardness measurements could result in wide usage of the methodology, especially in micromachining.

Nanosecond-LIBS has showed great promise for surface hardness measurements in many scientific articles [1], however similar works using femtosecond pulses are absent. Since femtosecond pulses are used for their advantages in material ablation, fs-LIBS for surface hardness measurements could yield advantages in application compared to ns-LIBS.

LIBS spectra was gathered from different specimens, having known surface hardness values. Plasma was induced with 1030nm and 343nm wavelength irradiation of Pharos femtosecond laser, pulsewidth 190fs, pulse energy of 0.13mJ. It is said that materials surface hardness has an impact on induced plasma temperature and ionisation degree [2], therefore we calculated plasma temperature T_e , as well as ionic/atomic spectra line relation and displayed the results in graphs in relation to known surface hardness values. Shadowgraphy was used to visualize shockwaves and measure the shockwave speed, which was also displayed in relation to surface hardness values (Fig.1).

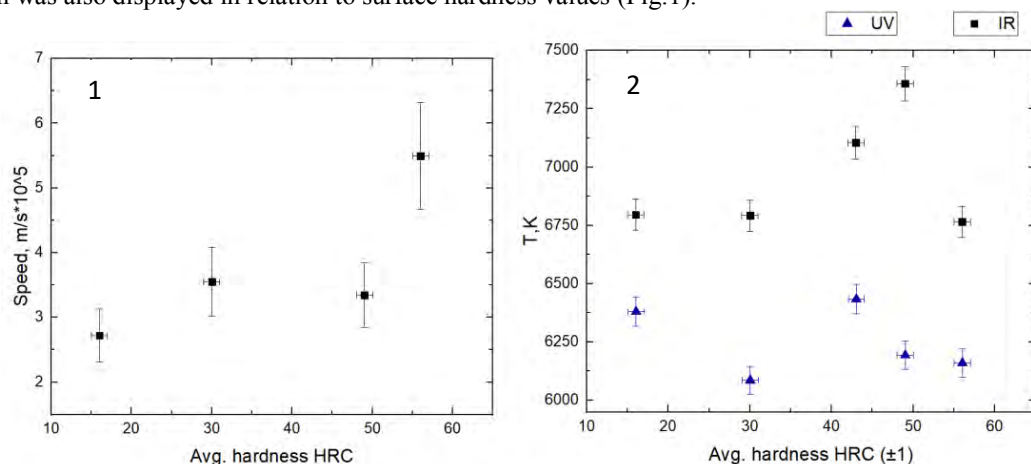


Fig 1. 1 – Shockwave speed in relation to surface hardness. 2 – Plasma temperature in relation to surface hardness, inducing plasma by UV and IR laser irradiation.

Using femtosecond infrared laser irradiation, evaluated plasma temperature values were higher than using ultraviolet light. In our case laser induced plasma temperature, as well as ionic/atomic spectra line ratio has no expressed dependence on materials surface hardness. Shockwave speed, however, tends to rise with surface hardness values.

The obtained results conclude that fs-LIBS could not be successfully applied for the measurements of materials surface hardness.

[1] K. Tsuyuki, S. Miura, N. Idris, K.H. Kurniawan, T.J. Lie, K. Kagawa, Measurement of Concrete Strength Using the Emission Intensity Ratio between Ca(II) 396.8 nm and Ca(I) 422.6 nm in a Nd:YAG Laser-Induced Plasma, *Appl Spectrosc*, 60(1):61-4 (2006).

[2] D. F. Mohamed and A. H. Galmed, Determination of Surface Hardness of Ti -based Alloys via Laser Induced Breakdown Spectroscopy (LIBS), *Arab Journal of Nuclear Sciences and Applications* 50(4), 142-155 (2017).

LASER-INDUCED GRAPHENE FORMATION FOR ELECTROCHEMICAL SENSOR APPLICATIONS

Aivaras Sartanavičius, Vytautas Žutautas, Rasa Pauliukaitė, Romualdas Trusovas

Department of Physics, Vilnius University, Lithuania
 Center for Physical Sciences and Technology, Lithuania
aivaras.sartanavicius@ff.stud.vu.lt

Laser-induced Graphene (LIG) is a simple method of interacting with the material to produce flexible components for energy storage devices, supercapacitors, water-splitting electrocatalysts, piezoelectric strain gauges, electrochemical biosensors, photodetectors, sensors etc. Furthermore, this process enables the production of a novel conducting polymer with less difficulty in integrating it with an electrode, which is highly helpful in flat or flexible systems.

In order to further extend the capabilities of LIG, the process combined selective laser pyrolysis and carbonisation on polyimide (PI) to produce graphene, which has better capabilities in the technical aspect of several standard used materials or used as an enhancing property for a prototype of electrochemical sensor.

The LIG was formed on the surface of the PI film using Atlantic picosecond laser (Ekspla). The laser pulse duration was 10 ps, the pulse repetition rate was 100 kHz, and the irradiation wavelengths were 355, 532 and 1064 nm. The beam and laser power were controlled to extract different scanning speeds, scan repetitions, focus, and powers. The PI film was placed at different focus ranges to obtain the lowest resistance (Ω) or sheet resistance (Ω/sq) on the film in a rectangular structure (1x1 or 1x2 cm).

Resistivity testing of the LIG products was carried out using a simple voltmeter and the 4-probe method. The products were first fabricated using different parameters, and then it was decided which parameters to use to select the best resistance results. The lowest achieved resistances can be seen in the figure 1 (made using parameters from table 1), these samples for prototypes do not crumble, and no additional damage is visible. At 355 nm, the surface resistance error is seen to be $\sim 10 \Omega/\text{sq}$ while at 532 nm it is in the range of $\sim 20\text{-}60 \Omega/\text{sq}$. The structure of the LIG was investigated using Raman spectroscopy and showed that the spectra of the 355 nm and 532 nm samples exhibit pronounced peaks characteristic of multilayer graphene, and the structure of 532 nm was found to be closer to graphene than at 355 nm.

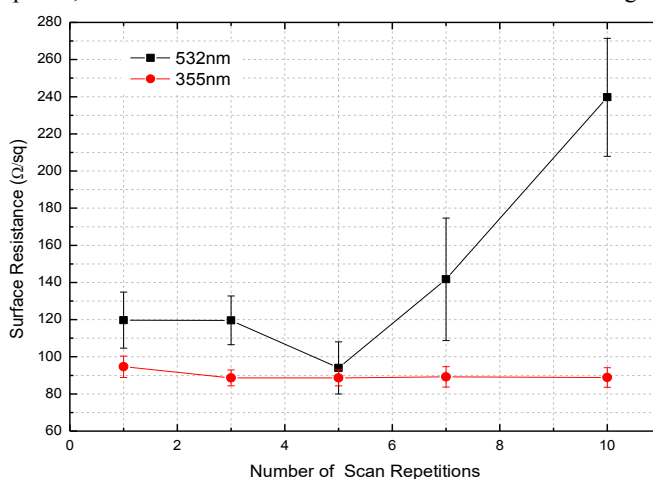


Fig. 1 532/355 nm - Resistance versus scan repetition (4-probe method)

Table 1 Parameters used to produce main prototype samples for potential sensors

Sample	LIG532	LIG355
Wavelength	532 nm	355 nm
Irradiation power	500 mW	200 mW
Scanning speed	50 mm/s	10 mm/s
Scan repetitions	5	5
Hatch	10 μm	10 μm
Position regarding focus	At the focus	4mm from the focus

Using picosecond laser irradiation, a multilayer graphene structure on a PI material has been successfully obtained using two different laser wavelengths (532 nm, 355 nm). Both types of samples were used to prototype pH sensors and were found to be suitable for pH sensor electrodes. The main advantages over other polymer-based pH sensors are that they have a shorter accumulation time (600 s), the sensor is reproducible, selective and stable for up to 70 days.

DEVELOPMENT OF SELECTIVE LASER SINTERING FOR CERAMIC ADDITIVE MANUFACTURING

Alireza Shahidi, Karolis Stravinskas, Genrik Mordas

3D-lab, Department of Laser Technologies, Center for Physical Sciences and Technology, Lithuania
alireza.shahidi@ftmc.lt

Additive manufacturing (AM) is a diverse group of manufacturing techniques that build objects by adding material in a layer-by-layer fashion. There are many ways of dividing the diverse family of ceramic AM techniques into sensible categories [1]. On this research a Selective Laser Sintering machine developed.

The developed system (shown in Fig. 1) includes a built platform and related elevator mechanism (1), powder chamber and elevator ball screw (2), roller feeder (3), transverse movement of the roller feeder by stepper motor (4), and XYZ CNC movement of the laser head (5). To ensure precise printing, we designed and fabricated a servo mechanism with a feeding ball screw.

The printing process for each layer begins by lowering the part platform by 40 microns, followed by upward movement of the material powder, typically twice the height of the part platform, to ensure that there is enough powder for the new layer. The roller feeder is then activated, and a timing belt mechanism moves to ensure a uniform distribution of the new layer. Finally, the XY ball screw CNC movement scans the predefined sections and sinters them according to the setup parameters. This process is carefully controlled to ensure the highest level of accuracy and repeatability.

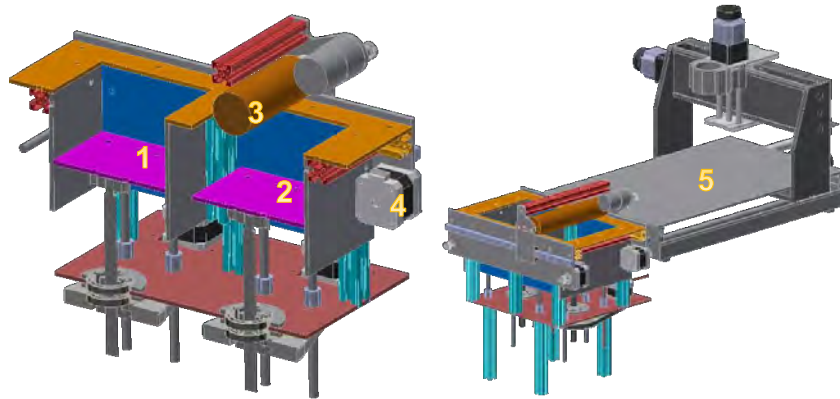


Figure 1) Components of the SLS system for ceramic AM

Ceramic materials are known for their ability to withstand a diverse range of working conditions. In order to account for these varying conditions, our system has been designed as a modular solution. This allows for flexibility in terms of air pressure, pipe diameter, nozzle diameter, and feeding screw specifications, ensuring that the system can be tailored to the specific needs of each material and condition.

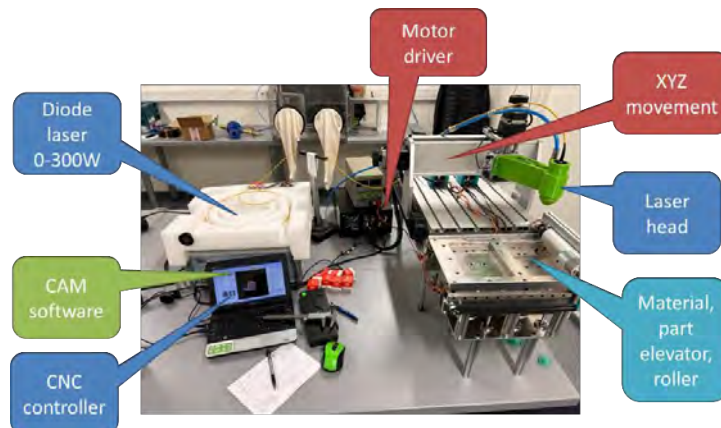


Figure 2) Whole SLS system by Laser, Chambers, XYZ CNC and controller

[1] Additive Manufacturing of Ceramics and Ceramic Composites via Robocasting By: Ezra Feilde , Centre for Advanced Structural Ceramics Department of Materials Imperial College London, 2017.

TERAHERTZ PASSIVE OPTICAL COMPONENTS REALIZING FREQUENCY-DIVISION DEMULTIPLEXING

Mateusz Kaluza^{1*}, Mateusz Surma¹, Pawel Komorowski², and Agnieszka Siemion¹

¹ Department of Physics, Warsaw University of Technology, Poland

² Institute of Microelectronics and Optoelectronics, Warsaw University of Technology, Poland
mateusz.kaluza.dokt@pw.edu.pl

The development of telecommunication systems requires fast, wireless signal transmission. Terahertz (THz) radiation frequencies allow to increase data transfer ratio compared to the ones used nowadays by end-users of telecommunication Wi-Fi system [1]. One of the ideas to achieve it, is an application of passive optical components for multiplexing and/or demultiplexing of radiation within the THz telecommunication system. This work presents components realizing the latter functionality – single-input multiple-output (SIMO) structures realized by a single diffractive optical element (DOE) redirecting the THz beam at a different angles for different frequencies and focusing it on a detector. Designed and manufactured SIMO structures might find application in spatial frequency-division demultiplexing in THz telecommunication systems.

DOEs allow for the desired beam shaping and manipulation according to the designer's idea [2]. Proposed SIMO structures are the combination of two different DOEs: diffraction grating and kinoform lens. The kinoform lens part corresponds to focusing of the incoming radiation into single focal spot, guaranteeing high diffraction efficiency of up to 100%. The second component – diffraction grating, allows for the spatial separation of beams of different THz frequencies previously traveling along a single optical channel. Images of gray-scale phase delay maps of designed elements are illustrated in Fig. 1 – top row. Elements were numerically simulated and then, based on these results, manufactured, which is presented in Fig. 1 – bottom row.

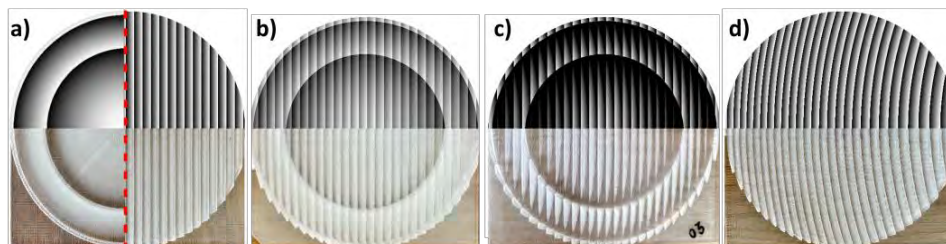


Fig. 1. The gray-scale phase delay maps and 3D printed single-input multiple-output (SIMO) elements. Structures were designed as a combination of two different types of diffractive optical elements (DOEs): phase diffractive lenses and phase blazed gratings in 4 various configurations. SIMO 1-4 corresponds to a) – d) images.

After numerical simulation tests, four different variants of SIMO (1-4) structures were manufactured using fused deposition modeling (FDM) 3D printing technology. All four lenses were manufactured from cyclic olefin copolymer (COC) material previously examined with THz time-domain spectroscopy [3] due to desired optical properties in the THz radiation range of that material (refractive index equal to about 1.5 and low absorption coefficient in the whole examined spectral range).

Fabricated lenses were verified experimentally and according to previously obtained simulation results, all four SIMO structures' performance corresponded to theoretical expectations. SIMO structures correctly separated spatially different THz frequencies and focused them into the -1st diffraction order concerning the designed focal length of 700 mm. Experimental results are presented in Fig. 2.

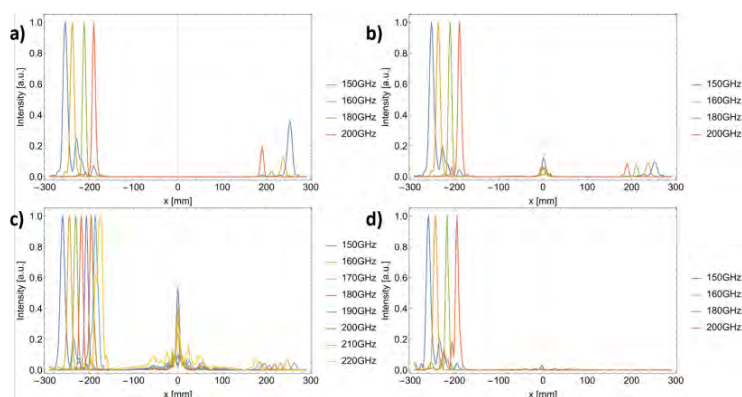


Fig.2 Experimental results for four SIMO structures demonstrating horizontal cross-section of intensity distribution along -1st, 0th, and 1st diffraction order for different THz frequencies. Presented data corresponds to Fig. 1 structures respectively.

[1] J. F. O'Hara, S. Ekin, W. Choi, I. Song, A perspective on terahertz next-generation wireless communications, *Technologies* 7, 43 (2019).

[2] A. Siemion, The magic of optics — an overview of recent advanced terahertz diffractive optical elements, *Sensors* 21, (2020).

[3] M. Kaluza, M. Surma et al., THz optical properties of different 3d printing polymer materials in relation to FTIR, Raman, and XPS evaluation techniques, 47th International Conference on Infrared 2022, ISSN 2162-2035, Millimeter and Terahertz Waves (IRMMW-THz), IEEE, 2022.

MULTIWAVELENGTH SURFACE-ENHANCED RAMAN SPECTROSCOPIC STUDY OF MAGNETO-PLASMONIC NANOPARTICLES

Aikaterini-Maria Gkouzi¹, Martynas Talaikis², Lina Mikoliūnaitė², Evaldas Stankevičius², Gediminas Niaura²

¹Faculty of Physics, Vilnius University, Lithuania

²Department of Organic Chemistry, Center for Physical Sciences and Technology, Lithuania
aikaterini-maria.gkouzi@tprs.stud.vu.lt

Surface-enhanced Raman spectroscopy (SERS) is an informative and non-destructive vibrational spectroscopy technique that allows for highly sensitive structural detection of low concentration analytes through the amplification of electromagnetic fields generated by the excitation of localized surface plasmons [1]. Whilst this technique has proved to be extremely useful in biomedical applications, SERS introduces some problems that need to be solved. These problems include weak reproducibility and contamination by organic materials such as reagents and stabilizers which are used for the chemical synthesis of the plasmonic part of nanoparticles. The chemical contamination can be avoided by producing nanoparticles in a cleaner way - in this case the laser ablation technique of target material in a solution that contains low concentration of salt for better nanoparticle stability. Another obstacle that appears frequently is the “coffee-ring” effect which occurs during the sample drying as a result of uneven material distribution [2]. To avoid this kind of problems, magnetic core (Fe₃O₄) – plasmonic shell (Ag, Au) hybrid nanoparticles are used. The magnetic core of the nanoparticles (Fe₃O₄) allows effortless spatial manipulation using magnet and results in homogeneous distribution of material on a surface. These properties permit more uniform spot-to-spot SERS intensity and higher reproducibility. Multiwavelength SERS spectroscopy was carried out on the reporter molecule 4-mercaptobenzoic acid (4-MBA) which was adsorbed on the smooth gold surface to investigate the enhancement capabilities of these hybrid magneto-plasmonic nanoparticles (Figure 1). In order to evaluate SERS enhancement capability of hybrid nanoparticles we calculated the ratio between SERS and Raman intensities of 4-MBA reporter molecule at the same spectroscopic setup. We found that the highest normalized SERS enhancement occurred at 633 nm, while the 785 and 830 nm excitations were moderately high.

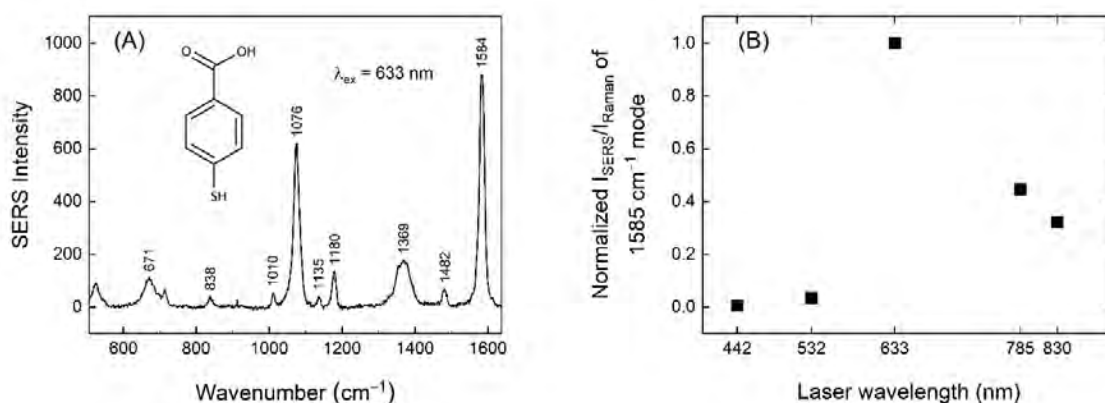


Fig. 1. (A) SERS spectrum of 4-MBA monolayer obtained by using hybrid magneto-plasmonic nanoparticles and 633 nm laser excitation wavelength. Inset shows 4-MBA structure. (B) Excitation wavelength dependence of the normalized SERS intensity of 1585 cm⁻¹ band from 4-MBA adsorbed on a smooth gold surface.

[1] Bhavya Sharma, Renee R. Frontiera, Anne-Isabelle Henry, Emilie Ringe, and Richard P. Van Duyne. SERS: Materials, applications, and the future, 15, 1-12 (2012).

[2] Mikoliūnaitė, Lina, Martynas Talaikis, Aleksandra Michalowska, Jorunas Dobilas, Voitech Stankevicius, Andrzej Kudelski, and Gediminas Niaura. Thermally Stable Magneto-Plasmonic Nanoparticles for SERS with Tunable Plasmon Resonance. *Nanomaterials*, 12, 1-16 (2022).

INVESTIGATION OF CONCENTRATION QUENCHING OF DYSPROSIUM IONS IN SILICATE-SUBSTITUTED FLUORAPATITE

Sara Targońska* and Rafał J. Wiglusz

Institute of Low Temperature and Structure Research, Polish Academy of Sciences, Okolna 2, 50-422 Wrocław, Poland
s.targonska@intibs.pl

In recent years, several studies have been conducted on rare-earth ions doped in various crystalline and non-crystalline materials in order to understand their spectroscopic properties. The majority of light sources are designed with doping of Dy³⁺ ions [1,2]. Luminescence properties of the Dy³⁺ ions are related to the intra configural *f-f* transition. White light can be created by mixing not only the three primary red, green, and blue colors. Additionally, it is important to gain the yellow emission source. There is possible to fabricate white light emission with suitable color temperature and chromaticity coordinates by adjusting the blue-to-yellow intensity ratio in Dy³⁺-doped luminescence materials, appropriately. Therefore, new nanocrystals doped with Dy³⁺ ions were proposed.

Microwave assisted hydrothermal techniques were used to synthesize silicon-substituted apatite doped with Dy³⁺ ions. The luminescence properties were investigated, including the UV-VIS absorption, and excitation spectra, emission spectra, and decay profiles. The spectra were used for further calculation.

According to XRD powder diffraction, obtained nanocrystals have hexagonal structures, with the *P6₃/m* space group. The size in the range of 20-80 nm was confirmed by the Rietveld calculations and TEM images. The EDX study revealed the presence of silicon and dysprosium elements with the concentration related to a theoretical estimate. This study is focused on spectroscopic properties of the obtained materials showing the critical concentration of the luminescence quenching. Radiative *f-f* transitions from the excited states to the ground states are responsible for the luminescence of RE³⁺ ions. In order to determine the critical radius between optically active ions there is needed to analyze the emission spectra. The highest luminescence intensity was observed for a 1 mol% Dy³⁺ ion doping. The critical distance was estimated to be equal to 10.79 Å. A value higher than 5 Å indicates that the interaction between active ions is a multipole-multipole.

An important factor analyzed for the potential light source is the emission color and correlated color temperature (CCT). Both parameters were evaluated. It was found that emission was characterized by the yellowish-green color, and CCT in the range of 4400-5600 K.

-
- [1] C.R. Kesavulu, C.K. Jayasankar, White light emission in Dy³⁺-doped lead fluorophosphate glasses, Mater. Chem. Phys. 130 (2011) 1078–1085. <https://doi.org/10.1016/j.matchemphys.2011.08.037>.
- [2] R. Shrivastava, Near White Light Emission and Concentration Quenching of Calcium Titanate Doped with Dysprosium (III) Phosphors, J. Fluoresc. 29 (2019) 369–374. <https://doi.org/10.1007/s10895-018-02344-2>.

HIGH RESOLUTION NMR STUDY OF 1-BUTYL 3-METHYLIMIDAZOLIUM CHLORIDE SOLUTIONS WITH VARIOUS SOLVENTS

Lukas Mikalauskas¹, Vytautas Klimavičius¹

¹Institute of Chemical Physics, Faculty of Physics, Vilnius University
lukas.mikalauskas@ff.stud.vu.lt

Ionic liquids (ILs) due to the trend of ecology and green energy are finding applications in industry and technology. Properties such as low vapour pressure, thermal stability and conductivity, non-volatility and tunability by changing the cation and anion make ILs very attractive systems in modern applications as well for research.

In this study high-resolution Nuclear Magnetic Resonance (NMR) was used to investigate the mixtures of 1-butyl 3-methylimidazolium Chloride [bmim][Cl] in various media. The media was chosen to act as hydrogen bonding donor/acceptor or as one which does not form hydrogen bonds as well different polarity solvents were investigated. Highly diluted [bmim][Cl] water/ dichloromethane/ acetonitrile/ methanol solutions were investigated by ¹H NMR (Fig 1.). The concentration range was from 10⁻⁶ to 10⁻² molar frequency.

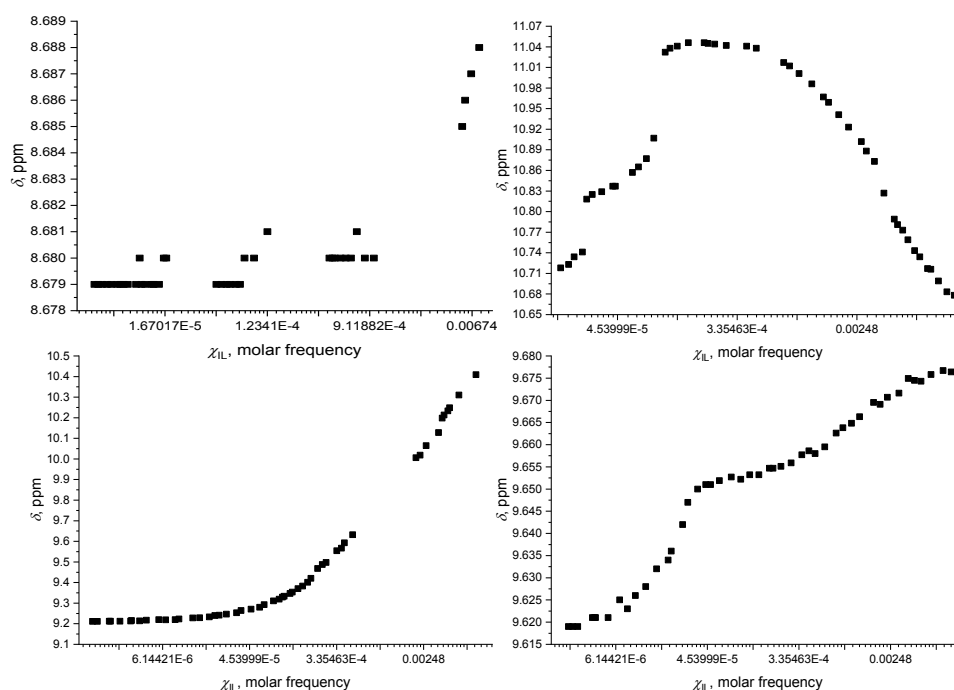


Fig. 1. The chemical shift dependency of H2 signal from concentration in highly diluted water (top left), dichloromethane (top right), acetonitrile (bottom left), methanol (bottom right).

It was found that the ¹H chemical shift reaches the plateau at 7.233*10⁻⁵/1.809*10⁻⁶/2.082*10⁻⁶ molar frequency concentrations for water/acetonitrile/methanol, respectively.

SPECTRAL PECULIARITIES OF HOT CARRIER PHENOMENON IN A SOLAR CELL

Ihor Zharchenko¹, Oleksandr Masalskyi^{1,2}, Jonas Gradauskas^{1,2}, Steponas Ašmontas¹, Algirdas Sužiedėlis¹, Aldis Šilėnas¹, Aurimas Čer. kus^{1,3}, Aleksej Rodin⁴

¹Laboratory of Electronic Processes, Center for Physical Sciences and Technology, Lithuania

²Department of Physics, Vilnius Gediminas Technical University, Lithuania

³Department of Mechatronics, Robotics and Digital Manufacturing, Vilnius Gediminas Technical University, Lithuania

⁴Laboratory of Solid State Lasers, Center for Physical Sciences and Technology, Lithuania

ihor.zharchenko@ftmc.lt

According to the Shockley–Queisser theory, photons with energy lower than the forbidden bandgap of a material do not contribute to net photoresponse of a solar cell. Photons with energy higher than the bandgap participate in photoresponse formation [1].

The present work was initiated by the fact that photons with energy smaller than the bandgap can induce photovoltage across a p-n junction, the hot carrier photovoltage, and its polarity is opposite to the classical one [2]. Moreover, calculations show that the 10% share of the total absorbed incident solar light in GaAs belongs to the below bandgap photons, and it strongly depends on carrier concentration and thickness of the layer [3].

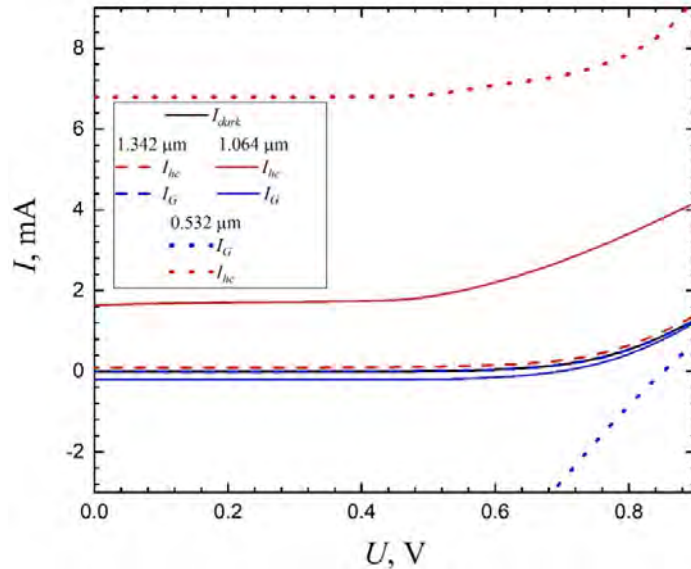


Fig. 1. I-V characteristics of GaAs p-n junction under laser illumination of 0.4 MW/cm² intensity and wavelengths: 0.532 μm (dotted lines), 1.064 μm (solid lines) and 1.342 μm (dashed lines).

The LPE-grown GaAs p-n diodes (forbidden energy gap is 1.42 eV) were illuminated with pulsed laser irradiation of the same 0.4 MW/cm² intensity having different wavelengths of 0.532, 1.064 and 1.342 μm. The obtained results reveal several noteworthy points. First, the 1.342 μm-long photons (0.92 eV) mainly contribute to the hot carrier current and do not have enough energy to induce notable classical generation-caused photoresponse. Second, under the action of the 1.064 μm-long (1.16 eV) photons, the hot carrier photoresponse dominates over the classical photocurrent caused by the two-photon absorption since the extra energy left after the excitation of ordinary electron-hole pair, i.e., 0.9 eV, adds to the intraband absorption-caused carrier heating process. Third, even illumination of the diode with laser light of 0.532 μm wavelength (photon energy 2.32 eV is higher than the bandgap) shows, in contrast to the classical theory, that the hot carrier photoresponse is still present and quite marked; most probably it is raised by the excess energy (0.9 eV) left after the classical interband absorption which is much stronger than the two-photon absorption.

It was shown that negative hot carrier effect manifested itself in the p-n junction in both cases, below and above bandgap photons. Thus, the theoretical maximum efficiency of a single junction solar cells (Shockley–Queisser limit) needs revision by taking into account the contribution of the hot carrier phenomenon within the entire solar spectral range.

[1] W. Shockley, H. J. Queisser, Detailed Balance Limit of Efficiency of p-n Junction Solar Cells, *J. of Appl. Phys.* **32**, 510-519 (1961).

[2] S. P. Ašmontas, J. Gradauskas, D. Šeliuta, Photoelectrical properties of nonuniform semiconductor under infrared laser radiation, *Nonresonant Laser-Matter Interaction conference, Proc. SPIE 4423*, 18-27 (2000).

[3] O. Masalskyi, J. Gradauskas, Pre-thermalizational effect of hot carriers on photovoltage formation in a solar cell, *Ukr. J. Phys. Opt.* **23**, 117-125 (2022).

THE WAVE CLIMATE PARAMETERS CHANGE IN NEARSHORE ALONG THE CURONIAN SPIT SEA COAST IN 2003-2019

Pranciškus Brazdžiūnas¹, Donatas Pupienis^{1,2}

¹ Department of Hydrology and Climatology, Vilnius University, Lithuania

² Laboratory of Geoenvironmental Research, Nature Research Centre, Lithuania
pranciskus.brazdziunas@chgf.stud.vu.lt

The shore formation is determined by hydro-aeolian processes and anthropogenic activities. The appearance, development or decline of coastal landforms (beach and foredune) depends on passive (geological framework, coastal morphology, amount of sediments, etc.) and active (wind, sea level, waves, currents) factors. The global sea level rise, increasing cyclonic activity and anthropogenic load lead to the intensification of coastal erosion. Modern active geomorphological processes - wind, waves, currents, etc. play an important role in shaping the coastal relief. The wave force in open nearshore can be used in assessment of an alongshore and cross-shore sediment transport magnitude and direction. Since the Curonian Spit Baltic Sea coast is open to wave activity, it is crucial to analyze the wave climate parameters change in space and time.

Previously the wave climate parameters (height, period, direction) in the Lithuania nearshore of the Baltic Sea was assessed by a visual method at three observation points - Klaipėda, Nida and Palanga [1]. However, the scientific researches [2, 3, 4] have revealed that visual wave monitoring data is insufficient for a correct assessment of the coastal processes.

The goal of this study was to investigate the Baltic Sea wave climate parameters change along the Curonian Spit nearshore during the 2003-2019 period.

To investigate the Baltic Sea wave climate parameters dynamic, the Baltic Sea wave hindcast data from the Copernicus Marine Environment Monitoring Service database were used. The wave parameters were computed with the wave spectral model WAM and surface forcing from ECMWF's ERA5 reanalysis products. This database covers 28 years of data (1993–2021), with the horizontal grid resolution of 1 nautical mile and provides hourly model data [5]. Mean values of wave parameters (significant wave height, mean wave direction, mean wave period) were analysed for every year at 24 coastal monitoring points.

The results revealed strong correlation between the changes of Baltic Sea wave parameters along the entire Curonian Spit nearshore which may mean that the highest and lowest waves usually occur at the same spots. The average wave height in the nearshore of the Curonian Spit reached 0.72 m. The highest waves prevailed in the nearshore between Pervalka and Preila, and the lowest in the nearshore between Lesnoe and Zelenogradsk settlements. It was found out that the change of prevailing wave direction is also homogeneous. The change of coastline and wave direction may be essential reasons creating differences of coast development in the different sections of the Curonian Spit Sea coast.

[1] L. Kelpšaitė, H. Herrmann, et al., Wave regime differences along the eastern coast of the Baltic Proper. *Proceedings of the Estonian Academy of Sciences*, **57(4)**, 225-231 (2008).

[2] D. Jarmalavičius, V. Šmatas, et al., Factors controlling coastal erosion during storm events. *Journal of Coastal Research*, (**75 (10075)**), 1112-1116 (2016).

[3] D. Jarmalavičius, G. Žilinskas, et al., Geologic framework as a factor controlling coastal morphometry and dynamics. *Curonian Spit, Lithuania. International Journal of Sediment Research*, **32(4)**, 597-603 (2017).

[4] D. Pupienis, I. Buynevich, et al., Spatial patterns in heavy-mineral concentrations along the Curonian Spit coast, southeastern Baltic Sea. *Estuarine, Coastal and Shelf Science*, **195**, 41-50 (2017).

[5] <https://marine.copernicus.eu>

STRUCTURAL ANALYSIS OF VALERIC ACID STRUCTURE USING MATRIX ISOLATION FTIR SPECTROSCOPY AND *AB INITIO* CALCULATIONS

Jogilė Mačytė¹, Rasa Platakytė¹, Joanna Stocka¹, Valdas Šablinskas¹

¹ Institute of Chemical Physics, Vilnius University, Saulėtekio av. 3, 10257 Vilnius, Lithuania
jogile.macyte@ff.stud.vu.lt

Valeric acid or pentanoic acid (C₅H₁₀O₂) is one of the simplest saturated carboxylic acids. Carboxylic acids are often studied using vibrational spectroscopy since they serve as very good model systems in order to understand processes in more complex molecular structures¹. Most of the last two-decade matrix isolation studies concentrate on hydrogen bond in the light acids, starting from formic and ending at propionic. The larger acids have been studied much less due to the additional complications² arising from possibility of having several different conformers, thus making assignment of the vibrational spectra far from straightforward. The main objective of this work is to identify the possible structures (see fig. 1) of the valeric acid using matrix isolation infrared spectroscopy combined with *ab initio* calculations.

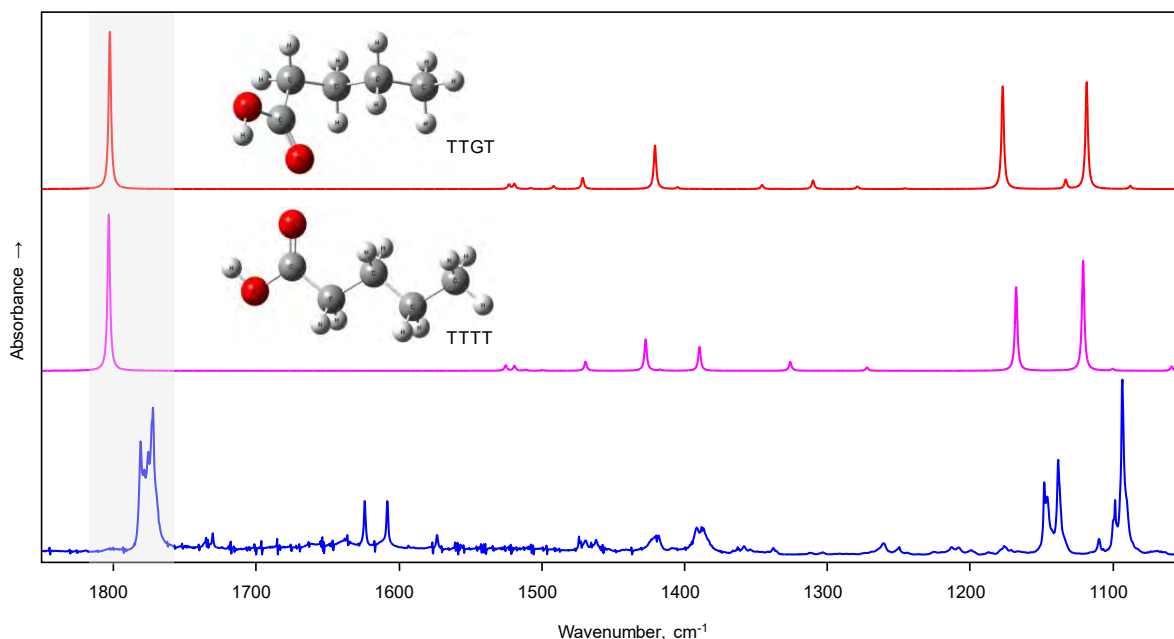


Fig. 1. FTIR absorption spectrum (lower curve) of valeric acid, isolated in argon matrix. The figure also shows the theoretically predicted spectra of conformers TTTT (upper curve) and TTGT (middle curve). The calculations were performed using MP2/cc-pVTZ theory level.

The theoretical calculations were carried out using two different methods. First of all, DFT calculations were performed using the B3LYP functional and an augmented Dunning correlation matched valence double zeta basis set. The further calculations were continued using the MP2 - Møller-Plesset expansion extension which contains truncated second orders, supplemented with the Dunning correlation matched basis set (triple zeta).

The MP2 calculations show that the TTGT conformation has the lowest energy. The second lowest energy conformer is TTTT, which is $\Delta E = 1.6$ k J/mol higher in energy than TTGT. Experimental FTIR spectra of valeric acid isolated in argon, nitrogen and neon matrices were recorded. Comparison of the experimental spectra with calculated ones of the two lowest energy conformers (see fig. 1) allowed us to identify bands belonging to the both conformers. The band corresponding to C=O stretching vibration at 1802 cm⁻¹ for TTGT and 1803 cm⁻¹ for TTTT conformer. In the experimental spectra, there are definitely more bands in the 1850-1750 cm⁻¹ spectral region than was predicted by the calculations. The 1772 cm⁻¹ band, for example, was assigned to the TTGT conformer band and 1773 cm⁻¹ assigned to TTTT conformer bands. Such findings allowed us to conclude that at least two conformers of valeric acid coexist in low temperature matrices, with different concentrations that can be explained taking in to account different stability of the conformers.

[1] J. Ceponkus et al. Lithuanian Journal of Physics, Vol. 49, No. 1, pp. 53–62 (2009)

[2] V. Šablinskas et al. Journal of Molecular Structure 976 (2010) 263–269

SOLAR CELL PERFORMANCE EVALUATION PECULIARITIES WITH LED – BASED SOLAR SIMULATORS

Darius Antonovič, Žygimantas Vosylius, Algirdas Novičkovas, and Vincas Tamošiūnas

Institute of Photonics and Nanotechnology, Vilnius University, LT – 10257, Vilnius, Lithuania
darius.antonovic@ff.stud.vu.lt

Solar simulators are tools that provide optical and spectral composition similar to sunlight intensity and are integral in the process of current – voltage (I-V) characterization of photovoltaic panels [1]. Compared to natural sunlight solar simulators have the advantage of being calibrated sources that can be changed on demand thus are not influenced by factors such as geographical location and climate conditions. Solar simulators have been traditionally manufactured using xenon short – arc lamps or metal halide discharge lamps; however, they require extensive maintenance and have a quite limited lifetime [2]. The development high – energy LED technologies has created new ways to design solar simulators that allow for the mitigation of the aforementioned issues due to the intrinsic properties of LEDs such as longevity, high efficiency and low operating voltages [3].

The “Sentaurus TCAD” program package consists of several programs out of which the most important one is “Sentaurus Device”. It allows to simulate numerically the performance of semiconductor – based optoelectronic devices under various illumination conditions [4].

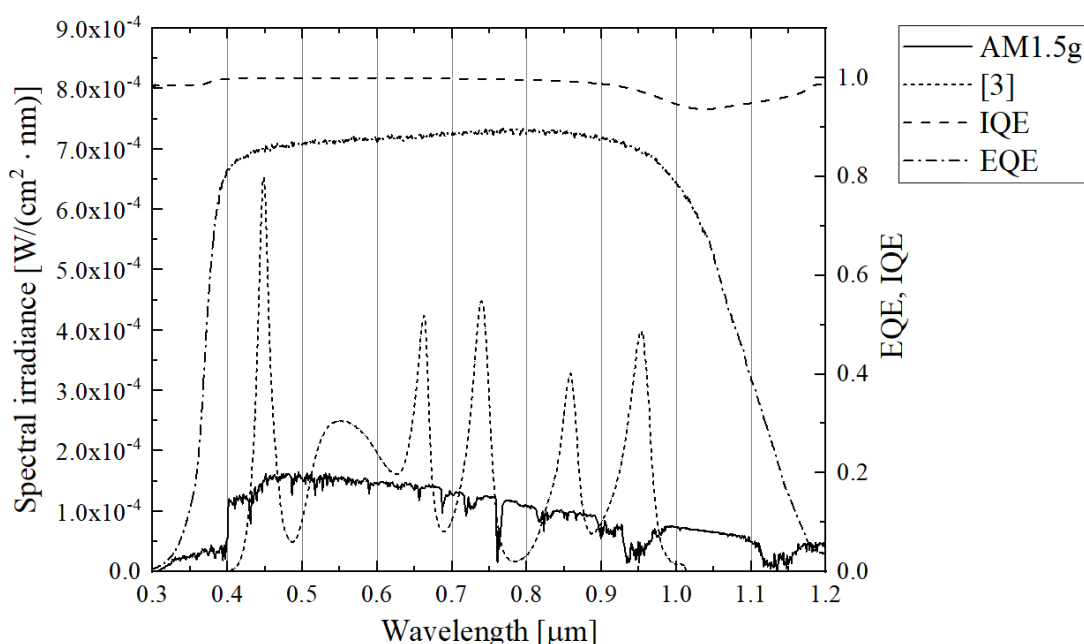


Fig. 1. Quantum efficiency spectra (right Y – axis) and illumination spectra (left Y – axis). “AM1.5g” denotes the reference global illumination spectra, [3] – the spectrum of a solely LED – based solar simulator.

In this contribution, we report on the evaluation of expected performance of solar cells under the illumination of various spectra that were calculated for LED – based solar simulators with varying layouts: from solely LED – based to hybrid solar simulators. We performed simulations for multiple solar cell types, including both single – junction and dual – junction ones.

Our simulation results reveal that substantial photocurrent differences might be expected even when solar simulators fully match newly defined [5] requirements for so-called A+ class solar simulators and constant irradiance is enforced. The origin of these deviations can be traced back to spectral contents of simulators and peculiarities of response of solar cells for photon energies either near the absorption edge of semiconductors or in the regions of strong absorption near the interfaces.

- [1] V. Esenda, Ş. Sağlam, B. Oral, *Light sources of solar simulators for photovoltaic devices: A review*, Renewable and Sustainable Energy Reviews **77**, 1240–1250 (2017).
- [2] E. López-Fraguas, J. M. Sánchez-Pena, R. Vergaz, *A Low-Cost LED – Based Solar Simulator*, IEEE Transactions on Instrumentation and Measurement **68**, (2019).
- [3] Ž. Vosylius, A. Novičkovas, K. Laurinavičius, V. Tamošiūnas, *Rational Design of Scalable Solar Simulators with Arrays of Light-Emitting Diodes*, IEEE Journal of Photovoltaics **12** (2022).
- [4] Synopsys Inc., *TCAD Documentation. Version S-2021.06* (2021).
- [5] <https://www.nrel.gov/grid/solar-resource/spectra-am1.5.html>

FEATURES OF FLUORESCENCE PROPERTIES OF NANODIAMONDS

Yaraslau Padrez¹, Lena Golubewa^{1,2}, Renata Karpicz¹

¹ Department of Molecular Compound Physics, Center for Physical Sciences and Technology, Lithuania

² Center for Photonics Sciences, Department of Physics and Mathematics, University of Eastern Finland, Finland
yaraslau.padrez@ftmc.lt

Nanodiamonds (NDs) are of great interest as promising materials with a high sensory potential for application in various fields of science and technology. Most of the exceptional mechanical, thermal and optical properties of NDs are inherited from bulk diamond or internal point defects such as lattice vacancies. Together with vacancies, random point defects (N, Si, etc.) that form various color centers have a wide range of unique properties, such as temperature-dependent PL (SiV centers) [1], spin-dependent PL (NV color centers), no blinking or photobleaching [2,3], sensitivity of color centers to radical formation and environmental chemical reactions or changes in pH values [4]. However, several properties could be additionally obtained because of specific steps of synthesis procedure or post-processing. These properties are associated with the ND's surface and can be sensitive to the changes of the external environment.

The goal of the present study was to investigate optical properties of NDs (Ray Techniques Ltd., Israel), obtained by pulsed laser ablation and post-processed to stabilize NDs in water, as well as to reveal the dependence of their properties on the structural features of NDs and their sensitivity to the pH value of water solutions. The NDs were characterized using transmission electron microscopy, atomic force microscopy, ATR-FTIR and Raman, steady-state and time-resolved fluorescence spectroscopies.

ND suspensions demonstrate a complex PL behavior which depends on the excitation wavelength, as it follows from Fig. 1 (A). The PL spectra were fitted with several Gaussian profiles allowing one to assume the presence of several PL centers in NDs. The positions of the PL maxima are slightly redshifted when the excitation wavelength increases.

The performed spectroscopic characterization of NDs reveals that NDs comprise sp³ cubic core covered with sp²-disordered clusters having size of 0.62 nm and decorated with wide range of oxygen-containing surface groups, including hydroxyl, ketone, carboxylic anhydride and carboxyl groups, without a pronounced predominance of any of them. The model is presented in Fig. 1 (B).

In the present study the revealed individual surface PL centers of NDs were shown to be pH-sensitive, and the dependence of the PL intensity on the pH was used to propose a calibration applicable for optical determination of the pH values in water solutions.

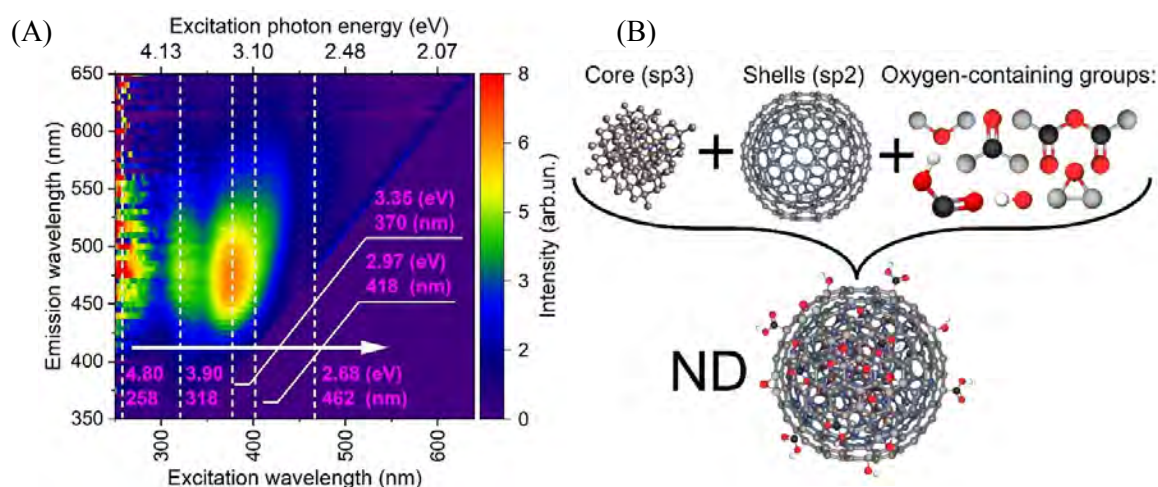


Fig. 1. (A) PLE-map of 0.04% ND water suspensions. Maxima on PLE spectra are marked with ticks, positions are represented in eV and nm. (B) The model of the nanodiamond structure.

Acknowledgments

This work was partially supported by Horizon Europe FLORIN (Project № 101086142).

- [1] L. Golubewa *et al.*, 'All-Optical Thermometry with NV and SiV Color Centers in Biocompatible Diamond Microneedles', *Adv. Opt. Mater.*, vol. n/a, no. n/a, p. 2200631, doi: 10.1002/adom.202200631.
- [2] S. V. Bolshedvorskii *et al.*, 'Single Silicon Vacancy Centers in 10 nm Diamonds for Quantum Information Applications', *ACS Appl. Nano Mater.*, vol. 2, no. 8, pp. 4765–4772, Aug. 2019, doi: 10.1021/acsnm.9b00580.
- [3] S.-J. Yu, M.-W. Kang, H.-C. Chang, K.-M. Chen, and Y.-C. Yu, 'Bright Fluorescent Nanodiamonds: No Photobleaching and Low Cytotoxicity', *J. Am. Chem. Soc.*, vol. 127, no. 50, pp. 17604–17605, Dec. 2005, doi: 10.1021/ja0567081.
- [4] M. J. Głowacki, M. Sawczak, A. Wcisło, M. Ficek, and R. Bogdanowicz, 'pH-Dependency of the Physical Properties of the Nitrogen-Vacancy Centers in Diamonds', in *Biophotonics Congress: Biomedical Optics 2020 (Translational, Microscopy, OCT, OTS, BRAIN)*, Washington, DC, 2020, p. JTh2A.11. doi: 10.1364/TRANSLATIONAL.2020.JTh2A.11.

ANALYSIS OF TIME-RESOLVED FLUORESCENCE SPECTRA FOR MOLECULAR SYSTEMS

Laura Lelevičiūtė¹, Andrius Gelžinis^{1,2}, Jevgenij Chmeliov^{1,2}, Leonas Valkūnas^{1,2}

¹Faculty of Physics, Vilnius University, Saulėtekio al. 9, LT-10222, Lithuania

²Department of Molecular Compound Physics, Center for Physical Sciences and Technology, Vilnius, Lithuania
laura.leleviciute@ff.stud.vu.lt

Fluorescence is a widely used method in various fields of science to easily analyze electronic excitation dynamics in molecular systems. Global and target analysis are used in order to extract meaningful data from time-resolved fluorescence spectra. The more complex the molecular system is, the more difficult it is to do so, hence the search for new and effective data analysis methods is still relevant to this day [1, 2]. In our study we use species associated kinetics method. Firstly we described the intensity of fluorescence as its' spectra and decay kinetics and postulated the shape of the spectra by Gaussian and pseudo-Voigt functions. Solving the optimization problem allowed us to obtain the spectra and then we used The Moore-Penrose pseudo inverse method [3] and calculated both decay kinetics and the intensity of fluorescence. This method was applied to the data of light harvesting complexes II – (LHCII) trimers and their aggregates, previously analyzed in Nature Plants article [4]. By introducing a more complex pseudo-Voigt function, we hoped to account for the asymmetry of fluorescence spectra in a straightforward way and get accurate results more easily.

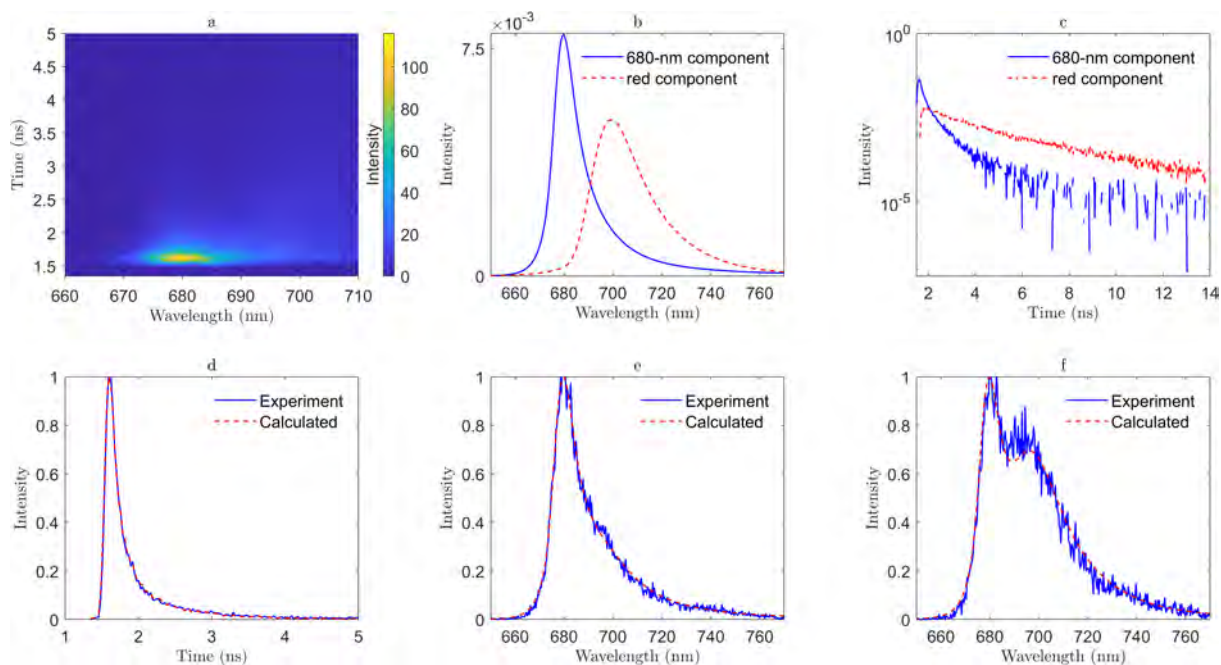


Figure 1. Time-resolved fluorescence measurements of LHCII aggregates at 100 K temperature using species associated kinetics with pseudo-Voigt function. a, Two-dimensional plot illustrating evolution of fluorescence intensity. b, Normalized fluorescence spectra. c, Normalized fluorescence decay kinetics. d, Vertical slice of experimental and calculated fluorescence intensities with $\lambda = 679 - 682$ nm wavelength interval. e, f, Horizontal slices of experimental and calculated fluorescence intensities with $t = 1.6 - 1.9$ ns and $t = 1.9 - 2.1$ ns time intervals respectively.

[1] J. R. Lakowicz, Principles of fluorescence spectroscopy, 2006.

[2] C. Slavov, H. Hartmann, and J. Wachtveitl, Implementation and evaluation of data analysis strategies for time-resolved optical spectroscopy, Analytical Chemistry, 2015, 87, 2328–2336.

[3] E. K. Chong and S. H. Zak, An introduction to optimization, 2013.

[4] J. Chmeliov, A. Gelžinis, E. Songaila, R. Augulis, C. D. Duffy, A. V. Ruban, and L. Valkunas, The nature of self-regulation in photosynthetic light-harvesting antenna, Nature Plants, 2016, 2, 16045.

AEROSOL PARTICLE NUMBER CONCENTRATION AND SIZE DISTRIBUTION DURING MIDSUMMER EVENT

Kamilė Kandrotaitė^{1,2}, Agnė Minderytė², Audrė Kalinauskaitė², Lina Davulienė², Lucja Janicka³, Vadimas Dudoitis², Iwona S. Stachlewska³, Steigvilė Byčėnkienė²

¹ Faculty of Physics, Vilnius University, Vilnius 01513, Lithuania

² Department of Environmental Research, Center for Physical Sciences and Technology, Vilnius 10257, Lithuania

³ Faculty of Physics, University of Warsaw, Warsaw 02093, Poland

kamile.kandrotaitė@ftmc.lt

According to the World Health Organization, air pollution is associated with ~7 million premature deaths worldwide annually [1]. The main sources of aerosol particle pollution in the cities are of anthropogenic origin [2], where today about 56% of the world's population lives (in Lithuania - 68%) [3]. In this way, urban air pollution is the biggest global environmental quality challenge in the context of health. Aerosol particles are a major component of urban air pollution and include a mixture of aerosol particles ranging in size from a few nanometers to tens of micrometers.

This study uses a Scanning Mobility Particle Sizer (SMPS, TSI 3936) and Aerodynamic Particle Sizer (APS, TSI 3321) for simultaneous measurement of particle number concentration (PNC) and size distribution in the summertime in urban environment (Vilnius). In this study, particles were classified into three modes based on particle diameter: nucleation mode (10-25 nm), Aitken mode (25–100 nm) and accumulation mode (100-1000 nm). The analyzed period was divided into three episodes based on measured aerosol particles mass concentration and prevailing wind direction: Episode 1 (June 1st – June 11th), Episode 2 (June 12th – June 23rd 11:00) and Episode 3 (June 25th – June 30th). The night of June 23-24th was classified as a special event due to wood burning in open bonfires in relation to St. John's Day (Midsummer) which is a national celebration in Lithuania and Latvia.

Monthly average total aerosol mass concentration for particles in the 10-16000 nm size range varied from 1.6 to 43.9 $\mu\text{g}/\text{m}^3$ (with maximum on June 23th 23:55). During Episodes 1, 2, and 3, the mean aerosol mass concentration was 14.7, 8.9, and 14.8 $\mu\text{g}/\text{m}^3$, respectively. In contrast, the mean monthly PNC in the same size range was $4.6 \times 10^3 \text{ \#/cm}^3$ (SD = 3.1×10^3), with an instantaneous maximum of $29.5 \times 10^3 \text{ \#/cm}^3$ (on June 7th 14:25). On Midsummer day, the average values of aerosol mass concentration and PNC were 16 $\mu\text{g}/\text{m}^3$ and $7.6 \times 10^3 \text{ \#/cm}^3$, respectively. Meanwhile, the maximum PNC value ($27 \times 10^3 \text{ \#/cm}^3$) on June 23th 23:55, indicated an extremely polluted midnight. In consequence of common tradition – bonfire night, on Midsummer it was caused mean mass and PNC increase by over 50% compared to the average mass and number concentration levels of the whole month of June.

The particles in Aitken mode had the largest input to the total PNC (Fig. 1). During Midsummer event a two-fold increase was observed in the mean Aitken mode particle number concentration compared to all episode concentration (Event - $4.1 \times 10^3 \text{ \#/cm}^3$ and 1-3 episode 2.4, 2.2, $1.5 \times 10^3 \text{ \#/cm}^3$, respectively). Our results reveal a significant contribution of open biomass burning to Aitken mode which can grow to larger sizes. Particles in nucleation mode were mainly derived from new particle formation [4], while Aitken mode particles were mainly influenced by biomass, biofuel combustion, anthropogenic emissions [5] and the growth of nucleation mode particles.

Increasing PNC of ultrafine particles due to biomass burning poses a great risk to human health, since there are no guidelines for ultrafine particles number concentrations.

Acknowledgment: Funding received by joint Lithuanian-Polish research project DAINA-2 grant "Importance of long-range transport of BIOMass burning emissions to local Smog events in Urban Environments (BIOSURE) supported by Narodowe Centrum Nauki (Grant no. 2020/38/L/ST10/00480) and the Research Council of Lithuania (Lietuvos mokslo taryba) (Grant no. S-LL-21-7)

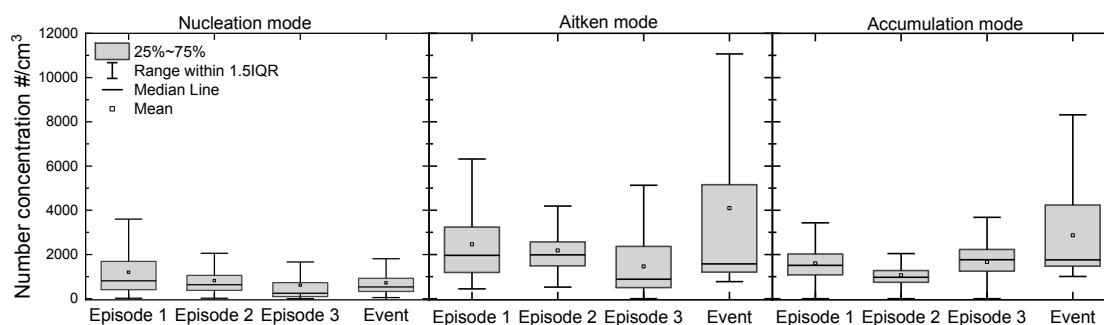


Fig. 1. Boxplots of number concentration during specified episodes and Midsummer event.

[1] https://www.who.int/health-topics/air-pollution#tab=tab_2 [3] <https://data.worldbank.org/indicator/SP.URB.TOTL.IN.ZS>

[2] Ali, M. et al., Pollution characteristics, mechanism of toxicity and health effects of the ultrafine particles in the indoor environment: Current status and future perspectives, *Critical Reviews in Environmental Science and Technology* (2022), 52:3, p.p. 436-473.

[4] Kulmala, Markku. (2003). How Particles Nucleate and Grow. *Science* (New York, N.Y.). 302. 1000-1. 10.1126/science.1090848.

[5] Zimmerman, Alyssa et al. (2020). Observations of new particle formation, modal growth rates, and direct emissions of sub-10 nm particles in an urban environment. *Atmospheric Environment*. 242. 117835. 10.1016/j.atmosenv.2020.117835.

A CASE STUDY OF EXTENSIVE BIOMASS BURNING RELATED BLACK CARBON EMISSIONS DURING MIDSUMMER EVE IN VILNIUS, LITHUANIA

Agnė Minderytė¹, Kamilė Kandrotaitė^{1,2}, Audrė Kalinauskaitė¹, Lina Davulienė¹, Lucja Janicka³, Vadimas Dudoitis¹, Iwona S. Stachlewska³, Steigvilė Byčėnkiėnė¹

¹ Department of Environmental Research, Center for Physical Sciences and Technology, Vilnius, Lithuania

² Faculty of Physics, Vilnius university, Lithuania

³ Institute of Geophysics, Faculty of Physics, University of Warsaw

agne.minderyte@ftmc.lt

Aerosol particles can scatter or absorb light depending on their chemical composition. Meanwhile, the chemical composition is highly dependent on the source [1]. It is widely known that sulphate and nitrate contribute significantly to light scattering. Even though there are numerous studies on aerosol particles originating from biomass burning, a consensus on the strength of the radiative effect of the aerosols has not been reached [2]. The case study investigates the impact of an extensive nationwide bonfire-burning event, associated with the celebration of Midsummer, on the aerosol black carbon (BC) mass concentration and optical properties at an urban background site. Aerosol BC mass concentration was measured using an Aethalometer (AE33, Magee Scientific); aerosol scattering properties were recorded using a Nephelometer (TSI model 3563); the aerosol particle number size distribution was evaluated using a condensation particle counter (CPC, TSI model 3085) and a differential mobility analyzer (DMA, TSI model 3085). The changes in aerosol BC source contribution, light absorption coefficient, absorption and scattering Ångström exponents (AAE and SAE, respectively), single scattering albedo (SSA), and particle number size distribution were analyzed during the period from 1st to 30th June 2022. The Midsummer celebration took place on the night of 23rd June when a 3-fold increase in the total BC mass concentration was observed. Moreover, the extensive bonfire burning resulted in a 7-fold increase in BC_{BB} (BC originated from biomass burning) level compared to the monthly average value. The high contribution of BC_{BB} to the total aerosol BC appears to increase aerosol light absorption. Thus, it performs a warming role in the atmosphere as the SSA value decreased to 0.62. This multi-parameter investigation focuses on the high pollution event when biomass-burning aerosols originated nationwide in a rather short time scale. The results provide a better perception of the biomass-burning-related aerosol characteristics in the ambient atmosphere and their impact on atmospheric radiative transfer.

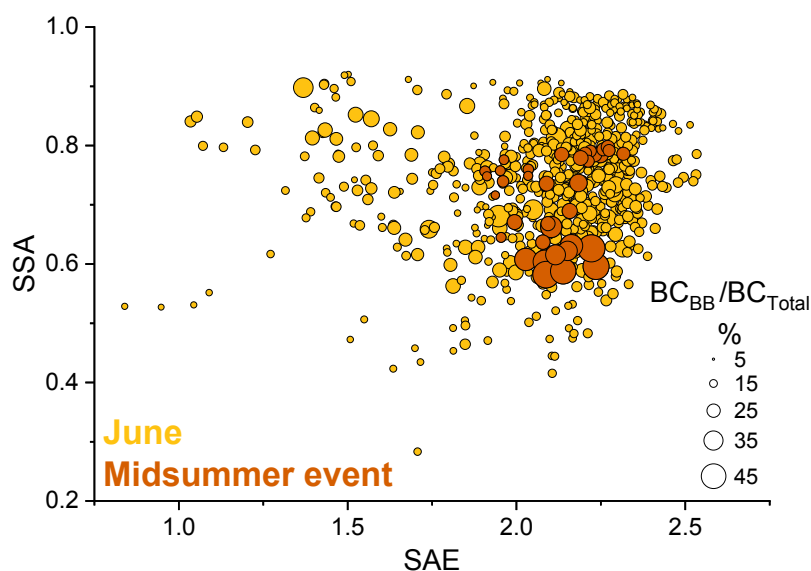


Fig. 1. Scatter plot of aerosol SSA and SAE together with BC_{BB} contribution to BC_{Total} .

[1] C. D.Cappa, K. R. Kolesar, X. Zhang et al., Understanding the optical properties of ambient sub- and supermicron particulate matter: results from the CARES 2010 field study in northern California, *Atmospheric Chemistry and Physics*, **16**, 6511–6535 (2016).

[2] V. Masson-Delmotte, P. Zhai, A. Pirani, S. L. Connors, C. Péan et al., IPCC 2021. Climate Change 2021: The physical science basis. Contribution of Working Group I to the sixth assessment report of the intergovernmental panel on climate change (2021).

CHARACTERIZATION OF Eu^{3+} ION-DOPED $\text{Sr}_{10}(\text{PO}_4)_6\text{F}_2$ FOR LUMINESCENCE-BASED TEMPERATURE SENSING

Katarzyna Szyszka and Rafal J. Wiglusz

Institute of Low Temperature and Structure Research, PAS, Okolna 2, PL-50-422 Wroclaw, Poland
k.szyszka@intibs.pl

Scientists around the world are constantly looking for new materials that can be applied in advanced photonic application as solid-state lighting or in medicine as theranostic materials. Phosphors based on rare-earth ions (RE^{3+}) are still in the spotlight due to their wide range of applications such as color displays, light-emitting diodes (LEDs), medical diagnostics, solar cells, non-invasive thermometry, and optical heating.

Materials belonging to a large family of apatite defined by the general chemical formula $\text{M}_{10}(\text{XO}_4)_6\text{Z}_2$ (e.g. $\text{M} = \text{Ca}^{2+}, \text{Sr}^{2+}$; $\text{XO}_4 = \text{PO}_4^{3-}, \text{SiO}_4^{4-}, \text{VO}_4^{3-}$; $\text{Z} = \text{OH}^-, \text{F}^-, \text{Cl}^-$) crystallize in the hexagonal system with the space group $P6_3/m$ [1–3]. The apatite lattice can be a host for luminescent active ions due to its excellent chemical and thermal stability.

Strontium fluorapatites ($\text{Sr}_{10}(\text{PO}_4)_6\text{F}_2$) doped with Eu^{3+} ions were obtained by microwave-hydrothermal method and heat-treated at 600 °C. Their structural and morphological properties were investigated by X-ray powder diffraction (XRD), scanning electron microscopy combined with energy-dispersive spectroscopy (SEM-EDS) as well as Fourier-transform infrared spectroscopy (FT-IR). The luminescence behavior of Eu^{3+} ions in $\text{Sr}_{10}(\text{PO}_4)_6\text{F}_2$ nanopowders was studied by using excitation, emission spectra, and luminescence decay time techniques. The electric dipole transition (${}^5\text{D}_0 \rightarrow {}^7\text{F}_2$) is the most intense in all prepared materials. The asymmetry parameter (R) was calculated and discussed. The temperature-dependent emission spectra of the as-prepared as well as annealed 1 mol% Eu^{3+} -doped $\text{Sr}_{10}(\text{PO}_4)_6\text{F}_2$ were measured in the temperature range from -193 °C to 600 °C and studied extensively.

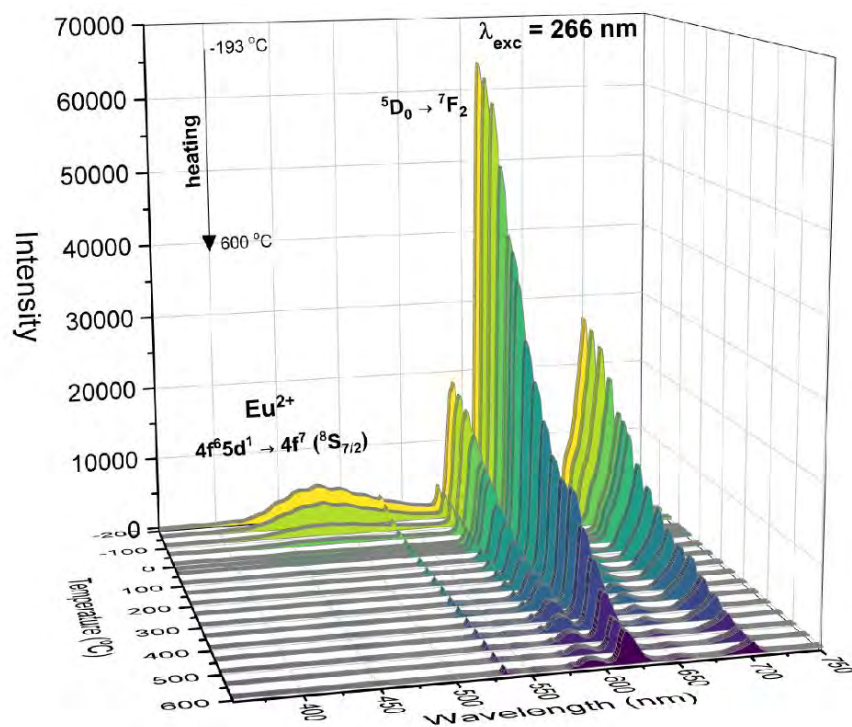


Fig. 1. The temperature-dependent emission spectra of the 1 mol% Eu^{3+} -doped $\text{Sr}_{10}(\text{PO}_4)_6\text{F}_2$ annealed at 600 °C in the temperature range from -193 to 600 °C.

- [1] H. Liu, L. Liao, J. Chen et al., Tunable luminescence properties and energy transfer of $\text{Ba}_3\text{NaLa}(\text{PO}_4)_3\text{F}:\text{Tb}^{3+}, \text{Sm}^{3+}$ phosphors with apatite structure, *J. Lumin.* **169**, 739–743 (2016).
- [2] S. Slimi, P. Loiko, A. Volokitina et al., Structure, optical properties and preferential site substitution of Eu^{3+} activated $\text{Ca}_8\text{NaBi}(\text{PO}_4)_6\text{F}_2$ red emitting phosphors prepared by modified Pechini process, *J. Lumin.* **241**, 118523 (2022).
- [3] K. Szyszka, N. Nowak, R.M. Kowalski et al., Anomalous luminescence properties and cytotoxicity assessment of $\text{Sr}_3(\text{PO}_4)_2$ co-doped with $\text{Eu}^{2+/3+}$ ions for luminescence temperature sensing, *J. Mater. Chem. C* **10**, 9092–9105 (2022).

POLARIZATION-BASED IDLER ELIMINATION: ENHANCING THE EFFICIENCY OF OPTICAL PARAMETRIC AMPLIFICATION

Gaudenis Jansonas^{1,2}, Rimantas Budriūnas^{1,2}, Gintaras Valiulis¹, Arūnas Varanavičius¹

¹Laser Research Center, Vilnius University, Lithuania

²Light Conversion Ltd., Lithuania
gaudenisjansonas@yahoo.com

The pump-to-signal conversion efficiency of the optical parametric amplifiers (OPA) is usually limited to about 20% and further amplification is accompanied by the degrading pulse and beam quality. Typically, the limiting factor here is the back-conversion process that (for Gaussian pulsed-beams) commonly starts at the full on-axis pump depletion. Back-conversion can be suppressed by eliminating the idler wave from the interaction before the pump wave is depleted. This was previously achieved by employing non-collinear pump recycling schemes [1] and idler absorption [2]. Nevertheless, when compared to the currently exploited standard solutions, these approaches tend to either consume a lot of space, demand exotic materials or lack tunability. In this work we propose and experimentally test a polarization-based idler elimination scheme for the suppression of the back-conversion in femtosecond OPA that is simple, compact, requires relatively inexpensive tools and preserves the wavelength tunability of the light source. This is achieved by using two consecutive crystals (see Fig. 1a.) cut for different nonlinear interaction types (type-I and type-II) in the same amplification stage. Idler wave, generated in the first crystal, cannot participate in the second interaction, because its polarization state is not supported by the nonlinear process. The enhanced idler amplification can also be achieved by rotating the type-II crystal for an interaction that satisfies the phase-matching conditions for o-polarized idler wave (see Fig. 1a.). We used a delay crystal in between the amplification crystals that compensates the temporal walk-off between pump and signal. This approach was tested by boosting the energy of the pre-amplified and temporally stretched white-light continuum.

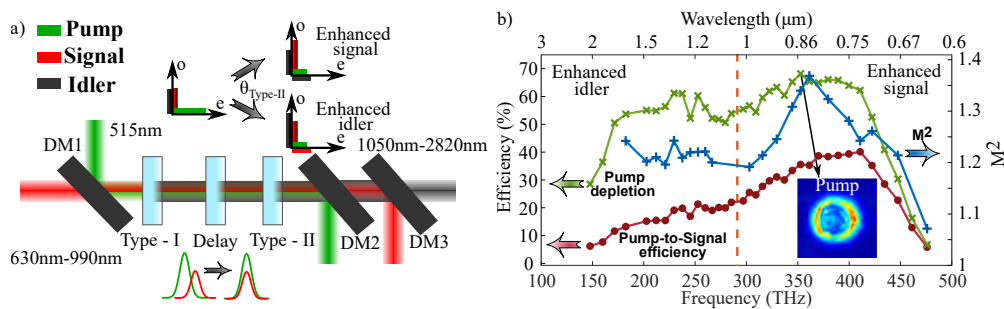


Fig. 1. a) - Booster amplification stage of the experiment. DM - dichroic mirror, θ - crystal polar angle. Electric field projections to ordinary o and extraordinary e polarization axes are also illustrated after type-I and type-II nonlinear interactions. b) - Pump-to-signal conversion efficiency, pump depletion and M^2 as a function of wavelength and frequency. The most depleted pump beam is illustrated in the inset.

In our experiments beta barium borate (β - $\text{Ba}(\text{BO}_2)_2$ - BBO) nonlinear crystals were employed. The main energy and output beam quality characteristics of the proposed booster amplifier are presented in Fig. 1b. Here pump-to-signal conversion efficiency, measured pump depletion after the DM2 and beam quality factor M^2 are plotted on the same frequency (wavelength) axis throughout the whole tuning range. The highest pump-to-signal energy conversion of 40% was obtained at 730 nm that corresponds to $M^2 = 1.25$. The maximal pump depletion value of 68% with corresponding $M^2 = 1.37$ was achieved at 850 nm. The rest of the M^2 curve qualitatively follows the pump depletion. The degree of the 68% pump depletion can be observed by looking at the output pump beam image after the last amplification crystal (inset of Fig. 1b.). Overall, Fig. 1b. favorably illustrates the capability to achieve pump-to-signal conversion efficiency of $\geq 30\%$ in the spectral range between 700 nm and 920 nm.

In conclusion, we have shown that the combination of type-I and type-II crystals enables one to achieve polarization-based idler elimination, which may greatly increase the conversion efficiency of short-pulse optical parametric amplification by suppressing the back-conversion process, and thus preserving the signal beam quality. In general, such two-crystal booster amplifier is cost-effective, has a broad tunability range and may serve as a convenient tool in many future nonlinear applications.

[1] M. Schultze et al., Multi- μJ , CEP-stabilized, two-cycle pulses from an OPCPA system with up to 500 KHz repetition rate, *Opt. Express* **18**, 27291 (2010).

[2] J. Ma, et al., Quasi-parametric amplification of chirped pulses based on a sm^{3+} -doped yttrium calcium oxyborate crystal, *Optica* **2**, 1006 (2015).

STUDY OF THE CALIBRATION OF CROC PIXEL DETECTORS WITH SENSORS

Kristijonas Mikas Silius¹, Marijus Ambrozus¹

¹ Faculty of Physics, Vilnius university, Lithuania
kristijonas.silius@ff.stud.vu.lt

The CMS or Compact Muon Solenoid experiment at CERN Large hadron collider (LHC) is a detector, designed to study various physical phenomena of colliding particles. One important part of the CMS detector is its Inner Tracker, which is responsible for measuring LHC produced particle trajectories. The Inner Tracker is made up of several layers of silicon pixels detectors to achieve high accuracy measurements.

To achieve better and more precise results, a new High Luminosity LHC (HL-LHC for short) upgrades are to be implemented by 2029 [1]. As a result, the CMS detector is also undergoing so called Phase-2 upgrade, to prepare it for the new collider.

HL-LHC will greatly increase its luminosity, meaning the currently achievable one billion collisions per second will increase to ten billion collisions [2]. So, the main goal of the upgrades is to increase the number of channels and improve the efficiency of the detectors. Therefore, the current detectors need to be replaced by ones with smaller pixels and higher granularity. Another essential factor is to make the parts much more resistant to radiation since the increased luminosity will do 10 times more radiational damage to the detectors than currently. The last important detail is to improve the read-out electronics, for the vastly increased rate of information.

The mentioned upgrades will provide several key benefits. Firstly, the higher number of channels will increase the effectiveness of the tracker, it will allow reconstruction and analysis of more particles. Furthermore, the improved pixel detector granularity is essential to measure and understand the properties of particles produced in LHC collisions more precisely.

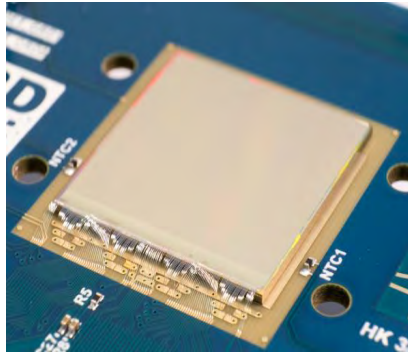


Fig. 1. RD53B chip on single chip test card [3].

Lithuanian scientists are working with the CMS Inner Tracker upgrade group to perform pixel detector prototype testing. The study to be presented focuses on calibration and system tests on RD53B CMS (also called CROC) pixel chip prototypes, which are developed for the Phase-2 CMS upgrade. We further explore and, in more detail, explain and present the work being completed in CERN.

This presentation will go more in-depth about the tests performed at CERN, using a radioactive source on a CROC chip with a sensor to study its trigger latency characteristics.

[1] CERN High Luminosity LHC Project. LS3 schedule change, <https://hilumilhc.web.cern.ch/article/ls3-schedule-change> (2022).

[2] I. Béjar Alonso et al. CERN. High-Luminosity Large Hadron Collider. Technical design report, <https://cds.cern.ch/record/2749422/files/127-117-PB.pdf> (2020).

[3] J. Christiansen, RD53 Collaboration. RD53B users guide: Introduction to RD53B pixel chip architecture, features and recommendations for use in pixel detector systems, https://cds.cern.ch/record/2754251/files/users_guide_v11.pdf (2021).

APPLICATION OF 3D VECTOR BUILDING DATA FOR DIFFRACTION MODELING IN WIRELESS NETWORKS

Karolis Stankevičius, Steponas Pilkauskas, Rimvydas Aleksiejūnas

Institute of Applied Electrodynamics and Telecommunications, Vilnius University, Lithuania
karolis.stankevicius@ff.vu.lt

New generations of wireless mobile networks are deployed in higher gigahertz frequencies close to sub-millimeter waves. Most popular frequency band for 5G networks is 3.5 GHz, but there are plans for 26 or 28 GHz bands and upper. Higher radio frequencies impose propagation problems especially in dense urban areas due to diffraction. Estimation of diffraction loss is essential in wireless network planning and optimization, where detailed building data is available. In the past, a raster-based building rooftop height data extracted from building footprints has been used down to 1 meter resolution [1]. For numerical evaluation of diffraction loss in case of raster-based input data, fast approximate algorithms are used such as XDraw and its various implementations [2]. Currently vector-based 3D city models with high level of detail attract a lot of interest. However, the analysis algorithms with vector data are slow and there are no efficient fast methods.

The aim of this work is to create fast numerical diffraction algorithm working with high accuracy vectorial 3D building data. This should allow to achieve higher precision of path loss predictions compared to raster-based calculations. In the proposed model, diffraction loss is estimated according to ITU-R P.526-15 recommendation model [3]. The method is based on finding clearance distance between the highest obstacle along the radio wave path and radio beam centerline. The clearance is used for estimating Fresnel diffraction integral giving diffraction loss due to obstructed path. This diffraction loss can be further combined with empirical drive-test calibrated propagation models such as Hata-type models.

The proposed algorithm is built on the principles of XDraw approach, but takes as input vector building data. It behaves as $\mathcal{O}(N^2)$ over time by analyzing propagation in rings starting at antenna location and progressing towards the edges of analysis area. The analysis area is divided into square matrix of points and each point is visited only once. For each point detailed geometric analysis is performed to find radio ray intersection with existing buildings and in addition reusing the diffraction results from previously visited points closer to antenna. Two approaches are proposed for approximations of previously calculated points: maximum obstacle and maximum roof diffraction loss. The maximum obstacle method retracts the spatial grid location with maximum diffraction loss from the previously visited points and recalculates diffraction. The maximum roof diffraction method takes into account limited number of first dominant roof plane diffraction calculations. The first method is more accurate, but the second method is faster.

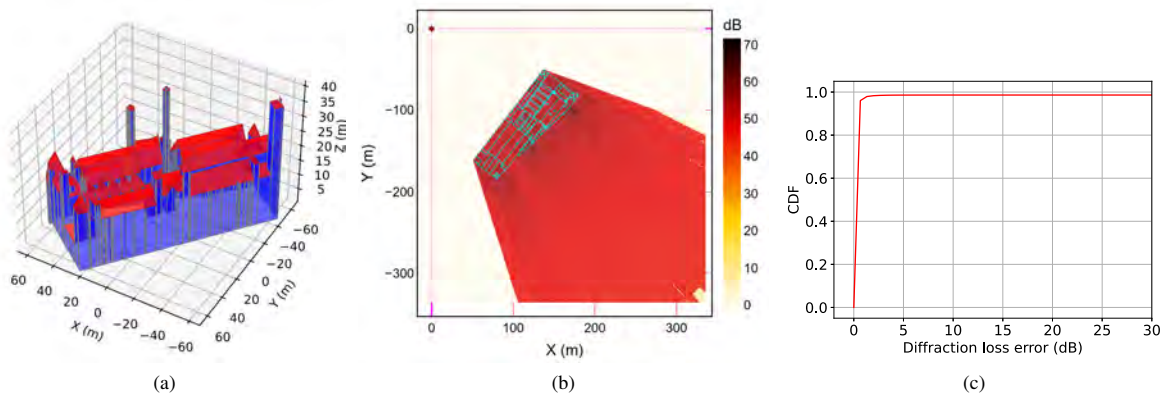


Fig. 1. Level of detail of vector building data (a), diffraction loss raster of the building (b) and cumulative distribution function (CDF) of error between exact and XDraw diffraction algorithms (c).

In this work, Amsterdam city 3D building data reconstructed from two-dimensional building footprints and LIDAR data is used [4]. Example of 3D building data is shown by polygons representing walls and roofs in Fig. 1a. The diffraction loss raster calculated from antenna located at zero coordinates is given in Fig. 1b and the difference between exact diffraction algorithms and XDraw implementation is illustrated in Fig. 1c. There are only few percents of coverage points with diffraction error extending above 5 dB.

- [1] A. Colpaert, E. Vinogradov, and S. Pollin, Aerial coverage analysis of cellular systems at LTE and mmWave frequencies using 3D city models, *Sensors*, **18**, no. 12, 4311 (2018).
- [2] J. Zhang, S. Zhao, and Z. Ye, Spark-enabled XDraw viewshed analysis, *IEEE J. Sel. Top. Appl. Earth Obs. Remote Sensing*, **14**, 2017-2029 (2021).
- [3] ITU-R, Propagation by diffraction, Recommendation ITU-R P.526-15 (2019).
- [4] R. Peters, B. Dukai, S. Vitalis, J. van Liempt, and J. Stoter, Automated 3D reconstruction of LoD2 and LoD1 models for all 10 million buildings of the Netherlands, *Photogrammetric Engineering & Remote Sensing*, **88**, no. 3, 165-170, (2022).

DIGITAL SIMULATION OF AGGLOMERATION OF SOLID PARTICLES FORMED DURING BIODIESEL COMBUSTION USING DEM

Darius Vainorius¹, Artūras Kilikevičius², Algis Džiugys¹

¹Laboratory of Heat Equipment Research and Testing, Lithuanian Energy Institute

²Institute of Mechanical Science, Faculty of Mechanical Engineering, Vilnius Gediminas Technical University
darius.vainorius@gmail.com

Keywords: Acoustic agglomeration, particularly, DEM

1. Introduction

The removal of harmful particulate matter (PM) is one of the most important tasks of environmental protection, as PM environmental pollution has a direct impact on human health. The greatest danger is caused by particles of type PM_{2.5}, which, due to their small size, do not remain in the upper respiratory tract of a person; they can penetrate the deeper respiratory tract or lungs and settle there. [1]. Emissions from various vehicles have recently become one of the main pollutants of the atmosphere. When comparing gasoline and diesel engines, the latter have higher PM emissions. [2]. Therefore, ways to reduce the release of PM into the environment are constantly being sought. One such method would be acoustic agglomeration [3]. The aim of this work is to better understand the influence of particle concentration and frequency on the acoustic agglomeration time of biodiesel particles.

2. Problem formulation, materials and methods

Vehicle emissions are an important source of PM with diameters $D_p \leq 2.5 \mu\text{m}$. To properly design acoustic equipment for PM removal, it is necessary to understand its behaviour. To solve this problem, we modified the conventional DEM method, where each particle is treated as an independent body moving in an incompressible viscous fluid. Particles moving in a fluid are characterised by a time t described by a changing displacement vector $x_p(t)$, and the equation of motion is:

$$m_p \ddot{x}_p(t) = F_{p,fl}(t) + F_{p,g}(t) \quad (1)$$

where $F_{p,fl}(t)$ – the total interaction force between the particles and the fluid acting in the direction of sound, $F_{p,g}(t)$ – gravity (including buoyancy) force [4]. The environment is a non-pressurised medium characterized by density $\rho_m = 1.293 \text{ kg/m}^3$ and dynamic viscosity $\mu_m = 0.0000183 \text{ Pa}\cdot\text{s}$. The properties of PM are chosen to match the properties and soot density produced during biodiesel $\rho_p = 1800 \text{ kg/m}^3$, and the diameter $D_p = \{0.5, 1, 2, 2.5\} \mu\text{m}$, distance between particles $5D_p$, frequency $f = \{500, 1000, 2000, 3000\} \text{ kHz}$.

3. Numerical results

The results show that the frequency change for smaller particles has a smaller influence on the acoustic agglomeration time than for larger particles (Figure 1).

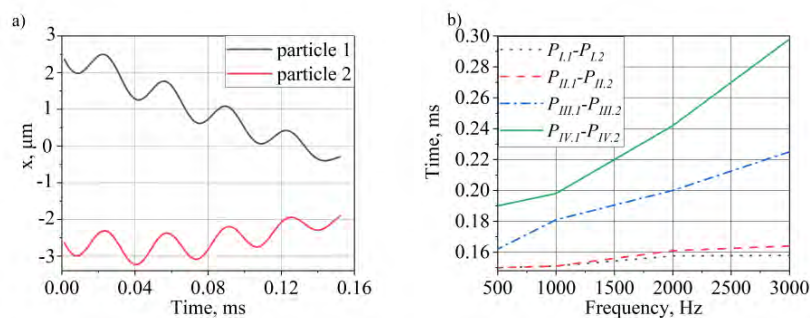


Figure 1. Time histories of two identical isolated particles a) diameter of the particle $D_p = 1 \mu\text{m}$ and frequency 3000 Hz b) dependence of the agglomeration time on the particle diameter when $P_{I,1} = P_{I,2} = 0.5 \mu\text{m}$, $P_{II,1} = P_{II,2} = 1 \mu\text{m}$, $P_{III,1} = P_{III,2} = 2 \mu\text{m}$ and $P_{IV,1} = P_{IV,2} = 2.5 \mu\text{m}$ and frequency.

The increase in frequency has a small effect on the agglomeration time of the smallest diameter particles in KD, the agglomeration time of $0.5 \mu\text{m}$ diameter increases by 3 percent and $1 \mu\text{m}$ by 8 percent, while the agglomeration time of particles with diameters of $2 \mu\text{m}$ and $2.5 \mu\text{m}$ increases by 41 and 57 %.

Acknowledgments

This project has received funding from the Research Council of Lithuania (LMTLT), agreement No [S-PD-22-69].

- [1] H. Omidvarborna, et. al., Recent studies on soot modelling for diesel combustion. *Renewable and Sustainable Energy Reviews*, 48, 635–647 (2015).
 [2] P. Trechera, et. al., Phenomenology of ultrafine particle concentrations and size distribution across urban Europe. *Environment International*, 172, 107744 (2023).
 [3] D. Zhou, Z. Luo, J. Jiang, H. Chen, M. Lu, M. Fang. Experimental study on improving the efficiency of dust removers by using acoustic agglomeration as pretreatment, *Powder Technology* 289, 52-59 (2016).
 [4] R. Kačianauskas, A. Maknickas, D. Vainorius. DEM analysis of acoustic wake agglomeration for mono-sized microparticles in the presence of gravitational effects. *Granular matter*. 19, 1-12 (2017).

RELATIVE OSCILLATOR STRENGTHS FOR LOW-LYING LEVELS OF Tm: EXPERIMENT AND THEORY

Adams Lapins¹, Maris Tamanis¹, Ilze Klincare¹, Ruvin Ferber¹, Gönül Başar², Sophie Kröger³, Andrey I. Bondarev⁴, Mikhail G. Kozlov⁵

¹Laser Centre, Faculty of Physics, Mathematics and Optometry, University of Latvia, 19 Rainis Blvd, LV-1586, Riga, Latvia

²Istanbul University, Faculty of Science, Physics Department, TR-34134 Vezneciler, Istanbul, Türkiye

³Hochschule für Technik und Wirtschaft Berlin, Wilhelminenhofstr. 75A, Berlin D-12459, Germany

⁴Helmholtz Institute Jena, Fröbelstieg 3, 07743 Jena, Germany

⁵St Petersburg Electrotechnical University LETI, Prof Popov Str 5, St Petersburg 197376, Russia

adams.lapins@lu.lv

We report on experimental data and ab initio calculations on transition strengths of atomic thulium (Tm). Transition probabilities of lanthanide atoms, e.g., Tm, along with other spectroscopic data, such as identified transitions and fine structure energy levels, determined hyperfine structure (hfs) constants, etc. are important both from point of view of fundamental physics, as well as for astrophysical purposes. Relative line intensity distributions were obtained in Tm emission spectra ranged from 400 nm to 700 nm [1] applying high-resolution Bruker IFS 125 HR Fourier-transform spectrometer at the Laser Centre of the University of Latvia. The ¹⁶⁹Tm emission spectra were produced in a hollow cathode discharge lamp in presence of either Ar or Ne buffer gases at different discharge current values. The nuclear spin of ¹⁶⁹Tm isotope is $I = \frac{1}{2}$ yielding a rather simple hfs, which has been studied experimentally by several authors (see [1] and references therein). Exploiting two different gases facilitated identification of those Tm lines, which exhibit completely overlapping hfs transitions. In present work we have determined relative intensity distributions in selected branches of Tm emission lines, which originate from a common upper level. We examined 3 branches from upper state levels with energies 32217.195 cm⁻¹, 33943.282 cm⁻¹, and 35682.251 cm⁻¹. An example of experimental relative intensity distribution from the level 35682.251 cm⁻¹ is presented in Fig. 1 (black crosses), along with ab initio calculations (red points). Calculations were done using a recently proposed modification of an approach that combines configuration interaction (CI) and many-body perturbation theory (MBPT) [2]. The ground state configuration of thulium is [Xe]4f¹³6s², so it was considered as a 15 active-electron system with a frozen Xe-like core. Due to a large number of the active electrons and opened f-shell the conventional CI approach can tackle only a relatively small configuration space (CS). In our approach, the active orbitals are divided into valence and virtual. The CS is constructed by making single and double excitations from few reference configurations to the valence orbitals and only single excitations to the virtual ones. Double excitations to the virtual orbitals are taken into account by means of MBPT. Once the many-electron wave functions of individual states are found, the transition amplitudes of the electric dipole lines are calculated using the formalism of transition matrix.

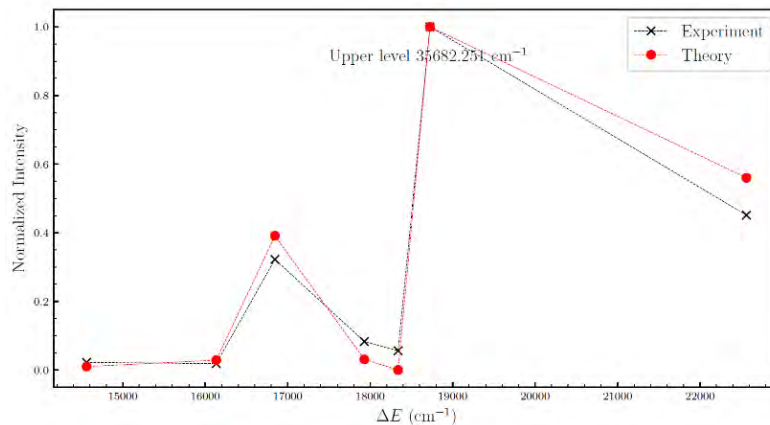


Fig. 1. Experimental and theoretical intensity distributions of emission lines from a common upper state level.

This study has been funded by Latvian Council of Science, project No. lzp-2020/1-0088 “Advanced spectroscopic methods and tools for the study of evolved stars” and by Scientific Research Projects Coordination Unit of Istanbul University, Project No.30048.

[1] Ş. Parlatan, İ. K. Öztürk, G. Başar, G. Başar, R. Ferber, S. Kröger, *Journal of Quantitative Spectroscopy & Radiative Transfer*, **287** 108195 (2022).

[2] M. G. Kozlov, I. I. Tupitsyn, A. I. Bondarev, and D. V. Mironova, *Phys. Rev. A* **105**, 052805 (2022).

CREATING FLUORESCENCE SPECTRA BASED ON THE FRANCK-CONDON FACTOR

Jaba Shainidze¹, Nugzar Gomidze¹

¹ Department of Physics, Batumi Shota Rustaveli State University, Batumi, Georgia
jabashainidze@gmail.com

The quantum theory of radiation pictures atoms with quantized energy levels interacting with an assembly of photons of varying frequencies ω . When the energy difference between two atomic states fulfills a resonance condition $\hbar\omega = E_1 - E_0$, three possible transition processes can occur: absorption, stimulated emission, and spontaneous emission. In the electric-dipole approximation, the transition rates for absorption and stimulated emission are given by [1]:

$$W_{abs} = W_{stim\ em} = \frac{4\pi^2}{3\hbar^2} \rho(\omega) |\langle 0|\mu|1\rangle|^2,$$

where μ is the electric dipole operator and $\rho(\omega)$ is the spectral density of the radiation field at frequency ω . The corresponding rate of spontaneous emission is:

$$W_{spont\ em} = \frac{4\omega^2}{3\hbar c^3} |\langle 0|\mu|1\rangle|^2.$$

All three radiative processes depend on the matrix element $\langle 0|\mu|1\rangle$ and therefore obey the same selection rules. A convenient measure of the intensity of a transition is the oscillator strength:

$$f_{0,1} = \frac{2m_e\omega}{3\hbar e} |\langle 0|\mu|1\rangle|^2,$$

makes spontaneous emission significant only for higher-energy transitions—in practice, only for optical frequencies and higher. The Figure 1 shows the transition-energy range of 0.1 to 10 eV, corresponding to radiation wavelengths of 12000 to 120 nm, which includes the visible region 380–750 nm, as well as parts of the infrared and ultraviolet (fig.1).

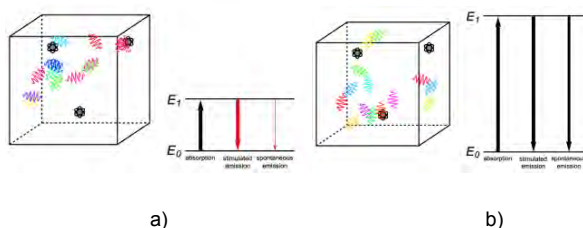


Fig.1. Demonstration of transition processes: a) transition in the infrared region $E_1 - E_0 = 0,2$ eV, $\lambda = 6200$ nm, $f_{0,1} = 0,5$; b) transition in the ultraviolet region $E_1 - E_0 = 10$ eV, $\lambda = 120$ nm, $f_{0,1} = 0,5$

At normal temperatures, only the $\nu = 0$ vibrational level of the ground state is occupied. When a molecule absorbs a photon in an electronic transition, the electrons can rearrange themselves much more rapidly than the much heavier nuclei (consistent with the Born–Oppenheimer approximation). Thus, electronic transition can be approximated by the vertical blue arrow to internuclear distances R in the excited state very close to its maximum value in the ground state. This leads to a mixture of several excited-state vibrational levels, predominated by the level that completely overlaps with the $U_0^{(0)}$ wavefunction. According to the Franck–Condon principle, the relative intensities of the individual vibrational peaks are proportional to the factors $|\langle U_{\nu_2}^{(1)} U_0^{(0)} \rangle|^2$. This gives rise to an absorption spectrum shown in blue. The relative intensity of the vibrational components depends on the molecular parameters of the two electronic states, but most sensitively on the difference between equilibrium internuclear distances, R_0 and R_1 .

A molecule excited in an electronically allowed transition will generally return to its ground electronic state, a process called *fluorescence*, within the order of a few nanoseconds. Before it does so, most of the excited molecules will decay to the lowest vibrational state $U_0^{(1)}$ by radiationless transition processes, such as internal collisional processes between molecules. These are represented in the upper curve by a series of black arrows. Fluorescence will then produce a series of peaks corresponding to different vibrational levels of the ground state, with intensities proportional to the Franck–Condon factors $|\langle U_{\nu_1}^{(0)} U_0^{(1)} \rangle|^2$. Because of the geometry of the energy curves, the fluorescent spectrum is very nearly a mirror image of the absorption spectrum, with the transitions $\nu_1 = 0 \leftrightarrow \nu_2 = 0$, meaning that this same transition occurs in both the absorption and fluorescence spectra [2].

[1] G. Videen, D. Ngo. Light Scattering from a Cell in Optics of Biological Particles. NATO Science Series, Series II: Mathematics, Physics and Chemistry, Vol. 238, (A. Hoekstra, V. Maltsev, and G. Videen, eds.), New York: Springer (2007).

[2] M. Khajishvili, N. Gomidze, J. Shainidze. Estimation SNR of CCD camera for OD medium. The Eurasia Proceedings of Science, Technology, Engineering & Mathematics (EPSTEM). ISBN:978-605-73797-9-5 ISSN: 2602-3199, 130-138 (2022).

ANALYSIS OF SPECTRAL LINES FOR STARS VIA SYNTHETIC SPECTRA

Dzmitry Viarbitski

Institute of Theoretical Physics and Astronomy, Physics Faculty, Vilnius University, Lithuania
dzmitry.viarbitski@ff.stud.vu.lt

Atmospheric parameters of stars are among the most important data received from a star. Processing the spectrum and knowing the class of the star allows you to find out such information as the temperature of the photosphere (T_{eff}), the acceleration of free fall on the surface ($\log(g)$), the metallicity ($[\text{Fe}/\text{H}]$) and the turbulent velocity (V_t). Thus, it becomes possible to obtain basic information about the state of the star and assume its further evolution [1- 4].

After the spectrum is obtained it is possible to process regions of the spectrum of a star at specific wavelengths that correspond to the lengths of the absorption bands of any element, it can be oxygen, nitrogen, or the most important element for studying, iron. To do this, the Python programming language software, as well as the Splat-VO program, were used.

By means of data selection, it is also possible to generate a synthetic spectrum using Moog and/or Turbospectrum softwares, if the entered data is correct, the resulting spectrum will coincide with the spectrum from the stars obtained by the observations and by using fitting algorithm. After the processing of the required number of wavelengths and the graph of the growth curve is satisfactory, the work is completed by overlaying the data in a spectrum and comparing it with the original one.

Using synthetic spectra is one way to analyze stellar spectra. Generating the spectra is slow, so trying out all possible combinations of the input parameters can take a very long time. The main advantage of this method is that it can also measure the abundances of molecules in stellar atmospheres, for example, CN and TiO. This is not possible with other methods and is why we use synthetic spectra.

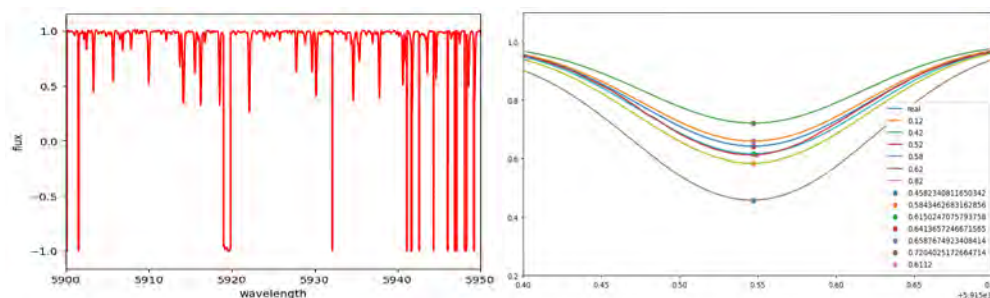


Fig. 1. Fragment of obtained spectrum in 5900-5950 Å wavelength diapason (graph from the left), process of comparing synthetic spectra with the real one (graph from the right)

[1] R. Brahm, A. Jordán, J. Hartman, G. Bakos, Monthly Notices of the Royal Astronomical Society, 467 (1), 971–984 (2017),
[2] P. de Laverny, A. Recio-Blanco, C. C. Worley, B. Plez, A&A, 544 A126 (2012).
[3] R. T. Coelho, Monthly Notices of the Royal Astronomical Society, 440 (2) 1027 (2014).
[4] M. Bergemann, R.-P. Kudritzki, B. Davies, GeoPlanet: Earth and Planetary Sciences, Determination of Atmospheric Parameters of B-, A-, F- and G-Type Stars, 217 (2014)

MULTITARGET REACTIVE MAGNETRON SPUTTERING TOWARDS THE PRODUCTION OF STRONTIUM MOLYBDATE THIN FILMS

Mindaugas Andrulevičius¹, Evgenii Artiukh², Gunnar Suchaneck², Sitao Wang², Nikolai A. Sobolev^{3,*}, Gerald Gerlach², Asta Tamulevičienė¹, Brigita Abakevičienė¹, and Sigita Tamulevičius¹

1 Institute of Materials Science, Kaunas University of Technology, 51423 Kaunas, Lithuania;

2 Solid State Electronics Laboratory, TU Dresden, 01062 Dresden, Germany;

3 Departamento de Física and i3N, Universidade de Aveiro, 3810-193 Aveiro, Portugal

* Correspondence: sobolev@ua.pt

X-ray photoelectron spectroscopy was used to study the direct synthesis of strontium and molybdenum oxide thin films deposited by multitarget reactive magnetron sputtering (MT-RMS). Sr and Mo targets with a purity of 99.9% and 99.5%, respectively, were cosputtered in an argon–oxygen gas mixture. The chamber was provided with an oxygen background flow plus an additional controlled oxygen supply to each of the targets. We demonstrate that variation in the power applied to the Mo target during MT-RMS enables the production of strontium and molybdenum oxide films with variable concentrations of Mo atoms. Both molybdenum and strontium were found in the oxidized state, and no metallic peaks were detected. The deconvoluted high-resolution XPS spectra of molybdenum revealed the presence of several Mo 3D peaks, which indicates molybdenum bonds in a lower valence state. Contrary to the Mo spectra, the high-resolution strontium Sr 3D spectra for the same samples were very similar, and no additional peaks were detected.

Conclusions:

(1) Survey XPS spectra showed all elements present in the deposited films and a small amount of atmospheric contaminants; in addition, the same elements were detected in EDX, Raman spectra, and XRD as well.

(2) Both Mo and Sr were found to be in the oxidized state, and no metallic peaks were detected. The deconvoluted high-resolution XPS spectra of molybdenum revealed the presence of several Mo 3D peaks, which indicated molybdenum bonds in a lower valence state. Contrary to the molybdenum spectra, the high-resolution strontium Sr 3D spectra for the same samples were very similar, and no additional peaks were detected.

(3) The oxygen spectra also showed a similar structure consisting mostly of a peak at approximately 530.5 eV, which represents oxygen bound to molybdenum (530.5 eV) or oxygen bound to strontium (530.4 eV). A small amount of typical atmospheric contaminants (C-O and H-O bonds) was also detected.

(4) Raman Scattering Spectroscopy revealed the presence of the MoO₃ phase in one of the deposited films.

(5) The XRD patterns showed the presence of a crystalline MoO₃ phase for the same sample, while the other samples were found in an amorphous state.

(6) The deposition of SrO-MoO₃ oxide films with variable concentrations of Mo atoms was achieved using a variation in power applied to the Mo target during MT-RMS. The obtained SrO-MoO₃ oxide films can be used as a starting material to produce SMO films via subsequent thermal treatment.

Funding: This research was funded by the European Union within the scope of the European project H2020-MSCA-RISE-2017-778308–SPINMULTIFILM. N.A.S. was supported also by project i3N, UIDB/50025/2020, and UIDP/50025/2020 and was financed by national funds through the Fundação para a Ciência e Tecnologia (FCT) and the Ministério da Educação e Ciência (MEC) of Portugal.



[1] Andrulevičius, M.; Artiukh, E.; Suchaneck, G.; Wang, S.; Sobolev, N.A.; Gerlach, G.; Tamulevičienė, A.; Abakevičienė, B.; Tamulevičius, S. Multitarget Reactive Magnetron Sputtering Towards the Production of Strontium Molybdate Thin Films. *Materials* 2023, 16, 2175. <https://doi.org/10.3390/ma16062175>

STUDY OF ELECTRICAL CHARACTERISTICS OF SILICON SENSORS FOR RADIOTHERAPY DOSE CONTROL

Augustas Baliukonis¹, Tomas Čeponis¹, Eugenijus Gaubas¹, Vytautas Rumbauskas¹, Marius Burkanas², Jonas Venius²

¹Institute of Photonics and Nanotechnology, Vilnius University, Saulėtekio av. 3, LT-10257, Vilnius, Lithuania

²National Cancer Institute, Santariškių 1, LT-08660, Vilnius, Lithuania

augustas.baliukonis@ff.stud.vu.lt

The *insitu* dose control during radiotherapy is important procedure in order to improve the treatment efficiency and avoid detrimental impact on healthy tissues, especially in high dose rate radiotherapy. Therefore, various dosimetry systems, dedicated for dose control during cancer specific treatment, are necessary. These systems require sensors for registering of ionizing radiation. The size of the sensors might also be critical to achieve sufficient spatial resolution. The most commonly used are pMOS (RADFET), direct ion storage (DIS), thermoluminescent (TL) and optically stimulated luminescent (OSL) sensors with specific advantages and drawbacks [1]. Silicon diodes have been used as radiotherapy beam dosimeters, mainly due to their good mechanical stability, high sensitivity per unit volume and high spatial resolution [2]. A new system for the *insitu* dose control during brachytherapy [3] is being developed at Vilnius University and National Cancer Institute. However, radiation tolerant sensors of rather small size, high speed and sensitivity are needed for this system.

In this work, the commercial Si sensors of *pin* structure and active area $S=0.35 \text{ mm}^2$ have been investigated in order to verify the suitability of the sensors for the brachytherapy system. Sensors were irradiated by 6 MeV electrons, 6 MeV X-rays in the dose range of 0.02 – 6 kGy at National Cancer Institute. Sensors response signals were measured under impact of electron radiation, X-rays and γ -rays by varying the irradiation flux. Irradiations by electrons and X-rays were performed by TrueBeam/Varian accelerator, while γ -rays were emitted from ^{192}Ir radionuclide. Current-voltage (I-V) and capacitance-voltage (C-V) characteristics were measured and analysed after irradiations.

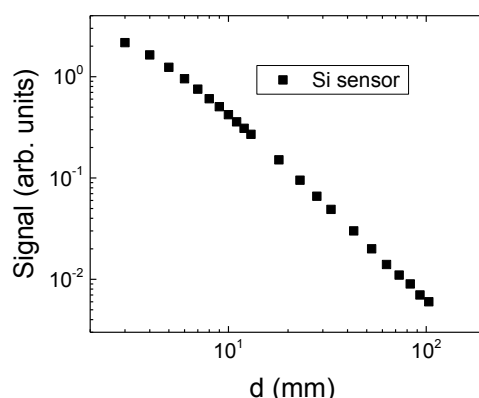


Fig. 1. Si sensor signal as a function of distance d from the ^{192}Ir radionuclide emitter.

Measurements of I-V characteristics showed that leakage current in sensors increases at highest irradiation doses. This phenomenon can be explained by increased density of radiation defects, which act as generation centres. Analysis of C-V characteristics showed slight variations of effective dopants density in irradiated samples. The sensitivity of sensors was sufficient for registering of signals at distances $d \geq 100 \text{ mm}$ between sensor and ^{192}Ir radionuclide emitter of activity $\approx 7.6 \text{ Ci}$ (Fig. 1). The largest radiation damage was observed after 6 MeV electrons irradiation.

[1] A. B. Rosenfeld, Semiconductor Detectors In Radiation Medicine: Radiotherapy And Related Applications. In S. Tavernier et al. (eds.), *Radiation Detectors for Medical Applications*, pp. 111-147 (Springer, Netherlands, 2006).

[2] T.C. dos Santos, W.F.P. Neves-Junior, J.A.C. Gonçalves, C.M.K. Haddad, C.C. Bueno, Evaluation of Rad-Hard Epitaxial Silicon Diode in Radiotherapy Electron Beam Dosimetry, *Radiat. Meas.* **46** (2011) 1662-1665.

[3] EPO application - APPARATUS AND METHOD FOR BRACHITHERAPY PLANNING, Authors: Eugenijus Gaubas, Tomas Čeponis, Kornelijus Pūkas, Vytautas Rumbauskas, Milta Užgirytė, Jonas Venius, Kęstutis Akelaitis, Aleksandras Cicinas. Application No. EP21210650.4, submission date: 2021 11 26.

ELECTROKINETIC PROPERTIES OF PLATINUM NANOPARTICLE MONOLAYERS DEPOSITED ON SOLID SURFACES

Kristina Sobol¹, Monika Wasilewska², Almira Ramanaviciene¹, Magdalena Ocwieja^{2*}

¹ NanoTechnas - Nanotechnology and Materials Science Center, Vilnius University, Lithuania

² Institute of Catalysis and Surface Chemistry Polish Academy of Science, Poland
kristina.sobol@chgf.stud.vu.lt

The primary objective of this study is to determine electrokinetic properties of platinum nanoparticle (PtNP) monolayers deposited on mica sheets under controlled conditions of pH, ionic strength and temperature using an electrokinetic cell applied in the streaming potential measurements. The platinum nanoparticles (PtNPs) used in the research were prepared by a chemical reduction method using sodium borohydride as a reducing agent of chloroplatinic acid and trisodium citrate as a stabilizing agent of formed nanoparticles. In the first stages of research, the PtNPs dispersed in the suspensions were characterized using dynamic light scattering and electrophoretic light scattering techniques. It was found that the PtNPs exhibit an average size equal to 22 ± 5 nm. The PtNPs were negatively charged, and their zeta potential was equal to -60 ± 3 mV and -48 ± 2 mV at ionic strength 10^{-4} and 10^{-2} M, respectively. The deposition process of PtNPs and formation of monolayers were conducted under controlled conditions of pH, ionic strength, and temperature. Because PtNPs as well as mica, used as a solid substrate, are negatively charged in a broad range of pH and ionic strength, an efficient formation of the monolayers was carried out after the modification of surface with cationic polyelectrolyte poly(allylamine hydrochloride) (PAH). The control of deposition time as well as ionic strength of PtNP suspension used in the experiments enable the formation of homogeneous monolayers. The structure and coverage of PtNP monolayers were determined based on the micrographs obtained from scanning electron microscopy (SEM).

In the next stage of studies, the electrokinetic properties of PtNP monolayers of given coverage were studied. Streaming potential E_s of mica sheets, bare and covered by platinum nanoparticle monolayers, was determined in the plane-parallel cell. E_s , occurring when an electrolyte solution of NaCl was flowing through the cell under regulated and constant hydrostatic pressure difference, was measured using the two Ag/AgCl electrodes connected to an electrometer [1]. The classical equations derived by Maryan Smoluchowski were used to convert streaming potential results into the surface zeta potential [2].

Different pH and ionic strength conditions were created to investigate the electrokinetic properties of PtNP monolayers and their stability over time. It was established that the electrokinetic properties of PtNP monolayers are dependent on the surface coverage. Dense PtNP monolayers of coverage equal to 25% were negatively charged in broad range of pH and ionic strength. Moreover, it was found that the desorption process of PtNPs from the monolayers was rather negligible. Thereby, with the use of streaming potential measurements the electrokinetic properties of monolayers were determined. The knowledge about these parameters should be useful for platinum-based catalysts and substrates used in modern spectroscopic techniques such as e.g., surface enhanced Raman spectroscopy (SERS) and tip enhanced Raman spectroscopy (TERS).

[1] M. Zembala, Z. Adamczyk, Measurements of streaming potential for mica covered by colloid particles, *Langmuir* 2000, 16, 1593-1602 (1999).
[2] T. Luxbacher, *The ZETA Guide: Principles of the streaming potential technique*. 27-30. (Anton Paar GmbH, 2014).

HIGH-SPEED DETECTION OF WATER CONTENT IN CRUDE OIL BY USING TERAHERTZ TIME-DOMAIN SPECTROSCOPY

Ihor Krapivin¹, Ramūnas Adomavičius¹

¹ Center for Physical Sciences and Technology, Savanorių Ave. 231, LT-02300, Vilnius, Lithuania
ihor.krapivin@ftmc.lt

The measurement of water content in crude oil is of great significance. The existence of water in crude oil can introduce serious problems in the petroleum refining process and transportation. Many measurement technologies have been developed for determining water content in crude oil. When it comes to different measurement technologies, the trade-off between measurement accuracy and speed is the first to be mentioned. For example, a water concentration measurement accuracy of about 0.05% can be achieved using a distillation method lasting several hours.

Recently, terahertz time-domain spectroscopy (THz TDS) has been successfully applied to measurements of water content in oil [1]. This methodology is comparable in accuracy to the distillation technique, but is characterized by a higher measurement speed. In our work, we further investigated the potential of the THz TDS methodology for measuring water content in oil. For greater certainty, absorption measurements were supplemented by refractive index studies (Fig. 1), as well as various types of oil were examined.

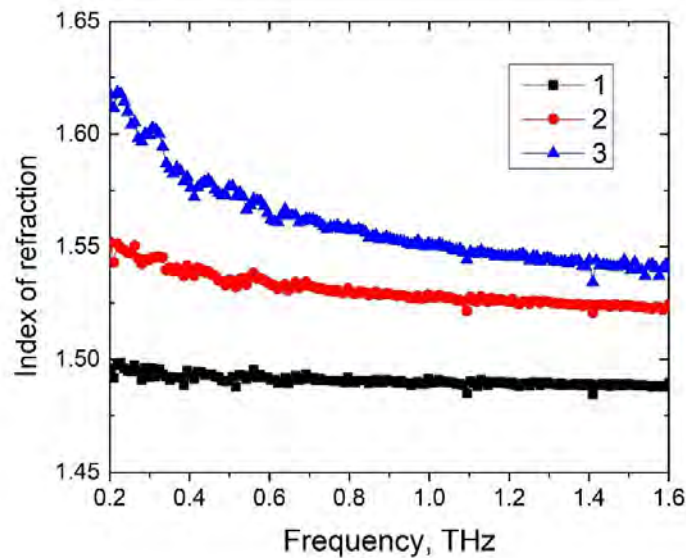


Fig. 1. Refraction index spectra of water-oil emulsion samples. A higher sample number corresponds to a higher water concentration.

In this work, it was shown that apart from the sample preparation time, the absorption and refractive index measurement of a single sample can be performed in 0.4 seconds without significantly compromising the measurement accuracy. This shows the perspective of the THz TDS methodology not only for laboratory measurements, but also for real-time oil monitoring in oil production and transportation facilities.

[1] J. Wu-Jun, Z. Kun et al., Experimental measurements of water content in crude oil emulsions by terahertz time-domain spectroscopy, *Applied Geophysics*, Vol. 10, 506-509 (2013).

AgAl mixed films for space applications

Ignas Bitinaitis¹, Alexandr Belosludtsev¹, Edvinas Petraitis¹, Anna Sytchkova²

¹ Center for Physical Sciences and Technology, Savanoriu ave. 231, Vilnius,

²Optical Coatings Group, ENEA Casaccia, via Anguillarese 301, Rome 00123, Italy

Ignas.Bitinaitis@ftmc.lt

We report a systematic investigation on the Silver-Aluminium (Ag-Al) mixed films properties and stability to radiation. Protected mixed metallic films were manufactured by magnetron sputtering. Deposited AgAl layer Al concentration was from 0 to 10 percent, maintaining constant layer thickness of 150 nm. Detailed investigation of proton radiation effect on silver-aluminum alloy films is conducted to understand how different aluminum concentrations affect film durability and performance in space applications.

Reflectance spectra were measured in 320 nm – 1300 nm wavelength range with the Photon RT spectrophotometer. Surface topography was measured using a Dimension Edge atomic force microscope (AFM) (Bruker) in tapping mode, over a 20 $\mu\text{m} \times 20 \mu\text{m}$ scan area. The AFM probe was an Al and diamond-like carbon (DLC) coated Si probe. Surface roughness evaluation was calculated using AFM measurement data.

Deposited samples reflectance spectra was measured at 8 degrees angle of reflectance. Decrease of reflectance is observed with increase of aluminum doping, likely due to influence of increased electron-to-atom ratio which red-shifts reflectance spectra due to interband transitions [1]. Generation of intermetallic phase of Ag₃Al at higher Al doping values is another likely reason for reflectance decrease [2]

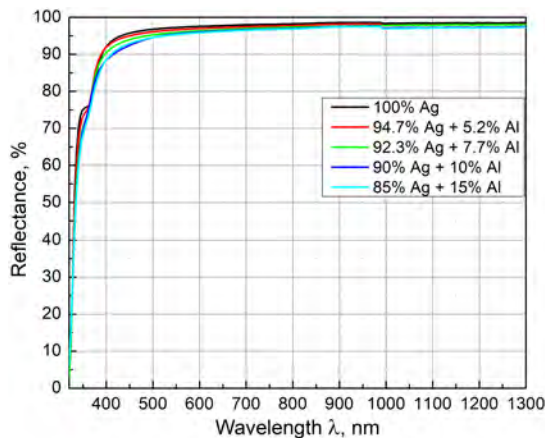


Fig. 1. Reflectance spectra of deposited Al-doped silver mirrors.

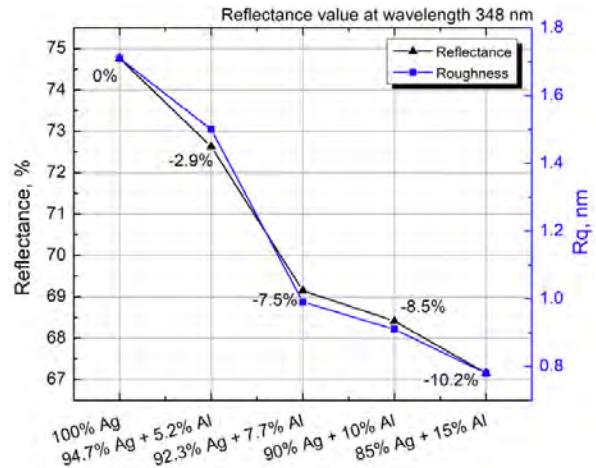


Fig. 2. Reflectance and roughness values dependence from Al doping. Reflectance value are for fixed wavelength at 348 nm.

Surface roughness decrease with the increasing Al doping is associated to property of aluminum grow which tends to be denser structure with smaller particles than Ag. This dense structure growth might be associated with lower Al diffusion rate, because metals with smaller diffusion rate exhibits higher nuclei density and smaller particle size [3]. Observed reflectance decrease in UV region is sharper compared to the VIS region (Fig. 1.)

From further radiation analysis it is observed AgAl films provide greater resistance to proton radiation, what makes such films favourable choice for space applications.

- [1] K.S.B. De Silva, V.J. Keast, A. Gentle, M.B. Cortie “Optical properties and oxidation of α -phase Ag–Al thin films” Australia. IOP Publishing, 2017;
- [2] R. E. Hummel “reflectivity of silver- and aluminium-based alloys for solar reflectors” USA.1981 Pergamon Press Ltd;
- [3] J D. Gu, C. Zhang, Y. Wu, L. J. Guo “Ultra-Smooth and Thermally-Stable Ag-Based Thin Films with Sub-Nanometer Roughness by Al Doping”. ACS Nano 2014.

PEROVSKITE SOLAR CELLS WITH MONOLAYER MODIFIED PTAA AND APPLICATION TO ALL-PEROVSKITE TANDEM SOLAR CELLS WITH EFFICIENCY OVER 25%

Daiva Tavgenienė^{1*}, Huan Bi², Yasuhiro Fujiwara², Chao Ding², Shahrir Razey Sahamir², Yoshitaka Sanehira², Ajay Kumar Baranwal², Kitamura Takeshi², Guozheng Shi², Gaurav Kapil², Zheng Zhang², Liang Wang², Takeru Bessho³, Hiroshi Segawa³, Saulius Grigalevicius¹, Qing Shen², Shuzi Hayase²

¹ Department of Polymer Chemistry and Technology, Kaunas University of Technology, Lithuania

² i-Powered Energy System Research Center (i-PERC), The University of Electro-Communications, Japan.

³ Research Center for Advanced Science and Technology, The University of Tokyo, Japan

daiva.tavgeniene@ktu.lt

Organic-inorganic perovskite solar cells (PSCs) have achieved a recorded power conversion efficiency (PCE) of 25.7%. [1] Thus, PSCs are considered to be the dominant player in the next-generation photovoltaic market. [2] So far, single-junction PSCs with narrow bandgap values have attracted attention. [3] As a member of perovskite materials, wide-bandgap perovskite (WBG-PVK) can't be ignored because it is important for tandem solar cells due to its matchable bandgap. [4] However, low PCE and the current of WBG-PSCs limited the efficiency of the tandem solar cell. So, it is necessary to further improve the PCE of wide bandgap PSCs.

Here, we demonstrate a series of SAMs with different alkyl chain lengths as interfacial modifiers to modify the PTAA and perovskite layer for improving the optoelectronic properties of PSCs by improving the quality of perovskite films and increasing the transport and extraction of interfacial carriers. The structures of the self-assembled monolayer materials (SAMs) is presented in Figure 1.

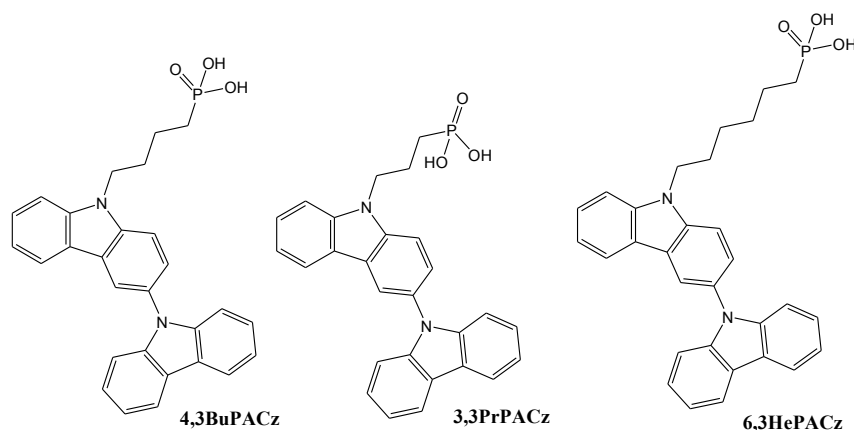


Fig. 1. New SAMs (named 3,3PrPACz, 4,3BuPACz, and 6,3HePACz)

In conclusion, several new SAMs (named 3,3PrPACz, 4,3BuPACz, and 6,3HePACz) have successfully been used to modify the interface between PTAA and WBG perovskite layer. The material with a linker group with four carbons gave the best results. The experimental results show that after the introduction of 4,3BuPACz, the quality of the perovskite thin film has significantly improved. Meanwhile, the grain size is increased, and the defects density of the films is also reduced. On the other hand, the introduction of the buffer layer can reduce the interfacial non-radiative recombination of the device and balance band offset between the perovskite and PTAA. Finally, 4,3BuPACz/PTAA-based PSCs achieved a high PCE of 16.57% with a bandgap of 1.77 eV. The target tandem solar cells gave a PCE of 25.24%, which is the highest PCE of tandem solar cells based on IZO. This work reveals a buried interface improvement mechanism with 4,3BuPACz/PTAA which can provide valuable guidance for developing effective SAMs buried layer materials.

Acknowledgements. The research was done under grant S-LJB-22-2 from Research Council of Lithuania.

[1] Access through internet: <https://www.nrel.gov/pv/cell-efficiency.html> (NREL, access)

[2] H. Bi, Y. Guo, M. Guo et al., Highly efficient and low hysteresis methylammonium-free perovskite solar cells based on multifunctional oteracil potassium interface modification, *Chemical Engineering Journal* **439**, 135671 (2022).

[3] S. Ma, G. Yuan, Y. Zhang et al., Development of encapsulation strategies towards the commercialization of perovskite solar cells, *Energy & Environmental Science* **15**, 13-55 (2022).

[4] K. Xiao, R. Lin, Q. Han et al., All-perovskite tandem solar cells with 24.2% certified efficiency and area over 1 cm² using surface-anchoring zwitterionic antioxidant, *Nature Energy* **5**, 870-880 (2020).

MATERNAL HIGH-FAT DIET: THE CHANGES OF OFFSPRING GUT MICROBIOTA AND BEHAVIOR

Adomas Smalskys¹, Gintarė Urbonaitė¹, Urtė Neniškytė^{1,2}

¹ Institute of Biosciences, Life Sciences Center, Vilnius University, Lithuania

² VU-EMBL Partnership Institute, Life Sciences Center, Vilnius University, Lithuania
adomas.smalskys@gmc.stud.vu.lt

Aims: A typical Western diet is excessively fatty, leading to a rapid increase in obesity in human population, including the women of reproductive age. There is growing evidence that maternal high-fat diet (mHFD) increases the risk of neurodevelopmental disorders in the offspring [1, 2, 3]. mHFD affects offspring neurodevelopment through various pathways, including changes in maternal metabolic status, increased chronic inflammation, or alterations in maternal and offspring gut microbiota [4, 5, 6]. Our aim was to evaluate whether mHFD increases maternal chronic inflammation and alters maternal metabolic status and gut microbiota, leading to the changes of offspring gut microbiota and abnormal offspring behavior.

Methods: Female C57Bl/6J mice were fed a control diet (CD, 10% fat) or high-fat diet (HFD, 60%) from weaning to lactation. Before mating, the metabolic status of the dams was evaluated by the body mass as well as glucose and insulin tolerance tests. The offspring were weaned to CD. After lactation, the concentration of maternal plasma insulin and proinflammatory cytokines were measured by ELISA tests. We investigated the behavioral phenotype of the offspring in three-chamber sociability, reciprocal social interaction, open field, marble burying, novel object recognition, and Barnes maze tests. To investigate gut microbiota, dam and offspring cecums were collected. Bacterial communities were determined by 16S rRNA amplicon sequencing.

Results: We determined that the consumption of HFD caused metabolic dysfunction but did not increase inflammation in the dams. mHFD changed the relative abundance of different gut bacteria genera in both dams and offspring. Decreased sociability was determined in both mHFD males and females although only males showed increased activity and only females showed decreased repetitive behavior.

Conclusions: Our findings demonstrated, that mHFD altered the composition of the offspring gut microbiota which may contribute to abnormal behavior in a sex-specific manner.

-
- [1] Li M, Fallin MD, Riley A, et al. The Association of Maternal Obesity and Diabetes With Autism and Other Developmental Disabilities. *Pediatrics*. 2016;137(2):e20152206. doi:10.1542/peds.2015-2206
- [2] Chen Q, Sjölander A, Långström N, et al. Maternal pre-pregnancy body mass index and offspring attention deficit hyperactivity disorder: a population-based cohort study using a sibling-comparison design. *Int J Epidemiol*. 2014;43(1):83-90. doi:10.1093/ije/dyt152
- [3] Rodriguez A. Maternal pre-pregnancy obesity and risk for inattention and negative emotionality in children. *J Child Psychol Psychiatry*. 2010;51(2):134-143. doi:10.1111/j.1469-7610.2009.02133.x
- [4] Buffington SA, Di Prisco GV, Auchtung TA, Ajami NJ, Petrosino JF, Costa-Mattioli M. Microbial Reconstitution Reverses Maternal Diet-Induced Social and Synaptic Deficits in Offspring. *Cell*. 2016;165(7):1762-1775. doi:10.1016/j.cell.2016.06.001
- [5] Sgritta M, Dooling SW, Buffington SA, et al. Mechanisms Underlying Microbial-Mediated Changes in Social Behavior in Mouse Models of Autism Spectrum Disorder. *Neuron*. 2019;101(2):246-259.e6. doi:10.1016/j.neuron.2018.11.018
- [6] Liu X, Li X, Xia B, et al. High-fiber diet mitigates maternal obesity-induced cognitive and social dysfunction in the offspring via gut-brain axis. *Cell Metab*. 2021;33(5):923-938.e6. doi:10.1016/j.cmet.2021.02.002

THE IMPACT OF STORAGE CONDITIONS AND EXTRAHENT CONCENTRATION ON THE CONTENT OF BIOACTIVE COMPOUNDS IN BEE BREAD AND POLLEN

Liveta Muliulytė, Vilma Kaškonienė, Audrius Maruška

Instrumental Analysis Open Access Centre, Faculty of Natural Sciences, Vytautas Magnus University, Vileikos 8, LT-44404 Kaunas, Lithuania
liveta.muliulyte@stud.vdu.lt

Natural foods are becoming more and more well-liked by the general population in today's globe as a result of the realization that they can help with disease prevention and treatment [1,2]. Polyphenols and flavonoids, which have the capacity to scavenge free radicals, are abundant in bee pollen and bee bread. Phenolic acids and flavonoids are probably the most studied classes of phenolic compounds. The ability of phenolic compounds, which are found naturally in plants, to successfully protect the body from free radicals is well established [3]. The beneficial properties of these substances include antioxidant, anticarcinogenic, antimicrobial, antiapoptotic, anti-atherosclerosis, anti-inflammation, cardiovascular protection, anti-aging, they also have an impact on the enhancement of endothelial function, inhibition of angiogenesis or even cell proliferation activity. The choice of solvent is one of the key factors leading to the selective extraction of secondary metabolites [4]. Solvents (extrahents) containing hydroxyl groups in their structure can form intramolecular hydrogen bonds with the hydroxyl groups of phenolic compounds, thereby increasing their solubility [5]. This research aims to compare the levels of bioactive compounds in samples of bee bread and bee pollen stored under different conditions, using different solvent concentrations for extraction.

Dried and frozen samples of bee bread and bee pollen were investigated in this study. The samples were collected in southern Lithuania, in the Lazdijai region, in July 2022. Extraction of bee bread and bee pollen was performed by the maceration method. Three different concentrations of extrahent were used: 70, 50, and 30% methanol. The total amount of phenolic compounds, flavonoids, and antiradical activity was evaluated using spectrophotometric methods [6]. The results were expressed in mg of rutin equivalents (RE) in 1 g of the sample.

The results showed that freezing had no significant effect on phenolic compounds, flavonoids, and antiradical activity in the bee bread. The content of tested parameters statistically ($p \leq 0.05$) increased by using a higher concentration of methanol. The total phenolic compounds varied from 42.11 mg RE/g to 93.62 mg RE/g, the flavonoids from 19.03 mg RE/g to 39.04 mg RE/g, and antiradical activity from 22.61 mg RE/g to 67.37 mg RE/g in the samples of bee bread. The highest levels of bioactive compounds were obtained at a methanol concentration of 70%. Nonetheless, both freezing and extrahent concentration had a significant impact on phenolic compounds content in bee pollen. In the extracts from dried material obtained using 70% methanol, the content of phenolic compounds was 99.95 mg RE/g, while in frozen – 83.85 mg RE/g. In 30% methanol extracts, phenolic compounds in dried material were 1.5 times higher than in the frozen bee pollen.

In conclusion, the highest amounts of the biologically active compounds were obtained using 70% methanol concentration. Freezing had no significant effect on the bioactive compounds in bee bread but had a compelling effect on bee pollen phenolic compounds. It is believable that different extrahents or even their mixtures may possess different both quantitative and qualitative extraction capabilities of biologically active compounds. The results also may be depended on the plant material, in our case on the botanical origin of bee bread or bee pollen. It would be recommended to optimize extraction solvent before the work with new plant material.

1. Gercek, Y. C., Celik, S., Bayram, A., Screening of plant pollen sources, polyphenolic compounds, fatty acids and antioxidant/antimicrobial activity from bee pollen, *Molecules* 27(1), 117 (2022).
2. Silla, E., Arnau, A., Tunon, I., Solvent effects on chemical systems. Handbook of solvents. Department of Physical Chemistry (2001).
3. Albuquerque, B. R., Heleno, S. A., Oliveira, M. B. P. P., Barros, L., Ferreira, I. C. F. R., Phenolic compounds: Current industrial applications, limitations and future challenges. *Food and Function* 12, 14–29 (2020).
4. Han, X., Shen, T., Lou, H., Dietary polyphenols and their biological significance. *International Journal of Molecular Sciences* 8, 950–988 (2007).
5. Abouda, Z., Zerdani, I. Kalalou, I., Faid, M., Ahami, M., The antibacterial activity of Moroccan bee bread and bee-pollen (fresh and dried) against pathogenic bacteria. *Research Journal of Microbiology* 6, 376–384 (2011).
6. Stankevičius, M., Akuneca, I., Jakobsonė, A., Maruška, A., Comparative analysis of radical scavenging and antioxidant activity of phenolic compounds present in everyday use spice plants by means of spectrophotometric and chromatographic methods, *Journal of Separation Science* 34 (11) 1261 – 12670 (2011).

ASSESSMENT OF THE INFLUENCE OF FERMENTATION WITH KOMBUCHA SCOBY ON THE BIOLOGICAL ACTIVITY OF PLANT MATERIAL

Greta Raškauskienė, Vilma Kaškonienė, Rūta Mickienė, Audrius Maruška

Instrumental Analysis Open Access Centre, Faculty of Natural Sciences, Vytautas Magnus University, Kaunas, Lithuania
greta.raskauskiene@stud.vdu.lt

Products of natural origins, such as medicinal and aromatic plants, are becoming more and more popular and are used in today's society, as an effective remedy due to their healing properties and lower risk of side effects [1]. The healing properties of plants depend not only on the quantity and quality of accumulated biologically active substances but also on the part of the plant. The plant part may be related to the limited release of biologically active compounds due to the different matrices, such as leaves, stems, or roots. Literature shows, that the biological activity of plant raw materials can be increased during fermentation. It is a low-cost system that ensures food safety and quality [2]. During fermentation, several biochemical changes occur that can affect the biological activity of the final product [3]. The impact of fermentation on the release of biologically active compounds depends on several factors, such as the specie and strain of microorganisms used for fermentation, conditions of fermentation (pH, temperature, duration), and fermenting matrix. To our knowledge, there are no literature data about the impact of kombucha SCOBY (*Symbiotic Culture of Bacteria and Yeast*) fermentation on the roots and bark of several plants grown in Lithuania.

The impact of fermentation with kombucha tea fungus (*Medusomyces gisevii*) beverage on roots of elecampane (*Inula helenium*), common dandelion (*Taraxacum officinale*), and valerian (*Valeriana officinalis*), as well as on the bark and acorns of the common oak (*Quercus robur*) and the acorns of the red oak (*Q. rubra*) was evaluated in this study. The plant material was fermented with kombucha beverage. After 48 h the liquid part was collected and is called "kombucha fraction", while the residues were extracted with 75% methanol, and the obtained extract is called "methanol extract". The total amounts of phenolic compounds, flavonoids, and antiradical activity were evaluated in kombucha fractions and methanol extracts by spectrophotometric methods [4]. Control samples were prepared in a similar way, just distilled water was used instead of kombucha. Results were expressed as rutin equivalents (mg RE/g).

Fermentation with kombucha beverage increased the content of biologically active compounds in the tested plants. The highest amount of phenolic compounds was determined in a fermented sample of common oak acorns (Fig. 1). The highest amount of flavonoids was detected in the fermented sample of common oak bark (2.22 and 3.54 mg RE/g before and after fermentation, respectively). An increase in anti-radical activity was found in all kombucha fractions after fermentation. However, the antiradical activity slightly decreased from 19.5 to 22.02 mg RE/g in the methanolic extract of common oak bark after fermentation.

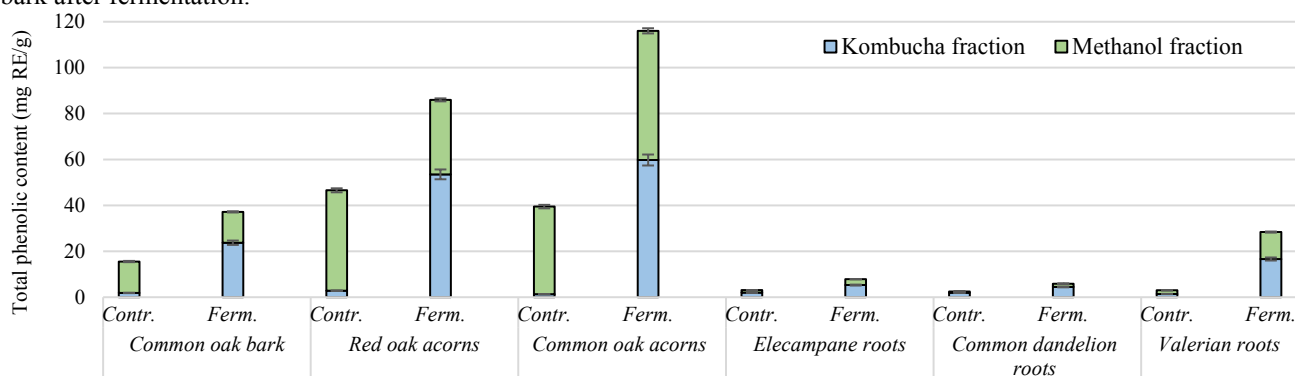


Fig. 1. Variation of total phenolic compounds content (mg RE/g) in the tested plants before (*Contr.*) and after (*Ferm.*) fermentation using kombucha SCOBY (n = 3; SSN ≤ 4.9%)

In conclusion, the fermentation had a positive effect on the sum of biologically active compounds determined in kombucha and methanol fractions together, where the content of biologically active compounds increased from 1.2 to 9 times. However, the variation activity of separate fractions was dependent on the plant.

- Jakubonienė, R., Ragažinskienė, O., Medicinal herbs. Ecology. Solar power. A community of full houses (2007).
- Villarreal-Soto, S. A., Beaufort S., et al., Understanding Kombucha Tea Fermentation: A Review, Journal of Food Science 83(3), 575-586 (2018).
- Chakravorty, S., Bhattacharya, S., et al., Kombucha tea fermentation: Microbial and biochemical dynamics, International Journal of Food Microbiology 220(2), 63-72 (2016).
- Kaškonienė, V., Kaškonas, P., Maruška, A., Volatile compounds composition and antioxidant activity of bee pollen collected in Lithuania, Chemical papers 69, 291-299 (2017).

FORMATION OF CALPROTECTIN (S100A8/S100A9) INHIBITS AGGREGATION OF S100A9 INTO AMYLOID COMPLEXES

Ieva Baronaitė, Darius Šulskis, Vytautas Smirnovas

Amyloid Research Sector, Institute of Biotechnology, Life Sciences Center, Vilnius University, Lithuania
ieva.baronaitė@chgf.stud.vu.lt

S100A8 and S100A9 are members of the S100 calcium-binding protein family. They are established as biomarkers of inflammation with various extracellular and intracellular functions [1]. Both of the proteins can be heavily upregulated in Alzheimer's disease (AD) patients' brain tissues [2]. S100A9 forms neurotoxic amyloid fibrils [3], which may contribute to the pathology of AD [4]. Differently from S100A9, S100A8 assembles into non-fibrillar aggregates in the brain tissues of transgenic APP or ageing wild-type mice [5]. Moreover, S100A8 and S100A9 are able to form heterodimeric complex (calprotectin (CP)). Calcified amyloidogenic fibrils of calprotectin can be found in the ageing prostate, which additionally emphasizes the connection between inflammation and amyloid deposits formation [6].

Assembly into amyloids is related to the changes in the protein's secondary structure. During the aggregation process, a transformation from the native state into cross β -sheet structures occurs [7]. However, existing evidence implies that S100A9 has a distinct aggregation pathway as S100A9 fibrils retain a significant amount of α -helical motives alongside β -sheets [3]. Thus, S100A9 amyloid fibrils structural propensities remain unclear. Moreover, there are no detailed studies of S100A8 and CP aggregation *in vitro*. Therefore, in this study, we were investigating S100A8 and S100A9 fibril's secondary structures and morphologies, as well as their aggregation rate dependence on protein concentration. Additionally, we examined CP formation influence on S100A8 and S100A9 aggregation.

In order to evaluate S100A8 and S100A9 aggregation propensities, Thioflavin T Fluorescence Assays were conducted under 37 °C. Aggregation kinetics results indicated that both proteins have a short lag-phase period and half-time values of the amyloid formation kinetics elevate notably in a concentration-dependent manner. However, distinct characteristics of S100A8 and S100A9 aggregation curves were observed, hence, formed aggregates were examined using Atomic Force Microscopy (AFM). AFM imaging indicated S100A8 aggregates as spherical oligomers, differently from S100A9 short worm-like fibrils. Lastly, we observed that CP formation inhibits S100A9 assembly into fibrils *in vitro*. In summary, our conducted research provides important and previously unknown insights into S100A8 and S100A9 aggregation, which is tightly connected to various pathologies.

[1] Pruenster, M., Vogl, T., Roth, J., & Sperandio, M., S100A8/A9: From basic science to clinical application, *Pharmacology and Therapeutics* 167, 120-131 (2016).

[2] Cristóvão, J. S., & Gomes, C. M, S100 Proteins in Alzheimer's Disease, *Frontiers in Neuroscience* 13, 463 (2019).

[3] Iashchishyn, I. A., Sulskis, D., Nguyen Ngoc, M., Smirnovas, V., & Morozova-Roche, L. A., Finke-Watzky Two-Step Nucleation-Autocatalysis Model of S100A9 Amyloid Formation: Protein Misfolding as "nucleation" Event, *ACS Chemical Neuroscience* 8(10), 2152–2158 (2017).

[4] Wang, C., Klechikov, A. G., Gharibyan, A. L., Wärmländer, S. K. T. S., Jarvet, J., Zhao, L., Jia, X., Shankar, S. K., Olofsson, A., Brännström, T., Mu, Y., Gräslund, A., & Morozova-Roche, L. A., The role of pro-inflammatory S100A9 in Alzheimer's disease amyloid-neuroinflammatory cascade, *Acta Neuropathologica* 127(4), 507-22 (2014).

[5] Lodeiro, M., Puerta, E., Ismail, M. A. M., Rodríguez-Rodríguez, P., Rönnbäck, A., Codita, A., Parrado-Fernandez, C., Maioli, S., Gil-Bea, F., Merino-Serrais, P., & Cedazo-Minguez, A., Aggregation of the inflammatory S100A8 precedes A β plaque formation in transgenic app mice: Positive feedback for S100A8 and A β productions, *Journals of Gerontology - Series A Biological Sciences and Medical Sciences* 72(3), 319-328 (2017).

[6] Yanamandra, K., Alexeyev, O., Zamotin, V., Srivastava, V., Shchukarev, A., Brorsson, A. C., Tartaglia, G. G., Vogl, T., Kaye, R., Wingsle, G., Olsson, J., Dobson, C. M., Bergh, A., Elgh, F., & Morozova-Roche, L. A., Amyloid formation by the pro-inflammatory S100A8/A9 proteins in the ageing prostate, *PLoS ONE* 4(5), e5562 (2009).

[7] Knowles, T. P. J., Vendruscolo, M., & Dobson, C. M., The amyloid state and its association with protein misfolding diseases, *Nature Reviews Molecular Cell Biology* 15 (6), 384-96, (2014).

PLASMA MiRNAs AS POTENTIAL BIOMARKERS FOR PREDICTING RADIATION-INDUCED HEART DISEASES IN LUNG CANCER PATIENTS

Paulina Kazlauskaitė^{1,2}, Ieva Vaicekuskaitė^{1,2}, Rasa Sabaliauskaitė¹, Sonata Jarmalaitė^{1,2}, Jonas Venius¹, Rita Steponavičienė¹

¹National Cancer Institute, LT-10257 Vilnius, Lithuania

²Institute of Biosciences, Life Sciences Center, Vilnius University, LT-08412 Vilnius, Lithuania

paulina.kazlauskaite@gmc.stud.vu.lt

Background: Lung cancer is the second most common malignancy and is the leading cause of cancer death in the world [1]. Improving cancer diagnostic and treatment methods would help to improve survivability. Currently, both non-small cell and small-cell lung cancer have various types of treatment, including radiotherapy as one of the main treatment options in all stages of lung cancer. Despite of that, thoracic radiotherapy for lung cancer has been linked to an increased risk of cardiac-related morbidity and mortality [2,3]. Currently available methods that predict radiation-induced heart disease (RIHD) are suboptimal. Identifying and developing biomarkers such as circulating plasma microRNAs (miRNAs) could improve the prediction of RIHD. Changes in miRNA expression levels could be a useful, non-invasive liquid biopsy tool for improved risk stratification and precise treatment planning.

The aim of this study was to identify miRNA expression changes in the plasma, taken from Lithuanian lung cancer patients, pre-and post-ionizing radiation treatment, in order to evaluate the effects of treatment on cardiac toxicity.

Methods: 12 pairs of lung cancer patients' plasma samples before and after radiotherapy were included in this study. MiR-1-3p, miR-21-5p, miR-24-3p, miR-29a-3p, miR-34a-5p and miR-222-3p were analyzed. MiRNA expression was examined by reverse transcription quantitative PCR. Results were normalized with exogenous cel-miR-39-3p control and relative expression was calculated.

Results: MiR-1-3p, miR-24-3p, miR-29a-3p, and miR-222-3p were downregulated, while miR-21-5p and miR-34a-5p were upregulated in lung cancer patients' plasma after radiation therapy. Moreover, after treatment, patients with higher natriuretic peptide serum concentration and troponin values showed significant differences in miRNA relative abundance compared to the norm of these indicators.

In conclusion, our study suggests that the identification of microRNA expression level changes in lung cancer patients' plasma before and after radiation therapy could be used for the early detection of RIHD and determine personalized radiation doses to the particular volume of the heart region to reduce toxicity to the heart. However, further analysis is required to validate these miRNAs as potential biomarkers for radiation-induced cardiac toxicity.

Acknowledgements: This study was supported by the National Cancer Institute research fund.

[1] Siegel, R., Miller, K., Fuchs, H. and Jemal, A., 2022. Cancer statistics, 2022. *CA: A Cancer Journal for Clinicians*, 72(1), pp.7-33.

[2] Hawkins, P., Sun, Y., Dess, R., Jackson, W., Sun, G., Bi, N., Tewari, M., Hayman, J., Kalemkerian, G., Gadgeel, S., Lawrence, T., Haken, R., Matuszak, M., Kong, F., Schipper, M. and Jolly, S., 2019. Circulating microRNAs as biomarkers of radiation-induced cardiac toxicity in non-small-cell lung cancer. *Journal of Cancer Research and Clinical Oncology*, 145(6), pp.1635-1643.

[3] Christina K. Speirs, Todd A. DeWees, Sana Rehman, Alerson Molotievski, Maria A. Velez, Daniel Mullen, Sandra Fergus, Marco Trovo, Jeffrey D. Bradley, Cliff G. Robinson, 2017. Heart Dose Is an Independent Dosimetric Predictor of Overall Survival in Locally Advanced Non-Small Cell Lung Cancer, *Journal of Thoracic Oncology*, 12(2), pp. 293-301.

ISOLATION OF ENDOPHYTIC MICROORGANISMS FROM BLUEBERRY FRUIT AND IDENTIFICATION BY SURFACE-ENHANCED RAMAN SPECTROSCOPY

Sofiya Asadchaya¹, Dorotėja Vaitiekūnaitė², Ingrida Bružaitė¹, Valentinas Snitka³

¹ Department of Chemistry and Bioengineering, Faculty of Fundamental Sciences, Vilnius Gediminas Technical University, Lithuania

² Lithuanian Research Centre for Agriculture and Forestry, Laboratory of Forest Plant Biotechnology, Institute of Forestry, Lithuania

³ Research Center for Microsystems and Nanotechnology, Kaunas University of Technology, Lithuania
sofiya.asadchaya@stud.vilniustech.lt

Endophytes are typically defined as microorganisms, that inhabit the plant endosphere asymptotically. They play specific roles in plant growth promotion and protection [1]. Endophytic microbes may help with nutrient acquisition, produce growth-enhancing hormones, fungicides, etc. Fruit endophytes can protect fruits against post-harvest diseases.

Blueberry fruits are consumed all over the world. They are also widely studied for their bioactive compounds [2], however, their endomicrobiota is not well studied, especially endophytes contained in the berries [3].

Surface-enhanced Raman spectroscopy (SERS) is a highly sensitive technique that enhances the Raman scattering of molecules supported by some nanostructured materials. Molecular characterization by SERS allows for easy separation of microorganisms and produces a lot of information about the composition of cells.

The aim of this study was to isolate endophytic microorganisms from commercially grown blueberries and to identify their molecular composition by SERS.

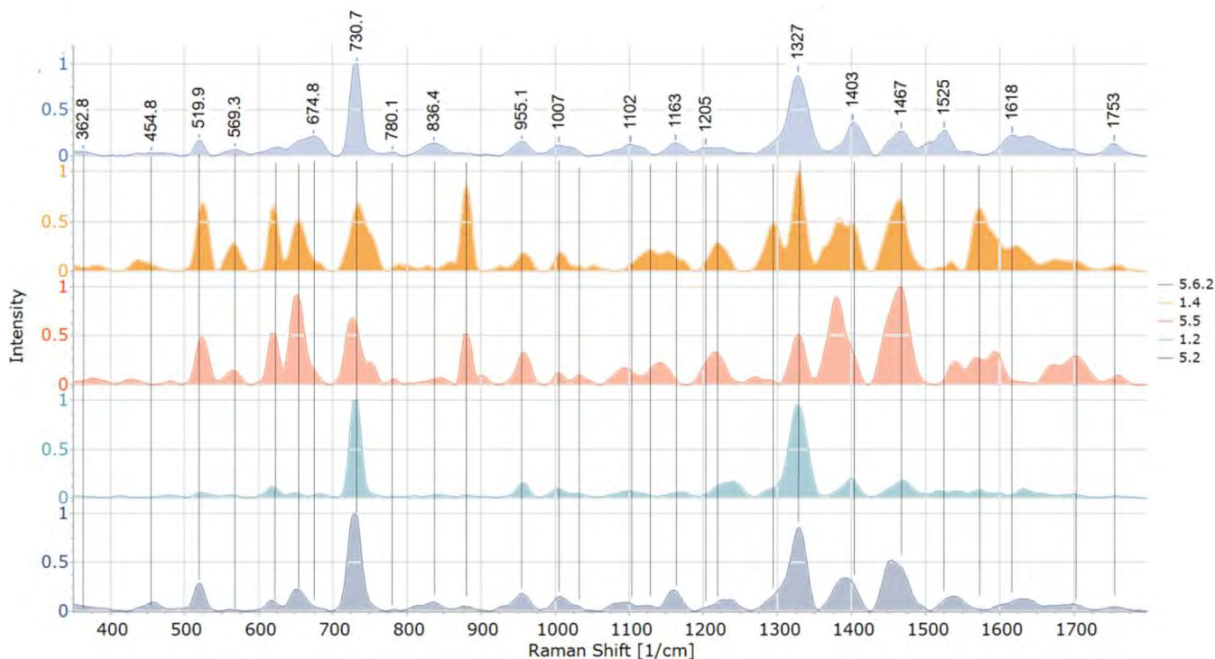


Fig. 1. SERS spectra (normalized to the highest peak) of all the bacterial isolates tested in this study at 532 nm excitation wavelength.

In this study, five microorganisms were isolated from blueberry fruit. It was 1.1 – *C. santamariae*, 5.5 – *Salmonella enterica*, 5.6.2 – *L. mesenteroides*, 1.2 – *Staphylococcus hominis*, and 5.2 – *S. cohnii* [4]. To our knowledge, *Candida* yeasts were not previously isolated from the blueberry endosphere.

[1] H. Rho, et al., Endophytes increased fruit quality with higher soluble sugar production in honeycrisp apple (*Malus pumila*), *Microorganisms* **8**, 1–17 (2020).

[2] P. Dró et al., Evaluation of bioactive compounds, minerals and antioxidant activity of lingonberry (*Vaccinium vitis-idaea* L.) fruits, *Molecules* **23**, 53 (2018).

[3] M.P. Nguyen, et al., Host species shape the community structure of culturable endophytes in fruits of wild berry species (*Vaccinium myrtillus* L., *Empetrum nigrum* L. and *Vaccinium vitis-idaea* L.), *FEMS Microbiol. Ecol.* **97**, 1–13 (2021).

[4] D. Vaitiekūnaitė, et al., Endophytes from blueberry (*Vaccinium* sp.) fruit: Characterization of yeast and bacteria via label-free surface-enhanced Raman spectroscopy (SERS), *Spectrochimica Acta Part A: Molecular and Biomolecular Spectroscopy* **275**, 121158 (2022).

QUANTUM DOTS TOXIC EFFECTS ON BROWN TROUT (*SALMO TRUTTA FARIO*)

Toma Černauskaitė^{1,2}, Gintarė Sauliūtė¹, Živilė Jurgelėnė¹

¹Laboratory of Ecotoxicology, Nature Research Centre, Lithuania

²Life Sciences Center, Vilnius University, Lithuania

toma.cernauskaite@gmc.stud.vu.lt

Quantum dots (QDs) are tiny semiconductor particles that are only a few nanometers in size. They are made of materials such as cadmium selenide (CdSe) and zinc sulfide (ZnS) [1]. QDs have unique electronic and optical properties that make them useful in a wide range of applications, but their small size also makes them more toxic than larger particles. This is because smaller particles have a higher surface-to-volume ratio, making them more reactive and more likely to interact with living cells. Additionally, smaller particles can more easily cross cell membranes and enter cells, where they can cause damage [2]. There is growing concern about their potential toxic effects on living organisms. The study of the toxic effects of quantum dots on brown trout (*Salmo trutta fario*) is an important contribution to the field.

Catalase (CAT) is an enzyme that catalyzes the breakdown of hydrogen peroxide (H₂O₂) into water and oxygen. This enzyme is vital in safeguarding cells from harm caused by an imbalance between the generation of reactive oxygen species (ROS) and the cells' ability to neutralize them [3]. When an organism is exposed to oxidative stress, the activity of CAT increases to neutralize the hydrogen peroxide that is produced as a result of the stress. Therefore, measuring the activity of CAT can provide an indication of the level of oxidative stress in a particular organism or tissue.

The aim of this study is to identify CAT activity in the liver of *Salmo trutta fario* after exposure to QDs. The CAT activity was measured using a colorimetric method. The results showed that exposure to QDs resulted in variation of CAT activity during exposure periods compared to the control group. Understanding the potential toxic effects of QDs on aquatic organisms is crucial for the protection of the environment, human health, and the sustainability of industries that rely on QDs.

Acknowledgements: This research was funded by the Research Council of Lithuania, Project registration No. MIP- 23-95.

-
- [1] R.E. Bailey, M.A. Smith, S. Nie. "Quantum dots in biology and medicine." *Physica E: Low-dimensional Systems and Nanostructures* 25.1 (2004).
[2] S. Singh, A. Dhawan, S. Karhana, M. Bhat, A.K. Dinda. "Quantum dots: An emerging tool for point-of-care testing." *Micromachines* 11.12 (2020).
[3] A. Nandi, L.J. Yan, C.K. Jana, N. Das. "Role of catalase in oxidative stress-and age-associated degenerative diseases." *Oxidative medicine and cellular longevity* (2019).

THE ACTIVITY OF HUMAN ANTIOXIDANT PROTECTION ENZYMES AFTER INFLUENCE OF TiO₂

Maryia Sadaunichuk¹, Aliaksandra Skarabhatava¹, Elena Venskaya¹, Natalia Aliakhnovich²

¹Institute of Biophysics and Cell Engineering of NAS of Belarus, 27 Akademicheskaya str., Minsk, Belarus

²Vitebsk State Order of Peoples' Friendship Medical University, Frunze Av., 27, Vitebsk, Belarus

mariasadovnichuk@gmail.com

In recent decades, the development of nanomaterials based on titanium oxide and their use in the household and medical fields has been carried out on an industrial scale. As a result, for now, there are problems in studying the bioavailability of titanium dioxide, as well as assessing their effects on cells and tissues of the human body.

The aim of this study is to evaluate the ability of human erythrocytes to accumulate titanium after exposure to titanium dioxide particles of different sizes (nano-, micro- and dietary particles), as well as to investigate the activity of antioxidant protection enzymes in erythrocytes after exposure to titanium dioxide.

Erythrocytes were separated from plasma by blood centrifugation at 2000 g, 5 minutes in PBS buffer pH 7.4. After separation erythrocytes were diluted to 2% hematocrit in the same buffer and loaded with titanium dioxide particles at the final concentration of 0,01 mg/ml and incubated for 3 hours at 37°C and permanent mixing. Analysis of the elemental composition of erythrocytes was realized by inductively coupled plasma atomic emission spectroscopy. Catalase and glutathione peroxidase activity were assessed by the standard methods [1, 2]. Statistical analysis was carried out using Wilcoxon test ($n=7$).

It was shown that after 3-h of incubation with the analyzed particles there was no reliable change of titanium content in the cells. The maximum values of titanium in erythrocytes were 1,57; 2,36 and 0,49 µg/L in treatment groups with nanoparticles, microparticles and dietary TiO₂ respectively, while in the control sample the average titanium content was 1,01 µg/L.

Analysis of the activity of antioxidant protection enzymes (glutathione peroxidase and catalase) revealed that after a 3-h load of TiO₂ cells, there was a decrease in the activity of the studied enzymes on average by 20% ($p<0.05$). However, the difference between the effects of different types of particles could not be identified.

Thus, we have found that the 3-h load of human erythrocytes by various types of titanium dioxide particles (nano-, microparticles and dietary titanium) does not lead to its accumulation in cells, nevertheless, it causes a decrease in the activity of enzymes of antioxidant protection.

[1] Method detection of catalase activity / M.A. Koroluk, M.I. Ivanova, I.G. Majorova, V.E. Tokareva // Lab. Sci. – 1988. – Vol. 1. – P. 16–19.

[2] Simple and specific method detection of glutathione peroxidase activity in erythrocytes / V.M. Moin // Lab. Sci. – 1986. – Vol. 12. – P. 724–727.

SYNTHESIS OF LIPOSOMAL CURCUMIN AND ITS CHARACTERIZATION IN VITRO

Austėja Kvedaraite^{1,2}, Simona Steponkienė¹, Vitalijus Karabanovas^{1,3}, Ričardas Rotomskis¹

¹Biomedical Physics Laboratory of National Cancer Institute, Vilnius, Lithuania

²Life Sciences Center, Vilnius University, Vilnius, Lithuania

³Department of Chemistry and Bioengineering, Vilnius Gediminas Technical University, Vilnius, Lithuania

austeja.kvedaraite@gmc.stud.vu.lt

Cancer is one of the most devastating diseases worldwide, accounting near 10 million deaths in 2020 [1]. In response to this issue, not only do therapeutic options are aimed to be improved but also prevention programs are being developed. For example, a chemopreventive substances are considered to lower a person's risk of (re)developing cancer [2]. However, minority of people, even if they are acknowledged of genetic predisposition to cancer, choose to use chemotherapy drugs because of severe side effects. Natural substances are thought to be free of severe side effects and would therefore be more accepted and used by the target group.

Curcumin is one of the naturally occurring substances that is considered to have anti-cancer properties [3], and therefore, having potential as a cancer chemopreventive agent. Nevertheless, curcumin is a hydrophobic compound and is poorly absorbed by a living organism. Encapsulation of curcumin in phospholipid liposomes could facilitate absorption since liposomes have a desired bioavailability and are biocompatible as well as biodegradable. However, the comparison of encapsulation techniques in terms of cellular uptake and localization in biological models is still limited.

The aim of our study was to evaluate the effect of liposomal curcumin on breast cancer cell line (MCF-7) and to identify liposomal curcumin localization in the cell. In our research we synthesized liposomal curcumin solution applying a thin-film and pH-differences methods. MCF-7 breast cancer cell line was used to evaluate liposomal curcumin effects on cancer cells. As a control, liposomes without curcumin were synthesized to eliminate the possible effect of liposomes. For the assessment of accumulation of liposomal curcumin in cancer cells, confocal microscopy imaging with fluorescent dyes labeling were applied. Particle size, zeta potential and encapsulation efficiency were assessed to characterize the liposomes.

The cell morphology, viability and proliferation test results showed toxicity of curcumin to breast cancer cell line and preliminary results from confocal microscopy images indicated an accumulation of curcumin in the cytoplasm at the lysosomal sites. No uptake of liposomal curcumin into the nucleus or mitochondria was observed. When it comes to comparison of synthesis methods, we found that liposomal curcumin solutions of both syntheses had similar effect on MCF-7 cells morphology, viability and proliferation, although thin-film synthesis resulted in higher yield. In conclusion, preliminary results suggest that liposomal curcumin has a potential as a chemopreventive agent, and a thin-film synthesis method is advantageous over the pH difference synthesis method.

ACKNOWLEDGEMENTS: We thank Vilius Poderys for technical assistance and Migle Ragelytė for refinement of synthesis protocols.

[1] Sung, H., Ferlay, J., Siegel, R. L., Laversanne, M., Soerjomataram, I., Jemal, A., & Bray, F. (2021). Global Cancer Statistics 2020: GLOBOCAN Estimates of Incidence and Mortality Worldwide for 36 Cancers in 185 Countries. *CA: A Cancer Journal for Clinicians*, 71(3), 209–249. <https://doi.org/10.3322/caac.21660>

[2] William, W. N., Heymach, J. V., Kim, E. S., & Lippman, S. M. (2009). Molecular targets for cancer chemoprevention. *Nature Reviews Drug Discovery*, 8(3), Article 3. <https://doi.org/10.1038/nrd2663>

[3] Shehzad, A., Wahid, F., & Lee, Y. S. (2010). Curcumin in Cancer Chemoprevention: Molecular Targets, Pharmacokinetics, Bioavailability, and Clinical Trials. *Archiv Der Pharmazie*, 343(9), 489–499. <https://doi.org/10.1002/ardp.200900319>

RELEASE STUDIES OF NISIN FROM NISIN-LOADED FUCOIDAN PARTICLES

Aiste Galinskaite¹, Ruta Gruskiene¹, Jolanta Sereikaite¹

¹ Department of Chemistry and Bioengineering, Vilnius Gediminas Technical University, Vilnius, Lithuania
aiste.galinskaite@stud.vilniustech.lt

Nisin is a cationic antimicrobial peptide, used in the food industry against gram-positive bacteria. The efficiency of this peptide could be reduced by environmental stresses, proteolysis, and undesirable interactions with food components. To overcome this problem, nisin can be encapsulated using lipids, proteins, or carbohydrates. Encapsulation also provides controlled release which plays a key role in improving the shelf life of foods [1]. It is important to research controlled antimicrobial peptide release from the particles to predict how long its antimicrobial effect will last. In this work, for the synthesis of particles fucoidan was used.

Fucoidan – anionic, sulfated polysaccharide produced by brown seaweed such as *Macrocystis pyrifera*, *Laminaria japonica*, and *Fucus vesiculosus*. It also has antitumor, antithrombotic, anti-inflammatory, anticoagulant, and antioxidant activity, which could also provide additional beneficial properties for food products [2].

This study researched *in vitro* release of nisin from nisin-loaded fucoidan particles. Release of the antimicrobial peptide was monitored using dialysis against 25 mM phosphate buffer solution at different pH (2, 6, and 8), temperatures (20 and 37 °C), and ionic strength (0; 0.1; 0.2 and 0.5 M of NaCl). As a control, the diffusion of non-encapsulated nisin through a membrane against phosphate buffer without NaCl was used. The greater influence of ionic strength was only observed at pH 2 at both temperatures. In this case, more nisin is released from the particles when the concentration of NaCl increases. At pH 6, the amount of released nisin increases with increasing ionic strength up to 0.2 M. However, further increasing the ionic strength slows down the release of nisin.

When investigating the influence of pH on the release, it was observed that more nisin is released at pH 6 (60–80% after 96 hours) at 20 °C. A similar amount of released peptide (10–40%) was observed at higher temperatures regardless of pH. Enhanced hydrophobic interactions could be a reason why higher temperatures did not induce the release of nisin.

[1] A. Bahrami, R. Delshadi, S. M. Jafari et al., Nanoencapsulated nisin: An engineered natural antimicrobial system for the food industry, Trends in Food Science & Technology 94, 20-31 (2019).

[2] J. Venkatesan, S. Anil, S. K. Kim, M. S. Shim. Seaweed polysaccharide-based nanoparticles: Preparation and Applications for Drug Delivery, Polymers 8 (2016).

THE APPLICATION OF PECTIN FOR THE PROTEOLYTIC STABILIZATION OF NISIN

Justė Čeičytė^{1*}, Aistė Galinskaitė¹, Rūta Gruškienė¹

¹ Department of Chemistry and Bioengineering, Vilnius Gediminas Technical University, Vilnius, Lithuania
juste.ceicyte@stud.vilniustech.lt

In the modern food industry, food preservation is extremely important. To this day the world still suffers from food contamination caused by bacteria, e.g. *Vibrio cholerae*, found in various types of seafood, or *Listeria*, associated with various ready-to-eat foods [1]. To solve the issue food industries are using synthetic preservatives or high amounts of salt or sugar. However, studies show that this type of conservation has caused harm to human health. Therefore, there is a need to find a substance that wouldn't cause bacterial resistance and would be naturally sourced. These requirements are met by bacteriocin–nisin.

Nisin is a small peptide made up of 34 amino acid residues, which is synthesized by the lactic acid bacteria *Lactococcus lactis* subsp. *lactis*. It aims to tackle both Gram-positive and certain Gram-negative bacteria due to its wide antimicrobial spectrum [2]. Nevertheless, nisin can be harmed by food-derived enzymes, which would result in a loss of antimicrobial activity. To ensure the stability of nisin, it could be coated with biopolymers [3]. In this work, pectin was used for particle preparation. Pectin is a complex anionic polysaccharide mainly composed of homogalacturonan (1→4 linked α -D-galacturonic acid and its methyl ester). According to its degree of esterification, pectin can be classified as high (> 50% esterified carboxyl groups) or low (< 50% esterified carboxyl groups) methoxyl pectin [4].

The aim of this study is to prepare nisin-loaded pectin particles and compare their proteolytic stability with free nisin. To encapsulate nisin three different types of anionic pectin biopolymer, i.e., high methoxyl pectin (HMP), low methoxyl pectin (LMP), and pectic acid (PecA) are used. The final concentration of pectin and nisin was 0,4 mg/ml. To test the proteolytic stability of the particles two distinct proteases were used, i.e., proteinase K and protease from *Rhizopus* sp. The first protease was dissolved in sodium dihydrogen phosphate dihydrate buffer solution at pH 7.5 and protease from *Rhizopus* sp. was dissolved in acetic acid buffer solution at pH 4. Nisin-loaded pectin and free nisin samples at pH 4 and 7 were prepared and were affected by proteinase K and protease from *Rhizopus* sp., respectively. Proteolysis was performed for 24 h at 37 °C. Finally, samples with proteolytic degradation products were analyzed by the capillary zone electrophoresis method using 7100 Capillary Electrophoresis unit (Agilent Technologies).

The appearance of new peaks in the electropherogram of proteolytically affected nisin was observed. If nisin-loaded pectin particles undergo proteolytic degradation, the profile of the electropherogram is the same as the sample containing only free nisin. The obtained results show that the area of peaks is obviously lower in nisin-loaded pectin particles compared with free nisin, especially when proteinase K is used. Thus, pectin could be successfully used to increase the resistance of nisin to the action of proteolytic enzymes.

Acknowledgments: This research was funded by the Research Council of Lithuania, Grant No. P-ST-22-42.

[1] F. Feldhusen, The role of seafood in bacterial foodborne diseases, *Microbes and Infection* **2**, 1651-1660 (2000).

[2] B. Özel, Ö. Şimşek, M. Akçelik, P.E.J Saris, Innovative approaches to nisin production, *Applied Microbiology and Biotechnology* **102**, 6299–6307 (2018).

[3] S. Ji, J. Lu, Z. Liu, D. Srivastava, A. Song, Y. Liu, I. Lee, Dynamic encapsulation of hydrophilic nisin in hydrophobic poly (lactic acid) particles with controlled morphology by a single emulsion process, *Journal of Colloid and Interface Science* **423**, 85–93 (2014).

[4] Wusigale, L. Liang, Y. Luo, Casein and pectin: Structures, interactions, and applications, *Trends in Food Science and Technology* **97**, 391–403 (2020).

ISOLATION AND CULTURE METHOD OF DERMAL CANINE FIBROBLASTS CELL LINE

Dawid Jeżewski¹, Nicole Nowak², Tomasz Gębarowski^{1,2}, Joanna Bubak³

¹Student Science Club Refectio, Wrocław University of Environmental and Life Sciences

²Department of Biostructure and Animal Physiology, Wrocław University of Environmental and Life Sciences, Kozuchowska 1/3, 51-631 Wrocław, Poland

²Department of Pathology, Wrocław University of Environmental and Life Sciences C. K. Norwida 31, 50-375 Wrocław, Poland

123527@student.upwr.edu.pl

Fibroblasts are the most common connective tissue cells, which can be found abundantly e.g. in reticular, loose or dense connective tissue forming structures like lymph nodes, tendons or skin layer. By producing reticular, collagen and elastic fibers but also components of the basic substance, they play an important role in wound healing and scar formation process [1]. This special properties of fibroblasts can be useful in the treatment of hard to heal wounds and tissue fractures. Research on the use of fibroblasts in the treatment of wounds has been conducted for many years [2,3,4]. Production of extracellular matrix components via fibroblasts can be also apply as alternative treatment in restoring the natural elasticity of scarred skin.

In order to understand and use the knowledge of how to treat wounds and scars with fibroblasts in veterinary medicine, a method of collecting, isolating and cultivating fibroblasts from tissue should be developed.

Isolation of cell line was conducted by collecting the material, and then via mechanical fragmentation of the material, cleaning the collected skin sample. The next step is transferring the material to test tubes with the medium that is stored in the incubator in a humidified atmosphere of 95% air and 5% CO₂ for 3 h at 37 °C. DMEM medium was used for cell culture, every 48h medium was changed.

The skin tissue was taken during the procedure mastectomy, from a Maltese dog, at age 6.

-
- [1] Driskell, Ryan R et al. "Distinct fibroblast lineages determine dermal architecture in skin development and repair." *Nature* vol. 504,7479 (2013): 277-281. doi:10.1038/nature12783
- [2] Kim WS, Park BS, Sung JH, Yang JM, Park SB, Kwak SJ, Park JS. Wound healing effect of adipose-derived stem cells: a critical role of secretory factors on human dermal fibroblasts. *J Dermatol Sci*. 2007 Oct;48(1):15-24. doi: 10.1016/j.jdermsci.2007.05.018. Epub 2007 Jul 23. PMID: 17643966.
- [3] Bainbridge P. Wound healing and the role of fibroblasts. *J Wound Care*. 2013 Aug;22(8):407-8, 410-12. doi: 10.12968/jowc.2013.22.8.407. PMID: 23924840.
- [4] Qian H, Shan Y, Gong R, Lin D, Zhang M, Wang C, Wang L. Fibroblasts in Scar Formation: Biology and Clinical Translation. *Oxid Med Cell Longev*. 2022 May 12;2022:4586569. doi: 10.1155/2022/4586569. PMID: 35602101; PMCID: PMC9119755.

ANTIMICROBIAL EXTRACTS AND ESSENTIAL OIL APPLICATION IN O/W EMULSION FORMATION

Jurga Andreja Kazlauskaitė^{1,2*}, Inga Matulytė^{1,2}, Jurga Bernatoniene^{1,2}

¹Department of Drug Technology and Social Pharmacy, Lithuanian University of Health Sciences, Lithuania.

²Institute of Pharmaceutical Technologies, Lithuanian University of Health Sciences, Lithuania.

jurga.andreja.kazlauskaitė@lsmu.lt

Plant extracts and essential oils are used in many fields, including the medical, chemical, pharmaceutical, and cosmetic industries [1]. Botanicals of plant origin, such as *Trifolium pratense* L. flowers, *Glycyrrhiza glabra* L. roots, and *Myristica fragrans* Houtt. essential oils are generally considered safe due to their natural source. It can prevent various degenerative diseases and possess many pharmacological activities such as antibacterial, anti-inflammatory, antiviral, antitumor, etc [2]–[4]. Antimicrobials of plant origin are promising options for treating infections phenolic compounds in plants can act synergistically and enhance valuable effects. These effects can be beneficiary in pharmaceutical forms.

The aim was to study the antimicrobial effects of two extracts (*Trifolium pratense* L. flowers, *Glycyrrhiza glabra* L. roots) and essential oil (*Myristica fragrans* Houtt.) and incorporate them together to create a stable emulsion.

Trifolium pratense L. flowers extract was prepared using ultrasound combined with thermal hydrolysis, and used solvent was 50 % ethanol solution. *Glycyrrhiza glabra* L. roots extract was done using ultrasound. The extraction solvent was water. *Myristica fragrans* Houtt. The essential oil was prepared by modified hydrodistillation [5]. The antimicrobial effects were investigated against standard cultures of non-spore bacteria (all bacteria were obtained from American Type Culture Collection (ATCC))—*Staphylococcus aureus* (ATCC 25923), *Staphylococcus epidermidis* (ATCC 12228), *Enterococcus faecalis* (ATCC 29212), *Escherichia coli* (ATCC 25922), *Klebsiella pneumoniae* (ATCC 13883), *Pseudomonas aeruginosa* (ATCC 27853), *Proteus vulgaris* (ATCC8427), *Bacillus cereus* (ATCC 6633) and fungus *Candida albicans* (ATCC 10231). Emulsion with extracts and essential oil was prepared using excipients (maltodextrin, inulin, and/ or gum Arabic) and sodium alginate solution. The solution was homogenized for 15 min at 5000 rpm using homogeniser. Emulsion stability was tested using a centrifuge, particles' size and distribution were assessed using Mastersizer.

Trifolium pratense L. extract (33 mg/ml) inhibited the growth of *Staphylococcus epidermidis*, *Staphylococcus aureus*, and *Bacillus cereus*. Obtained results showed that this extract inhibits Gram-positive bacteria more than Gram-negative. The growth of other pathogens was not inhibited. *Glycyrrhiza glabra* L. extract (11 mg/ml) had expressed antimicrobial activity against Gram-positive bacteria: *Staphylococcus aureus*, *Staphylococcus epidermidis*, *Enterococcus faecalis*, and *Bacillus cereus*. Additionally, it suppressed the growth of the fungus *Candida albicans*. Essential oils are volatile liquids, so it is difficult to determine their effect due to evaporation. Nevertheless, essential oil (30 µg) suppressed the growth of *Staphylococcus aureus*, *Bacillus cereus*, *Escherichia coli*, and *Klebsiella pneumoniae*.

Six emulsion samples were prepared, and their stability was evaluated. Emulsion, which was prepared additionally using maltodextrin, inulin, gum arabic (ratio 62:43:15), alginate, all the extracts and essential oil, was the most stable, and its centrifugation index was 100%. *Myristica fragrans* Houtt. essential oil drop diameter in the emulsion was 0.571 µm. Evaluated percentiles were measured: D10 was 0.328 ± 0.051 µm, D50 was 0.46 ± 0.03 µm, and D90 was 0.89 ± 0.094 µm.

All of the extracts were more susceptible to Gram-negative bacteria than Gram-positive, but increasing extract concentration results can be more effective, so plant extracts should be concentrated in the final product in order to have a wide range antimicrobial agent. Created stable emulsion with both extracts and suspended essential oil can be used as the final pharmaceutical form or incorporated in other products for therapeutic benefits.

Acknowledgments

The authors would like to thank Open Access Centre for the Advanced Pharmaceutical and Health Technologies (Lithuanian University of Health Sciences) and for the opportunity to use modern infrastructure and perform this research. The authors declare no conflicts of interest.

This work was supported by the Research council of Lithuania (grant no. 09.3.3-ESFA-V-711-01-0001).

[1] Wojdylo, A.; Oszmianski, J.; Czemerys, R. Antioxidant Activity and Phenolic Compounds in 32 Selected Herbs. *Food Chem.* **2007**, *105* (3), 940–949. <https://doi.org/10.1016/j.foodchem.2007.04.038>.

[2] Kanadys, W.; Baranska, A.; Jedrych, M.; Religioni, U.; Janiszewska, M. Effects of Red Clover (*Trifolium Pratense*) Isoflavones on the Lipid Profile of Perimenopausal and Postmenopausal Women—A Systematic Review and Meta-Analysis. *Maturitas* **2020**, *132* (October 2019), 7–16. <https://doi.org/10.1016/j.maturitas.2019.11.001>.

[3] Gomaa, A. A.; Abdel-Wadood, Y. A. The Potential of Glycyrrhizin and Licorice Extract in Combating COVID-19 and Associated Conditions. *Phytomedicine Plus* **2021**, *1* (3), 100043. <https://doi.org/10.1016/j.phyplu.2021.100043>.

[4] Ashokkumar, K.; Simal-Gandara, J.; Murugan, M.; Dhanya, M. K.; Pandian, A. Nutmeg (*Myristica Fragrans* Houtt.) Essential Oil: A Review on Its Composition, Biological, and Pharmacological Activities. *Phyther. Res.* **2022**, *36* (7), 2839–2851. <https://doi.org/10.1002/ptr.7491>.

[5] Kazlauskaitė, J. A.; Matulytė, I.; Marksa, M.; Lelesius, R.; Pavilonis, A.; Bernatoniene, J. Application of Antiviral, Antioxidant and Antibacterial *Glycyrrhiza Glabra* L., *Trifolium Pratense* L. Extracts and *Myristica Fragrans* Houtt. Essential Oil in Microcapsules. *Pharmaceutics* **2023**, *15* (2), 464. <https://doi.org/10.3390/pharmaceutics15020464>.

COLLAGEN-CONTAINING ENZYME-ELECTROPHORESIS IN DETECTION OF PROTEOLYTIC ACTIVITY IN BLOOD PLASMA OF DONORS WITH DIFFERENT TITERS OF ANTI-SARS-COV-2 IGG

Maryna Kalashnikova, Daryna Krenytska, Olexiy Savchuk

Educational and Scientific Centre "Institute of Biology and Medicine" Taras Shevchenko National University of Kyiv
m.kalashnikova2507@gmail.com

Background. Sodium dodecyl sulfate–polyacrylamide gel electrophoresis (SDS-PAGE) has been proved to be a high efficient method to distinguish proteins with molecular masses. There are a lot of different modifications of this method to satisfy certain purposes. In this way, the technique of substrate-containing SDS-PAGE was developed to examine the proteolytic activity in samples. However, there is a necessity to optimize this method for using collagen as a substrate. [1].

The aim of the research was based on finding out appropriate conditions for conducting collagen-containing SDS-PAGE by altering the main such as an incubation time, degree for sample dilution, concentrations of a separation gel and collagen solution.

Materials and methods. Tris, glycine, sodium dodecyl sulfate, acrylamide, N,N'-Methylenebisacrylamide, ammonium persulfate, N,N,N',N' – tetramethylethylenediamine were used to make gels (Sigma, USA). After electrophoretic separation gels were washed in 2.5% Triton X-100 and incubated at 37 °C for 12 hours. Samples for the experiment were blood plasma of donors, who had suffered from COVID-19, with various titers of anti- SARS-CoV-2 IgG and were received from the "BIOPHARMA-PLASMA" company (Kyiv, Ukraine). During electrophoresis two types of samples were used: 1) plasma with streptokinase (ps) which was added into a plasma; 2) plasma without streptokinase (p0). In both cases, euglobulin fractions were obtained. All samples were diluted with the standard SDS-PAGE sample buffer. [2]. Glycerine was replaced by sucrose and dithiothreitol was removed at all to preserve enzyme activity.

Results. We had analyzed an effect of changing each of the parameters on the accuracy of this test. It was determined that the mixing ps samples with treatment buffer in the ratio 1:16 forms a larger number of evenly distributed bands. In comparison, dilution of the same ps samples by 4 and 8 times led to their concentration in one part of the plate with the formation of unclear bands. Moreover, the most accurate dilution of p0 samples was 8-fold, which produced clear and evenly distributed bands.

We explored an appropriate concentration of a separation gel by its variation: 10%, 12%, 15% and 18%. It was found that only 15% resolving gel prevented migration of samples, markers and a substrate during the experiment. In addition, we examined that using collagen solution with a concentration 2 mg/ml prevented its migration.

The time of extending the electrophoretic separation after the front line of the samples exited the gel into the electrophoresis buffer was altering between two options: 10 and 15 minutes. An accommodation of markers and samples was more correct when an elongation time was 15 minutes than 10 minutes. Also, it provided better washing after staining for undigested substrate with Coomassie Blue (**Figure 1**).

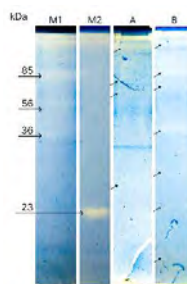


Figure 1. Collagen zymograms of p0 samples (A, B) and ps samples (C, D). Lane M1, M2 – molecular-weight markers. In all cases, p0 and ps samples were mixed with treatment buffer in the ratio 1:8 and 1:16, in accordance; 15% SDS-PAGE with 2 mg/ml collagen solution and the time of elongation was 15 minutes.

Conclusion. This study was focused on discovering set of parameters for collagen-containing enzyme-electrophoresis which will provide this test with appropriate conditions. We can state that new modification of collagen-containing enzyme-electrophoresis method which includes mixing ps samples with treatment buffer in the ratio 1:16 and p0 samples in the ratio 1:8, preparing 15% separating gel with adding 2mg/ml collagen solution and elongation of the electrophoresis for 15 minutes can be useful for different research.

[1] L. Ostapchenko, O. Savchuk, N. Burlova-Vasileva, Enzyme electrophoresis method in analysis of active components of haemostatis system, *Advances in Bioscience and Biotechnology*, 2, 20-26 (2011).

[2] I. Nikolaieva, Yu. Dudkina, D. Oliinyk, O. Oskyrko, O. Marushchak, T. Halenova, O. Savchuk, Amphibian skin secretions: a potential source of proteolytic enzymes, *Biotechnologia Acta*, 11 (5), 42-48 (2018).

INHIBITOR PROTEINS OF CRISPR-CAS BACTERIAL IMMUNITY

Dovydas Januška¹, Tomas Šinkūnas¹

¹Department of Protein-Nucleic Acids Interactions, Institute of Biotechnology, Life Sciences Center, Vilnius University, Lithuania
dovydas.januska@chgf.stud.vu.lt

CRISPR-Cas are bacterial and archaeal defense systems that provide resistance against phages and other invasive genomic elements. Short DNA fragments of extracellular origin are inserted within repeated sequences of the CRISPR locus. The CRISPR transcript is matured into small crRNA molecules, which, together with Cas proteins, assemble an effector complex destined to detect and destroy foreign nucleic acids [1]. The bacteriophages evolved small anti-CRISPR (Acr) proteins, which block CRISPR-Cas protection [2]. To date, over 100 Acr families have been discovered, but only a fraction of them have been studied in detail [3]. Recently, Acr proteins have been utilized to regulate CRISPR-Cas editing tools, demonstrating their immense practical potential.

Our research object is the Acr proteins inhibiting the type I-F CRISPR-Cas system from *Aggregatibacter actinomycetemcomitans*. The system encodes a ribonucleoprotein complex, termed Cascade, which binds foreign DNA and then recruits the Cas2/3 nuclease to destroy the invader [4]. We show Acr proteins blocking the CRISPR-Cas system in bacterial cells. We employ biochemical assays for the analysis of their molecular mechanisms. Our findings provide insight into the inhibitory mechanism of these previously uncharacterised proteins.

-
- [1] Hille, F., & Charpentier, E. CRISPR-Cas: Biology, mechanisms and relevance, *Philosophical Transactions of the Royal Society B: Biological Sciences*, 371(1707), 20150496 (2016).
- [2] Yu, L., & Marchisio, M. A. Types I and V anti-CRISPR proteins: From phage defense to eukaryotic synthetic gene circuits, *Frontiers in Bioengineering and Biotechnology*, 8 (2020).
- [3] Bondy-Denomy, J., Davidson, A. R., Doudna, J. A., Fineran, P. C., Maxwell, K. L., Moineau, S., Peng, X., Sontheimer, E. J., & Wiedenheft, B. A unified resource for tracking Anti-CRISPR Names, *The CRISPR Journal*, 1(5), 304–305 (2018).
- [4] Koonin, E. V, Makarova, K. S. and Zhang, F. Diversity, classification and evolution of CRISPR-Cas systems, *Current opinion in microbiology*, 37, pp. 67–78 (2017).

CLONING, PURIFICATION AND *IN VIVO* ACTIVITY OF A NOVEL BACTERIAL DEFENSE SYSTEM

Marija Duchovskyte¹, Dalia Smalakyte¹, Gintautas Tamulaitis¹

¹ Institute of Biotechnology, Life Sciences Center, Vilnius University, Lithuania
marija.duchovskyte@chgf.stud.vu.lt

To avert frequent viral infections, prokaryotes have developed numerous defense systems. It was found that in bacterial and archaeal genomes phage defense systems tend to be clustered in regions called “defense islands” [1]. This observation led to identification of novel antiviral systems by examining uncharacterized genes located in close vicinity to genes encoding well-known bacterial defense systems. One of recently discovered systems that assists bacteria to conquer phage infection is named Septu [2].

Septu defense system, isolated from bacteria of *Bacillus* genus, consists of two proteins – PtuA, which contains ATPase domain, and HNH nuclease PtuB [2]. Surprisingly, Septu system of *B. thuringiensis* provides protection from not only *B. subtilis* but also *E. coli* phages [3]. In this study we present results of purification of proteins encoded by PtuAB operon and *in vivo* activity against *E. coli* phages of *B. thuringiensis* Septu defense system.

-
- [1] K. S. Makarova, Y.I. Wolf, S. Snir, E. V. Koonin. Defense islands in bacterial and archaeal genomes and prediction of novel defense systems. *J Bacteriol* 193(21), 6039-56 (2011).
- [2] S. Doron, S. Melamed, G. Ofir, A. Lopatina, M. Keren, G. Amitai, R. Sorek. Systematic discovery of antiphage defense systems in the microbial pangenome. *Science* 359(6379) (2018).
- [3] A. Stokar-Avihail, T. Fedorenko, J. Garb, A. Leavitt, A. Milman, G. Shulman, N. Wojtania, S. Melamed, G. Amitai, R. Sorek. Discovery of phage determinants that confer sensitivity to bacterial immune systems. *bioRxiv* (2022).

INVESTIGATION OF ANTIMICROBIAL PEPTIDE PEDIOCIN

Julija Petravičiūtė¹, Ramunė Stanevičienė², Elena Servienė², Jolanta Sereikaitė¹

¹ Department of Chemistry and Bioengineering, Vilnius Gediminas Technical University, Lithuania

² Nature Research Centre, Lithuania

julija.petraviciute@stud.vilniustech.lt

The food industry is at a crossroad between the production of healthy organic food which is usually prone to microorganisms that cause foodborne diseases, and the making of products with exceptional organoleptic properties and long shelf life but containing harmful chemicals such as artificial preservatives. This problem can be solved by implementing the use of bacteriocins. These compounds are small antimicrobial peptides ribosomally synthesized by lactic acid bacteria (LAB). Bacteriocins act as natural preservatives that kill bacteria closely related to their producer strain [1]. This specialty makes these peptides applicable as an alternative for antibiotics or anticancer agents as bacteriocins are target-oriented and rarely interact with the cells outside of their activity spectrum [2,3].

One of the most studied bacteriocins is pediocin. This heat-stable non-modified peptide exhibits bacteriostatic and bactericidal activity against gram-positive bacteria, especially *Listeria monocytogenes* [4], by forming pores in the target membrane [5]. Pediocin has been purified using different methods [6]. However, the yields acquired have been lower than expected. In addition, the continued experiments suggest that the studied pediocin produced by *Pediococcus acidilactici* JEM-1 has a lower molecular weight than the theoretical one. Therefore, the aim of this study is to find and perform efficient purification methods for the characterization of the pure pediocin. The previously employed single-step purification of ion-exchange chromatography is adjusted by replacing the SP-Sepharose resin with CM-Sepharose in order to avoid the interaction between the resin and colored impurities from the bacteria culture media. Moreover, the purification is supplemented with a dialysis step which is necessary to eliminate salts and the aforementioned impurities. The effectiveness of the methods is assessed by measuring antimicrobial activity. These procedures will be followed by the optimization of the purification scheme and the investigation of the final product.

[1] S. Ennahar, T. Sashihara, K. Sonomoto, A. Ishizaki, Class IIa bacteriocins: biosynthesis, structure and activity, *FEMS Microbiology Reviews*, **24** (1), 85–106 (2000).

[2] B. Fernandez, C. Le Lay, J. Jean, I. Fliss, Growth, acid production and bacteriocin production by probiotic candidates under simulated colonic conditions, *Journal of Applied Microbiology*, **114** (3), 877–885 (2013).

[3] S. Kaur, S. Kaur, Bacteriocins as Potential Anticancer Agents, *Frontiers in Pharmacology* **6** (NOV) (2015).

[4] S. V. Balandin, E. V. Sheremeteva, T. V. Ovchinnikova, Pediocin-Like Antimicrobial Peptides of Bacteria, *Biochemistry (Moscow)* **84** (5), 464–478 (2019).

[5] J. M. Rodríguez, M. I. Martínez, J. Kok, Pediocin PA-1, a wide-spectrum bacteriocin from lactic acid bacteria, *Critical Reviews in Food Science and Nutrition*, **42** (2), 91–121 (2002).

[6] B. Vijay Simha, S. K. Sood, R. Kumariya, A. K. Garsa, Simple and rapid purification of pediocin PA-1 from *Pediococcus pentosaceus* NCD 273 suitable for industrial application, *Microbiological Research*, **167** (9), 544–549 (2012).

YEAST SURFACE DISPLAY OF *ACINETOBACTER BAUMANNII* BLP1 PROTEIN C-TERMINAL FRAGMENT

Ieva Šapronytė¹, Arūnė Verbickaitė¹, Indrė Dalgėdienė², Julija Armalytė³, Rasa Petraitytė-Burneikienė¹

¹ Institute of Biotechnology, Department of Eukaryote Gene Engineering, Life Sciences Center, Vilnius University, Lithuania

² Institute of Biotechnology, Department of Immunology, Life Sciences Center, Vilnius University, Lithuania

³ Institute of Biosciences, Life Sciences Center, Vilnius University, Lithuania

ieva.sapronyte@gmc.stud.vu.lt

Acinetobacter baumannii is a gram-negative bacterium, that is widespread in hospitals and causes soft tissue infections such as pneumonia and meningitis, or sepsis in immunocompromised patients. The clinical *A. baumannii* infection treatment has become challenging due to rapid emergence of multidrug-resistant strains [1]. In 2017, the World Health Organization named *A. baumannii* as a top priority pathogen in critical need of new therapeutic approaches [2]. Additionally, the COVID-19 pandemic has increased the rate of coinfections or secondary infections caused by multidrug-resistant *A. baumannii* that are directly associated with poor clinical outcomes, prolonged hospitalization, and higher mortality risk [3].

Vaccination is a promising strategy for preventing *A. baumannii* infections. Currently, there are no vaccine candidates that have stepped into clinical trials. The development of vaccines is complicated by a thick polysaccharide capsule that protects the bacterium and shields most outer membrane proteins from immune recognition [4]. Nonetheless, some proteins, such as Blp1, can penetrate the capsule, enabling the pathogen to adhere to host epithelium cells and form biofilms. Previous studies using active and passive immunizations have shown that surface-exposed C-terminal 711 amino acid length fragment of Blp1 is a suitable vaccine candidate and protects mice from *A. baumannii* infection. Conveniently, within this fragment, a stretch of 163 amino acids is conserved and therefore fit as a universal antigen to target the most prevalent *A. baumannii* clinical strains [5].

The yeast surface display technology has potential in prototyping of oral vaccines against various pathogens. The display of antigens on the yeast surface occurs through cell wall proteins, such as α -agglutinin. *Saccharomyces cerevisiae* cell wall protein α -agglutinin consists of two subunits Aga1 and Aga2. The antigen is expressed as a fusion with Aga2 subunit, linked by two disulfide bonds to cell wall-anchored Aga1 subunit. Importantly, *S. cerevisiae* has GRAS (Generally Recognized As Safe) status, which allows its use in food and drug production. Finally, it is worth noting that the immunostimulatory properties of yeast cell wall major component β -glucan allow yeast cells to serve not only as a vaccine carrier but also as an immune adjuvant [6].

The aim of this study was to immobilize the C-terminal fragment of *A. baumannii* Blp1 protein on the surface of *S. cerevisiae*. Fusion protein composed of conserved 163 amino acid fragment of the target protein and Aga2 subunit was displayed on yeast cell surface. Antigen expression and display was confirmed by western blot analysis and visualized by immunofluorescence microscopy. Flow cytometry analysis indicated that 48.5% of singlets displayed the conserved fragment of *A. baumannii*. These initial results provide compelling evidence that the yeast surface display technology has bright prospects in development of oral vaccine candidate against *A. baumannii*.

[1] N. A. Mat Rahim, H. Y. Lee, U. Strych et al. Facing the challenges of multidrug-resistant *Acinetobacter baumannii*: progress and prospects in the vaccine development. *Human Vaccines & Immunotherapeutics*. 17(10), 3784 (2021).

[2] World Health Organization. Guidelines for the prevention and control of carbapenem-resistant Enterobacteriaceae, *Acinetobacter baumannii* and *Pseudomonas aeruginosa* in health care facilities. Geneva: World Health Organization (2017).

[3] K. Rangel, S. G. De-Simone. *Acinetobacter baumannii* during COVID-19: What Is the Real Pandemic? *Pathogens*. 12(1), 41 (2023).

[4] P. S. Gellings, A. A. Wilkins, L. A. Morici. Recent Advances in the Pursuit of an Effective *Acinetobacter baumannii* Vaccine. *Pathogens*. 9(12), 1066 (2020).

[5] J. Skemiškytė, E. Karazijaitė, J. Deschamps et al. Blp1 protein shows virulence-associated features and elicits protective immunity to *Acinetobacter baumannii* infection. *BMC Microbiology* 19(1), 1–12 (2019).

[6] Y. Tan, L. Chen, K. Li et al. Yeast as carrier for drug delivery and vaccine construction. *Journal of Controlled Release* 346, 358–379 (2022).

TOWARDS SIDE-EFFECT FREE ANTICANCER THERAPY

Reda Rulinskaitė¹, Rūta Palepšienė¹, Saulius Šatkauskas¹, Renaldas Raišutis², Martynas Maciulevičius¹

¹Biophysical Research Group, Vytautas Magnus University, Lithuania
²Ultrasound Research Institute, Kaunas University of Technology, Lithuania
reda.rulinskaite@vdu.lt

In cancer treatment, the primary goal is to find an effective way to reduce the size of a cancerous tumor by leaving no side effects. Since bleomycin is cytotoxic, it is frequently used in chemotherapy to treat cancer [1]. Despite the fact that bleomycin reduces or stops the growth of a tumor, drug can lead to severe or fatal side effects, such as pulmonary injury progressing into pulmonary fibrosis [2]. Chemotherapy has a variety of side effects that slow down the time necessary for recovery.

Calcium (Ca^{2+}) ions are immensely vital for normal cell and tissue function being an intracellular second messenger that is involved in signal transduction pathways and many cellular metabolic processes [3]. Ca^{2+} is currently used in anti-cancer treatment: calcium electroporation has been proven to be an effective anti-cancer treatment method [4].

Sonoporation (SP) involves non-invasive application of medical ultrasound (US) in combination with microbubbles (MBs) in order to attain spatio-temporally controlled anticancer drug delivery to cells and tissues. Although SP could have greater potential in treating cancer than electroporation, Ca^{2+} delivery and possible applications for sonotherapy are poorly investigated. The employment of Ca^{2+} for cancer treatment would allow to significantly diminish detrimental side-effects, imposed by conventional cytotoxic drugs.

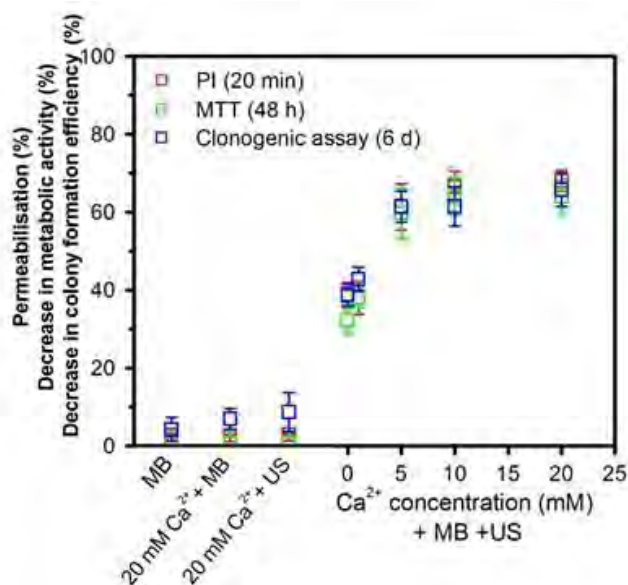


Fig. 1. Similar levels of membrane permeabilization (propidium iodide (PI) assay, 20 min), metabolic activity (MTT test, 48h) and cell viability (clonogenic assay, 6 days) evaluated in different groups after Ca^{2+} delivery via SP.

Our preliminary data indicate that Ca^{2+} (5 mM) induces rapid (within 20 min) cell death of Chinese hamster ovary cells as cell viability assays, performed at different time periods, indicate similar results (Fig. 1). Fast cellular response after Ca^{2+} delivery via SP would offer new opportunities for initiating effective and rapid (< 20 min) cell death by intrinsic Ca^{2+} activated mechanisms as compared to slow (24 - 72 h) cell death, induced by chemo- or gene therapy [5].

- [1] L. M. Mir, S. Orłowski, J. Belehradek, C. Paoletti, Electrochemotherapy potentiation of antitumour effect of bleomycin by local electric pulses, *European Journal of Cancer and Clinical Oncology* **27**, 68-72 (1991).
[2] N. Saccone, J. Bass, M. L. Ramirez, Bleomycin-Induced Lung Injury After Intravenous Iron Administration, *Cureus*, **14** (2022).
[3] L. Conrard, D. Tyteca, Regulation of Membrane Calcium Transport Proteins by the Surrounding Lipid Environment, *Biomolecules* **9**, 513 (2019).
[4] S. K. Frandsen, M. Vissing, J. Gehl, A Comprehensive Review of Calcium Electroporation - A Novel Cancer Treatment Modality, *Cancers* **12**, 290 (2020).
[5] M. Maciulevičius, D. Navickaitė, S. Chopra, B. Jakštys, S. Šatkauskas, Sudden Cell Death Induced by Ca^{2+} Delivery via Microbubble Cavitation, *Biomedicines* **9**, 32 (2021).

MICROFLUIDIC CHIP FABRICATION FOR ELECTROPORATION OF CELLS

Kamilė Kasperavičiūtė¹, Eivydas Andriukonis¹, Arūnas Stirke¹

¹ Vilnius university, Life Sciences Center, 7 Saulėtekio Ave, Vilnius, Lithuania

² Laboratory of Bioelectrics, Center for Physical Sciences and Technology, Saulėtekio av. 3, Vilnius, Lithuania

kamile.kasperaviciute@gmc.stud.vu.lt

Microfluidics is a new technique to produce high sensitivity, high speed, high throughput, and cost-efficient analysis by manipulating fluids using microfabricated channel and chamber structures. Additionally, its use in high-level chemical, biological and physical analyses and affordable point-of-care assays are rapidly expanding [1]. The capacity to regulate cell microenvironment factors at pertinent length and time scales is one of microfluidics' main advantages [2]. Microfluidics and the creation of microfluidic chips is key to development of molecular sensors based on bioassays, such as immunoassay, cell separation, DNA amplification, imitation of biological and physiological conditions, membrane systems and other analysis. Microfluidic chip channels and chambers usually are made via high precision methodologies such as lithography and then transferred to a castable material such as silicone (polydimethylsiloxane - PDMS) or other. Currently, due to rapid expansion in desktop resin printers, fast prototyping of microfluidic devices or small scale production became much more accessible. Herein, we present PDMS casting methodologies and tooling for advanced, high quality, and dimensional accuracy PDMS microfluidic devices for electroporation of cells and fast laboratory oriented applications. Methodologies are oriented for secondary clear resin casting (such polymers as Off-stoichiometry thiol-ene polymer) using PDMS master molds for microfluidic device manufacturing.

[1] Ren, Kangning, Jianhua Zhou, and Hongkai Wu. 2013. "Materials for Microfluidic Chip Fabrication." *Accounts of Chemical Research* 46 (11): 2396–2406. <https://doi.org/10.1021/ar300314s>.

[2] Young, Edmond W. K., and David J. Beebe. 2010. "Fundamentals of Microfluidic Cell Culture in Controlled Microenvironments." *Chemical Society Reviews* 39 (3): 1036–48. <https://doi.org/10.1039/B909900J>.

IDENTIFICATION AND HETEROLOGOUS BIOSYNTHESIS OF NOVEL BACTERIOCINS WITH THE ANTI-PHYTOPATHOGENIC BACTERIAL ACTIVITY

Gabija Smulkaitė¹, Arnoldas Kaunietis¹

¹Department of Microbiology and Biotechnology, Institute of Biosciences, Life Sciences Center, Vilnius University, Vilnius, Lithuania
gabija.smulkaite@gmc.stud.vu.lt

An increasing antimicrobial resistance among phytopathogenic bacteria has shown significant problems in the soil ecosystem, since these pathogens can cause variety of plant diseases as well as economic damage to various plant crops. In 2019, losses from phytopathogen-caused illnesses in five major crops, wheat, rice, maize, potato, and soybean, were 10.2 %, 10.8 %, 8.5 %, and 8.9 %, respectively [1]. Current methods used to control these plant pathogens are chemicals, which could be harmful for the environment and threatening to human health [2]. Therefore, bacteriocins, a heterogeneous group of ribosomally synthesized antimicrobial peptides with the ability to kill closely related or a diverse range of bacteria species, could be used to overcome this problem [3]. Bacteriocins are much safer to use than some of the chemicals, moreover, due to their specificity towards purposive targets it comes off with no side effects.

The aim of this study was to identify bacteriocins that are secreted by microorganisms that have been isolated from the soil and may have an impact on phytopathogenic bacteria. 63 isolates were isolated from the soil and screened in order to evaluate their antibacterial activity against 9 phytopathogenic bacteria strains, such as *Pectobacterium carotovorum*, *Xanthomonas vesicatoria*, etc. We successfully identified two bacteria strains: *Streptomyces* sp. AB3 and *Bacillus* sp. DM1.10 that produce antibacterial substances. Genome analysis of AB3 and DM1.10 strains revealed gene clusters associated with bacteriocin biosynthesis. One of the AB3 gene clusters is presumably responsible for biosynthesis of a lasso peptide type bacteriocin. In this study, we describe heterologous expression of genes responsible for the lasso peptide bacteriocin biosynthesis in *Escherichia coli* cells.

-
- [1] Savary S, Willocquet L, Pethybridge SJ, Esker P, McRoberts N, Nelson A. The global burden of pathogens and pests on major food crops. *Nat Ecol Evol.* 2019;3(3):430-439.
[2] Rooney WM, Chai R, Milner JJ, Walker D. Bacteriocins Targeting Gram-Negative Phytopathogenic Bacteria: Plantibiotics of the Future. *Front Microbiol.* 2020;11:575981.
[3] Holtmark I, Eijsink VG, Brurberg MB. Bacteriocins from plant pathogenic bacteria. *FEMS Microbiol Lett.* 2008;280(1):1-7.

CHARACTERIZATION OF NOVEL CRISPR-CAS12 EFFECTOR COMPLEXES

Brigita Duchovska¹, Greta Bigelytė¹, Rimantė Žedaveinytė¹, Arūnas Šilanskas¹, Tautvydas Karvelis¹

¹Department of Protein-DNA Interactions, Institute of Biotechnology, Vilnius University, Lithuania
brigita.duchovska@gmc.stud.vu.lt

CRISPR–Cas (Clustered Regularly Interspaced Short Palindromic Repeats – CRISPR associated protein) – prokaryotic defence systems, which provide resistance against foreign mobile genetic elements and have a wide range of genome editing and other biotechnological applications. Due to their ease of programmability, Cas9, and Cas12a, representative effector proteins of class 2 CRISPR-Cas systems, became the most commonly used CRISPR-Cas molecular tools in genome engineering to date [1]. Guided by short and easily interchangeable RNA molecules, these proteins can be programmed to target any DNA sequence of need. However, in *in vivo* therapy, the delivery of such nucleases to cells is limited by the capacity of adeno-associated viruses (AAVs) and the packaging of large Cas12a (850-1400 aa) or Cas9 (1000-1600 aa) nuclease-coding genes into these carriers remains complicated [2]. As a result, recent efforts have focused on expanding the number and characterizing new CRISPR-Cas systems to identify nucleases with novel properties. Smaller CRISPR-Cas nucleases in particular are being sought to treat hereditary genetic disorders *in vivo* using AAV although the functional diversity of these compact nucleases remains poorly explored.

Here, we describe a selection of novel Cas12 protein candidates, ranging from 500-700 aa in size. Using a selection of biochemical approaches, we characterize key elements of such Cas12 effectors complexes and their activities on nucleic acid targets. Altogether, this study expands the CRISPR-Cas toolbox and provides a thorough characterization of DNA target elements, needed for successful RNA-guided interference.

[1] Makarova, K. S., Wolf, Y. I., Iranzo, J., Shmakov, S. A., Alkhnbashi, O. S., Brouns, S. J. J., Charpentier, E., Cheng, D., Haft, D. H., Horvath, P., Moineau, S., Mojica, F. J. M., Scott, D., Shah, S. A., Siksnyš, V., Terns, M. P., Venclovas, Č., White, M. F., Yakunin, A. F., ... Koonin, E. V. (2020). Evolutionary classification of CRISPR–Cas systems: A burst of class 2 and derived variants. *Nature Reviews Microbiology*, 18(2), 67–83. <https://doi.org/10.1038/s41579-019-0299-x>

[2] Holkers, M., Maggio, I., Henriques, S. F. D., Janssen, J. M., Cathomen, T., & Gonçalves, M. A. F. V. (2014). Adenoviral vector DNA for accurate genome editing with engineered nucleases. *Nature Methods*, 11(10), 1051–1057. <https://doi.org/10.1038/nmeth.3075>

INHIBITION OF BACTERIAL ANTIVIRAL CRISPR-CAS SYSTEM

Melita Graužinytė¹, Tomas Šinkūnas¹

¹Department of Protein-Nucleic Acids Interactions, Institute of Biotechnology, Life Sciences Center, Vilnius University,
Lithuania
melita.grauzinyte@gmc.stud.vu.lt

The battle between bacteria and bacteriophages has led to the development of defense mechanisms such as the CRISPR-Cas system by bacteria. This system uses ribonucleoprotein complexes to detect and destroy the DNA of invading phages [1]. To counteract this defense, bacteriophages encode small repressors called anti-CRISPR (Acr) proteins. These Acr proteins interact with the effector complex, preventing either the recognition or hydrolysis of DNA [2]. CRISPR-Cas has become a valuable tool for genome editing, while Acr proteins have been used to regulate this tool in both prokaryotes and eukaryotes [3]. To date, more than 100 Acr families have been identified. However, the molecular mechanism is characterized only for a small fraction of these proteins [4].

Here, we analyse Acr proteins that inhibit the type I-F CRISPR-Cas system from *Pseudomonas aeruginosa*. We identified the Acr protein blocking the system in bacterial cells. Then, purified the protein and by employing biochemical methods we studied its interplay with the CRISPR-Cas components. Our findings provide insight into the molecular mechanism of this uncharacterized Acr protein.

-
- [1] Liu, T. Y., & Doudna, J. A. (2020). Chemistry of Class 1 CRISPR-Cas effectors: Binding, editing, and regulation. *Journal of Biological Chemistry*, 295(42), 14473–14487.
- [2] Bondy-Denomy, J., Pawluk, A., Maxwell, K. L., & Davidson, A. R. (2013). Bacteriophage genes that inactivate the CRISPR/Cas bacterial immune system. *Nature*, 493(7432), 429–432.
- [3] Marino, N. D., Pinilla-Redondo, R., Csörgő, B., & Bondy-Denomy, J. (2020). Anti-CRISPR protein applications: natural brakes for CRISPR-Cas technologies. *Nature Methods* 2020 17:5, 17(5), 471–479.
- [4] Jia, N., & Patel, D. J. (2021). Structure-based functional mechanisms and biotechnology applications of anti-CRISPR proteins. *Nature Reviews Molecular Cell Biology* 2021 22:8, 22(8), 563–579.

VIABILITY OF *E. COLI* COMPETENT CELLS USING CRYOPROTECTANTS

¹Saulė Rapalytė, ¹P. Šimonis, ¹Greta Gančytė, ¹Arūnas Stirke

¹Laboratory of Bioelectronics, Center for Physical Sciences and Technology, Lithuania
s.rapalyte@gmail.com

Effective method for bacteria transformation is using pulsed electric field (PEF), known as electroporation. PEF affects plasma membrane causing pores to form in it thus enhancing cells' permeability to various extracellular substances. While performing electro-transformation exogenous DNA is inserted into a competent cell by means of reversible electroporation – in viable cells foreign genes are inherited upon cell division [1]. *Escherichia coli* cells, commonly used for electro-transformation, are stored in cold temperatures. However, freezing causes intracellular water crystallization which is lethal [2]. Water crystallisation damage can be minimized by using cryoprotectants, such as glycerol and trehalose.

Mentioned cryoprotectants were used to investigate their impact on *E. coli* viability after freezing. Different pulsed electric field strength values were tested to find optimal parameters for glycerol and trehalose insertion to prepare competent *E. coli* cells for further transformation efficiency studies.

Experiments were done with *E. coli* strain DH5 α . Bacteria were grown until 0.5 OD, then centrifuged and resuspended in one of three electroporation solutions: 20% glycerol, 0.1 M trehalose, and MiliQ water was used for control samples. *E. coli* suspension, held in ice bath during the whole experiment, was electroporated with single electric field pulse with duration of 100 μ s and field strength up to 20 kV/cm. Immediately after electroporation cells were transferred to a freezer with -80 °C for a 7 day period. Then cells were defrosted, transferred to a SOC medium and incubated for one hour in 37 °C, serial dilutions and plating were performed after. Cells were plated on agar medium and grown for two days in 30 °C temperature. Counted colony forming units (CFU) were used to evaluate *E. coli* viability (Fig. 1).

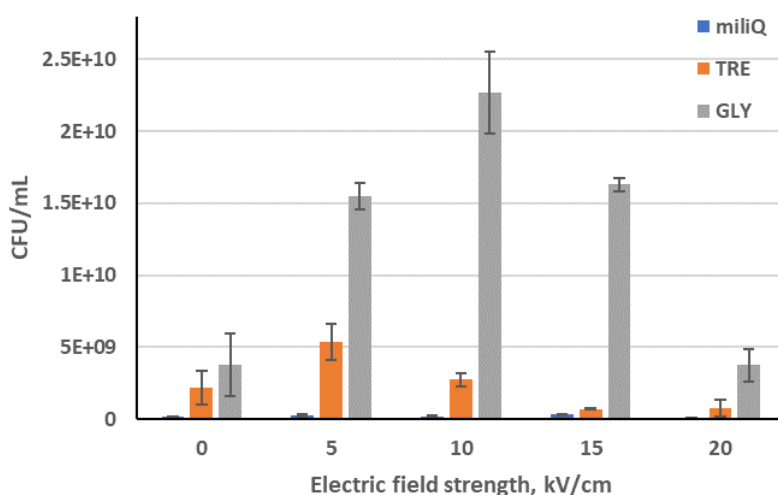


Fig. 1. *E. coli*, incubated in 0.1 M trehalose (depicted in orange), 20 % glycerol (depicted in grey) and miliQ (depicted in blue) prior to freezing, viability dependence on electric field strength.

Results revealed that *E. coli* viability after freezing does depend on both cryoprotective substances inserted into cells and electric field strength application used to insert these cryoprotectants. It was shown that electroporating cells with 5 kV/cm electric field strength before freezing had increased their viability in MiliQ and trehalose solutions, however, bacteria in glycerol solution were affected negatively. For glycerol 10 kV/cm strength was most effective in achieving higher colony unit forming count. *E. coli* viability has significantly diminished after being treated with stronger electric fields due to electroporation itself causing irreparable damage prior to freezing.

To conclude, cryoprotectants that were inserted into *E. coli* during electroporation before freezing have a positive impact on cells' viability.

[1] T. Kotnik, W. Frey, M. Sack, S. Haberl Megličič, M. Peterka, D. Miklavčič, "Electroporation-based applications in biotechnology", Cellpress, TIBTEC-1273; No. of Pages 9, (2015)

[2] P. Mazur, "Freezing of living cells: mechanisms and implications", American Journal of Physiology-Cell Physiology 1984 247:3, C125-C142, (1984)

MILK PERMEATE AS AN ALTERNATIVE TO ISOPROPYL β -D-1-THIOGALACTOPYRANOSIDE FOR THE INDUCTION OF RECOMBINANT PROTEIN SYNTHESIS

Aurimas Greičius¹, Renata Gudiukaitė¹

¹ Institute of Biosciences, Life Sciences Center, Vilnius University, Saulėtekis ave. 7., LT-10257 Vilnius, Lithuania
aurimas.greicius@gmc.stud.vu.lt

The use of Isopropyl β -D-1-thiogalactopyranoside (IPTG) has been the primary method to induce recombinant protein synthesis in systems operating with the lac repressor. However, IPTG has limitations due to its toxicity to cells as well as its cost. This poster aims to present that milk permeate (MP), a waste product of the dairy industry that is produced when milk is filtered to remove most of its fat, is a viable alternative to IPTG.

As the biotechnology industry continues to grow, competition raises the bar to find cheaper and more sustainable alternatives to currently used practices. The most popular inducer of recombinant protein synthesis, namely IPTG, has an astonishing cost of around 100\$ per gram. On the other hand, the price of MP is as low as 10\$ per 25 kg. Thus, using MP alleviates the cost issues arising from the use of IPTG while adhering to circular economy principles.

It has been shown that IPTG not only itself is toxic, but also exacerbates the toxicity of substrates, causing additional stress to host cells, whereas using the natural inducer of P lac drastically alleviates the stress without compromising the efficiency of induction [1]. Milk permeate, primarily composed of lactose, is thought to have similar stress alleviation to that of lactose when compared to IPTG, thus MP appears to be a better alternative to IPTG especially for longer induction times.

In this study, experiments using MP as an inducer for recombinant protein synthesis were carried out. First, optimal conditions for recombinant synthesis were found, followed by experiments which revealed that MP indeed produces recombinant proteins, using two control inducers: lactose and IPTG. Synthesis induction of a variety of recombinant proteins was performed, their length varied from 23 kDa to 99 kDa. As the synthesized recombinant proteins were enzymes, it was additionally shown that the proteins resulting from the induction with MP were active, using Zymography methods.

Acknowledgements: This research has received funding from the Research Council of Lithuania (LMTLT), project registration no. P-SV-22-160.

[1] Dvorak, P., Chrast, L., Nikel, P.I. et al. Exacerbation of substrate toxicity by IPTG in *Escherichia coli* BL21(DE3) carrying a synthetic metabolic pathway. *Microb Cell Fact* 14, 201 (2015).

IMAGING OF GLUCOSE OXIDASE ACTIVITY BY SCANNING ELECTROCHEMICAL MICROSCOPY

Tomas Mockaitis¹, Wojciech Nogala², Agnė Boguševičė³, Kasparas Kižys¹, Inga Morkvėnaitė-Vilkončienė¹

¹Center for Physical Sciences and Technology, Department of Chemical Engineering and Technology Lithuania

²Institute of Physical Chemistry, Polish Academy of Sciences, Poland

³Panevėžys Republic Hospital, Department of Surgery, Lithuania

tomas.mockaitis@ftmc.lt

Since its discovery in 1928, glucose oxidase (GOx) is still one of the most studied enzymes worldwide because of its various industrial applications: textile bleaching, food and baking industry or for the production of gluconic acid, but the most well-known application of glucose oxidase is its use in daily and continuous glucose sensors for diabetes management [1]. GOx may also find applications in glucose/O₂ biofuel cell or self-power sensors [2]. The greatest benefits of glucose oxidase over other sugars enzymes for bioelectrochemical applications are its high specificity for glucose, low redox potential (~ -0.42V vs. Ag/AgCl at pH 7.4) and good thermostability [3]. These properties allow scanning electrochemical microscopy (SECM) to efficiently exploit the unique properties of such enzymes using probes. SECM employs ultramicroelectrodes (UMEs) that can be moved in the proximity of a surface while recording a faradaic current, which depends on both the topography and the electrochemical activity of the surface itself [4].

The aim of this study was to determine GOx activity with different K₃[Fe(CN)₆] concentrations (0.5, 0.75, 1.0, 1.5, 2.0 mM) using tip generation – substrate collection mode scanning electrochemical microscopy of oxygen reduction electrocatalysts. Glucose concentration was 10 mM and Au UME (5 μM) was used as a probe for SECM measurements.

[1] N. Mano, Engineering glucose oxidase for bioelectrochemical applications, *Bioelectrochemistry*, **128**, 218 – 240 (2019).

[2] N. Mano, & A. de Poulpique, O₂ Reduction in Enzymatic Biofuel Cells, *Chemical Reviews*, **118**, 2392 – 2468 (2018).

[3] S.Vogt, M. Schneider, H. Schäfer-Eberwein, & G. Nöll, Determination of the pH Dependent Redox Potential of Glucose Oxidase by Spectroelectrochemistry, *Analytical Chemistry*, **86**, 7530 – 7535 (2014).

[4] A. Soldà, G. Valenti, M. Marcaccio, M. Giorgio, P. G. Pelicci, F. Paolucci, & S. Rapino, Glucose and lactate miniaturized biosensors for SECM-based high-spatial resolution analysis: a comparative study, *ACS sensors*, **2**(9), 1310 – 1318 (2017).

DEVELOPMENT OF MONOCLONAL ANTIBODIES AGAINST ANTIBIOTIC RESISTANCE PROTEINS OXA-48, OXA-134, SME-3, ADC-144 AND SHV-42

Gabija Lauciūtė¹, Vytautas Rudokas¹, Laima Čepulytė¹, Karolina Juškaitė¹, Martynas Simanavičius¹, Aurelija Žvirblienė¹

¹Department of Immunology, Institute of Biotechnology, Life Sciences Center, Vilnius University, Lithuania
gabija.lauciute@gmc.vu.lt

Antimicrobial resistance (AMR) is the largest global health threat in the 21st century and it requires urgent measures. Major reasons behind the emergence of AMR - misusing and overusing different antibacterial agents in healthcare settings [1]. One of the steps in limiting the spread of AMR is accurate diagnostics of the disease and prescription of effective antibiotics. Currently applied diagnostic methods include phenotyping, biochemical, and genotyping methods which tend to be expensive and protracted. Immunodetection, on the other hand, is a rapid, specific, and sensitive method for identifying resistance factors. However, the lack of highly specific monoclonal antibodies (MABs) limits the development of immunodiagnostic tests.

The aim of this study was to generate and characterize MABs against five antibiotic resistance factors – β -lactamases OXA-48, OXA-134, SHV-42, ADC-144, and SME-3, which are widespread in pathogenic *Enterobacteriaceae* and confer resistance to carbapenems, penams and cephalosporins [2,3,4]. Using hybridoma technology three specific anti-OXA-48, three specific anti-OXA-134, two specific anti-SHV-42, two specific anti-ADC-144, and three specific anti-SME-3 MABs secreting cell lines were developed. Ten out of thirteen generated MABs were shown to have high affinity towards respective antigens and twelve recognize linear epitopes. One anti-OXA-134, one anti-SME-3, and one anti-ADC-144 monoclonal antibody pair were shown to have the potential to be applied in the development of antibiotic resistance factors detection tools.

[1] World Health Organization (2020) Antibiotic resistance [Fact sheet] <https://www.who.int/news-room/fact-sheets/detail/antibiotic-resistance>.

[2] Evans, B.A., Amyes, S.G.B. (2014) OXA β -Lactamases. *Clinical Microbiology Reviews*. 27(2), 241–263.

[3] Mulvey MR, Bryce E, Boyd D, Ofner-Agostini M, Christianson S, Simor AE, Paton S; Canadian Hospital Epidemiology Committee, Canadian Nosocomial Infection Surveillance Program, Health Canada. Ambler class A extended-spectrum beta-lactamase-producing *Escherichia coli* and *Klebsiella* spp. in Canadian hospitals. *Antimicrob Agents Chemother*. 2004 Apr;48(4):1204-14.

[4] Queenan AM, Shang W, Schreckenberger P, Lolans K, Bush K, Quinn J. SME-3, a novel member of the *Serratia marcescens* SME family of carbapenem-hydrolyzing beta-lactamases. *Antimicrob Agents Chemother*. 2006 Oct;50(10):3485-7.

PRO-INFLAMMATORY PROTEIN S100A9 ALTERS MEMBRANE ORGANIZATION BY DISPERSING ORDERED DOMAINS

Rimgailė Tamulytė¹, Evelina Jankaitytė¹, Zigmantas Toleikis², Darius Šulskis², Marija Jankunec¹

¹Institute of Biochemistry, Life Sciences Center, Vilnius University, Vilnius, Lithuania

²Institute of Biotechnology, Life Sciences Center, Vilnius University, Vilnius, Lithuania

rimgaile.tamulyte@bchi.stud.vu.lt

Pro-inflammatory, calcium-binding protein S100A9 is localized in the cytoplasm of a wide range of cells and regulates several intracellular and extracellular processes [1]. One of them is the participation in the inflammation associated with the pathogenesis of Alzheimer's disease (AD) [2]. The number of studies on the impact of S100A9 in co-aggregation processes with amyloid-like proteins is increasing. However, the interest in the interaction mechanism of protein S100A9 with biological membranes is still limited. In this work various biomimetic membrane models as lipid vesicles in solution and tethered lipid bilayers (tBLMs) were used to examine the interaction between the protein and the membrane surface. For this purpose we employed atomic force microscopy (AFM) and fluorescence spectroscopy techniques. Our results indicate that the damage induced by S100A9 in a calcium-free environment is mainly determined by membrane fluidity rather than by negatively charged lipids (Fig. 1). The most significant loss of integrity was observed in lipid bilayers composed of lipid mixture (brain total lipid extract). Furthermore, we demonstrate that the presence of Ca²⁺ ions promotes the membrane disruption induced by S100A9. These results might broaden the understanding of S100A9 interactions with lipid membrane and potentially affect the development of new diagnostic and therapeutic approaches for AD or other related diseases.

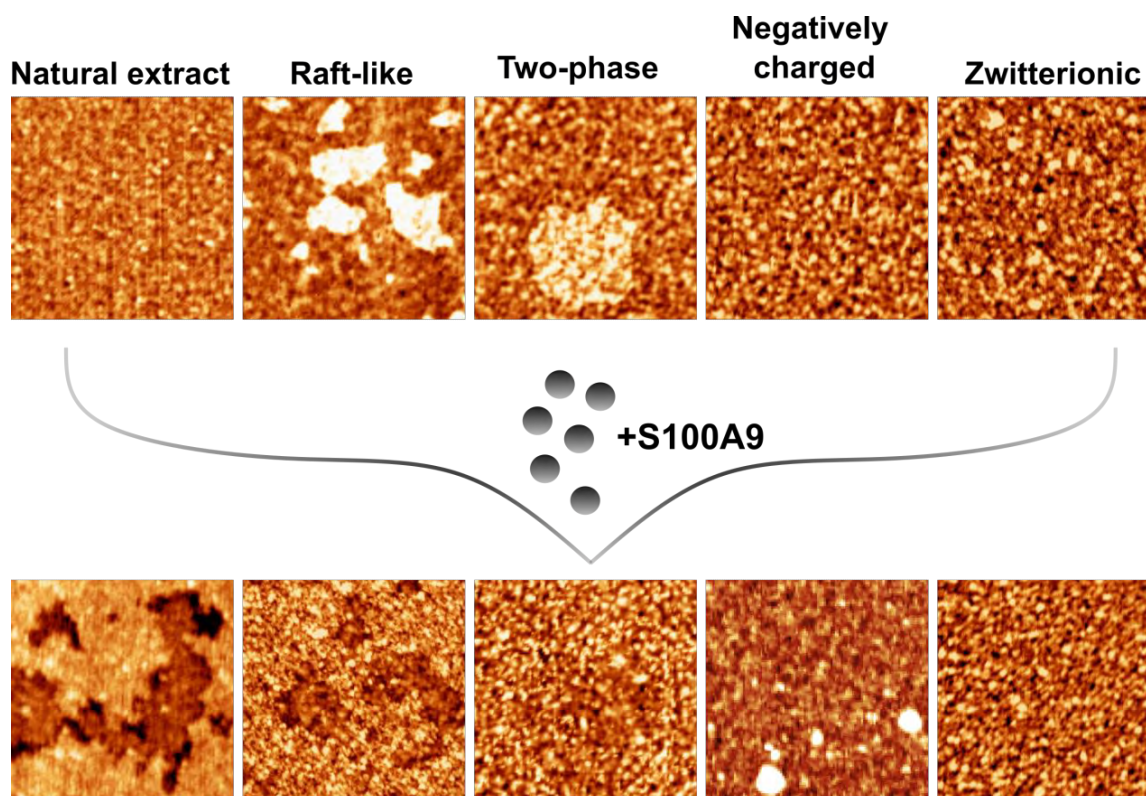


Fig. 1. AFM observation of phase-specific S100A9 interaction with tBLMs in a calcium-free environment. Lipid bilayers of different compositions were used: negatively charged, zwitterionic, composed of natural brain total lipid extract, enriched in raft-like or gel-like domains [3].

[1] C. Wang, I.A. Iashchishyn, J. Pansieri et al., S100A9-Driven Amyloid-Neuroinflammatory Cascade in Traumatic Brain Injury as a Precursor State for Alzheimer's Disease. *Sci Rep* **8**, 12836 (2018).

[2] T.Y. Ha, K.A. Chang, J.A. Kim et al., S100a9 knockdown decreases the memory impairment and the neuropathology in Tg2576 mice, AD animal model. *PLoS one* **5**, e8840 (2010).

[3] R. Tamulytė, E. Jankaitytė, Z. Toleikis et al., Pro-inflammatory protein S100A9 alters membrane organization by dispersing ordered domains. *BBA Biomembranes* **1865**, 184113 (2022).

SYNTHESIS OF *SACCHAROMYCES CEREVISIAE* L-BC VIRUS-LIKE PARTICLES IN *ESCHERICHIA COLI*

Kamilė Vaišaitė¹, Enrika Celitan¹, Saulius Serva¹

¹Vilnius university, Life Sciences Center, Vilnius, Lithuania
kamile.vaisaite@chgf.stud.vu.lt

Virus-like particles (VLPs) are multiprotein structures that mimic naturally occurring virions but lack genetic material and, therefore, are unable to replicate and cause infection. The major application of VLPs is vaccines and delivery of drugs, other bio- and nanomaterials [1]. Being known for cost-effective cultivation, high levels of protein expression and rapid cell growth, *Escherichia coli* is the most widely used bacterial expression system for VLP synthesis [2].

Two species of the virus family *Totiviridae*, L-A and L-BC, are presently known to infect *Saccharomyces cerevisiae*. They are double-stranded RNA viruses which pack their genomes into a capsid composed of a single major coat protein Gag and Gag-Pol fusion protein. Previous research has shown that Gag modification by Mak3-Mak10-Mak31 N-acetyltransferase complex is essential for L-A viral assembly, while L-BC can persist in host cells which lack the N-acetyltransferase complex [3]. Since L-BC Gag protein does not require N-acetylation, attempts to produce its VLPs in bacteria have been made.

The main aim of this study was to synthesize recombinant L-BC Gag protein that would successfully self-assemble into VLPs in *E. coli*. The L-BC Gag encoding sequence was incorporated into a bacterial expression vector and protein synthesis was initiated by double inducing system. The particles were purified from *E. coli* lysate by ultracentrifugation through sucrose cushion and cesium chloride, with a yield of 0.34 mg protein/g dry cell weight. Dynamic light scattering (DLS) method confirmed that L-BC Gag protein self-assembled into VLPs, the diameter of which was found to be 40.4±1.57 nm. This result is comparable to the diameter of native L-BC virions (38.5 nm), recently observed in another study [4]. Further research regarding cytotoxicity and stability of the synthesized VLPs is in progress before considering these VLPs as nanodelivery system.

[1] S. Nooraei, H. Bahrulolum, Z. Hoseini et al., Virus-like particles: preparation, immunogenicity and their roles as nanovaccines and drug nanocarriers, *Journal of Nanobiotechnology* 19:1, 19(1), 1–27 (2021).

[2] X. Huang, X. Wang, J. Zhang et al., *Escherichia coli*-derived virus-like particles in vaccine development, *Npj Vaccines* 2:1, 2(1), 1–9 (2017).

[3] R.B. Wickner, T. Fujimura, & R. Esteban, Viruses and prions of *Saccharomyces cerevisiae*, *Advances in Virus Research*, 86, 1 (2013).

[4] D. Grybchuk, M. Procházková, T. Füzik et al., Structures of L-BC virus and its open particle provide insight into Totivirus capsid assembly, *Communications Biology* 5, 847 (2022).

ACTION POTENTIALS IN *NITELLOPSIS OBTUSA* RHIZOIDS

Ilvika Maleckaitė¹, Vilmantas Pupkis¹, Indrė Lapeikaitė¹, Vilma Kisnierienė¹

¹Department of Neurobiology and Biophysics, Vilnius University, Vilnius, Lithuania
ilvika.maleckaite@gmc.stud.vu.lt

Characean internodal cells have been used by leading scientists in search of the mechanism of plant action potentials (APs) since the early 20th century [1]. High amplitude (up to 150 mV) and long duration (tens of seconds) of characean APs make them suitable to be registered extracellularly [2] and intracellularly [3] and used in biophysical research. However, electrical signaling of *Nitellopsis obtusa* unicellular chloroplast-free rhizoids, which anchor the body of algae to the substrate, has not been described previously. Therefore, wider research and analysis of rhizoids' properties would contribute to the extensive application of *Nitellopsis obtusa* cells, since rhizoids and internodal cells are distinct – rhizoids do not need constant lighting nor chloroplasts to carry out their functions [4].

Since the parameters describing electrical signaling of internodal cells of *Nitellopsis obtusa* have been characterized in detail, we aimed to explore the same parameters in their rhizoids as well. Electrophysiological experiments were conducted using intracellular microelectrode and two pair current clamp method placing an oblong cylinder-shaped rhizoid of *Nitellopsis obtusa* along the chamber with electrically isolated compartments.

Results show that *Nitellopsis obtusa* rhizoids are, in fact, excitable and their APs are more rapid. In comparison to the APs of internodal cells, APs of rhizoids do not have the overshoot (peak is negative) and the excitation threshold is more hyperpolarized: the amplitude of action potentials of rhizoids varies around 100 ± 3 mV, threshold: -140 ± 2 mV and peak: -40 ± 2 mV (n=28).

Summarizing current clamp results we affirm that neither constant lighting nor chloroplasts are needed for rhizoids in order to generate action potentials which can contribute to the algae's physiology, for example, gravitational sensing. However, further analysis of rhizoids' electrical active and passive properties should be carried out in order to determine additional possible applications of *Nitellopsis obtusa* rhizoids along the internodal cells in biophysical research.

[1] K. Umrath, Untersuchungen über plasma und plasmaströmung an Characeen. Protoplasma 9: 576– 597 (1930).

[2] T. Tabata, T. Sibaoka. Conduction velocity and blockage of action potential in Chara internodal cells. Plant Cell Physiol 28 (7): 1187– 1194 (1987).

[3] V. Kisnieriene, K. Trębacz. Evolution of long-distance signaling upon plant terrestrialization: comparison of action potentials in Characean algae and liverworts. Annals of Botany 130 (4): 457–475 (2022).

[4] JZ. Kiss. Gravitropism in the rhizoids of the alga Chara: a model system for microgravity research. Biol Bull 192:134–136 (1997).

Formation of tethered bilayer lipid membranes on gold surface probed by SEIRAS

Vaidas Pudžaitis¹, Martynas Talaikis², Gediminas Niaura^{1,2}

¹ Department of Organic chemistry, Center for Physical Sciences and Technology, Lithuania

² Institute of Biochemistry, Life Sciences Center, Vilnius University

vaidas.pudzaitis@ftmc.lt

Tethered bilayer lipid membranes (tBLMs) are widely used as a convenient biological membrane-mimicking platform to study biochemical and biophysical processes with great potential for biomedical applications [1]. Submembrane water reservoir plays an important role in tBLMs functionality and is affected by the composition and structure of anchoring self-assembled monolayers (SAMs). However, detailed molecular level information on the structure and formation in a solution of mixed SAMs used for tBLM construction is rather scarce [2]. That is largely due to the limited availability of techniques that are able to directly probe electrode/solution interface at the molecular level.

In this work, we used surface-enhanced infrared absorption spectroscopy (SEIRAS) for direct in-situ observation of two processes at gold-solution interface: mixed SAM monolayer formation from thiols (WC14 (20-(tetradecyloxy)-3,6,9,12,15,18,22-heptaohexatriacontane-1-thiol) and ME (2-mercaptoethanol)) followed by the development of lipid bilayer from multilamellar vesicles of deuterated phospholipid and cholesterol (DPPC-d₆₂/cholesterol-d₇).

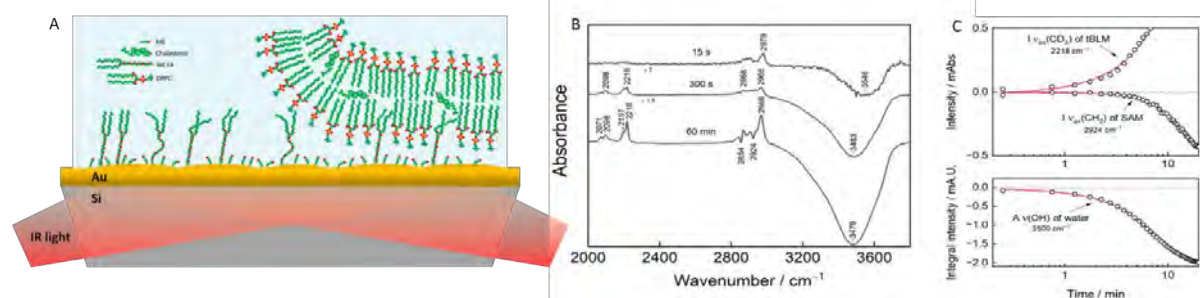


Fig. 1. (A) Pictorial representation of tBLM study using SEIRAS methodology. (B) SEIRAS-difference spectra captured at different times during the formation of the lipid layer of DPPC-d₇₅ and cholesterol-d₇ (60/40 mol%) on mixed SAM composed of WC14 and ME (30/70 mol%) in aqueous solution. (C) The dependence of $\nu_{\text{as}}(\text{CD}_3)$ of lipid layer, $\nu_{\text{as}}(\text{CH}_2)$ of SAM, and $\nu(\text{OH})$ of water spectral intensity on tBLM formation time.

Our study revealed that ethyleneglycol chains of long-chain thiol in SAM are in the predominant amorphous state, while alkyl chains are in the disordered state providing the required flexibility for the formation of the bilayer. The bilayer is formed in two stages (Fig 1A), first through lipid adsorption and simultaneous removal of water from the surface, and second through the lipid membrane inner layer insertion/interaction with SAM, resulting in structural changes of monolayer alkyl chains. We show, that around 60 minutes are required for the full development of the lipid bilayer formed from vesicles composed of a mixture of partially deuterated compounds DPPC-d₆₂/cholesterol-d₇.

[1] B.A. Cornell, V.L.B. Braach-Maksvytis et al., A biosensor that uses ion-channel switches, *Nature* **387**, 580 (1997).

[2] G. Valincius, D.J. McGillivray et al., Molecular-scale structural and functional characterization of sparsely tethered bilayer lipid membranes, *J. Phys. Chem. B*, **110**, 10213 (2006).

GLUCOSE DECORATED BOVINE SERUM ALBUMINE STABILIZED GOLD NANOCLUSTERS

Šantalė Šaliūtė^{1,2}, Greta Jarockytė¹, Vilius Poderys¹

¹ Biomedical Physics Laboratory, National Cancer Institute, P. Baublio str. 3b, LT-08406 Vilnius, Lithuania

² Department of Physics, Vilnius University, Saulėtekio ave. 9, LT-10222, Vilnius, Lithuania
santale.saliute@ff.stud.vu.lt

Gold nanoclusters (Au NCs) are promising nanocompounds that consists of from several to hundreds gold atoms. Stabilizing nanoclusters with proteins such as bovine serum albumin (BSA) may improve their biocompatibility, biodistribution and colloidal stability. Au NCs exhibit a long photoluminescence lifetime suggesting that they can be capable of reactive oxygen species generation [1]. Due to this, Au NCs are highly attractive as photosensitizer for photodynamic therapy. However, publications showed poor accumulation of Au NCs in cancer cells [2]. In order to improve uptake, Au NCs could be modified with molecules which would target to cancer cells. Usually, cancer cells have higher metabolism and glucose uptake compared to healthy cells. Moreover, they overexpress glucose transport proteins (Glut) which are assigned to be involved in increased transport of glucose in cells [3]. Therefore, glucose decorated BSA-Au NCs (Glu-BSA Au NCs) would be more likely accumulated by cancer cells.

In this study we investigated optical properties and colloidal stability of Glu-BSA Au NCs.

Glu-BSA gold nanoclusters were synthesized according to the previously reported procedure with slight modifications [3]. The optical properties were studied using absorption and fluorescence spectrometers. Photoluminescence spectrum of Glu-BSA gold nanoclusters solution ($\lambda_{\text{ex}} = 405 \text{ nm}$) has two bands in the visible region: a main peak with a maximum at 650 nm and another band of lower intensity at 480 nm. The photoluminescence excitation spectrum of a Glu-BSA Au NCs solution ($\lambda_{\text{em}} = 650 \text{ nm}$) had a band at about 500 nm and a gradual slope towards a region of longer wavelengths. Additionally, colloidal stability of nanoclusters had been studied for 6 weeks after synthesis using the same methods. Photoluminescence spectrum is almost the same 6 weeks after synthesis suggesting that Glu-BSA Au NCs solution stays stable for more than a month. To sum up, synthesized Glu-BSA gold nanoclusters have photoluminescence in red region, which fall into optical tissue transparency window. Also Glu-BSA Au NCs are stable and can be used for further studies and be investigated as photosensitizers for reactive oxygen species generation in cancer cells.

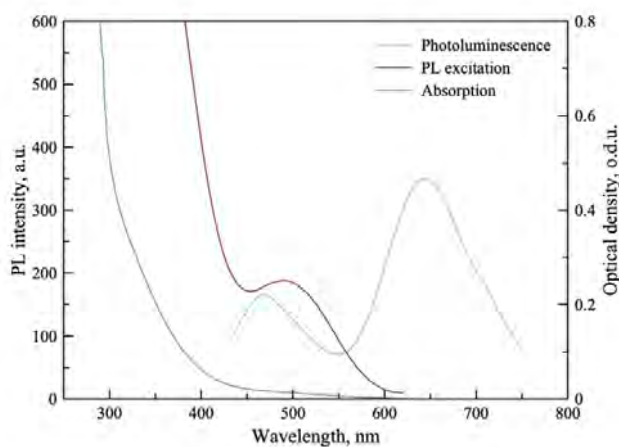


Fig. 1. Absorption (blue), PL excitation ($\lambda_{\text{em}} = 650 \text{ nm}$) (dark red), PL emission ($\lambda_{\text{ex}} = 405 \text{ nm}$) (green) spectra of Glu-BSA Au NCs.

[1] P. Zhang, X. X. Yang, Y. Wang, N. W. Zhao, Z. H. Xiong, and C. Z. Huang, "Rapid synthesis of highly luminescent and stable Au₂₀ nanoclusters for active tumor-targeted imaging in vitro and in vivo," *Nanoscale*, vol. 6, no. 4, pp. 2261–2269, 2014.

[2] X. Wen, P. Yu, Y.-R. Toh, A.-C. Hsu, Y.-C. Lee, and J. Tang, "Fluorescence Dynamics in BSA-Protected Au 25 Nanoclusters," *J. Phys. Chem. C*, vol. 116, no. 35, pp. 19032–19038, Sep. 2012.

[3] Sanjay Singh, "Glucose decorated gold nanoclusters: A membrane potential independent fluorescence probe for rapid identification of cancer cells expressing Glut receptors," *Colloids and Surfaces B: Biointerfaces*, vol. 155, pp. 25–34, 2017.

LOCALISED IMPEDANCE OF ANTI - HUMAN GROWTH HORMONE ANTIBODIES FOR THE DEVELOPMENT OF AN IMPEDIMETRIC IMMUNOSENSOR

Timas Merkelis^{1,2}, Antanas Zinovičius^{2,3}, Inga Morkvėnaitė - Vilkončienė^{2,3}, Arūnas Ramanavičius^{1,2}

¹ Department of Chemistry and Geosciences, Vilnius University, Lithuania

² National Center for Physical Sciences and Technology, Lithuania,

³ Vilnius Gediminas Technical University, Lithuania

timas.merkelis@chgf.stud.vu.lt

Since Clark and Lyons published their work in 1962, a number of analytical chemistry researchers have been fascinated by the development of biosensors, which can be a fast and cheap way to conduct clinical, chemical, environmental or pharmaceutical research [1]. Electrochemical biosensors are devices that detect biological reactions happening at the electrode – solution interface and utilise transducers to transform chemical energy into electric signals. These devices could be used to detect various biological molecules, such as: proteins, antibodies, aptamers, or even entire cells [1]. One type of an electrochemical biosensor is an impedimetric sensor. These devices track biological reactions by measuring impedance changes at certain frequencies as biological reactions progress. Electrochemical impedance spectroscopy (EIS) is a widely used method for characterising and quantifying these types of interface reactions [1].

EIS as a method for tracking biological reactions has a few advantages. Firstly, it utilises currents of small amplitudes to disrupt a system from equilibrium, only causing minimal damage to the system in the process. It can be used to measure impedance with or without the presence of a redox pair, measuring faradaic processes in the former variant and non-faradaic processes in the latter. Biosensors that use both types of measurement have been developed in the past [2]. Faradaic sensors typically track changes in charge transfer resistance that stems from electrostatic interactions between charge carriers and biological molecules, while non – faradaic sensors measure changes in the electric double layer capacity that occur during biological reactions at the interface.

EIS is limited by a few requirements that are needed to obtain a valid impedance spectrum. These are causality- meaning the response of our system must be caused by the applied alternating potential. Linearity - the voltammetric curve must be linear in the chosen potential range. Stability- the system must return to its original state after any measurement. And finally, finity- meaning out impedance spectrum has to have finite values as frequency approaches 0 and infinity, as well as all frequencies in between. The biggest issue with biosensors has been their stability, since biological systems in electrochemical cells rarely retain stability for extended periods of time [2].

In this work, we utilise local EIS with scanning electrochemical microscopy (SECM) to analyse anti-human growth hormone (anti - HGH) antibodies modified with gold nanoparticles as a potential tool for developing a biosensor for the HGH protein. A functional HGH biosensor could provide a non – invasive method for testing HGH blood levels in humans.

[1] Bahadir, E. B., & Sezgintürk, M. K. (2016). A review on impedimetric biosensors. *Artificial Cells, Nanomedicine and Biotechnology*, 44(1), 248–262. <https://doi.org/10.3109/21691401.2014.942456>

[2] Xi, F., Gao, J., Wang, J., & Wang, Z. (2011). Discrimination and detection of bacteria with a label-free impedimetric biosensor based on self-assembled lectin monolayer. *Journal of Electroanalytical Chemistry*, 656(1–2), 252–257. <https://doi.org/10.1016/j.jelechem.2010.10.025s>

LIPOPOLYSACCHARIDES AND PROPERTIES OF THEIR AQUEOUS SOLUTIONS

Aistė Stičinskaitė¹, Lina Ragelienė¹

¹ Department of Biochemistry, Faculty of Natural Sciences, Vytautas Magnus University, Lithuania
aiste.sticinskaite@stud.vdu.lt

Lipopolysaccharide (LPS) is the major surface membrane component present in almost all Gram-negative bacteria and it is essential to both the form and function of the outer membrane. Lipopolysaccharides are known to be responsible for the production of various inflammatory cytokines produced by monocytes and macrophages. The role of LPS in Gram-negative bacterial diseases and its widespread application in various cell stimulation experiments provide a conceptual framework for studies targeting the isolation, purification, and detailed characterization of chemical interactions and structure of LPS. The main problem with LPS purification protocols is the contamination of the final product with proteins and nucleic acid, which hinders further quality assurance of the studies. Although, the structure and pathophysiological functions of LPS have been extensively studied, the studies of physical properties such as aggregation of LPS in aqueous solution are limited. According to other researches there is evidence that only endotoxin in aggregated structure is biologically active [1].

During the study, *E.coli* bacteria were grown in a bioreactor. The experiments have been performed in two different conditions: in the first group bacterial cell lysis was achieved by ultrasound applications, and in the second group methanol-chloroform extraction was executed. Further steps were identical for both groups, which included enzymatic LPS protein purification, dialysis and lyophilization. Quantity and degree of purification was determined in both groups. Concentration of LPS was identified by spectrophotometry and Limulus amoebocyte lysate (LAL) test. Aggregation of LPS molecules, like any other micellization of an amphiphilic molecule, can only be characterized under specific conditions. The aim of this study was to determine critical micelle concentration (CMC) in water and phosphate buffer at different temperatures using conductometry.

Conductometrically determined critical micelle formation concentration of LPS in water at room temperature (21°C), 37°C and 50°C. Comparative analysis of CMC between two separate methods of LPS purification at different temperatures was performed.

[1] M. Mueller, B. Lidner, S. Kusumoto et al., Aggregates are the biologically active units of endotoxin, *The Journal of biological chemistry* **279**, 26307–26313, (2004).

INVESTIGATION OF TETRAPHENYLPHOSPHONIUM CATION UPTAKE BY ELECTROPORATED *S. CEREVISIAE* YEASTS

Greta Gančytė¹, Povilas Šimonis¹, Aurelijus Zimkus², Arūnas Stirke¹

¹Laboratory of Bioelectronics,
Center for Physical Sciences and Technology,
Saulėtekio al. 3, Vilnius, Lithuania

²Department of Biochemistry and Molecular biology
Life Sciences Center, Vilnius University
Saulėtekio al. 7, Vilnius, Lithuania
greta.gancyte@gmail.com

Historically the budding yeasts *Saccharomyces cerevisiae* have been viewed as a prototype of eukaryotic cells, ideally suited for use in studies of many basic phenomena of eukaryotic life [1]. The *S. cerevisiae* yeast cells are surrounded by a cell wall, which provides them with protection from osmotic stress and is also important for their defense against toxic compounds, for self-recognition and for aggregation [2]. Permeability of yeast cells can be changed using many various methods. These include treatment of the cells chemically by adding reducing agents or antibiotics. Permeability can also be changed by increasing the external mechanical pressure on the cells. Pulsed electric field (PEF) treatment is known to cause plasma membrane permeabilization, an effect known as electroporation [3]. Tetraphenylphosphonium salts (for example, tetraphenylphosphonium bromide [TPPBr]) are frequently used in the measuring the membrane potential of prokaryotic and eukaryotic cells. The use of a potentiometric ion-selective electrode is also a convenient method for the quantitative evaluation of the permeability of the yeast cell wall and membrane [4].

In this study we, firstly, constructed a TPP⁺ ion selective electrode. Secondly, we measured TPP⁺ ion uptake by electroporated yeast cells, dependence on electric field strength. Experiments were performed with wild type SEY6210 strain. Cells were grown until 1 OD, transferred to electroporation buffer (20 mM TRIS, 1 M sorbitol, pH = 7.4) with 1 : 3 ratio by mass, then yeast suspension was exposed to single electric field pulse with duration of 150 μs and field strength of 2,9 kV/cm, 4,5 kV/cm or 5,9 kV/cm. 100 μL of 1 × 10⁻⁴ M TPP⁺ was added to the cell suspension (final volume 200 μL) at different time intervals after PEF (Δt = 5, 10, 20, 30, 40, 50, 60, 80, 120 and 180 seconds). It was then incubated for 3 minutes at room temperature and centrifuged in order to obtain cell free supernatant. The quantity of TPP⁺ absorbed by the yeast cells was measured potentiometrically and expressed as the accumulation percentage, where 100% is the maximum concentration of TPP⁺ that can be accumulated in yeast.

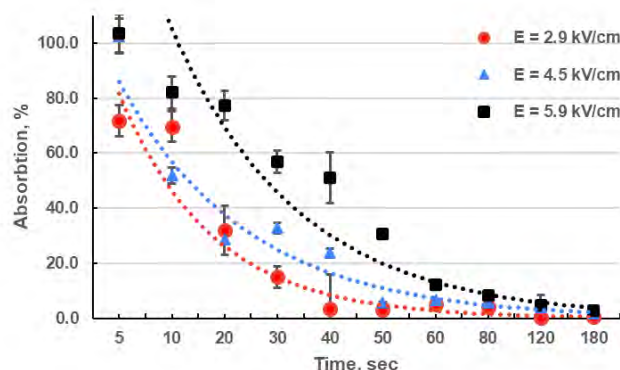


Fig. 1. TPP⁺ absorption dependence over time after PEF. The y axis represents the relative TPP⁺ amount accumulated in the yeast cells; the x axis represents the TPP⁺ injection time after PEF treatment. The dashed curves were obtained using Stirke. A. *et al.* methodology [3].

It was shown that quantitative TPP⁺ uptake by yeasts can be measured using our constructed selective electrode. Recovery dependence on electric field strength was observed (Fig. 1), stronger PEF application caused higher TPP⁺ absorption. Further experimentation of various mutant yeast strains with focus on cell wall components influence on TPP⁺ absorption will be evaluated. With future studies we plan to evaluate yeasts cell wall structure influence on electroporation kinetics.

[1] Breitenbach M, Jazwinski SM, Laun P. 2012. Aging research in yeast. Dordrecht, The Netherlands: Springer.

[2] Levin DE. 2011. Regulation of cell wall biogenesis in *Saccharomyces cerevisiae*: The cell wall integrity signaling pathway. *Genetics* 189:1145–1175.

[3] A. Stirke, R. Celiesiute-Germaniene, A. Zimkus, N. Zurauskiene, P. Simonis, A. Dervinis, A. Ramanavicius, and S. Balevicius, “The link between yeast cell wall porosity and plasma membrane permeability after PEF treatment.” *Scientific reports* vol. 9, 14731, (2019)

[4] Arunas Stirke, Aurelijus Zimkus, Almira Ramanaviciene, Saulius Balevicius, Nerija Zurauskiene, Gintautas Saulis, Larisa Chaustova, Voitech Stankevici, Arunas Ramanavicius, et al. Electric field-induced effects on yeast cell wall permeabilization. *Bioelectromagnetics*. 2014;35:136–144. doi: 10.1002/bem.21824.

EFFECTS OF HUMAN CHORIONIC GONADOTROPIN ON ENDOMETRIAL STROMAL CELLS DECIDUALIZATION

Deimantė Žukauskaitė, Erika Girniūtė, Rūta Navakauskienė

Department of Molecular Cell Biology, Institute of Biochemistry, Life Sciences Center, Vilnius University, Lithuania
deimante.zukauskaitė@gmc.vu.lt

Synchronized biochemical cross-talking between embryo and endometrium is critical for successful embryo implantation. One of the first embryo-secreted factors which signal endometrium about embryo presence is human chorionic gonadotropin (hCG). It was shown that hCG contributes to endometrium decidualization, differentiating tissue to a receptive state, and regulates maternal immunotolerance of the embryo and vascularization of the tissue [1-3].

This study analyzed how hCG affects endometrial stromal cell properties depending on its concentration *in vitro*. For endometrial stromal cells' decidualization, it was used established *in vitro* decidualization protocol by using db-cAMP and MPA. hCG effect in different concentrations was evaluated alone and in combination with decidualization stimulus.

Firstly, hCG and decidualization effects for cellular metabolic activity and viability were assessed. Gene expression analyses were conducted to evaluate hCG impact for decidualization markers (*IGFBP1*, *PRL*), apoptotic factors (*BAX*, *BCL2*, *BAK1*), DNA methylation regulators (*TET1*, *TET2*, *TET3*), and signaling molecules (*IL-11*, *IL-6*, *IL-1β*). Finally, ELISA was performed to confirm the results for prolactin. Results revealed that decidualization induction together with hCG increased the metabolic activity of cells, however, more prolonged exposure with hCG decreased it. Moreover, decidualization markers gene expression analysis revealed that an additive exposure with hCG slightly elevated these genes' expression compared to cells treated only with decidualization stimulus.

In conclusion, we demonstrated that hCG affects endometrial stromal cells and influence decidualization process in dose- and time-dependent manner.

-
- [1] Evans J., The role of hCG in endometrial receptivity and embryo implantation, In L. A. Cole, & S. A. Butler (Eds.), 100 Years of Human Chorionic Gonadotropin: Reviews and New Perspectives, 153-166, (2020).
[2] Ogino MH, Tadi P., Physiology, Chorionic Gonadotropin. In: StatPearls [Internet]. Treasure Island (FL): StatPearls Publishing, (2022).
[3] Hajipour H, Farzadi L, Roshangar L, Latifi Z, Kahroba H, Shahnazi V, et al., A human chorionic gonadotropin (hCG) delivery platform using engineered uterine exosomes to improve endometrial receptivity, *Life Sci*, **275**, 119351, (2021).

ATTEMPTS TO INHIBIT EFFLUX OF ANTIFUNGALS IN *CANDIDA* SPP. YEASTS

Eglė Vansevičiūtė¹, Guoda Jarašiūtė¹, Rimantas Daugelavičius^{1,2}

¹Department of Biochemistry and ²Research Institute of Natural and Technological Sciences, Vytautas Magnus University, Kaunas, LITHUANIA
egle.vanseviciute@vdu.lt

The number of dangerous and fatal infections caused by pathogenic *Candida* yeasts is increasing rapidly every year. One of the biggest problems encountered in treating these infections is the ability of cells to acquire resistance to known antifungal drugs. The most common mechanism of resistance is multidrug resistance pumps. Usually, in resistant strains activity of such pumps is upregulated, leading to increased antifungal drug efflux out of cells. Because of that, the concentrations of drugs within the cells are too low to inhibit the growth of pathogenic *Candida* yeasts. One possible way to increase the concentrations of antifungals inside the cells is an inhibition of the activity of efflux pumps, using alternative substrates, i.e. drugs used for the treatment of chronic diseases.

The aim of this study was to evaluate the ability of statins - drugs to lower the level of cholesterol in the blood – to inhibit the efflux of antifungals. The effects of statins alone or in combinations with antifungals were tested against different strains of *C. glabrata* and *C. albicans*, including strains mutant in ABC family efflux pumps – CDR1 and CDR2. The efficiency of the statins was determined using the microdilution method and electrochemical measurements. The results of our experiments revealed that three of chosen statins (atorvastatin, fluvastatin, and rosuvastatin) at tested concentrations (0,5 - 256 µg/ml) had no fungicidal activity against *C. glabrata* and *C. albicans*. At the same time, combinations with known antifungals (fluconazole and nystatin) reduced the growth of tested cells used in this study.

These findings show that statins strengthen the effects of antifungal drugs and might be helpful in the treatment of *Candida* infections.

TRICHODERMA REESEI AND PRODUCTION OF HYDROLYTIC ENZYMES

Augustinas Andziulis¹, Rimantas Daugelavičius^{1,2}

¹Department of Biochemistry, Vytautas Magnus University, Lithuania

²Research Institute of Natural and Technological Sciences, Vytautas Magnus University, Lithuania
Augustinas.andziulis@stud.vdu.lt

Currently, most of the world's energy needs are met by fossil fuel resources. Several different technologies can be used to transition to more sustainable energy sources. Cellulose is the most abundant organic material in the biosphere. Therefore, the isolation and industrial use of cellulases could be used in the production of biofuels from organic cellulose sources.

Trichoderma reesei is a mesophilic, filamentous fungus, known for its efficient production of cellulase enzymes, which are necessary for breaking down crystalline cellulose into glucose. In 1950 it was isolated in the Solomon Islands from decaying textiles. *T. reesei* produces three main types of cellulolytic enzymes: endoglucanase, cellobiohydrolase, and β-glucosidase. Endoglucanase shears internal connections in cellulose, cellobiohydrolase cleaves cellobiosyl units from the non-reducing end of cellulose, and β-glucosidase cleaves glycosyl units from the non-reducing end of cellulose oligosaccharides. These enzymes work synergistically to depolymerize cellulose and convert it into glucose [1]. However, the close relationship between lignin and cellulosic biomass can create barriers to the enzymatic hydrolysis of cellulose into fermentable sugars. Hemicellulose and lignin prevent cellulosic enzymes from functioning, inhibiting enzyme structure and reducing matrix pore size. The crystalline structure of cellulose with a glucan chain stops the hydrolysis process. Different pretreatment methods have specific effects on different lignocellulosic components. However, a significant number of them can create some kind of obstacles to the action of cellulases [2].

In our study we used RTS-1C bioreactor for cultivation of *T. reesei* ATCC 26921 cells. When growing *T. reesei* preculture in the bioreactor, it was important to create a constant aeration, to maintain optimal pH and to ensure the optimum temperature. After ensuring the optimal preculture growth conditions, the developed methodology was applied to the cultivation of cellulase-producing cultures. In the further cultivation of enzyme-producing cultures, it is planned to study the influence of the processing of cellulose raw materials on the final yield of enzymes, also to investigate different additives that can increase the excreted amount of the enzyme or the increase enzyme activity. It is expected to optimize the cultivation, enzyme production and purification technologies to provide convenient, cost-effective, and efficient conditions, as well as to investigate the specificities of the culturing of the culture in the bioreactor.

[1] Shoemaker, S., et al., Characterization and properties of cellulases purified from *Trichoderma reesei* strain L27, *Bio/Technology* **1.8**, 687-690 (1983)

[2] Kumar, Anil, et al., Multifarious pretreatment strategies for the lignocellulosic substrates for the generation of renewable and sustainable biofuels: A review. *Renewable Energy*, **160**, 1228-1252 (2020)

INVESTIGATION OF DCMU EFFECT ON *NITELLOPSIS OBTUSA* AUTOFLUORESCENCE

Aušrinė Navickaitė¹, Vilmantas Pupkis¹, Saulius Bagdonas²

¹ Department of Neurobiology and Biophysics, Vilnius University, Vilnius, Lithuania

² Laser Research Center, Vilnius University, Vilnius, Lithuania
ausrine.navickaite@gmc.stud.vu.lt

Recording of the fluorescence emitted from chlorophyll molecules is a frequently used tool to monitor photosynthetic performance, as photochemical reactions and emission are in direct competition for excitation energy. Therefore, changes in the photosynthetic rate will cause complementary changes in the intensity of the emitted fluorescence [1]. However, various factors affect emission signals in a similar way. Further investigation of fluorescence parameters is therefore needed to improve their diagnostic potential in practical applications.

Pairing an optical fiber system with a controlled stepper motor enabled registration of autofluorescence signals along Characean alga *Nitellopsis obtusa* internodes in 1 mm intervals. A low intensity (< 1 mW) LED light source emitting at 405 nm was used for excitation. To determine fluorescence parameters best suited to monitor photosynthetic performance under conditions of an external stress, algae were immersed overnight in a 100 μM solution of 3-(3,4-dichlorophenyl)-1,1-dimethylurea (DCMU). This compound interrupts photosynthetic electron transport [2] and should affect the recorded emission spectra. Since it is unknown whether DCMU alters the effect of other environmental factors on fluorescence parameters, the data obtained after DCMU treatment were compared with signals registered in untreated internodes kept under different lighting conditions: darkness, natural daylight, intense (photosynthetic photon flux density of 829 $\mu\text{mol m}^{-2} \text{s}^{-1}$) white LED light.

Two peaks at 680 nm and 739 nm were observed in the autofluorescence spectrum of *N. obtusa* (Fig. 1A). Fluorescence intensity values recorded at these wavelengths showed variations along the cell corresponding to changes in the fluorescence intensity ratio between 680 nm and 750 nm (F680/F750). These variations were observed regardless of lighting conditions. Emission spectra of algae treated with 100 μM DCMU displayed an altered shape, but the recorded intensity remained similar to that of untreated cells. Further investigation of the relationship between maximum fluorescence intensity (at 680 nm) and the F680/F750 ratio revealed a clear separation of DCMU affected algae (Fig. 1B). These results confirm that DCMU interferes with photosynthetic performance, either by affecting it in a way other than that due to the changing conditions of external lighting, or by directly altering this reaction. Therefore, the relationship found between selected fluorescence parameters provides a model for predicting light-induced changes in the emission spectra of algal cells. Nevertheless, more data are needed to confirm whether the model is suitable for assessing the effect of other environmental factors on photosynthetic performance.

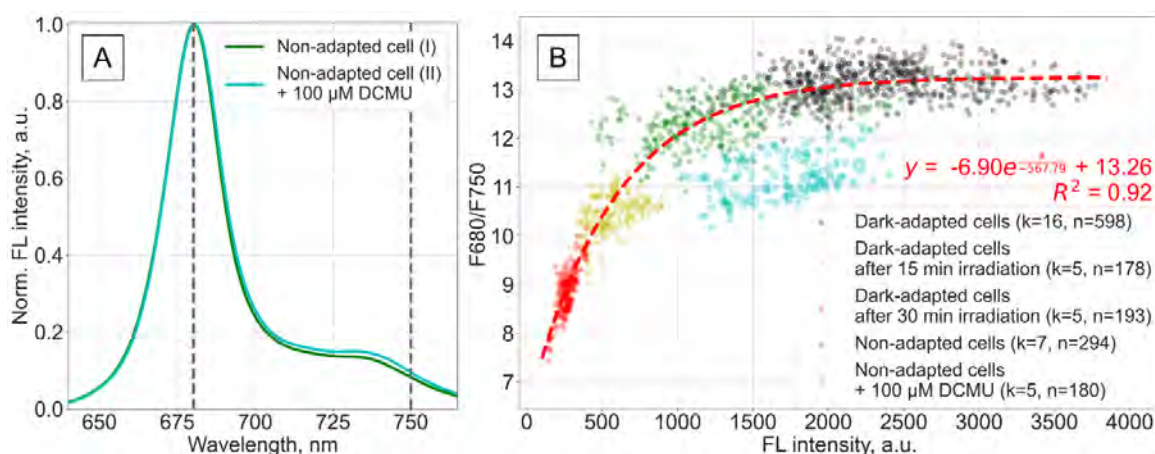


Fig. 1. DCMU effect on *N. obtusa* autofluorescence (FL) spectrum (A) and the relationship between peak FL intensity (680 nm) and F680/F750 ratio in algae kept under different conditions (B); k – number of cells, n – number of registered spectra.

[1] N. R. Baker, Chlorophyll Fluorescence: A Probe of Photosynthesis In Vivo, Annual Review of Plant Biology 59(1), 89-113 (2008).

[2] D. Kirilovsky, A. W. Rutherford, A. L. Etienne, Influence of DCMU and ferricyanide on photodamage in photosystem II, Biochemistry 33(10), 3087-3095 (1994).

ACTIVITY AND CRYSTALLIZATION OF TYPE III CRISPR-CAS ASSOCIATED RING NUCLEASE

Danas Klimavičius¹, Dominik Rafalski², Matthias Bochtler^{2,3}, Gintautas Tamulaitis^{1,4}

¹Institute of Biotechnology, Life Sciences Center, Vilnius University, Lithuania

²International Institute of Molecular and Cell Biology, Poland

³Institute of Biochemistry and Biophysics PAS, Poland

⁴Life Sciences Center European Molecular Biology Laboratory Partnership Institute, Vilnius University, Lithuania
danas.klimavicius@gmc.vu.lt

Type III CRISPR-Cas systems employ Csm or Cmr ribonucleoprotein complexes to cleave RNA [1] and DNA [2] to confer immunity against viruses and foreign plasmids. After recognition of target RNA Csm/Cmr complex also synthesizes 3-6 nt cyclic oligoadenylates (cOA) from ATP [3]. cA₄ or cA₆ allosterically activates CARF domain-containing accessory proteins. Bioinformatic analysis revealed that in prokaryotic genomes CARF domain could be fused with different putative DNases, RNases, adenosine deaminase and other domains [4]. Together with Csm/Cmr these auxiliary effectors provide immunity to the host. However, they could be toxic to a cell and result a dormancy or an altruistic cell death. To avoid host damage, the cOA concentration is tightly regulated by (i) cOA synthesis that is controlled through target RNA degradation by Csm complex [2], (ii) cOA degradation by specialized enzymes called ring nucleases [5,6].

Several uncharacterized CRISPR-associated genes were hypothesized to possess ring nuclease activity [4]. In this study we present results to demonstrate that Csx20 family proteins act as ring nucleases *in vitro* and *in vivo*. We also share results of our crystallization attempts in order to determine nuclease structure and mechanism.

-
- [1] G. Tamulaitis, M. Kazlauskienė, E. Manakova, C. Venclovas, A. O. Nwokeoji, M. J. Dickman, P. Horvath, V. Siksnys, 2014, *Mol. Cell*, 4, p. 506–517.
- [2] M. Kazlauskienė, G. Tamulaitis, G. Kostiuk, Č. Venclovas, V. Siksnys, 2016, *Mol. Cell*, 2, p. 295–306.
- [3] M. Kazlauskienė, G. Kostiuk, Č. Venclovas, G. Tamulaitis, V. Siksnys, 2017, *Science* 357(6351), p. 605–609.
- [4] K. S. Makarova, A. Timinskas, Y. Wolf, A. B. Gussow, V. Siksnys, Č. Venclovas, E. V. Koonin, 2020, *Nucleic Acids Res.*, 16, p. 8828–8847.
- [5] J. S. Athukoralage, C. Rouillon, S. Graham, S. Grüşchow, M. F. White, 2018, *Nature*, 7726, p. 277–280.
- [6] D. Smalakyte, M. Kazlauskienė, J. Havelund, A. Ruksenaite, A. Rimaite, G. Tamulaitiene, N. J. Færgeman, G. Tamulaitis, V. Siksnys, 2020, *Nucleic Acids Res.*, 16, p. 9204–9217.

STUDIES ON ENERGY TRANSFORMATION IN HALOARCUA HISPANICA IN LIGHT AND DARK PHASES

Tomas Stanevičius¹, Rimantas Daugelavičius^{1,2}

¹Department of Biochemistry and ²Research Institute of Natural and Technological Sciences, Vytautas Magnus University,
Kaunas, Lithuania

tomas.stanevicius1@stud.vdu.lt

Heavy metal pollution has become a great concern due to its adverse effects on the ecological system and human health. Major increase in heavy metal are caused by intensive human activities and economic development. For this reason, when extracting salts from mineral water that are necessary to produce other products such as food supplements, cosmetics, and laboratory reagents, pollutants are also extracted.

Haloarchaea are unique microorganisms resistant to environmental and osmotic stresses and thrive in their habitats despite extreme salinities. The results of previous studies have shown that the concentration of calcium and magnesium ions in the medium affects the stability of the membranes of *Haloarcula hispanica* and their energetic activity related to the efficiency of electron transport through the respiration chain in the plasma membrane [1]. The knowledge of microorganisms living in hypersaline environments is still limited and further investigation is needed to determine energy transformation methods and environmental adaptation conditions. To extend the results of these studies, experiments with high concentrations of Ca²⁺ and Mg²⁺ salts in archaeal environments are needed. Due to particularly high concentrations of Ca²⁺ and Mg²⁺ salts in the medium, the concentrations of pollutants, especially heavy metal ions, also increase, cause morphological changes in archaea and inhibit their reproduction. This forces archaea as bioindicators in the studies of purity of Ca²⁺ and Mg²⁺ salts isolated from natural resources, i.e., mineral waters.

Monitoring the dissolved oxygen concentration changes in the *H. hispanica* incubation medium, it is possible to follow the respiratory activity of cells, register the effect of substances – components of the medium. Observing the decrease of dissolved oxygen concentration in medium of archaea growing in light, it is not easy to assay the ion transport activity, as light activates light-driven proton pumps, which cause reduction of archaea respiration. This effect was interpreted as the result of competition between two energy yielding systems: the light-driven rhodopsin proton pumps and the respiratory chain. During the dissolved oxygen measurements, it was found that additional factors, in parallel to light, also affect the archaea's oxygen uptake such as cell preparation for measurements; stock suspension storage conditions; or medium for measurement. Based on *H. hispanica* respiration measurements, a new method for biotesting of calcium and magnesium salts was developed.

[1] Kellermann, M. Y., et al., Important Roles for Membrane Lipids in Haloarchaeal Bioenergetics. *Biochimica et Biophysica Acta (BBA) - Biomembranes*, 1858(11), 2940-2956 (2016).

EXPRESSION OF SELECTED HISTONE METHYLATION-ASSOCIATED GENES IS ASSOCIATED WITH ADVANCED PROSTATE CANCER

Greta Meidutė¹, Rūta Maleckaitė¹, Kristina Daniūnaitė¹

¹Institute of Biosciences, Life Sciences Center, Vilnius University, Vilnius, Lithuania
greta.meidute@gmc.stud.vu.lt

Prostate cancer (PCa) is the most commonly diagnosed male malignancy and the 5th leading cause of cancer-related death in men [1]. Most tumors tend to grow slowly and are low-grade with relatively lower risk of recurrence, whereas others are aggressive and significantly affect patients' life quality. PCa prognosis is primarily based on prostate-specific antigen (PSA) testing, however, it lacks accuracy in differentiating between indolent and aggressive forms of the disease [2]. Aberrant expression of histone methylation-associated genes (HMs), like histone lysine methyltransferases (KMTs) and demethylases (KDMs), has emerged as one of the major research areas in search of prognostic PCa biomarkers [3]. Being epigenetic regulators themselves, these genes could also be regulated by epigenetic mechanisms, one of which is by small regulatory RNAs, like microRNAs (miRNAs), at the post-transcriptional level. Therefore, investigation of HM gene expression together with their potential regulatory miRNAs could provide novel insights into the epigenetic mechanisms underlying PCa progression.

The present study was aimed at the analysis of 5 selected HM genes (*KDM5D*, *KMT5A*, *KDM7B*, *KMT1E* and *KDM5A*) and 6 potential regulatory miRNAs (miR-7-5p, miR-9-5p, miR-149-5p, miR-186-5p, miR-425-5p, and miR-618). In total, 186 prostate tissue samples (123 PCa, 47 noncancerous prostate tissues (NPT), and 16 benign prostate hyperplasia (BPH) samples) were included in the study. MiRNAs, which can potentially target the HM gene transcripts, were identified by *in silico* analysis, using data from 7 databases (Fig. 1). Expression of the selected miRNAs was evaluated in a subset of the samples (36 PCa and 6 NPT) from the same cohort. All HM genes and miRNAs were quantified by means of probe-based real-time PCR.

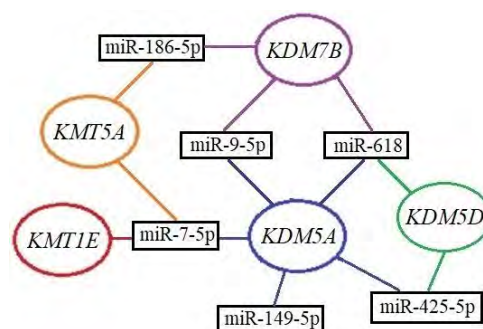


Fig. 1. MiRNA interaction with selected HM genes.

The results of our study revealed differences in HM gene expression among the histological sample groups. *KMT5A* was highly expressed in BPH as compared to both PCa and NPT (both $p < 0.0001$), whereas the expression of *KMT1E* in tumors was lower than in NPT and BPH ($p < 0.0001$ and $p = 0.0178$, respectively). Lower expression of *KDM5D* and *KDM5A* was associated with higher pathological tumor stage pT ($p = 0.0342$ and $p = 0.0338$, respectively). *KDM7B* had generally low expression in all samples, nevertheless, it was significantly different between pT2 and pT3 cases ($p = 0.0178$). No associations were found between HM genes expression and patient's age, prostate mass, and serum PSA levels (all $p > 0.0500$). Lower *KMT5A*, *KMT1E* and *KDM5A* expression was associated with biochemical disease recurrence (BCR; $p = 0.0172$, $p = 0.0003$ and $p < 0.0001$, respectively). Expression analysis of the selected miRNAs showed no differences between PCa and NPT and no associations were found with the HM genes expression (all $p > 0.0500$). Also, none of the miRNAs was associated with the BCR status ($p > 0.0500$).

In summary, the present study revealed significant expression differences of *KMT5A*, *KMT1E* and *KDM5A* in prostatic tissues, as well as some associations with the advanced disease parameters, suggesting these genes as potential PCa biomarkers. The analyzed miRNAs were not associated with the putative target genes. However, further investigation in larger independent cohorts is needed to confirm our findings.

[1] Global Cancer Observatory; <https://gco.iarc.fr> (World Health Organisation, France, 2021).

[2] N. Terada, S. Akamatsu, T. Kobayashi et al., Prognostic and predictive biomarkers in prostate cancer: latest evidence and clinical implications. *Ther Adv Med Oncol.* 2017 Aug;9(8):565-573.

[3] A. Mehdi, D. Cheishvili, A. Arakelian et al., DNA methylation signatures of Prostate Cancer in peripheral T-cells. *BMC Cancer.* 2020 Jun 23;20(1):588.

CRISPR-CAS PROTOSPACER INTERACTION WITH ADAPTATION COMPLEX

Viktoras Ragožius¹, Inga Songailienė^{1,2}, Lina Malinauskaitė¹

¹EMBL Partnership Institute, Life Sciences Centre, Vilnius University, Lithuania

²Institute of Biotechnology, Life Sciences Centre, Vilnius University, Lithuania
viktoras.ragozius@gmc.stud.vu.lt

CRISPR (Clustered Regularly Interspaced Short Palindromic Repeats) and their associated genes (*cas*) provide an adaptive immunity against exogenous nucleic acids in bacteria and archaea [1]. During the adaptation a recognition of a short motif known as a PAM (protospacer-adjacent motif) initiates the binding of adaptation complex to a target DNA. Adaptation complex cleaves out a segment of the target DNA and generates a protospacer. After duplication of the repeat, protospacer is inserted into the leader end of the CRISPR array and becomes a spacer [2]. Therefore, the main purpose of this research was to investigate how the sequence of a protospacer affects the adaptation process.

In this study the adaptation complex was co-expressed in *E. coli* BL21(DE3) cells and purified using a two-step affinity chromatography. Afterwards, *in vitro* integration assay was carried out. In total 7 different protospacers were analysed. All sequences of protospacers contained an identical segment for the integration into CRISPR array. However, they differed from one another at their 5' and/or 3' ends.

Here we purified a functional adaptation complex and showed that the sequence of a protospacer has an impact for the interaction with adaptation complex. Protospacer that contained sticky ends and double-stranded PAM had the best integration efficiency, which indicates a stronger interaction with adaptation complex.

Taking everything into account, these results provide insight into the mechanism of adaptation complex and protospacer interaction affecting the process of adaptation.

[1] J.Y. Wang, P. Pausch, J.A. Doudna, Structural biology of CRISPR-Cas immunity and genome editing enzymes, *Nature Reviews Microbiology* **20**, 641-656 (2022).

[2] K.S. Makarova, Y.I. Wolf, J. Iranzo et al., Evolutionary classification of CRISPR-Cas systems: a burst of class 2 and derived variants, *Nature Reviews* **18**, 67-83 (2020).

INVESTIGATION OF DEEP EUTECTIC SOLVENTS FOR LIGNOCELLULOSIC BIOMASS PRE-TREATMENT

Monika Paulauskaitė¹, Justinas Babinskas¹, Inga Matijošytė¹

¹Sector of Applied Biocatalysis, Institute of Biotechnology, Life Sciences Center, Vilnius University, Lithuania
monika.paulauskaite@chgf.stud.vu.lt

Fluctuating fuel prices, climate change, soil and ecosystem degradation, and growing world population are motivating the researchers to explore new technologies that lessen the society's dependence on the ecological capacity of Earth. Lignocellulosic biomass is recognized as one of the largest sources of sustainable and renewable organic material on Earth that could be used to produce fuels and bio-based products [1]. Effective fractionation of biomass into its main components (cellulose, hemicellulose and lignin) is essential in order to achieve efficient utilization of lignocellulosic materials. Pre-treatment is considered to be the most important step for obtaining an efficient conversion of biomass into value-added products; nevertheless, it is also one of the most expensive steps in a biorefinery process [2].

Deep eutectic solvents (DES) are a mixture of two or more compounds with a significantly lower melting point compared to the starting materials. DES are made by combining an appropriate hydrogen bond acceptors (HBA) and hydrogen bond donors (HBD) in specific molar ratios (Fig. 1.).

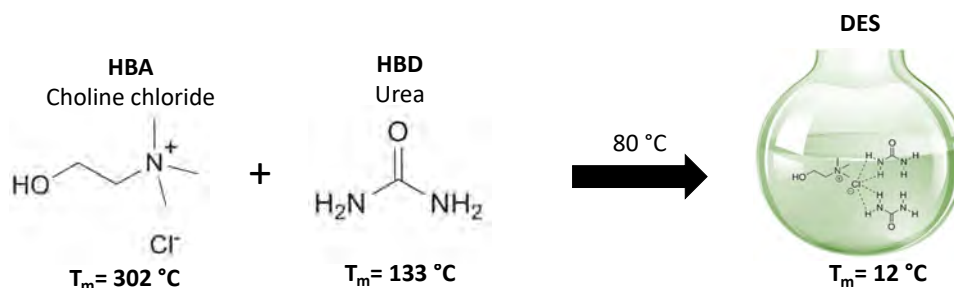


Fig. 1. Formation of choline chloride and urea DES.

DES have attracted the attention of the scientific community due to their ability to process and selectively dissolve biomass components to yield polysaccharides and lignin [3]. DES have many advantages over organic solvents commonly used in chemical and biochemical processes: negligible vapor pressure, non-flammability, high chemical and thermal stability, low toxicity, biodegradability, recyclability, and low price, among others [4]. DES have been recognized as a promising solvent for biomass pre-treatment, although DES applications toward biomass are still in its nascent stage.

In this project, we explored synthesis of four different choline chloride-based DES using urea, lactic acid, citric acid and linoleic acid as HBD. To confirm formation of DES, we used attenuated total reflectance – Fourier transform infrared spectroscopy. Furthermore, we studied DES properties and application in lignocellulose (wheat straw) processing.

[1] Nanda, S., Azargohar, R., Dalai, A. K. & Kozinski, J. A. An assessment on the sustainability of lignocellulosic biomass for biorefining. *Renew. Sustain. Energy Rev.* **50**, 925–941 (2015).

[2] Mussatto, S. I. & Dragone, G. M. Chapter 1 - Biomass Pretreatment, Biorefineries, and Potential Products for a Bioeconomy Development. in *Biomass Fractionation Technologies for a Lignocellulosic Feedstock Based Biorefinery* (ed. Mussatto, S. I.) 1–22 (Elsevier, 2016). doi:10.1016/B978-0-12-802323-5.00001-3.

[3] Hansen, B. B. *et al.* Deep Eutectic Solvents: A Review of Fundamentals and Applications. *Chem. Rev.* **121**, 1232–1285 (2021).

[4] Ailing, W., Xueliang, Z., Zhuangzhi, Z., Changping, L. & Xuefang, Z. Deep Eutectic Solvents to Organic Synthesis. *Prog. Chem.* **26**, 784 (2014).

PROTEIN AND ALGAE EFFECT ON THE PHOTOSTABILITY OF Cd- AND Cu-BASED QUANTUM DOTS

Emilija Januškaite¹, Agnė Kalnaitytė^{1,2}, Saulius Bagdonas^{1,2}

¹ Biophotonics Group, Laser Research Center, Vilnius University, Saulėtekio 9, bld. 3, LT – 10222, Vilnius, Lithuania

² Institute of Ecology, Nature Research Centre, Akademijos str. 2, LT – 08412, Vilnius, Lithuania
emilija.januskaite@gmc.stud.vu.lt

Nano-sized quantum dots (QDs) are widely used in various fields of science and engineering, including biomedicine. Although QDs may have a protective shell and surface ligands, prolonged exposure to the environment and/or light affects their structure and spectroscopic properties [1]. After decomposition, toxic metals (e.g., Cd) from the core of QDs can enter the environment, so less toxic alternatives such as Cu-based QDs are considered, despite poorer optical performance than Cd-QDs. Protein molecules can coat QDs and improve their spectroscopic properties [2], however, more research is needed to understand whether the mechanism of action of algae is similar to proteins and how they both affect the photostability of QDs.

In this work we studied the optical density (OD) and photoluminescence (PL) spectra of CdSe/ZnS-COOH (Invitrogen, USA) and CuInS/ZnS-COOH (Nanooptical Materials, USA) QDs in a model biological medium containing bovine serum albumin (BSA) or unicellular algae *Scenedesmus quadricauda* when exposed to light. Samples of QDs (concentration of both QDs was 4 nM) were prepared in deionized water (dw) with BSA (concentration 100 μ M) and in MWC algae growth medium with unicellular algae (concentration about 10^5 cells/ml). The samples were held in a 12-well plate during light irradiation, and collimated violet LED light ($404 \text{ nm} \pm 9 \text{ nm}$, 30 mW/cm^2) was directed at the sample from a distance of 8 cm. In all media, fractionated exposure was given at intervals of 1.8 J/cm^2 and 3.6 J/cm^2 to achieve a partial cumulative dose of up to 36 J/cm^2 .

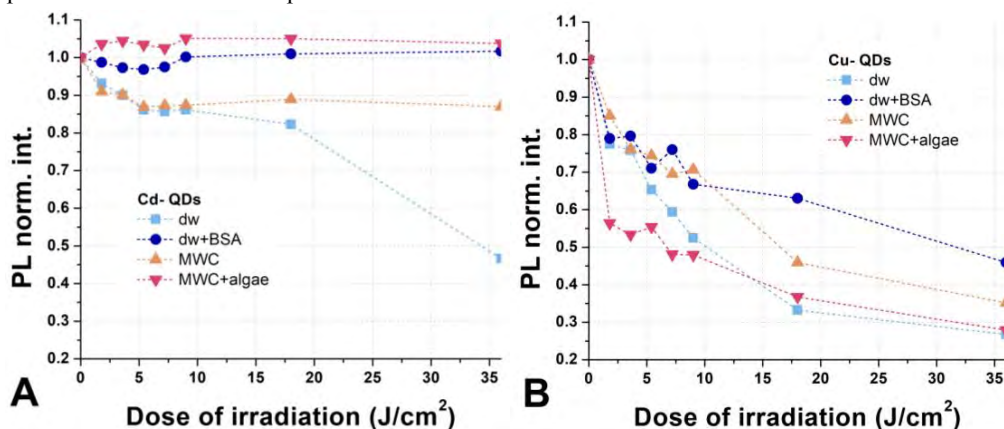


Fig. 1. Decrease in PL of Cd- and Cu- based QDs at the value of the spectral peak (about 622 nm and 550 nm, respectively) depending on the irradiation dose in various media. The excitation wavelength was 405 nm.

Cu-based QDs samples had a higher initial OD than Cd-based QDs, but Cd-based QDs showed a higher PL quantum yield, a narrower and more intense PL spectrum. The presence of BSA in the medium led to a higher OD and PL intensity of Cd- QDs, as well as to a bathochromic shift of PL spectrum, while in the samples with algae, there was no decrease in the PL intensity and no spectral shift. A decrease in the OD and the PL intensity and the absence of spectral shifts were registered in the samples of Cu-QDs both with BSA and with algae. After exposure to light, the spectroscopic properties of Cd-QDs were more stable in all studied media compared to the samples with Cu-QDs (Fig. 1). The presence of BSA increased the photostability of both QDs: BSA practically protects Cd-QDs from a photoinduced decrease in the PL intensity, and the decrease in the PL intensity in Cu- QDs samples was slower than in the dw sample without BSA. Although the MWC medium increased the photostability of the spectroscopic properties of both QDs compared to dw, the decrease in the PL intensity of Cu-QDs with algae after initial doses was greater than in MWC medium alone. On the contrary, the PL intensity of Cd-QDs with algae slightly increased after the initial irradiation doses and remained stable during the experiment. Cu- QDs appeared to be less photostable in general. The presence of algae in the medium further reduced their photostability, while BSA slightly stabilized the PL intensity at higher exposures. In the case of Cd- QDs, the presence of BSA or algae led to increased PL intensity of the samples.

This work was funded by the Research Council of Lithuania, Project No. S-MIP-20-22.

- [1] A. Kalnaitytė, S. Bagdonas, R. Rotomskis, *The dose-dependent photobleaching of CdTe quantum dots in aqueous media*, Journal of Luminescence, 201, pp. 434-441, 2018.
[2] V. Poderys, M. Matulionytė, A. Selskis, R. Rotomskis, *Interaction of Water-Soluble CdTe Quantum Dots with Bovine Serum Albumin*, Nanoscale Res. Lett., 6:9, 2011.

OVARIAN CANCER CELL LINES EXHIBIT DIFFERENTIAL STEMNESS-RELATED PROTEIN AND GENE EXPRESSION IN 2D AND 3D MODELS

Eglė Žymantaitė^{1,2}, Agata Mlynska²

¹ Life Sciences Centre, Vilnius University, Lithuania

² Immunology Laboratory, National Cancer Institute, Vilnius, Lithuania

egle.zymantaite@gmc.stud.vu.lt

Epithelial ovarian cancer (EOC) in most developed countries is the leading cause of death among gynaecological malignancies. The high level of heterogeneity of this cancer plays a big role in the lack of successful treatments [1]. To improve our understanding of epithelial ovarian tumour biology and behaviour it is important to adopt a suitable culture system. Usually, the majority of in vitro experiments are performed in two-dimensional (2D) cancer cell line monolayer cultures. Even though the 2D model is commonly used, it does not fully reflect the tumour complexity therefore more sophisticated models should be adopted. Cancer cell microstructures formed as three-dimensional (3D) spheroids closer represent the main characteristics of in vivo tumours, such as cell-cell interactions, hypoxia and pH rate, exposure to nutrients and metabolites, and gene expression profiles [2]. In our study, we aimed to adopt and optimize the 3D culture conditions of four different EOC cell lines: A2780, SKOV3, COV362, OV7. Next, we compared the gene and protein expression profiles between 3D and widely used 2D cell culture models by performing flow-cytometry (FACS) and analyzing the expression of genes related to stemness properties, epithelial-mesenchymal transformation and interaction with the immune system by quantitative real-time PCR (qPCR).

EOC spheroids were measured and observed in different growth conditions and at a different seeding density as a starting point (Fig. 1). We noticed that the A2780 cell line formed no spheroids in our culture conditions and as such this cell line was excluded from further analysis. After optimization when the best cell count and conditions were determined, protein and gene expression profile evaluation was performed. We found out that the OV7 cell line had the upregulated TGF- β pathway and epithelial-mesenchymal transformation-related genes. Next, we compared the gene and protein expression in respective 2D and 3D cultures, where we found substantial differences.

In conclusion, for each cell line, we characterized its gene and protein expression profile in 2D and 3D culture conditions.

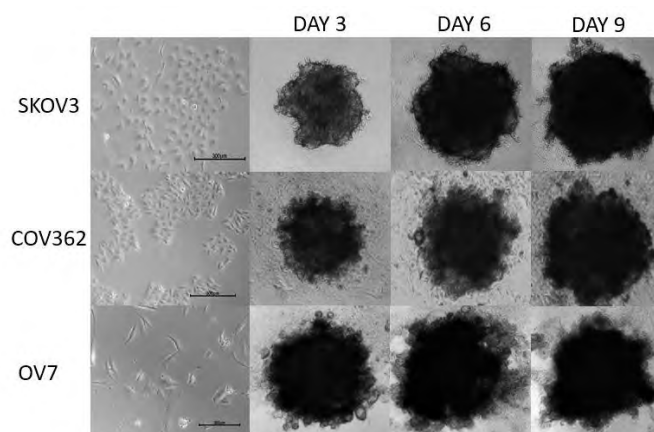


Fig.1. Epithelial ovarian cancer cell line SKOV3, COV362, OV7 spheroids on different culturing days.

[1] Kossai M, Leary A, Scoazec J, -Y, Genestie C: Ovarian Cancer: A Heterogeneous Disease. *Pathobiology* 2018;85:41-49.

[2] Gheyntchi E, Naseri M, Karimi-Busheri F, Atyabi F, Mirsharif ES, Bozorgmehr M, Ghods R, Madjd Z. Morphological and molecular characteristics of spheroid formation in HT-29 and Caco-2 colorectal cancer cell lines. *Cancer Cell Int.* 2021 Apr 13;21(1):204. doi: 10.1186/s12935-021-01898-9. PMID: 33849536; PMCID: PMC8042991.

PLASMA INDUCED CHANGES IN STEVIA REBAUDIANA ANTIOXIDANT ACTIVITY

Augustė Judickaitė, Erika Endriulaitytė, Rasa Žūkiene

Department of Biochemistry, Vytautas Magnus University, Lithuania
auguste.judickaite@vdu.lt

The *Stevia rebaudiana* plant produces steviol glycosides, a non-caloric sweeteners that are not metabolized in the human body. In addition to the sweet taste, it has various applications for health improvement acts as antihyperglycemic, anticancerous, antihypertensive agent and prevents bacterial and fungi growth [1]. The increasing demand of such products like stevia sweeteners is also putting pressure on the need to improve stevia agronomical traits, such as seed germination, disease resistance and biomass [2]. It has been proven that seed treatment with cold plasma had positive effects on these traits, however changes in the biosynthesis of secondary metabolites are not yet fully understood [3]. The aim of this study was to determine low-pressure plasma (CP)-, dielectric barrier discharge plasma (DBD)-, and vacuum-induced changes in antioxidant activity and concentrations of flavonoids and phenolic compounds in stevia leaves.

The extracts from stevia leaves were prepared by using 70% ethanol and ultrasound (1h) extraction. The concentration of flavonoids was measured using adjusted spectrophotometric FC method [3]. For determination of phenolic compounds another spectrophotometric method was chosen using reagent consisting of 96% ethanol; 33% acetic acid; 5% hexamethylenetetramine and 10% aluminum chloride [3]. DPPH activity measured according to the standardized protocol [3].

Results shows that CP exposure decreases antioxidant activity after 2- and 7-min. exposure (CP2; CP7) compared to unexposed (Control) group, $p < 0.05$. Although longer (CP7) exposure of decreased activity less than shorter exposure length (Table 1). A similar tendency was observed in decrease of phenolic compounds concentration (Table 1). Positive tendency was captioned in flavonoid concentration compared to the control group (Table 1). On the other hand, exposure of DBD shows tendency in flavonoid concentration decrease with longer exposure lengths (Table 1). However, longer DBD exposure (DBD7) increased antioxidant activity ($p < 0.05$). Tendency in phenolic compounds concentration increase after DBD exposure is also consistent with increased antioxidant activity (Table 1).

	Flavonoid conc., mg GAE/g	Phenolic compounds conc., mg GAE/g	Antioxidant activity, mg RUE/g
Control	48.8 ± 11.2	102.0 ± 18.0	124.1 ± 5.0
V5	58.8 ± 11.0	136.1 ± 4.2	111.0 ± 11.3
CP2	58.8 ± 6.3	55.4 ± 4.9	27.5 ± 9.2*
CP5	61.5 ± 18.7	78.0 ± 33.9	57.2 ± 30.1
CP7	73.7 ± 3.5	89.6 ± 13.0	69.4 ± 9.7*
DBD2	86.2 ± 1.7	97.3 ± 10.2	53.5 ± 21.0
DBD5	47.1 ± 4.2	62.7 ± 1.8	46.3 ± 6.4
DBD7	46.0 ± 12.6	103.6 ± 19.8	142.3 ± 22.5*

Table 1 Flavonoid; phenolic compounds concentrations and antioxidant activity in stevia leaves, mg/g
 * $p < 0.05$

The results suggests that antioxidant activity correlates with the concentration of phenolic compounds rather than the concentration of flavanoids. DBD7 group shows the strongest antioxidant activity, while CP exposure only decreased it. Studies had shown that plasma-induced changes are dependent on the origin of plant and length of exposure. It was also confirmed that seeds exposure with CP and DBD has a positive effect on antioxidant activity [4,5,6]. Therefore, the standartization of

different plasma application is needed for different plant species. It could be concluded that stevia seeds treatment with dielectric barrier discharge plasma for 7 min has positive effect on antioxidant activity in stevia leaves. However, further research is needed to determine underlying mechanisms of the changes.

- [1] A. K. Yadav, et al. A review on the improvement of stevia [*Stevia rebaudiana* (Bertoni)]. Canadian journal of plant science **91.1**, 1-27 (2011).
 [2] A. Kumari, V. Kumar, N. Malhotra. *Stevia rebaudiana*. *Himalayan Medicinal Plants* p. 199-221 (Academic Press, Science Direct (2021)).
 [3] A. Judickaitė, et al. The potential of cold plasma and electromagnetic field as stimulators of natural sweeteners biosynthesis in stevia rebaudiana bertoni. *Plants* **11.5**, 611 (2022).
 [4] W. Saengha, et al. Cold plasma treatment on mustard green seeds and its effect on growth, isothiocyanates, antioxidant activity and anticancer activity of microgreens. *International journal of agriculture & biology* **25**, 667-676 (2021).
 [5] V. Sirgedaitė-šėžienė, et al. Changes in Content of Bioactive Compounds and Antioxidant Activity Induced in Needles of Different Half-Sib Families of Norway Spruce (*Picea abies* (L.) H. Karst) by Seed Treatment with Cold Plasma. *Antioxidants* **11.8**, 1558 (2022).
 [6] M. Keshavarz, et al. Enhancement of polyphenolic content extraction rate with maximal antioxidant activity from green tea leaves by cold plasma. *Journal of Food Science* **85.10**, 3415-3422 (2020).

PHYSICOCHEMICAL CHARACTERIZATION AND RELEASE PROPERTIES OF HYDROGEL WITH NIMESULIDE LOADED ON NANOHYDROXYAPATITE

Katarzyna Wiglusz¹ and Rafal J. Wiglusz²

¹ Department of Basic Chemical Sciences, Wroclaw Medical University, Poland;

² Institute of Low Temperature and Structure Research, Polish Academy of Sciences, Wroclaw, Poland

katarzyna.wiglusz@umw.edu.pl

Nimesulide (N-(4-Nitro-2-phenoxyphenyl)methanesulfonamide, empirical formula C₁₃H₁₂N₂O₅S) is a non-steroidal anti-inflammatory drugs (NSAIDs) to be treated for pain and inflammation. It can also perform antipyretic activities [1].

The aim of the study was to prepare and characterize the hydrogel carbopol containing active component - nimesulide loaded on the nanohydroxyapatite matrix for skin application.

The obtained gel with the nimesulide incorporated on the nanohydroxyapatite was tested in terms of pH, viscosity, homogeneity and the polymer-active substance interactions that take place in the preparation were considered.

The spectroscopic, rheological, thermogravimetric analysis and swelling studies were performed to evaluate the effect of on drug release and stability of the hydrogel. Greater swelling was observed at a pH slightly higher than the physiological pH of the skin. The results revealed that 50% wt. drug was released from the hydrogel in 6 h at pH 5.6 and 32°C (Fig. 1).

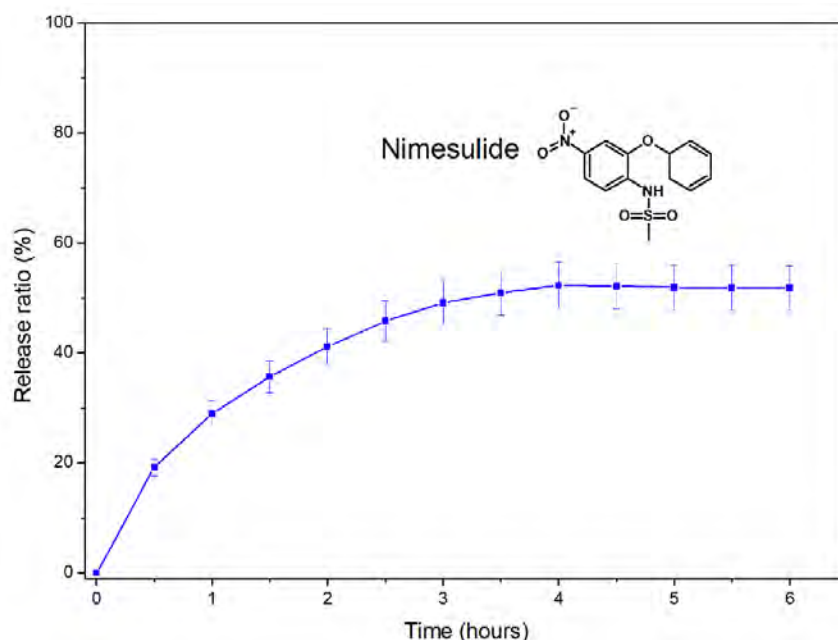


Fig. 1. Nimesulide release test for Carbopol hydrogel at pH=5.6 and 32°C and the chemical structure of nimesulide.

The rheograms for the formulation was measured at 25 and 32°C and corresponding as a storage temperature and a skin temperature, respectively.

The rheological properties and extended the nimesulide release of hydrogel make a potential candidate for controlled delivery of the drug.

[1] Singla AG, Chawia AM, Sing A (2000) Review. Nimesulide: some pharmaceutical and pharmacological aspects — an update. *J Pharm Pharmacol* 52: 467–486

APPLICATION OF MOUSE ORGANOTYPIC HIPPOCAMPAL SLICE CULTURES TO INVESTIGATE NEURONAL SIALYLATION

Ugne Kisieliute¹, Ugne Kuliesiute^{1,2}, Urte Neniskyte^{1,2}

¹Institute of Biosciences, Life Sciences Centre, Vilnius University, Vilnius, Lithuania

²VU-EMBL Partnership Institute, Life Sciences Centre, Vilnius University, Vilnius, Lithuania
ugne.kisieliute@gmc.stud.vu.lt

Precise and tight regulation of the number of synapses is a crucial factor for healthy nervous system development. Atypical abundance or disposal of synapses in the brain may lead to neurodevelopmental disorders, such as autism, schizophrenia, or epilepsy [1]. Microglia, the main phagocytes of CNS, regulate synapse pruning to selectively eliminate or strengthen the subset of synapses by “eat me” – “spear me” distinction determined by specific neuronal markers. Sialic acid – a monosaccharide, which typically terminates the structures of glycoconjugates that compose neuronal glycoalyx, has a particular importance in neuron-microglia interaction. In the presence of neuronal sialic acid microglial phagocytic activity is actively inhibited, while desialylation of neurons promotes their phagocytosis *in vitro* [2]. However, the potential role of sialic acid in synapse pruning as a local specific marker on synapses has not been determined yet.

We used mouse organotypic hippocampal slice cultures as a platform to define how sialylation provides a selective mechanism for the maintenance and strengthening of necessary synapses. We applied bioorthogonal CLICK chemistry to metabolically label *de novo* synthesised sialic acid on the surface of excitatory neurons [3]. We used chemical inhibitors (1S,2R)-1-((3S,4R,5R,6S)-3-acetamido-4,6-diacetoxy-5-fluoro-6-(methoxycarbonyl)tetrahydro-2H-pyran-2-yl)propane-1,2,3-triyl triacetate (3FAX) and 2-deoxy-2,3-didehydro-N-acetylneuraminic acid (DANA) targeting either sialic acid synthesis or desialylation, respectively, to alter neuronal sialylation.

Mouse organotypic hippocampal slice cultures were established and used as an *ex vivo* system allowing to study metabolic processes of neuronal sialylation. The visualization and quantitative analysis of newly synthesized sialic acids on dendrites of excitatory neurons showed specificity of metabolic sialic acid labelling. The inhibition of sialyltransferases by 3FAX significantly reduced neuronal sialylation, while sialidase inhibition by DANA led to increased sialylation levels. Our results indicated that neuronal sialylation can be chemically modulated *ex vivo* allowing the precise assessment of sialic acid abundance on the neuronal structures, such as dendrites and individual synapses.

In conclusion, we demonstrated the applicability of mouse organotypic hippocampal slice cultures as a robust model to investigate *de novo* synthesis and the turnover of sialic acid in the mouse developing brain *ex vivo*. Moreover, our system enables to target and characterise the exact role of the enzymes involved in neuronal sialylation and desialylation in synaptic pruning.

[1] Sakai, J. (2020). How synaptic pruning shapes neural wiring during development and, possibly, in disease. *Proceedings of the National Academy of Sciences of the United States of America*, 117(28), 16096–16099.

[2] Brown GC, Neher JJ. Microglial phagocytosis of live neurons. *Nature Reviews Neuroscience*. 2014 Apr;15(4):209–16.

[3] Baskin, J. M., & Bertozzi, C. R. (2007). Bioorthogonal click chemistry: Covalent labeling in living systems. In *QSAR and Combinatorial Science* (Vol. 26, Issues 11–12, pp. 1211–1219).

STRUCTURAL VARIABILITY OF PRION PROTEIN AMYLOID FIBRILS UNDER DIFFERENT AGITATION CONDITIONS

Egle Pociute, Kamile Mikalauskaite, Vytautas Smirnovas

Amyloid Research Sector, Institute of Biotechnology, Life Sciences Center, Vilnius University
egle.pociute@gmc.stud.vu.lt

Amyloidogenic peptides and proteins have a property to convert from their native functional states into fibrillar amyloid aggregates. This property is associated with neurodegenerative disorders, such as Alzheimer's or Parkinson's diseases, as well as prionopathies [1]. It has been observed that the environment conditions in which amyloid aggregation takes place have an important effect on fibril polymorphism. Moreover, amyloid aggregates have recently been shown to have the property to adopt more than one different conformation under the same environmental conditions [2]. One example of such environmental conditions, whose effect on amyloid structural variability is not fully understood, is agitation.

In this work, we examined the effect of three different agitation conditions on the aggregation kinetics of mouse prion protein fragment (MoPrP 89-230) and analyzed the secondary structure of the resulting fibrils.

Protein MoPrP 89-230 samples were incubated under three agitation conditions (200, 400 and 600 RPM) at 37°C, under denaturing conditions (2 M guanidinium hydrochloride, 50 mM sodium phosphate, pH 6.0). The kinetics of aggregation were determined by recording the fluorescence intensity of the amyloidophilic dye thioflavin-T (ThT). The secondary structure of fibrils was determined by analyzing each sample's FTIR spectra.

The results suggest that the intensity of agitation has a minimal influence on primary nuclei formation and that the rate of elongation does to scale with the level of agitation. In all three cases, a diverse collection of secondary structures (at least three structure types) were observed, with the highest variability detected under 200 RPM agitation conditions.

[1] Chiti F, Dobson CM. Protein Misfolding, Amyloid Formation, and Human Disease: A Summary of Progress Over the Last Decade. *Annu Rev Biochem.* 2017 Jun 20;86:27-68. doi: 10.1146/annurev-biochem-061516-045115. Epub 2017 May 12. PMID: 28498720.

[2] Ziaunys M, Sneideris T, Smirnovas V. Formation of distinct prion protein amyloid fibrils under identical experimental conditions. *Sci Rep.* 2020 Mar 12;10(1):4572. doi: 10.1038/s41598-020-61663-2. PMID: 32165692; PMCID: PMC7067779

THE EFFECT OF dGAE FRAGMENT CONCENTRATION ON ITS SELF-AGGREGATION AND ASSOCIATION WITH TAU PROTEIN

Urte Venclovaite, Kamile Mikalauskaite, Vytautas Smirnovas

Amyloid Research Sector, Institute of Biotechnology, Life Sciences Center, Vilnius University, Lithuania
urte.venclovaite@chgf.stud.vu.lt

Protein aggregation into amyloid fibrils is associated with several widespread neurodegenerative disorders. Alzheimer's disease is one of the most prominent cases, with an ever-increasing number of afflicted patients. The disorder is characterized by memory loss and is considered to be caused by amyloid- β extracellular plaques and neurofibrillary tangles made from hyperphosphorylated Tau. The main physiological function of the Tau protein is to maintain microtubule dynamics and promote polymerization. *In vitro* Tau protein filament formation is induced by the presence of polyanions such as heparin. A truncated form of Tau protein (dGAE), which can assemble into filaments without polyanions, forms a proteolytically stable core region in full-length Tau paired helical filament (PHF) [1]. The dGAE fragment could serve as a model system for the search for inhibitors of Tau protein aggregation [2].

Considering the rise of Alzheimer's disease incidences worldwide, understanding the process of amyloid aggregation is a crucial step in developing drugs. Research of dementia is heavily focused on the process of how pathogenic Tau can spread throughout the brain, as it may provide a key therapeutic target for slowing the development of tauopathies. There are a lot of disputed questions concerning the physiological and pathological consequences of PHF-core Tau self-assembly, therefore we aim to elucidate the influence of dGAE fragment on Tau protein aggregation.

Tau 2N4R gene was inserted into pET Champion His-SUMO vector by TA cloning method to create the ULP1-cleavable N-terminally His-SUMO-tagged Tau. The recombinant His-SUMO-tagged Tau (2N4R isoform) protein was purified by immobilized metal affinity chromatography and consequently cleaved by the ULP1 protease to remove His-SUMO-tag. A truncated form of Tau protein (297-391) (dGAE) was purified by cation exchange chromatography. Both proteins were purified further by size-exclusion chromatography. We used purified Tau 2N4R protein and dGAE fragment for monitoring the amyloid aggregation process. All performed aggregation kinetics were followed using a thioflavin-T fluorescence assay. Atomic force microscopy was performed to analyze the morphology of the formed aggregates. We used FTIR spectroscopy to observe the differences in secondary structures of the dGAE fragment and dGAE+Tau protein aggregates.

Looking at the results we can see the aggregation halftime and lag time decrease when dGAE fragment concentration increases. Thus, the results obtained confirm the fact that is stated in the articles that at higher concentrations the dGAE fragment aggregates faster. The apparent rate constant varies within error at different concentrations. *In vitro* FTIR analysis indicates that the soluble Tau protein is a natively unfolded protein dominated by random coil structure, whereas Alzheimer PHFs show an increase in the level of β -structure. The results support a model in which the repeat domain of Tau (which lies within the core of PHFs) adopts an increasing level of β -structure during aggregation. FTIR spectra show that when dGAE aggregates, the resulting dGAE fibrils associate with monomeric Tau protein.

[1] Maina, M.B. et al. (2021) "Oxidative stress conditions result in trapping of PHF-core tau (297–391) intermediates," *Cells*, 10(3), p. 703. Available at: <https://doi.org/10.3390/cells10030703>.

[2] Al-Hilaly, Y.K. et al. (2020) "Tau (297-391) forms filaments that structurally mimic the core of paired helical filaments in alzheimer's disease brain," *FEBS Letters*, 594(5), pp. 944-950. Available at: <https://doi.org/10.1002/1873-3468.13675>.

ACTION POTENTIAL EXCITATION THRESHOLD HYPERPOLARIZATION IN *NITELLOPSIS OBTUSA* CELL AFTER EXPOSURE TO IP₃

Judita Januzaitė¹, Vilmantas Pupkis¹, Indre Lapeikaite¹, Vilma Kisnieriene¹

¹Department of Neurobiology and Biophysics, Vilnius University, Vilnius, Lithuania
judita.januzaitė@gmc.stud.vu.lt

The giant algae *Nitellopsis obtusa* cells generate action potentials (APs) in response to mechanical stimulation, injury, or direct electrical stimulation. Each internodal segment is a single large cell, up to 10 cm and more in length suitable for biophysical research. The possibility of determining the excitation threshold and its alterations in *N. obtusa* cells allows linking the effect of many chemicals to the Ca²⁺-dependent initiation of excitation.

Inositol 1,4,5-trisphosphate (IP₃) mobilizes Ca²⁺ from internal stores in animal cells during excitation. In plants an excitation-related IP₃-induced release of Ca²⁺ from isolated vacuoles has been observed [1]. However, a direct link between an increase in the intracellular level of IP₃ and the regulation of AP excitation threshold value is yet to be demonstrated.

We have used two-pair current clamp microelectrode technique to evaluate the AP excitation threshold (E_{th}). The cylinder-shaped *N. obtusa* internodal cell was placed in a chamber with electrically isolated compartments. APW (Artificial Pond Water) solution for control and 75 μM IP₃ solution for exposure were used.

Results show that 30 min exposure to IP₃ increases the excitability of *Nitellopsis obtusa* by hyperpolarizing the excitation threshold (Fig. 1). Spontaneous APs were also observed after the exposure to IP₃.

This investigation supports the proposition that IP₃ increases the excitability of the single cell by releasing Ca²⁺ from internal stores. Further research should be done for the rest of the AP parameters.

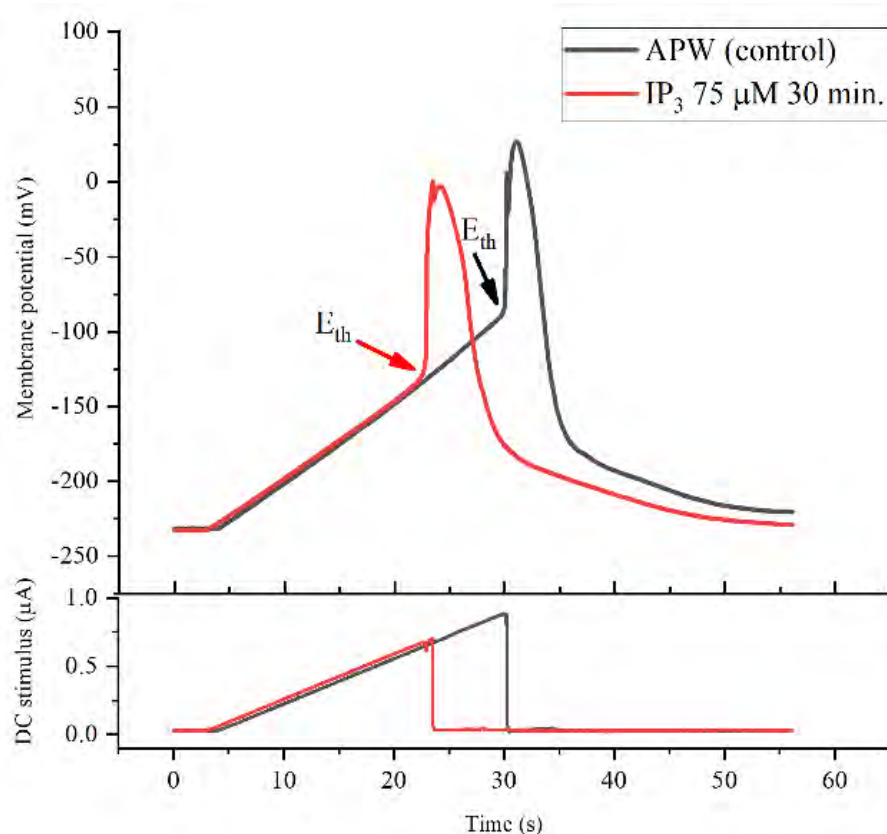


Fig. 1 Electrically induced action potentials of *Nitellopsis obtusa* internodal cell in standard conditions and after the 30 min exposure to 75 μM IP₃. E_{th} – excitation threshold.

[1] Thiel, G., MacRobbie, E. A., & Hanke, D. E., Raising the intracellular level of inositol 1, 4, 5-trisphosphate changes plasma membrane ion transport in characean algae, *EMBO Journal*, **9**(6), 1737-1741 (1990).

ELECTROCHEMICAL METHOD FOR HYBRIDISATION SIGNAL AMPLIFICATION OF METHYLENE BLUE-LABELLED DNA OLIGONUCLEOTIDES

Justina Gineitytė, Dalius Ratautas

Department of Bioanalysis, Institute of Biochemistry, Life Sciences Center, Vilnius University, Saulėtekio al. 7, LT-10257, Vilnius, Lithuania

Justina.Gineityte@gmc.vu.lt

Nucleic acid detection and quantification are crucial steps in many biotechnological and clinical applications, including disease diagnosis, genetic engineering, and personalized medicine. Current nucleic acid detection methods, such as polymerase chain reaction (PCR) and quantitative PCR (qPCR), usually employ optical signal readout methods [1]. Electrochemical readout could provide comparable or better sensitivity, specificity, cost-effectiveness, and simplicity, possibly faster sample-to-answer times. However, electrochemical nucleic acid sensors have limitations. One of the challenges – achieving clinically or technologically relevant detection limits – often requires complicated designs. The designs may involve surface damaging voltametric techniques (usually suitable only for end-point measurements) and the use of expensive nanomaterials.

In this study, we developed an electrochemical system for real-time detection of nucleic acid hybridisation. The target, single-stranded DNA (ssDNA) labelled with methylene blue (MB), was captured at a gold electrode by an immobilized complementary probe, resulting in an increase in oxidation current during constant potential amperometry measurements. The detection was enabled by the use of ascorbic acid (AA) as a freely diffusing signal amplifier [2]. AA reduced MB to leucomethylene blue (LB), which was oxidized back to MB at the electrode by applying an appropriate potential, creating a cyclical electrocatalytic amplification of the signal (Fig. 1). The resulting biosensor provides real-time hybridisation measurements with 1-second temporal resolution, enabling electrochemical readout of a redox-tagged oligonucleotide hybridisation signal. When compared to previously used hybridisation evaluation technique that employed cyclic voltammetry without signal amplification [3], the new method offers several advantages: (1) temporal resolution was improved from 20 s to 1 s; (2) assay time was reduced from 15 min to 5 min; (3) LOD was reduced by half to 5 nM.

In summary, the development of this electrochemical hybridisation biosensor brings a new level of simplicity, sensitivity, and speed to nucleic acid detection and quantification. Real-time signal readout allows using this tool for studying heterogenous hybridisation. Such biosensors have the potential to greatly improve biotechnological applications by providing more efficient and accurate results cost-effectively.

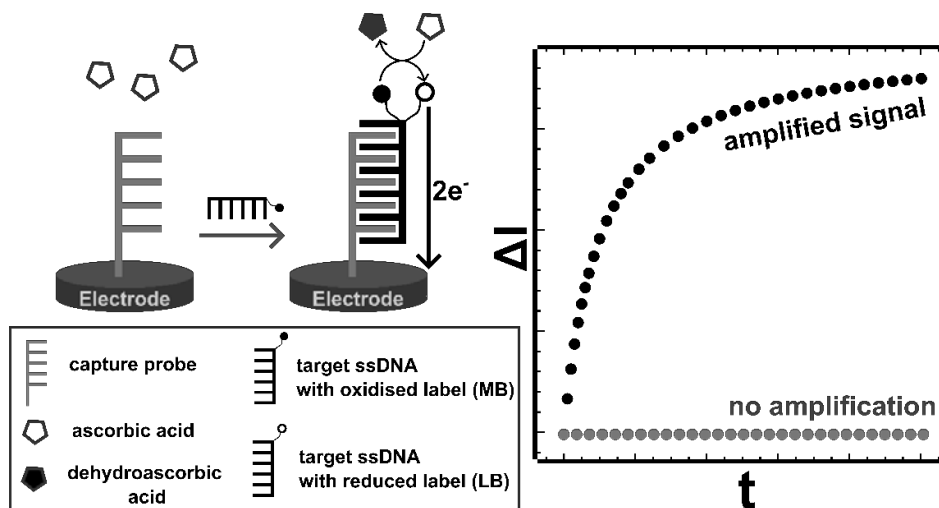


Fig. 1. Amperometric nucleic acid hybridisation monitoring enabled by signal amplification. Left – target oligonucleotide hybridisation and signal amplification scheme, legend below. Right – illustration of recorded current in case no signal amplification is employed, and in case the signal is amplified by ascorbic acid.

[1] Botella, J. R. Point-of-Care DNA Amplification for Disease Diagnosis and Management. *Annual Review of Phytopathology* **60**, 1–20 (2022).

[2] Mowry, S. & Ogren, P. J. Kinetics of Methylene Blue Reduction by Ascorbic Acid. *J. Chem. Educ.* **76**, 970 (1999).

[3] Serapinas, S. *et al.* Biosensor prototype for rapid detection and quantification of DNase activity. *Biosensors and Bioelectronics* **213**, 114475 (2022).

EVALUATION OF THE INFLUENCE OF SOLVENT AND STEPWISE EXTRACTION ON THE AMOUNT OF PHENOLIC AND FLAVONOID COMPOUNDS IN OAK ACORN EXTRACTS

Aurelija Kondratavičiūtė, Vilma Kaškonienė, Rūta Mickienė, Audrius Maruška

Instrumental Analysis Open Access Centre, Faculty of Natural Sciences, Vytautas Magnus University, Lithuania
aurelija.kondrataviciute@stud.vdu.lt

Oaks (*Quercus*) are widely distributed trees throughout the Northern Hemisphere, including Lithuania. These trees have a special fruit – acorns. The phytochemical potential, nutritional value, and biological activity of oak acorns are promising approaches in the management and treatment of various diseases [1]. There are naturally growing oaks and introduced oak species in Lithuania. Knowing that the common oak (*Quercus robur* L.) is a naturally growing oak in Lithuania, its fruits were selected for research. Furthermore, the fruits of red oak (*Quercus rubra* L.) were selected simultaneously because it is well adapted and widely introduced oak species in Lithuania.

Scientific literature [2] shows that all *Quercus* spp. acorns accumulate phytochemical compounds (phenolic compounds, volatile organic compounds, tocopherols, sterols, aliphatic alcohols, and fatty acids) that determine antioxidant and antibacterial properties. It is believable that the solvents of acorn extracts could significantly affect their biological activity [3]. Therefore, it is necessary to find the most optimal solvent, which would allow to extract the largest amounts of biologically active compounds and at the same time would be the most economical. For this reason, solvents such as bidistilled water (ddH₂O), methanol (MeOH), and ethyl acetate (EtOAc) were chosen to investigate. Stepwise extraction is also evaluated additionally. Total phenolic compounds and flavonoid content were evaluated in prepared extracts by spectrophotometric tests [4].

The study showed that the antioxidant properties of acorns depended on the species of oak and sample extraction method (Fig. 1). During the first extraction step, the MeOH solvent showed significantly ($p \leq 0.05$) higher amount of phenolic compounds compared to EtOAc. During the second step, it can be seen from the results that both ddH₂O and MeOH had better properties to extract biological amounts of phenolic compounds (Fig. 1). This may be because many biologically active compounds remain after the first step extraction, and both the second and third extractions from the same raw material allow the extraction of large amounts of biologically active compounds. The same trend is repeated in the extracts of the third step extraction. The amount of flavonoids in acorns (range from 0.23 to 3.42 mg/g) is significantly lower than that of phenolic compounds (range from 0.92 mg/g to 45.42 mg/g). The EtOAc-MeOH-ddH₂O extraction sequence was found to extract the highest amounts of total phenolics and flavonoids from both oak acorns (120.23 mg/g).

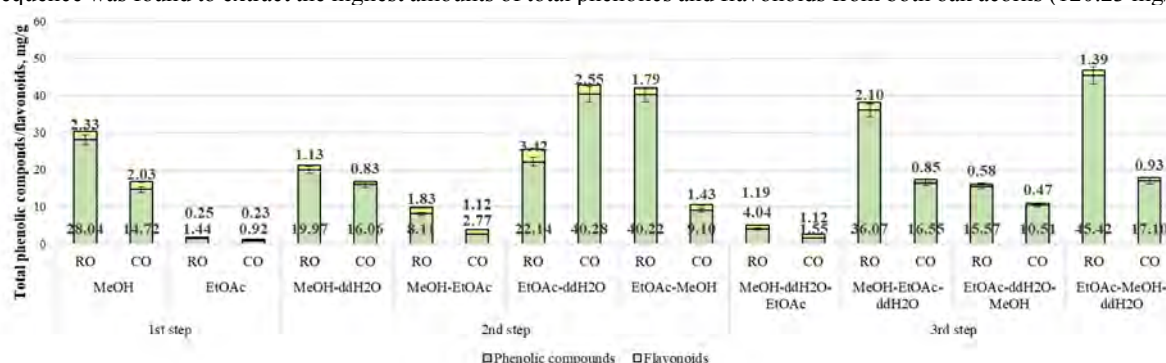


Fig. 1. Total amount of phenolic compounds and flavonoids extracted from *Q. rubra* (red oak) and *Q. robur* (common oak) acorns using different solvents and stepwise extraction (RO – red oak, CO – common oak, MeOH – methanol, EtOAc – ethyl acetate, ddH₂O - bidistilled water; n=3).

In the assessment of the amounts of bioactive compounds in different solvents and extraction methods, it can be stated that the methods used affected the amounts of phytochemical compounds, which can result in increased antioxidant activity. It is likely that the proper solvent and extraction conditions can be used to further enhance phytochemical levels in acorns.

Acknowledgments: This project has received funding from the Research Council of Lithuania (LMTLT), agreement No. S-ST-22-66.

- [1] Vinha, A.F., Barreira, J.C.M., Costa, A.S.G., et al., A new age for *Quercus* spp. fruits: review on nutritional and phytochemical composition and related biological activities of acorns. *Comprehensive Reviews in Food Science and Food Safety*, **15**(6), 947–981 (2016).
- [2] Burlacu, E., Nisca, A., Tanase, C. A comprehensive review of phytochemistry and biological activities of *Quercus* species. *Forests* **11**(9), 904 (2020).
- [3] Ngo, T. V., Scarlett, C. J., Bowyer et al., Impact of different extraction solvents on bioactive compounds and antioxidant capacity from the root of *Salacia chinensis* L. *Journal of Food Quality*, **1**, 1–8 (2017).
- [4] Adaškevičiūtė, V., Kaškonienė, V., Barčauskaitė, K., et al., The impact of fermentation on bee pollen polyphenolic compounds composition. *Antioxidants* **11**, 645 (2022).

EVALUATION OF THE IMPACT OF VARIOUS TREATMENT METHODS ON BEE-COLLECTED POLLEN BIOLOGICAL ACTIVITY

Lukas Asanavičius, Ieva Krivaitė, Vilma Kaškonienė, Nicola Tiso, Audrius Sigitas Maruška

Instrumental Analysis Open Access Center, Vytautas Magnus University, Lithuania
lukas.asanavicius@stud.vdu.lt

Bee pollen is a natural product made by bees (*Apis mellifera*). The main component of bee pollen is pollen collected from various plants, such as dandelion, rape, clover, lime, willow, and many more. Collected pollen is first treated with bee saliva enzymes, such as amylase and catalase, then stuck together by nectar and formed into small granules which are called bee pollen. Bee pollen is rich in a plethora of nutrients, vitamins, minerals, and phenolic compounds which have positive effects on human health [1]. Unfortunately, the bioavailability of bee pollen is rather limited, due to a specific pollen wall, which is named exine. This exine wall is made out of sporopollenin, which makes the wall extremely elastic, sturdy, and resilient to chemical degradation. Due to the exine wall resilience to chemical degradation, humans only digest roughly 10-15% of bee pollen [2].

Several methods were described for the improvement of the bioavailability of bee pollen in the scientific literature, such as fermentation with kombucha [3], lactic acid bacteria [4], enzymatic hydrolysis [5], ultrasonic treatment and enzymatic hydrolysis together with ultrasonic treatment [5, 6]. All these methods showed promising results in the increase of bee pollen bioavailability, although, it is quite difficult to compare various treatment methods applied in different studies and select a better one due to the different parameters used during the experiments, such as temperature, bacteria culture, treatment time, ultrasonic frequency and different bee pollen botanic and geographic origin.

The aim of the present study was to evaluate and compare the impact of different bee pollen treatment methods on their biological activity. In this project, a Lithuanian bee pollen sample was treated with tibico (water kefir) and kombucha (tea fungus) symbiotic cultures of bacteria and yeast, tibico and kombucha mixture, pure lactic acid bacteria (*Bifidobacterium infantis*), hydrolytic enzymes, ultrasound, or ultrasound combined together with previously mentioned methods of the treatment. The changes in total phenolic compound content were evaluated in the samples before and after the treatment by spectrophotometric tests [7].

Results showed that all applied methods allowed to increase the release of biologically valuable bee pollen compounds. The increased level depended on the treatment method, however, the impact of bee pollen botanical origin should also be considered in future studies.

Acknowledgments: This project has received funding from the Research Council of Lithuania (LMTLT), agreement No. S-ST-22-62.

-
- [1] B. Denisov ir M. Denisov-Pietrzyk., Biological and therapeutic properties of bee pollen: a review, *Journal of the Science of Food and Agriculture* **96**, 4303-4309 (2016).
- [2] J. Brooks ir G. Shaw, Sporopollenin: A review of its chemistry, palaeochemistry and geochemistry, *Grana* **17**, 91-97 (1978).
- [3] E. Utoiu, F. Matei, A. Toma et al., Bee collected pollen with enhanced health benefits, produced by fermentation with kombucha consortium, *Nutrients* **10(10)**, no. 1365 (2018).
- [4] V. Kaškonienė, V. Adaškevičiūtė, P. Kaškonas et al., Antimicrobial and antioxidant activities of natural and fermented bee pollen, *Food Bioscience* **34**, no. 100532 (2020).
- [5] C. Zuluaga-Dominguez et al., Effect of enzymatic hydrolysis on structural characteristics and bioactive composition of bee-pollen, *Journal of Food Processing and Preservation* **43(7)**, 360-365 (2019).
- [6] J. Dong et al., Cell wall disruption of rape bee pollen treated with combination of protamex hydrolysis and ultrasonication, *Food Research International* **75**, 123-130 (2015).
- [7] V. Adaškevičiūtė, V. Kaškonienė, K. Barčauskaitė et al. The impact of fermentation on bee pollen polyphenolic compounds composition, *Antioxidants* **11(4)**, no. 645 (2022).

INVESTIGATING BODIPY-BASED SENSORS FOR MEASURING MICROVISCOSITY IN HUMAN BREAST CANCER CELLS

Džiugas Jurgutis^{1,2}, Greta Jarockytė^{1,2}, Aurimas Vyšniauskas³, Ričardas Rotomskis¹, Vitalijus Karabanovas^{1,4}

¹ Biomedical Physics Laboratory, National Cancer Institute, Vilnius, Lithuania

² Life Sciences Center, Vilnius University, Vilnius, Lithuania

³ State Research Institute Center for Physical Sciences and Technology, Vilnius, Lithuania

⁴ Department of Chemistry and Bioengineering, Vilnius Gediminas Technical University, Vilnius, Lithuania

dziugas.jurgutis@nvi.lt

Microviscosity of subcellular components is a critical factor in ensuring the structural and functional stability of cells, and regulating the diffusion of biomolecules within cells. Significant microviscosity alterations have been observed during various intracellular processes, such as apoptosis, differentiation, or diseases, such as diabetes or cancer [1]. However, microviscosity values within human breast cancer cells have yet to be determined. By measuring these values, it could be possible to identify different subtypes of breast cancer cells, therapy-resistant tumour cells, or cancer stem cells based on the microviscosity of their organelles.

Intracellular microviscosity measurements can be performed by utilising viscosity-sensitive fluorophores – molecular rotors, together with fluorescence lifetime imaging microscopy (FLIM). In molecular rotors, the degree of intramolecular rotation affects the efficiency of non-radiative relaxation from the excited state. Therefore, in micro-environment that is less viscous (e.g., cytoplasm), non-radiative decay dominates, resulting in a decrease of fluorescence intensity and lifetime of molecular rotors [1,2]. Molecular rotors based on boron-dipyrromethene or BODIPY framework are the most widely used due to their ease of functionalisation, photostability and biocompatibility. Recently, it was demonstrated that the functionalisation of *meso*-phenyl BODIPY (BDP-H) with a –NO₂ group results in a viscosity-sensor (BDP-NO₂) with an extremely wide viscosity-sensitivity range (0.5–50 000 cP) (Fig. 1.) [2]. However, optical properties of BDP-NO₂ in aqueous media and the ability of both molecules to sense microviscosity in cells have not been evaluated before.

The aim of our study was to determine the optical properties of BDP-NO₂ and BDP-H in aqueous media, and to investigate the applicability of these molecules to monitor microviscosity in the organelles of MCF-7 and MDA-MB-231 human breast cancer cells by FLIM.

Optical properties of BDP-NO₂ and BDP-H were determined in ethanol and 7.4 pH phosphate-buffered saline. Human breast cancer cells were imaged with a laser-scanning confocal microscope. Fluorescence lifetimes of BDP-H in live cancer cells were determined using a time-correlated single photon-counting based FLIM. BDP-H calibration curve obtained at 40 °C in toluene-castor oil mixtures of varying viscosity was used to convert fluorescence lifetime values to microviscosity.

Our findings indicate that BDP-NO₂ molecules form aggregates in aqueous media, thus the molecular rotor is unsuitable for biological systems. In contrast, the BDP-H molecular rotor exhibits better solubility in aqueous media and is more suitable for microviscosity measurements in live cells. Furthermore, BDP-H accumulates in lipid droplets and cytosol of MCF-7 and MDA-MB-231 cells and exhibits monoexponential fluorescence decays. By utilising BDP-H with FLIM, we were able to measure lipid droplet microviscosity in human breast cancer cell lines of different malignancy, and for the first time demonstrate a significant difference between the lipid droplet microviscosity in MCF-7 and MDA-MB-231 cancer cells [3]. We anticipate that microviscosity of lipid droplets will become a valuable biomarker for identifying the malignancy of cancer cells, and that the BDP-H molecular rotor could be used for this purpose.

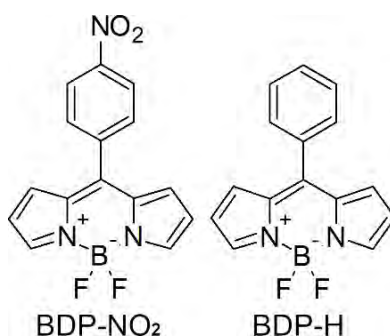


Fig. 1. The molecular structures of BDP-NO₂ and BDP-H molecular rotors investigated in this work [3].

[1] Kuimova, M. K. Mapping viscosity in cells using molecular rotors. *Phys. Chem. Chem. Phys.* 14, 12671–12686 (2012).

[2] Toliautas, S. et al. Enhancing the Viscosity-Sensitive Range of a BODIPY Molecular Rotor by Two Orders of Magnitude. *Chemistry – A European Journal* 25, 10342–10349 (2019).

[3] Jurgutis, D. et al. Exploring BODIPY-Based Sensor for Imaging of Intracellular Microviscosity in Human Breast Cancer Cells. *International Journal of Molecular Sciences* 23, 5687 (2022).

BIOCHEMICAL CHARACTERIZATION OF SARS-COV-2 3-CHYMOTRYPSIN-LIKE PROTEASE

Kamilė Čerepenkaitė, Aurelija Mickevičiūtė, Asta Zubrienė

Department of Biothermodynamics and Drug Design, Institute of Biotechnology,
Life Sciences Center, Vilnius University, Saulėtekio 7, Vilnius, Lithuania
kamile.cerepenkaite@chgf.stud.vu.lt

In 2020, the global pandemic of COVID-19 was caused by a highly contagious and occasionally fatal severe acute respiratory syndrome coronavirus 2 (SARS-CoV-2). The virus regularly causes mild upper respiratory tract illness, sometimes leading to life-threatening conditions. The search for chemical substances that would act as antiviral drugs against SARS-CoV-2 has been of great importance.

The assembly of mature SARS-CoV-2 viral particles is mediated by main or 3-chymotrypsin like protease (Mpro or 3CLpro). It is one of the 29 proteins encoded in the SARS-CoV-2 genome, responsible for the cleavage of polyproteins in 11 conserved sites. 3CLpro is intensively explored as a potential drug target for the inhibition of viral replication¹. Both synthetic compounds and natural substances are investigated as possible antiviral drug candidates using *in silico*-based, *in vitro* and *in vivo* approaches².

To obtain 3CLpro proteins, two recombinant plasmids were designed and expressed in *E. coli*. The proteins were purified by affinity chromatography and their catalytic efficiency was determined using *in vitro* enzyme inhibition assay and later compared with commercially available wild-type 3CLpro. 3CLpro showing the greatest activity was chosen to determine the thermal properties of the protein and screen more than 250 flavonoids as potential 3CLpro inhibitors using fluorescent thermal shift assay. The compounds that stabilized or destabilized the protein were further investigated using FRET-based enzymatic assay. Consequently, several flavonoids were identified as inhibitory compounds and their K_d values were determined by dose-response analysis (Fig. 1), suggesting that naturally derived compounds could be considered potential 3CLpro inhibitors.

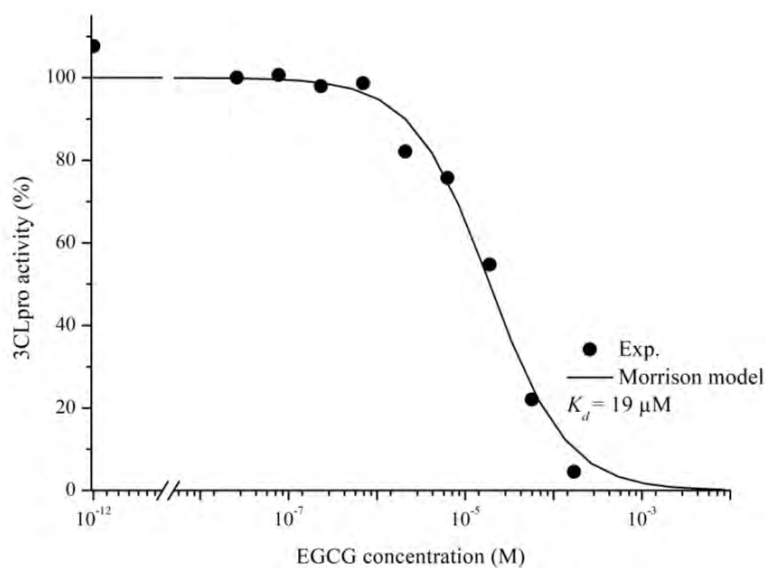


Fig. 1. Dose-response curve of 3CLpro inhibition with epigallocatechin gallate.

[1] Mengist HM, Dilnessa T, Jin T. Structural Basis of Potential Inhibitors Targeting SARS-CoV-2 Main Protease. *Front Chem.* 2021;9. doi:10.3389/fchem.2021.622898

[2] Hu, Q. et al. The SARS-CoV-2 main protease (Mpro): Structure, function, and emerging therapies for COVID-19. *MedComm vol. 3* Preprint at <https://doi.org/10.1002/mco2.151> (2022).

PROTOTYPE OF ANTIMICROBIAL PHOTOINACTIVATION TO PROTECT AGAINST FUNGI PHYTOPATHOGENS AND EXTEND THE SHELF-LIFE OF STRAWBERRY FRUITS IN GREENHOUSES

Goda Mažeikaite¹, Irina Buchovec¹, Pranciškus Vitta¹

¹Institute of Photonics and Nanotechnology, Faculty of Physics, Vilnius, Lithuania
goda.mazeikaite@ff.stud.vu.lt

Strawberry fruits contain vitamins, minerals, dietary fibers, phenolic antioxidants, and other bioactive compounds, making them an essential part of the nutritional pyramid. On the other hand, fresh products are one of the main sources of foodborne illness [1]. Strawberries need plenty of sunlight and well-drained soil, suggesting them to be grown in greenhouses in northern regions. However, in greenhouses the environmental conditions ideal for mould phytopathogens is usually present. Therefore, this project aimed to develop a prototype system of antimicrobial photoinactivation (API) suitable for industrial applications to protect against fungi phytopathogens and extend the shelf-life of strawberry fruits. API is a modern biophotonic technology based on the interaction of a non-toxic photosensitizer (PS), molecular oxygen, and low doses of harmless light of a suitable wavelength to match the PS absorption region. [2].

A special LED-based irradiation system prototype for the photoactivation experiments was developed at the Institute of Photonics and Nanotechnology of Faculty of Physics in Vilnius University. The construction of the prototype frame was adjusted for the usage in greenhouse since the prototype complies with electrical, mechanical and UV protection requirements (Fig 1. A).

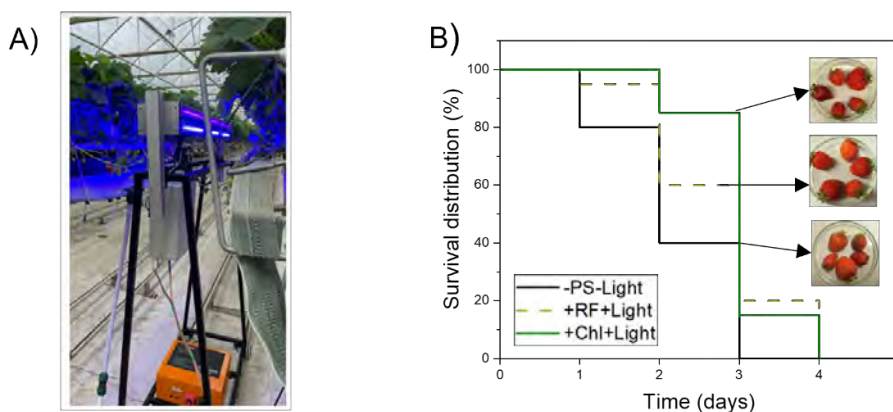


Fig. 1. LED-based irradiation system prototype demonstration in the greenhouse (A) and evaluation of shelf-life (storage at 20 ± 2 °C) of strawberries treated by API (B): -PS-Light -soaked in distilled water (without RF and Chl) and non-irradiated; +RF+Light – soaked in 1.1×10^{-4} mol/L RF solution and irradiated; +Chl+Light – soaked in 1.5×10^{-4} mol/L Chl solution and irradiated. Irradiation conditions: two irradiation steps by 30 min with 440 nm (40 ± 5 mW/cm²)/402 nm (30 ± 5 mW/cm²) combined light.

We used natural and water-soluble PSs magnesium chlorophyllin (Chl) and riboflavin (RF). Berries were soaked in the 1.5×10^{-4} mol/L Chl and 1.1×10^{-4} mol/L RF solutions for 5 seconds and dried in the dark for 30 min. Then samples were irradiated with combination of 440 nm (40 ± 5 mW/cm²)/402 nm (30 ± 5 mW/cm²) light for 30 min (Step 1). Afterwards, the berries were turned over and irradiated again for 30 min (Step 2). All samples (irradiated and non-irradiated) were stored at room temperature (20 ± 2 °C). The surface temperature of berries was tracked during the light illumination. The shelf-life of berries was evaluated visually from the surface color changes and infected spots.

Results indicated that the treatment of strawberries with RF- and Chl-based API could prolong the shelf-life of strawberries compared to the control. On the third day of storage, all non-irradiated strawberries were infected. Meanwhile, the shelf-life of strawberries soaked in PS solutions and irradiated with the constructed prototype was extended by one day. No impact on the strawberry color or firmness was found after the irradiation. The temperature increase on the berries' surface did not exceed 40 °C (the temperature at which proteins' denaturation may already happen). Experimental data support the idea that constructed LED-based irradiation system prototype, together with natural PSs RF and Chl can be used in future for strawberry decontamination and shelf-life expansion in greenhouses.

[1] US Food and Drug Administration (2022) <https://www.fda.gov/food/consumers/what-you-need-know-about-foodborne-illnesses>

[2] Denis, et al. An introduction to photoantimicrobials: photodynamic therapy as a novel method of microbial pathogen eradication. in science against microbial pathogens: communicating current research and technological advances; formatex research center: badajoz, spain, pp. 675–682, 2011.

FERREDOXIN:NADP⁺ OXIDOREDUCTASE FROM *RHODOPSEUDOMONAS PALUSTRIS*: STEADY-STATE KINETICS AND POTENTIOMETRIC CHARACTERISTICS

Gintarė Maurutyte¹, Mindaugas Lesanavičius¹, Daisuke Seo², Narimantas Čėnas¹

¹ Department of Xenobiotics Biochemistry, Institute of Biochemistry, Life Sciences Center, Vilnius University, Lithuania

² Division of Material Sciences, Graduate School of Natural Science and Technology, Kanazawa University, Japan
gintare.maurutyte@chgf.stud.vu.lt

Ferredoxin:NADP⁺ oxidoreductases (FNRs, EC 1.18.1.2) are flavoenzymes classified as dehydrogenases – electrontransferases acting in electron transfer in plastids, mitochondria and bacteria. FNR catalyzed two electron transfer from two equivalents of reduced ferredoxin to NADP⁺ is the final step of electron transfer in photosynthesis, while electron transfer in the opposite direction is implicated in nitrogen fixation or isoprenoid biosynthesis. After the transfer of a single electron to the oxidant a FAD semiquinone forms. *Rhodospseudomonas palustris* is a Gram-negative purple nonsulfur bacterium exhibiting the ability to switch its metabolism between four different modes [1]. *R. palustris* ferredoxin:NADP⁺ oxidoreductase (*RpFNR*) belongs to novel subgroup of glutathione reductase-like FNRs resembling thioredoxin reductase. The key differences from other FNRs are a native homodimeric structure and NADP(H) binding domain being inserted between the two segments of an FAD binding domain.

By combining steady-state kinetics and photosensitization methods, here we present a study on the *RpFNR* catalyzed oxidation of NADPH in the presence of nonphysiological electron acceptors commonly considered to be xenobiotic compounds, often found as environmental pollutants or various drugs. These compounds exhibit redox-cycling behavior under aerobic conditions and this is considered to be the basis of their prooxidant cytotoxicity.

Based on the reactions of *RpFNR* with the 3-acetylpyridine adenine dinucleotide phosphate redox couple, we estimated the two-electron reduction midpoint potential of the FAD cofactor to be -0.285 V. 5-DeazaFMN-sensitized photoreduction revealed a -0.017 V separation of the redox potentials between the first and second electron transfer events. The mechanism of oxidation of *RpFNR* by several different groups of nonphysiological electron acceptors was examined. Quinone reductase and nitroreductase reactions proceed via a ping-pong mechanism. The k_{cat}/K_m values of quinones and aromatic *N*-oxides towards *RpFNR* increase with their single-electron reduction midpoint potential with a parabolic dependence. The same is true for nitroaromatic compounds, albeit their reactivity is lower and the increase is linear, owing to their electron self-exchange constants being lower by several orders of magnitude. This then illustrates that the reactivity is governed by the energetics of the compounds and not their structural features. A mixed single- and two-electron reduction was characteristic of quinones, whereas nitroaromatics were reduced entirely in a single-electron way. The calculated electron transfer distances in the reaction with quinones and nitroaromatics were close to the ones obtained in the studies of *Anabaena* and *Plasmodium falciparum* FNRs highlighting similar “intrinsic” reactivities [2,3].

[1] F. W. Larimer, P. Chain, L. Hauser et al., Complete genome sequence of the metabolically versatile photosynthetic bacterium *Rhodospseudomonas palustris*, Nat. Biotechnol. **22**, 55-61 (2004).

[2] Ž. Anusevičius, M. Martínez-Júlvez, C. G. Genzor et al., Electron transfer reactions of *Anabaena* PCC 7119 ferredoxin:NADP⁺ reductase with nonphysiological oxidants, Biochim. Biophys. Acta – Bioenerg. **1320**, 247-255 (1997).

[3] M. Lesanavičius, A. Aliverti, J. Šarlauskas et al., Reactions of *Plasmodium falciparum* ferredoxin:NADP⁺ oxidoreductase with redox cycling xenobiotics: a mechanistic study, Int. J. Mol. Sci. **21**, 3234 (2020).

CRYSTALLIZATION AND X-RAY STRUCTURAL ANALYSIS OF THSB PROTEINS FROM BACTERIAL ANTIVIRAL SYSTEM THOERIS

Deividas Vilutis¹, Arūnas Šilanskas¹, Mindaugas Zaremba¹, Giedrė Tamulaitienė¹

¹Department of Protein-Nucleic Acid Interactions, Institute of Biotechnology, Life Sciences Center, Vilnius University, 7 Saulėtekio Ave, LT- 10257 Vilnius
deividas.vilutis@gmc.vu.lt

Recently, bacterial antiviral systems have been shown to cluster side-by-side in bacterial genomes, forming 'defence islands', which lead to an explosion of new discoveries of prokaryotic antiviral systems [1, 2]. One of these new systems is named after the ancient Egyptian deity of protection and fertility, *Thoeris*. This system consists of two genes, *thsA* and *thsB*. The ThsB proteins share homology with the Toll-interleukin receptor (TIR) domains, and in prokaryotic genomes the homologous *thsB* genes are often located side-by-side in a single operon. Two types of ThsA are found: the first (TH1) consists of SIR2 and SLOG domains, the second (TH2) of transmembrane and Macro domains [2].

During bacteriophage infection, ThsB proteins of TH1 Thoeris system have been shown to produce the signalling molecule 1'-3'gcADPR from NAD⁺ [3-5]. These molecules are bound by the SLOG domain of the ThsA protein, which activates the NADase activity of the SIR2 domain when bound. Thus, when the phage infects the bacterium, the Thoeris system consumes all of the cell's NAD⁺, leading to cell death (Fig. 1.). To date, it is not yet known how ThsB recognises bacteriophage infection and how these proteins are activated to synthesise the signalling molecule [3].

Based on protein sequence ThsBs are classified into 7 phylogenetic clusters. To gain more insight into the function of the ThsB proteins, we decided to determine X-ray structures of ThsBs belonging to 3 different clusters – c2, c3 & c5. For this type of analysis, protein crystals are required, which are obtained by performing crystallization experiments with the purified recombinant protein. Crystal structures of the selected ThsB proteins would provide the basis for further studies on the recognition of bacteriophage infection and the regulation of the enzymatic activity of the ThsB proteins.

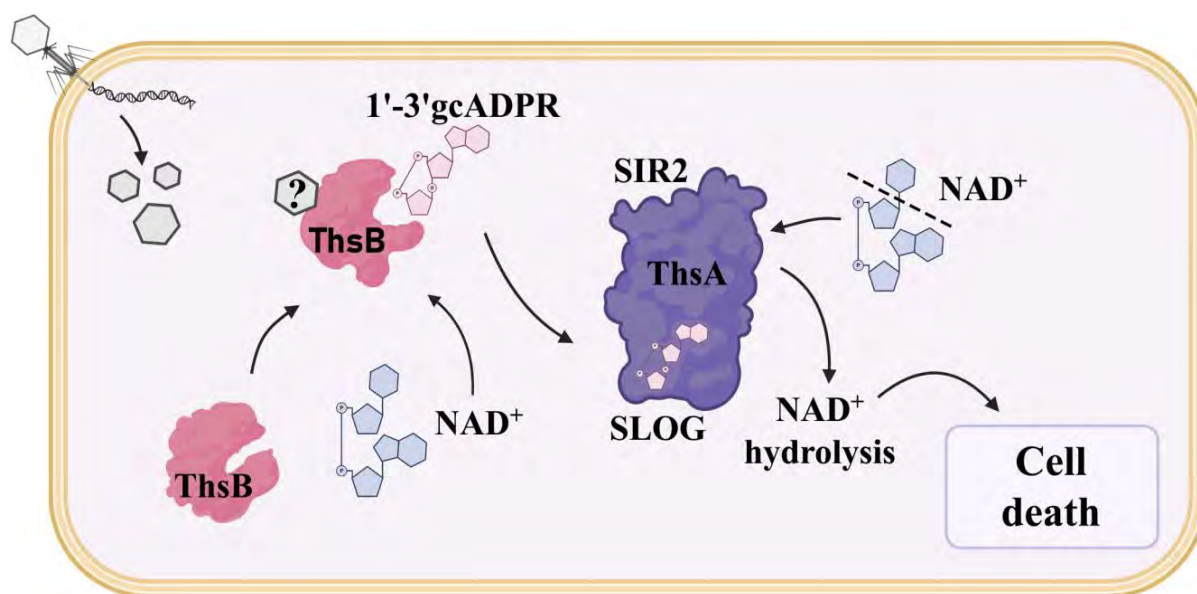


Fig. 1. Proposed mechanism of action of the TH1 Thoeris antiviral system.

[1] Makarova, K. S., Wolf, Y. I., Snir, S., & Koonin, E. V. (2011). Defense islands in bacterial and Archaeal genomes and prediction of novel defense systems. *Journal of Bacteriology*, 193(21), 6039-6056.

[2] Doron, S., Melamed, S., Ofir, G., Leavitt, A., Lopatina, A., Keren, M., Amitai, G., & Sorek, R. (2018). Systematic discovery of antiphage defense systems in the microbial pangenome. *Science*, 359(6379).

[3] Ofir, G., Herbst, E., Baroz, M., Cohen, D., Millman, A., Doron, S., Tal, N., Malheiro, D. B., Malitsky, S., Amitai, G., & Sorek, R. (2021). Antiviral activity of bacterial TIR domains via immune signalling molecules. *Nature*, 600(7887), 116-120.

[4] Leavitt, A., Yirmiya, E., Amitai, G., Lu, A., Garb, J., Morehouse, B. R., Hobbs, S. J., Kranzusch, P. J., & Sorek, R. (2022). Viruses inhibit TIR gcADPR signaling to overcome bacterial defense.

[5] Manik, M. K., Shi, Y., Li, S., Zaydman, M. A., Damaraju, N., Eastman, S., Smith, T. G., Gu, W., Masic, V., Mosaiab, T., Weagley, J. S., Hancock, S. J., Vasquez, E., Hartley-Tassell, L., Kargios, N., Maruta, N., Lim, B. Y., Burdett, H., Landsberg, M. J., ... Kobe, B. (2022). Cyclic ADP ribose isomers: Production, chemical structures, and immune signaling. *Science*, 377(6614).

UNCOVERING THE ROLE OF 5'-NAD-RNA HYDROLYSIS-ASSOCIATED PROTEINS IN *ESCHERICHIA COLI*

Gytė Tupikaitė¹, Gabrielė Olendraite¹, Renatas Krasauskas¹, Milda Mickutė¹, Giedrius Vilkaitis¹

¹Department of Biological DNA Modification, Institute of Biotechnology, Life Sciences Center, Vilnius
gyte.tupikaite@gmc.vu.lt; gabriele.olendraite@gmc.vu.lt

Modification at the 5'-end of RNA was thought to be a distinguishing feature of eukaryotes. Eukaryotic mRNA is known to possess a 7-methylguanosine cap (m⁷G) at the 5'-end, which protects the transcript from degradation and plays an essential role in its maturation, localization, and transcription [1]. However, it is now established that prokaryotes have a diverse 5'-end modification repertoire that comprises 30 different molecules. One of the most abundant 5'-RNA conjugates in *Escherichia coli* is nicotinamide adenine dinucleotide (NAD) [2]. The main known function of this non-canonical cap in prokaryotes is the protection of RNA from degradation [3], but only a few proteins have been found capable of regulating 5'-NAD capping.

Members of the Nudix superfamily, previously shown to have decapping activity on the canonical eukaryotic m⁷G cap, are known to be among the proteins in prokaryotes capable of removing the 5'-NAD-RNA cap. In *Escherichia coli* bacteria Nudix hydrolase NudC can hydrolyze 5'-NAD-RNA to 5'-P-RNA, initiating RNA degradation by RNase E [4]. However, as it is unclear how this protein interacts with RNA, our laboratory identified one of the potential partners cold-shock DEAD-box RNA helicase – DeaD. Although the molecular function of these proteins has been extensively studied, further research is necessary to fully comprehend their significance on bacterial physiology and the importance of this noncanonical cap.

In this study, we aimed to extend current knowledge about 5'-NAD-RNA hydrolysis-associated proteins by analyzing the impact of *E. coli* Nudix hydrolase NudC and its partner DeaD on bacterial growth (i), motility (ii), and the quantity of 5'-NAD-modified and unmodified RNA (iii). The effect of these protein on bacterial growth was examined by growing *E. coli* strains at optimal and cold shock temperature and it was found that helicase DeaD is crucial for bacteria growth at low temperature. For the first time, we demonstrated that hydrolase NudC can decrease bacterial swimming intensity at both optimal and low temperatures by carefully analysing the *E. coli* strain movement phenotype in a semi-liquid medium. Using Northern hybridization method, we successfully showed that both proteins and their complex affect not only the quantity of 5'-NAD cap-modified sRNA, but also the amount of total sRNA. Knowing that selective RNA degradation is one of the key factors in gene expression which affects rapid cell response to environmental change, deeper understanding of the specific mechanisms by which 5'-NAD-RNA capping contributes to gene expression would provide further insight into the regulatory networks underlying bacterial physiology and the broader implications of RNA modifications in cellular processes.

[1] E. Grudzien-Nogalska, M. Kiledjian, New insights into decapping enzymes and selective mRNA decay, *Wiley Interdisciplinary Reviews: RNA* 8(1), 1757-7012 (2017).

[2] Y. G. Chen, W. E. Kowtoniuk et al., LC/MS analysis of cellular RNA reveals NAD-linked RNA, *Nature Chemical Biology* 5(12), 879-881 (2009).

[3] A. Jäschke, K. Höfer et al., Cap-like structures in bacterial RNA and epitranscriptomic modification, *Current Opinion in Microbiology* 30, 44-49 (2016).

[4] S. Doamekpor, S. Sharma et al., Recent insights into noncanonical 5' capping and decapping of RNA, *Journal of Biological Chemistry* 298(8), 102171 (2022).

SIGNIFICANCE OF NOTCH SIGNALING PATHWAY IN COLORECTAL CANCER HCT116 AND ENDOMETRIAL CANCER KLE CELL LINES

Darija Šachova¹, Viktorija Stučytė¹, Eglė Žalytė¹, Violeta Jonušienė¹

¹ Department of Biochemistry and Molecular Biology, Institute of Biosciences, Vilnius University Life Sciences Center, Lithuania

darija.sachova@gmc.stud.vu.lt

Both colorectal cancer (CRC) and endometrial cancer (EC) remain among the most commonly diagnosed cancer types in the general population of humans [1, 2]. Depending on the cancer progression, the tumour may be surgically removed or treated with chemotherapeutics. However, chemotherapy response rates for advanced CRC and EC remain low, primarily due to intrinsic or acquired chemoresistance. Despite already described molecular mechanisms, there are other significant biochemical traits that are essential to understand in order to develop efficient therapy.

In recent years, an increasing number of studies have linked the development of malignant cells to dysregulation of signaling pathways in these cells. One such mechanism is the evolutionary conserved pathway known as Notch signaling, which is involved in the cell differentiation, proliferation and apoptosis processes. In mammals, the Notch pathway consists of four corresponding receptors (NOTCH 1-4) and five ligands (DLL1,3,4 and JAG1,2). Ligand and Notch receptor interaction activates γ -secretase protein complex, resulting in cleavage of the transmembranous Notch receptors and subsequent release of the intracellular domain (NICD). The NICD translocates into the nucleus and activates the transcription of Notch target genes by forming an activator complex with transcription factor CSL [3]. Alterations in Notch signaling pathway are proven to result in either suppressive or stimulating effect on tumor development in various cancer types, which makes it a viable therapeutic target.

To gain more insight into the significance of Notch signaling, we examined the impact of pathway suppression achieved by inhibiting γ -secretase both in colorectal cancer cells HCT116 and chemoresistant sublines HCT116/FU, HCT116/OXA as well as endometrial cancer cells KLE. We investigate the alteration of viability rate and other changes in target cell lines after applying γ -secretase inhibition alone or in combination with chemotherapeutic drugs, such as Oxaliplatin in case of colorectal cancer cells and Cisplatin and Paclitaxel in endometrial cancer cells.

This work was supported by the project MSF-JM-17/2022.

[1] Coll-de la Rubia E, Martinez-Garcia E, Dittmar G, Gil-Moreno A, Cabrera S, Colas E. Prognostic Biomarkers in Endometrial Cancer: A Systematic Review and Meta-Analysis. *J Clin Med.* 2020;9:

[2] Baidoun F, Elshiwly K, Elkerai Y, Merjaneh Z, Khoudari G, Sarmini MT, Gad M, Al-Husseini M, Saad A. Colorectal Cancer Epidemiology: Recent Trends and Impact on Outcomes. *Curr Drug Targets.* 2021;22:998-1009.

[3] Anusewicz D, Orzechowska M, Bednarek AK. Notch Signaling Pathway in Cancer-Review with Bioinformatic Analysis. *Cancers (Basel).* 2021;13:

STRUCTURAL AND FUNCTIONAL STUDIES OF THOERIS ANTIPHAGE DEFENSE SYSTEM

Dziugas Sabonis¹, Giedrius Sasnauskas¹, Audrone Ruksenaite¹, Arunas Silanskas¹, Gal Ofir², Rotem Sorek², Mindaugas Zaremba¹, Virginijus Siksnys¹, Giedre Tamulaitiene¹

¹ Institute of Biotechnology, Life Sciences Center, Vilnius University, Saulėtekio av. 7, LT-10257, Vilnius, Lithuania.

² Department of Molecular Genetics, Weizmann Institute of Science, Rehovot 7610001, Israel.

dziugas.sabonis@gmc.vu.lt

Prokaryotic antiviral (antiphage) defense system research is a rapidly developing field. In recent years, known arsenal of antiphage systems has expanded to over a hundred of confirmed unique instances [1]. Detailed investigation of these systems reveals unique molecular pathways and deepens our knowledge about microorganism ecology. However, only a small number of antiphage systems are characterized in depth.

Thoeris is a bacterial antiviral defense system composed of two genes *thsA* and *thsB*. ThsB protein contains Toll/interleukin-1 receptor (TIR) domain which is a canonical component of animal and plant immune systems. ThsA is composed of a sirtuin-like (SIR2) and SLOG domains [2]. Representative structures of ThsA and ThsB proteins and their functional studies were published recently [3, 4]. ThsB protein recognizes phage infection and produces a signaling molecule cyclic ADP ribose isomer 1''-3' gcADPR [5]. 1''-3' gcADPR is then bound by the ThsA SLOG domain and activates NAD⁺ hydrolysis by the SIR2 domain resulting in NAD⁺ depletion and host cell death [4]. However, it was not clear how binding of the signaling molecule turns on NADase activity of ThsA. In this work we reconstituted Thoeris enzymatic activities *in vitro* and using structural and biochemical methods showed the ThsA activation mechanism.

[1] Tesson, F., Hervé, A., Mordret, E., Touchon, M., d'Humières, C., Cury, J., & Bernheim, A. (2022). Systematic and quantitative view of the antiviral arsenal of prokaryotes. *Nature Communications* 2022 13:1, 13(1), 1–10.

[2] Doron, S., Melamed, S., Ofir, G., Leavitt, A., Lopatina, A., Keren, M., Amitai, G., & Sorek, R. (2018). Systematic discovery of antiphage defense systems in the microbial pangenome. *Science*, 359(6379),

[3] Ka, D., Oh, H., Park, E., Kim, J. H., & Bae, E. (2020). Structural and functional evidence of bacterial antiphage protection by Thoeris defense system via NAD⁺ degradation. *Nature Communications*, 11(1), 1–8.

[4] Ofir, G., Herbst, E., Baroz, M., Cohen, D., Millman, A., Doron, S., Tal, N., Malheiro, D. B. A., Malitsky, S., Amitai, G., & Sorek, R. (2021). Antiviral activity of bacterial TIR domains via immune signalling molecules. *Nature*, 600(7887), 116–120.

[5] Leavitt, A., Yirmiya, E., Amitai, G., Lu, A., Garb, J., Herbst, E., Morehouse, B. R., Hobbs, S. J., Antine, S. P., Sun, Z. Y. J., Kranzusch, P. J., & Sorek, R. (2022). Viruses inhibit TIR gcADPR signalling to overcome bacterial defence. *Nature* 2022 611:7935, 611(7935), 326–331.

INVESTIGATION OF THE PHOTOPHYSICAL PROPERTIES OF THE CHLOROPHYLLIN-CHITOSAN COMPLEX

Gabrielė Vasiliauskaitė¹, Irina Buchovec²

¹Department of Neurobiology and Biophysics, Vilnius University, Vilnius, Lithuania

²Institute of Photonics and Nanotechnology, Faculty of Physics, Vilnius University

Saulėtekio av. 3, Vilnius, Lithuania

gabriele.vasiliauskaite@gmc.stud.vu.lt

Emerging microbiological food safety issues is an increasing problem worldwide. As stated by the United States Food and Drug Administration, there are over 48 million cases of foodborne illness each year [1]. The high resistance of microbes to disinfecting agents has led to the development of alternative antimicrobial technologies. In this context, antimicrobial photodynamic inactivation (API) seems promising. The API principle is based on the combination of a non-toxic photosensitizer (PS) with light irradiation and molecular oxygen [2]. In order to enhance the antimicrobial efficiency of API, the combination of the API with the effects of biologically active agents, such as biodegradable and bactericidal biopolymer chitosan (CHS) is used [3]. The aim of this study was to make a photoactive chlorophyllin-chitosan complex (Chl-CHS) and to investigate the photophysical properties of the complex.

In the first stage of the work, several solutions were prepared: aqueous stock solution of CHS (pH 2.5 at 20 °C) containing 1% of CHS and 0.18% of HCl (Fig. 1A) and stock solution of 0.05% Chl (Fig. 1B). Afterwards, the stock solution of Chl-CHS complex (pH 2.5 at 20 °C) containing 1% of CHS, 1.5×10^{-5} M Chl and 0.18% of HCl was prepared by drop-wise addition of aqueous 0.05% Chl solution into rapidly spinning aqueous solution containing 1.25% of CHS and 0.23% of HCl (Fig. 1C)[3]. To investigate Chl-CHS aggregates, the complex solution was added to the phosphate-buffered saline buffer (PBS, pH ~ 7.4) and 0.9% NaCl (NaCl aqueous solution pH ~ 5.5).

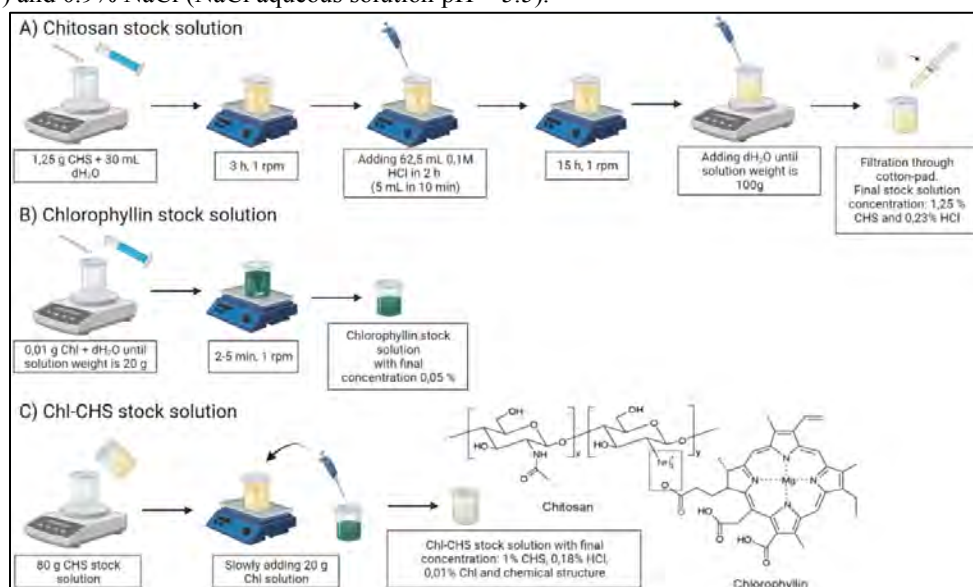


Fig. 1. Schematic illustration of chitosan (A), chlorophyllin (B) and chlorophyllin-chitosan complex (C) stock solutions preparation.

More different sizes of particles (size from 200 nm to 700 nm) were detected after aggregate measurements in the Chl-CHS complex in PBS at pH 7 than in NaCl (size from 200 nm to 400 nm) when the pH of the solution was only 5.5. It could be explained by the CHS being protonated at acidic pH and more residues becoming available. For further research, more photophysical properties of the Chl-CHS complex should be analysed, such as the dependence of photostability from solution pH and used irradiation dose.

[1] FDA, Food and Drug Administration, 2020 <https://www.fda.gov/>.

[2] A. Rapacka-Zdonczyk, et al. Factors Determining the susceptibility of Bacteria to Antibacterial Photodynamic Inactivation, *frontiers in Medicine* (2021).

[3] I. Buchovec, et al. Effective photosensitization-based inactivation of Gram(-) food pathogens and molds using the chlorophyllin-chitosan complex: towards photoactive edible coatings to preserve strawberries, *Royal Society of Chemistry* (2016).

LACTICASEIBACILLUS CASEI BL23 NON-CODING SLCB2236- SMALL RNA – MEDIATED RESPONSE TO ENVIRONMENTAL STRESSES

Odilija Safinaite¹, Renatas Krasauskas¹, Giedrius Vilkaitis¹

¹ Department of Biological DNA Modification, Institute of Biotechnology, Life Sciences Center Vilnius University, Lithuania

odilija.safinaite@gmc.stud.vu.lt

Lactocaseibacillus casei is a gram-positive lactic acid bacteria that can adapt to a wide range of environmental conditions. These bacteria are used as probiotics in fermented products and have beneficial effects on human health [1]. *L. casei* is an attractive research target as it can be used not only for food fermentation but also for various industrial applications such as the production of pharmaceuticals or biofuels [2]. Moreover, although the entire genome of *L. casei* BL23 has been sequenced [3], there is still not much known about the genes that determine environmental adaptation.

It is widely accepted that small non-coding RNA molecules (sRNAs) play one of the most important roles in the post-transcriptional regulation of gene expression by complementary binding to the target mRNA or protein itself. Changes induced by these molecules usually determine the amount or activity of the protein in the cell, which affects adaptation to the environment [4, 5]. With this in mind, we analysed sLCB2236-sRNA, which is conserved in all *L. casei* bacteria and is a potential regulatory molecule that could help bacteria adapt to environmental changes. Thus, the aim of this work was to determine the effects of sRNA deletion (sLCB2236-) on bacterial stress adaptation.

For this purpose, an *L. casei* Δ sLCB2236- deletant was constructed using CRISPR-Cas9^{D10A} nickase and, with wild-type and a deletant with reconstituted sRNA, seeded on agarised MRS media supplemented with different stressors such as ethanol, NaCl, H₂O₂, EDTA, Penicillin G, lysozyme, and bile acid. Furthermore, the agarised MRS media with bacteria was stored at different temperatures. The results showed that overexpression of sRNA increases bacterial resistance to ethanol stress, although it does not affect bacterial growth under other stresses.

In conclusion, we suggest that sLCB2236- is important for the adaptation of *L. casei* to ethanol-induced stress. In addition, this means that sLCB2236- could be suitable for research to confer ethanol resistance on other beneficial microorganisms that do not have this ability.

-
- [1] T. C. Pimentel, L. R. Brandão, M. P. de Oliveira, W. K. da Costa, & M. Magnani, Health benefits and technological effects of *Lactocaseibacillus casei*-01: An overview of the scientific literature, *Trends in Food Science & Technology*, 114, 722–737 (2021).
- [2] X. Song, H. Huang, Z. Xiong, L. Ai, & S. Yang, CRISPR-Cas9^{D10A} Nickase-Assisted Genome Editing in *Lactobacillus casei*, *Applied and environmental microbiology*, 83(22), e01259-17 (2017).
- [3] A. Mazé, G. Boël, M. Zúñiga, A. Bourand, V. Loux, M. J. Yebra et al., Complete genome sequence of the probiotic *lactobacillus casei* strain BL23, *Journal of Bacteriology*, 192(10), 2647–2648 (2010).
- [4] G. Storz, J. Vogel, & K. M. Wassarman, Regulation by small RNAs in bacteria: expanding frontiers, *Molecular cell*, 43(6), 880–891 (2011).
- [5] M. G. Jørgensen, J. S. Pettersen, & B. H. Kallipolitis, sRNA-mediated control in bacteria: An increasing diversity of regulatory mechanisms, *Biochimica et biophysica acta. Gene regulatory mechanisms*, 1863(5), 194504 (2020).

STUDY OF NEW ANTI-PHAGE DEFENSE SYSTEMS

Viktorija Rainytė¹, Paulius Toliušis¹, Mindaugas Zaremba¹

¹ Department of Protein - DNA Interactions, Vilnius University Life Sciences Center, Lithuania
viktorija.rainyte@gmc.stud.vu.lt

Bacteriophages are incredibly diverse and widespread viruses that constantly threaten bacteria. The continuing coevolutionary fight between bacteria and their viral predators has resulted in the development of sophisticated and diverse array of bacterial defense mechanisms such as well known restriction-modification and CRISPR-Cas systems. Discovery of these systems led to the development of precise molecular tools used in genetic engineering and genome manipulation, thus the identification of novel defense systems may result in the development of new tools for manipulating cells and genomes. On the basis of the discovery that anti-phage defense systems frequently form so-called "defence islands" in bacterial genomes, several groups have employed computational methods to detect new uncharacterized defense systems [1, 2].

Here, we present research of nine of these newly discovered systems which have well known nuclease, NTPase and DNA/RNA helicase domains. We showed that these systems are active and possess resistance against bacteriophages. Also, we successfully cloned these systems into high-copy plasmid DNAs and showed protein expression studies.

[1]Vassallo, C.N. *et al.* (2022) "A functional selection reveals previously undetected anti-phage defence systems in the E. Coli pangenome," *Nature Microbiology*, 7(10), pp. 1568–1579.

[2]Millman, A. *et al.* (2022) "An expanded arsenal of immune systems that protect bacteria from phages," *Cell Host & Microbe*, 30(11).

SYNTHESIS OPTIMIZATION OF ADOMET ANALOGUE FOR PHOTOCLEAVABLE GENE LABELING

Mindaugas Matonis¹, Martynas Malikėnas²

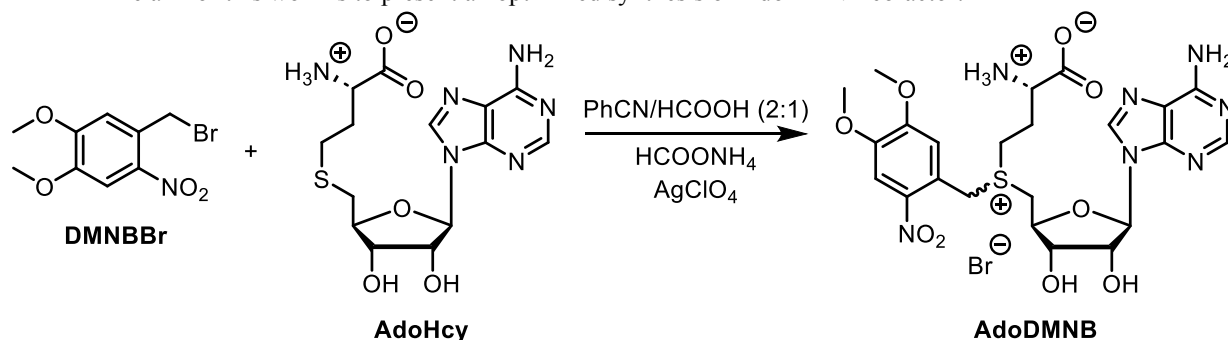
¹Faculty of Chemistry and Geosciences, Vilnius University, Lithuania

²Institute of Biotechnology, Vilnius University, Lithuania

mindaugas.matonis@chgf.stud.vu.lt

DNA methylation is a predominant epigenetic modification that regulates gene expression without altering the original DNA sequence [1]. In DNA, m⁵C leads to inactivation of transcriptional start sites, while its oxidative removal recovers gene expression [2]. The reaction occurs via methyltransferase (MTase) catalyzed S_N2 transfer of an activated sulfonium-bound methyl group from the cofactor S-adenosyl-L-methionine (SAM) to targeted DNA bases, S-adenosyl-L-homocysteine (SAH) serving as a leaving group [1][3]. The use of photolabile and reactive groups instead of methyl may lead to an easy way to make genetic modifications. Unfortunately, synthetic cofactors with functional groups other than methyl suffer from abysmal stability in the physiological medium and the limited literature on synthesis of the cofactors indicates unsatisfactory yields. Although DMNB is one of the functional groups that is stable in the physiological medium and shows promising application in gene labeling, synthesis yields are poor and need to be further optimized.

The aim of this work is to present an optimized synthesis of AdoDMNB cofactor.



Scheme 1. Synthesis of photocleavable group containing AdoMet cofactor analogue (AdoDMNB).

References:

- [1]. S. Klimašauskas and E. Weinhold, "A new tool for biotechnology: AdoMet-dependent methyltransferases," *Trends Biotechnol.*, vol. 25, no. 3, pp. 99–104, 2007, doi: 10.1016/j.tibtech.2007.01.006.
- [2]. F. Michailidou, N. Klöcker, N. V. Cornelissen, R. K. Singh, A. Peters, A. Ovcharenko, D. Kümmel, A. Rentmeister, *Angew. Chem. Int. Ed.* 2021, 60, 480. DOI: 10.1002/anie.202012623.
- [3]. G. Lukinavičius, M. Tomkuvienė, V. Masevičius, and S. Klimašauskas, "Enhanced chemical stability of AdoMet analogues for improved methyltransferase-directed labeling of DNA," *ACS Chem. Biol.*, vol. 8, no. 6, pp. 1134–1139, 2013, doi: 10.1021/cb300669x.

APPLICATION OF IMMOBILIZED FRUCTOSE DEHYDROGENASE ONTO MODIFIED GOLD NANOPARTICLES FOR D-TAGATOSE BIOSENSOR

Milda Stachnevičiūtė¹, Julija Razumienė¹, Marius Butkevičius¹

¹ Department of Bioanalysis, Institute of Biochemistry, Life Sciences Center, Vilnius University, Saulėtekio av. 7, LT-10257 Vilnius, Lithuania
milda.stachneviute@chgf.stud.vu.lt

During past years rare sugars, such as D-tagatose have drawn attention due to their ability to replace naturally occurring sugars that lead to obesity, hypertension, diabetes, etc. Nonetheless, heavy consumption of D-tagatose is shown to have negative effects, therefore quantitative and qualitative determination in various media is an important challenge [1]. Currently, only a few methods are used to detect D-tagatose: colorimetric, mass spectrometric and chromatographic. Unfortunately, these methods are complicated and do not allow for easy and fast analysis, so the aim of this work is to develop a sensor that can perform real-time analysis of D-tagatose synthesis in a bioreactor. Efficient direct electron transfer (DET) from an enzyme layer to the electrode is a highly desirable feature in biosensors, as it allows for a mediator-free system, which increases the sensitivity and selectivity of such a system and reduces its cost [2]. In our study we used D-fructose dehydrogenase (EC 1.1.99.11) from *Gluconobacter industrius* – an enzyme that catalyzes D-fructose oxidation to 5-keto-D-fructose. Despite the fact that this enzyme is very selective, after immobilization, its selectivity decreases and a new property of oxidizing D-tagatose appears. This feature allows to construct a D-tagatose bioelectrochemical sensor.

In this study we have constructed a stable biosensor and have shown its viability in a simulated bioreactor. Several different systems were tested: the surface of the working electrode with added gold nanoparticles (AuNP) was modified with thiol compounds with different functional groups – 4-mercapto phenol, 4-mercaptobenzoic acid, 4-methyl benzenethiol and 4-amino thiophenol. It was demonstrated that different thiols not only affect enzyme adsorption but also determine other properties of the biosensor, for example, detection linear range, sensitivity. Also, the long-term stability was investigated.

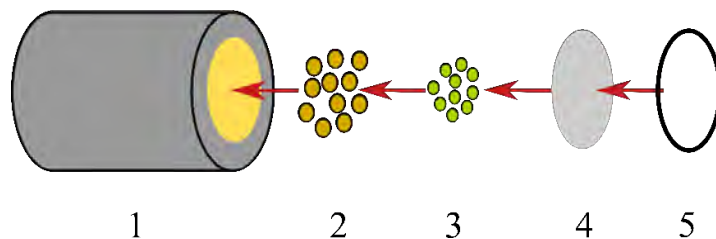


Fig.1 Simplified scheme of the D-tagatose biosensor: 1 — gold electrode, 2 — AuNPs modified with thiols 3— layer of FDH, 4—terylene film, 5—rubber ring.

[1] E. Voitechovič *et al.*, 'Bioamperometric Systems with Fructose Dehydrogenase From *Gluconobacter japonicus* for D-Tagatose Monitoring', *Electroanalysis*, vol. 33, no. 6, pp. 1393–1397, 2021, doi: 10.1002/elan.202060573.

[2] I. Šakinytė, M. Butkevičius, V. Gurevičienė, J. Stankevičiūtė, R. Meškys, and J. Razumienė, 'Reagentless D-Tagatose Biosensors Based on the Oriented Immobilization of Fructose Dehydrogenase onto Coated Gold Nanoparticles- or Reduced Graphene Oxide-Modified Surfaces: Application in a Prototype Bioreactor', *Biosensors*, vol. 11, no. 11, p. 466, Nov. 2021, doi: 10.3390/bios11110466.

THE DEVELOPMENT AND CHARACTERIZATION OF AN L-AMINO ACIDS BIOSENSOR

Deimantė Stakelytė^{1,2}, Justas Miškinis¹, Dalius Ratautas^{1,2}

¹Life Sciences Center, Vilnius University, Vilnius, Lithuania

²Department of Chemistry and Bioengineering, Vilnius Gediminas Technical University, Saulėtekio av. 11, 10223, Vilnius, Lithuania

deimante.stakelyte@stud.vilniustech.lt

Amino acids are of great interest due to their key role in human health. Increased levels of total plasma L-amino acids can be related to fructose intolerance, kidney failure, and ketoacidosis [1]; while lowered levels of total amino acids plasma can be a sign of nephrotic syndrome, Huntington's disease, rheumatoid arthritis and also fever [1]. Hence, the determination of L-amino acids in bodily fluids is of great importance. Enzymes are biocatalysts that increase the rate of biochemical reactions. Therefore, they are commonly used in the field of biosensors in the development of enzymatic biosensors. Due to the long history of enzyme-based biosensors, various biosensors can be produced on the basis of enzyme specificity.

The aim of this research was to develop an L-amino acids biosensor using immobilized L-amino acid oxidase from *Crotalus adamanteus*. L-amino acid oxidase is a flavoenzyme that catalyzes the oxidative deamination of L-amino acids to α -keto acids producing ammonia and hydrogen peroxide [2]. The resulting hydrogen peroxide diffuses to the surface of the working electrode, on which the electrochemical oxidation of hydrogen peroxide occurs. The immobilization of L-amino acid oxidase was achieved using bovine serum albumin, as a stabilizing agent and glutaraldehyde, as a cross-linking agent. The electrochemical performance of the sensor for detecting L-amino acids was investigated by cyclic voltammetry and chronoamperometry. The response to L-amino acids was linear in the range of 0.1 mM to 1 mM, correlation coefficient was 0.9998, sensitivity was 7073 $\mu\text{A mM}^{-1} \text{cm}^{-2}$, calculated limit of detection was 0.1 mM. To add more, after 40 days the biosensor still demonstrated more than 70 % of the initial activity indicating a good overall stability. The developed biosensor was tested on artificial and real samples and demonstrated fast assessment in analyzing amino acid levels in diluted serum samples obtained from patients undergoing renal replacement therapy.

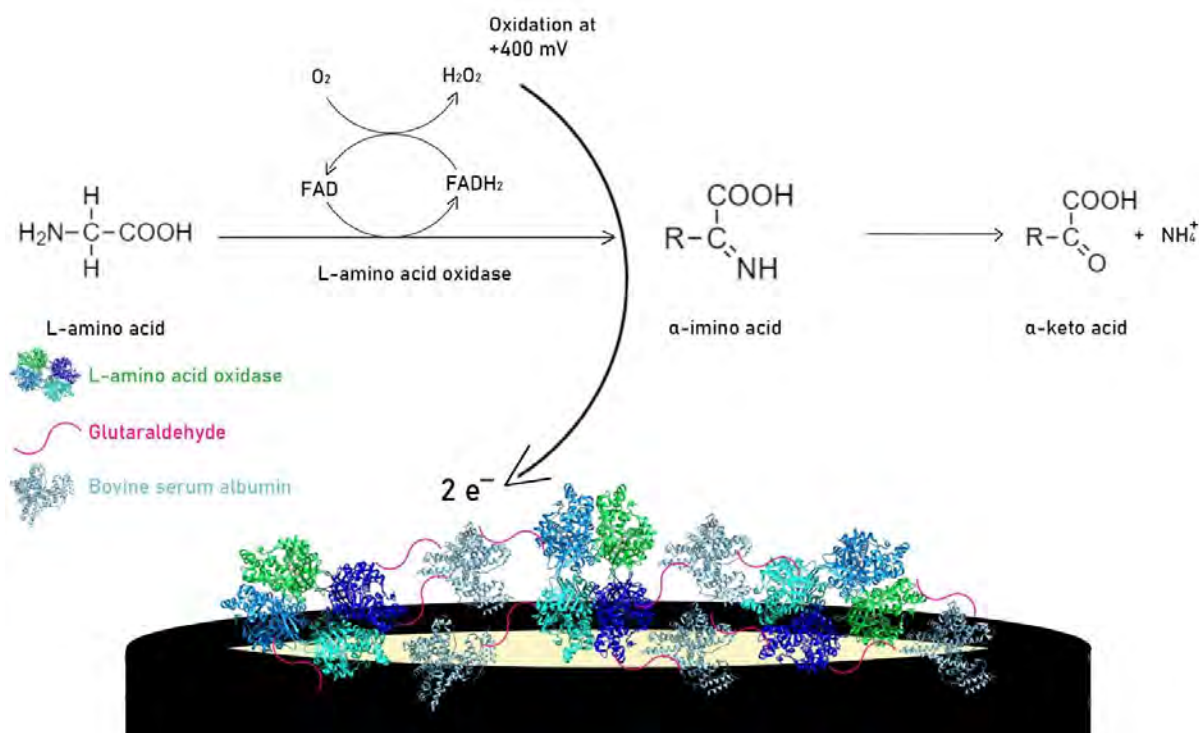


Fig. 1. Schematic representation of this biosensor.

[1] K. Moulae and G. Neri, "Electrochemical amino acid sensing: A review on challenges and achievements," *Biosensors*, vol. 11, no. 12, pp. 1–54, 2021, doi: 10.3390/bios11120502.

[2] D. Wellner and A. Meister, "Studies on the mechanism of action of L- amino acid oxidase," *J Biol Chem*, 1961, doi: [https://doi.org/10.1016/S0021-9258\(18\)64085-2](https://doi.org/10.1016/S0021-9258(18)64085-2).

A FLUORIMETRIC METHOD FOR NUCLEIC ACID CONTENT DETERMINATION BASED ON PROPIDIDIUM IODIDE STAINING

Rammukund Kishore Kumar¹, Dr. Baltramiejus Jakštys²

¹Department of Biology, Vytautas Magnus University, Lithuania

²Department of Biology, Drugs and gene delivery cluster, Vytautas Magnus University, Lithuania
rammukund.kishore-kumar@vdu.lt

Several molecular biology protocols rely on accurate nucleic acid detection and quantification. Eventhough several developments in nucleic acid stains, labels and other detection strategies have been made [1], these rely on expensive reagents and kits. When it comes to nucleic acid staining, two important factors that must be considered include sensitivity and selectivity of the method used. We describe a sensitive and selective method for fast nucleic acid quantification based on staining with the fluorescent probe, propidium iodide (PI).

Propidium iodide is a membrane impermeant dye that intercalates between base pairs in polynucleotides. It binds stoichiometrically to nucleic acids with the emission fluorescence intensity being proportional to the amount of nucleic acid in the sample [2]. Once the dye binds to nucleic acids, it undergoes a fluorescence enhancement of approximately 20-30 fold [3]. Propidium iodide staining has been employed previously in the analysis of apoptosis using flow cytometry [2], but here we describe a method to fluorometrically quantify nucleic acids (preferentially) in solution present along with contaminating biomolecules.

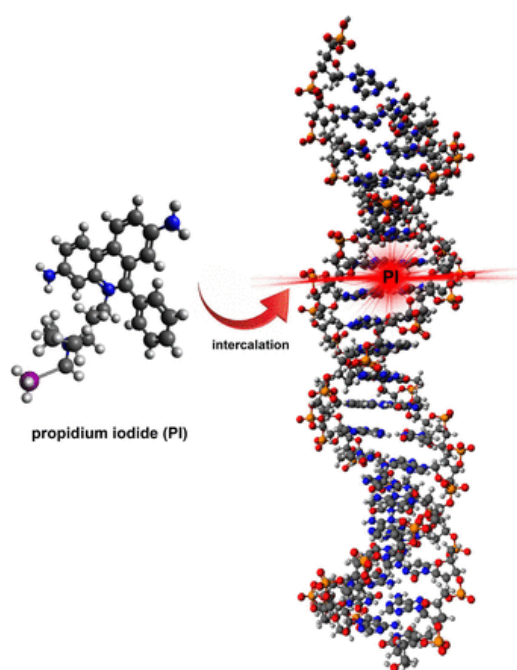


Fig. 1. Diagram showing PI intercalation between DNA bases [4]

CHO (Chinese Hamster Ovary) cells grown in RPMI-1640 medium supplemented with 1% L-glutamine, 10% FBS and 1% penicillin streptomycin were used as the model to study PI fluorescence emission dynamics vs PI concentration. The cells were suspended in a HEPES-based buffer and sonicated at 300-400W for 2-3s to completely disrupt the cell membrane and release their total nucleic acid (RNA + DNA) content. The results reveal a plateau in emission fluorescence intensity at PI concentrations - 40 μ M/ml, 20 μ M/ml, 12 μ M/ml and a roughly 50% decline in emission fluorescence intensity at 1 μ M/ml. We hypothesize that this decrease is a consequence of difference in selectivity of PI at low concentrations where it prefers to bind to DNA over RNA due to structural differences. Further investigations employing selective enzymatic degradation of nucleic acids will reveal the exact picture and we hope to achieve the same before the conference.

[1]Kricka, L. J. (2002). *Stains, labels and detection strategies for nucleic acids assays. Annals of Clinical Biochemistry*, 39(2), 114–129. doi:10.1258/0004563021901865

[2]Riccardi, C., & Nicoletti, I. (2006). Analysis of apoptosis by propidium iodide staining and flow cytometry. *Nature Protocols*, 1(3), 1458–1461. doi:10.1038/nprot.2006.238

[3] <https://assets.thermofisher.com/TFS-Assets/LSG/manuals/mp01304.pdf>

[4]Paulina Tomaszewska, Till K. Pellny, Luis Miguel Hernández, Rowan A. C. Mitchell, Valheria Castiblanco, José J. de Vega, Trude Schwarzacher, Pat (J.S.) Heslop-Harrison, bioRxiv 2021.03.26.437252; doi: <https://doi.org/10.1101/2021.03.26.437252>

SYNTHESIS OF AMINO ACID AND NUCLEOSIDE CONJUGATES

Kamilė Butkutė¹, Martyna Koplūnaitė¹, Rolandas Meškys¹

¹ Department of Molecular Microbiology and Biotechnology, Institute of Biochemistry, Life Sciences Center, Vilnius University

kamile.butkute@gmc.stud.vu.lt

Nucleosides are vital molecules that play functional and structural roles in organisms. Modification of these compounds can have a significant impact on their biological properties, as well as their potential toxicity and ability to serve as substrates for a diverse range of enzymes [1,2]. Among the diverse methods for designing prodrugs, amino acid and nucleoside conjugates, particularly phosphoramidate derivatives, have demonstrated substantial potential as effective antiviral agents [3]. The conjugation of nucleosides and amino acids serves to enhance biopharmaceutical properties and solubility of nucleosides, too [4].

In this study, we synthesized novel 2'-deoxycytidine *N*⁴-amino acid-acylated derivatives (Fig. 1. Product 1) and *N*-(4-(2'-deoxycytidinyl))amino acid amides (Fig. 1. Product 2) – the conjugates of amino acid and nucleoside. For synthesis of these conjugates we modified 2'-deoxycytidine with L-tyrosine, D-tyrosine, L-lysine and D-lysine. The synthesis of blocked amino acid-nucleoside conjugates was performed in a three-step process, including amino acid blocking, activation of the amino acid, and synthesis of the final compound via formation of an amide bond. The initial step involved the protection of the amino group of selected amino acids using di-*tert*-butyl dicarbonate. The Boc-protected amino acids were treated with NHS and DCC to generate activated amino acid esters. Reaction of these NHS-esters and 2'-deoxycytidine resulted in formation of *N*⁴-acyl-Boc-2'-deoxycytidine nucleosides (yield of 24-48%).

The synthesized nucleosides were deprotected using a catalyst-free method by heating at reflux in water. During the deprotection step the *N*⁴-acylated 2'-deoxycytidines underwent rearrangement to the corresponding *N*-(4-(2'-deoxycytidinyl))amino acid amides (yield of 20-63%).

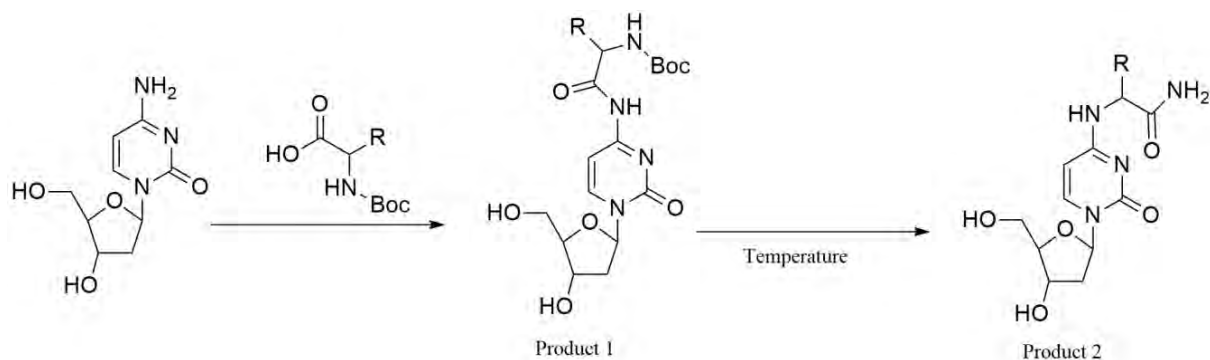


Fig. 1. Synthesis of amino acid and 2'-deoxycytidine conjugates.

- [1] Laponi MJ, Rivero CW, Zinni MA, Britos CN, Trelles JA, New developments in nucleoside analogues biosynthesis: A review, *Journal of Molecular Catalysis B: Enzymatic* **133**, 218-233 (2016).
- [2] Mahmoud S, Hasabelnaby S, Hammad S, Sakr T, Antiviral nucleoside and nucleotide analogs: a review, *Journal of Advanced Pharmacy Research* **2**, 73-88 (2018).
- [3] Li P, Ramsay Shaw B, Synthesis of Nucleoside Boranophosphoramidate Prodrugs Conjugated with Amino Acids, *The Journal of Organic Chemistry* **70** (6), 2171-2183 (2005).
- [4] Koplūnaitė M, Butkutė K, Meškys R, Tauraitė D, Synthesis of pyrimidine nucleoside and amino acid conjugates, *Tetrahedron Letters* **61**, 49 (2020).

ELECTROCHEMICAL INVESTIGATION OF PHOSPHOLIPID MEMBRANE DAMAGE INDUCED BY S100A9 PROTEIN

Evelina Jankaitytė¹, Darius Šulskis², Vytautas Smirnovas², Rima Budvytytė¹, Gintaras Valinčius¹

¹ Institute of Biochemistry, Life Sciences Center, Vilnius University, Vilnius, Lithuania

² Institute of Biotechnology, Life Sciences Center, Vilnius University, Vilnius, Lithuania

evelina.jankaityte@bchi.stud.vu.lt

Increased accumulation of misfolded proteins in the brain is a hallmark of several neurodegenerative disorders. In Alzheimer's disease (AD) abnormal levels of naturally occurring proteins clump together to form plaques that accumulate in the brain and disrupt functions of neurons [1]. S100A9 protein has amyloid-like properties and can be found in senile plaques together with amyloid beta peptide (A β). S100A9 is involved in the formation of aggregates and inflammatory processes [2]. One prevailing hypothesis suggests that toxic effect of amyloids is accomplished through a membrane disruption mechanism, which leads to loss of synaptic efficiency, neuronal dysfunction, and degeneration [3].

Biomimetic lipid bilayer systems are a useful tool for modelling specific properties of cellular membranes. In this work the interaction between S100A9 protein and tethered bilayer lipid membranes (tBLMs) was studied. Here we formed tBLMs and optimised their properties. The aim of our work was to use tBLM as a membrane model for studying S100A9 protein-induced membrane damage. Atomic force microscopy (AFM) was used for characterization of S100A9. By employing electrochemical impedance spectroscopy (EIS) we monitored membrane damage caused by protein. We observed that S100A9 aggregates at different stages of oligomerization exhibit different ability to impair integrity of phospholipid membranes. In addition, the effect of S100A9 protein depends on the lipid composition of the membrane.

[1] Li M, Chen L, Lee DHS, Yu LC, Zhang Y. *Progress in Neurobiology*. 2007; 83(3):131-139.

[2] Wang C, Klechikov AG, Gharibyan AL, Warmalander SKTS, Jarvet J, Zhao L, Xueen J, Shankar SK, Olofsson A, Brannstrom T, Mu Y, Graslund A, Morozova-Rpche LA. *Acta Neuropathologica*. 2013; 127(4):507-522.

[3] Kotler SA, Walsh P, Brender JR, Ramamoorthy A. *Chemical Society Reviews*. 2014; 43(19):6692-6700.

ARCHAEOGLOBUS FULGIDUS ARGONAUTE PROTEIN RECOGNIZES GUIDE AND TARGET STRANDS IN A SEQUENCE-SPECIFIC MANNER

Reda Pocevičiūtė^{1*}, Edvardas Golovinas¹, Elena Manakova¹, Mindaugas Zaremba¹

¹ Department of Protein-Nucleic Acids Interactions, Vilnius University, Lithuania
reda.poceviuciute@gmc.stud.vu.lt

Argonaute proteins (Ago) are found in all domains of life. Eukaryotic Argonautes (eAgo) are the catalytic core of RNA interference machinery, whereas prokaryotic Argonautes (pAgo) provide innate immunity to exogenous nucleic acids, such as plasmid or bacteriophage DNA. All pAgo share a similar mechanism of action, they use DNA or RNA guides to recognize complementary DNA or RNA targets. Upon target recognition, pAgo either cleaves the target strand or employs effector proteins, which leads to degradation of invading nucleic acids or, in some cases, cell death [3,4]. Knowledge of preferred guides and targets reveals valuable information about how pAgo obtain their guides and recognize invading nucleic acids.

The object of this study is an archaeal Argonaute protein AfAgo from *Archaeoglobus fulgidus*. Several groups published crystal structures of AfAgo with various nucleic acid substrates [2]. Therefore, it served as a structural Argonaute model in RNA interference studies. Although AfAgo was widely-studied, recently new features of AfAgo were described, such as ability to form homodimers and create DNA loops [1]. Latest crystal structure of AfAgo obtained in our group revealed several base specific contacts with three terminal base pairs of guide-target duplex. In addition to that, we showed that in vivo AfAgo binds RNA guides (gRNA) enriched in 5'-AUU sequence. Studies show that similarly to eAgo, pAgo may exhibit specificity to the guide strand 5' terminal nucleotide and respective complementary target strand nucleotide. However, this is the first example of more extensive specificity towards guide and target sequence [3].

In this study we compare AfAgo affinity towards RNA guides with different 5'-end sequence using electrophoretic mobility shift assay (EMSA). Results provide experimental evidence that AfAgo specifically recognizes RNA guides with 5'-AUU sequence. We also demonstrate that AfAgo:gRNA binary complex preferentially binds complementary DNA targets. These results challenge previous knowledge about AfAgo, since it was thought that AfAgo uses ssDNA guides and recognizes DNA targets, possibly due to the use of nonoptimal 5'-sequence guides in experiments [2].

[1] Golovinas, E., Rutkauskas, D., Manakova, E., Jankunec, M., Silanskas, A., Sasnauskas, G., & Zaremba, M. (2021). Prokaryotic Argonaute from *Archaeoglobus fulgidus* interacts with DNA as a homodimer. *Scientific Reports*, 11(1), 4518. DOI: 10.1038/s41598-021-83889-4

[2] Ma, J.-B., Yuan, Y.-R., Meister, G., Pei, Y., Tuschl, T., & Patel, D. J. (2005). Structural basis for 5'-end-specific recognition of guide RNA by the *A. fulgidus* Piwi protein. *Nature*, 434(7033). DOI: 10.1038/nature03514

[3] Ryazansky, S., Kulbachinskiy, A., & Aravin, A. A. (2018). The Expanded Universe of Prokaryotic Argonaute Proteins. DOI: 10.1128/mBio

[4] Zaremba, M., Dakineviciene, D., Golovinas, E., Zagorskaitė, E., Stankunas, E., Lopatina, A., Sorek, R., Manakova, E., Ruksenaite, A., Silanskas, A., Asmontas, S., Grybauskas, A., Tylenyte, U., Jurgelaitis, E., Grigaitis, R., Timinskas, K., Venclovas, Č., & Siksnyš, V. (2022). Short prokaryotic Argonautes provide defence against incoming mobile genetic elements through NAD⁺ depletion. *Nature Microbiology*, 7(11), 1857–1869. DOI: 10.1038/s41564-022-01239-0

STUDY OF THE STABILITY OF POTENTIAL DRUG CARRIERS, GRAPHENE QUANTUM DOTS AND DOXORUBICIN AGGREGATES BY OPTICAL METHODS

Martynas Zalieckas,^{1,2} Vilius Čirgelis,² Renata Karpicz²

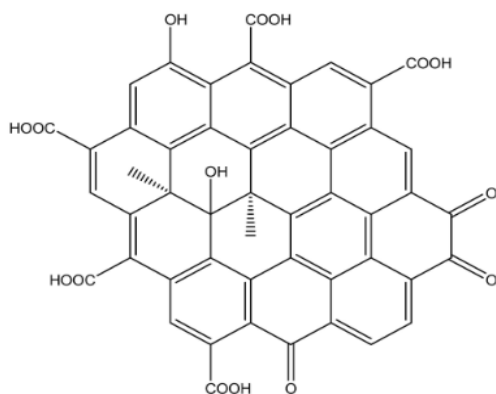
¹ Faculty of Fundamental Sciences, Vilnius Gediminas Technical University, Saulėtekio Ave. 11, LT-10223 Vilnius, Lithuania

² Center for Physical Sciences and Technology, Saulėtekio Ave. 3, LT-10257 Vilnius, Lithuania.
martynas.zalieckas@stud.vilniustech.lt

Doxorubicin (DOX) is an antibiotic of the anthracycline class widely used in cancer chemotherapy. This drug successfully inhibits the proliferation of cancer cells, but its effectiveness is limited by insufficient tissue penetration and high toxicity. Attempts are being made to solve this problem by creating and improving various carriers with the help of nanotechnology, which help the drug reach cancer cells effectively, causing as few side effects as possible.

Recently, graphene quantum dots (GQDs) have received special attention from scientists. GQDs are graphene nanoparticles with unique properties such as extremely low toxicity, chemical stability, biocompatibility, and excellent photoluminescence. Also, due to its extremely small size, it easily penetrates biological membranes. Due to these properties, GQDs have great potential in biomedicine, e.g., biosensor development, bioimaging, and most importantly, they are good drug nanocarriers. The properties of GQDs, especially the interaction with doxorubicin (fig. 1), are still under investigation.

A



B

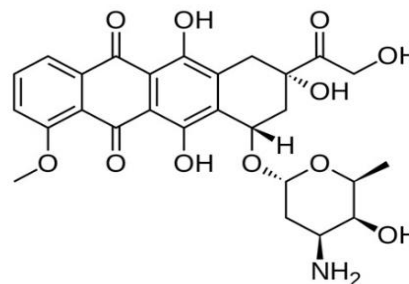


Fig. 1. Chemical structure of graphene quantum dots (A) and doxorubicin (B).

During this study, the absorption and fluorescence spectra of GQD and DOX, as well as the quenching kinetics, were measured in different pH environments using stationary spectrophotometry methods. The aim of the study is to evaluate the changes in the absorption and fluorescence spectra of GQD and DOX, and to investigate the stability of the formation of aggregates of these compounds over time in different pH environments.

MODULATION OF SPECIFIC DNMT1 ACTIVITY BY KINASE INHIBITORS IN MURINE EMBRYONIC STEM CELLS

Radvilas Bendorys¹, Liepa Gasiulė¹, Vaidotas Stankevičius¹

¹ Department of Biological DNA Modification, Institute of Biotechnology, Life Sciences Center, Vilnius University, Lithuania
radvilas.bendorys@gmc.vu.lt

5-methylcytosine (5mC) is a major biological DNA modification that is involved in mammalian development and disease. DNA methylation in cells is catalyzed by a collective activity of DNA methyltransferase (Dnmt) proteins, explicitly Dnmt1, Dnmt3a, and Dnmt3b, which transfer the methyl group from S-adenosyl-L-methionine (SAM or AdoMet) to the cytosine base in the DNA CpG sequence, while levels of DNA modification are regulated by the modulation of the amount of the individual enzyme or its catalytic efficiency. Despite recent advances, the precise role of each methyltransferase in the maintenance of cellular epigenomic status remains unclear.

Classically, mouse embryonic stem cells (mESCs) are cultured in the presence of leukemia inhibitory factor (LIF), which sustains the naive state of pluripotency but exhibit a significant heterogeneity. When mESCs are cultured in the presence of LIF and two additional kinase inhibitors (2i; MEK/ERK pathway inhibitor PD0325091 and Gsk-3 inhibitor CHIR99021), they can maintain a more homogeneous ground state of pluripotency. Furthermore, mESCs grown in LIF medium maintain a relatively high level of DNA 5mC, whereas 2i maintains mESC genomic DNA hypomethylation by promoting Dnmt3a and Dnmt3b protein degradation [1]. However, the regulation of specific Dnmt1 activity by individual MEK/ERK or Gsk-3 pathways is unknown.

In this work we aimed to evaluate a specific Dnmt1 activity in mouse embryonic stem E14tg2a cells after the treatment with 2i or each kinase inhibitor individually. For this purpose, we used a novel Dnmt1-specific genome tagging platform [2] to assess 5mC, 5azidoC and Dnmt gene expression levels in cells exposed to corresponding inhibitor. HPLC-MS analysis revealed that the levels of genomic DNA 5mC significantly decreased when E14tg2a cells were cultured with both or individual kinase inhibitors. Similarly, 5azidoC levels were significantly decreased in cells cultured with 2i, whereas the treatment with single inhibitor yielded different outcome: the MEK/ERK pathway inhibitor PD0325091 significantly reduced Dnmt1-specific genome tagging in cells, while CHIR99021 had no effect on 5azidoC levels. Real-time qPCR analysis unveiled that *Dnmt1* and *Uhrf1* mRNA expression remained stable after treatment with a single kinase inhibitor or their combination.

In summary, MEK/ERK signaling pathway is important in the regulation of Dnmt1 activity in mouse embryonic cells. As a result, the application of Dnmt1-specific genome tagging platform could be further expanded to investigate the regulation of catalytic Dnmt1 activity *in cellulo* by a variety of signaling pathways or particular “druggable” proteins.

[1] Sim Y.J., Kim M.S., Nayfeh A., Yun Y.J., Kim S.J., Park K.T., Kim C.H., Kim K.S. (2017) 2i maintains a naive ground state in ESCs through two distinct epigenetic mechanisms. *Stem Cell Rep.* 8:1312–1328

[2] Stankevičius V, Gibas P, Masiulionytė B, Gasiulė L, Masevičius V, Klimašauskas S, Vilkaitis G (2022) Selective chemical tracking of Dnmt1 catalytic activity in live cells. *Mol Cell* 82:1053–1065.e8

HALIDE METHYLTRANSFERASE AS AN EFFICIENT TOOL FOR CHEMOENZYMATIC COFACTORS SYNTHESIS

Goda Jankauskaitė¹, Bernadeta Masiulionytė¹, Giedrius Vilkaitis¹

¹Department of Biological DNA Modification, Institute of Biotechnology, Life Sciences Center, Vilnius University, Lithuania
goda.jankauskaite@gmc.vu.lt

Methylation of DNA cytosines or adenines, RNA adenines or riboses, histone amino acids are pivotal epigenetic mechanisms that are paramount importance for various biological processes including mammalian embryonic development, normal regulation of transcription, chromatin structure, disease pathogenesis and other. Aberrations in the methylation mechanisms usually cause cellular processes dysregulations which usually provoke human diseases such as neurodegenerative disorders, cancer and others [1, 2].

A large family of *S*-adenosyl-L-methionine (AdoMet)-depended methyltransferases (MTases) catalyzes the enzymatic methylation mechanism. These enzymes are widely used as a biotechnological tool for biomolecules such as DNA, RNA, proteins or small molecules specific targeting to deciphering epigenetic or biological processes and their regulation. Moreover, methyltransferases are used as a tool for chemoenzymatic production of small compounds such as pharmaceutical, vanillin or artificial compounds [3, 4]. To pave the way for a broader utilization of MTases in area of chemical and synthetic biology to produce various compounds we used halide methyltransferases (HMT) for deeper analysis of enzymatic parameters and HMT-based system for AdoMet cofactor synthesis. We analyzed HMT enzymes from different organisms and off-the-shelf reagent methyl iodide for chemoenzymatic synthesis of cofactor AdoMet. Furthermore, we showed that HMT-based system in enzyme cascades with various DNA methyltransferases could be used for specific DNA targets methylation. We proposed that wider utilization of promiscuous HMT could broaden a high-throughput approaches for chemoenzymatic synthesis of AdoMet cofactors *in vitro* or even *in vivo*.

-
- [1] M. V. C. Greenberg and D. Bourc'his, 'The diverse roles of DNA methylation in mammalian development and disease', *Nat Rev Mol Cell Biol*, vol. 20, no. 10, Art. no. 10, Oct. 2019, doi: 10.1038/s41580-019-0159-6.
- [2] K. D. Robertson, 'DNA methylation and human disease', *Nat Rev Genet*, vol. 6, no. 8, Art. no. 8, Aug. 2005, doi: 10.1038/nrg1655.
- [3] M. Tomkuvienė, M. Mickutė, G. Vilkaitis, and S. Klimašauskas, 'Repurposing enzymatic transferase reactions for targeted labeling and analysis of DNA and RNA', *Curr Opin Biotechnol*, vol. 55, pp. 114–123, Feb. 2019, doi: 10.1016/j.copbio.2018.09.008.
- [4] C. Liao and F. P. Seebeck, 'S-adenosylhomocysteine as a methyl transfer catalyst in biocatalytic methylation reactions', *Nat Catal*, vol. 2, no. 8, Art. no. 8, Aug. 2019, doi: 10.1038/s41929-019-0300-0.

RESEARCH ON CELL PLASMA MEMBRANE PERMEABILIZATION, RESEALING AND CELL VIABILITY AFTER ELECTROPORATION

Dominykas Makarovas¹, Baltramiejus Jakštys², Saulius Šatkauskas^{2*}

¹ Biochemistry Cathedral, Faculty of Natural Sciences, Vytautas Magnus University, Kaunas, Lithuania

² Research on Delivery of Medicine and Genes Group, Research Institute of Natural and Technological Sciences, Vytautas Magnus University, Kaunas, Lithuania
dominykas.makarovas@stud.vdu.lt

Electroporation (EP) is the process when cell plasma membrane gets permeabilized due to applied short, high amplitude electrical pulses. It is thought, that increased cell plasma membrane permeability is increased due to formation of electropores [1]. However, the actual mechanism of electroporeabilization remains unclear. The main electric pulse parameters that affect electroporation efficiency are pulse intensity, duration and pulse number. If any of parameter is too high, the outcome leads to a decrease in cell viability [2]. For cells to remain vital after EP, cells must restore their plasma membrane integrity. Recent studies demonstrate the importance of annexin family proteins that are fundamental proteins for injured plasma membrane repair. One of the most abundant proteins from the annexins family is the annexin A4. Through over 40 years of research on electroporation phenomenon there are barely a few investigations on protein impact on cell plasma membrane recovery. In this work we aimed to figure out how calcium affects wild type MCF7 cells, in which annexin A4 gene is fully functional compared with MCF7-ANXA4- knock out (KO) cells in which this gene expression was disturbed, after electroporation.

We used MTS method to determine cell viability. Cell plasma membrane repair and electroporeabilization dynamics were evaluated using flow cytometry measuring propidium iodide positive cells. CaCl₂ concentration was 2 mM. Cells were electroporated with 1 of 100 μs duration electric pulses at varying pulse intensities.

Collected results showed that wild type MCF7 and MCF7-ANXA4- KO cells respond to electroporation at the same or very similar pattern. On the other hand, we determined that calcium did not affect propidium iodide electrotransfer but decreased cell viability and disrupted cell plasma membrane repair process leading to higher amounts of electroporeabilized cell amounts. These results suggest that annexin A4 might be not that crucial to cell plasma membrane repair after EP.

[1] Neumann E., Ridder M. S., Wang Y., Hofschneider P.H. (1982). Gene transfer into mouse lyoma cells by electroporation in high electric fields. *EMBO*, 1(7): 841-845.

[2] Jakštys B., Jakutavičiūtė M., Uždavinytė D., Šatkauskienė I., Šatkauskas S. (2020). Correlation between the loss of intracellular molecules and cell viability after cell electroporation. *Bioelectrochemistry*, 135: 107550.

TITANIUM VS STAINLESS-STEEL ELECTRODES IN ELECTROPORATION: COMPARING CELL TRANSFECTION, PERMEABILITY, PORE RESEALING AND VIABILITY

Dominyka Gabulaitė¹, Baltramiejus Jakštys², Saulius Šatkauskas²

¹Biochemistry Cathedral, Faculty of Natural Sciences, Vytautas Magnus University, Kaunas, Lithuania

²Research on Delivery of Medicine and Genes Group, Research Institute of Natural and Technological Sciences, Vytautas Magnus University, Kaunas, Lithuania
dominyka.gabulaite@stud.vdu.lt

During electroporation (EP), short electric pulses increase cells permeability, thus leading to emphasized material transfer to cells like drugs and genes or intracellular molecules extracted from cells. One can find EP daily utilized in biotechnology, food industry and medicine. However, during pulsing metal ions get released from anode electrode and cause contamination of electroporated sample with these metal ions leading to changes in medium pH, cell viability, quench fluorescence of fluorophores etc. [1]. Scientist demonstrated that electrodes made from alloys, like aluminum, copper, contaminate samples with metal ions more significantly compared to stainless steel or more inert electrodes [2]. Moreover, it was determined that release of metal ions depend on electric pulse parameters [3]. However, we were unable to find titanium electrodes being used for EP. Here we compare stainless steel to titanium electrodes impact on cell electropermeabilization, gene electrotransfer, viability and pore resealing in regards to changing pulse duration and intensity, but maintaining the same pulse power.

Chinese hamster ovarian (CHO) cells were electroporated between titanium or stainless-steel electrodes with 0,1, 0,5 and 1 ms duration high voltage (HV) electric pulses. Flow cytometry was used to measure the amounts of cells that were permeabilized or irreversibly electroporated by determining number of propidium iodide (PI) positive cells (PI⁺). Transfection was performed using pEGFP-N1 plasmid and measured using flow cytometry 24 hours after EP. Cell viability was evaluated using colorimetric MTS assay 24 hours after treatments.

Results revealed that titan and stainless-steel electrodes give nearly identical amount of permeable CHO cells after EP. Similar tendencies were noticed measuring gene electrotransfer and pore resealing efficacies and cell viability cells electroporated between titanium electrodes gave similar results as cells electroporated between stainless-steel electrodes.

Overall, EP of CHO cells with different duration of 0.1 ms, 0.5 ms and 1 ms HV pulses bearing the same power output revealed no significant difference in results using titan either stainless-steel electrodes concerning electropermeabilization, gene electrotransfer, pore resealing efficacies and cell viability. Our data emphasize that using titanium electrodes for EP one may expect the same results as using stainless-steel electrodes.

[1] R. R. Rodaitė, R. Saulė., V. Snitka, G. Saulis, Release of Iron Ions from the Stainless-Steel Anode Occurring During High-Voltage Pulses and Its Consequences for Cell Electroporation Technology, *IEEE Transactions on Plasma Science* **42** 249-254 (2014).

[2] A. Vižintin, J. Vidmar, J. Ščančar, D. Miklavčič, Effect of interphase and interpulse delay in high-frequency irreversible electroporation pulses on cell survival, membrane permeabilization and electrode material release, *Bioelectrochemistry* **134** 107523 (2020).

[3] A. Vižintin, S. Marković, J. Ščančar, & D. Miklavčič, Electroporation with nanosecond pulses and bleomycin or cisplatin results in efficient cell kill and low metal release from electrodes. *Bioelectrochemistry* **140**, 107798 (2021).

LYSOZYME AMYLOID FIBRIL STRUCTURAL VARIABILITY DEPENDENCE ON INITIAL PROTEIN FOLDING STATE

Kamile Mikalauškaite, Mantas Ziaunys, Vytautas Smirnovas

Amyloid Research Sector, Institute of Biotechnology, Life Sciences Center, Vilnius University, Vilnius, Lithuania
kamile.mikalauškaite@gmc.vu.lt

Aggregation of amyloid proteins through the formation of amyloid fibrils is associated with various amyloidoses, including neurodegenerative disorders such as Alzheimer's, Parkinson's or prion diseases. Although for many years scientists have been trying to find out the mechanisms of aggregation and the factors affecting them, but this field is still strongly developed and not fully explored. Studies show that various environmental conditions such as protein concentration, ionic strength of the solution, pH or temperature can change the course of aggregation and affect the conformation of the resulting amyloid fibrils [1]. It has been observed that the polymorphism of prion protein fibrils is influenced by the initial folding form of the protein [2]. In this work, we wanted to investigate whether the variability of the fibril structures formed by one of the model proteins - hen egg white lysozyme - changes depending on the initial folding form of the protein, at a temperature lower or higher than the melting temperature.

Four temperatures (50, 55, 60, 65 °C) were chosen based on the results of the melting assay of lysozyme under experimental conditions (PBS buffer solution containing 2 M guanidine hydrochloride, pH 7.4). To better determine the variability of the secondary structures of the resulting fibrils, a full 96-well plate of identical lysozyme samples was analyzed at each temperature condition. Aggregation was performed at a constant 600 rpm agitation, using the fluorescent dye thioflavin-T (ThT). The conformations of the resulting amyloid fibrils were analyzed using Fourier transform infrared spectroscopy (FTIR) and atomic force microscopy (AFM).

The results of the study showed that the initial form of protein folding affects not only aggregation parameters such as lag time or apparent rate constant, but also the variability of the secondary structure of the resulting amyloid fibrils, the fluorescence intensity of bound-ThT and the processes of self-replication. In addition, these changes occur in a small temperature range where the protein's folding form changes.

[1] Sakalauskas, A.; Ziaunys, M.; Smirnovas, V. Concentration-dependent polymorphism of insulin amyloid fibrils. *PeerJ* 2019, 7, e8208.

[2] Ziaunys, M.; Sakalauskas, A.; Mikalauškaite, K.; Snieckute, R.; Smirnovas, V. Temperature-dependent structural variability of prion protein amyloid fibrils. *Int. J. Mol. Sci.* 2021, 22, 5075.

ENZYMATIC ELECTROCHEMICAL BIOSENSOR FOR EXTRACELLULAR GLUTAMATE DETECTION IN BIOFLUIDS

Roberta Stefanovič¹, Vidutė Gurevičienė², Julija Razumienė^{2*}

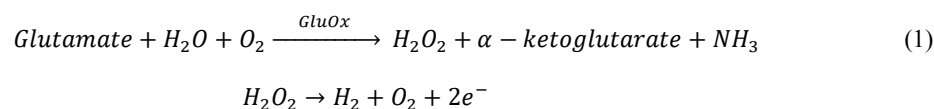
¹ Department of Neurobiology and Biophysics, Vilnius University, Lithuania

² Department of Bioanalysis, Vilnius University, Lithuania
roberta.stefanovic@gmc.stud.vu.lt

Glutamate (Glu) is the most abundant excitatory neurotransmitter in the human central nervous system (CNS) which plays a major role in metabolic signalling pathways involved in learning and memory. Whereas excess Glu concentrations in synapses can excite neurons to the point of cell death in a process referred to as **excitotoxicity**. Powerful uptake systems (glutamate transporters) prevent excessive activation of Glu receptors present on the surface of brain cells by continuously removing Glu from the extracellular brain fluid. Neurodegenerative diseases known to be associated with expressing excess glutamate exciting nerve cells include Parkinson's disease, Alzheimer's disease and Huntington's disease [1]. Whereas insufficient brain glutamate concentration is thought to result in trouble concentrating, mental exhaustion, insomnia, and low energy. Therefore it is essential our CNS maintains moderate extracellular glutamate concentrations. Extracellular glutamate concentration estimates conducted *in vitro* from tissue slices vary around 0.02–0.1 μM [2].

An option to facilitate real-time, continuous monitoring of analytes such as glutamate is by use of **enzymatic electrochemical sensors**. Enzymatic sensors provide potential for obtaining high measurement sensitivity. However, they are often expensive and decrease in stability over time, resulting in a signal reduction causing inaccuracies in measurement. **Biosensors** are the biological manipulation of electrochemical sensors, where a biological analyte is detected on a bioreceptor. In order to obtain plausible sensitivity and prove biosensor reliability it is essential to assess its technical suitability by accurately optimizing its detection conditions, such as electrolyte solution parameters and provide reassurance that the measured analyte is undeniably glutamate.

Therefore the approach to detect extracellular glutamate levels was using first generation biosensors to utilize the reaction enzyme - glutamate oxidase (GluOx). When the analyte (glutamate) is detected a reduction–oxidation (redox) reaction takes place, indirectly producing an electron through the production of hydrogen peroxide [3]. The following reactions occur, Eq (1):



The used three-electrode potentiometric sensor consists of a platinum (Pt) working electrode on which the redox reaction occurs; a silver chloride (AgCl) reference electrode as an electrode which has a stable and well-known electrode potential (acts as a dynamic baseline to compare the measured potentials of the other electrodes); a titanium (Ti) counter electrode which provides a means of applying input potential to the working electrode. The electrodes were submerged in different concentration acid/base/salt electrolyte solutions to optimize which buffer pH would ensure electrical neutrality and allow ions to migrate with minimal resistance. Electrodes were connected to a data processor to relay the results

As a **result**, we present a first generation GluOx Pt electrode biosensor with an adjusted membrane which specifically measures glutamate levels in mouse brain tissue. Biosensor results assure reliability by providing high sensitivity measurements and a low limit of detection (LOD) for hydrogen peroxide (up to 0.05 μM) while submerging electrodes in a 10 mM, pH 5.5 electrolyte solution.

Considering Glu is linked to various neurodegenerative diseases and mental health disorders its **significance** as a biological marker and fast methods of sensing [Glu] in biofluids remains a perspective and important matter to elaborate in future research.

[1]Lewerenz J, Maher P. Chronic Glutamate Toxicity in Neurodegenerative Diseases-What is the Evidence? *Front Neurosci.* 2015 Dec 16;9:469. doi: 10.3389/fnins.2015.00469. PMID: 26733784; PMCID: PMC4679930.

[2]Moussawi K, Riegel A, Nair S, Kalivas PW. Extracellular glutamate: functional compartments operate in different concentration ranges. *Front Syst Neurosci.* 2011 Nov 24;5:94. doi: 10.3389/fnsys.2011.00094. PMID: 22275885; PMCID: PMC3254064.

[3]Schultz J, Uddin Z, Singh G, Howlader MMR. Correction: Glutamate sensing in biofluids: recent advances and research challenges of electrochemical sensors. *Analyst.* 2020 Jun 15;145(12):4369–4371. doi: 10.1039/d0an90050h. Erratum for: *Analyst.* 2020 Jan 21;145(2):321–347. PMID: 32432607.

STAT3 SIGNALING PATHWAY AS A POTENTIAL PREDICTIVE TARGET IN TRIPLE-NEGATIVE BREAST CANCER

Aistė Gerulaitytė^{1,2}, Justas Burauskas^{1,2}, Agnė Šeštokaitė¹, Monika Drobnienė¹, Rasa Sabaliauskaitė¹, Sonata Jarmalaitė¹

¹ National Cancer Institute, Vilnius, Lithuania

² Vilnius University, Lithuania

aiste.gerulaityte@nvi.lt

Breast cancer is the most common neoplasm worldwide and is the leading cause of cancer deaths among women. Triple-negative breast cancer (TNBC) is the most aggressive subtype with the lowest 5-year survival rates accounting for 12-18% of all breast cancers. TNBCs have a much higher recurrence and metastasis as a result of not being eligible for current treatment options due to the lack of estrogen, progesterone receptor, and human epidermal growth factor receptor 2 [1]. This aggressive cancer contributes to the overall shortened survival of patients diagnosed with TNBC [2].

Considering the absence of molecular targets, neoadjuvant chemotherapy (NAC) remains the standard of care for patient treatment. However, the effectiveness of treatment is unpredictable, as patients frequently develop resistance. For this reason, there is a growing need to develop novel non-invasive molecular predictive approaches for this disease [3]. It has become evident that the development of TNBC chemoresistance is based on the elaborate interplay of the tumor microenvironment, drug efflux, and cancer stem cells. Alterations of multiple signaling pathways govern these interactions [2]. Recent evidence from clinical trials and preclinical studies have demonstrated a pivotal role of the STAT3 (signal transducer and activator of transcription 3) signaling pathway in the initiation, progression, and metastasis of TNBC [3].

The aim of this study was to evaluate the expression of *STAT3*, *ALDH1A1*, *NFIB*, *UPF3A*, *BCL-2*, and *R-RAS-2* genes in serial plasma samples before and after NAC. Gene expression changes were used to determine associations with clinical features of TNBC patients and to analyze *STAT3*, *ALDH1A1*, *NFIB*, *UPF3A*, *BCL-2*, and *R-RAS-2* expression as potential biomarkers for predictive purposes.

In this study, we used reverse transcription quantitative PCR to determine *STAT3*, *ALDH1A1*, *NFIB*, *UPF3A*, *BCL-2*, and *R-RAS-2* expression in paired 122 blood plasma samples of TNBC patients before and after NAC. We determined that a combination of expression changes of *STAT3*, *BCL-2*, and *R-RAS-2* could be used as a predictive biomarker panel to determine TNBC patients that show a more positive response to NAC ($p=0.0012$, $p=0.0098$ and $p<0.0001$, respectively).

Overall, understanding how the expression changes of these genes influence the course response to NAC in TNBC patient plasma potentially could be used as non-invasive molecular biomarkers for treatment effectiveness.

-
- [1] E. A. O'Reilly *et al.*, "The fate of chemoresistance in triple negative breast cancer (TNBC)," *BBA Clin.*, vol. 3, pp. 257–275, Jun. 2015, doi: 10.1016/J.BBACLI.2015.03.003.
- [2] M. Nedeljković and A. Damjanović, "Mechanisms of Chemotherapy Resistance in Triple-Negative Breast Cancer-How We Can Rise to the Challenge," *Cells*, vol. 8, no. 9, Aug. 2019, doi: 10.3390/CELLS8090957.
- [3] J. J. Qin, L. Yan, J. Zhang, and W. D. Zhang, "STAT3 as a potential therapeutic target in triple negative breast cancer: a systematic review," *J. Exp. Clin. Cancer Res.* 2019 381, vol. 38, no. 1, pp. 1–16, May 2019, doi: 10.1186/S13046-019-1206-Z.

THE EFFECT OF SOWING DENSITY ON THE CHEMICAL COMPOSITION AND ANTIOXIDANT ACTIVITY OF INDUSTRIAL HEMP (*CANNABIS SATIVA* L.) ROOTS

Dovilė Motiejauskaitė¹, Karolina Barčauskaitė¹

¹ Lithuanian Research Centre for Agriculture and Forestry, Institute of Agriculture Instituto Al. 1, Akademija, Kėdainiai distr, Lithuania
dovile.motiejauskaite@lammc.lt

Cannabis sativa L. is well known for its secondary metabolites such as cannabinoids, terpenes and phenolic compounds [1]. However, despite being one of the oldest cultivated crops, hemp remains highly controversial due to its psychoactive properties, and research on it is still lacking. Although data on *Cannabis sativa* L. inflorescences, leaves and stems are increasing, the roots remain an extremely understudied part of the plant. Hemp roots have been used in medicine since the beginning of our era. They were mostly used to treat fever, gout, arthritis, joint pain and inflammation [2]. However, only from 0.001 to 0.004% of cannabinoids are found in the roots, so research on them is not so relevant, as most of today's scientists focus mainly on the cannabinoids. Nevertheless, looking at the history of hemp roots use, it is worth investigating their chemical composition and biological activity [3]. Therefore, the goal of this study was to evaluate the influence of sowing density on the chemical composition and antioxidant activity of *Cannabis sativa* L. roots.

The experiment was conducted in 2022 at the experimental base at Lithuanian Research Center for Agriculture and Forestry located in Central Lithuania (55°24' N, 23° 52' E, 65 m asl) on an *Endogleyic Endo- stagnic Endocalcaric Luvisol* (Loamic) soil according to WBR [4]. Industrial hemp variety *Felina32* (French national hemp grower association) was sown in two densities (15 and 35 kg ha⁻¹). Harvest was carried out manually at full maturity on the 19th of September. Dried hemp roots were ground using a coffee beans mill. 1 g of *Cannabis sativa* L. roots flour was extracted with 10 mL 70% methanol solution and placed into an ultrasonic bath at room temperature for 1 hour. Extracts were filtered through a 45 µm nylon filter and kept at 4°C until analysis. The extracts were used to determine total polyphenolic compounds (TPC), total flavonoids (TFC), total polyphenolic acid (TPA) content and antioxidant activity by DHHP assays.

The results revealed that higher sowing density decreased biologically active compounds in hemp roots. Increasing the density from 15 to 35 kg ha⁻¹ the total amount of polyphenolic compounds decreases by approximately 2.42 times (from 10.77 ± 1.36 to 4.45 ± 0.98 mgRUE g⁻¹ DW), total flavonoid content about 6.65 times (from 14.51 ± 0.75 to 2.18 ± 0.13 mgRUE g⁻¹ DW) and total polyphenolic acid content decreases from 9.49 ± 0.54 to 0.96 ± 0.33 mgCAE g⁻¹ DW it is almost 10 times. Accordingly, the antioxidant activity also decreased.

In conclusion, the performed research shows that lower sowing density has a positive effect on the chemical composition of hemp roots as they can accumulate larger amounts of biologically active substances.

-
- [1] C. Kornpointner *et al.*, Chemical composition and antioxidant potential of *Cannabis sativa* L. roots, *Ind Crops Prod*, vol. 165, Jul. 2021.
[2] N. R. Ryz, D. J. Remillard, and E. B. Russo, Cannabis Roots: A Traditional Therapy with Future Potential for Treating Inflammation and Pain, *Cannabis and cannabinoid research*, vol. 2, no. 1. NLM (Medline), pp. 210–216, 2017.
[3] D. Jin, K. Dai, Z. Xie, and J. Chen, Secondary Metabolites Profiled in Cannabis Inflorescences, Leaves, Stem Barks, and Roots for Medicinal Purposes, *Sci Rep*, vol. 10, no. 1, Dec. 2020.
[4] Food and Agriculture Organization of the United Nations, *World reference base for soil resources 2014 : international soil classification system for naming soils and creating legends for soil maps*. FAO, 2014.

GENOTOXICITY AND CYTOTOXICITY ASSESSMENT OF MICROPLASTICS ON FISH

Agnė Bučaitė^{1,2}, Milda Stankevičiūtė¹

¹Laboratory of Ecotoxicology, Nature Research Centre, Vilnius Lithuania

²Vilnius University Life Sciences Centre, Institute of Biosciences, Vilnius Lithuania
agne.bucaite@gamtc.lt

Microplastics (MPs) have been frequently found in the aquatic ecosystems around the world and may constitute a serious threat to the environment. Only a few papers have examined their ecological consequences on freshwater animals, even though several studies have shown direct negative effects on marine organisms [1]. Toxic potential of waterborne pollutants must be accurately assessed to regulate and control pollution in aquatic environments. Fish are frequently used in aquatic ecotoxicology studies due to their ecological significance, adaptability, easy breeding, and ease of maintenance in laboratory settings [2]. The gills of fish are multipurpose organs that perform gas exchange, osmoregulation, trace metal transport, and waste excretion. It is also the primary place where contaminants are absorbed by fish [3]. Polystyrene (PS) is among the most extensively manufactured plastics in the world [4]. It is also one of the most commonly found MPs in aquatic environments, and because of its large molecular weight and structural stability, PS is commonly deemed as nonbiodegradable [5].

The aim of this study is to investigate chronic genotoxic and cytotoxic effects of PS MPs at environmentally relevant concentrations on erythrocytes in rainbow trout (*Oncorhynchus mykiss*) gills. Samples were collected by spreading freshly dissected gills on to a microscopic slide. Cytogenetic analysis was carried out using erythrocyte nuclear abnormalities assay with criteria described by Baršienė *et al.* [6], Fenech *et al.* [7] and Heddle *et al.* [8]. For this analysis 4000 intact erythrocytes were analyzed for each slide/fish. The formation of micronuclei (MN), nuclear buds (NB), nuclear buds on filament (NBf), blebbed nuclei (BL) cells were assessed as genotoxicity endpoints, as well as 8-shaped and bean-shaped nuclei, fragmented apoptotic (FA) and bi-nucleated (BN) cells as cytotoxicity endpoints. Data analysis was performed using R [9] software (version 4.2.2).

There were no significant differences in the frequencies of any observed nuclear abnormalities although mean differences between PS and control (CTRL) groups ranged from -0.0270 ‰ (NBf) to 0.0612 ‰ (BL). A standardized effect size (Cohen's d) for measuring the difference between two group means was also calculated. Effect size ranged from negligible ($|d| < 0.2$) to medium (for BL $|d| = 0.52$). The investigation of relationships between observed cytogenetic endpoints in rainbow trout using principal component analysis (PCA) yielded two principal components (PCs) which explained 47.98% of the total variance. In PC1 NB and 8-shaped nuclei had the highest contribution to variance (37.31% and 33.82% respectively). Afterwards, PCA was done in each group separately to observe group specific contributions to variance. In conclusion, environmentally realistic concentrations of PS MP did not induce genotoxic or cytotoxic effects in fish gill erythrocytes. This study in no way contradicts all the previous research on MP toxicity but highlights the use of environmentally realistic concentrations to assess the practical ecological impact of plastic pollution.

Study was funded by the Research Council of Lithuania through the project S-MIP-21-10 (MULTIS).

-
- [1] X. Li *et al.*, "From marine to freshwater environment: A review of the ecotoxicological effects of microplastics," *Ecotoxicol. Environ. Saf.*, vol. 251, p. 114564, Feb. 2023, doi: 10.1016/j.ecoenv.2023.114564.
 - [2] K. A. Bawa-Allah, A. Otitoloju, and C. Hogstrand, "Cultured rainbow trout gill epithelium as an in vitro method for marine ecosystem toxicological studies," *Heliyon*, vol. 7, no. 9, p. e08018, Sep. 2021, doi: 10.1016/j.heliyon.2021.e08018.
 - [3] S. Schnell *et al.*, "Procedures for the reconstruction, primary culture and experimental use of rainbow trout gill epithelia," *Nat. Protoc.*, vol. 11, no. 3, Art. no. 3, Mar. 2016, doi: 10.1038/nprot.2016.029.
 - [4] "Plastics - the Facts 2022 • Plastics Europe," *Plastics Europe*. <https://plasticseurope.org/knowledge-hub/plastics-the-facts-2022/> (accessed Jan. 12, 2023).
 - [5] R. Liu *et al.*, "Biodegradation of polystyrene (PS) by marine bacteria in mangrove ecosystem," *J. Hazard. Mater.*, vol. 442, p. 130056, Jan. 2023, doi: 10.1016/j.jhazmat.2022.130056.
 - [6] J. Baršienė, A. Rybakovas, G. Garnaga, and L. Andreikėnaitė, "Environmental genotoxicity and cytotoxicity studies in mussels before and after an oil spill at the marine oil terminal in the Baltic Sea," *Environ. Monit. Assess.*, vol. 184, no. 4, pp. 2067–2078, Apr. 2012, doi: 10.1007/s10661-011-2100-0.
 - [7] M. Fenech *et al.*, "HUMN project: detailed description of the scoring criteria for the cytokinesis-block micronucleus assay using isolated human lymphocyte cultures," *Mutat. Res.*, vol. 534, no. 1–2, pp. 65–75, Jan. 2003, doi: 10.1016/s1383-5718(02)00249-8.
 - [8] J. A. Heddle *et al.*, "Micronuclei as an index of cytogenetic damage: Past, present, and future," *Environ. Mol. Mutagen.*, vol. 18, no. 4, pp. 277–291, 1991, doi: 10.1002/em.2850180414.
 - [9] R Core Team, "R: A language and environment for statistical computing." R Foundation for Statistical Computing, Vienna, Austria. [Online]. Available: <https://www.R-project.org/>

EFFECTS OF PATHOGENIC OOMYCETES ON ATLANTIC SALMON EMBRYOS

Eglė Gadeikytė^{1,2}, Gintarė Sauliutė¹, Arvydas Markuckas², Milda Stankevičiūtė¹

¹Nature Research Centre, Akademijos St. 2, LT-08412 Vilnius, Lithuania

²Vilnius University, Life Sciences Center, Saulėtekio av. 7, 10223 Vilnius, Lithuania
egle.gadeikyte@gmc.stud.vu.lt

Oomycetes, or water moulds, are fungal – like microorganisms that include many pathogens that cause devastating diseases in freshwater aquaculture and natural environment. Diseases caused by oomycetes may affect numerous fish species (especially salmonid), including fish eggs [1]. For this reason, that the oomycetes are among the most problematic group of disease-causing organisms in both agriculture and aquaculture, they represent a recurrent threat for global food security and results in major economic losses and serious damage to natural ecosystems [2]. At present, fish farmers are struggling to control this pathogen and currently there is still lack of information, how to prevent and treat oomycete-related diseases. Based on previous research a disease causes oxidative stress in naturally infected fish [3]. Thus, changes in antioxidant systems of aquatic organisms can serve as indicators for a variety of stressors exposures related to oxidative stress [3]. So, use of biomarkers helps to assess the negative effects of oxidative stress. In this study, as biomarkers were used enzymes, like catalase and glutathione S-transferase. Catalase (CAT) was one of the first enzymes proposed to be an effective biomarker of oxidative stress, which protects tissues against damage by hydrogen peroxide [4], and glutathione S-transferase (GST) – ideal organ damage indicator, also protects organisms from peroxidative damage, moreover this enzyme been used in detoxification of toxicants including pesticides, cyclic hydrocarbons, oil and other xenobiotics, because they help to eliminate the oxidative by-products [5].

The aim of this study was to evaluate the toxicity of oomycetes to *Salmo salar* L. embryos by evaluating changes in the activity of antioxidant enzymes - CAT and GST. The results of this study showed significant changes of CAT and GST activity in *S. salar* embryos, after exposure to different species of pathogenic oomycetes. Therefore, oxidative stress biomarkers are very useful in diseases ethology and environmental toxicological studies [1].

Acknowledgments

This research was funded by the Research Council of Lithuania, Project No. S-MIP-21-10, MULTIS.

-
- [1] A. Miljanović *ir kt.*, „Bioactive compounds in fluid propolis preparations inhibit different life stages of pathogenic oomycetes *Aphanomyces astaci* and *Saprolegnia parasitica*“, *Aquaculture*, t. 552, p. 737982, bal. 2022, doi: 10.1016/j.aquaculture.2022.737982.
- [2] L. Derevnina *ir kt.*, „Emerging oomycete threats to plants and animals“, *Philosophical Transactions of the Royal Society B: Biological Sciences*, t. 371, nr. 1709, p. 20150459, gruodž. 2016, doi: 10.1098/rstb.2015.0459.
- [3] M. D. Baldissera *ir kt.*, „Oxidative stress in liver of grass carp *Ctenopharyngodon idella* naturally infected with *Saprolegnia parasitica* and its influence on disease pathogenesis“, *Comparative Clinical Pathology*, t. 29, nr. 2, p. 581–586, bal. 2020, doi: 10.1007/s00580-019-03090-y.
- [4] O. Yu. Vasylykiv, O. I. Kubrak, K. B. Storey, ir V. I. Lushchak, „Catalase activity as a potential vital biomarker of fish intoxication by the herbicide aminotriazole“, *Pesticide Biochemistry and Physiology*, t. 101, nr. 1, p. 1–5, rugs. 2011, doi: 10.1016/j.pestbp.2011.05.005.
- [5] J. Bhagat, B. Ingole, ir N. Singh, „Glutathione s-transferase, catalase, superoxide dismutase, glutathione peroxidase, and lipid peroxidation as biomarkers of oxidative stress in snails: A review“, t. 13, p. 336–349, saus. 2016.

BIOANALYTICAL METHOD FOR THE DETERMINATION OF PSYCHOACTIVE SUBSTANCES IN BIOLOGICAL SPECIMENS

Nerijus Karlonas

The State Forensic Medicine Service, Toxicology Laboratory, Didlaukio 86E, LT-08303 Vilnius, Lithuania
nerijuskarlonas@yahoo.com

Sample preparation is one of the most important steps in the majority of bioanalytical procedures to determine trace psychoactive substances in biological samples with complex matrices. An ideal biological sample preparation technique should be simple, inexpensive, efficient, selective, and compatible with various bioanalytical techniques [1]. It should give a recovery as high as possible, use the minimum amount of solvent, and be environmentally friendly. Therefore, researchers are making great efforts to develop rapid, accurate, precise, and sensitive bioanalytical methods for the determination of psychoactive substances and their metabolites in real biological samples [1-3].

Therefore, the main aim of my study was the development of a new sensitive and specific bioanalytical method based on fast gas chromatography with negative-ion chemical ionization mass spectrometry (GC/NICI-MS) using a mixed-mode solid phase extraction for the identification and quantification of psychoactive substances in biological samples. Moreover, the speed of the analytical separation was emphasized by modifying various GC/NICI-MS parameters. The fully validated bioanalytical method was applied for the identification and quantification of several psychoactive substances in real whole blood and urine samples.

The proposed GC/NICI-MS method coupled with a mixed-mode solid phase extraction, and derivatization by N-(tert-butyltrimethylsilyl)-N-methyltrifluoroacetamide:acetonitrile:ethyl acetate mixture (20:40:40 (v/v/v)) was shown to be useful for the analysis of psychoactive substances in biological samples. For that purpose, the derivatization step using different silylation reagents, duration, and temperature was investigated. This method is the fastest among the others reported up to now [2,3]. Under the optimized GC conditions derivatives of analytes were completely separated within 3.9 min. Sensitive and specific NICI-MS detection combined with fast GC resulted in a sharp and symmetric peak shape of the target analyte while maintaining sufficient resolution.

One of the greatest challenges with a residue analysis of psychoactive substances is the selection of a sorbent suitable to achieve an acceptable sensitivity to all compounds characterized by different physicochemical properties. In this research, a mixed-mode polymeric sorbent with ion-exchange properties was applied. This sorbent is capable of hydrophilic-lipophilic and ion-exchange interactions [2,4,5], and therefore it is suitable for achieving an efficient extraction of all herein-investigated analytes by a single extraction step. For that reason, biological sample preparation conditions including a selection of the solvent for washing and elution steps, pH values were optimized. To the best of my knowledge, this method has been used for the first time for the optimization of sample preparation at pH 1.0.

The developed bioanalytical method for the determination of psychoactive substances in biological samples was validated following the recommendations for new methods [2,6,7]. The linear relationships with the correlation coefficients (r^2) better than 0.996 were evaluated. It was determined that extraction efficiency ranged from 82.9 (± 6.2) % to 94.6 (± 3.4) %. The precision (RSD) for psychoactive substances was 4.08 - 9.52 %, while the accuracy was in the range of 93.0 - 106.3 %. The developed method provides significant advantages in comparison with other previously published methods [7-9]. It shows higher sensitivity (the limit of detection ≤ 0.62 ng mL⁻¹) in biological samples. Moreover, this bioanalytical method has several advantages: elimination of interferences, low volume of samples (0.2 mL), a multi-residue analysis, and very fast chromatographic separation of analytes (3.9 min). According to the results, the developed bioanalytical method is accurate, precise, effective, selective, sensitive, and specific enough to detect analytes after a long time of use of a single oral administration of some psychoactive substances. Furthermore, this method enables reaching the highest specificity for major analytes and meets the requirements of good laboratory practice, especially when applied to pharmacodynamic investigations. Ultimately, the developed bioanalytical method has been applied in routine toxicological analysis during the investigation of both clinical and forensic cases.

For more information about my research

This research was published in my doctoral dissertation (Solid-phase extraction and fast gas chromatography for a residue analysis of sedative-hypnotic drugs in biological samples), license agreement no. VU-ETD-4 (10-04-2015).

The author has declared no conflict of interest

-
- [1] A. Y. Simão, M. Antunes, H. Marques, T. Rosado, S. Soares, J. Gonçalves, M. Barroso, M. Andraus, et al. *Bioanalysis* **12**, 1557-1595 (2020).
 - [2] N. Karlonas, A. Padaruskas, A. Ramanavicius, A. Ramanaviciene. *Journal of Separation Science* **36**, 1437-1445 (2013).
 - [3] C. Margalho, A. Castanheira, F. C. Real, E. Gallardo, M. L. Rivadulla. *Journal of Chromatography B* **1020**, 14-23 (2016).
 - [4] N. Fontanals, F. Borrull, R. M. Marcé. *Journal of Chromatography A* **1609**, 460531 (2020).
 - [5] N. Karlonas, A. Ramanavicius, A. Ramanaviciene. *Journal of Separation Science* **37**, 551-557 (2014).
 - [6] N. Karlonas, A. Padaruskas, A. Ramanavicius, Z. Minkuviene, A. Ramanaviciene. *Chemija* **23**, 91-99 (2012).
 - [7] J. Pum. *Advances in Clinical Chemistry* **90**, 215-281 (2019).
 - [8] L. Ambach, A. H. Redondo, S. König, V. Angerer, et al. *Bioanalysis* **7**, 1119-1136 (2015).
 - [9] A. Orfanidis, H. G. Gika, G. Theodoridis, O. Mastrogianni, N. Raikos. *Journal of Analytical Toxicology* **45**, 28-43 (2021).

STUDY OF THE EFFECT OF CHEMOTHERAPEUTICS ON HUMAN COLORECTAL CANCER CELL SUBLINES

Ieva Norkaitytė¹, Eglė Žalytė¹, Aušra Sasnauskienė¹

¹Department of Biochemistry and Molecular Biology, Institute of Biosciences, Vilnius University Life Sciences Centre, Lithuania
ieva.norkaityte@gmc.stud.vu.lt

Approximately 1.9 million new cases of colorectal cancer are diagnosed each year [1]. Oxaliplatin (OxaPt) and 5-fluorouracil (5-FU) are the main chemotherapeutics for colorectal cancer, but the development of chemoresistance is almost inevitable. In recent years, it has been established that the incidence of OxaPt and 5-FU resistance can be attributed to the alterations in drug transport, evasion of apoptosis, changes in the cell cycle and DNA-damage repair machinery [2].

One of the ways to study the mechanisms of cancer resistance to chemotherapeutics is by comparing transcriptome and proteome between drug-resistant cancer cell sublines and the parental cell line. In this study, parental human colorectal adenocarcinoma cells DLD-1 were cultured in a medium containing either OxaPt or 5-FU to create sublines that were resistant to each drug. The sublines have the respective names DLD/Oxa and DLD/FU. DLD/Oxa and DLD/FU cells were further characterized by assessing their sensitivity to chemotherapeutic drugs. Cell sensitivity to drug treatment was assayed by two methods, colony forming assay and crystal violet method. Both methods indicated and increased DLD/Oxa cell resistance to OxaPt, but only colony forming assay showed an increased DLD/FU resistance to 5-FU.

Also, to further investigate the drug resistance of the parental and cell sublines mentioned above, combinations of drugs named FOLFOX and FOLFIRI were developed. While 5-FU used as single agent in patients with metastatic colorectal cancer has an objective response rate at a very low percentage, the administration of combinations of irinotecan with 5-FU or OxaPt with 5-FU is speculated to result in increased response rate and improved survival [3]. Cells were treated with drugs according to the standard FOLFOX and FOLFIRI clinical regimens and cell viability was determined with crystal violet staining.

In conclusion, we believe that OxaPt and 5-FU-resistant DLD-1 cell line sublines DLD/Oxa and DLD/FU will be a valuable tool for colorectal cancer studies in the future.

[1] Sung, H., Ferlay, J., Siegel, R. L., Laversanne, M., Soerjomataram, I., Jemal, A., & Bray, F. (2021). Global Cancer Statistics 2020: GLOBOCAN Estimates of Incidence and Mortality Worldwide for 36 Cancers in 185 Countries. *CA Cancer J Clin*, 71(3), 209-249. doi: 10.3322/caac.21660

[2] Azwar, S., Seow, H. F., Abdullah, M., Faisal Jabar, M., & Mohtarrudin, N. (2021). Recent Updates on Mechanisms of Resistance to 5-Fluorouracil and Reversal Strategies in Colon Cancer Treatment. *Biology (Basel)*, 10(9). doi: 10.3390/biology10090854

[3] Mohelnikova-Duchonova B, Melichar B, Soucek P. FOLFOX/FOLFIRI pharmacogenetics: the call for a personalized approach in colorectal cancer therapy. *World J Gastroenterol*. 2014 Aug 14;20(30):10316-30. doi: 10.3748/wjg.v20.i30.10316

THE ANALYSIS OF ANTIBIOTIC RESISTANCE AND VIRULENCE GENES IN CLINICAL AND ENVIRONMENTAL ISOLATES OF OPPORTUNISTIC PATHOGEN *STENOTROPHOMONAS MALTOPHILIA*

Radvilė Drevinskaitė¹, Laurita Klimkaitė¹, Julija Armalytė¹

¹ Institute of Biosciences, Life Sciences Center, Vilnius University, Vilnius, Lithuania
radvile.drevinskaite@gmc.stud.vu.lt

Stenotrophomonas maltophilia is an aerobic gram-negative multidrug-resistant bacterium widely distributed in natural and clinical environments. This opportunistic pathogen is associated with various infectious diseases, mostly respiratory, urinary tract, bloodstream infections [1]. Catheter insertion, severe traumatic injuries, burns and other factors can increase the risk of infections caused by *S. maltophilia* [2]. *S. maltophilia* is characterized by innate resistance to various classes of antibiotics, such as β -lactams, aminoglycosides, macrolides, chloramphenicol, tetracyclines, therefore infections caused by this bacterium are difficult to treat. Despite the wide spectrum of infections caused by *S. maltophilia* there is still little known about its other virulence factors. The ability to form biofilms, pili, adhesins, flagella, as well as various enzymes are mostly suggested virulence factors of *S. maltophilia* [3].

The aim of this study was to compare the prevalence of antibiotic resistance and virulence factors encoding genes in clinical and natural isolates of *S. maltophilia*. Antibiotic resistance and virulence factors encoding genes detection was performed on a total of 75 *S. maltophilia* isolates, consisting of 42 environmental and 33 clinical isolates from Lithuania. All clinical isolates were isolated from patients, environmental isolates were isolated from different sources such as soil, water bodies, fish gut.

Detection of the antibiotic resistance genes showed that genes providing resistance to β -lactams (*bla*_{L1} and *bla*_{L2}) and aminoglycosides (*phT*, *aph(3')-IIc* and *aph(6)*) were commonly detected in both environmental and clinical *S. maltophilia* isolates. The *qnr* gene conferring resistance to quinolone class antibiotics was detected in majority clinical, but only two environmental isolates. The higher prevalence of resistance genes in clinical isolates can be related to the intensive use of antibiotics in clinical settings. The *hly* gene encoding hemolysin was found in almost all clinical and nearly half of the natural isolates. The protease encoding *stmpr2* gene was detected in almost all isolates, whereas the protease encoding *stmpr1* gene was more abundant in clinical isolates.

[1] J. S. Brooke, Advances in the Microbiology of *Stenotrophomonas maltophilia*. *Clinical Microbiology Reviews* **34**, e00030-19 (2021).

[2] J. S. Brooke, *Stenotrophomonas maltophilia*: an Emerging Global Opportunistic Pathogen. *Clin Microbiol Rev* **25**, 2–41 (2012).

[3] A. A. Adegoke, T. A. Stenström et al., *Stenotrophomonas maltophilia* as an Emerging Ubiquitous Pathogen: Looking Beyond Contemporary Antibiotic Therapy. *Frontiers in Microbiology* **8** (2017).

MECHANISM OF CRISPR-CAS3 HELICASE USING MAGNETIC TWEEZERS

Miglė Šarpilo¹, Algirdas Toleikis¹

¹Vilnius University, Life Science Center, 7 Saulėtekio Ave, Vilnius, Lithuania

migle.sharpilo@gmail.com

CRISPR-Cas provides RNA-guided adaptive immunity against invading genetic elements. CRISPR systems consist of multiple Cas proteins, which are responsible for CRISPR-dependent cell immunity mechanisms. The effector complex in CRISPR I-E consists of Cascade and Cas3. Cascade is responsible for foreign DNA targeting. Meanwhile, Cas3, which possesses helicase and nuclease activity, is a key protein of the system, necessary for crRNA-guided interference of virus proliferation.

Although single-component Class 2 CRISPR systems, such as type II Cas9 are widely used for genome-editing, the research on multi-component Class 1 proteins of the same system has been less developed. Components of the I-E CRISPR system have already been used as a genome-editing tool to generate big deletions. However, the detailed mechanism by which Cas3 achieves its function is not well understood. The aim of this study is to elucidate the mechanism of Cas3 unwinding. We are using single-molecule force microscopy, namely, magnetic tweezers, to probe the mechanical aspects of Cas3 unwinding activity. Greater knowledge of the Cas3 mechanism of action would improve the application of Cas3 as a tool for genome editing.

ACUTE TOXIC EFFECTS CAUSED BY THE CO-EXPOSURE OF NANO/MICROPARTICLES AND HYDROXYCHLOROQUINE IN *SALMO TRUTTA* AT EARLY DEVELOPMENT

Augustas Morkvėnas^{1,2}, Živilė Jurgelėnė³, Reda Dzingelevičienė⁴, Nerijus Dzingelevičius⁵, Małgorzata Szultka-Młyńska⁶, Bogusław Buszewski^{6,7}, Vitalijus Karabanovas^{1,2}

¹Biomedical Physics Laboratory, National Cancer Center, Baublio 3b, LT-08406, Vilnius, Lithuania

²Department of Chemistry and Bioengineering, Vilnius Gediminas Technical University, Saulėtekio Ave. 11, LT-10223 Vilnius, Lithuania

³Nature Research Center, Akademijos St. 2, LT-08412 Vilnius, Lithuania

⁴Faculty of Health Sciences, Klaipėda University, H. Manto Street 84, LT-92294 Klaipėda, Lithuania

⁵Marine Research Institute of Klaipėda University, LT-92295 Klaipėda, Lithuania

⁶Department of Environmental Chemistry and Bioanalytics, Faculty of Chemistry, Nicolaus Copernicus University, Gagarina 7, 87-100 Torun, Poland

⁷Interdisciplinary Centre of Modern Technologies, Nicolaus Copernicus University, 87-100 Torun, Poland
augustas.morkvenas@vilniustech.lt

The COVID-19 pandemic has brought to light the urgent need for personal protective equipment (PPE) and has also exacerbated the ongoing issue of plastic pollution as a result. The increased use of plastic PPE, combined with the use of antibiotics and antiviral pharmaceuticals in hospitals to treat COVID-19 patients and the unregulated use of these substances in households, has resulted in the release of large amounts of contaminants into rivers and coastal waters [1–3].

The current understanding of the impact of nano/micro-sized plastics and pharmaceuticals, particularly those used for COVID-19 treatment and prevention, on aquatic organisms and the environment is limited. More research is needed to determine the physico-chemical changes of these new contaminants, their penetration abilities through the protective barriers of organisms, and the health status of these organisms. Our study aimed to investigate the bioaccumulation and acute toxicity of different size carboxylate-modified nano/microplastics in combination with the pharmaceutical hydroxychloroquine on *Salmo trutta* embryos and larvae. The results of spectroscopic measurements showed that the stability of the colloidal plastics exhibited a size-dependent pattern. By using confocal fluorescence microscopy, we demonstrated that nano/microplastics in combination with hydroxychloroquine could penetrate through the external protective tissues of embryos and larvae. Additionally, we found that changes in the biological parameters of the exposed organisms depend on the type of chemical material, the duration of treatment and the stage of development of the affected organisms. The findings of this study highlight the need for further research on the long-term impact of nano/microplastics on aquatic organisms, particularly on the potential interactions between these particles and other contaminants. This will help in the development of more effective management strategies to mitigate the negative effects of pollution arising during emergency situations.

This project has received funding from the European Regional Development Fund (project No 13.1.1-LMT-K-718-05-0014) under a grant agreement with the Research Council of Lithuania (LMTLT), and it was funded as part of the European Union's measure in response to the COVID-19 pandemic.

[1.] Mohamed BA, Fattah IMR, Yousaf B, Periyasamy S. Effects of the COVID-19 pandemic on the environment, waste management, and energy sectors: a deeper look into the long-term impacts. *Environ Sci Pollut Res.* 2022 Jul;29(31):46438–57.

[2.] Peng Y, Wu P, Schartup AT, Zhang Y. Plastic waste release caused by COVID-19 and its fate in the global ocean. *Proc Natl Acad Sci USA.* 2021 Nov 23;118(47):e2111530118.

[3.] Benson NU, Bassey DE, Palanisami T. COVID pollution: impact of COVID-19 pandemic on global plastic waste footprint. *Heliyon.* 2021 Feb;7(2):e06343.

EVALUATION OF CHEMICAL COMPOSITION AND RADICAL SCAVENGING OF MEDICAL PLANTS ACCUMULATING BIOACTIVE COMPOUNDS USING SPECTROMETRIC AND CHROMATOGRAPHIC METHODS

Domantas Armonavičius¹, Mantas Stankevičius¹, Ona Ragažinskienė², Audrius Maruška¹

¹ Instrumental Analysis Open Access Centre, Faculty of Natural Sciences, Vytautas Magnus University, 8 Vileikos Street, 44404 Kaunas, Lithuania

² Kaunas Botanical Garden of Vytautas Magnus University, 6 Ž.E. Žilberto Street, 46324 Kaunas, Lithuania
domantas.armonavicius@vdu.lt

Cancer is an immense health issue that has a drastic impact on millions of individuals around the world. It is one of the leading causes of death and profoundly affects people both personally and socially. Even with recent advancements in cancer treatments, the search for more successful and less hazardous therapies remains essential. Substances from natural sources, like medical plants, might provide an encouraging response to the cancer issue, and their capacity to prevent or treat cancer is still being investigated. Therefore, research on natural antioxidants (polyphenols, including ellagitannins) found in plants is relevant globally as it holds the potential to provide alternative solutions to the ongoing challenge of cancer treatment.

For this study, 14 medicinal plants were collected from the Kaunas Botanical Garden of Vytautas Magnus University at various stages of growth. In total, there were 26 sample specimens. Different parts of *Juglans regia*, *Juglans nigra*, *Quercus robur* and *Epilobium angustifolium*, such as grass, leaves, pericarp, fruit and bark, were obtained. For the spectrometric and chromatographic methods, methanolic extracts were prepared.

Total phenolic and flavonoid contents and free radical-scavenging assay were determined using a UV-VIS spectrometer. To harmonize results, all spectrophotometric analysis results were calculated in rutin equivalents (mg of rutin standard per 1 g of dry raw material: RE mg/g). Total phenolic content was determined using the Folin-Ciocalteu colorimetric method, the content of total flavonoids was determined by the AlCl₃ colorimetric method, and radical scavenging activity of all medical plant extracts was assessed using DPPH radical scavenging method [1].

The separation and identification of phenolic compounds were carried out using a modular HPLC system consisting of a mobile phase binary pump, autoinjector, chromatographic column, UV detector and data processing system. Mobile phases were as follows: A—bidistilled water, acidified with trifluoroacetic acid (0.05% vol.) and B—methanol. Following mobile phase gradient was applied: from 0 min. to 4 min., component B concentration is changed from 5% to 30%, on 20 min. B is set to 43%; on 30 min. B is set 50%, on 40 min.—B is set to 95% and hold for 5 min. Flow rate: 0.75 mL/min, injection volume 10 µL. Compounds were determined using an external standards method according to the retention times [2].

Future studies will include the extraction and fractionation of anticancer ellagitannins accumulating plants using different strategies. The research will also develop and adapt solid-phase anticancer plant separation equipment and raw materials for quality assessment. Anticancer studies of the extract fractions will also be performed using *in vitro* cancer cell lines.

[1] K. Bimbraitė-Survilienė, M. Stankevičius, S. Šuštauskaitė, A. Gėgotek, A. Maruška, E. Skrzydlewska, Z. Barsteigienė, I. Akuņeca, O. Ragažinskienė and A. Lukošius, Evaluation of Chemical Composition, Radical Scavenging and Antitumor Activities of *Satureja hortensis* L. Herb Extracts, *Antioxidants* **10** (1), 1-15 (2021).

[2] M. Stankevičius, I. Akuņeca, I. Jākobsone and A. Maruška, Analysis of phenolic compounds and radical scavenging activities of spice plants extracts, *Food Chem. Technol.* **44**, 85-91 (2010).

PECULIARITIES OF MOSQUITO LARVAE DISTRIBUTION IN DIFFERENT WATER BODIES

Kristina Valavičiūtė-Pocienė¹, Rasa Bernotienė¹

¹ Laboratory of Entomology, Nature Research Centre, Lithuania
Kristina.valaviciute@gamtc.lt

The diversity of blood-sucking mosquitoes is high - 3,593 species are currently known worldwide [1], and these insects are involved in the transmission of different pathogens of birds and mammals. Due to a wide range of larval habitats mosquitoes are able to inhabit vast territories [2, 3, 4], however, knowledge on the habitat preferences of certain mosquito species is still lacking. This information is of great importance for vector control strategies [5] and for forecasting mosquito-borne diseases.

We collected 5392 mosquito larvae in 2021 March-October and 2022 April-June from 134 water bodies located throughout Lithuania. Physical and chemical parameters of water bodies (the size, bottom coverage, water temperature, pH, amount of NO₂, and NO₃ in water etc.) were measured. 25 mosquito species have been identified, the most abundant being *Aedes cinereus*, *Ochlerotatus cantans*, *Oc. sticticus* and *Oc. cataphylla*.

Here we evaluated mosquito species diversity, seasonality and the impact of investigated parameters on the larval abundance of certain mosquito species. Statistical analysis showed that the temporality of water bodies and the time of the year are among the most important parameters for the abundant development of some mosquito species. This research will help to understand the local mosquito distribution and will help to lay the groundwork for the renewal of Lithuanian mosquito fauna research.

[1] R. E. Harbach, Mosquito Taxonomic Inventory. Available at: <http://mosquito-taxonomic-inventory.info/>. Accessed April 15, 2022.

[2] N. Becker, D. Petric, C. Boase, J. Lane, M. Zgomba, C. Dahl, A. Kaiser, *Mosquitoes and their control* (Kluwer Academic/Plenum Publishers, New York, 2003).

[3] G. Valkiūnas, R. Kazlauskienė, R. Bernotienė, D. Bukauskaitė, V. Palinauskas, T. A. Iezhova, Haemoproteus infections (Haemosporida, Haemoproteidae) kill bird-biting mosquitoes. *Parasitology Research*, **113**(3), 1011–1018 (2014).

[4] E. Wegner, The characteristics of the most troublesome mosquito species (Diptera: Culicidae) in Poland. *Fragmenta Faunistica*, **52**(2), 157–179 (2009).

[5] S. T. Mereta, D. Yewhalaw, P. Boets, A. Ahmed, L. Duchateau, N. Speybroeck, P. L. Goethals, Physico-Chemical and biological characterization of anopheline mosquito larval habitats Diptera: Culicidae: Implications for malaria control. *Parasites and Vectors*, **6**(1), 1–16 (2013).

RESPONSE OF ENTOMOPATHOGENIC NEMATODE *STEINERNEMA FELTIAE* TO 1-NONENE, THE VOLATILE OF INSECT CADAVERS

Deimantė Tiškevičiūtė^{1,2}, Rasa Čepulytė², Vincas Būda²

¹Vilnius University, Life Sciences Centre

²Nature Research Centre, Institute of Ecology, Laboratory of Chemical and Behavioral Ecology
deimante.tiskeviciute@gamtc.lt

Entomopathogenic nematodes (EPN) are lethal parasites of insects and are applied for controlling economically important pests. Although usage of these environmentally friendly biopesticides has many advantages, its efficiency in the field depends on various factors, especially on chemical compounds in the soil. These chemicals navigate EPN to find a suitable insect host [1]. Volatiles are emitted by healthy insects as well as by EPN infected cadavers [2]. It was found that insect larvae release different volatile blends depending on the infecting EPN species. 1-Nonene was emitted during any infection tested [3]. In this study we tested the response of EPN *Steinernema feltiae* to 1-nonene by using a two-choice assay to reveal the possible effect on its behavior. We found that 1-nonene can repel or attract EPN depending on the compound concentration. Thus, 1-nonene plays an essential role in the behavior of the EPN and our results contribute to a better knowledge of the EPN, widely used as a biopesticide.

-
- [1] Lee, J.H., Dillman, A.R., and Hallem, E.A. Temperature-dependent changes in the host-seeking behaviors of parasitic nematodes. *BMC Biol* 14, 36 (2016).
- [2] Zhang, X., Machado, R.A., Doan, C.V., Arce, C.C., Hu, L., and Robert, C.A. Entomopathogenic nematodes increase predation success by inducing cadaver volatiles that attract healthy herbivores. *eLife* 8, e46668 (2019).
- [3] Grunseich, J.M., Aguirre, N.M., Thompson, M.N., Ali, J.G., and Helms, A.M. Chemical Cues from Entomopathogenic Nematodes Vary Across Three Species with Different Foraging Strategies, Triggering Different Behavioral Responses in Prey and Competitors. *J Chem Ecol* 47, 822–833 (2021).

TRANSCRIPTOMIC AND MUTATIONAL ANALYSIS OF GYNEGOLOGIC CELL LINES AND TUMORS

Ieva Vaicekauskaitė^{1,2}, Daiva Dabkevičienė^{1,2}, Julija Šimienė^{1,2}, Diana Žilovič^{1,2}, Rūta Čiurlienė², Sonata Jarmalaitė^{1,2}, and Rasa Sabaliauskaitė²

¹ Institute of Biosciences, Life Sciences Center, Vilnius University, Vilnius, Lithuania

² National Cancer Institute, Vilnius, Lithuania

ieva.vaicekauskaite@nvi.lt

Ovarian cancer (OC) has the second highest rate of death among all gynecological cancers [1]. The high mortality rates are attributed to the lack of specific symptoms and appropriate screening biomarkers for OC. Chromatin remodeling complex gene *ARID1A* is the second most frequently mutated gene in gynecologic cancers, while NOTCH/WNT pathway is involved in both the development and cancerogenesis of gynecologic organs, thus *ARID1A* and NOTCH/WNT members could be useful as biomarkers in gynecologic malignancy diagnostic biomarkers [2].

In this pilot study two OC cell lines SKOV3 and A2780 as well 51 gynecologic tumors (32 high-grade serous OC (HGSOC), 9 other OC cases, 1 endometrial cancer, and 9 benign ovarian tumors) were investigated for NOTCH/WNT pathway as well as SWI/SNF chromatin remodeling complex gene *ARID1A* mRNA expression analysis using qPCR. *ARID1A* and NOTCH/WNT pathway gene *CTNNB1*, *FBXW7*, and *PPP2R1A* predicted mutations were analyzed using targeted NGS, while cell line mutations were analyzed using publicly available databases. Mutation pathogenicity prediction was conducted on VarSome [3] and VarCards [4] databases.

We detected significant *NOTCH3* downregulation in HGSOC/clear-cell OC model cell culture SKOV3 when compared to endometrial type OC cell line A2780. Both cell lines had mutations in *ARID1A* mutations, while SKOV3 also had *FBXW7* mutations. HGSOC tissue mRNA expression was significantly downregulated when compared to benign gynecologic tumors. Lower WNT gene *CTNNB1* expression was significantly associated with tumor stage ($p=0.02$, Mann-Whitney test) while *ARID1A* expression showed a tendency positive correlation with good prognosis (HR:3.4, 95% CI: 1.1-10.2). In all 15 alterations were detected in 13 OC tissues. Of them, 10 *ARID1A* alterations were detected in 6 HGSOC and 6 other OC tissues. At least 50% of detected *ARID1A* mutations were predicted as pathogenic by *in silico* analysis.

In summary, *ARID1A* and NOTCH/WNT pathway mutational and transcriptional changes are abundant in OC tissues. Next, these promising biomarkers should be further analyzed in a non-invasive samples type in order to adapt their use as OC biomarkers.

[1] F. Bray, J. Ferlay, I. Soerjomataram et al., Global cancer statistics 2018: GLOBOCAN estimates of incidence and mortality worldwide for 36 cancers in 185 countries, *CA. Cancer J. Clin.* 68, 394-424 (2018).

[2] Bocchicchio, S., Tesone, M. and Irusta, G., Convergence of Wnt and Notch signaling controls ovarian cancer cell survival, *J. Cell. Physiol.* 234, 22130–22143 (2019).

[3] C. Kopanos, V. Tsiolkas, A. Kouris et al., VarSome: the human genomic variant search engine, *Bioinformatics* 35, 1978-1980 (2018).

[4] J. Li, L. Shi, K. Zhang K et al., VarCards: An integrated genetic and clinical database for coding variants in the human genome, *Nucleic. Acids. Res.* 46, D1039–D1048 (2018)

QUANTITATIVE ANALYSIS OF MICRORNAS IN 4NQO-TREATED LEUKOCYTES OF PATIENTS WITH TYPE 1 DIABETES MELLITUS

Bernadeta Kaminskaite¹, Laura Siauliene², Zydruone Visockiene², Kristina Daniunaite¹

¹Institute of Biosciences, Life Sciences Center, Vilnius University, Vilnius, Lithuania;

²Vilnius University Hospital Santaros Klinikos, Vilnius, Lithuania
bernadeta.kaminskaite@gmc.stud.vu.lt

Type 1 diabetes mellitus (T1DM), also known as insulin-dependent diabetes, is a metabolic disorder characterized by blood hyperglycemia. In this condition, the pancreas makes little-to-no insulin, therefore, the treatment is directed towards managing the amount of glucose in blood. Chronic hyperglycemia damages, dysfunctions, and causes side effects in a variety of organs and tissues (peripheral nerves, kidneys, eye retina, heart, etc.) [1]. The formation of reactive oxygen species (ROS) and the consequent oxidative stress play a pivotal role in the development of diabetes complications. Increased ROS levels are known to disrupt pancreatic β -cell mitochondrial function, resulting in decreased insulin release; however, the underlying epigenetic regulatory mechanisms are still poorly understood [2]. MicroRNAs (miRNAs), as one of major regulators of gene expression, play important roles in various cellular processes, including those directly associated with diabetes pathogenesis. Several miRNAs have been identified as potential biomarkers for the assessment of complication risk, however, the currently available data are contradictory [3].

The present study was aimed to evaluate the expression of four selected miRNAs – miR-16-5p, miR-17-5p, miR-106a-5p, miR-223-3p – in leukocyte samples obtained from 40 patients with advanced T1DM and to assess the effect of 4-nitroquinoline 1-oxide (4NQO), mimicking ROS in cells. For comparison, 21 non-diabetic patients (NDP) were also included in the study as a control group. Expression levels of selected miRNAs were quantified by means of real-time PCR using TaqMan-based assays after reverse transcription of all miRNAs.

Expression of the analyzed miRNAs did not differ between T1DM and NDP groups (all $p > 0.0500$), however, there were some associations with disease complications and clinical-pathological patients' parameters. Notably, after 4NQO treatment, miR-16-5p and miR-106a-5p levels were generally decreased in individuals diagnosed with chronic kidney disease and nephropathy than without a corresponding diagnosis (all $p < 0.0500$; Fig. 1). In patients with nephropathy, similar associations were also detected for miR-17-5p and miR-223-3p. 4NQO-induced down-regulation of the latter miRNA was confirmed in this patients' group, whereas no effect was observed in the T1DM individuals without the complication. Furthermore, miR-17-5p was differentially expressed between 4NQO-untreated cases with and without nephropathy, whereas only a weak tendency was observed for miR-223-3p in the same comparison ($p > 0.0500$).

In conclusion, the preliminary data of our study indicate the potential role of the analyzed miRNAs in the development of kidney-related T1DM complications. However, further analysis of larger independent cohorts, followed by functional experiments, would be needed to confirm the findings.

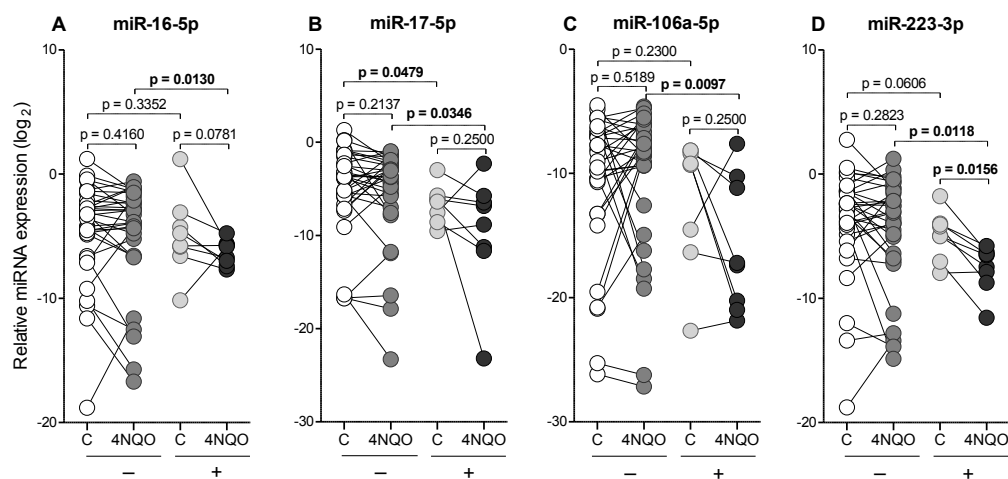


Fig. 1. MiRNA expression in leukocytes of T1DM patients according to the manifestation of nephropathy and 4-nitroquinoline 1-oxide (4NQO) treatment. A-D – miR-16-5p, miR-17-5p, miR-106a-5p, and miR-223-3p, respectively. +/- – patients with/without nephropathy; C – 4NQO-untreated leukocytes (treatment control). Circles represent individual samples, connecting lines indicate sample pairs.

[1] Ohiagu, F. O., Chikezie, P. C., & Chikezie, C. M. (2021). Pathophysiology of diabetes mellitus complications: Metabolic events and control. *Biomedical Research and Therapy*, 8(3).

[2] Darenskaya, M. A., Kolesnikova, L. I., & Kolesnikov, S. I. (2021). Oxidative Stress: Pathogenetic Role in Diabetes Mellitus and Its Complications and Therapeutic Approaches to Correction. In *Bulletin of Experimental Biology and Medicine* (Vol. 171, Issue 2).

[3] Kim M, Zhang X. The Profiling and Role of miRNAs in Diabetes Mellitus. *J Diabetes Clin Res*. 2019;1(1):5-23.

IDENTIFICATION OF CYTOGENETIC POTENTIAL OF THE FISH PATHOGEN *SAPROLEGNIA PARASITICA* USING ERYTHROCYTIC NUCLEAR ABNORMALITY TEST

Eva Kutys^{1,2}, Milda Stankevičiūtė¹

¹Laboratory of Ecotoxicology, Nature Research Centre, Vilnius, Lithuania

²Vilnius University Life Sciences Centre, Institute of Biosciences, Vilnius, Lithuania

eva.kutys@gmc.stud.vu.lt

Many Stramenopile species belonging to the oomycetes (water molds) of the genus *Saprolegnia* infect fish and other aquatic vertebrates and invertebrates in aquaculture farms and natural habitats. *Saprolegnia parasitica* is one of the main causes of saprolegniasis disease, which is the second most economically important infection in aquaculture [1]. *S. parasitica* is responsible for up to 10% of salmonids mortality in fish farms however there is no effective way of treating saprolegniasis since the restriction of malachite green dye for its carcinogenic and teratogenic effect [1], [2]. For a long time, *S. parasitica* was thought to be an opportunistic pathogen that infects only immunosuppressed, wounded, or dead fish and cannot harm healthy salmonid embryos, however evidence of *S. parasitica* being a primary pathogen has recently emerged. Moreover, some researchers believe that *S. parasitica* is able to suppress immune response in fish [3].

The main objective of this work was to assess genotoxic and cytotoxic effects caused by *S. parasitica* to sea trout (*Salmo trutta trutta*) embryos erythrocytes using micronucleus and other nuclear abnormalities test. The results showed that *S. parasitica* causes genotoxic and cytotoxic lesions in the erythrocytes of *S. trutta trutta* embryos, indicating its pathogenicity.

This study was funded by the Research of Council of Lithuania through the project MULTIS, No. S-MIP-21-10

[1] Phillips, A. J., Anderson, V. L., Robertson, E. J., Secombes, C. J. & van West, P. New insights into animal pathogenic oomycetes. *Trends in Microbiology* **16**, 13–19 (2008).

[2] Lee, K., Wu, J. & Cai, Z. Determination of malachite green and leucomalachite green in edible goldfish muscle by liquid chromatography–ion trap mass spectrometry. *Journal of Chromatography B* **843**, 247–251 (2006).

[3] van West, P. *Saprolegnia parasitica*, an oomycete pathogen with a fishy appetite: new challenges for an old problem. *Mycologist* **20**, 99–104 (2006).

IL-1B AND IL-4 CONCENTRATION IN SERA OF PANCREATIC CANCER PATIENTS' VS HEALTHY CONTROL

Kornelija Jencevičiūtė¹, Arenida Bartkevičienė¹, Aldona Jasukaitienė¹ Jason Matthews²,
Antanas Gulbinas¹, Žilvinas Dambrauskas¹

¹ Laboratory of chiralurgical gastroenterology, Digestive System Research Institute, Lithuanian University of Health Sciences, Kaunas, Lithuania

² Faculty of Medicine, University of Oslo, Oslo, Norway
Kornjenc0314@kmu.lt

Introduction. Pancreatic Cancer (PC) is one of the biggest challenges in today's oncology. Based on WHO GLOBOCAN 2020 estimates, pancreatic cancer has ranked the 11th most common cancer in the world counting 495 773 new cases and causing 466 003 deaths. PC is 7th leading cause of cancer-related deaths worldwide [1]. PC is currently treated with a combination of surgery, chemotherapy and radiation therapy in selected cases which results in long-term survival only in a small percentage of patients. Cancer therapies that incorporate immunotherapy-based techniques have become increasingly common in recent years. IL-1b and IL-4 are members of the cytokine family, with a pivotal role in the activation and regulation of immune response and progression of cancer. Tumor cell-derived IL-1b promotes pancreatic tumor proliferation, immune suppression, neoangiogenesis [2]. However, IL-1b, produced by M1 macrophages, have antitumoral properties and help to activate cytotoxic T cells, which can induce cancer cell death [3]. IL-4, produced by regulatory T Cells, induce differentiation of monocytes into M2 macrophages, which exhibit tumor-promoting capabilities involving immuno-suppression, angiogenesis, metastasis [4]. M1/M2 ratio are known to correlate with patients' longevity, higher level of M2 associating with poor prognosis [5].

Aim. The purpose of this research was to study if and how differed IL-1b and IL-4 levels in sera of cancer patients compared with healthy control.

Materials and methods. Main material of this study was sera from pancreatic cancer (PC) patients - 11 subjects and 15 healthy donors (HC). Blood from 3ml vacutainers with SST (serum clot activator) were left at room temperature for one hour before centrifugation at 2500g in 4°C 20min. After centrifugation first layer before gel was sera. We collected 2ml sera into krio tubes, stored it in -80°C temperature until bead-based multiplex assay. On the day of assay all previously frozen sera samples were centrifuged at 16000g 4°C 4min and diluted according to the manufacturer's protocol for Human Premixed Multi-Analyte Kit (Luminex). 96well plate with target antibodies for IL1b and IL4 cytokines was read using a Luminex 100 analyzer. Statistical analysis was performed using GraphPad (version 9.01; GraphPad Software Inc., La Jolla, CA, USA) software. The data are presented as medians with MIN/MAX values from 26 subjects grouped to PC and HC. Nonparametric Mann-Whitney test was used for comparison of concentration levels between groups. Statistical significance was defined as p<0.05. Correlation was calculated by Spearman method.

Results. IL-1b and IL-4 concentrations in sera were increased in pancreatic cancer patients' group vs healthy control. Only IL-1b data was statistically significant (p<0.05). Correlation data showed weak positive association between IL-1b and IL-4 concentration (by Spearman coef.).

Conclusions. The increase of IL-1b and IL-4 in sera of pancreatic cancer patients might be associated with enhanced production of these cytokines in the tumor microenvironment and tumor-associated macrophages (TAMs). Free cytokine burst in cancer patients' sera showed us fight between pro-inflammatory and anti-inflammatory responses.

[1] <https://gco.iarc.fr/today/fact-sheets-cancers>

[2] Daoxiang Zhang, Lin Li, Hongmei Jiang, Qiong Li, Andrea Wang-Gillam, Jinsheng Yu, Richard Head, Jingxia Liu, Marianna B. Ruzinova, Kian-Huat Lim; Tumor-Stroma IL1β-IRAK4 Feedforward Circuitry Drives Tumor Fibrosis, Chemoresistance, and Poor Prognosis in Pancreatic Cancer. *Cancer Res* 1 April 2018; 78 (7): 1700–1712. <https://doi.org/10.1158/0008-5472.CAN-17-1366>

[3] Van Dalen, F.J.; Van Stevendaal, M.H.M.E.; Fennemann, F.L.; Verdoes, M.; Ilina, O. Molecular Repolarisation of Tumour-Associated Macrophages. *Molecules* 2019, 24, 9. <https://doi.org/10.3390/molecules24010009>

[4] Lankadasari, M.B., Mukhopadhyay, P., Mohammed, S. et al. TAMing pancreatic cancer: combat with a double edged sword. *Mol Cancer* 18, 48 (2019). <https://doi.org/10.1186/s12943-019-0966-6>

[5] Hu, H., Hang, J.J., Han, T. et al. The M2 phenotype of tumor-associated macrophages in the stroma confers a poor prognosis in pancreatic cancer. *Tumor Biol.* 37, 8657–8664 (2016). <https://doi.org/10.1007/s13277-015-4741-z>

ASSESSMENT OF BREX PROTEINS IN ANTIVIRAL DEFENCE

Aistė Petrauskaitė¹, Justė Adomaitytė¹, Tomas Šinkūnas¹

¹Department of Protein – DNA Interactions, Institute of Biotechnology, Life Sciences Center Vilnius University, Vilnius
aiste.petrauskaite@gmc.stud.vu.lt

Bacteriophages are the most abundant biological entity in the biosphere, and they are responsible for the destruction of 20-40 % of bacterial cells each day [1]. This evolutionary pressure drives the emergence of diverse bacterial defence systems, one of which is the BREX (Bacteriophage Exclusion). This system is spread in about 10 % of prokaryotic genomes, yet its detailed defence mechanism remains to be elucidated [2].

Our research object is the type I BREX (BREX1) system, which is encoded in the six gene cluster: *brxA-brxB-brxC-pglZ-brxL-pglX*. This system methylates host DNA at certain sequences, protecting it from autoimmunity. The non-methylated DNA of bacteriophages triggers BREX1, which blocks the phage's proliferation (Fig. 1). We have previously showed that deletion of certain BREX1 genes resulted in cytotoxicity [3]. This suggests that some BREX1 proteins participate in autoregulation of the immune response, while other might act as effectors interfering with the vital process of the cell. Here, we assess cell viability by expressing various combinations of BREX1 genes thus seeking to identify the effector and regulator proteins of the BREX1 immunity.

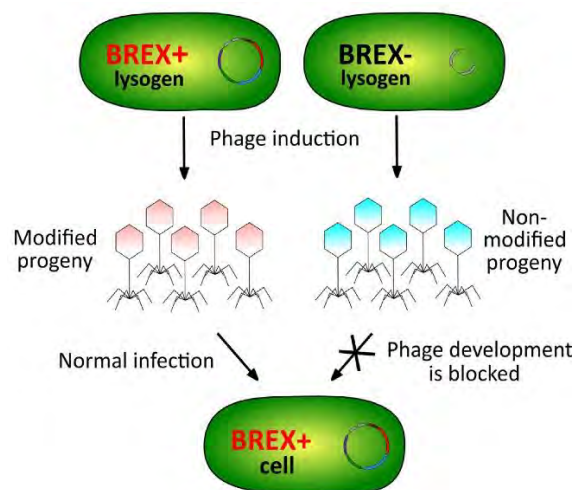


Fig. 1 Graphical representation of BREX1 mechanism of action. Adapted from [3].

-
- [1] L.-C. Fortier and O. Sekulovic, 'Importance of prophages to evolution and virulence of bacterial pathogens', *Virulence*, vol. 4, no. 5, pp. 354–365, Jul. 2013, doi: 10.4161/viru.24498.
- [2] T. Goldfarb *et al.*, 'BREX is a novel phage resistance system widespread in microbial genomes', *EMBO J.*, vol. 34, no. 2, pp. 169–183, Jan. 2015, doi: 10.15252/embj.201489455.
- [3] J. Gordeeva *et al.*, 'BREX system of Escherichia coli distinguishes self from non-self by methylation of a specific DNA site', *Nucleic Acids Res.*, vol. 47, no. 1, pp. 253–265, Jan. 2019, doi: 10.1093/nar/gky1125.

TNF- α AS A NOVEL BIOMARKER FOR POSTOPERATIVE COMPLICATIONS IN LEFT-SIDE COLORECTAL CANCER SURGERY

Kornelija Rauduvytė^{1,2}, Agata Mlynska³, Žilvinas Gricius⁴, Agnė Šeštokaite^{5,6}, Simona Rūta Letautienė^{4,7}, Kristina Žukauskaitė^{5,8}, Audrius Dulskas^{2,4}, Rasa Sabaliauskaitė⁶, Augustinas Baušys²

¹ Department of Human and Medical Genetics, Faculty of Medicine, Vilnius University, Lithuania

² Department of Abdominal Surgery and Oncology, National Cancer Institute, Vilnius, Lithuania

³ Laboratory of Immunology, National Cancer Institute, Vilnius, Lithuania

⁴ Faculty of Medicine, Vilnius University, Vilnius, Lithuania

⁵ Institute of Biosciences, Life Sciences Center, Vilnius University, Vilnius, Lithuania

⁶ Laboratory of Genetic Diagnostic, National Cancer Institute, Vilnius, Lithuania

⁷ Diagnostic and Interventional Radiology Department, National Cancer Institute, Vilnius, Lithuania

⁸ Medical University of Graz, Graz, Austria

kornelija.rauduvyte@gmc.stud.vu.lt

Colorectal cancer (CRC) is one of the most common types of cancer worldwide. Surgery remains the only potentially curative treatment option for it. Despite recent medical progress, postoperative complications still occur in about 40-50% of CRC patients [1]. There is a lack of tools that could reliably predict postoperative complications before the surgery. Therefore, this study aims to investigate a variety of biomarkers for postoperative outcomes after left-side CRC surgery.

In this prospective longitudinal study, 40 patients undergoing left-side CRC surgery were included. Blood samples were collected on the baseline, postoperative day 6 and 30. ELISA and RT-qPCR were performed to evaluate 13 serum cytokines and 2 plasma miRNAs expression as biomarkers for postoperative outcomes. Univariate and multivariate logistic regression analyses were performed to adjust for common risk factors (age, gender, CCI, TNF- α , IL-8, tumor size, lymph node status, white blood cells and c-reactive protein concentration).

Patients who suffered postoperative complications (n = 16; 40%) were found to have an increased baseline serum median of TNF- α (50.39; IQR = 2.37–590.50 pg/mL vs 2.28; IQR = 2.28–14.16 pg/mL, p = 0.009) and IL-8 (15.88; IQR = 5.16–49.96 pg/mL vs 7.06; IQR = 3.84–13.26 pg/mL, p = 0.031). At univariate analysis, TNF- α , gender and CCI were identified as potential risk factors associated with postoperative complications (p < 0.1). Multivariate analysis confirmed a higher than 2.47 TNF- α level (OR = 15.97; 95% CI 2.30–337.13, p = 0.018) and male gender (OR = 9.48; CI 1.44–189.46, p = 0.047) as risk factors for postoperative complications after CRC resections. Results presented here suggest that serum TNF- α could be used to identify high-risk surgical CRC patients.

In conclusion, our study demonstrated that patients with an increased TNF- α level are at a higher risk for postoperative complications after left-side CRC surgery.

[1] Warps, A. K., Tollenaar, R. A. E. M., Tanis, P. J., & Dekker, J. W. T. (2022). Postoperative complications after colorectal cancer surgery and the association with long-term survival. *European Journal of Surgical Oncology*, 48(4), 873–882. <https://doi.org/10.1016/j.ejso.2021.10.035>

FUNGAL DIVERSITY ON INVASIVE *CYTISUS SCOPARIUS* L. PLANTS IN LITHUANIA

Dovilė Čepukoit¹, Ieva Rinkevičiūtė¹, Daiva Burokienė¹

¹ Laboratory of Plant Pathology, Nature Research Center, Lithuania
dovile.cepukoit@gamtc.lt

Globalization, landscape alteration and climate change are factors that make it easier for alien organisms to overcome geographical barriers and unfavorable environmental conditions in a new area. All over the world these species cause biological, economic and social problems. *Cytisus scoparius* is an invasive plant in Lithuania. Along with this plant, its pathogenic fungi are introduced into new areas. Their diversity has still not been evaluated. This type of data is lacking for further studies on the interaction between invasive and native plants.

Fungi of the genus *Diaporthe* are plant, human or other mammal pathogens, endophytes and saprotrophs. It is an economically important group of pathogenic microorganisms that cause diseases for agricultural, wild and ornamental plants. Based on morphology, it is difficult to distinguish the species of this genus due to phenotypic plasticity. In Lithuania *Diaporthe* fungi was not yet intensively studied. The main aim of this work was to assess the diversity of fungi on *C. scoparius*.

During the study, 44 samples of damaged *C. scoparius* plants were collected in 9 different areas of Lithuania, from which 235 fungal cultures were isolated. After evaluating the characteristics and micromorphological features of fungal colonies, they were assigned to 78 morphological groups. All representatives of these morphogroups were identified by molecular methods. Different genera were identified according to the ITS sequence using ITS1 and ITS4 primers [1]: *Kalmusia*, *Diaporthe*, *Fusarium*, *Alternaria*, *Chondrostereum*, *Neonectria*, *Eutypa*, *Epicoccum*, etc. The most common genera on *C. scoparius* are *Kalmusia*, *Diaporthe* and *Fusarium*. To identify the fungi of the genus *Diaporthe* to species, their ACT, CAL, TEF-1 and TUB genes were sequenced using ACT-512F/ACT-783R, CAL-228F/CAL737R, EF1-728F/EF1-986R [2], Bt-2a/BT-2b [3] primers. It showed that several different species of *Diaporthe* are associated with *C. scoparius*. To sum up, microbiota studies provide new information about the prevalence of fungal microorganisms on invasive plants in Lithuania and give more data on the potential threat to local ecosystems.

[1] T. J. White, T. Bruns, S. Lee, J. Taylor, Amplification and direct sequencing of fungal ribosomal RNA genes for phylogenetics, PCR protocols: a guide to methods and applications **18**, 315-322 (1990).

[2] I. Carbone, L. M. Kohn, A method for designing primer sets for speciation studies in filamentous ascomycetes, *Mycologia* **91**, 553-556 (1999).

[3] N. L. Glass, G. C. Donaldson, Development of primer sets designed for use with the PCR to amplify conserved genes from filamentous ascomycetes, *Applied and environmental microbiology* **61**, 1323-1330 (1995).

STABLE ISOTOPES IN YOUR HAIR CAN TELL WHAT YOU ATE AND HOW YOU LIVED

Raminta Skipitytė¹, Andrius Garbaras¹

¹ Isotopic Research Laboratory, Center for physical sciences and technology, Lithuania
raminta.skipityte@ftmc.lt

Carbon ($\delta^{13}\text{C}$) and nitrogen ($\delta^{15}\text{N}$) stable isotope ratios in human tissues are related to individual dietary habits as well as environmental and physiological factors. Typically, carbon provides information on the primary energy source, while nitrogen allows discrimination among trophic levels [1]. Due to easy and non-invasive sampling, hair is a good tissue for modern human analyses. In forensic science, stable isotope ratios of human remains such as hair are mainly used for geographical allocation [2]. Therefore, knowledge of the impact of various factors on stable isotope distribution in human tissues is an important component in the interpretation of the analytical results of stable isotopes.

In this study, modern human hair samples were analyzed to show the dietary differences according to their dietary practice and the main food source (plant, meat, or fish). People who reported a low-meat or vegetarian diet $\delta^{13}\text{C}$ values range from -19.9 to -18.7 ‰, the average is -19.3 ± 0.4 ‰, while $\delta^{15}\text{N}$ values range from 9.3 to 9.9 ‰ and do not exceed 10 ‰, the average is 9.6 ± 0.2 ‰. Meanwhile, people whose diet is dominated by meat and fish products, average $\delta^{13}\text{C}$ is higher -18.9 ± 0.9 ‰, ranging from -20.4 to -17.9 ‰. The average $\delta^{15}\text{N}$ value is also higher 10.5 ± 0.6 ‰, ranging from 9.5 to 11.2 ‰.

According to $\delta^{15}\text{N}$, those who eat more meat and fish have higher nitrogen stable isotope values to compare with vegetarians or those who eat meat occasionally, these groups differed statistically significantly (Kruskal-Wallis test $p < 0.05$) (Fig. 1). A modern human hair isotopic study reveals that $\delta^{15}\text{N}$ values of those who eat fish and meat has $\delta^{15}\text{N}$ values > 10 ‰. A further study on modern human hair samples showed changes in retrospective life history according to segmental hair measurements.

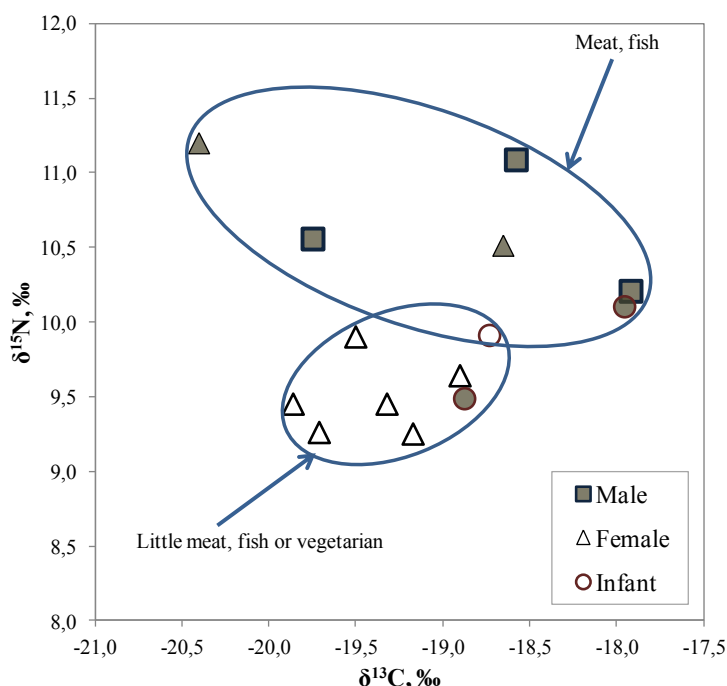


Fig. 1. Carbon and nitrogen stable isotope ratio values of human hair samples; a diet that represents a lot of meat/fish (solid symbols) and little meat/fish or vegetarians (hollow symbols).

In addition, the present stable isotope data set in Lithuania could be enlarged including samples of different contexts that may help in the interpretation of carbon and nitrogen stable isotope results of modern or ancient humans in view of dietary preferences, region, or health issues.

-
- [1] F. Hülsemann, C. Lehn et al., Global spatial distributions of nitrogen and carbon stable isotope ratios of modern human hair, *Rapid Communications in Mass Spectrometry*, 29(22), 2111-2121 (2015).
[2] C. M. O'reilly, R. E. Hecky et al., Interpreting stable isotopes in food webs: recognizing the role of time averaging at different trophic levels, *Limnology and oceanography*, 47(1), 306-309 (2002).

VEGETARIAN OR EATING MEAT? STABLE ISOTOPES REVEAL THE DIETARY HABITS OF MODERN AND ANCIENT HUMANS IN LITHUANIA

Raminta Skipitytė¹, Rimantas Jankauskas²

¹ Isotopic Research Laboratory, Center for physical sciences and technology, Lithuania

² Institute of Biomedical Sciences, Vilnius University, Lithuania

raminta.skipityte@ftmc.lt

The stable isotope ratio method is considered as a “golden standard” in modern [1] and archaeological [2] dietary studies. In general, carbon isotopic ratios reveal food sources and nitrogen – trophic levels with isotopic enrichment at each trophic level. Thus, in stable isotope ecology, “you are what you eat plus a few permil” [3].

In this work, stable isotopes were applied in the fields of ecology, archaeology, and forensics. Modern human hair samples were analyzed to show dietary differences in people according to their diets (vegetarians, eating meat or fish). The modern human hair study revealed that $\delta^{15}\text{N}$ values of those who eat fish and meat are higher ($> 10\text{‰}$) and the known keratin-collagen fractionation factor allows the use of these results to compare with archaeological data, where only bone tissue usually survive. Therefore, modern studies can help to better understand the dietary practices in the past.

In a further archaeological study, preserved human from various regions and historical periods bone collagen and bioapatite samples were analyzed to find out more about dietary practices in the past. Stable isotope data showed that humans during the I-II millennium in Lithuania relied on C_3 photosynthetic plants and terrestrial animal food sources. There were significant differences between humans from different regions (urban, rural, and coastal) (Fig. 1).

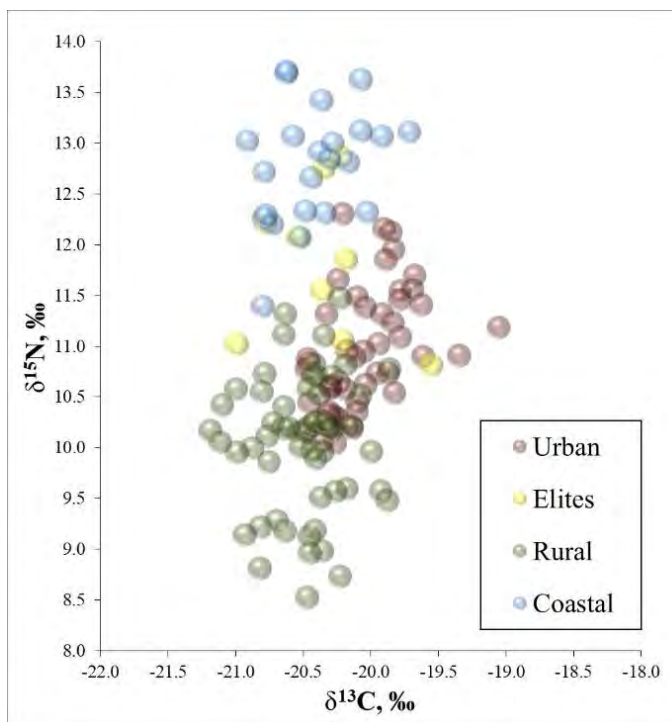


Fig. 1. Carbon ($\delta^{13}\text{C}$) and nitrogen ($\delta^{15}\text{N}$) stable isotope values in urban (15th – 17th c.), social elite (16th – 17th c. and 19th a.), rural (13th – 19th c.) and coastal (19th c.) populations.

Based on archaeological human bone collagen analysis, the influence of biological factors (men-women); the importance of diachronic factors (I – II millennia); the influence of technological factors (agricultural development) factors; as well as the importance of social and cultural factors (dietary characteristics of rural, urban people, social elites) on the distribution of their stable isotope values were determined.

Therefore, in this presentation, the potential of the stable isotope ratio method will be exemplified by the modern and archaeological investigations.

[1] L. Balčiauskas, V. Stirkė et al., Stable isotope analysis supports omnivory in bank voles in apple orchards, *Agriculture*, 12(9), 1308 (2022).

[2] R. Skipitytė, K. Lidén, et al., Diet patterns in medieval to early modern (14th-early 20th c.) coastal communities in Lithuania, *Anthropologischer Anzeiger*, 77(4), 299-312 (2020).

[3] B. Fry, *Stable isotope ecology*, Vol. 521, New York, Springer (2006).

STRUCTURAL ANALYSIS OF *SIW14*, PROTEIN AFFECTING [PSI+] PRION APPEARANCE IN *SACCHAROMYCES CEREVISIAE*

Gvidas Katauskas¹, Justina Versockienė¹, Audrius Gegeckas¹, Eglė Lastauskienė¹

¹ Department of Microbiology and Biotechnology, Institute of Biosciences, Life Sciences Center, Vilnius University, Vilnius, Lithuania
gvidas.katauskas@gmail.com

Prions are altered conformation proteins, capable of causing other natively folded proteins to change conformation. Prions are the causative agent in mammalian (including humans) diseases, termed spongiform encephalopathies. Some neurodegenerative diseases pathologies are also thought to be connected to native protein misfolding into prions.

Among unicellular organisms, both are known to form and transmit prions. To date, the best explored system for prions is in yeast model organism *Saccharomyces cerevisiae*, where prions were discovered before the prion term was even coined [1]. The work in this organism has yield data, that certain genes antagonize or accelerate appearance of prions. Those genes usually code for chaperones and their cofactors. In 2017, a new gene with anti-prion effect was discovered – *SIW14*. Siw14 is inositol polyphosphate β-pyrophosphatase. The mechanism of anti-prion effect of *SIW14* is unknown [2]. A phosphatase in humans with Siw14-like activity is yet to be found.

This work explores the structural requirements of Siw14 protein to antagonize Sup35 misfolding into [PSI+] prion in yeast *S. cerevisiae*. Mutants, carrying *SIW14* mutations (N-terminal, C-terminal/phosphatase domain, catalytically inactive Siw14 with C214S mutation in active site) were introduced in *siw14Δ* cells overexpressing Sup35-GFP and their ability to antagonize *de novo* appearance of [PSI+] prion was assessed by *adel* suppression phenotypic test and fluorescent microscopy.

The prionization tests show that functional Siw14 phosphatase domain is necessary for anti-prion activity. N-terminal domain, and catalytically inactive C214S mutant failed to prevent prion formation and had prionization rates similar to that of *siw14Δ* cells. Fluorescent constructs of Siw14 display diffused localization in cells, irrespective of cell's prion status.

The data shows that phosphatase activity of Siw14 is essential for prion antagonization, but mechanism of suppression is yet to be discovered. Future work should explore how Siw14 prevents prion appearance, if anti-prion system is dependent on inositol pyrophosphates or if actin defects in *siw14Δ* cell are affecting prion appearance rates.

[1] R. B. Wickner. [URE3] as an altered URE2 protein: evidence for a prion analog in *Saccharomyces cerevisiae*. *Science* **264**, 566-569 (1994).

[2] R. B. Wickner, A. C. Kelly, E. E. Bezsonov, and H. K. Edskes. [PSI+] prion propagation is controlled by inositol polyphosphates, *Proceedings of the National Academy of Sciences*, 114(40), E8402–E8410 (2017).

EVALUATION OF SEVERAL *IN VITRO* RESEARCH METHODOLOGY STEPS FOR NONCODING CIRCULAR RNA QUANTIFICATION

Marta Tamošiūnaitė¹, Rūta Maleckaitė¹, Kristina Daniūnaitė^{1*}

¹ Institute of Biosciences, Life Sciences Center, Vilnius University, Vilnius, Lithuania
marta.tamosiunaite@gmc.stud.vu.lt

Noncoding circular RNAs (circRNAs) are a class of single-stranded noncoding RNAs formed in a circular form during non-canonical splicing or back-splicing [1]. Initially thought to be the result of splicing errors, circRNAs are now widely recognized as important gene expression regulators, although very little is known about their specific roles in or outside the cell. Previous studies have shown that most of the currently annotated circRNAs are involved in various pathologies and in the carcinogenesis as well, being potential cancer biomarkers and, thus, the attractive research target [2]. However, their molecular analyses are not perfected, yet.

In the present study, we aimed to evaluate several steps of RNA sample preparation for circRNA analysis in order to determine the optimal workflow. The yield and quality of the purified RNA were compared among three different RNA extraction kits (coded *M*, *P*, and *Z*). Also, circular and linear transcripts of the same genes (13 transcripts in total) were quantified in two different cellular fractions: nuclear and cytoplasmic RNA. The efficacy of RNase R treatment step was assessed by comparing quantities of linear transcripts. The selected circRNA and linear targets were analyzed by means of real-time PCR using the QuantStudio™ 7 Pro Real-Time PCR System (Applied Biosystems™, Thermo Fisher Scientific). All analyses were performed using six cancer cell lines.

Our preliminary results revealed that although the yield and quality of purified RNA were comparable among the kits, relatively higher quantities of the same circRNA targets were obtained with the *P* kit. Among the analyzed circRNA targets, the majority were detected in higher relative amounts in the cytoplasmic RNA fraction than in the nuclear one (e.g. *circFOXO3* and *circHIPK3*). However, some circRNAs were found in similar quantities in both cellular fractions (e.g. *circNRIP1*). The majority of the circRNA targets were detected in higher relative amounts when the RNase R treatment step was performed as compared to untreated samples (e.g. *circUBAP2* and *circCSNK1G3*). However, quantities of several other circRNAs showed the opposite tendency (e.g. *circFAT1* and *circNRIP1*).

In conclusion, our preliminary data indicate no significant differences in the yield and quality of the circRNA fraction comparing the three RNA extraction kits. The RNase R treatment reduced the amount of linear transcripts in the total RNA fraction, but not all the analyzed circRNAs were enriched uniformly, raising concern for biased data.

[1] Kristensen, L. S., Andersen, M. S., Stagsted, L. V. W., Ebbesen, K. K., Hansen, T. B., & Kjems, J. (2019). The biogenesis, biology and characterization of circular RNAs. *Nature reviews. Genetics*, 20(11), 675–691.

[2] Burd, C. E., Jeck, W. R., Liu, Y., Sanoff, H. K., Wang, Z., & Sharpless, N. E. (2010). Expression of linear and novel circular forms of an INK4/ARF-associated non-coding RNA correlates with atherosclerosis risk. *PLoS genetics*, 6(12), e1001233.

THE EFFECTS OF GRAPHENE OXIDE AND METAL MIXTURES ON FRESHWATER BROWN TROUT (*SALMO TRUTTA* L.) SWIMMING BEHAVIOUR

Tomas Makaras¹, Sergej Semčuk²

¹ Nature Research Centre, Akademijos Str. 2, 08412, Vilnius, Lithuania

²SRI Center for Physical Sciences and Technology, Saulėtekio Av. 3, 02300 Vilnius, Lithuania

Tomas.makaras@gamtc.lt

The increasing use of these carbon nanomaterials in a range of industries highlights the necessity to examine their environmental destiny as well as their potential toxicity to living organisms. In a real-world scenario, where the risk of these nanomaterials being developed and accidentally discharged into the environment is quite high, the toxicity of graphene-based nanomaterials must be investigated individually and in combination with other chemicals for a more associated risk differentiation of these materials [1].

The potential short-term impact of graphene oxide (GO) and four common metals (Zn, Cu, Ni, and Cr) in a complex mixture (MIX) on the swimming behaviour of freshwater brown trout (*Salmo trutta* L.) was examined. Fish juveniles were treated individually in open-field tanks for 2-hours to single and combined exposure of GO (1, 10 and 20 mg L⁻¹) and MIX (Zn²⁺ – 100, Cu²⁺ – 10, Ni²⁺ – 34 and Cr^{3+/6+} – 10 µg L⁻¹, respectively) solution. MIX was produced in accordance with the maximum-allowable-concentrations (MAC) for certain metals in European rivers and lakes [2].

The results (Figure 1 and 2) showed that single and combined GO and MIX treatment had a substantial influence on the behavioural responses of fish juveniles, increasing swimming activity by 19-61%. Fish juveniles exposed to GO and MIX showed opposite responsive tendency, where interaction between GO and MIX intensified the trace elements effects by significantly increasing (from 1.8 to 2.8-fold) swimming activity in juveniles compared to those exposed to MIX. These findings show that GO modulate the toxicity of metal pollutants in complex mixture at the biological scale.

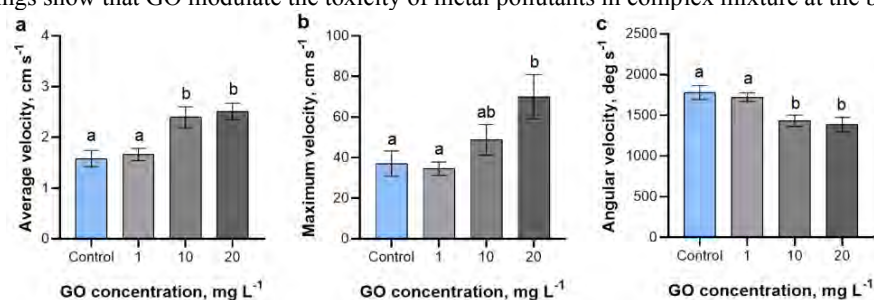


Fig. 1. Changes in swimming activity endpoints (a,b and c) (mean ± SEM, n = 16) of brown trout (*S. trutta*) juveniles after the short-term (2 h) exposure to different graphene oxide (GO) concentrations.

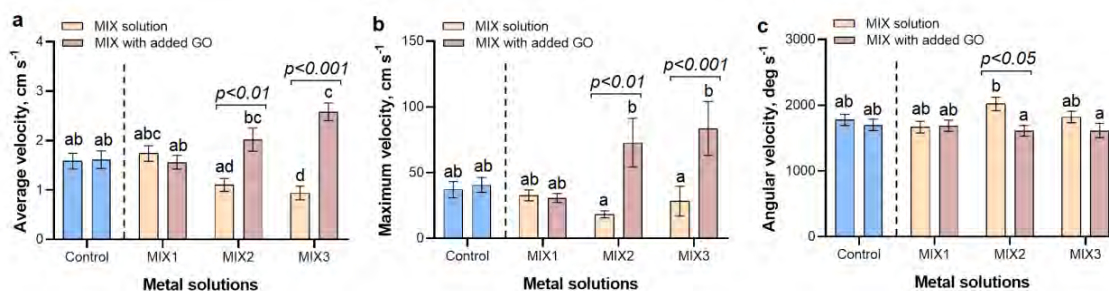


Fig. 2. Changes in swimming activity endpoints (a,b and c) (mean ± SEM, n = 16) of brown trout (*S. trutta*) juveniles after the short-term (2 h) exposure to metal solutions with and without added GO. MIX1 denotes the concentrations of Zn, Cu, Ni, and Cr in a solution produced at maximum-allowable-concentration (MAC) levels (Directive 2013/39/EU). MIX2 and MIX3 represent metal concentrations in mixture that are 10 and 20-fold higher than MAC, respectively.

Acknowledgement

This work was funded by the Research Council of Lithuania, Project No. S-MIP-22-51.

[1] X. Liu, R. Ma et al. Graphene oxide-based materials for efficient removal of heavy metal ions from aqueous solution: A review. *Environmental Pollution* **252**, 62–73 (2019).

[2] Directive 2013/39/EU Directive of the European Parliament and the Council of the European Union for environmental quality standards in the field of water policy (WFD), (2013).

THE PHYSICOCHEMICAL PROPERTIES OF CHITOSAN VARY DEPENDING ON THE LIVING SOURCE AND THE FUNCTIONS PERFORMED

Aurelija Ramanauskaitė¹, Vykintas Baublys¹, Povilas Mulerčikas^{2*}

¹ Department of Biology, Faculty of Natural Science, Vytautas Magnus University, Kaunas, Lithuania

² Agriculture academy, Vytautas Magnus University, Kaunas, Lithuania

aurelija.ramanauskaite@vdu.lt (10 point)

Chitosan is a widespread biopolymer, found in the cuticles of arthropods, the cell walls of fungi, and the skeletal structures of insects. The applicability of chitosan covers many areas: medicine, pharmacy, food/feed, agriculture, textile and water purifications. Previous studies show that the properties of chitosan depend on the source from which it was isolated. Herein, we produced chitosan from corneal lens and rest part of the head of *Laphria flava* to compare the physicochemical properties between them.

We proved the purity of the obtained chitosan samples by using Fourier-transform infrared spectroscopy (FT-IR). Thermogravimetric analysis (TGA) and Scanning electron microscope (SEM) were used to determine the properties of the obtained chitosan. TGA analysis showed similar results for both samples. 3D chitosan isolated from insect cornea lens has a unique compound structure - hexagonal-circular shape. The outer surface of the membrane is characterized by papillae forms; however, there are small hexagonal holes on the inner sides.

Considering all the results, it has been noted that the physicochemical properties of chitosan vary according to the living source and body parts and functions performed.

Keywords: *Laphria flava*, chitin, chitosan, insect eyes

EVALUATION OF THE SALMONID SENSITIVITY TO THE PATHOGENIC OOMYCETES AT THE EARLY DEVELOPMENT STAGE

Gabrielė Oželytė^{1,2}, Gintarė Sauliūtė¹, Arvydas Markuckas², Milda Stankevičiūtė¹

¹Nature Research Centre, Akademijos St. 2, LT-08412 Vilnius, Lithuania

²Vilnius University, Life Sciences Center, Saulėtekio av. 7, 10223 Vilnius, Lithuania

gabriele.ozelyte@gmc.stud.vu.lt

Oomycetes are saprophytic opportunists found in freshwater bodies that can cause diseases in wild and farm-raised salmonid fish all around the world [1]. Oomycetes *Saprolegnia* species cause the majority of cases of saprolegniasis, a disease characterized by immunosuppression, that affects salmonid in the early stages of development [2][3][4]. In countries with large-scale fish farming oomycete infections are mainly a problem during the egg incubation period [5]. It is estimated that saprolegniasis outbreaks are responsible for large-scale fish mortalities up to 50%, which is a major problem for fish welfare and the economic sustainability of fish farming [1][6]. Oomycetes cause oxidative stress resulting in the production of reactive oxygen species (ROS) [7]. To prevent or minimize the production of free radicals, organisms activate the antioxidant defense system which includes enzymes such as catalase (CAT) and metallothioneins (MTs) [4][8].

This study aimed to evaluate responses of oxidative stress biomarkers such as CAT activity and MTs induction in *Salmo trutta fario* exposed to pathogenic oomycetes at an early stage of development. During the experiment, there were no significant changes in catalase (CAT) activity. In contrast, the study found higher MTs induction in *S. trutta fario* embryos exposed to *S. ferax* and decreased MTs levels when exposed to *S. parasitica*. It is worth mentioning, that more than two enzymes play a role in the antioxidant defense system, and additional research should be conducted to better understand the components involved in preventing and regulating oxidative stress in pathogenic oomycetes-infected fishes.

Acknowledgments

This research was funded by the Research Council of Lithuania, Project No. S-MIP-21-10, MULTIS.

-
- [1] M. N. Sarwar, Md J. Hossain, T. Nasrin, T. Naznin, Z. Hossain, and M. M. Rahman, Molecular identification of oomycete species affecting aquaculture in Bangladesh, *Aquac. Fish.* **4**(3), 105–113 (2019).
- [2] D. Pavic et al., Tracing the oomycete pathogen *Saprolegnia parasitica* in aquaculture and the environment, *Sci. Rep.* **12**(1), 16646 (2022).
- [3] L. Boddy, Chapter 9 - Interactions with Humans and Other Animals, in *The Fungi* (Third Edition), Third Edition., Academic Press, 293–336 (2016).
- [4] M. B. Baldissera et al., Oxidative stress in liver of grass carp *Ctenopharyngodon idella* naturally infected with *Saprolegnia parasitica* and its influence on disease pathogenesis, *Comp. Clin. Pathol.*, **29**(2), 81–586 (2020).
- [5] M. M. Songe et al., '*Saprolegnia diclina* IIIA and *S. parasitica* employ different infection strategies when colonizing eggs of Atlantic salmon, *Salmo salar* L', *J. Fish Dis.*, **39**(3), 343–352, Mar. (2016).
- [6] T. Korkea-Aho, T. Wiklund, C. Engblom, A. Vainikka, and S. Viljamaa-Dirks, Detection and Quantification of the Oomycete *Saprolegnia parasitica* in Aquaculture Environments, *Microorganisms*, **10**(11), 2186 (2022).
- [7] E. Zahran and E. Risha, Protective role of adjuvant and potassium permanganate on the oxidative stress response of Nile tilapia (*Oreochromis niloticus*) challenged with *Saprolegnia ferax*, *SpringerPlus*, **2**(1), 94 (2013).
- [8] F. Ma'rifah, M. R. Saputri, A. Soegianto, B. Irawan, and T. W. C. Putranto, The Change of Metallothionein and Oxidative Response in Gills of the *Oreochromis niloticus* after Exposure to Copper, *Anim. Open Access J. MDPI*, **9**(6), 353 (2019).

EFFECTS OF MICROGRAVITY ON THE PHYSIOLOGY OF MICROORGANISMS AND RESISTANCE TO CHEMICAL AND PHYSICAL AGENTS

Irmantas Arūnas Čiužas¹, Eglė Lastauskienė¹, Justina Versockienė¹, Vitalij Novickij², Gediminas Staigvila²

¹ Institute of Biosciences, Life Sciences Center, Vilnius University, Saulėtekio Av. 7, LT-10257 Vilnius, Lithuania

² Faculty of Electronics, Vilnius Gediminas Technical University, Vilnius, Lithuania
irmantas.ciuzas@gmc.stud.vu.lt

Long-range space missions will become a reality in the future, due to this, it is important for scientists to find a solution to protect astronauts from a variety of pathogenic microorganisms that undergo physiological and phenotypical changes in microgravity [1]. In this work, the effect of microgravity on the resistance of *Saccharomyces cerevisiae* and *Candida lusitaniae* to chemical and physical agents was measured by comparing cells grown under normal gravity and simulated microgravity.

The study attempted to evaluate chemical and physical factors such as resistance to formic and acetic acids, antifungal compounds, namely amphotericin B and nystatin dihydrate, and electric shock. Microgravity was simulated using a rotary cell culture system, chemical resistance was assessed using the microplate dilution method, and the cells were exposed to an electric shock by a pulsed electric field generator.

The obtained results did not show a significant difference between *S. cerevisiae* cells grown under normal gravity and microgravity treated with organic acids, antifungal compounds, and electric shock. *C. lusitaniae* cells grown in microgravity showed a 16.2-fold increase in resistance to electric shock, but there was no difference between the minimal inhibitory concentration values.

To conclude, yeast cells grown in microgravity can be differently effected by physical agents. For better understanding of microgravity's effects, it is important to carry out more studies with different types of cells and prolonged exposure to microgravity.

[1] Milojevic, T., & Weckwerth, W. (2020). Molecular Mechanisms of Microbial Survivability in Outer Space: A Systems Biology Approach. *Frontiers in Microbiology*, 11. <https://doi.org/10.3389/fmicb.2020.00923>

THE EFFECT OF MATERNAL HIGH-FAT DIET ON OFFSPRING RETINA

Neda Ieva Biliūtė¹, Gintarė Urbonaitė¹, Guoda Laurinavičiūtė², Urtė Neniškytė^{1,3}

¹ Institute of Biosciences, Life Sciences Center, Vilnius University, Lithuania

² Institute of Biomedical Sciences, Faculty of Medicine, Vilnius University, Lithuania

³ VU-EMBL Partnership Institute, Life Sciences Center, Vilnius University, Lithuania

neda.biliute@gmc.stud.vu.lt

Aim: Today Western diet has increasing content of fats, and this leads to increasing obesity rates. Many studies show that maternal high-fat diet causes chronic inflammation which can lead to neurodevelopmental disorders of the offspring [1, 2, 3]. It has been shown that the retina, as a part of central nervous system, is also affected in the individuals consuming high-fat diet [4, 5, 6]. However, there are no studies investigating the effect of maternal high-fat diet on the retina of the offspring. In this study we aim to determine whether maternal high-fat diet leads to retinal changes in the offspring.

Methods: We fed female C57Bl/6J mice with a control diet (10% fat) or high-fat diet (60% fat) from weaning to lactation. The offspring were weaned to CD. The eyeballs of the offspring were collected, fixed with 4% PFA, cryoprotected and sliced using cryotome. Retinal ganglion cells, Müller cells and microglia cells were labeled immunohistochemically using anti-RBPMS, anti-GFAP and Iba1 antibodies, respectively.

Results: We evaluated the thickness of retinal layers, density of retinal ganglion cells and microglia cells, GFAP and Iba1 signal area. The measurements were compared between the groups of offspring. No significant changes were found in the layer thicknesses of the peripheral retina. Outer nuclear layer of the central retina was significantly thicker in male offspring of maternal high-fat diet group compared to the male offspring of maternal control diet group. Density of the retinal ganglion cell did not differ significantly between the groups. There were no significant differences in the GFAP signal area and Iba1 signal area between the groups. Microglia density was significantly higher in maternal high-fat diet female offspring compared to maternal control diet female offspring in peripheral and central retina. However, in the male offspring the microglia density was lower in the maternal high-fat diet group in the peripheral retina. Iba1 signal area was significantly larger in the peripheral retina of maternal high-fat diet female offspring and significantly lower in peripheral retina of maternal high-fat diet male offspring compared to maternal control diet offspring. No significant differences in Iba1 signal area were found on central retina of female and male offspring.

Conclusions: Our findings showed that maternal high-fat diet had a gender-specific effect on the morphology of offspring retina and activation of microglia in the retina.

Funding: This work was supported by the Science Promotion Fund of Vilnius University.

[1] S. S. Kang, A. Kurti, D. A. Fair, and J. D. Fryer, 'Dietary intervention rescues maternal obesity induced behavior deficits and neuroinflammation in offspring', p. 12, 2014.

[2] R. D. Oades, A.-M. Myint, M. R. Dauvermann, B. G. Schimmelmann, and M. J. Schwarz, 'RAestetaerchntion-deficit hyperactivity disorder (ADHD) and glial integrity: an exploration of associations of cytokines and kynurenine metabolites with symptoms and attention', p. 19, 2010.

[3] M. Maes, R. Verkerk, S. Bonaccorso, W. Ombelet, E. Bosmans, and S. Scharpé, 'Depressive and anxiety symptoms in the early puerperium are related to increased degradation of tryptophan into kynurenine, a phenomenon which is related to immune activation', *Life Sciences*, vol. 71, no. 16, pp. 1837–1848, Sep. 2002, doi: 10.1016/S0024-3205(02)01853-2.

[4] D. A. Clarkson-Townsend, A. J. Douglass, A. Singh, R. S. Allen, I. N. Uwaifo, and M. T. Pardue, 'Impacts of high fat diet on ocular outcomes in rodent models of visual disease', *Experimental Eye Research*, vol. 204, p. 108440, Mar. 2021, doi: 10.1016/j.exer.2021.108440.

[5] R. C.-A. Chang *et al.*, 'High-Fat Diet-Induced Retinal Dysfunction', *Invest. Ophthalmol. Vis. Sci.*, vol. 56, no. 4, p. 2367, Apr. 2015, doi: 10.1167/iovs.14-16143.

[6] J.-J. Lee *et al.*, 'High-Fat Diet Induces Toll-Like Receptor 4-Dependent Macrophage/Microglial Cell Activation and Retinal Impairment', *Invest. Ophthalmol. Vis. Sci.*, vol. 56, no. 5, p. 3041, May 2015, doi: 10.1167/iovs.15-16504.

ADHESION OF MAMMALIAN CELL LINES ON POLYCARBONATE MEMBRANE

Paulina Kizinievič^{1,2}, Neringa Bakutė¹, Arūnas Stirke^{1,3}

¹Center for Physical Science and Technology, Department of Functional Materials and Electronics, Bioelectrics Laboratory, Sauletekio av. 3, LT-10257 Vilnius

²Institute of Biosciences, Life Sciences Center, Vilnius University, Sauletekio av. 7, LT-10257 Vilnius

³Institute of Solid State Physics, Micro and Nanodevices Laboratory, University of Latvia, Kengaraga str. 8, LV-1063, Riga, Latvia

paulina.kizinievic@gmc.stud.vu.lt

Successful mammalian cell adhesion is an important aspect of cell life cycle, proliferation, and signalling. In laboratories, researchers mostly use dishes which usually are pre-treated by suppliers for an enhanced adhesion of cells. There is a lot known about cell adhesion [1], however, some experiments require for the cells to grow on unconventional special surfaces. When using a specific substrate or surface for cell adhesion, it is necessary to experimentally find out which conditions would ensure a sufficient adhesion of a certain cell line. In our example, we are using polycarbonate membrane, which will be implemented into a microfluidics chip for electroporation of adherent cells and plasmid DNA inside of it.

Our objective is to prepare polycarbonate membrane by modifying it to facilitate adhesion of mammalian cells on it. Polycarbonate membrane is available commercially in different thicknesses and containing pores in different sizes. Oxygen plasma is known to increase the number of oxygen-containing groups, such as peroxide, hydroxyl, carboxyl groups on a substrate or surface, which makes the surface even more hydrophilic and ensures attachment of adhesion molecules [2]. We have tested an influence of oxygen plasma treatment for cell adhesion after membrane was also coated with poly-D-lysine. The results showed that only one fifth of cells attach to polycarbonate membrane without oxygen plasma treatment, meanwhile, more than 90 per cent of cells adhered on membrane with oxygen plasma treatment.

Next, we have tested the influence of other adhesion molecules - type I collagen and fibronectin for cell adhesion on polycarbonate membrane pre-treated with oxygen plasma. Our results showed that there is no significant difference in numbers of adherent cells between different adhesion molecules used; the mammalian cells easily attach to polycarbonate membrane which was coated with poly-D-lysine and any adhesion molecule (or their combinations) mentioned above. With the indication of our results, we conclude, that oxygen plasma treatment is a necessary step to induce cell adhesion on polycarbonate membrane; also, coating polycarbonate membrane with any adhesion molecules (fibronectin, collagen I and poly-D-lysine) is sufficient for achieving a required level of cell adhesion on polycarbonate membrane.

[1] Sobiepanek, A. (2020). Different Types of Surface modification used for Improving the Adhesion and Interactions of Skin Cells. Open Access Journal of Biomedical Science, 2(1);

[2] Daum, R., Mrcic, I., Hutterer, J., Junginger, A., Hinderer, S., Meixner, A. J., Gauglitz, G., Chassé, T., & Schenke-Layland, K. (2021). Fibronectin adsorption on oxygen plasma-treated polyurethane surfaces modulates endothelial cell response. Journal of Materials Chemistry B, 9(6), 1647–1660.

IN VITRO EVALUATION OF STEM CELL DIFFERENTIATION ON 3D BIOPRINTED HYDROGELS FOR URETHRAL TISSUE ENGINEERING

Andrius Buivydas¹, Povilas Barasa¹, Egidijus Šimoliūnas¹, Natalija Krestnikova², Virginija Bukelskienė¹

¹ Department of Biological Models, Institute of Biochemistry, Life Sciences Center, Vilnius University, Lithuania

² Department of Molecular Cell Biology, Institute of Biochemistry, Life Sciences Center, Vilnius University, Lithuania
andrius.buivydas@gmc.stud.vu.lt

The urethra is an important component of the urinary system that facilitates the passage of urine from the bladder to the outside of the body. Effective repair of damaged urethra is essential for restoring normal urination function and preventing long-term complications[1]. Current treatment of urethral damage involves surgical intervention, with recurrent treatment often necessary. To improve treatment, we set out to use 3D printing to manufacture an artificial urethral tissue which would be suited to a patient's individual needs and would be optimal for cell proliferation, migration and differentiation into healthy urethral tissue.

Gelatin methacrylate (GelMA) and silk fibroin (SF) are two biocompatible and biodegradable polymers that have been utilized in the development of hydrogels for biomedical applications where they can serve as artificial tissues[2]. GelMA is denatured collagen modified with methacrylate, it is commercially accessible and can undergo a photoinitiated radical reaction to form a tough 3D structure[3]. Polymerized GelMA is a solid but it is not rigid enough to implant into tissues during an operation. For this reason, it was decided to combine the GelMA with silk fibroin, which when denatured forms beta-sheets and can therefore make the whole composite mechanically stronger.

The first step in creating the hydrogel was optimising the printing of the GelMA-SF construct without any cells. The workflow of printing the hydrogels consists of firstly mixing GelMA and SF, then sonicating the mixture to denature the silk fibroin, then performing the 3D printing into a non-newtonian fluid and finally using UV light to polymerize GelMA-SF into a firm, tubularized structure.

To achieve this, various component combinations of the GelMA-SF mixture and the parameters for 3D printing itself were tested. Ultimately, we found that GelMA and SF should be mixed with 10% and 5% concentrations, respectively, to consistently successfully print GelMA-SF hydrogels (fig 1.). To analyze the surface (fig 2.) of the printed construct SEM (scanning electron microscopy) was used. The acquired images show that the hydrogels' surface is uneven and has a large surface area both of which are optimal for cell migration and proliferation.



Fig 1. Successfully printed hydrogels submerged in PBS

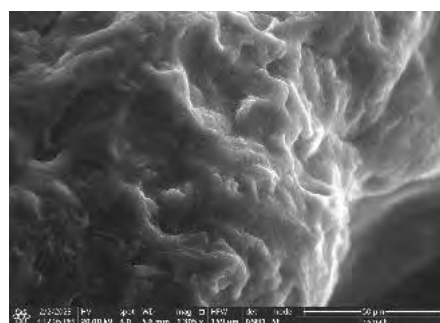


Fig 2. Surface pictures of a GelMA-SF hydrogel acquired using a SEM microscope

The next step of the project is to print a cell-laden GelMA-SF hydrogel. RASC (rabbit adipose stem cells) and RBMC (rabbit buccal mucosa cells) primary cells were seeded onto the hydrogel and differentiated towards the epithelial lineage for 2 weeks. Induced and spontaneous epithelial differentiation was evaluated by measuring gene expression levels of epithelial differentiation markers *Ck14*, *Cadh1* and *Ocln*, and our results showed that both RASC and RBMC cells exhibit reduced expression of *Ck14* after 2 weeks of differentiation on GelMA-SF hydrogels, which is a sign that the stem cells successfully became non-proliferative epithelial cells[4].

To summarize, our results show that 3D bioprinting of cell-laden GelMA-SF hydrogels with subsequent cell differentiation into epithelial tissue could be a promising method for manufacturing artificial urethral tissue. *In vivo* experiments will be performed to further evaluate our findings.

[1] "Urethral Injuries | Conditions | UCSF Health." <https://www.ucsfhealth.org/conditions/urethral-injuries> (accessed Feb. 02, 2023).

[2] J. O. Buitrago et al., "Silk fibroin/collagen protein hybrid cell-encapsulating hydrogels with tunable gelation and improved physical and biological properties," *Acta Biomater*, vol. 69, pp. 218–233, Mar. 2018, doi: 10.1016/j.actbio.2017.12.026.

[3] S. Bupphathong, C. Quiroz, W. Huang, P. F. Chung, H. Y. Tao, and C. H. Lin, "Gelatin Methacrylate Hydrogel for Tissue Engineering Applications—A Review on Material Modifications," *Pharmaceuticals*, vol. 15, no. 2. MDPI, Feb. 01, 2022. doi: 10.3390/ph15020171.

[4] H. Alam, L. Sehgal, S. T. Kundu, S. N. Dalal, and M. M. Vaidya, "Novel function of keratins 5 and 14 in proliferation and differentiation of stratified epithelial cells," *Mol Biol Cell*, vol. 22, no. 21, pp. 4068–4078, Nov. 2011, doi: 10.1091/mbc.E10-08-0703.

INVESTIGATIONS OF THE EFFECTS OF POLYSTYRENE NANOPARTICLES ON ROOT CELLS OF *ALLIUM CEPA* BY MOLECULAR METHODS

Gabija Zinkevičiūtė, Asta Stapulionytė

Institute of Biosciences, Life Sciences Center, Vilnius University, Lithuania
gabija.zinkeviciute@gmc.stud.vu.lt

Plastic is synthetic or semi-synthetic material that is used to make various items. A lot of us probably could not imagine life without plastic, because it is everywhere in our households. The reason why it is so commonly used, it's because plastic is lightweight, durable and inexpensive to make. During 70 years period worldwide plastic production grew enormously – in the 1950s around 1.7 million tons of plastics per year were produced, in 2021 the number increased to 390.7 million tons. And numbers are still growing. Plastics remain in the environment for hundreds of years and degrade into microparticles (< 5000 nm in diameter), and further into nanoparticles (< 100 nm in diameter). It is known that nanoparticles can penetrate organisms through pinocytosis, phagocytosis or passive transport [1].

Since nanoparticles enter living organisms and accumulate in the food chain, it is important to investigate their potentially harmful effects on those organisms. Our research purpose is to determine whether polystyrene nanoparticles have a genotoxic effect on *Allium cepa* (common onion) at DNA level.

We have been growing onions in suspensions with polystyrene nanoparticles of various concentrations. The nanoparticles were from 50 to 100 nm in size. DNA was extracted from onion roots. For DNA purification we used Thermofisher GeneJet Plant Genomic DNA Purification Mini Kit. For this research, the ISSR-PCR method was used to evaluate whether polystyrene nanoparticles induce polymorphisms in onion DNA.

In conclusion, we observed the genotoxic effects of various concentrations of polystyrene nanoparticle suspensions in *Allium cepa* (common onion) root cells.

[1] Kik K, Bukowska B, Sicińska P. Polystyrene nanoparticles: Sources, occurrence in the environment, distribution in tissues, accumulation and toxicity to various organisms. *Environ Pollut.* 2020 Jul;262:114297

RESEARCH OF GENOTOXIC EFFECTS INDUCED BY POLYSTYRENE NANOPARTICLES IN *ALLIUM CEPA* ROOT MERISTEM CELLS

Agnė Kilnaitė, Asta Stapulionytė

Institute of Biosciences, Life Sciences Center, Vilnius University, Lithuania
agne.kilnaite@gmc.stud.vu.lt

Polystyrene nanoparticles, also known as nanoplastics, have become a significant environmental issue in recent years due to their increasing abundance and potential harm to the environment and wildlife. They can come from a variety of sources, including the breakdown of larger plastic products and the release of microbeads from personal care products. The small size of nanoplastics allows them to evade filtration systems and persist in the environment, including water and soil. This signifies that they can remain in the environment for a long time, can be transported over large distances by wind, water, and other means and can easily enter the food chain [1]. Overall, the problem of polystyrene nanoparticles is serious because of the potential harm they can cause to wildlife, human health, and the environment.

Plants play a crucial role in the ecosystem, and understanding the effects of nanoparticles on their cells can provide valuable insights into the impact of these particles on the environment and the food chain. To further understand the potential genotoxic effects of polystyrene nanoparticles, a cytogenetic study on *Allium cepa* root meristem cells was conducted. The common onion is generally used as a model organism in cytogenetic studies due to its well-studied root system and ease of cultivation [2]. Solutions containing various concentrations of polystyrene nanoparticles were tested and the length of onion roots was examined. A plant bioassay, called *Allium* test, was applied to determine the mutagenic potential of polystyrene nanoparticles, ratio of chromosome aberrations, mitotic index and micronuclei frequencies were observed and compared with results of the negative control.

The findings of this study are expected to contribute to a better understanding of the potential dangers of polystyrene nanoparticles and their impact on the ecosystem. By investigating the effects of these particles on the environment, the study aims to provide valuable insights into the need for proper disposal methods and to raise awareness about the importance of environmental conservation.

[1] Gigault, J., Halle, A. T., Baudrimont, M., Pascal, P.-Y., Gauffre, F., Phi, T.-L., El Hadri, H., Grassl, B., & Reynaud, S. (2018). Current opinion: What is a nanoplastic? *Environmental Pollution* (Barking, Essex: 1987), 235, 1030–1034.

[2] Leme, D. M., & Marin-Morales, M. A. (2009). *Allium cepa* test in environmental monitoring: A review on its application. *Mutation Research/Reviews in Mutation Research*, 682(1), 71–81.

THE EFFECTS OF HUMAN MENSTRUAL BLOOD MESENCHYMAL STEM CELL GROWTH FACTORS ON CHONDROGENESIS IN VITRO

Paulina Bialaglovyte¹, Rokas Miksiunas¹, Ignas Lebedis¹, Jolita Pachaleva¹, Eiva Bernotiene¹,
Almira Ramanaviciene^{2,3}, Giedrius Kvederas⁴, Ilona Uzieliene¹

¹Department of Regenerative Medicine, State Research Institute Centre for Innovative Medicine, Vilnius, Lithuania

²Department of Immunology, State Research Institute Centre for Innovative Medicine, LT-08406 Vilnius, Lithuania;

³NanoTechnas – Center on Nanotechnology and Materials Sciences, Faculty of Chemistry and Geosciences, Vilnius university, Naugarduko g. 24, LT-03225 Vilnius, Lithuania;

⁴The Clinic of Rheumatology, Traumatology Orthopaedics and Reconstructive Surgery, Institute of Clinical Medicine of the Faculty of Vilnius University, Vilnius, Lithuania.

paulinabialaglovyte@gmail.com

Mesenchymal stem cells (MSCs) have been widely used in regenerative medicine due to their capability of differentiating and self-renewing [1]. These cells are being isolated from different tissues, including bone marrow, dental pulp, adipose tissue, etc.. Menstrual blood MSCs (MenSCs) are much less characterized, however, they are known to possess more pronounced stem cell properties, as compared to classical bone marrow MSCs (BMMSCs). MenSCs exhibit a higher proliferation rate and a broader differentiation capacity [2,3]. Although MenSCs is an attractive alternative to BMMSCs, their use for cartilage tissue regeneration is still under consideration and research. Also, MenSCs are known to possess large amounts of growth factors responsible for an effective endometrium regeneration, which might be a potential co-stimulant for other tissue regeneration [2,3].

The aim of the study is to evaluate the chondrogenic differentiation capacity of MenSCs and their ability to stimulate BMMSCs chondrogenesis in co-culture conditions, analyzing levels of chondrogenesis-related growth factors.

This study was performed in compliance with all bioethical requirements. Cells were isolated from healthy human menstrual blood (n=3) and bone marrow (n=3) samples. MenSCs and BMMSCs were characterized according to stem cell surface marker expression (flow cytometry) and adipogenic/osteogenic differentiation capacity (Oil-Red/Alizarin). Chondrogenic differentiations of MenSCs and BMMSCs were stimulated with transforming growth factor-beta (TGF- β 3), activin A, insulin-like growth factor 1 (IGF-1), bone morphogenetic protein-2 (BMP-2) and their combinations. The results of this study indicate that TGF- β 3 significantly stimulated chondrogenic response in BMMSCs, as compared to other growth factors, while chondrogenic differentiation of MenSCs was much weaker and stimulated with combination of activin A and TGF- β 3. For co-culture conditions, MenSCs were seeded in 24 well plates, while BMMSCs were seeded in 0.4 μ m membrane inserts placed into wells with seeded MenSCs. After co-cultures with MenSCs, secretion of TGF- β 3, activin A, BMP-2 and IGF-1 was analyzed (ELISA) and chondrogenic differentiation of BMMSC pellets was evaluated according to cartilage oligomeric matrix protein (COMP) cultured in chondrogenic medium for 3, 7, 21 days, and immunohistochemical analysis of collagen type II. The results demonstrated that chondrogenic differentiation of BMMSCs was more pronounced in co-culture with MenSCs, as compared to single BMMSCs cultures, which have resulted in a significant secretion of COMP and production of collagen type II in BMMSCs chondrogenic pellets. The amounts of growth factor release (TGF- β 3, activin A and IGF-1) was also higher in co-culture conditions, which demonstrated the importance of cell co-stimulation.

In conclusion, MenSCs may turn out to be a promising population of stem cells for the development of cell-based technologies to stimulate chondrogenesis in vitro.

[1] Behr B, Ko SH, Wong VW, Gurtner GC, Longaker MT. Stem cells. *Plast Reconstr Surg.* 2010 Oct;126(4):1163-1171. doi: 10.1097/PRS.0b013e3181ea42bb. PMID: 20555302.

[2] Meng, X.; Ichim, T.E.; Zhong, J.; Rogers, A.; Yin, Z.; Jackson, J.; Wang, H.; Ge, W.; Bogin, V.; Chan, K.W.; et al. Endometrial regenerative cells: a novel stem cell population. *J. Transl. Med.* 2007, 5, 57.

[3] Uzieliene I, Bagdonas E, Hoshi K, Sakamoto T, Hikita A, Tachtamisevaite Z, Rakauskiene G, Kvederas G, Mobasheri A, Bernotiene E. Different phenotypes and chondrogenic responses of human menstrual blood and bone marrow mesenchymal stem cells to activin A and TGF- β 3. *Stem Cell Res Ther.* 2021 Apr 29;12(1):251. doi: 10.1186/s13287-021-02286-w.

Un-Settling Virome of *Saccharomycetales* Yeast: Dispersal within Species

Kristupas Paulius¹, Aleksandras Konovalovas¹, Saulius Serva¹

¹Department of Biochemistry and Molecular Biology, Institute of Biosciences, Life Sciences Center, Vilnius University, Vilnius, Lithuania
kristupas.paulius@gmc.stud.vu.lt

Since the development of Holobiont worldview, it has become difficult to see species living in isolation: there are many points of interaction that favor collaborative survival strategies among organisms. One such example may be observed in so-called *killer yeasts*, where cells are provided with biocidal properties by a system of double-stranded RNA (dsRNA) viruses. The goal of this research was to find such symbiotic groups throughout wild *Saccharomycetales* yeast and define their virome by homologically overlaying the indicated viral sequences, and analyzing them using bioinformatic tools. The unveiled findings may assist us in comprehending interspecies communication and viral transmission within distant biological organisms.

Our group evaluated 407 wild yeast strains from various natural environments in Lithuania. Incubation on selective medium and RNA gel electrophoresis revealed that more than 10% (N = 47) of the selected colonies exhibited a killer phenotype. Only yeast belonging to different species were investigated further. Twenty distinct dsRNAs were obtained after purifying viral genomes from the chosen strains. They were all sequenced using *Oxford Nanopore Technologies* and characterized by applying *CLANS (CLuster ANalysis of Sequences)* tool. The findings show that a broader range of viruses — not only belonging to yeasts — are present in different strains, including non-yeast totiviruses and *Mitoviridae sp.*, generally found in filamentous fungi. This implies that dsRNA genomes are considerably more distributed throughout the organisms and that their modes of function are yet to be deciphered.

EFFECTS OF SURFACE ROUGHNESS ON THE GIANT MAGNETORESISTANCE PERFORMANCE IN MAGNETIC SANDWICHES

Aleksandre Melikadze¹, Lali Kalandadze¹, Nugzar Gomidze¹

¹Department of Physics, Batumi Shota Rustaveli State University, Georgia
Aleksander.melikadze@gmail.com

Since the discovery of Giant magnetoresistance, the theoretical treatment of this effect became the subject of much attention. It is one of the most engrossing discoveries in thin-film magnetism, which combines both huge technological potential and deep fundamental physics. It is considered that the effect of giant magnetoresistance is due to the spin-dependent scattering of charge carriers in the volume of magnetic layers and at their boundaries, and its amplitude depends on the degree of roughness of the outer and interlayer boundaries. Despite a large number of both experimental and theoretical works, in which the influence of the state of outer boundaries and interfaces on the magnitude of the giant magnetoresistance was studied, conclusions do not coincide [1-5]. The need to resolve these contradictions should be carried out within the framework of an extended theoretical study of the giant magnetoresistance effect using more complex models for describing the interaction of charge carriers with the structure and interlayer boundaries. This was the subject of our study. As an example, we have considered a three-layer film Fe/Cr/Fe consisting of ferromagnetic metal layers of different thicknesses separated by a nonmagnetic ultrafine metal layer. The results of numerical calculation within the framework of the semiclassical approximation shown that the specular scattering of charge carriers by the interlayer and outer boundaries insignificantly increases the amplitude of the giant magnetoresistance effect due to the fact that they do not lose their spin information when reflected from the surfaces. However, it should be noted that in the case when scattering centers are concentrated at the interlayer boundary, this leads to screening of charge carriers and, accordingly, to a decrease in the effect.

-
- [1] Yu.O. Shkurdoda, L.V. Dekhtyaruk, A.G. Basov, A.M. Chornous, et al., The giant magnetoresistance effect in Co/Cu/Co three-layer films, *Journal V. 477*, Pages 88-91, 2019. <https://www.sciencedirect.com/science/article/abs/pii/S0304885318329597>
- [2] M.C. Cyrille, S. Kim, M.E. Gomez et al., Enhancement of perpendicular and parallel giant magnetoresistance with the number of bilayers in Fe/Cr superlattices // *Rev. B:– 2000.– V.62, №5*. pp. 3361 – 3367. (2000) DOI: <https://doi.org/10.1103/PhysRevB.62.3361>
- [3] D. Olligs, D.E. Burgler, Y.G. Wang et al. Roughness - induced enhancement of giant magnetoresistance in epitaxial Fe/Cr/Fe (001) trilayers, *Europhysics Lett. V.59, №3*, pp.458 – 464. (2002) [10.1209/epl/i2002-00217-9](https://doi.org/10.1209/epl/i2002-00217-9)
- [4] Bae Seongtae, J. Jack H., P.J. Chen, Dependence of physical properties and giant magnetoresistance ratio on substrate position during rf sputtering of NiO and Fe₂O₃ for bottom spin valves *J. Appl. Phys. Lett. V.81, №12*. P. 2208 – 2210. (2002)
- [5] Bae, S., Chen, P., Egelhoff Jr., W. and Judy, J. Effects of Sputtering Angle on Surface Roughness, Chemical Composition and Giant Magnetoresistance Properties of NiO and α -Fe₂O₃ Bottom Spin-Valves, *IEEE Transactions on Magnetics* (Accessed February 1, 2023) <https://www.nist.gov/publications/effects-sputtering-angle-surface-roughness-chemical-composition-and-giant>

CHEMOPREVENTIVE ACTIVITY OF LINSEED OIL ETHYL ESTERS FOR GLIOMA TUMOR CELL PANEL TCP-1018™

Nikoła Hauzer¹, Maciej Janeczek², Tomasz Gębarowski²

¹ Students' Scientific Society of Veterinary Biotechnology „Refectio”, Department of Biostructure and Animal Physiology, Wrocław University of Environmental and Life Sciences, Kozuchowska 1/3, 51-631 Wrocław, Poland

² Department of Biostructure and Animal Physiology, Wrocław University of Environmental and Life Sciences, Kozuchowska 1/3, 51-631 Wrocław, Poland
123516@student.upwr.edu.pl

Glioma is the most common and malignant type of primary brain tumor. The prognosis for the burdened patients depends on their age, performance status, and tumor stage. However, most cases, even with low malignancy, have a poor survival rate with optimal therapy.

Currently, the management of glioma is challenging and requires multidisciplinary treatment.

Nearly two-thirds of gliomas are highly malignant lesions, which account for a disproportionate share of the morbidity and mortality associated with brain tumors.[1]

The aim of the study was to determine the toxicity of 20% flaxseed oil ester emulsions, with different final concentrations from 0.2% to 5%, against 5 types of glial tumor.

A Glioma Tumor Cell Panel TCP-1018™ consisting of 5 glial tumor cell lines of varying genetic complexity was used for the study. HTB-14 cell line with epithelial morphology, isolated from a malignant glioma from a male patient; A172 cell line isolated from brain tissue from a male patient; HTB-15 cell line with mixed morphology, isolated from a 50-year-old man with stage IV glioma; HTB-12 astrocytoma cell line isolated from a 72-year-old man; and HTB-148 neuroglioma cell line isolated from a 37-year-old man.

The experiments were carried out using 20% linseed oil ester emulsions with final concentrations ranging from 0.2% to 5%. After 24 h of incubation, the SRB assay (sulforhodamine B assay) used to assess cell proliferation based on measurement of cellular protein content was performed. The test was performed according to the National Cancer Institute (NCI) recommendations. This was followed by analysis using LIVE/DEAD fluorescent staining to determine cell viability.

The performed experiment proved that the emulsion showed high activity on all cell lines. It had the strongest cytotoxic effect on cancer cells of the HTB-14, SW 1088 and A172 cell lines, for the HTB-15 line only at its highest concentration. The results suggest that the tested emulsion at the lowest concentrations causes cytostatic effect, while at higher concentrations it causes cytotoxic effect, in other words, leads to apoptosis or necrosis of the cell.

[1] Norden AD, Wen PY. Glioma therapy in adults. *Neurologist*. 2006 Nov;12(6):279-92. doi: 10.1097/01.nrl.0000250928.26044.47. PMID: 17122724.

ISOLATION OF STEM CELLS OBTAINED FROM HUMAN SUBCUTANEOUS ADIPOSE TISSUE

Emilia Kamińska¹, Weronika Gołabek¹, Nikola Hauzer¹, Maciej Janeczek²,
Tomasz Gębarowski²

¹Students' Scientific Society Department of Biostructure and Animal Physiology, Wrocław University of Environmental and Life Sciences, Koźuchowska 1/3, 51-631 Wrocław, Poland

²Department of Biostructure and Animal Physiology, Wrocław University of Environmental and Life Sciences, Koźuchowska 1/3, 51-631 Wrocław, Poland
123550@student.upwr.edu.pl, 121504@student.upwr.edu.pl

Adipose tissue is a type of connective tissue found in many places in the body - around internal organs, bone marrow, breast tissue, and under the skin. Adipose tissue stem cells (ASCs) are obtained easier than other types of multipotent mesenchymal stem cells (MSCs). That is why subcutaneous tissue can be harvested during various procedures, including minimally invasive procedures such as liposuction. During liposuction, 100 ml to 3000 ml of adipose tissue is obtained, which contains about 1×10^6 mesenchymal stem cells/200 ml of fat[1]. The process of cell isolation, the target of the study, provides the basis for further use of SVF (Stromal Vascular Fraction), which can differentiate into other cell types, including adipocytes, chondroblasts, myoblasts and osteoblasts[2].

The fat collected from the patient is placed in sterile bottles and transported to the laboratory in a thermos containing cooling cartridges. The isolation process should begin by pouring the material into 500ml conical centrifuge tubes and centrifuging at an acceleration of 1200-2000g for 5 minutes. After the first centrifugation, two fractions appear in the conical centrifuge tube - the upper fraction is fat, and the lower fraction contains, among other things, blood. Above the upper fraction is a layer of oil, which should be removed. The upper fraction (fat) should be transferred to a new tube, and then Collagenase II solution (1g in 10ml PBS) is added to the homogenized tissue in a ratio of 1:1 or 1:2, later centrifuge at an acceleration of 1260g for 5 minutes. Incubation of fat in the Collagenase II solution is done horizontally, on a rocker, and should last about 40-60 minutes at 37°C. During the incubation, the connections between cells are destroyed. After this time, the tube should be centrifuged again at an acceleration of 1360g for 5 minutes. The next step is to pellet the top layer of tissue to access the bottom layer. On its bottom, after rinsing with DMEM (Dulbecco's Modified Eagle Medium) and centrifuging 400g for 5 minutes, a pellet containing SVF that can initiate multipotent stromal cell culture or be used as a finished therapeutic product. After pelleting the supernatant, the resulting pellet should be resuspended in the complete mesenchymal stem cell culture media and then transferred to a culture bottle. The culture should be incubated at 37°C under 5% CO₂, which will allow the cells to multiply correctly and adhere to the plastic bottom of the bottle.

The above-described process is the result of the development of a universal scheme for the isolation of stem cells for their further use in cell therapies. Examples of the use of these cells include the treatment of hard-to-heal wounds, extensive burns, osteoarthritis, or nerve injuries[3].

[1] Witkowska-Zimny, M., & Walenko, K. (2011). *Stem cells from adipose tissue. Cellular and Molecular Biology Letters*, 16(2). doi:10.2478/s11658-011-0005-0

[2] Rodriguez, A.-M., Elabd, C., Amri, E.-Z., Ailhaud, G., & Dani, C. (2005). *The human adipose tissue is a source of multipotent stem cells. Biochimie*, 87(1), 125-128. doi:10.1016/j.biochi.2004.11.007

[3] Chu, D.-T., Nguyen Thi Phuong, T., Tien, N. L. B., Tran, D. K., Minh, L. B., Thanh, V. V., ... Thi Nga, V. (2019). *Adipose Tissue Stem Cells for Therapy: An Update on the Progress of Isolation, Culture, Storage, and Clinical Application. Journal of Clinical Medicine*, 8(7), 917. doi:10.3390/jcm8070917

DETERMINATION OF INCREASE IN THE DEGREE OF HESPERIDIN DISSOLUTION IN THE COMPOSITION OF A CENTRIFUGALLY FORMED SOLID DISPERSION SYSTEM

Vadym Lisovyi^{1,2}, Artem Kharchenko¹, Andriy Goy¹, Viktoriia Plavan², Volodymyr Bessarabov¹

¹Department of Industrial Pharmacy, Kyiv National University of Technology and Design, Ukraine

²Department of chemical technology and resource saving, Kyiv National University of Technology and Design, Ukraine
v.lisovyi@kyivpharma.eu

Hesperidin is a flavanone glycoside obtained from the skin of citrus fruits. This compound has an anti-inflammatory and antioxidant effect [1]. An obstacle in the use of this glycoside is its low solubility in water, therefore, to increase solubility, centrifugally formed solid dispersion systems (SDS) from pharmaceutically acceptable polymers with hesperidin in the composition are being developed. This material is devoted to checking the solubility of one of the SDS.

Methodology: the study of dissolution profiles was carried out according to the methodology of the European Pharmacopoeia (EPH) 8.0 (2.9.3) [2]. Apparatus 2 (a paddle apparatus) and Vankel Varian VK7000 dissolution test equipment with a VK750D external water heater were used. The volume of the dissolution medium was 500 ml ±1%. The temperature of the dissolution medium is 37.0±0.5 °C. The speed of rotation of the stirring element, the blade, was 50 rpm. Sampling was carried out at the indicated time (5, 10, 15, 30, 45, 60, 90, 120 minutes after the start of the test) from the area in the middle between the surface of the dissolution medium and the upper part of the rotating blade, at no closer than 1 cm from the vessel wall. The selected aliquot for analysis (5 ml) was compensated with an equal volume of fresh dissolution medium heated to a temperature of 37.0±0.5 °C [2].

During the SDS dissolution test of hesperidin, buffer solutions with a controlled value of the hydrogen index (pH) were used. A medium with hydrochloric acid pH 1.20±0.05, acetate buffer solution pH 4.50±0.05 and phosphate buffer solution pH 6.80±0.05 were used. The pH value was monitored at the beginning and end of the test.

Quantitative determination of hesperidin released from SDS was carried out according to the calibration chart spectrophotometrically according to the validated method. The method of quantitative determination of hesperidin meets all acceptance criteria. The quantitative determination of the hesperidin content in SDS is based on the qualitative reaction of hesperidin with ferric (III) chloride, while a colored compound is formed, the maximum optical absorption of which is observed at a wavelength of 602 nm.

The solution was characterized by the value Q (degree of dissolution), which is calculated by Eq. (1):

$$Q (\%) = \frac{(\text{API concentration at the specified time,g/l})}{(\text{Nominal content of API,g/l})} * 100 \% \quad (1)$$

The degree of release of hesperidin from SDS was compared with the degree of solubility of pure hesperidin.

When comparing the dissolution profiles of pure hesperidin and hesperidin in the composition of SDS in an environment with a pH of 1.2, it was found that SDS has a significantly higher degree of dissolution compared to pure hesperidin. In the first 5 min, the degree of dissolution of hesperidin in SDS is 38.2±2.5%, while for pure hesperidin Q=5.5±0.5% (p<0.05). At 45 minutes, the degree of dissolution of hesperidin in the composition of SDS reached a value of 51.5%, which is 8.3 times more than the degree of dissolution of pure hesperidin.

When conducting an experiment in an acetate buffer medium of pH 4.5, it was established that the degree of hesperidin release from SDS in the first 5 minutes is about 50.0%. 10 minutes after the start of the experiment, the degree of dissolution of hesperidin released from SDS was 65.0%, which is 12.0 times higher than the degree of dissolution of pure hesperidin under identical conditions (p<0.05).

In a phosphate buffer with a pH of 6.8, hesperidin in SDS is released much more slowly, but has a higher degree of solubility than pure hesperidin (14.0% in SDS versus 5.0% in pure hesperidin). The dissolution profile of hesperidin in SDS increased over an hour and after one hour was 4.0 times higher than the degree of dissolution for pure hesperidin.

The results of the study indicate that SDS with hesperidin in the composition allows to achieve a greater degree of solubility than that of pure hesperidin. Hesperidin from SDS is best released in acetate buffer (pH 4.5), the degree of solubility in 60 minutes reaches 65.0%. In an acidic environment, an 8.3-fold increase in the degree of solubility of hesperidin in SDS was achieved compared to pure hesperidin.

[1] R. Cao, Y. Zhao, Z. Zhou, X Zhao, Enhancement of the water solubility and antioxidant activity of hesperidin by chitoooligosaccharide, Journal of the Science of Food and Agriculture **98**(6), 2422-2427 (2018).

[2] European Pharmacopoeia. 8th edition. Vol. 2. Strasbourg (FR): Directorate for the Quality of Medicines and HealthCare of the Council of Europe (EDQM); Dissolution test for solid dosage form, 288-295 (2013).

INHIBITION OF NOVOCAINE HYDROLYSIS IN HUMAN SERUM BY HESPERIDIN IN VITRO

Dmytro Oliinyk, Volodymyr Bessarabov, Galyna Kuzmina, Vadym Lisovyi, Anastasiia Behdai,
Vladyslav Udovytskyi

Department of Industrial Pharmacy, Kyiv National University of Technologies and Design, Ukraine
oliinyk.do@knutd.edu.ua

Despite the development of modern approaches to the design and modification of new molecules, the nomenclature of local anesthetics has remained constant over the past two decades. The difficulty of developing new molecules with anesthetic effect is explained by the relative complexity of their mechanism of action, which in turn determines specific requirements for the physicochemical properties of these compounds. An alternative is to optimize existing anesthetic drugs to control pain effects of various origins and treat chronic neuropathic pain syndromes.

Novocaine is a common local anesthetic that is a reference anesthetic in ambulatory practice, which is well studied, with known sympatholytic, anti-inflammatory, and moderate toxic effects. However, the short duration of analgesic action of novocaine is a significant disadvantage compared to other alternatives, such as lidocaine. The relatively short duration of action is due to the structure of the molecule: novocaine is an aminoester, which, unlike amides, is metabolized by plasma esterases, namely butyrylcholinesterase [1-3]. The possibility of increasing the duration of local anesthetic action necessitates the search for inhibitors of the process of decomposition of novocaine by butyrylcholinesterase, as the main enzyme that prevents long-term anesthesia. The flavonoid hesperidin can be considered as a potential inhibitor of butyrylcholinesterase.

The efficiency and prospects of using hesperidin to create a new pharmaceutical composition based on novocaine were studied by determining the kinetics of novocaine hydrolysis by human serum butyrylcholinesterase. The study was based on the spectrophotometric kinetic method *in vitro*.

The working solution was a mixture of phosphate buffer (pH=7.6) and lyophilized blood serum solution (Czech Republic, Erba Lachema s.r.o.) in the ratio of 1400 μL : 50 μL , respectively. Dimethyl sulfoxide was used as a solvent for flavonoids. 30 μL of the required concentration of hesperidin solution was added to the working solution and incubated for 5 min at 37 °C. Hesperidin was tested at concentration points of 5, 25, 50, and 100 μM . After incubation, 50 μL of novocaine solution (10 μM) was added to obtain a total volume of 1530 μL of reaction mixture. As a control solution, 1530 μL of a mixture identical in composition to the working solution in the test samples, but not containing the flavonoid, was used. Immediately after the addition of novocaine, measurements were made using a SPECORD 200 UV spectrophotometer (Analytic Jena, Germany) at 290 nm for 30 min. The signal was detected at intervals of 75 seconds. Each concentration point was tested 3 times.

The rate of decomposition of novocaine by butyrylcholinesterase in the presence of a flavonoid was determined by calculating the first-order rate constant (K_H^1). The data were calculated and visualized using standard methods in Microsoft Excel for Microsoft 365 software.

Hesperidin was found to inhibit human serum butyrylcholinesterase at all test concentrations. The greatest inhibition effect was found when hesperidin was added to the mixture at a concentration of 100 μM , at which the rate constant of novocaine hydrolysis significantly ($p \leq 0.05$) decreased by 1.6 times ($K_{H(100)}^1 = 0,82 \pm 0,03 \times 10^{-3}$ 1/s) compared to the value of the corresponding rate constant of novocaine hydrolysis in the mixture without the flavonoid ($K_{H(0)}^1 = 1,39 \pm 0,01 \times 10^{-3}$ 1/s).

Hence, hesperidin can be considered a promising active pharmaceutical ingredient of a long-acting pharmaceutical composition based on novocaine.

[1] L. Ombregt, Procaine: Principles of treatment. A System of Orthopaedic Medicine, Science Direct. **e.5**, 83–115 (2013).

[2] O. Lockridge, Review of human butyrylcholinesterase structure, function, genetic variants, history of use in the clinic, and potential therapeutic uses, *Pharmacology & therapeutics* **148**, 34–46 (2015).

[3] J. Yuan, J. Yin, E. Wang, Characterization of procaine metabolism as probe for the butyrylcholinesterase enzyme investigation by simultaneous determination of procaine and its metabolite using capillary electrophoresis with electrochemiluminescence detection, *Journal of chromatography A*, **1154(1-2)**, 368–372 (2007).

STUDY OF THE KINETICS OF THE RELEASE OF NIMESULIDE FROM A POLYMER SOLID DISPERSION SYSTEM

Viktoriiia Lyzhniuk, Vadym Lisovyi, Volodymyr Bessarabov, Galyna Kuzmina, Viktor Kostiuk, Andriy Goy

Department of industrial pharmacy, Kyiv National University of Technologies and Design, Ukraine
v.lyzhniuk@kyivpharma.eu

Nowadays, non-steroidal anti-inflammatory drugs (NSAIDs) are one of the most used symptomatic drugs in the modern world, as they can simultaneously exhibit anti-inflammatory, antipyretic, analgesic and antirheumatic effects [1]. Among the wide variety of NSAIDs, nimesulide-based drugs are among the most frequently used in practice for the treatment of various conditions of pain, fever, and inflammation. This active pharmaceutical ingredient (API) is able to affect a large number of mediators involved in inflammatory processes. Nimesulide, like most nonsteroidal anti-inflammatory APIs, belongs to class II according to the biopharmaceutical classification, that is, it is characterized by high permeability, but has low solubility in water (~0.01 g/l) [2]. In this regard, nimesulide is slowly released from solid oral dosage forms, and accordingly, the rate of its absorption from the gastrointestinal tract into the blood is also slowed down. This creates prerequisites for the use in medical practice of excessive doses of nimesulide and the occurrence of undesirable side effects. Therefore, increasing the solubility of nimesulide while maintaining high permeability to biological membranes is an actual issue.

In recent years, the formation of solid dispersion systems (SDS), which represent the dispersion of one or more active ingredients in an inert carrier in a solid state, is considered to be the most useful pharmaceutical technology for increasing the solubility, absorption, and therapeutic efficacy of hydrophobic APIs. Particles in solid dispersions have a reduced size, mostly amorphous state, as well as a higher degree of porosity and wettability, which allows to significantly increase the solubility of sparingly soluble APIs [3].

That is why, to increase the solubility of nimesulide, the technology of solid dispersion systems was applied. SDS of nimesulide was formed by solvent evaporation using polyvinylpyrrolidone K-25 (PVP K-25) as a polymer carrier. The study of dissolution profiles was carried out on a VK7000 vane dissolution device with a VK750D water heater (Vankel, USA) according to the method EPh 8.0 (2.9.3). The volume of the dissolution medium was 900 ml, the speed of rotation of the blade was 50 rpm, and the temperature was 37 °C. When studying dissolution profiles of nimesulide, it was taken into account that API is a weak acid with low solubility in water, so the use of standard media with low pH values (1.2 and 4.5) for comparison of dissolution profiles is unacceptable. Therefore, the research was carried out in buffer environments with a pH of 6.8; 7.5 and 7.8 (phosphate buffer solutions). The concentration of nimesulide was determined by the spectrophotometric method in the ultraviolet region on an OPTIZEN POP UV/VIS spectrophotometer (Mecasys, South Korea) at a wavelength of 400 nm. "Aulin", granules for oral suspension, 100 mg/2 g, was used as a comparison drug (Angelini Pharma, Czech Republic).

According to the results of the "Dissolution" test, it was established that the formation of SDS by solvent evaporation had a significant effect on improving the solubility of nimesulide. When studying the kinetics of the release of nimesulide in a buffer medium of pH=6.8, a more intense release of nimesulide from SDS was observed in the first minutes compared to the original drug. The degree of release of nimesulide from SDS in the first 5 min. was about 14%, while the comparison drug showed only 8% API release. For 10 min. during the test, the degree of release of nimesulide from SDS increased to 16%, while the indicators of "Aulin" remained at the same level. At the end of the experiment, the degree of dissolution of nimesulide was 18%, and "Aulin" was only 11% ($p < 0.05$). In the buffer environment pH=7.5, the degree of release of nimesulide from the polymer SDS in the first 5 minutes was 55%, which is 1.3 times more compared to the original drug "Aulin". After 90 min. from the beginning of the study, the degree of nimesulide released from the SDS composition was more than 77%, while "Aulin" showed only 59% ($p < 0.05$). The degree of release of nimesulide from SDS in buffer medium pH=7.8 is also higher than that of "Aulin". At the beginning of the experiment (5 min.), the degree of release of nimesulide from SDS was 1.44 times higher compared to the original drug. At the end of the study, the degree of nimesulide released from the SDS composition was more than 90%, while "Aulin" showed 80% ($p < 0.05$).

It was concluded that the introduction of nimesulide into a solid dispersion system based on a water-soluble polymer carrier by the method of solvent evaporation improves the degree of release of nimesulide in all studied buffer media in comparison with the original drug, and the obtained SDS can be used as an API for the preparation of a highly soluble anti-inflammatory drug.

[1] A. Bruno, S. Tacconelli, P. Patrignani, Variability in the response to non-steroidal anti-inflammatory drugs: mechanisms and perspectives, *Basic Clin Pharmacol Toxicol* **114**(1), 56-63 (2014).

[2] K. D. Rainsford, Consensus Report Group on Nimesulide. Nimesulide—a multifactorial approach to inflammation and pain: scientific and clinical consensus, *Current medical research and opinion* **22**(6), 1161-1170 (2006).

[3] X. Zhang, H. Xing, Y. Zhao, Z. Ma, Pharmaceutical dispersion techniques for dissolution and bioavailability enhancement of poorly water-soluble drugs, *Pharmaceutics* **10**(3), 74 (2018).

PROOXIDANT PROPERTIES OF LORATADINE AND DESLORATADINE IN THE CHEMICAL SYSTEM OF AUTO-OXIDATION OF ADRENALINE

Daryna Taran, Volodymyr Bessarabov, Roman Smishko, Vadym Lisovyi, Galyna Kuzmina, Vladyslav Strashnyi

Department of Industrial Pharmacy, Kyiv National University of Technology and Design, Ukraine
d.taran@kyivpharma.eu

Neurodegenerative diseases (NDD) are a major health problem for the elderly. It is known that active forms of oxygen play a certain role in the pathogenesis of NDD.

According to the analysis of literary sources, it was found that some drugs, in particular antihistamines, show additional anti-inflammatory activity, which makes them promise in the treatment of neurodegenerative diseases. It is also known that antagonists of H₁-receptors show an antioxidant effect, inhibiting free radical reactions. Therefore, it is advisable to study the antioxidant activity of the most commonly used antihistamine drugs, such as loratadine and desloratadine. Loratadine is an effective, non-sedating antihistamine drug of the second generation of long-term action with a rapid and pronounced antiallergic effect and selective activity against peripheral H₁-receptors [1]. Desloratadine is a selective antagonist of H₁-histamine receptors of the third generation, which is an active metabolite of loratadine, and has anti-inflammatory and antioxidant properties [2].

The aim of the article: study of the effect of loratadine and desloratadine on the chemical system of autoxidation of adrenaline.

Materials and methods of research. Determination of the activity of loratadine and desloratadine in the chemical system of autoxidation of adrenaline was carried out *in vitro* spectrophotometrically [3]. The absorbance was measured for 7 minutes from the moment of adding low concentrations of adrenaline (230 μM) to the alkaline solution at intervals of 15 s. A 0.2 M carbonate buffer with a pH of 10.65 was used as an alkaline environment. The research was conducted at a temperature of 25.0°C. Kinetic studies were carried out on an OPTIZEN POP UV spectrophotometer (Mesasys, South Korea) with a built-in thermostat (thermostatic accuracy 25.0±0.1°C) in quartz glass cuvettes with an optical layer thickness of 1 cm at a wavelength of λ=347 nm.

Research results. The reaction rate of the formation of an intermediate product of autoxidation of adrenaline in the presence of loratadine (in the first sample) and desloratadine (in the second sample) in concentrations of 25, 50 and 100 μM in the system was investigated. The measurement was performed three times for each concentration. Quantitative expression of reaction rates was carried out by calculating the first-order rate constant (K_n^1) according to Eq. (1):

$$k_n^1 = \frac{1}{t} \cdot \ln \frac{D_\infty - D_0}{D_\infty - D_t} \quad (1)$$

where t – reaction time;

D_∞ – value of the absorbance after the end of the reaction;

D_0 – value of the absorbance at the beginning of the reaction;

D_t – the value of the absorbance at a certain point in time.

It was established that loratadine reliably accelerates the autoxidation reaction of adrenaline by 35%, 45% and 53% at concentrations of 25, 50 and 100 μM, respectively: $k_n^1(0) = (1.018 \pm 0.590) \cdot 10^{-3} \text{ s}^{-1}$; $k_n^1(25) = (1.370 \pm 0.028) \cdot 10^{-3} \text{ s}^{-1}$; $k_n^1(50) = (1.478 \pm 0.037) \cdot 10^{-3} \text{ s}^{-1}$; $k_n^1(100) = (1.579 \pm 0.021) \cdot 10^{-3} \text{ s}^{-1}$ ($p \leq 0,05$).

In turn, desloratadine reliably accelerates the auto-oxidation reaction of adrenaline, but not so intensively - by 13%, 15% and 18% at concentrations of 25, 50 and 100 μM, respectively: $k^1(0) = (1.018 \pm 0.590) \cdot 10^{-3} \text{ s}^{-1}$; $k_n^1(25) = (1.152 \pm 0.013) \cdot 10^{-3} \text{ s}^{-1}$; $k_n^1(50) = (1.117 \pm 0.013) \cdot 10^{-3} \text{ s}^{-1}$; $k_n^1(100) = (1.204 \pm 0.012) \cdot 10^{-3} \text{ s}^{-1}$ ($p \leq 0,05$).

Conclusions.

1. Loratadine and desloratadine stimulate the formation of superoxide radicals in the chemical system of autoxidation of adrenaline.
2. When the concentration of loratadine increases, the values of the rate constants of the first order of autoxidation of adrenaline increase up to 10%, and therefore this effect depends on the concentration of API.
3. Desloratadine does not so actively stimulate the formation of superoxide radicals in comparison with loratadine, its pro-oxidant effect is 23% less than that of loratadine.

[1] G. A. Jalbani, K. Aamir, A. M. Shaikh, M. A. Unar, R. Ashraf, F. M. Soomro, To evaluate and compare the effects of first generation anti-histamine (chlorpheniramine maleate) and second generation anti-histamine (loratadine) on isolated trachea of rabbit, J Pak Med Assoc **54**, 556-561 (2004).

[2] G. W. Canonica, F. Tarantini, E. Compalati, M. Penagos, Efficacy of desloratadine in the treatment of allergic rhinitis: a metaanalysis of randomized, double-blind, controlled trials, Allergy **62**(4), 359-366 (2007).

[3] T.V. Sirota, Novel approach to the study of adrenaline auto-oxidation and its use for the measurements of superoxide dismutase activity, Vopr. Med. Khim. **45**(3), 263-272 (1999).

CONCENTRATIONS OF FIBRINOGEN AND D-DIMER IN BLOOD PLASMA OF DONORS WITH VARIOUS TITERS OF ANTI-SARS-CoV-2 IgG

Antonina Rachkovska, Daryna Krenytska, Vitaliy Karbovskiy

Educational and Scientific Centre "Institute of Biology and Medicine" Taras Shevchenko National University of Kyiv
tonia01128@gmail.com

Background. Some clinical cases of long-term COVID-19 have been reported, which can be caused by micro- and macrothrombotic complications that persist after recovery. Although more information has been gathered on coagulation disorders during COVID-19, the post-COVID-19 period is unknown. Fibrinogen and D-dimer are the primary parameters for detecting an imbalance in the conversion of soluble fibrinogen and the cleavage of insoluble fibrin clots. Clinical data describe higher concentrations of fibrinogen and D-dimer that may lead to COVID-19 coagulopathy in ill patients [1, 2].

The aim of our research was to establish the concentration of fibrinogen and D-dimer in donor groups who recovered from COVID-19 depending on the titers of anti-SARS-CoV-2 IgG in the blood plasma.

Materials and methods. People who had suffered from COVID-19 agreed to be donors of blood plasma for biotechnological purposes at the "BIOPHARMA-PLASMA" company (Kyiv, Ukraine). Blood plasma was collected from donors who had recovered from COVID-19 3-6 months ago. Donors were checked by screening tests before blood plasma was used to produce targeted biotechnological drugs. We were sent the blood plasma of donors with determined anti-SARS-CoV-2 IgG titers for scientific research. The Abbott SARS-CoV-2 IgG serological assay was used to determine the titers of anti-SARS-CoV-2 IgG in blood plasma. We had donor groups with anti-SARS-CoV-2 IgG titers: 0 (n = 20), 10 ± 3 (n=20), 55 ± 5 (n=20), 65 ± 5 (n=20), 75 ± 5 (n=20), 85 ± 5 (n=20), 95 ± 5 (n=20), 125 ± 5 (n=20) and 175 ± 5 (n=20) Index (S/C). The concentration of fibrinogen was measured by the Clauss method. The concentration of D-dimer was determined by sandwich-type immunochemiluminescent assay using the D-dimer Test Kit for CLIA Maglumi (Snibe Co., Ltd., China).

Results. We examined the coagulation parameters in each donor group. We then identified the maximum and minimum concentrations of fibrinogen and D-dimer among donor groups with titers of anti-SARS-CoV-2 IgG ≥ 10 ± 3 Index (S/C). The donor group with titer of anti-SARS-CoV-2 IgG 0 Index (S/C) was chosen as a reference point.

We found that all donor groups with titers of anti-SARS-CoV-2 IgG ≥ 10 ± 3 Index (S/C) had higher concentrations of fibrinogen and D-dimer than in donors with titer – 0 Index (S/C).

The maximum concentration of fibrinogen was characterized for the donor group with titer of anti-SARS-CoV-2 IgG 10 ± 3 Index (S/C) that was higher by 107.4 % than in donors with titer - 0 Index (S/C). The minimum was determined in donor group with titer of anti-SARS-CoV-2 65 ± 5 Index (S/C), which was an increase by 32.1 % than in donors with titer - 0 Index (S/C), **Table 1**.

Table 1. Concentration of fibrinogen in blood plasma of donor groups

Donor group with titer of anti- SARS-CoV-2 IgG, Index (S/C)	Concentration of fibrinogen, mg/dL
0	238.70 ± 37.12
10 ± 3	495.13 ± 52.04
65 ± 5	315.24 ± 36.09

The maximum concentration of D-dimer was demonstrated in donor group with titer of anti-SARS-CoV-2 IgG 55 ± 5 Index (S/C) that was increase by 440 % than in donors with titer - 0 Index (S/C). The minimum was defined in donors with titers - 85 ± 5 and 175 ± 5 Index (S/C). Both had an increase of concentration D-dimer by 120 % than in donors with titer - 0 Index (S/C), **Table 2**.

Table 2. Concentration of D-dimer in blood plasma of donor groups

Donor group with titer of anti- SARS-CoV-2 IgG, Index (S/C)	Concentration of D-dimer, µg·FEO/L
0	0.10 ± 0.05
55 ± 5	0.54 ± 0.20
85 ± 5	0.22 ± 0.06
175 ± 5	0.22 ± 0.06

Conclusion. Our study focused on detecting key changes in coagulation parameters depending on the titers of anti-SARS-CoV-2 IgG. According to the described results, we may confirm the defect of the coagulation profile in donor groups with titers of anti-SARS-CoV-2 IgG ≥ 10 ± 3 Index (S/C). Therefore, it is necessary to carry out the additional *in vitro* and *in vivo* research with purified anti-SARS-CoV-2 IgG.

1. Aggarwal, M., Dass, J., Mahapatra, M. (2020). Hemostatic Abnormalities in COVID-19: An Update. Indian journal of hematology & blood transfusion: an official journal of Indian Society of Hematology and Blood Transfusion, 36(4), 616–626.

2. Kasinathan, G., Sathar, J. (2020). Haematological manifestations, mechanisms of thrombosis and anti-coagulation in COVID-19 disease: A review. Annals of medicine and surgery (2012), 56, 173–177. <https://doi.org/10.1016/j.amsu.2020.06.035>

CO-PRECIPIATION SYNTHESIS OF SAMARIUM-GADOLINIUM CO-DOPED CERIA THIN FILMS

Elessar Mhana^{1*}, Jurgita Čyvienė³, Brigita Abakevičienė^{2,3}

¹Faculty of Chemical Technology, Kaunas University of Technology, K. Baršausko st. 59, 51423 Kaunas, Lithuania

²Institute of Materials Science, Kaunas University of Technology, K. Baršausko st. 59, 51423 Kaunas, Lithuania

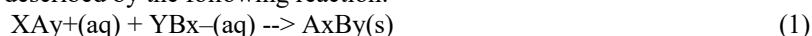
³Department of Physics, Kaunas University of Technology, Studentų st. 50, 51368 Kaunas, Lithuania

*elemha@ktu.lt

Renewable energy sources have dominated the primary fields in green energy applications over the past decade. Due to their high generated electrical efficiency, low activation loss, high quantity of chemical energy conversion to electric power, longevity, and lack of corrosion in the structural sections, solid oxide fuel cells (SOFCs) are one of the most widely utilized groups of fuel cells [1, 2]. Depending on the electrolyte material, sofc can operate in a wide temperature range (400 – 1000 °C).

Compared to other types of electrolytes, ceria-based materials show the highest ionic conductivity in low-temperature SOFC. Research and literature indicate that Gd and Sm, either as single or co-doped systems, increase conductivity more than other rare earth dopants in ceria-based electrolytes [3]. Samarium-Gadolinium-doped ceria (SGDC, stoichiometric formula $Ce_{0.825}Sm_{0.0875}Gd_{0.0875}O_{2-δ}$) nanopowders were synthesized using co-precipitation synthesis method, since it allows one to obtain fine nanopowders with controlled homogeneity, and the method is relatively fast and inexpensive.

Samarium (III) nitrate hexahydrate ($Sm(NO_3)_3 \cdot 6H_2O$, 99.9%, Sigma-Aldrich), Gadolinium (III) nitrate hexahydrate ($Gd(NO_3)_3 \cdot 6H_2O$, 99.9%, Sigma-Aldrich), and cerium (III) nitrate hexahydrate ($Ce(NO_3)_3 \cdot 6H_2O$, 99.0%, Fluka) were used as the source of metal cations. Oxalic acid ($C_2H_2O_4$, $\geq 99.0\%$, Sigma-Aldrich) and ammonium hydroxide (NH_4OH , 25%, Sigma-Aldrich) were used as precipitating agents, and the solvent was distilled water. As a result of strong supersaturation, the products formed during synthesis become insoluble. Precipitation occurs when supersaturation conditions are met, which is described by the following reaction:



where $+/-$ is the valence for metal cations and oxidizer ions, A and B are the initial molecules, AB is the final product, and x and y are free atoms and radicals. The synthesis scheme is shown in Figure 1.

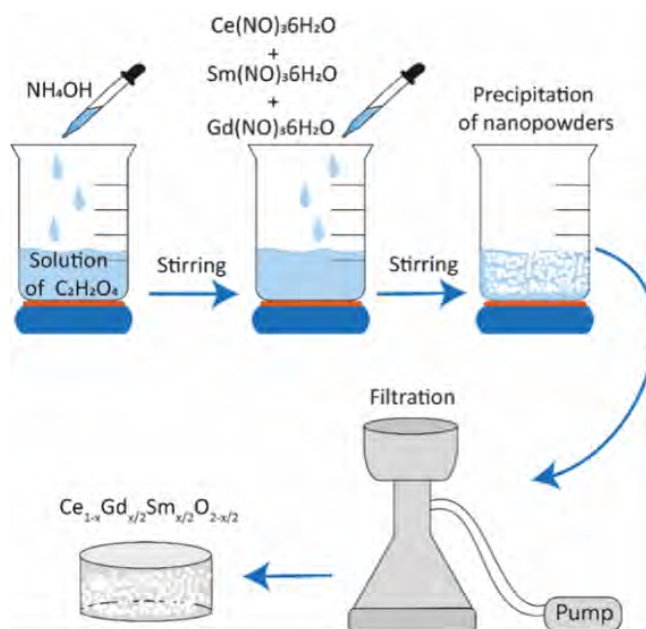


Fig. 1. Scheme of co-precipitation synthesis of ceria-based ceramic nanopowders

Acknowledgements. The research was funded by DAINA-2 project of a bilateral research funding programme by the Research Council of Lithuania (LMT) No. P-LL-21-124 and National Science Centre (NCN) No. UMO-2020/38/L/ST8/00513.

[1] MAHAPATRA, M.K.; P. SINGH, Fuel Cells. Energy Conversion Technology., 2013. DOI 10.1016/B978-0-08-099424-6.00024-7

[2] LINDORFER, J.; D.C. ROSENFELD; H. BÖHM, Fuel cells: Energy conversion technology., Elsevier Ltd, 2020. DOI 10.1016/B978-0-08-102886-5.00023-2

[3] COLES-ALDRIDGE, A. V.; R.T. BAKER., Oxygen ion conductivity in ceria-based electrolytes co-doped with samarium and gadolinium. Solid State Ionics. 2020. Vol. 347, p. 115255. DOI 10.1016/j.ssi.2020.115255.

OPEN READINGS | 2023

ORGANIZERS



Faculty of
Physics



SPIE. STUDENT
CHAPTER
VILNIUS
UNIVERSITY

OPTICA
Advancing Optics and Photonics Worldwide

STUDENT CHAPTER
VILNIUS UNIVERSITY



MEDIA PARTNER

LRT | .lt

PARTNER

Go Vilnius

SPONSORS



BROLIS



Altechna



MONO SPEKTRA

Optoteka

